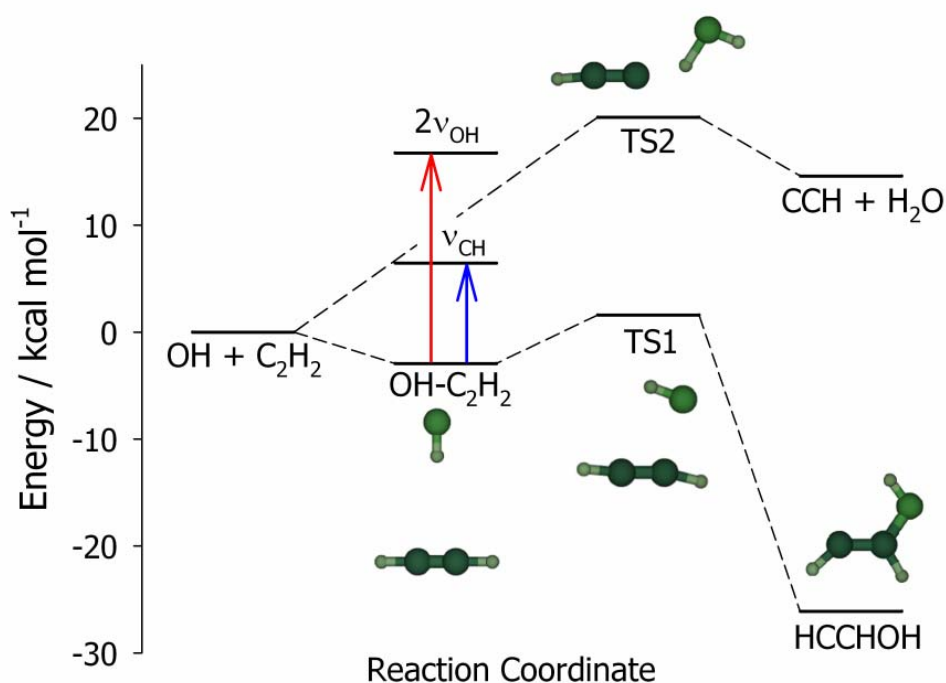


26th Annual Combustion Research Conference



Airlie Conference Center
Warrenton, Virginia
May 31 – June 3, 2005



Office of Basic Energy Sciences

Chemical Sciences, Geosciences & Biosciences Division

Cover Image: Addition and abstraction pathways for OH + acetylene reaction, showing IR excitation of reactant complex in the OH overtone stretch and asymmetric CH stretch fundamental regions. (*“Intermolecular Interactions of Hydroxyl Radicals on Reactive Potential Energy Surfaces”*, **Marsha I. Lester**, p160.)

FOREWORD

The achievement of National goals for energy conservation and environmental protection will rely on technology more advanced than we have at our disposal today. Combustion at present accounts for 85% of the energy generated and used in the U.S. and is likely to remain a dominant source of energy for the coming decades. Achieving energy conservation while minimizing unwanted emissions from combustion processes could be greatly accelerated if accurate and reliable means were at hand for quantitatively predicting process performance.

The reports appearing in this volume present work in progress in basic research contributing to the development of a predictive capability for combustion processes. The work reported herein is supported by the Department of Energy's Office of Basic Energy Sciences (BES) and in large measure by the chemical physics program. The long-term objective of this effort is the provision of theories, data, and procedures to enable the development of reliable computational models of combustion processes, systems, and devices.

The development of reliable models for combustion requires the accurate knowledge of chemistry, turbulent flow, and the interaction between the two at temperatures and pressures characteristic of the combustion environment. In providing this knowledge, the research supported by BES addresses a wide range of continuing scientific issues of long standing.

- For even the simplest fuels, the chemistry of combustion consists of hundreds of reactions. Key reaction mechanisms, the means for developing and testing these mechanisms and the means for determining which of the constituent reaction rates are critical for accurate characterization are all required.
- For reactions known to be important, accurate rates over wide ranges of temperature, pressure and composition are required. To assess the accuracy of measured reaction rates or predict rates that would be too difficult to measure, theories of reaction rates and means for calculating their values are needed. Of particular importance are reactions involving open shell systems such as radicals and excited electronic states.
- To assess the accuracy of methods for predicting chemical reaction rates, the detailed, state-specific dynamics of prototypical reactions must be characterized.
- Methods for observing key reaction species in combustion environments, for interpreting these observations in terms of species concentrations, and for determining which species control the net reactive flux are all required
- Energy flow and accounting must be accurately characterized and predicted.
- Methods for reducing the mathematical complexity inherent in hundreds of reactions, without sacrificing accuracy and reliability are required. Methods for reducing the computational complexity of computer models that attempt to address turbulence, chemistry, and their interdependence and also needed.

Although the emphasis in this list is on the development of mathematical models for simulating the gas phase reactions characteristic of combustion, such models, from the chemical dynamics of a single molecule to the performance of a combustion device,

require validation by experiment. Hence, the DOE program represented by reports in this volume supports the development and application of new experimental tools in chemical dynamics, kinetics, and spectroscopy.

The success of this research effort will be measured by the quality of the research performed, the profundity of the knowledge gained, as well as the degree to which it contributes to goals of resource conservation and environmental stewardship. In fact, without research of the highest quality, the application of the knowledge gained to practical problems will not be possible.

The emphasis on modeling and simulation as a basis for defining the objectives of this basic research program has a secondary but important benefit. Computational models of physical processes provide the most efficient means for ensuring the usefulness and use of basic theories and data. The importance of modeling and simulation remains well recognized in the Department of Energy and is receiving support through the Scientific Discovery through Advanced Computing (SciDAC) initiative; several work-in-progress reports funded through SciDAC are included in this volume.

During the past year, this program has benefited greatly from the involvement of Dr. Richard Hilderbrandt, program manager for Chemical Physics and for Computational and Theoretical Chemistry, and Dr. Eric Rohlfing, team leader for the Fundamental Interactions programs. Finally, the efforts of Sophia Kitts, Kellye Sliger and Rachel Smith of the Oak Ridge Institute for Science Education and Diane Marceau of the Division of Chemical Sciences, Geosciences, and Biosciences, Office of Basic Energy Sciences in the arrangements for the meeting are also much appreciated.

Frank P. Tully, SC-141
Division of Chemical Sciences, Geosciences, and Biosciences
Office of Basic Energy Sciences

May 31, 2005

Wednesday, June 1, 2005
Evening Session
Phillip R. Westmorland, Chair

6:15 pm	<i>“Chemical Kinetic Modeling of Combustion Chemistry”</i> , Charles K. Westbrook.....	314
6:45 pm	<i>“Comprehensive Mechanisms for Combustion Chemistry: Experiment Modeling, and Sensitivity Analysis”</i> , Frederick L. Dryer	63
7:15 pm	<i>“Kinetics and Dynamics of Combustion Chemistry”</i> , David L. Osborn	233
7:45 pm	Break	
8:00 pm	<i>“Time-Resolved Infrared Absorption Studies of the Dynamics of Radical Reactions”</i> , R. G. Macdonald.....	183
8:30 pm	<i>“Hydrocarbon Radical Thermochemistry: Gas-Phase Ion Chemistry Techniques”</i> , Kent M. Ervin	73
9:00 pm	<i>“Determination of Accurate Energetic Database for Combustion Chemistry by High-Resolution Photoionization and Photoelectron Methods”</i> , C. Y. Ng	225

Thursday, June 2, 2005

7:00 am **Breakfast**

Morning Session
Robert S. Barlow, Chair

8:15 am	<i>“Investigation of Non-Premixed Turbulent Combustion”</i> , Stephen B. Pope.....	241
8:45 am	<i>“Multiple-Time-Scale Kinetics”</i> , Michael J. Davis	59
9:15 am	<i>“Computational and Experimental Study of Laminar Flames”</i> , Mitchell D. Smooke	277
9:45 am	Break	
10:15 am	<i>“Combustion Chemistry”</i> , Nancy J. Brown	17
10:45 am	<i>“High Energy Processes”</i> , Alan R. Kerstein.....	148
11:15 am	<i>“Large Eddy Simulation of Turbulence-Chemistry Interactions in Reacting Flows”</i> , Joseph C. Oefelein	229
12:00 pm	Lunch	

Thursday, June 2, 2005
Afternoon and Evening Session
Terry A. Miller, Chair

5:15 pm	<i>“Picosecond Nonlinear Optical Diagnostics”</i> , Thomas B. Settersten 269
5:45 pm	<i>“Investigation of Polarization Spectroscopy and Degenerate Four-Wave Mixing for Quantitative Concentration Measurements”</i> , Robert P. Lucht..... 179
6:15 pm	Break
6:30 pm	<i>“Photoinitiated Processes in Small Hydrides”</i> , Curt Wittig 322
7:00 pm	<i>“Photodissociation and Photoionization of Radicals and Closed-Shell Hydrocarbons”</i> , Daniel Neumark..... 222
7:30 pm	Cash Bar
8:00 pm	Dinner

Friday, June 3, 2005

7:00 am *Breakfast*

Morning Session
Robert E. Continetti, Chair

8:15 am	<i>“Intermolecular Interactions of Hydroxyl Radicals on Reactive Potential Energy Surfaces”</i> , Marsha I. Lester 164
8:45 am	<i>“Single-Collision Studies of Energy Transfer and Chemical Reaction”</i> , James J. Valentini..... 307
9:15 am	<i>“Probing Radical Intermediates of Bimolecular Combustion Reactions”</i> , Laurie J. Butler 21
9:45 am	Break
10:00 am	<i>“Large Amplitude Motion as a Generator of Intramolecular Energy Transfer”</i> , David S. Perry 237
10:30 am	<i>“Experimental Characterization of the Potential Energy Surfaces for Conformational Isomerization in Aromatic Fuels”</i> , Timothy S. Zwier 334
11:00 am	<i>Closing Remarks</i>
11:30 am	Lunch

Table of Contents

<i>Photoelectron Photoion Coincidence Studies: Heats of Formation of Ions, Molecules, and Free Radicals</i> Tomas Baer	1	<i>Hydrocarbon Radical Thermochemistry: Gas-Phase Ion Chemistry Techniques</i> Kent M. Ervin	73
<i>Turbulence-Chemistry Interactions in Reacting Flows</i> Robert S. Barlow	5	<i>Experimental Kinetics and Mechanistic Investigations of Hydrocarbon Radicals Relevant to Combustion Modeling</i> Askar Fahr	77
<i>Theoretical Studies of Combustion Dynamics</i> Joel M. Bowman	9	<i>Spectroscopic and Dynamical Studies of Highly Energized Small Polyatomic Molecules</i> Robert W. Field	80
<i>Very High Pressure Single Pulse Shock Tube Studies of Aromatic Species</i> Kenneth Brezinsky	13	<i>Scanning Tunneling Microscopy Studies of Chemical Reactions on Graphite Surfaces</i> George Flynn	84
<i>Combustion Chemistry</i> Nancy J. Brown	17	<i>Quantitative Imaging Diagnostics for Reacting Flows</i> Jonathan H. Frank	88
<i>Probing Radical Intermediates of Bimolecular Combustion Reactions</i> Laurie J. Butler	21	<i>Mechanism and Detailed Modeling Of Soot Formation</i> Michael Frenklach	92
<i>Joint Theoretical and Experimental Study of Key Radicals in Hydrocarbon Combustion</i> Barry K. Carpenter	25	<i>Chemical Dynamics In The Gas Phase: Quantum Mechanics Of Chemical Reactions</i> Stephen K. Gray	96
<i>Ion Imaging Studies of Chemical Dynamics</i> David W. Chandler	29	<i>Computer-Aided Construction of Chemical Kinetic Models</i> William H. Green, Jr.	100
<i>Direct Numerical Simulation and Modeling of Turbulent Combustion</i> Jacqueline H. Chen, Evatt R. Hawkes, and Ramanan Sankaran	33	<i>High-Resolution Spectroscopic Probes of Chemical Dynamics</i> Gregory E. Hall	104
<i>Turbulent Combustion</i> Robert K. Cheng	37	<i>Flame Chemistry and Diagnostics</i> Nils Hansen	108
<i>Dynamics and Energetics of Elementary Combustion Reactions and Transient Species</i> Robert E. Continetti	41	<i>Spectroscopy and Kinetics of Combustion Gases at High Temperatures</i> Ronald K. Hanson and Craig T. Bowman	112
<i>Flame Sampling Photoionization Mass Spectrometry</i> Terrill A. Cool	45	<i>Theoretical Studies of Potential Energy Surfaces</i> Lawrence B. Harding	116
<i>State Controlled Photodissociation Of Vibrationally Excited Molecules And Hydrogen Bonded Dimers</i> F.F. Crim	49	<i>Chemical Accuracy From Ab Initio Molecular Orbital Calculations</i> Martin Head-Gordon	120
<i>Spectroscopy and Dynamics of Vibrationally Excited Transient Radicals</i> Hai-Lung Dai	52	<i>Laser Studies of Combustion Chemistry</i> John F. Hershberger	124
<i>Bimolecular Dynamics of Combustion Reactions</i> H. Floyd Davis	56	<i>Product Imaging of Molecular Dynamics Relevant to Combustion</i> P. L. Houston	129
<i>Multiple-time-scale kinetics</i> Michael J. Davis	59	<i>Terascale High-Fidelity Simulations of Turbulent Combustion with Detailed Chemistry</i> Hong G. Im, Arnaud Trouvé, Christopher J. Rutland, Jacqueline Chen	133
<i>Comprehensive Mechanisms for Combustion Chemistry: Experiment, Modeling, And Sensitivity Analysis</i> Frederick L. Dryer	63	<i>Ionization Probes of Molecular Structure and Chemistry</i> Philip M. Johnson	137
<i>Laser Photoelectron Spectroscopy of Ions</i> G. Barney Ellison	67		

<i>Investigating the chemical dynamics of bimolecular reactions of dicarbon and tricarbon molecules with hydrocarbons in combustion flames</i> Ralf I. Kaiser	140	<i>Dynamics of Activated Molecules</i> Amy S. Mullin	214
<i>Dynamical Analysis of Highly Excited Molecular Spectra</i> Michael E. Kellman	144	<i>Reacting Flow Modeling with Detailed Chemical Kinetics</i> Habib N. Najm	218
<i>High Energy Processes</i> Alan R. Kerstein	148	<i>Photodissociation and Photoionization of Radicals and Closed-shell Hydrocarbons</i> Daniel Neumark	222
<i>Kinetics of Combustion-Related Processes at High Temperatures</i> J. H. Kiefer	152	<i>Determination of Accurate Energetic Database for Combustion Chemistry by High-Resolution Photoionization and Photoelectron Methods</i> C. Y. Ng	225
<i>Theoretical Chemical Kinetics</i> Stephen J. Klippenstein	156	<i>Large Eddy Simulation of Turbulence-Chemistry Interactions in Reacting Flows</i> Joseph C. Oefelein	229
<i>Time-Resolved FTIR Emission and Advanced Light Source Studies of Photofragmentation, Radical Reactions, and Aerosol Chemistry</i> Stephen R. Leone	160	<i>Kinetics and Dynamics of Combustion Chemistry</i> David L. Osborn	233
<i>Intermolecular Interactions of Hydroxyl Radicals on Reactive Potential Energy Surfaces</i> Marsha I. Lester	164	<i>Large Amplitude Motion as a Generator of Intramolecular Energy Transfer</i> David S. Perry	237
<i>Theoretical Studies of Molecular Systems</i> William A. Lester, Jr.	168	<i>Investigation of Non-Premixed Turbulent Combustion</i> Stephen B. Pope	241
<i>Quantum Dynamics of Fast Chemical Reactions</i> John C. Light	171	<i>Optical Probes of Atomic and Molecular Decay Processes</i> S.T. Pratt	245
<i>Kinetics of Elementary Processes Relevant to Incipient Soot Formation</i> M. C. Lin	175	<i>Photoinitiated Reactions of Radicals and Diradicals in Molecular Beams</i> Hanna Reisler	249
<i>Investigation of Polarization Spectroscopy and Degenerate Four-Wave Mixing for Quantitative Concentration Measurements</i> Robert P. Lucht	179	<i>High Accuracy Calculation of Electronic Structure, Molecular Bonding and Potential Energy Surfaces</i> Klaus Ruedenberg and Mark S. Gordon	253
<i>Time-Resolved Infrared Absorption Studies of the Dynamics of Radical Reactions</i> R. G. Macdonald	183	<i>Active Thermochemical Tables – Thermochemistry for the 21st Century</i> Branko Ruscic	257
<i>Quantum chemical studies of chemical reactions related to the formation of polyaromatic hydrocarbons and of spectroscopic properties of their key intermediates</i> Alexander M. Mebel	187	<i>Theoretical Studies of Elementary Hydrocarbon Species and their Reactions</i> Henry F. Schaefer III	261
<i>Flash Photolysis-Shock Tube Studies</i> Joe V. Michael	191	<i>Spectroscopy and Dynamics of Transient Species</i> Trevor J. Sears	265
<i>Particle Diagnostics Development</i> H. A. Michelsen	195	<i>Picosecond Nonlinear Optical Diagnostics</i> Thomas B. Settersten	269
<i>Chemical Kinetics and Combustion Modeling</i> James A. Miller	199	<i>Theoretical Studies of Potential Energy Surfaces and Computational Methods</i> Ron Shepard	273
<i>Detection and Characterization of Free Radicals Relevant to Combustion Processes</i> Terry A. Miller	202	<i>Computational and Experimental Study of Laminar Flames</i> M. D. Smooke and M. B. Long	277
<i>Reaction Dynamics in Polyatomic Molecular Systems</i> William H. Miller	206	<i>Universal and State-Resolved Imaging Studies of Chemical Dynamics</i> Arthur G. Suits	281
<i>Gas-Phase Molecular Dynamics: Theoretical Studies Of Combustion-Related Chemical Reactions</i> James T. Muckerman	210	<i>Elementary Reaction Kinetics of Combustion Species</i> Craig A. Taatjes	285

<i>The Extraction of Underlying Molecular Vibrational Dynamics from Complex Spectral Regions</i> H.S. Taylor	289
<i>Theoretical Chemical Dynamics Studies of Elementary Combustion Reactions</i> Donald L. Thompson	291
<i>Elementary Reactions of PAH Formation</i> Robert S. Tranter	295
<i>Variational Transition State Theory</i> Donald G. Truhlar	299
<i>Kinetic Database for Combustion Modeling</i> Wing Tsang	303
<i>Single-Collision Studies of Energy Transfer and Chemical Reaction</i> James J. Valentini	307
<i>Molecular Dynamics as seen through Rydberg States</i> Peter M. Weber	310
<i>Chemical Kinetic Modeling of Combustion Chemistry</i> Charles K. Westbrook and William J. Pitz	314
<i>Probing Flame Chemistry with MBMS, Theory, and Modeling</i> Phillip R. Westmoreland	318
<i>Photoinitiated Processes in Small Hydrides</i> Curt Wittig	322
<i>Theoretical Studies of the Reactions and Spectroscopy of Radical Species Relevant to Combustion Reactions and Diagnostics</i> David R. Yarkony	326
<i>Gas-Phase Molecular Dynamics: Quantum Molecular Dynamics of Combustion Reactants and Molecular Spectroscopy Calculations</i> Hua-Gen Yu	330
<i>Experimental Characterization of the Potential Energy Surfaces for Conformational Isomerization in Aromatic Fuels</i> Timothy S. Zwier	334
Participants	338
Author Index	342

Progress report – March, 2005
**Photoelectron Photoion Coincidence Studies: Heats of Formation of Ions,
Molecules, and Free Radicals**

Tomas Baer (baer@unc.edu)
Department of Chemistry
University of North Carolina
Chapel Hill, NC 27599-3290
DOE Grant DE-FG02-97ER14776

Program Scope

The photoelectron photoion coincidence (PEPICO) technique is utilized to investigate the dissociation dynamics and thermochemistry of energy selected medium to large organic molecular ions. Extensive modeling of the dissociation rate constant using the RRKM theory or variational transition state theory (VTST) is used in order to determine the dissociation limits of energy selected ions. These studies are carried out with the aid of molecular orbital calculations of both ions and the transition states connecting the ion structure to their products. The results of these investigations yield accurate heats of formation of ions and free radicals. In addition, they provide information about the potential energy surface that governs the dissociation process. Isomerization reactions prior to dissociation are readily inferred from the PEPICO data.

The PEPICO Experiment

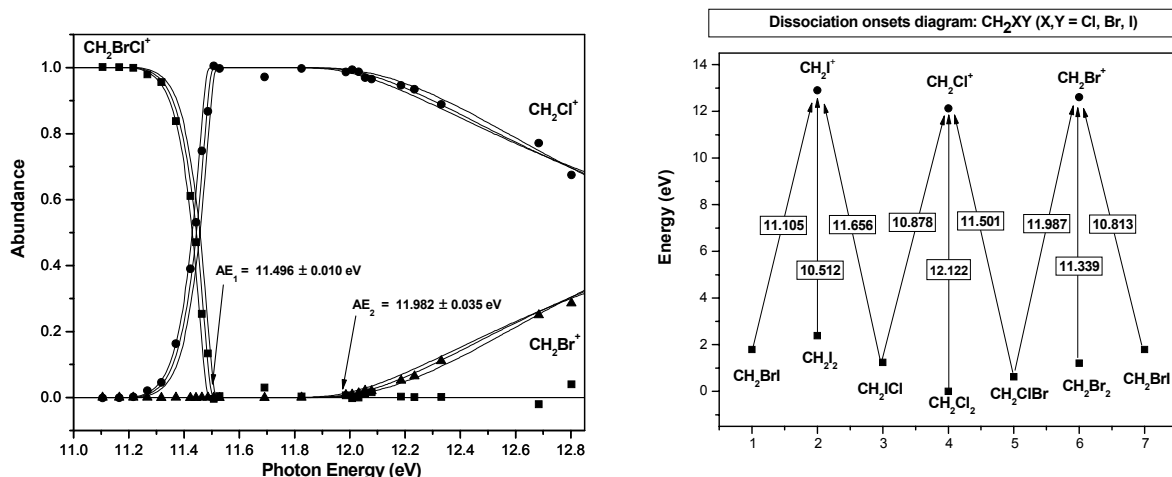
The threshold photoelectron photoion coincidence (TPEPICO) experiment in Chapel Hill is carried out with a laboratory H₂ discharge light source. Threshold electrons are collected by focusing them into a 1.5 mm hole that discriminates against electrons with perpendicular velocity components. The TPEPICO spectrometer incorporates a velocity focusing detector for threshold electrons and a separate detector for hot electrons so that two TPEPICO spectra are simultaneously collected. The ion TOF is either a linear version or a reflectron for studying H loss processes. This apparatus is now producing beautiful results. The purpose of the reflectron is to permit us to look at slower ion dissociation rates. The electrons provide the start signal for measuring the ion time of flight distribution. When ions dissociate in the microsecond time scale, their TOF distributions are asymmetric. The dissociation rate constant can be extracted by modeling the asymmetric TOF distribution. A high-resolution version of this experiment is currently being constructed in collaboration with an atomic physics group using an imaging detector for the electrons at the Chemical Dynamics Beamline of the ALS. When combined with coincidence ion detection, the results permit the measurement of ion dissociation limits to within 1 meV or 0.1 kJ/mol.

Recent Results

The Heats of Formation of CH₂XY, X, Y = Cl, Br, and I

The literature heats of formation for the dihalomethanes are in terrible shape. Some have only been measured once, others are only estimated. The error bars on some of the mixed dihalides are ± 20 kJ/mol. By measuring the onsets for the first and second dissociation limits by TPEPICO, it was possible to extract the heats of formation of all six molecules. The key to this achievement is the ability to determine quantitatively the second dissociation limit. The breakdown diagram for one of the dihalides is shown in the figure. The first onset can be

determined to within ± 10 meV. The only adjustable parameter is the 0 K onset. The rest of the curve is determined by the thermal energy distribution at 298 K. The second onset is much less sharp and must be modeled with transition state frequencies. The two parameter fit results in errors on the order of ± 30 meV (3 kJ/mol).



Figures 1 and 2. The breakdown diagram for CH_2BrCl showing the fractional abundance of the ions as a function of the ion internal energy. The onset data for all six dihalomethanes are plotted in Figure 2. The zero for the energy scale is the energy for $\text{CH}_2\text{Cl}_2 + 2 \text{ Br} + 2 \text{ I}$.

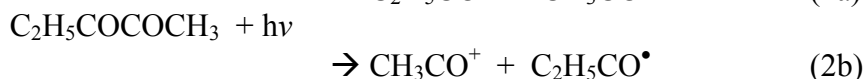
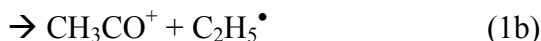
Figure 2 shows the first and second onsets for all of the dihalo methanes. By measuring all of the first and second onsets, it is possible to obtain the heats of formation of the ionic fragments as well as the neutral precursors, using the well established heat of formation of CH_2Cl_2 . It is interesting that we have 8 unknowns but 9 onset measurements. This means that the system is over determined, which helps reduce the errors in the derived heats of formation. The results are shown in the Table. This is the first consistent set of energies for this important class of molecules. Several of the literature values (e.g. CH_2I_2) contained major errors.

Species	$\Delta_f H^0_{0K}$	$\Delta_f H^0_{298K}$	$H^0_{298K} - H^0_{0K}$	$\Delta_f H^0_{298K}$ (lit.)
CH_2Cl_2	- 88.7	- 95.5 \pm 1.3	11.87	- 95.5 \pm 1.3
CH_2Br_2	24.5	3.2 \pm 2.7	12.69	4.7 \pm 8.3
CH_2BrCl	- 30.5	- 44.6 \pm 2.0	12.27	- 44.8 \pm 8.3
CH_2BrI	70.4	55.0 \pm 2.7	12.98	57.2 \pm 20
CH_2I_2	117.0	107.5 \pm 3.2	13.25	118.0 \pm 21
CH_2ICl	18.8	10.7 \pm 1.9	12.47	13.6 \pm 20

The Heats of Formation of the Propionyl ion and Radical and 2,3 Pentanedione by Threshold Photoelectron Photoion Coincidence Spectroscopy

The dissociative photoionization onsets for the formation of the propionyl ion ($\text{C}_2\text{H}_5\text{CO}^+$) and acetyl ion (CH_3CO^+) were measured from energy selected butanone and 2,3-pentanedione ions using the technique of threshold photoelectron photoion coincidence (TPEPICO)

spectroscopy. We use two starting molecules and three reactions to establish the heats of formation of the propionyl radical ($C_2H_5CO^\bullet$), the propionyl ion ($C_2H_5CO^+$), and $C_2H_5COCOCH_3$ (2,3-pentanedione). The reactions involved are:



The heat of formation of butanone is known to within 1 kJ/mol, as are the heats of formation of CH_3^\bullet , $C_2H_5^\bullet$, CH_3CO^+ , and CH_3CO^\bullet , the latter two in part from our previous study of this radical and its ion. The onset for reaction 1a establishes the propionyl ion heat of formation. The onset for reaction 1b confirms that our analysis of competitive reactions is valid. The derived onset agreed with the thermochemically known onset to within 1 kJ/mol. The onset for reaction 2a establishes the heat of formation of the di-ketone because the product heats of formation are known from reaction 1a and our previous studies for the acetyl radical. Finally, the onset for reaction 2b establishes the heat of formation of the propionyl radical.

The results are summarized in Table 2

Species	$\Delta_f H_{0K}^0$ ^a	$\Delta_f H_{298K}^0$ ^a	Other Experimental $\Delta_f H_{298K}^0$	Theoretical $\Delta_f H_{298K}^0$	$H_{298K}^0 - H_{0K}^0$
Propionyl ion	632.4 ± 1.4	618.6 ± 1.4	617.8	617.9 618	14.9°
Propionyl radical	-18.0 ± 3.4	-31.7 ± 3.4	-32.3 ± 4.2 -34.3 ± 8	-33.3	15.7°
2,3-pentanedione	-320.7 ± 2.5	-343.7 ± 2.5		-338.3 -348	24.7°

Future Plans

At the present time, we are investigating the dissociative photoionization of PEt_3 , where Et = ethyl. This molecule dissociates in a sequential manner by losing C_2H_4 in the following sequence of reactions:



The interest in this system is that the heats of formation of PEt_3 , $HPEt_2$, and H_2PEt have never been measured. By measuring the energy required to convert any of these three molecules to the final products, $PH_3^+ + nC_2H_4$, we can determine the starting material's heat of formation because the energetics of the final product are well established. In addition, it affords us a chance to model sequential reactions on a system that can be accessed from three different molecules, H_3-nPEt_n ($n = 0, 1, 2, 3$).

We continue to be involved in the constructing of a velocity focusing TPEPICO experiment in collaboration with an atomic physics group at the ALS. This will incorporate an imaging plate for either electrons or ions and a straight TOF for the other particle. Of particular interest to us is to obtain a full photoelectron spectrum between 0 and 1 eV in coincidence with the ions. This experiment will permit us for the first time to measure the distribution of zero energy electrons in Franck-Condon gaps, a problem that has been unresolved since its discovery

some 20 years ago. In addition, we will be able to collect TPES with a resolution of 1 meV. The experimental set-up will be available for all people interested in carrying out TPEPICO experiments at the ALS.

Publications from DOE supported work 2003 – 2005

B. Sztaray and T. Baer, The suppression of hot electron in threshold photoelectron photoion coincidence spectroscopy using velocity focusing optics, *Rev. Sci. Instrum.* **74** 3763-3768 (2003)

X.M. Qian, T. Zhang, C. Chang, P. Wang, C.Y. Ng, Y-H Chiu, D.J. Levandier, S. Miller, R.A. Dressler, T. Baer, and D.S. Peterka, High-resolution state-selected ion-molecule reaction studies using pulsed field ionization photoelectron-secondary ion coincidence method, *Rev. Sci. Instrum.* **74** 4096-4109 (2003)

T. Baer and B. Sztaray, The statistical theory for unimolecular decay of organic and organometallic ions, volume 4, *Encyclopedia of Mass Spectrometry*, Elsevier, (2005) Pp. 9-18.

W.K. Lewis, B.E. Applegate, J. Sztáray, B. Sztáray, T. Baer, R.J. Bemish, and R.E. Miller, Electron impact ionization in helium nanodroplets: Controlled fragmentation by active cooling of molecular ions, *J. Am. Chem. Soc.* **126** 11283-11292 (2004)

E.A. Fogleman, H. Koizumi, J. Kercher, B. Sztaray, and T. Baer, The Heats of Formation of the Acetyl radical and Ion obtained by Threshold Photoelectron Photoion Coincidence, *J. Phys. Chem. A* **108** 5288-5294 (2004)

H. Koizumi and T. Baer, The heats of formation of *t*-butyl isocyanide and other alkyl isocyanides by photoelectron photoion coincidence spectroscopy, *J. Phys. Chem. A* **108** 5956-5961 (2004)

A. Bodi, J. P. Kercher, T. Baer, and B. Sztáray On the Parallel Mechanism of the Dissociation of Energy-Selected $\text{P}(\text{CH}_3)_3^+$ Ions, *J. Phys. Chem. B* **109** xxxx – xxxx (2005).

Adam Brooks,^a Kai-Chung Lau,^b C.Y. Ng,^b and Tomas Baer^a The C_3H_7^+ Appearance Energy from 2-Iodopropane and 2-Chloropropane Studied by Threshold Photoelectron Photoion Coincidence, *European J. of Mass Spectrom.*, in press (2005)

A.F. Lago, J.P. Kercher, A. Bodi, B. Sztáray, B. Miller, D. Wurzelmann, and T. Baer, The heats of formation of the dihalomethanes, CH_2XY , (X,Y = Cl, Br, and I), by threshold photoelectron photoion coincidence, *J. Phys. Chem. A* **109** 1802-1809 (2005)

J.P. Kercher, E.A. Fogleman, H. Koizumi, B. Sztáray, and T. Baer, The Heats of Formation of the Propionyl ion and Radical and 2,3 Pentanedione by Threshold Photoelectron Photoion Coincidence Spectroscopy, *J. Phys. Chem. A* **109** 939-946 (2005)

T. Baer, B. Sztáray, J. P. Kercher, A.F. Lago, A. Bödi, C. Skull, and D. Palathinkal, Threshold Photoelectron Photoion Coincidence Studies of Parallel and Sequential Dissociation Reactions, *Phys. Chem. Chem. Phys.* In press (2005)

Turbulence-Chemistry Interactions in Reacting Flows

Robert S. Barlow
Combustion Research Facility
Sandia National Laboratories, MS 9051
Livermore, California 94551
barlow@ca.sandia.gov

Program Scope

This program is directed toward achieving a more complete understanding of turbulence-chemistry interactions in flames. In the Turbulent Combustion Laboratory (TCL) at the CRF, simultaneous line imaging of spontaneous Raman scattering, Rayleigh scattering, and two-photon laser-induced fluorescence (LIF) of CO is applied to obtain spatially and temporally resolved measurements of temperature, the concentrations of all major species, and mixture fraction (ξ), as well as gradients in these quantities in hydrocarbon flames. The instantaneous three-dimensional orientation of the turbulent reaction zone is also measured by imaging of OH LIF in two crossed planes, which intersect along the laser axis for the multiscale measurements. These combined data characterize both the thermo-chemical state and the instantaneous flame structure, such that the influence of turbulent mixing on flame chemistry may be quantified. Our experimental work is closely coupled with international collaborative efforts to develop and validate predictive models for turbulent combustion. This is accomplished through our visitor program and through an ongoing series of workshops on Turbulent Nonpremixed Flames (TNF). Within the CRF we are collaborating with Joe Oefelein to use highly-resolved large-eddy simulations (LES) of our experimental flames in order to gain greater fundamental understanding of dynamic, multi-scale, flow-chemistry interactions.

Recent Progress

Recent experimental work has focused on two areas: 1) the progression toward global extinction in piloted jet flames of $\text{CH}_4/\text{H}_2/\text{air}$ mixtures at high Reynolds number, and 2) the effects of spatial averaging and experimental noise in measurements of scalar dissipation. Both investigations are being conducted in collaboration with university research groups and experiments have included student visitors, which is consistent with the operation of the CRF as a User Facility.

Progressive Extinction in Piloted $\text{CH}_4/\text{H}_2/\text{Air}$ Jet Flames

Accurate prediction of localized extinction in turbulent flames is broadly recognized as one of the essential requirements for robust predictive combustion models, but few modeling approaches have so far demonstrated this capability when compared to detailed multiscale experiments. Both experimental and computational studies have shown that the degree of localized extinction becomes very sensitive to boundary conditions as a flame approaches global extinction. The piloted CH_4/air flames, which have been the primary targets for models that address extinction, include too few cases to rigorously test the ability of models to predict the progression of localized extinction as a flame series moves from a fully burning state toward blowout.

In collaboration with Henri Ozarovsky and Peter Lindstedt (Imperial College) we conducted multiscale measurements in a series of CH₄/H₂/air jet flames in order to provide more refined data on this progression toward blowout. CH₄ and H₂ were used in equal proportions (by volume) and this fuel flow was partially premixed with air. This mixture allows for operation of a fully burning piloted jet flame at higher Reynolds numbers ($Re \geq 60,000$) than can be achieved using CH₄/air. Local extinction was introduced and then progressively increased by decreasing the flow rate to the premixed pilot flame. A total of 18 cases were measured, including 6 pilot flow rates for each of 3 fuel mixtures (equivalence ratio, $\phi = 3.17, 2.5,$ and 2.1 in the jet fluid). The progression of local extinction in the $\phi = 3.17$ series is illustrated in Fig. 1, which shows scatter plots of temperature and CH₄ mass fraction. Analysis of the experimental data and pdf calculations of these flames are both in progress, with the focus of the calculations being on the performance of mixing models in predicting the progress of localized extinction.

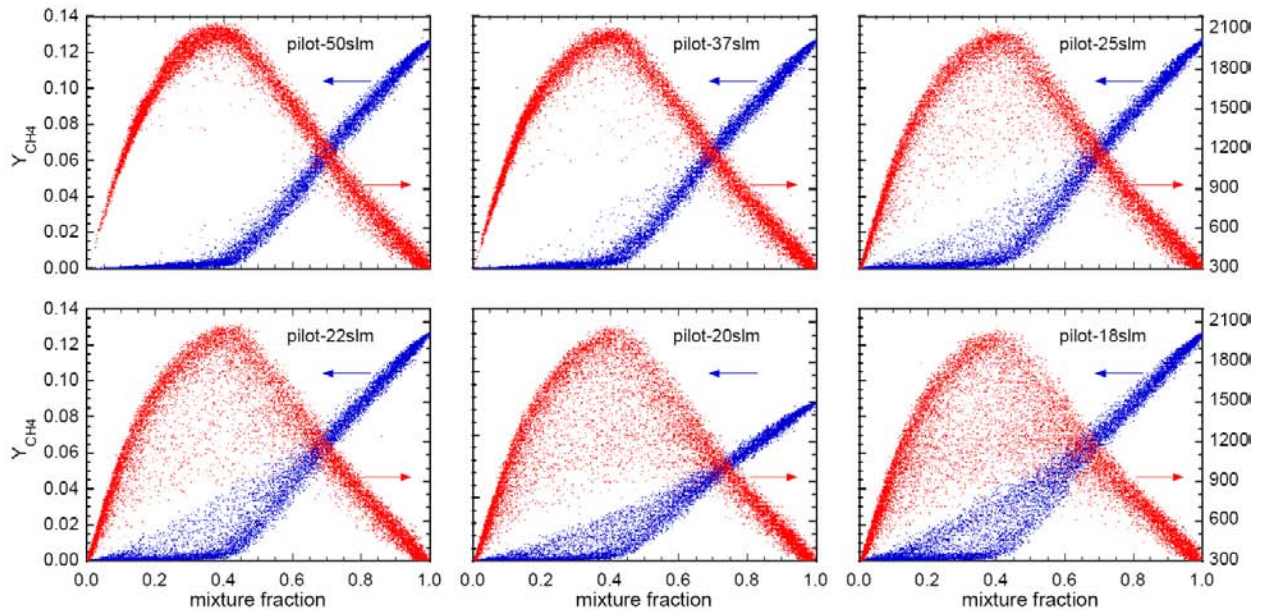


Fig. 1. Measured temperature and CH₄ mass fraction in six piloted flames of CH₄/H₂/air at Reynolds number 60,000. All data are from a streamwise location of $x/d=4$, and each data set comprises roughly 60,000 samples. The degree of local extinction is increased by reducing the pilot flow rate.

Effects of Noise and Spatial Averaging in Scalar Dissipation Measurements

We have made significant progress toward quantifying the combined effects of experimental noise and spatial averaging on laser-based measurements of scalar dissipation in turbulent flames. Because scalar dissipation, $\chi = 2D_\xi(\nabla\xi \cdot \nabla\xi)$ or $\chi_r = 2D_\xi(\partial\xi/\partial r)^2$ for the radial contribution, is determined from the square of the measured gradient in mixture fraction, ξ , experimental noise in the mixture fraction measurements always increases the apparent measured mean scalar dissipation value. This is true in both laminar and turbulent flames. Quantitative knowledge of this noise contribution is essential if experimental scalar dissipation results are to be used to test and validate scalar dissipation models for turbulent combustion computations. Investigations are being carried out in collaboration with Dirk Geyer (Technical University of Darmstadt), Noel Clemens (UT Austin), and Guanghua Wang (new Sandia postdoc).

Experiments were conducted during 2004 to quantify noise statistics in measurements of mixture fraction in laminar flames and to determine the effect of noise on scalar dissipation measurements in turbulent flames. An enclosed laminar jet flame burner was constructed to eliminate flame unsteadiness. Noise in the measurements of mixture fraction was demonstrated to scale as the inverse of the square root of laser energy and to have a normal distribution around the mean. Analysis shows and measurements confirm that in steady laminar flows or flames experimental noise contributes an additive term to the measured scalar dissipation, such that the apparent mean scalar dissipation is given by $\langle \chi_n \rangle = \langle \chi \rangle + D_\xi (\sigma_\xi / 2\Delta r)^2$, where $\langle \chi \rangle$ is the noise-free scalar dissipation obtained from the gradient of the averaged mixture fraction profile, D_ξ is the mixture diffusivity, σ_ξ is the mixture fraction noise at each location, and Δr is the data spacing in the radial (flame-normal) direction. Figure 2a demonstrates agreement between the measured and analytical noise terms and also shows that the noise contribution is roughly a 10% effect in this laminar flame, where the maximum scalar dissipation is roughly 27 s^{-1} .

Analysis of the noise contribution to scalar dissipation measurements in turbulent flames is more complex. However, preliminary results suggest that noise is not a significant issue for the present experimental system, which was specifically developed to achieve high precision in the measurements of mixture fraction. Measurements at representative locations in the well-know CH_4/air piloted flame D were repeated using 1, 2, and 4 Nd:YAG lasers (factor of ~ 2 overall difference for noise in the mixture fraction measurement). The conditional mean and rms of scalar dissipation showed no significant dependence on laser energy, indicating that true turbulent fluctuations in scalar dissipation dominate the contribution from noise and that the relative accuracy of the instantaneous scalar dissipation measurements increase with increasing dissipation. Representative results are shown in Fig. 2b.

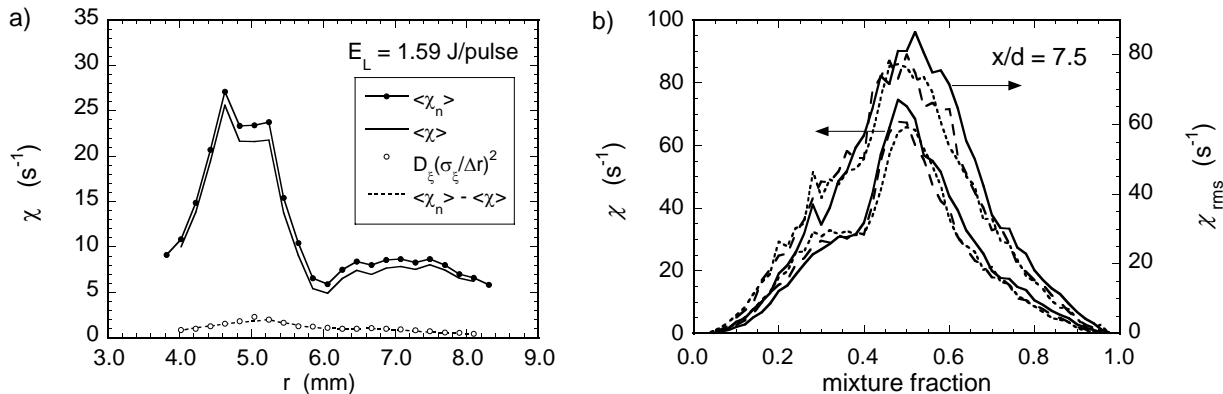


Fig. 2. a) Noise contribution to the measured scalar dissipation in a steady laminar CH_4/air jet flame. b) Conditional mean and rms scalar dissipation measured at $x/d=7.5$ in piloted flame D using four laser energy levels: 1.59 J/pulse (solid), 0.79 J/pulse (dashed), 0.42 J/pulse (dotted).

Future Plans

Completion of work on the combined effects of noise and spatial averaging on measurements of scalar dissipation in turbulent flames is our highest near-term priority. This will allow quantitative evaluation of model predictions of scalar dissipation in the Sandia piloted flames. Preliminary comparisons conducted at the TNF7 Workshop (July 2004) revealed significant disagreement among model results for piloted flame D, highlighting the need for reliable scalar dissipation measurements. A more detailed comparison of measured and modeled

results on scalar dissipation is planned for TNF8 (Heidelberg 2006). An important aspect of this work will be to compare measured scalar dissipation statistics and instantaneous scalar fields with results from highly-resolved LES (Oefelein) where the sub-grid scale contribution to scalar dissipation is expected to be small compared to the resolved scalar dissipation. More generally, the use of closely coupled experimental and LES research is expected to be a major theme of future investigations of fundamental processes of turbulent combustion, including both nonpremixed and premixed flames.

Experiments are in progress or are planned for several turbulent flame configurations, including the jet flames of $\text{CH}_4/\text{H}_2/\text{N}_2$ (the DLR flames) with emphasis on scalar vs. thermal dissipation, lifted methane flames in air with emphasis of the scalar structure of edge flames in the stabilization region, confined swirling premixed $\text{CH}_4/\text{H}_2/\text{air}$ flames, bluff-body and swirl stabilized jet flames (collaboration with Sydney University), and turbulent stratified premixed flames (collaboration with TU Darmstadt). All of these studies are aligned with the ongoing TNF Workshop process to systematically and collaboratively address fundamental aspects of turbulent combustion from experimental and computational perspectives in order to accelerate the development of science-based predictive models for complex combustion systems.

BES Supported Publications (2003 - present)

Y. Zheng, R.S. Barlow, J.P. Gore, "Measurements and Calculations of Spectral Radiative Intensities for Turbulent Non-Premixed and Partially Premixed Flames," *ASME J. Heat Transfer*, **125**, 678-696 (2003).

Y. Zheng, R. S. Barlow, J.P. Gore, "Spectral Radiative Properties of Turbulent Partially Premixed Flames," *ASME J. Heat Transfer*, **125**, 1065-1073 (2003).

A.N. Karpetis, T.B. Settersten, R.W. Schefer, and R.S. Barlow, "Laser Imaging System for Determination of Three-Dimensional Scalar Gradients in Turbulent Flames," *Optics Lett.* **29**, 355-357 (2004).

A.R. Masri, P.A.M. Kalt, R.S. Barlow, "The compositional structure of swirl-stabilized turbulent nonpremixed flames," *Combust. Flame* **137**, 1-37 (2004).

R.S. Barlow, A.N. Karpetis, "Measurements of Scalar Variance, Scalar Dissipation, and Length Scales in Turbulent Piloted Methane/Air Jet Flames," *Flow Turb. Combust.*, **72**, 427-448 (2004).

A.N. Karpetis and R.S. Barlow, "Measurements of Flame Orientation and Scalar Dissipation in Turbulent Partially Premixed Methane Flames," *Proc. Combust. Inst.* **30**, 665-672 (2005).

R.S. Barlow, A.N. Karpetis, "Scalar Length Scales and Spatial Averaging Effects in Turbulent Piloted Methane/Air Jet Flames," *Proc. Combust. Inst.* **30**, 673-680 (2005).

K. Kohse-Hoinghaus, R. S. Barlow, M. Alden, J. Wolfrum, "Combustion at the Focus: Laser Diagnostics and Control," *Proc. Combust. Inst.* **30**, 89-123, (2005) (invited plenary paper).

R.S. Barlow, J.H. Frank, A.N. Karpetis, J.-Y. Chen, "Piloted Methane/Air Jet Flames: Transport Effects and Aspects of Scalar Structure," *Combust. Flame*, (submitted).

R. Cabra, J.-Y. Chen, R.W. Dibble, A.N. Karpetis, R.S. Barlow, "Lifted Methane-Air Jet Flames in a Vitiated Coflow," *Combust. Flame*, (submitted).

Web-Based Information

<http://www.ca.sandia.gov/CRF/staff/barlow.html>

<http://www.ca.sandia.gov/TNF>

Research Page

TNF Workshop

Theoretical Studies of Combustion Dynamics

Joel M. Bowman
Cherry L. Emerson Center for Scientific Computation and
Department of Chemistry, Emory University
Atlanta, GA 30322, jmbowma@emory.edu

Program Scope

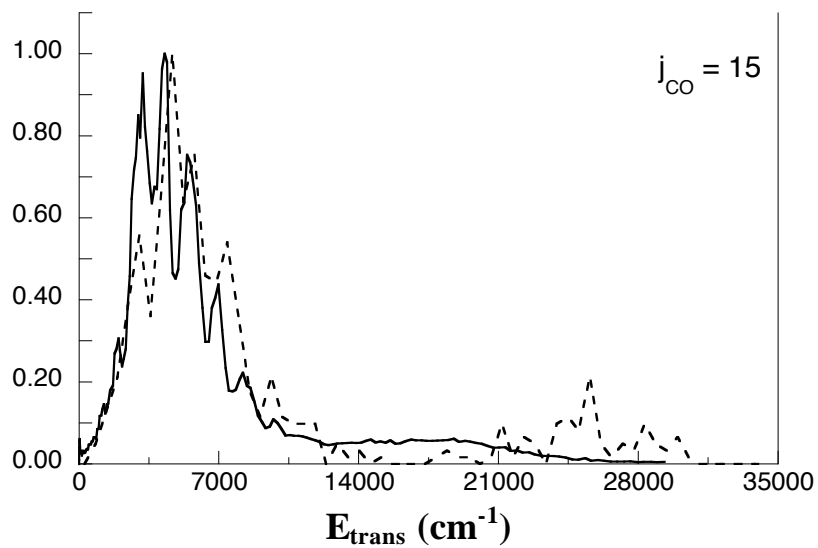
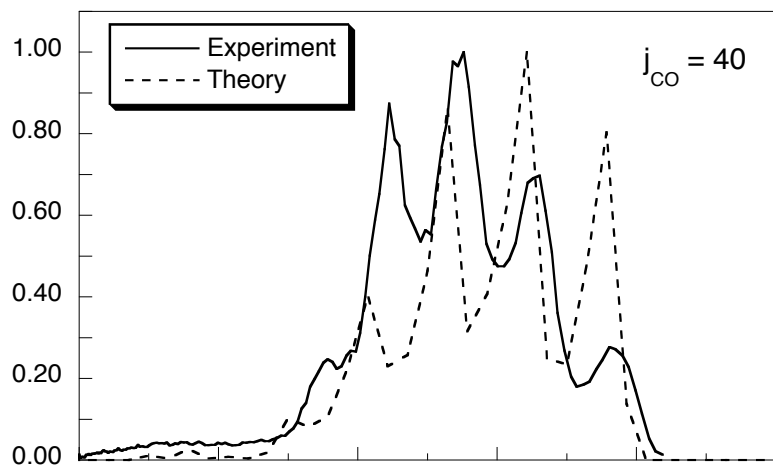
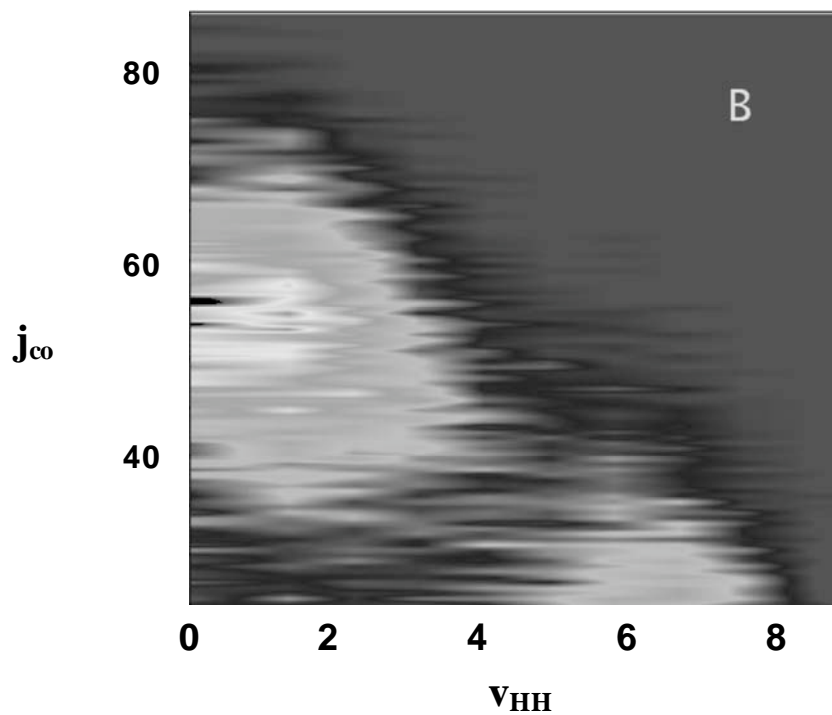
The research supported by the Department of Energy is to develop and apply methods to study the dynamics of chemical processes of importance in gas-phase combustion. These include quantum and quasiclassical calculations of bimolecular and unimolecular reactions and the *ab initio*-based potentials that govern these reactions. Recent work has resolved a puzzle about the photodissociation of H_2CO and in the process has widened our understanding of chemical reactivity. Additional completed work has looked at a careful comparison of the quantum and two types of quasiclassical calculations of the $\text{O}(^3\text{P})+\text{HCl}$ reaction on two potential energy surfaces.

Recent Progress

The roaming H atom: photodissociation of H_2CO

The photodissociation dynamics of formaldehyde has been of great interest, both experimentally¹⁻⁴ and theoretically.⁵⁻⁹ We recently completed a global potential surface (PES) for H_2CO , in collaboration with L. B. Harding.¹⁰ This surface describes both the molecular and $\text{H}+\text{HCO}$ radical channels, as well as the *cis* and *trans* isomers HCOH . The surface was used in several dynamical studies of the photodissociation of H_2CO as well as the bimolecular reaction of $\text{H} + \text{HCO} \rightarrow \text{H}_2 + \text{CO}$. The most interesting, completed calculations were those done in collaboration with Arthur Suits' group. They measured the CO and H_2 time of flight distributions for known quantum states of CO following photodissociation at $30\,340\text{ cm}^{-1}$. These experiments were done to examine a curious feature in the CO rotational distribution reported by Moore and co-workers¹¹ in 1993. This was a shoulder in low rotational states and which was not expected nor seen in dynamics calculations done at that time. Suits was able to correlate this weak bimodal feature with very highly excited vibrational states of H_2 (v up to 7). With the availability of a global PES we were able to perform quasiclassical dynamics calculations of the photodissociation at this energy and were quite pleased to see this feature in the calculations.¹² This is shown in the image plot where j_{CO} is plotted against v_{HH} . As seen there is a weak peak at j_{CO} around 10 and j_{CO} of 7 and a much more intense peak at around $j_{\text{CO}} = 55$ and $v_{\text{HH}} = 0$. The comparison with the experimental time-of-flight (TOF) distributions shows very good agreement and indicates in another fashion the correlation of low j_{CO} with high v_{HH} and vice-versa. (The quasiclassical TOF distribution was obtained by first binning the vibration/rotation states of CO and H_2 and then calculating the quantized translational energy.)

It remained to understand the source of the puzzling peak at low j_{CO} and high v_{HH} . This was done by examining trajectories leading to these products. What we found were "roaming" H atom trajectories. These are trajectories "heading" to the $\text{H}+\text{HCO}$ products but where the H atom orbits the HCO fragment until a favorable H-atom abstraction configuration is reached and then abstraction occurs at a large HH distances leading to vibrationally excited H_2 . (A movie of this trajectory can be found at <http://www.chemistry.emory.edu/faculty/bowman/news/index.html>). These trajectories, leading to the $\text{H}_2 + \text{CO}$ products completely by-pass the conventional transition state for this reaction and present another striking example of chemical reactivity that is not governed by the conventional transition state model.



Very recently we reported calculations of the branching ratio of the molecular and radical products as a function of the total energy.¹³

Quantum and Quasiclassical dynamics of the $O(^3P)+HCl$ reaction on $^3A''$ and $^3A'$ potential energy surfaces

We have completed quantum and quasiclassical reactive scattering studies of this reaction on both the $^3A''$ and $^3A'$ potential energy surfaces.¹⁴ We tested the standard quasiclassical binning and the so-called Gaussian binning and found much better agreement with the quantum results using the latter method.

Future Plans

We plan to continue dynamics studies of H_2CO photodissociation on the triplet surface T_1 , with a focus on the $H+HCO$ products, which also correlate with this surface. It is known that there is a barrier (of order 4 kcal/mol) on this surface¹⁵ and this is expected to play an identifiable role in translational energy distribution compared to the one arising from dissociation on S_0 . Our goal is to calculate the relevant parts of the full dimensional T_1 PES and perform the relevant dynamics to determine the internal and translational energy distributions of the radical products.

References

1. For a review up to 1983, see, C. B. Moore and J. C. Weisshaar, *Ann. Rev. Phys. Chem.* **34**, 525 (1983).
2. (a) T. J. Butenhoff, K. L. Carteton and C. B. Moore, *J. Chem. Phys.* **92**, 377 (1990); (b) W. F. Polik, D. R. Guyer and C. B. Moore, *J. Chem. Phys.* **92**, 3453 (1990); (c) R. D. Zee, M. F. Foltz, and C. B. Moore, *J. Chem. Phys.* **99**, 1664 (1993).
3. A. C. Terentis and S. H. Kable, *Chem. Phys. Lett.* **258**, 626 (1996).
4. L. R. Valachovic, M. F. Tuchler, M. Dulligan, Th., Droz-George, M., Zyrianov, A. Kolessov, H. Reisler, and C. J. Wittig, *J. Chem. Phys.* **112**, 2752 (2000).
5. Y. Chang, C. Minichino, and W. H. Miller, *J. Chem. Phys.* **96**, 4341 (1992).
6. Y. Yamaguchi, S. S. Wesolowski, T. J. Huis, H. F. Schaefer, *J. Chem. Phys.* **108**, 5281 (1998).
7. D. Feller, M. Dupuis, and B. C. Garrett, *J. Chem. Phys.* **113**, 218 (2000).
8. (a) X. Li, J. M. Millam and H. B. Schlegel, *J. Chem. Phys.* **113**, 10062 (2000); (b) W. Chen, W. L. Hase, and H. B. Schlegel, *Chem. Phys. Lett.* **228**, 436 (1994).
9. T. Yonehara and S., J. Kato *Chem. Phys.* **117**, 11131 (2002).
10. X. Zhang, S. Zou, L. B. Harding, and J. M. Bowman, *J. Phys. Chem. A*, **108**, 8980 (2004)
11. R. D. van Zee, M. F. Foltz, C. B. Moore, *J. Chem. Phys.* **99**, 1664 (1993).
12. S. A. Lahankar, S. K. Lee, S. D. Chambreau, A. G. Suits, X. Zhang, J. Rheinecker, L. B. Harding and J. M. Bowman, *Science* **306**, 1158 (2004).
13. X. Zhang, J. L. Rheinecker, and J. M. Bowman, *J. Chem. Phys.* **122**, 114313 (2005).
14. T. Xie, J. M. Bowman, J. W. Duff and M. Braunstein, and B. Ramachandran, *J. Chem. Phys.* **122**, 014301 (2005).
15. Y. Yamaguchi, S. S. Wesolowski, T. J. van Huis, and H. F. Schaefer III, *J. Chem. Phys.* **108**, 5281 (2002).

PUBLICATIONS SUPPORTED BY THE DOE (2002-present)

The challenge of high resolution dynamics: Rotationally mediated unimolecular dissociation of HOCl, J. M. Bowman, in *Accurate Description of Low-Lying Electronic States*, edited by M. Hoffman (ACS, Washington, DC, 2002).

A quasiclassical trajectory study of O(¹D)+HCl reactive scattering on an improved *ab initio* surface, K. M. Christoffel and J. M. Bowman, *J. Chem. Phys.* **116**, 4842 (2002).

Reduced dimensionality quantum calculations of acetylene \leftrightarrow vinylidene isomerization, S.-L. Zou and J. M. Bowman, *J. Chem. Phys.* **116**, 6667 (2002).

Resonances in the O(³P)+HCl reaction due to Van der Waals minima, T. Xie, D. Wang, J. M. Bowman, and D. E. Manolopoulos, *J. Chem. Phys.* **116**, 7461 (2002).

Overview of reduced dimensionality quantum approaches to reactive scattering, J. M. Bowman, *Theor. Chem. Acc.* **108**, 125 (2002).

Full dimensionality quantum calculations of acetylene \leftrightarrow vinylidene isomerization, S. Zou and J. M. Bowman, *J. Chem. Phys.* **117**, 5507 (2002).

A new *ab initio* potential energy surface describing acetylene/vinylidene isomerization, S. Zou and J. M. Bowman, *Chem. Phys. Lett.* **368**, 421 (2003).

Full-dimensionality quantum calculations of acetylene \leftrightarrow vinylidene isomerization, S.-L. Zou, J. M. Bowman, and A. Brown, *J. Chem. Phys.* **118**, 10012 (2003).

A scaled *ab initio* potential energy surface for acetylene and vinylidene, D. Xu, H. Guo, S.-L. Zou, and J. M. Bowman, *Chem. Phys. Lett.* **377**, 582 (2003).

Quantum calculations of the rate constant for the O(³P) + HCl reaction on new *ab initio* ³A'' and ³A' surfaces, T. Xie, J. M. Bowman, K. A. Peterson, and B. Ramachandran, *J. Chem. Phys.* **119**, 9601 (2003).

A global *ab initio* potential energy surface for formaldehyde, X.-B. Zhang, S.-L. Zou, L. B. Harding, and J. M. Bowman, *J. Phys. Chem. A* **108**, 8980 (2004).

Calculation of converged rovibrational energies and partition function for methane using vibrational-rotational configuration interaction, A. Chakraborty, D. G. Truhlar, J. M. Bowman, and S. Carter, *J. Chem. Phys.* **121**, 2071 (2004).

The roaming atom: Straying from the reaction path in formaldehyde decomposition, D. Townsend, S. A. Lahankar, S. K. Lee, S. D. Chambreau, A. G. Suits, X. Zhang, J. Rheinecker, L. B. Harding and J. M. Bowman, *Science* **306**, 1158 (2004).

Construction of a global potential energy surface from novel *ab initio* molecular dynamics for the O(³P) + C₃H₃ reaction, S. C. Park, B. J. Braams, and J. M. Bowman, *J. Theor. Comput. Chem.* **4**, 163 (2005).

Quasiclassical trajectory studies of the dynamics of H₂CO on a global *ab initio*-based potential energy surface, J. L. Rheinecker, X. Zhang, and J. M. Bowman, *Mol. Phys.* **103**, 1067 (2005).

Quasiclassical trajectory study of formaldehyde: H₂CO \rightarrow H₂+CO, H+HCO, X. Zhang, J. L. Rheinecker, and J. M. Bowman, *J. Chem. Phys.* **122**, 114313 (2005).

Quantum and quasi-classical studies of the O(³P) + HCl \rightarrow OH + Cl(²P) reaction using benchmark potential surfaces, T. Xie, J. M. Bowman, J. W. Duff and M. Braunstein, and B. Ramachandran, *J. Chem. Phys.* **122**, 014301 (2005).

Enhancement of tunneling due to resonances in pre-barrier wells in chemical reactions, J. M. Bowman, *Chem. Phys.* **308**, 255 (2005).

Very High Pressure Single Pulse Shock Tube Studies of Aromatic Species

Prof. Kenneth Brezinsky (PI)
Department of Mechanical Engineering (M/C 251),
University of Illinois at Chicago,
2039, Engineering Research Facility,
842, W. Taylor St., Chicago, IL 60607.
Kenbrez@uic.edu

Program Scope

Aromatic species form a significant percentage of commercial fuels such as gasoline and aviation fuels. Despite their abundance there is a very limited experimental database against which combustion models can be developed and validated, more so under conditions relevant to practical combustion viz. high pressures/high temperatures. Consequently the primary focus of this research program is aimed at understanding the oxidation and pyrolysis chemistry of aromatic molecules and radicals with the aim of developing a comprehensive kinetic model at conditions that are relevant to practical combustion devices.

The experimental approach uses a very high pressure single pulse shock tube to obtain experimental data over a wide pressure range in the high pressure regime, 5-1000 bars, at pre-flame temperatures and a broad spectrum of equivalence ratios. Stable species sampled from the shock tube are analyzed using standard chromatographic techniques using GC/MS and GC/TCD-FID. Experimental data from the HPST (stable species profiles) and data from other laboratories (if available) are simulated using kinetic models (if available) to develop a comprehensive model that can describe aromatics oxidation and pyrolysis over a wide range of experimental conditions.

The principal focus of our work during this grant period has been

- A. **Toluene Oxidation** - The development and validation of a comprehensive chemical kinetic model to describe the high pressure oxidation of toluene.
- B. **Toluene and Benzene Pyrolysis** – Experimental and modeling studies on the high pressure thermal decomposition of toluene and benzene.

Apart from these detailed experimental and modeling studies on the primary aromatics (our principal research focus) we have also performed work on

- C. **Ethane Combustion** – We have extended our earlier experimental work on ethane oxidation and pyrolysis and our current experimental database spans pressures from 5-1000 bars and temperatures from 1000-1450K. The data has been used to successfully develop a comprehensive model.
- D. **PAH Thermochemistry** – A new quantum chemical based cost effective technique has been developed to estimate $\Delta H_f^0_{298K}$ for a variety of aromatics, PAHs and their radicals with excellent accuracy (< 1 kcal/mol deviations). The simple but effective technique shows comparable accuracies to recently developed higher order (more parameters) schemes.
- E. **Shock Tube Characterization** - The validity of conventional treatments applied to the evaluation of experimental parameters behind the reflected shock wave – assumption of constant P and T, neglect of real gas effects and of the effects of continuing reactions during shock wave quenching, have been examined. The conventional treatments were all found to be valid.

Recent Progress

A. Toluene Oxidation

Toluene forms a significant percentage of commercial fuels and because of its abundance has been suggested in recent fuel workshops to be the primary single ring aromatic gasoline surrogate^{1,2}. The development and validation of a comprehensive chemical kinetic model to describe the high pressure oxidation of toluene is the first step in our research program aimed at elucidating reaction pathways/mechanisms and developing detailed models to describe the oxidation and pyrolysis of primary aromatic species and radicals.

Experimental data³ were obtained over a wide range of pressures from 25-610 bars in the temperature range 1200-1500 K at nominal reaction times of 1.5 ms for stoichiometric ($\Phi=1$) and fuel rich

($\Phi=5$) oxidation. The data set spans the first such high pressure kinetic measurements for the oxidation of toluene. Dilute reagent mixtures with initial toluene concentrations from 8- 85 ppm were used in these experiments. The experimental data were simulated using current literature models for toluene oxidation the KBG Model⁴ and the Dagaut et al. model⁵. Preliminary modeling³ indicated that the KBG model⁴ which is based on our prior work forms a good starting point for the development of a more comprehensive model valid over a wide range of conditions. A more detailed discussion of the experimental data and the model simulations is available in a recent publication³. The high pressure experimental data formed the basis of a more detailed modeling study⁶. The conventional tools of sensitivity analyses and reaction path analyses were used to identify the major contributors to fuel decay and intermediates growth at such high pressures. Several modifications were made to the KBG model⁴ to better reflect the HPST experimental data. The modified model⁶ was also successfully used to simulate the lower temperature (<1200K, 1atm) data from the Princeton turbulent flow reactor⁴ as well as ignition delay measurements made by Burcat et al.⁷ over a wide range of conditions (P=2-8 atm, 1300 K<T<1800 K) thereby extending the capability of the developed model and making it comprehensive over a wide range of conditions.

B. Toluene and Benzene Pyrolysis

The toluene oxidation work⁶ highlighted the importance of the pyrolytic pathways (especially for fuel rich conditions) involving toluene, benzene, the benzyl and phenyl radicals. Consequently, to isolate the contributions of the pyrolytic channels, complementary experimental and modeling studies were performed on benzene and toluene pyrolysis at high pressures. Experimental data were obtained for the pyrolysis of benzene⁸ and toluene⁹ at pressures of 25 and 50 bars over the temperature range 1200-1900 K. An array of intermediates was observed in these experiments. The experimental data were used to obtain rate coefficients for overall decay of the fuel (benzene and toluene) which was in line with earlier measurements at lower temperatures.

The experimental data for benzene pyrolysis were simulated using the high pressure toluene model developed in our lab⁶. Being more of an oxidative model, the model contained steps for the pyrolysis that were not well characterized for phenyl radical decomposition. Therefore, the model was updated by incorporating pyrolytic decay steps for phenyl and the modified model⁸ was able to simulate the experimental decay of benzene as well as C₂H₂ (the primary intermediate) growth accurately.

The toluene pyrolysis data was initially simulated using this modified model⁸. The modeling in this case was complicated due to the large uncertainties involving the branching ratios of the primary decay steps in toluene dissociation. Consequently we have also undertaken a complementary modeling study of H atom ARAS measurements from prior work on toluene pyrolysis by Braun-Unkloff et al.¹⁰ along with our own toluene decay profiles to obtain more reliable measures for the primary dissociation rates. Furthermore the model⁸ does not incorporate the chemistry to describe the formation of single and multi ring aromatics observed in the experiments such as phenylacetylene, p-xylene and indene and consequently a series of steps were added to describe their formation. The toluene pyrolysis modeling is a work in progress and has shown encouraging results⁹.

C. Ethane Combustion

We have continued our earlier studies on ethane combustion and have obtained experimental data over a wide pressure range from 5-1000 bars at temperatures from 1000-1450 K for stoichiometric ($\Phi=1$) oxidation, fuel rich ($\Phi=5$) oxidation and pure pyrolysis. The data set is the most extensive of its kind in the high pressure regime. Prior simulation and modeling efforts^{11, 12} were not able to explain the entire data set and consequently a more detailed modeling study was undertaken. The model¹³ developed as part of this work is able to simulate the entire data set and is the first such model that can describe ethane combustion over such a wide range of pressures and temperatures. Furthermore the model was tested against species measurements and ignition delays for ethane combustion by Hidaka et al.¹⁴ in a shock tube as well as species measurements for natural gas oxidation in a jet stirred reactor and ignition delay measurements in a shock tube reported by Bakali et al.¹⁵ and in general is able to make good predictions of these data sets thereby extending the validity of the model and making it comprehensive.

D. PAH Thermochemistry

The experimental and modeling work on aromatics combustion has highlighted the importance of accurate thermochemistry for aromatics, PAH species and their radicals. Reliable thermochemical information ($\Delta H_f^0_{298K}$) is available for single ring aromatics and PAHs with 3-4 rings. However there is a dearth of information on larger stable PAHs as well as aromatic/PAH radicals. Future experimental and modeling work on larger aromatic species in our lab would require as the first step a better description of the thermochemistry of these larger aromatics and PAHs. Consequently a simple DFT based [B3LYP/6-

31G(d)] cost effective scheme (small basis set) has been developed to predict ΔH_f^0 for a variety of aromatics, PAH and their radicals (55 species in the test set) with mean deviations from experimental ΔH_f^0 being less than 1 kcal/mol (chemical accuracy). The scheme involves an extension of the widely used bond separation isodesmic reaction scheme¹⁶ which predicts ΔH_f^0 for small hydrocarbons accurately. A new reaction scheme referred to as the “Ring Conserved Isodesmic Reaction” scheme¹⁷ has been developed and it involves an indirect parametrization of resonance to identify a unique isodesmic reaction to use when determining heats of reaction from low level quantum chemical calculations. The method compares favourably against an optimized homodesmic reaction scheme developed in recent work by Yu et al.¹⁸.

E. Shock Tube Characterization

Detailed chemical kinetic simulations¹⁹ have been performed to assess the validity of the conventional approach (constant T and P) to characterize the conditions behind the reflected shock wave in a single pulse shock tube. The conventional approach was found to be accurate as long as the pressure rise in the reflected shock wave is within 15%. The effects of reaction quenching were also analyzed and were found to be insignificant for the stable species profiles. Real gas effects at elevated pressures in the shock tube were found to be insignificant for dilute reagent systems used in the shock tube as long as data were obtained over a wide temperature range.

Future Plans

Heating systems were installed to the mixture rig and the GC injection rigs previously. Recently we have also added a heating system to the entire shock tube and sampling apparatus that would permit the shock tube to be heated to temperatures upto 150°C. This would allow the use of higher concentrations of fuel mixtures as well as permit the sampling and analysis of heavy condensates. This would also facilitate experiments to be performed on larger aromatic and PAH molecules.

Currently the modeling work on toluene pyrolysis is in progress. Experiments are to be initiated on the oxidation and pyrolysis of xylenes as a natural extension of our work on toluene oxidation. The xylenes are present in fuels in comparable amounts to toluene and consequently this work is of practical importance. The experimental database on xylene oxidation is limited and currently there exists no detailed kinetic model to describe its combustion. Experiments are also proposed to be conducted on the oxidation of benzene. The high temperature chemistry of the oxidation of benzene still remains unclear with the most recent models²⁰ unable to describe the phenol and cyclopentadiene profiles. The benzene oxidation work will also help clarify the importance of the phenyl oxidation decay routes to phenoxy and the benzoquinones. The benzene oxidation data set can be used to refine the benzene oxidation sub-chemistry in the comprehensive toluene model⁶ developed in prior work in this laboratory. The experimental work will also be augmented by ab-initio quantum chemical calculations to assess the importance of the mechanistic routes involved. Furthermore the derived energetics from the ab-initio calculations can be used to obtain the required high pressure limiting rate constants (k_{∞}) using standard statistical theories.

References

1. Farrell J. T., NIST Fuels Workshop, NIST, Gaithersburg, Maryland, **September 4-5 2003**.
2. Manion, J. A. Combustion Kinetics Databases for Real Fuels; International Workshop on CHEMKIN in Combustion, Chicago, **July 25 2004**.
3. Sivaramakrishnan R., Tranter R. S., Brezinsky K., Combustion and Flame, 139,340-350, **2004**.
4. Klotz S. D., Brezinsky K., Glassman I., Proc. Combust. Inst., 27 (1) 337-344, **1998**.
5. Dagaut P., Pengloan G., Ristori A., Phys. Chem. Chem. Phys., 4, 1846-1854, **2002**.
6. Sivaramakrishnan R., Tranter R. S., Brezinsky K., Proc. Combust. Inst., 30, 1165-1173, **2005**.
7. Burcat A., Snyder C., Brabbs T., *Ignition Delay Times of Benzene and Toluene with Oxygen in Argon Mixtures*, NASA TM 87312, **1986**.
8. Sivaramakrishnan R., Vasudevan H., Tranter R. S., Brezinsky K., In Press, Combustion Science and Technology, **2005**.
9. Sivaramakrishnan R., Vasudevan H., Tranter R. S., Brezinsky K., Paper C07, Proceedings of the Fourth Joint Meeting of the US Sections of the Combustion Institute, **2005**.
10. Braun-Unkoff, M.; Frank, P.; Just, TH. Proc. Combust. Inst., 22, 1053-1061, **1988**.
11. Tranter R.S., Sivaramakrishnan R., Brezinsky K., Allendorf M.D., Phys. Chem. Chem. Phys. 4, 2001-2010, **2002**.

12. Tranter R.S., Ramamoorthy H., Raman A., Brezinsky K., Allendorf M.D., Proc. Combust. Inst., 29, 1267-1275, **2002**.
13. Tranter R. S., Raman A., Sivaramakrishnan R., Brezinsky K., Int. J. Chem. Kin., 37, 306-331, **2005**.
14. Hidaka Y., Sato K., Hoshikawa H., Nishimori T., Takahashi R., Tanaka H., Inami K., Ito N., Combust. Flame, 120, 245-264, **2000**.
15. El Bakali A., Dagaut P., Pillier L., Desgroux P., Pauwels J.-F., Rida A., Meunier A., Combust. Flame, 137(1/2), 109-128, **2004**.
16. Raghavachari, K.; Stefanov, B. B.; Curtiss, L. A. J. Chem. Phys., 106, 6764-6767, **1997**.
17. Sivaramakrishnan R., Tranter R. S., Brezinsky K. J. Phys. Chem. A, 109, 1621-1628, **2005**.
18. Yu J., Raman S., Green Jr. W. H. J. Amer. Chem. Soc. 126, 12685-12700, **2004**.
19. Tang W., Brezinsky K., Manuscript Submitted, Int. J. Chem. Kin., **2005**.
20. Da Costa I., Fournet R., Billaud F., Battin-Leclerc F. Int. J. Chem. Kin., 35, 503-524, **2003**.

Publications based on the DOE supported work (2003 - Current):

1. Sivaramakrishnan R., Tranter R. S., Brezinsky K., "High Pressure, High Temperature Oxidation of Toluene", Combustion and Flame, 139, 340-350, 2004.
2. Sivaramakrishnan R., Tranter R. S., Brezinsky K., "A High Pressure Model for the Oxidation of Toluene", Proceedings of the Combustion Institute, 30, 1165-1173, 2005.
3. Sivaramakrishnan R., Tranter R. S., Brezinsky K., "Ring Conserved Isodesmic Reactions: A New Method for Estimating the Heats of Formation of Aromatics and PAHs", J. Phys. Chem. A, 109, 1621-1628, 2005.
4. Tranter R. S., Raman A., Sivaramakrishnan R., Brezinsky K., "Ethane Oxidation and Pyrolysis from 5 bar to 1000 bar: Experiments and Simulation", Int. J. Chem. Kin., 37, 306-331, 2005.
5. Sivaramakrishnan R., Vasudevan H., Tranter R. S., Brezinsky K., "A Shock Tube Study of the High Pressure Thermal Decomposition of Benzene", Submitted, Combustion Science and Technology, 2005.
6. Tang W., Brezinsky K., "Chemical Kinetic Simulations behind Reflected Shock Waves", Submitted, Int. J. Chem. Kin., March 2005.
7. Sivaramakrishnan R., Tranter R. S., Brezinsky K., "An Experimental and Modeling Study of the High Pressure Pyrolysis of Toluene in a Single Pulse Shock Tube", In Preparation for Submission to J. Phys. Chem. A, 2005.

Presentations based on the DOE supported work (2003 - Current):

1. Tranter R.S., Sivaramakrishnan R., Durgam S., Vasudevan H. and Brezinsky K., "High Temperature, High Pressure Oxidation of Toluene", Third Joint Meeting of the U.S. Sections of The Combustion Institute, March, 2003.
2. Sivaramakrishnan R., Tranter R. S., Brezinsky K., "High Pressure Oxidation of Toluene", Paper 544h, AIChE Annual Meeting, November 21 2003, San Francisco, CA.
3. Sivaramakrishnan R., Vasudevan H., Raju A. S. K., Tranter R. S., Brezinsky K., "A High Pressure Model for Aromatics Oxidation and Pyrolysis", Proceedings of the 2004 Technical Meeting of the Central States Section of the Combustion Institute, March 2004, Austin, Texas.
4. Sivaramakrishnan R., Vasudevan H., Tranter R. S., Brezinsky K., "The High Pressure Pyrolysis of Benzene and Toluene in a Single Pulse Shock Tube-Experiments and Modeling", Proceedings of the Fourth Joint Meeting of the U. S. Sections of the Combustion Institute, Paper C07, Philadelphia, March 2005.
5. Sivaramakrishnan R., Tranter R. S., Brezinsky K., "Accurate Thermochemistry using a New Ring Conserved Isodesmic Reaction Scheme-A DFT study of Aromatics and PAHs", Proceedings of the Fourth Joint Meeting of the U. S. Sections of the Combustion Institute, Paper A09, Philadelphia, March 2005.
6. Tang W., Brezinsky K., "Rigorous Chemical Kinetic Simulations behind Reflected Shock Waves", Proceedings of the Fourth Joint Meeting of the U. S. Sections of the Combustion Institute, Paper C42, Philadelphia, March 2005.

Posters based on the DOE supported work (2003 - Current):

1. Raman A., Sivaramakrishnan R., Tranter R. S., Brezinsky K., "Comprehensive Study of Ethane Oxidation and Pyrolysis", Poster presented at the 2004 Chicago Joint Conference on the Environment, April 6-7 2004, UIC, Chicago, Illinois.

COMBUSTION CHEMISTRY
Principal Investigator: Nancy J. Brown
Environmental Energy Technologies Division
Lawrence Berkeley National Laboratory
Berkeley, California, 94720
510-486-4241
NJBrown@lbl.gov

PROJECT SCOPE

Combustion processes are governed by chemical kinetics, energy transfer, transport, fluid mechanics, and their complex interactions. Understanding the fundamental chemical processes offers the possibility of optimizing combustion processes. The objective of our research is to address fundamental issues of chemical reactivity and molecular transport in combustion systems. Our long-term research objective is to contribute to the development of reliable combustion models that can be used to understand and characterize the formation and destruction of combustion-generated pollutants. We emphasize studying chemistry at both the microscopic and macroscopic levels. To contribute to the achievement of this goal, our current activities are concerned with three tasks: Task 1) developing models for representing combustion chemistry at varying levels of complexity to use with models for laminar and turbulent flow fields to describe combustion processes; Task 2) developing tools to probe chemistry fluid interactions; and Task 3) modeling and analyzing combustion in multi-dimensional flow fields.

RECENT PROGRESS

Task 1: Developing models for representing combustion chemistry at varying levels of complexity to use with models for laminar and turbulent flow fields to describe combustion processes (with Shaheen R. Tonse and Marcus Day) Describing the evolution of species concentration during combustion in more sophisticated laboratory scale burners requires that the computational burden attributable to solving the chemical rate equations must be reduced. We continue to develop an approach that can contribute to this problem, PRISM (Piecewise Reusable Implementation of Solution Mapping). PRISM is an economical and accurate approach for implementing complex kinetics into high fidelity fluids codes. PRISM is an approach to mechanism reduction that draws upon factorial design, statistics and numerics, caching strategies, data structures, and long term reuse of chemical kinetic calculations. In PRISM a solution-mapping technique is invoked, in which the result of time-integrating the chemical rate equations (ODEs) is parameterized by a set of algebraic polynomial response surfaces in C , the N_s+1 chemical composition space. The solution-mapping is done piecewise after dividing the space into N_s+1 dimensional hypercubes with a distinct polynomial parameterization for each. Subsequent calculations in an existing hypercube result in an inexpensive polynomial evaluation rather than an ODE time-integration. The more reuse a hypercube has, the greater the economical gain in CPU time. We have chosen the polynomial order to be quadratic with cross-terms, to give sufficient accuracy. The number of polynomial coefficients scales as $(N_s+2)^2$. The coefficient values are determined by integrating the ODEs at various points in the hypercube

and then performing a regression calculation, hence the number of ODE calls has to be greater than the number of coefficients. We continue to investigate the application of dynamic reduction schemes on more complex chemistry like the 33 species CH₄/Air system. The dimensional reduction method achieves dynamical chemical mechanism reduction through exploitation of diverse time scales that obtain during combustion.

Dynamic dimensional reduction is based on identifying and isolating chemical species that have both fast time-scales and low concentration. The inspiration comes from the steady-state approximation and Intrinsic Low Dimensional Manifold (ILDM) concepts in which concentrations of fast species tend to depend on the concentrations of slow species. The reduction scheme for separating species into the classes fast and low in contrast to slow species has been optimized for the 33 species CH₄/Air system (dimensionality is 34; 33 species and temperature). We work with a prototype flame system that consists of a flame sheet that interacts with vortices of different strengths. We frequently determine dimensional reductions of the 33 species to 4 species, and very infrequently observe conditions with more than 10 species.

We determine improved efficiencies of a factor of 2 for the vortex flame system. The hypercubes for which we compute polynomials have average reuses of 700-900, and they require 0.1 of the total chemistry CPU time. In contrast, there are also many cubes which have very little reuse (nominally in the range 5 to 10). There are no polynomials constructed for these hypercubes yet they require 0.9 of the total chemistry CPU time due to their high dimensionality (34) and the high cost of ODE solves. Stated another way, the per-call cost of an ODE solve is about 20 times more than a PRISM call, and approximately 1/3 the total calls to chemistry are handled by the ODE solver.

We also examined strategies that optimize the tradeoff between hypercube size and the polynomial order to increase the reuse for hypercubes for which polynomials are calculated. Larger cubes with some cubic polynomials did not prove promising. Variable sized cubes with respect to the temperature dimension were considered whereby larger values of ΔT at higher temperatures using three different meshing schemes were evaluated and did not result in acceptable accuracy. We continue to investigate the impact of various cube sizes for specific species on the accuracy/efficiency optimization. We have identified regions of CCN where high re-use occurs and have only calculated polynomials in these regions, and this does improve accuracy. The impact of hypercube size on mass and enthalpy conservation is also being explored.

The advantage of using dynamic reduction without polynomial construction is under active investigation. Species are separated dynamically into the slow and fast/low classes, the classification of species is invariant within a hypercube, and a non-stiff solver provides sufficient accuracy for the time evolution of the slow species. The steady state approximation has been implemented in the past for chemical reduction methods. Species identified as being in steady state are subsequently excluded from chemical kinetic time integration calculations, and instead are treated as being in equilibrium with the remaining species, which are included in the time integration. A short-coming of the traditional approach is that different species are in steady state as the mixture evolves through chemical composition space. This evolution is influenced by the initial and boundary conditions as well as the chemistry and fluid mechanics. We have developed a method, in which the partitioning of species into steady state is dynamic, and changes with the initial and

boundary conditions, chemistry, and fluid mechanics. The methodology builds upon the PRISM approach in which chemical composition space is divided into hypercubes, with a different treatment for each hypercube. We refer to the new approach as the Dynamic Steady State Approximation (DYSSA) Method. The method gives a factor of 5 computational advantage for the 33 species CH₄/Air chemistry.

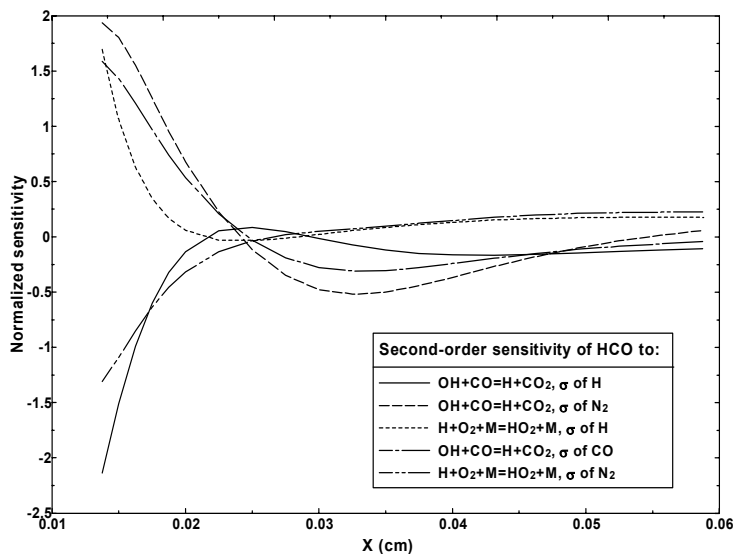
Task 2: Developing tools to facilitate building and validating chemical mechanisms (Nancy Brown and Kenneth Revzan). We completed a study of the sensitivity of dependent variables in three different flame systems to transport properties and their underlying molecular parameters, and a paper describing the study has been accepted for publication. Major findings of the study are indicated in the subsequent paragraphs.

Influential transport properties are as important in flame modeling as influential reaction rates. Hence, transport and rate parameters must be considered in concert when building or validating chemical mechanisms using 1-D premixed laminar flames. Failure to consider sensitivity to transport could result in errors in the transport properties being compensated for by adjusting chemical rate parameters. When combustion is not premixed, it is likely that transport property sensitivity will become even more influential.

Transport parameter importance is found to vary according to the independent variable being considered and the flame type. The influence of parameter values on the sensitivity magnitudes appears to be more important than the approach used to compute the transport properties. The number of significant sensitivities to transport parameters increases for the progression: flame temperature, flame velocity, reactant species, product species, and intermediate radical species. Many dependent variables have significant sensitivities to the pure species thermal conductivities of N₂, O₂, and the fuel. Significant sensitivity is observed with respect to the thermal diffusion ratios of H₂N₂ and H₂,N₂ for the cases when H₂ is the fuel, and it would appear important to compute improved values of this for temperatures less than 1000 K, where these properties are important.

Large sensitivities to the collision diameters of several species are observed, and significant sensitivity to well depths, although observed, is less and more rare. In general, large sensitivity is not observed with respect to μ , the dipole moment or α , the molecular polarizability. As molecular complexity increases, the theoretical foundation for the calculation of thermal conductivity coefficients becomes less robust and tends to depend on parameterizations of the translational-rotational interactions (i.e., Z_{rot}). Sensitivity to Z_{rot} is not significant.

The Jacobian of the original PREMIX solution cannot be used for the brute force sensitivity calculations performed for the purpose of algorithm checking. The Jacobian of the original PREMIX is calculated by using current values of the parent solution elements and the *previous* values of the diffusion velocities and thermal conductivities. The problem solution produced by the use of this compromise Jacobian is adequate, but the sensitivities are not. For the calculation of transport property sensitivities, the correct Jacobian must be calculated after recalculating the transport parameters *after* each incrementation, which is extremely computationally intensive. Sensitivities calculated with the original PREMIX Jacobian can differ from those of the correct Jacobian by approximately 50%, and they can be larger and smaller than the correct values.



Normalized second-order sensitivities of the mole fraction of HCO, in the HCO concentration range of interest, with respect to the most important A-factors and collision diameters for the CO/H₂/Air flame using TRANLIB and its parameters as a function of distance from the burner surface are shown in the Figure for a C₂H₄/Air flame. Second-order coefficients are significant for a number of dependent variables, and computing and

evaluating them provides insight regarding the potential for compensating errors in the model.

PUBLICATIONS

S.R. Tonse and N.J. Brown, "Dimensionality Estimate of the Manifold in Chemical Composition Space for a Turbulent Premixed H₂+air Flame." International Journal of Chemical Kinetics 36, pp 326-336, 2004. Also LBNL Report No. 52058.

N.J. Brown and K.L. Revzan, "Comparative Sensitivity Analysis of Transport Properties and Reaction Rate Coefficients." In press, International Journal of Chemical Kinetics, 2004. Also LBNL Report No. 55671.

Tonse, S.R., Moriarty, N.W., Frenklach, M., and Brown, N.J., "Computational Economy Improvements in PRISM." Intl. J. Chem. Kin. Vol. 35, pp 438-452 (2003). Also Lawrence Berkeley National Laboratory Report No. LBNL-48858.

Tonse, S.R. and Brown, N.J., "Computational Economy Improvements in PRISM." Proceedings The 3rd Joint Symposium of the U.S. Sections of the Combustion Inst. Paper-B36 (2003). Also Lawrence Berkeley National Laboratory Report No. LBNL-48858.

Probing Radical Intermediates of Bimolecular Combustion Reactions

Laurie J. Butler
The University of Chicago, The James Franck Institute
5640 South Ellis Avenue, Chicago, IL 60637
L-Butler@uchicago.edu

I. Program Scope

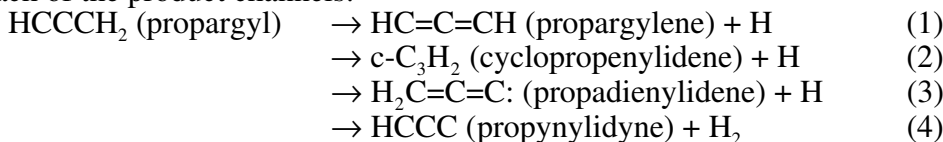
Polyatomic radical intermediates play a key role in a wide range of combustion processes. Our DOE-supported work investigates competing product channels in photodissociation processes used to generate radical intermediates important in combustion and develops new methodology to investigate the unimolecular dissociation and isomerization channels of the nascent radicals.¹⁻⁵ Our new work for DOE begun this year, described in more detail below, focuses on probing the radical intermediates of bimolecular reactions that proceed through an addition/insertion mechanism. Our techniques allow us to generate selected polyatomic radical isomers with a well-defined internal energy distribution in the ground electronic state and then resolve the branching between dissociation and isomerization channels of the radical as a function of the radical's internal energy. In contrast to other methodologies which produce the radicals in a molecular beam source and then access the dissociation channels of the radical by exciting it with a UV photon, this method does not require one to electronically excite the radical, so offers a more direct probe of the radical's ground electronic state dissociation dynamics. The experiments offer a key probe of the radical intermediates important along bimolecular reaction coordinates. Generating the radical intermediates dispersed by velocity and thus by internal energy and then measuring the velocity of the reaction products allows us to identify the product branching as a function of internal energy in the radical intermediate for energies that span the lowest energy product channels. Our experimental studies use a combination of techniques including analysis of product velocity and angular distributions in a crossed laser-molecular beam apparatus, coupled with either electron bombardment or tunable vacuum ultraviolet photoionization detection, and, most recently, velocity map imaging of the dissociation products and the energetically stable radical intermediates. Much of the work serves to test and develop our fundamental understanding of chemical reaction dynamics and to benchmark the accuracy of emerging electronic structure methods developed to predict the energetic barriers between the radical intermediate and each product channel.

II. Recent Progress

Our work this year initiated studies of the product channels accessed from the key radical intermediates in several bimolecular reactions that proceed through an addition/insertion mechanism. The experiments described in Section A below probe the product branching from the propargyl radical intermediate of the $\text{CH}(X^2\Pi) + \text{C}_2\text{H}_2$ reaction and the $\text{C}(^3\text{P}) + \text{C}_2\text{H}_3$ reaction. The first set of experiments, done in collaboration with Dr. Jim Lin at Taiwan's National Synchrotron Radiation Research Center (NSRRC) in March 2005 by my student Laura McCunn, evidence the competing $\text{H} + \text{C}_3\text{H}_2$ and $\text{H}_2 + \text{C}_3\text{H}$ product channels of the reaction. The experiments in Section B outline our investigation of the $\text{CH}_3\text{O} + \text{CO} \rightarrow \text{CH}_3 + \text{CO}_2$ reaction by accessing the CH_3OCO radical intermediate. This study, also in collaboration with Jim Lin, was initiated in the summer of 2004 and is presently being prepared for publication. Finally, Section C describes our newest experiments on one of the key radical intermediates of the $\text{O} + \text{propargyl}$ reaction. We introduced single VUV ionization detection of radical species in our photofragment imaging apparatus to detect the energetic onset for dissociation of the CH_2CHCO radical intermediate predicted by Bowman and coworkers to lead to a vinyl + CO product channel for that reaction.

A. Product Branching from the Propargyl Radical Intermediate of the $\text{CH}(X^2\Pi) + \text{C}_2\text{H}_2$ Reaction and the $\text{C}(^3\text{P}) + \text{C}_2\text{H}_3$ Reaction

Our work this year began our investigation of the competing $\text{H} + \text{C}_3\text{H}_2$ and $\text{H}_2 + \text{C}_3\text{H}$ product channels of the $\text{CH}(X^2\Pi) + \text{C}_2\text{H}_2$ reaction and the $\text{C}(^3\text{P}) + \text{C}_2\text{H}_3$ reaction. Our approach to probing dynamics on the potential energy surface of the $\text{CH}(X^2\Pi) + \text{C}_2\text{H}_2$ reaction and the $\text{C}(^3\text{P}) + \text{C}_2\text{H}_3$ reaction is to investigate the dynamics from the propargyl radical intermediate along the reaction coordinate. The experiments are designed to determine the energetic barriers to each of the product channels:



Several theoretical studies have provided predictions for the barrier energies and, in some cases, branching ratios predicted for these product channels. The most recent theoretical study, A. M. Mebel, S. H. Lin, and R. I. Kaiser, *J. Phys. Chem. A* **105**, 11549-11559 (2001), indicates that in the $\text{C}(^3\text{P}) + \text{C}_2\text{H}_3$ reaction, whether the $\text{C}(^3\text{P})$ atom adds to the carbon atom with an unpaired electron or to the $\text{C}=\text{C}$ bond, the entrance channel addition complexes rapidly isomerize to the propargyl radical isomer. Thus, bimolecular reactive scattering events which evolve through addition complexes should access the same product channels as do internally excited ground state propargyl radicals undergoing unimolecular decomposition. The $\text{CH}(X^2\Pi) + \text{C}_2\text{H}_2$ reaction also proceeds through a propargyl radical intermediate and is predicted to access the same product channels. Importantly, the collisional stabilization of the propargyl intermediate in this nearly gas-kinetic reaction is one of the dominant sources of propargyl radicals in combustion systems, and the self-reaction of the propargyl radicals are key to soot formation. Peeters and co-workers' earlier theoretical work, L. Vereecken, K. Pierloot, and J. Peeters, *J. Chem. Phys.* **108**, 1068-1080 (1998), on that reaction thus treats many of the same transition states as Mebel, but at a lower level of electronic structure theory.

Our experiments this year used the photodissociation of propargyl chloride at 157 nm to generate the propargyl radical intermediate of these reactions with internal energies spanning the theoretically-predicted energetic barriers to those product channels. The Cl atom and the nascent propargyl radicals are produced under collision-free conditions with the internal energy and velocity of each of the nascent propargyl radicals determined from measuring the velocities of the momentum-matched Cl atom. The propargyl radicals formed in C-Cl bond fission events that partition less than 18 kcal/mol to relative kinetic energy have an internal energy sufficient to surmount the lowest product channel barrier (predicted to be the $\text{c-C}_3\text{H}_2 + \text{H}$ product channel), while smaller velocity propargyl radicals have enough internal energy to access the competing product channels. Our experiments detect the HCCCH, the $:\text{CCCH}_2$, and the $\text{c-C}_3\text{H}_2$ products in reactions 1-3 and the CCCH product of reaction 4 with tunable VUV ionization and simultaneously resolve the velocities of these products. Momentum conservation dictates that the velocity of these heavy partners to H and H_2 products respectively have a nearly identical velocity to the radical intermediate that dissociated to give that product. Thus, our experiments offer the chance to determine the energetic barrier to each of these competing product channels. We are currently analyzing the data but our preliminary results indicate that the HCCC (propynylidyne) + H_2 product channel is competitive with the $\text{H} + \text{C}_3\text{H}_2$ product channels. An HCl elimination channel in the photolytic precursor complicates the data analysis, but our data resolves the velocity distribution of the HCl co-product so the C_3H_2 products of this reaction in the precursor can be separated from the C_3H_2 products formed in the competing product channels of the propargyl radical intermediate. This data promises to provide the only experimental benchmark for the theoretically predicted barriers in this important reaction. (The carbene and biradical products are difficult to treat theoretically, so for instance even the CASPT2 energies

for the three $\text{H} + \text{C}_3\text{H}_2$ product channels differ substantially from the energies given in Mebel's papers.) We thank Barney Ellison for stimulating our interest in this system at the 2004 contractor's meeting.

B. Investigating the $\text{CH}_3\text{O} + \text{CO} \rightarrow \text{CH}_3 + \text{CO}_2$ Reaction by Accessing the CH_3OCO Radical Intermediate

While the reaction $\text{OH} + \text{CO} \rightarrow \text{H} + \text{CO}_2$, proceeding through the HOCO radical intermediate, has been extensively studied, experimental work on the analogous $\text{CH}_3\text{O} + \text{CO} \rightarrow \text{CH}_3 + \text{CO}_2$ reaction is relatively limited. A CH_3OCO radical intermediate is indicated both in studies which collisionally stabilize the reaction intermediate and in several theoretical studies of the minima and transition states along the reaction coordinate. Our work this year investigated the dynamics of this reaction by initiating the reaction from the CH_3OCO radical intermediate in the ground electronic state. The nascent vibrationally excited radicals produced from the photodissociation of chloromethylformate at 193 nm were formed with a distribution of internal energies which allowed access to the low barrier $\text{CH}_3\text{O} + \text{CO}$ entrance channel of the bimolecular reaction and the higher barrier but exothermic $\text{CH}_3 + \text{CO}_2$ product channel of the bimolecular reaction. An RRKM estimate of the product branching averaged over our radical's internal energy distribution predicts a product branching of $\text{CH}_3 + \text{CO}_2:\text{CH}_3\text{O} + \text{CO}$ of 4% if one uses the barrier energies predicted by B. Wang et al., B. Wang, H. Hou, and Y. Gu, *J. Phys. Chem. A* **103**, 8021-8029 (1999). This branching ratio is predicted to be about 0.5% if one uses the higher QCISD(T)/barrier energy and transition state frequencies of Francisco, and over 15% if one uses the B3LYP prediction of Zhou et al. Our data resolves two product channels of the photolytic precursor, the required $\text{Cl} + \text{CH}_3\text{OCO}$ product channel and a competing $\text{CH}_3 + \text{OCOC}$ product channel. Using photoionization detection of the CH_3O , CH_3 and CO_2 products we probe the branching to the entrance and exit channels of the bimolecular reaction.

C. Accessing the CH_2CHCO Radical Intermediate of the $\text{O}({}^3\text{P}) + \text{C}_3\text{H}_3$ Reaction

Very little experimental work has been done on the $\text{O} + \text{propargyl}$ radical reaction, and it is predicted to be quite complex. While Slagle and coworkers, I. R. Slagle, G. W. Gmurczyk, L. Batt, and D. Gutman, *Symp. Int. Combust. Proc.* **23**, 115-121 (1991), have investigated the total reaction rate, little is known about the product branching. Recent crossed molecular beams work using LIF detection of the OH product, S. -K. Joo, L. -K. Kwon and J. -H. Choi, *J. Chem. Phys.* **120**, 2215-2224 (2004), sought to experimentally detect only the $\text{OH} + \text{C}_3\text{H}_2$ product channels. They included a theoretical prediction for the product branching based on calculated transition states for the decomposition of various possible radical intermediates formed in this reaction and concluded that the dominant product channel should be propynal + H. At the 2004 contractor's meeting Bowman presented preliminary computational results on this system that indicates the reaction could proceed through a $\text{CH}_2=\text{CH}\dot{\text{C}}\text{O}$ radical intermediate to form a much more exothermic product channel, vinyl + CO. This channel was missed in Choi's theoretical work. This motivated our new experiments on this system, using a velocity map imaging technique to determine the energetic barrier between the $\text{CH}_2=\text{CH}\dot{\text{C}}\text{O}$ radical intermediate and the vinyl + CO product channel.

Prior work in my group³ used photofragment translational spectroscopy to investigate the primary and secondary dissociation channels of acryloyl chloride ($\text{CH}_2=\text{CHCOCl}$) excited at 193 nm. The data evidenced three primary photodissociation channels. The dominant C-Cl fission channel produced nascent CH_2CHCO radicals with internal energies ranging from 23 to 66 kcal/mol. Not resolving any signal at the parent mass of CH_2CHCO , the results showed that the nascent CH_2CHCO radicals were unstable and dissociated to form $\text{CH}_2\text{CH} + \text{CO}$. These results suggested an upper limit of about 23 kcal/mol to the energetic barrier between the $\text{CH}_2=\text{CH}\dot{\text{C}}\text{O}$

radical intermediate and the vinyl + CO product channel that was in agreement with our G3//B3LYP barrier height of 22.4 kcal/mol to within experimental and computational uncertainties. The preliminary results of Bowman at the UB3LYP/6-311G(d,p) level of theory gave a higher zero-point-corrected barrier of 26.6 kcal/mol, however. Thus we sought to renew our investigation of this system by photolytically generating the radicals with a lower distribution of internal energies so the results could directly determine the barrier energy.

Our experiments this spring generated CH_2CHCO radicals from the photodissociation of acryloyl chloride at 235 nm, producing nascent radicals with internal energies ranging from 5 to 28 kcal/mol as determined from the momentum-matched Cl atom velocities in our product velocity map imaging apparatus. We detected the Cl $^2\text{P}_{1/2}$ and $^2\text{P}_{3/2}$ atoms state-selectively with 2+1 REMPI. We then resolved the velocities of all the CH_2CHCO radicals formed stable to dissociation to vinyl + CO by detecting the surviving radicals using 157 nm photoionization and velocity map imaging. Comparison of the total recoil kinetic energy distribution, determined from the weighted sum of the two state-resolved Cl atom spectra, with the recoil kinetic energy distribution derived from the surviving CH_2CHCO radical spectrum determined the threshold internal energy for dissociation of the CH_2CHCO radical intermediate. The experimental results give 21 ± 2 kcal/mol for the zero-point-corrected barrier to the unimolecular dissociation of the CH_2CHCO radical to form $\text{CH}_2\text{CH} + \text{CO}$. Getting this high-quality result required taking care to reduce ion density to eliminate space-charge effects and taking difference spectra to eliminate contributions from 157 nm photodissociation products. The result is in good agreement with the calculated G3/B3LYP barrier to within the substantial uncertainty in the experiments and calculations, but considerably lower than the UB3LYP predicted barrier of 26.6 kcal/mol.

III. Future Plans

We are collaborating with F. Blase at Haverford College to develop a synthetic route for the photolytic precursor to the second key radical intermediate in the O + propargyl reaction, the $\text{HC}\equiv\text{CCH}_2\text{O}^\cdot$ radical intermediate. We hope to photolytically generate the $\text{HC}\equiv\text{CCH}_2\text{O}^\cdot$ radical intermediate in our imaging apparatus and resolve both the velocities of any energetically stable radicals produced and the velocities of the $\text{C}_3\text{H}_2\text{O}$ products from the H atom loss channel of this intermediate. These experiments test the theoretically-predicted pathway to a much higher energy product channel for the O + propargyl reaction. I also anticipate further work on the propargyl radical intermediate of the CH + acetylene reaction using our imaging apparatus with tunable VUV ionization of the C_3H_2 product isomers.

IV. Publications Acknowledging DE-FG02-92ER14305 (2003 or later)

1. Photodissociation Dynamics of Ethyl Ethynyl Ether: A new ketenyl radical precursor, M. J. Krisch, J. L. Miller, L. J. Butler, H. Su, R. Bersohn, and J. Shu, *J. Chem. Phys.* **119**, 176-186 (2003).
2. Photodissociation of allyl- d_2 iodide excited at 193 nm: Stability of highly rotationally excited H_2CCDCH_2 radicals to C-D fission, D. E. Szpunar, Y. Liu, M. McCullagh, L. J. Butler, and J. Shu, *J. Chem. Phys.* **119**, 5078-5084 (2003).
3. The 193 nm photodissociation of acryloyl chloride to probe the unimolecular dissociation of CH_2CHCO radicals and CH_2CCO , D. E. Szpunar, J. L. Miller, L. J. Butler and F. Qi., *J. Chem. Phys.* **120**, 4223-30 (2004).
4. Competing Pathways in the 248 nm Photodissociation of Propionyl Chloride and the Barrier to Dissociation of the Propionyl Radical, L. R. McCunn, M. J. Krisch, K. Takematsu, L. J. Butler, and J. Shu, *J. Phys. Chem. A* **108**, 7889-7894 (2004).
5. C-Cl bond fission dynamics and angular momentum recoupling in the 235 nm photodissociation of allyl chloride, Y. Liu and L. J. Butler, *J. Chem. Phys.* **121**, 11016-11022 (2004).

**Joint Theoretical and Experimental Study of
Key Radicals in Hydrocarbon Combustion.
(DE-FG02-98ER14857)**

PI: Barry K. Carpenter
Department of Chemistry and Chemical Biology
Cornell University Ithaca, NY 14853-1301
E-mail: bkc1@cornell.edu

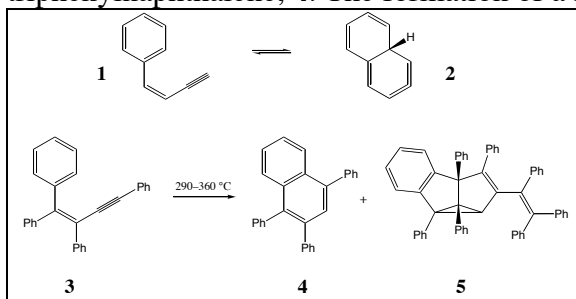
Reaction of Matrix-Isolated Vinyl Radical with O₂

In collaboration with the group of Mingfei Zhou at Fudan University, we have studied the reaction of vinyl radical with O₂ in an argon matrix between 4 and 25K.² The vinyl radical was produced by high-frequency discharge from a Tesla coil through C₂H₄. The formation of the vinylperoxy radical was supported by infrared spectroscopy and anharmonic vibrational frequency calculations on a variety of isotopomers, generated from ¹⁸O₂, C₂D₄, ¹³C₂H₂, and H₂¹³C¹²CH₂. IR absorptions at 1140.7 and 875.5 cm⁻¹ (for the ¹H, ¹²C, and ¹⁶O isotopes) were assigned respectively to the O–O stretch and =CH₂ out-of-plane bending vibrations of *s-trans* vinylperoxy radical.

Visible-light irradiation of the vinylperoxy radical led to formation of the hydrogen-bonded complex H₂COH---CO. Time-dependent DFT and multistate CASPT2-g3 calculations suggest that this occurs by two photochemical reactions. The first converts vinylperoxy to dioxiranylmethyl. The dioxiranylmethyl radical then absorbs a second photon (the longest-wavelength absorption being calculated to be at 443 nm) to isomerize formyloxymethyl. The next step of the reaction – fragmentation of formyloxymethyl to CHO + CH₂O – appears not to be a photochemical process, since the longest-wavelength absorption calculated for formyloxymethyl is at 306 nm. Instead, we hypothesize that the >90 kcal/mol of heat released by the dioxiranylmethyl → formyloxymethyl conversion cannot be absorbed fast enough by the Ar matrix to prevent thermal fragmentation of formyloxymethyl. The resulting matrix-trapped CHO and CH₂O pair undergo H-atom transfer in the final step to generate the observed H₂COH---CO complex.

New Mechanism of C–C Bonding in Hydrocarbons Related to Soot Formation

In collaboration with the group of Henning Hopf at Braunschweig, we have studied the mechanism of isomerization and dimerization of (*Z*)-1-phenylbutenyne (**1**) – a hydrocarbon of the type often invoked in PAH and soot formation.³ Hopf's group has shown that pyrolysis of tetraphenylbutenyne, **3**, leads to formation of triphenylnaphthalene, **4**. The formation of a new aromatic ring in this isomerization



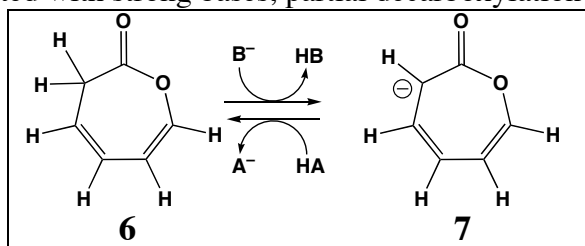
is of potential relevance to PAH formation, and looks structurally plausible. Much less obvious is the mechanism of formation of the polycyclic dimer, **5**. Through a series of DFT and CASPT2 calculations on the reactions of **1**, we have provided evidence that there is a common first step in both naphthalene and dimer formation.

It involves cyclization of the reactant to give a strained and reactive allene (compound **2** when **1** is the reactant). Cyclic allenes of this kind are known to undergo addition to

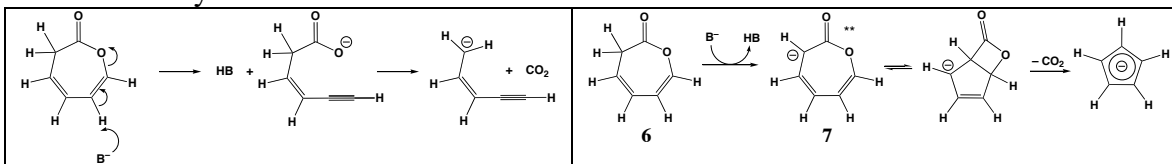
unsaturated hydrocarbons with very low barriers, and so this mechanism provides a new pathway for C–C bond creation that does not involve the radical intermediates usually considered necessary for PAH formation.

Synthesis and Gas-Phase Acidity Measurements of 2(3H)-Oxepinone

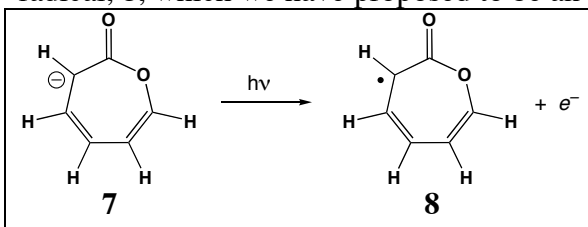
In collaboration with the group of Christopher Hadad at The Ohio State University, we have synthesized 2(3H)-oxepinone (**6**) and have determined its gas-phase acidity in a flowing afterglow. The result is $\Delta_{298}H_{\text{acid}} = 352 \pm 2$ kcal/mol, which agrees well with the B3LYP/aug-cc-pVTZ value of 349.2 kcal/mol. The anion, **7**, appears to be stable when generated in near-thermoneutral conditions, since acidity measurements determined by both forward (deprotonation of **6**) and reverse (reprotonation of **7**) reactions afford the same value.⁴ However, when **6** is deprotonated with strong bases, partial decarboxylation is observed. Two plausible mechanisms have been considered for this process. One is that stronger bases open up an E_2 -elimination channel. The other is that the excess internal energy of **7** arising from exothermic deprotonation allows it to



surmount a barrier for unimolecular decarboxylation. DFT calculations suggest that the rate-limiting barriers to these two mechanisms differ by only 2 kcal/mol, which is within the uncertainty of the calculations.



The significance of the generation of anion **7**, and the determination of the gas-phase acidity of precursor **6**, is that photodetachment of **7** would generate the 2-oxepinoxy radical, **8**, which we have proposed to be an important intermediate in the phenyl + O₂ reaction. Determination of the IP of anion **7**, along with calorimetric evaluation of the heat of formation of precursor **6** and the acidity measurement that we have already made would afford an experimental determination of the heat of formation of



radical **8**. The first photoelectron spectroscopy experiments on **7** are planned for April in Carl Lineberger's group.

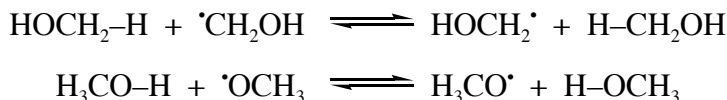
Theoretical Analysis of Hydrogen-Atom-Transfer Reactions

Hydrogen-atom-transfer (HAT) reactions are vital steps in a wide variety of important processes, including hydrocarbon combustion. Despite their prevalence and apparent simplicity, much remains to be understood about these reactions. For example, all credible levels of *ab initio* electronic structure theory, as well as the limited number of experiments that have been done, show that the barrier for transfer of an O–H hydrogen from methanol to CH₃[•] is lower than that for transfer of a C–H hydrogen, despite the fact that the O–H bond is 8.5 kcal/mol stronger. (This is true only in the gas phase. In liquid methanol the transfer of the C–H hydrogen is favored because the O–H is hydrogen

bonded.) The literature explanation for this phenomenon invokes a so-called polar effect, in which ionic valence-bond configurations provide added stabilization to the HAT transition state for the O–H transfer:



However, Jim Mayer’s group at the University of Washington has shown that a wide variety of HAT reactions have barriers that can be correlated by a simple Marcus expression. This correlation includes the O–H and C–H HAT reactions of methanol. Since the Marcus relationship includes no special “polar effect” term, one might be suspicious of any explanation that relies on it. The explanation provided by the Marcus correlation is that the reaction-enthalpy term, which derives from the bond dissociation energies, is more than compensated by a difference in the self-exchange barriers for the reactions:



The barrier for the degenerate transfer between carbons is much higher than that for transfer between oxygens. But this explanation, in turn, raises the question about what controls self-exchange barriers. We have addressed that question in collaboration with Jim Mayer’s group and the group of Wes Borden at the University of North Texas.⁵ That there is an interesting question to consider is revealed both by the computed barrier heights in Table 1 and the subsequent figure showing the geometries of the transition structures.

Table 1. Computed bond-dissociation enthalpies (BDE) for X–H, and activation enthalpies (ΔH^\ddagger) and potential energy barriers (ΔE^\ddagger) for the reaction $\text{X-H} + \text{X}^\bullet \rightarrow \text{X}^\bullet + \text{H-X}$. All values are in kcal/mol. The MPW1K calculations used the 6-31+G(d,p) basis set while the UCCSD(T) calculations used cc-pVTZ.

X	X–H BDE		Self-Exchange Barriers				
			MPW1K		CBS-QB3		UCCSD(T)
	Exptl.	CBS	ΔH^\ddagger	ΔE^\ddagger	ΔH^\ddagger	ΔE^\ddagger	ΔE^\ddagger
CH ₃	105.0	105.3	15.2	16.8	15.8	17.4	18.1
NH ₂	107.6	107.6	9.7	11.0	9.4	10.6	11.4
OH	118.8	119.1	6.5	8.6	7.7	9.4	8.9
F	136.3	137.1	11.9	16.0	14.0	17.9	17.8
OOH	87.8	87.8	9.9	12.5	8.5	10.9	12.9
ONH ₂	–	77.6	10.9	12.9	8.1	10.2	14.5

One sees from the data in Table 1 that the magnitudes of the self-exchange barriers show no discernable dependence on the X–H bond strength, and, perhaps more surprisingly, no obvious relationship to the position of the heavy atoms in the periodic table. Furthermore, the optimized geometries of the transition structures look, at first sight, to

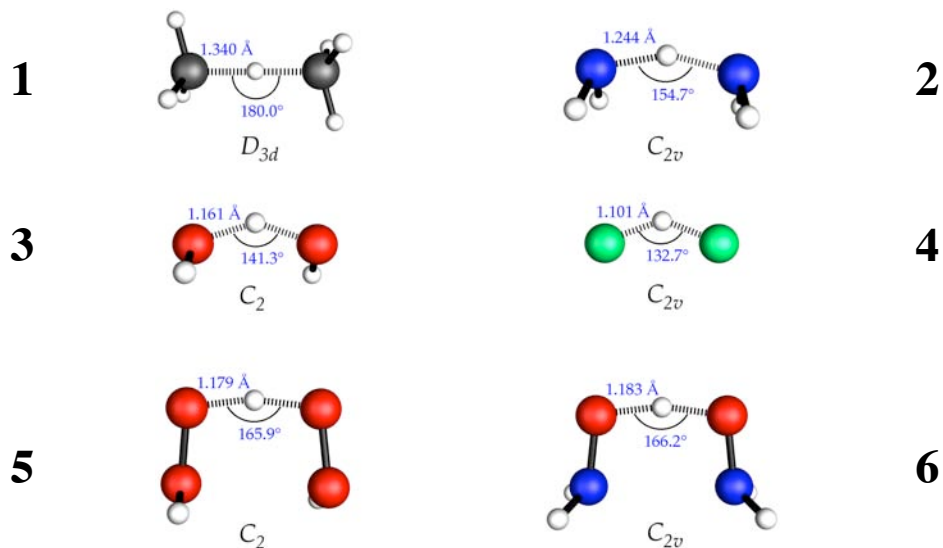


Figure 1. UCCSD(T)/cc-pVTZ optimized geometries for the degenerate HAT reactions considered in Table 1. The numbers indexing each structure correspond to the rows of Table 1.

be far from those that would minimize steric repulsion among all of the atoms involved. The underlying physical factors that lead to these unusual results have been analyzed by assembling the HAT transition structures in five conceptual steps. First, X–H is distorted so that the ancillary atoms attached to X adopt the TS geometry. Second, the bond to the transferring hydrogen is broken. Third, the acceptor X* is distorted so that its ligands adopt the TS geometry. Fourth, the two distorted X* are brought into their TS relationship, with triplet coupling. Finally, the H atom that was dissociated in step two is added back with singlet coupling to each X* and with a geometry that completes the TS. This analysis has revealed the importance in the X–H–X complex of direct X···X interactions, both attractive and repulsive, that influence the barrier heights and TS geometries. Attempts to turn these results into a quantitative model that can predict barrier heights of degenerate HAT reactions, and thence, through the Marcus relationship, of nondegenerate HAT reactions are under way.

Recent Publications Acknowledging DOE-BES Support

1. “Nonstatistical Dynamics in Thermal Reactions of Polyatomic Molecules,” *Ann. Rev. Phys. Chem.* **2005**, 56, 57.
2. “Reaction of Vinyl Radical with Oxygen: A Matrix Isolation Infrared Spectroscopic and Theoretical Study,” Yang, R.; Yu, L.; Jin, X.; Zhou, M.; Carpenter, B. K. *J. Chem. Phys.* **2005**, 122, 014511.
3. “A Computational Investigation of the Reactivity of a Hexadienyne Derivative,” Litovitz, A. E.; Carpenter, B. K.; Hopf, H. *Org. Lett.* **2005**, 7, 507.
4. “The Gas-Phase Acidity of 2(3H)-Oxepinone: A Step Towards an Experimental Heat of Formation for the 2-Oxepinoxy Radical,” Kroner, S. M.; DeMatteo, M. P.; Hadad, C. M.; Carpenter, B. K. *J. Am. Chem. Soc.* **2005**, 127, in press.
5. “Factors Controlling the Barriers to Degenerate Hydrogen Atom Transfers,” Isborn, C.; Hrovat, D. A.; Borden, W. T.; Mayer, J. M.; Carpenter, B. K. *J. Am. Chem. Soc.* **2005**, 127, in press.

Ion Imaging Studies of Chemical Dynamics

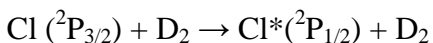
David W. Chandler
Combustion Research Facility, mail Stop 9054, Sandia National Laboratories,
Livermore, CA 94551-0969
chand@sandia.gov

Scope of Program

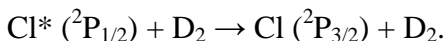
The goal of this program is to study the dynamics of fundamental collisional processes. In the past year I have studied the adiabatic and non-adiabatic collisions between Cl atoms and hydrogen molecules and the translationally and rotationally inelastic collisions of atom/ diatom systems for the production of ultra cold molecules. We have also finished a study of the half collisions or NO/Ar van der Waals dimers.

Progress Report

In the last year we have performed two related studies. We have determined limits on the cross section for both electronically non-adiabatic excitation and quenching in the Cl (2P_j) + D₂ system. Our experiment incorporates crossed molecular beam (CMB) scattering with state selective Cl ($^2P_{1/2,3/2}$) detection and velocity mapped ion imaging. By colliding atomic chlorine with D₂, we address the propensity for collisions that result in a change of the spin-orbit level of atomic chlorine either through electronically non-adiabatic spin-orbit excitation:



or through electronically non-adiabatic spin-orbit quenching:



In the first part of the study, we obtain an estimate of an upper limit for the electronically non-adiabatic spin-orbit excitation cross section at a collision energy of 5.3 kcal/mol, which lies above the energy of the reaction barrier (4.9 kcal/mol). Our analysis and simulation of the experimental data determines an upper limit for the excitation cross section as $\sigma_{\text{NA}} \leq 0.012 \text{ \AA}^2$. In the second part of the study we investigate the propensity for electronically non-adiabatic spin-orbit quenching of Cl* following a collision with D₂ or He. We perform these experiments at collision energies above and below the energy of the reaction barrier. By comparing the amount of scattered Cl* in our images to the amount of Cl* lost from the atomic beam we obtain the maximum cross section for electronically non-adiabatic quenching as $\sigma_{\text{NA}} \leq 15 \text{ \AA}^2$ for a collision energy of 5.7 kcal/mol. Our experiments show the probability for electronically non-adiabatic quenching in Cl* + D₂ to be indistinguishable at the level we have been able to measure to that for the kinematically identical system of Cl* + He.

In addition to those studies we have investigated electronically non-adiabatic spin-orbit quenching for $\text{Cl}^* (^2\text{P}_{1/2}) + \text{H}_2$ which is the required first step for the reaction of Cl^* to produce ground state $\text{HCl} + \text{H}$ products. In these experiments we collide $\text{Cl} (^2\text{P})$ with H_2 at a series of fixed collision energies using a crossed molecular beam machine with velocity mapped ion imaging detection. Through an analysis of our ion images, we determine the probability for electronically adiabatic scattering and for electronically non-adiabatic scattering, quenching. We determine the following quenching cross sections $\sigma_{\text{quench}}(2.1 \text{ kcal/mol}) = 26 \text{ \AA}^2$, $\sigma_{\text{quench}}(4.0 \text{ kcal/mol}) = 21 \text{ \AA}^2$, and $\sigma_{\text{quench}}(5.6 \text{ kcal/mol}) = 14 \text{ \AA}^2$. In these experiments, we form an atomic beam of Cl/Cl^* through photolysis of Cl_2 at 420 nm by focusing a laser (Coherent Infinity ND:YAG/OPO) at the throat of a supersonic expansion of $\sim 5\%$ Cl_2 in a carrier gas. Atomic Cl then collides with H_2 from a supersonic expansion of neat H_2 . Both molecular beams are formed using homebuilt piezoelectric valves. The molecular beams counterpropagate giving a collision geometry of 180° in these experiments. We state-selectively ionize atomic Cl or Cl^* using resonance enhanced multiphoton ionization (REMPI). The Cl^+ ions are detected using velocity mapped ion imaging.

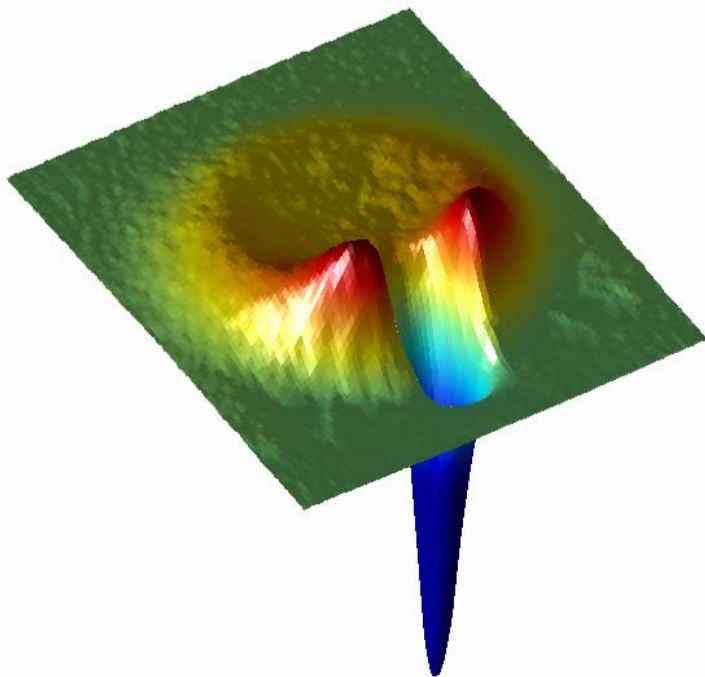


Figure 1. Example ion image for $\text{Cl} + \text{H}_2$ scattering after subtraction of the unscattered Cl beam spot. The dominant circular ridge in the front of the image is forward scattered Cl resulting from electronically adiabatic rotationally elastic collisions with H_2 . The large negative dip in the image corresponds to the amount of Cl scattered out of the atomic beam.

For these experiments, we collect data by collecting pairs of ion images. Each pair of ion images has one image with Cl/Cl^* and the H_2 collider overlapped in time and one image with the H_2 delayed in time and only Cl/Cl^* present. After collecting each of the two individual images for 2-5s we subtract the Cl only image from the $\text{Cl} + \text{H}_2$ image and repeat this process ~ 30 -60 times. In the Cl only image, the atomic beam spot is slightly more intense because no Cl has been lost due to scattering with H_2 . Fig. 1 shows the

result when we subtract the Cl only ion image from the Cl + H₂ ion image. The image in Fig. 1 has two important features. First, we see Cl which was scattered out from the atomic beam and detected by the experiment as a positive ring in this image. Second, after subtraction the atomic beam spot appears as a large negative region in the image.

Collisional Cooling of Molecules

We report the cooling of nitric oxide molecules in a single collision between an argon atom and an NO molecule at collision energies of 5.65 ± 0.36 kJ/mol and 14.7 ± 0.9 kJ/mol in a crossed molecular beam apparatus. We have produced in significant numbers ($\sim 10^8$ molecules cm⁻³ per quantum state) translationally cold NO(²Π_{1/2}, v'=0, j'=7.5) molecules in a specific quantum state with an upper-limit laboratory-frame rms velocity of 14.8 ± 1.1 m/s, corresponding to a temperature of 406 ± 28 mK. The translational cooling results from the kinematic collapse of the velocity distribution of the NO molecules after collision. We present experimental evidence to show that increasing the collision energy by a factor of ~ 2.6 does not change the velocity spread of the cold NO molecules. Similarly, the energy condition for producing the cold NO does not depend on the energy of the Ar beam. However, the energy of the Ar beam does shift the scattering angle at which the cold molecules appear.

This work was done in collaboration with Professor James Valentini of Columbia University.

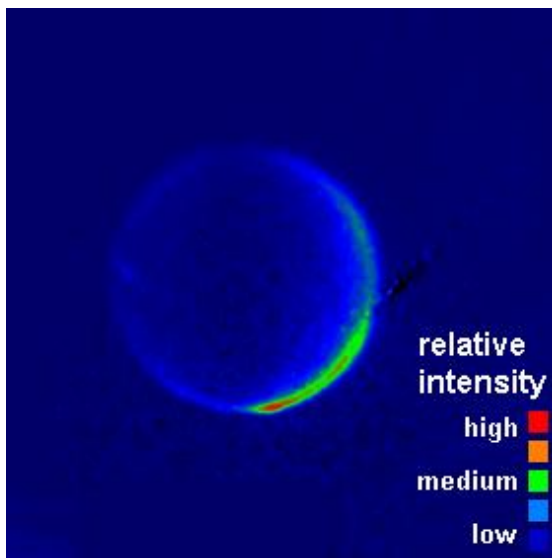


Figure 2. Image of NO(j=7.5) collision product showing slowly moving molecules as an intense spot at the bottom of the image.

Future Directions

The collisional cooling of molecules to millikelvin temperatures represents a new way of creating single quantum states of translationally cold molecules. We propose to further investigate this technique for cooling molecules and are in the process of building up two

experiments associated with this effort. One is to use the slowly moving molecules that are produced with a very narrow velocity distribution to perform molecular interferometer experiments. We also plan on utilizing the same physics of cooling of a molecule by collision with an atom of the same mass to stop molecules. A cloud alkali atoms that will be trapped in a Magneto Optical Trap (MOT) and a molecule of the same mass as the atom will be collided with the stopped atoms. Some fraction of those molecules will transfer all of their momentum to the atom and will replace the atom in the trap.

Publications:

- 1) B. F. Parsons and D. W. Chandler, "On the Dissociation of van der Waals Clusters of X₂-cyclohexane (X=O, Cl) Following Charge Transfer Excitation in the Ultraviolet" J. Phys. Chem. A, V. 107, p. 10544 (2003).
- 2) E. A. Wade, K.T. Lorenz, J. L. Springfield, and D. W. Chandler, "Collisions of HCl with Rare Gas and Molecular Colliders" J. Phys. Chem. A, V. 107, p. 4976 (2003).
- 3) M. Elioff, J. J. Valentini and D. W. Chandler, "Production of cold molecules by crossed molecular beam scattering" Science, vol. 302, p 1940 (2003).
- 4) Raarup, MK; Chandler, DW; Olsthoorn, RCL; Schmidt, T "Single Molecule FRET microscopy of conformational changes in the RNA of Alfalfa mosaic virus." Biophysics Journal v. 84, p. 299A (2003).
- 5) Elioff, MS; Valentini, JJ; Chandler, DW; "Formation of NO(j '=7.5) molecules with sub-kelvin translational energy via molecular beam collisions with argon using the technique of molecular cooling by inelastic collisional energy-transfer." European Phys. J. D; v.31, no.2, p.385 (2004).
- 6) Wade, EA; Lorenz, KT; Chandler, DW; Barr, JW; Barnes, GL; Cline, JI, "Ion imaging studies of product rotational alignment in collisions of NO (X-2 Pi(1/2), j=0.5) with Ar"; Chem. Phys. v.301, no.2-3, p.261(2004).
- 7) Parsons, BF; Chandler, DW; Sklute, EC; Li, SL; Wade, EA "Photodissociation dynamics of ArNO clusters" J. of Phys. Chem. A; vol.108, no.45, p.9742-9 (2004).
- 8) Parsons B. F. and Chandler D. W. "An Investigation of Non-Adiabatic Interactions in Cl (2Pj) + D₂ via Crossed Molecular Beam Scattering." Accepted J. Chem. Phys. 2005.

Direct Numerical Simulation and Modeling of Turbulent Combustion

Jacqueline H. Chen, Evatt R. Hawkes, and Ramanan Sankaran

Sandia National Laboratories, Mail Stop 9051

Livermore, California 94551-0969

Email: jhchen@sandia.gov

Program Scope

The goal of this research program is to gain fundamental insight into unsteady flow/chemistry interactions that occur in turbulent combustion, and to develop and validate combustion models required in various engineering CFD approaches including Reynolds Averaged Navier-Stokes (RANS) and Large-eddy simulation (LES). In this work a high-fidelity numerical approach known as direct numerical simulation (DNS), which resolves all of the scales in the scalar and velocity fluctuations, is used to efficiently investigate fine-grained physical phenomena associated with interactions between convective and diffusive transport with detailed chemistry in the combustion of hydrogen and hydrocarbon fuels.

Recent Progress

In the past year we have made efficiency gains with our MPP DNS code S3D on NERSC's IBM SP and on ORNL's CrayX1. Significant gains (10-fold increase in efficiency) were obtained on the CrayX1 by vectorization of key chemistry and thermochemistry modules in the code. With these gains in performance along with a large computer allocation through the DOE FY05 INCITE award, we are performing 3D simulations of turbulent flames with detailed chemistry for the first time. While costly, these simulations enable both turbulence dynamics and chemical reaction to be accurately represented concurrently, thus opening new realms of possibility for understanding turbulence-chemistry interactions and the development of models. We have also continued to perform 2D DNS of turbulent autoignition with compression heating and turbulent nonpremixed and premixed combustion. Several of our accomplishments in the past year are summarized below.

Parametric Study of Ignition Front Propagation in a Constant Volume With Temperature Inhomogeneities^{9,10}

A parametric study of the autoignition of a thermally stratified lean hydrogen-air mixture was performed. The parametric study focused on the influence of the amplitudes and length scales of the initial temperature fluctuations and the presence of turbulence. The primary goal was to understand the effect of these parameters on the mode of combustion and on the performance of a model that is applicable to weakly stratified ignition, the multi-zone model. The combustion mode was understood by visual comparison of the observed heat release fields, and by two diagnostic techniques that we developed [9]. The first diagnostic technique was based on tracking the speed of the advancing combustion wave, and comparison of this with a nominal deflagration speed to determine the significance of molecular transport effects within the ignition front. The second technique was to use the comparison of the mixing time-scale with the ignition delay time to determine the influence of passive scalar mixing changing the probability density of temperature in the domain. These diagnostic techniques were applied to the data and used to explain the performance of the multi-zone model. In all cases the observed performance could be adequately explained using these simple arguments.

The parametric study in the RMS temperature fluctuation revealed that this parameter has a strong influence on the observed combustion mode, and on the timing and duration of heat release. Larger temperature fluctuation amplitudes were found to increase the combustion duration and advance the ignition timing. More volumetric, homogeneous combustion was observed for lower amplitudes whereas higher amplitude cases showed evidence of combustion in fronts. Using the flame speed diagnostic, it was found that higher amplitudes led to a greater prevalence of molecular transport within the fronts (i.e. deflagrations). The performance for the multi-zone model was linked to the effects of passive scalar dissipation and the prevalence of deflagrations. Very good performance was obtained in cases without significant deflagrations and when passive scalar mixing had been mostly accounted for by making the comparison of the model with the DNS at a point in time when ignition had just begun. Predictions deteriorated as the prevalence of deflagrations increased, i.e. at higher amplitudes.

The parametric study in the initial temperature fluctuation length scale without turbulent velocity fluctuations showed that larger length scales lead to thicker front structures, and a decrease in the importance of molecular transport effects both in deflagrations and through passive scalar mixing. The multi-zone model showed excellent predictions in the cases with larger length scales. The parametric study of the initial length scales with turbulent velocity fluctuations, where the turbulence time scale was kept constant, showed an increased range of scales in the larger length scale cases. Turbulence had a strong effect in elongating and folding the initial hot spots. Surprisingly it was found that the importance of deflagrations was roughly independent of the initial length scale. This was explained considering the fact that the turbulence time scale was the same for each case and using the well known characteristic of turbulence that molecular dissipation timescales tend to scale with the turbulence integral timescale. The multi-zone model predictions for the cases with turbulence were significantly worse than those without turbulence, and furthermore showed a counter-intuitive trend that predictions did not improve with increasing length scale, which was explained considering the roughly equal importance of deflagrations occurring in the ignition fronts.

Quantification of Differential Diffusion in Nonpremixed Systems⁸

Most attempts to quantify the amount of differential diffusion (DD) are based on the differences between different definitions of the mixture fraction. We have developed a general method for evaluating DD in premixed and nonpremixed flames based on the conservation of elemental mass fractions. These measures form a basis for analyzing DD. Casting these in terms of a mixture fraction gives insight into DD in nonpremixed flames, and provides a single measure of DD. In both 1D strained methane-air and hydrogen-air flames and in 2D DNS of spatially-evolving turbulent CO/H₂-air and methane-air jet flames we found that DD is largely affected by production of hydrogen in the flame zone of hydrocarbon flames. We also found that for a given definition of mixture fraction, our DD measure is well approximated by considering only the contributions from hydrogen and methane in methane-air flames. Finally, in the context of large-eddy simulation, the DNS data were spatially filtered and analyzed to determine the significance of DD relative to convection and sub-filter terms in the filtered mixture fraction equation. We found that as filter size increases, the importance of DD relative to molecular diffusion on the filter scale decreases.

*Evaluation of Models for Flame Stretch Due to Curvature in the Thin Reaction Zones Regime*⁶

We performed direct numerical simulations to study modeling assumptions for the curvature propagation component of flame stretch in the thin reaction zones regime of turbulent premixed combustion, a regime in which small eddies can penetrate the preheat zone but not the thinner fuel breakdown zone. Closure models for the combustion term in Reynolds-averaged Navier-Stokes (RANS) simulation and large-eddy simulation (LES) of premixed combustion exploit estimates of the total flame stretch to arrive at a final model. Specifically, in the G-equation, thickened flame, and flame surface density approaches, the total flame stretch requires closure. We focused on the modeling assumptions of Peters that were explicitly derived for the thin reaction zones regime. We found that the mean stretch is dominated by stretch due to correlations of flame speed with curvature, and specifically the effects of tangential diffusion. The modeling assumptions of Peters were found to provide an improvement over the assumptions of a constant flame speed, or a flame speed governed by the linear relationship with stretch at small and steady stretch. However, for the DNS conditions (time scale ratio of turbulence eddy turnover to flame time) considered, we found that diffusive-thermal effects remain well into the thin reaction zones regime, and the suggestions of Peters generally overpredict the mean compressive stretch. We introduced an effective diffusivity for flame stretch and evaluated it for the methane-air DNS. We found that the effective diffusivity was comparable to the mass diffusivity for flames with a large ratio of flame time to eddy turnover time. Finally, we examined the length scales contributing to stretch and found that while most of the flame area has a radius of curvature greater than the laminar flame thickness, most stretch occurs in more tightly curved flame elements. This result implies that steady or small curvature models are unlikely to be successful at capturing the stretch response of a premixed flame in this regime. This also has implications for modeling in LES, with regard to the application of equilibrium on total stretch at the subgrid scales.

Future Plans

3D Direct Numerical Simulations of a Temporally Evolving Planar Jet Flame with Detailed Chemistry (INCITE Goal) – Extinction and Reignition Dynamics

We plan to perform a three-dimensional turbulent DNS of a nonpremixed CO/H₂/N₂-air flame with detailed chemistry. This simulation, the first in a series of different Reynolds numbers, will be targeted at providing fundamental insight into key outstanding issues related to modeling of turbulent nonpremixed combustion: extinction and reignition, flow and flame unsteadiness, the correlation of strain rate and scalar dissipation rate, differential diffusion of species, and turbulent mixing with finite-rate chemistry. Through collaboration with experimentalists and modelers of the Turbulent Nonpremixed Flame Workshop, we also plan to gather statistics required to further improve or validate different modeling approaches. One aspect we will focus on initially is to understand the mechanisms of extinction and reignition in a turbulent environment. Unlike previous DNS studies with simpler chemistry, the proposed configuration with detailed chemistry will permit reignition to occur by flame propagation in directions normal or tangential to the stoichiometric surface of the extinguished flame or by autoignition. We plan to collaborate with Jonathan Frank of SNL on unsteady laminar flame experiments and computations that also examine, in a more controlled environment, competing reignition modes following local extinction. We plan to perform a priori and a posteriori testing of subgrid combustion and mixing models for large-eddy simulations (LES) performed in the same

configuration by Joe Oefelein of SNL. In anticipation of performing the INCITE run we have successfully optimized key kernels in our DNS code, S3D, on NERSC's IBM SP and on ORNL's CrayX1 architectures. While optimization on the IBM SP resulted in modest gains, vectorization of S3D on the CrayX1 resulted in a ten-fold increase in code efficiency. S3D was found to scale well on both platforms. To prepare for the INCITE run, we have performed many test calculations ranging from 3 to 40 million grid points to identify the optimal physical and numerical parameters to allow us to study extinction and reignition dynamics.

Characterization of Turbulent Mixing Effects on HCCI Combustion Modes and Model Validation

We plan to make use of advanced optical diagnostic measurements in engines LES to characterize turbulence and scalar fluctuation amplitudes and length scales in real engine configurations (both in the core of the charge and in boundary layers which may have very different characteristics). These scalar and velocity distributions will be used to initialize DNS of HCCI combustion exhibiting multi-stage ignition. These DNS will help us understand the influence of different mixture composition and temperature stratifications on the ignition timing and burn rate. In particular we plan to investigate the influence of scalar dissipation on the negative temperature coefficient regime ignition behavior. The DNS data will also be used for a priori testing of HCCI combustion models including unsteady flamelets, conditional moment closure, and transported PDF approaches.

BES Publications (2003-2005)

1. T. Echekki and J. H. Chen, "Direct Numerical Simulation of Autoignition in Non-homogeneous Hydrogen-Air Mixtures," *Combust. Flame*, **134**:169-191. (2003).
2. J. C. Sutherland and C. A. Kennedy, "Improved Boundary Conditions for Viscous, Reacting, Compressible Flows," *J. Comp. Phys.* **191**:502-524 (2003).
3. C. A. Kennedy and M. H. Carpenter, Additive "Runge-Kutta Schemes for Convective-Diffusion-Reaction Equations," *Appl. Num. Math.* **44**:139-181 (2003).
4. E. R. Hawkes and J. H. Chen, "Direct Numerical Simulation of Hydrogen Enriched Lean Premixed Methane/Air Flames," *Combust. Flame*, **138**: 242-258. (2004).
5. S. Liu, J. C. Hewson, J. H. Chen, and H. Pitsch, "Effects of Strain Rate on High-Pressure Nonpremixed N-Heptane Autoignition in Counterflow," *Combust. Flame*, **137**:320-339 (2004).
6. E. R. Hawkes and J. H. Chen, "Evaluation of Models for Flame Stretch in the Thin Reaction Zones Regime," *Proceedings of the Combustion Institute*, **30**, pp. 647-655. (2004).
7. J. C. Sutherland, P. J. Smith, and J. H. Chen, "A Generalized Method for A Priori Evaluation of Combustion Reaction Models," in preparation *Combust. Flame*, (2004).
8. J. C. Sutherland, P. J. Smith, and J. H. Chen, "Quantification of Differential Diffusion in Nonpremixed Systems," to appear in *Combust. Theory and Modeling*, (2005).
9. J. H. Chen, E. R. Hawkes, R. Sankaran, S. D. Mason, and H. G. Im, "Direct Numerical Simulation of Ignition Front Propagation in a Constant Volume With Temperature Inhomogeneities, Part I: Fundamental Analysis and Diagnostics", submitted to *Combust. Flame*, (2004).
10. E. R. Hawkes, R. Sankaran, P. Pebay, and J. H. Chen, "Direct Numerical Simulation of Ignition Front Propagation in a Constant Volume With Temperature Inhomogeneities, Part II: Parametric Study", submitted to *Combust. Flame*, (2004).
11. R. Sankaran, H. G. Im, E. R. Hawkes, and J. H. Chen, "The Effects of Nonuniform Temperature Distribution on the Ignition of a Lean Homogeneous Hydrogen-Air Mixture," *Proceedings of the Combustion Institute*, **30**, pp. 875-882. (2004).
12. R. Seiser, J. H. Frank, S. Liu, J. H. Chen, R. J. Sigurdsson, and K. Seshadri, "Ignition of Hydrogen in Unsteady Nonpremixed Flows," *Proceedings of the Combustion Institute*, **30**, pp. 423-430. (2004).
13. E. R. Hawkes and J. H. Chen, "Comparison of Direct Numerical Simulations of Lean Premixed Methane-Air Flames with Strained Laminar Flame Calculations", submitted to *Combust. Flame*, (2004).

Turbulent Combustion

Robert K. Cheng
Environmental Energy Technologies Div.
Lawrence Berkeley National Laboratory
70 –109, 1 Cyclotron Rd.
Berkeley, CA 94720
E-mail : rkcheng@lbl.gov

Scope

This research program focuses on lean premixed combustion: an advanced low emission energy technology for heating and power systems. Combustion processes in these systems are turbulent and are not sufficiently well characterized or understood to guide turbulent combustion theories and computational methods. Our objective is to investigate experimentally the coupling of turbulence with burning rate, flame stability, extinction and pollutant formation. The goal is to provide for energy technologies the chemical and fluid mechanical scientific underpinnings that can be captured in models and simulations that will become accurate and reliable tools for predicting combustion process performance. This effort is responsive to DOE's mission to "foster a secure and reliable energy system that is environmentally and economically sustainable." Our approach is to conduct detailed measurements of the spatial structures of the turbulent scalar and velocity fields of laboratory flames over a wide range of fuel/air ratios, flow velocities and turbulence intensities. The analysis and interpretation are guided by a theoretical concept of classifying premixed flames according to the initial turbulence and thermo-chemical conditions. Specific goals for FY 06-08 will be (1) to obtain experimental data and analyses for direct comparison with device scale ($O(10\text{ cm})$) 3D time dependent numerical simulations with comprehensive chemistry and (2) elucidate the fundamental processes in turbulent premixed flames at elevated initial pressures and temperatures.

Recent Progress

The relocation of our laboratory to a larger space was a major undertaking in FY04-05. The old laboratory was decommissioned in May 2004 and the new laboratory was not commissioned until November. To date, only three of the four experimental stations are operable. The fourth, being a station for investigation of high pressure flame, is still under construction and is expected to be commissioned early in FY06. During the transitional period, our work continued with emphasis on collaborating with developers of computational simulations of laboratory premixed turbulent flames. As reported previously, the Center of Computational Sciences and Engineering (CCSE) led by John Bell at LBNL has successfully simulated one of our premixed turbulent v-flames. The methodology was based on low Mach number approach for second order Navier-Stokes equations to eliminate the acoustic time steps while maintaining compressibility to consider the effects due to heat release. With this approach, the CCSE team simulated for the first time a device scale $O(10\text{ cm})$ flame in 3D and with time dependence using Adaptive Mesh Refinement (AMR) and full chemistry.

A primary objective of our first study was to determine, by direct comparison with our particle image velocity (PIV) data, the mesh refinement levels necessary to predict the overall scalar field (flame brush) and flowfields (mean and rms velocities). The simulation was carried out in two parts. Inflow conditions were generated in a separate nonreacting simulation of the upstream turbulent flow produced by a perforated plate in a circular nozzle. For the reacting flow region, a $(12\text{ cm})^3$ domain was used. It was found that, with the low Mach number implementation, a 3-level adaptive grid hierarchy, with a finest-level grid spacing, $\Delta x = 312.5\ \mu\text{m}$, was capable of predicting with remarkable fidelity the major features of the experimental results. Differences between the growth rates of the simulated and measured turbulent flame brush thicknesses were within experimental uncertainties and the mean flame brush angles differ by only 2° . The results confirm that the AMR low Mach number implementation is well-suited for our laboratory flames.

The overall flowfield of the simulated v-flame also shows that the simulation captured the important physical features. These include the deflection of the flow from outward to inward across the flame brush, a flow acceleration along the burner axis, apparent increase in turbulence intensity across the flame fronts and buoyancy effects. However, there exist quantitative differences between the simulated and measured results. This was clearly shown when comparing the radial velocity profiles at various distances downstream of the stabilizer. Whereas the measurements show a velocity deficit along the burner axis generated by the wake of the flame stabilizer, the simulated results show instead an acceleration. Another noticeable difference is the simulation overpredicting the degree of flow deflection through the flame brush. To investigate the causes of these discrepancies, additional sets of experiments were performed to determine the sensitivity of the flame to the initial and side boundary conditions. These experiments consisted of flame stabilized by rods of various sizes with and without a co-flow.

In the simulation, a co-flow of 1 m/s (compared to mainflow velocity of 3 m/s) was used to accelerate the transient effect associated with initiating the computation. This co-flow is absent in the original experiments. However, by adding this co-flow to the burner, the flame and its flowfield do not show a noticeable change except for a weakening of the mixing shear regions at the edge of the reactants. The results obtained with different stabilizer rods including a heated wire of 0.7 mm, the original 1.3 mm rod and a larger 3.2 mm rod shows more significant effects. The flame and flowfield characteristics show that the growth rates of the flame brushes and evolution of the flame wrinkles are influenced by the shear regions of the stabilizer wakes. Within the shear wake region, flame wrinkle development and flame front dynamics were impeded. As the size of the wake region is proportional to the size of the stabilizer, the flame brush produced by the larger rod has a comparatively slower growth rate. Moreover, the velocity deficit on the centerline persists far downstream. In contrast, the effects due to the stabilizer wake region are not considered in the simulation because a hydrodynamic flow around the flame stabilizer was assumed. As a result, there is no velocity deficit downstream of the simulated stabilizer and heat release across the flame fronts contributes directly to the formation of an accelerating flow along the centerline instead of being dragged down by the recirculation zone. The approximation for a hydrodynamic flow around the stabilizer was necessary because of the significant increases in complexity and computational resources associated with simulating the highly unsteady recirculating shear flow formed in the wake. Nevertheless, the experiments

obtained with different stabilizer rods indicate a trend that is consistent with the simulated results being an idealized case with no wake influences.

We also note that the bulk of flame is entirely outside the wake and that its dynamics are determined predominantly by its interaction with the reactant flow turbulence. Therefore, we are developing analytical tool for further examination to infer these interactions from the simulated results as well as from the experimental results. These will include such parameters as flame front curvature and the flame surface density, which is often used to quantify the combustion intensity in low Mach number premixed flames. In both cases 2D comparisons between simulations and experiments are relatively straightforward but it will be possible from the simulation data to extend the investigation to obtain a complete 3D description of flame front curvature and surface density, both of which are very difficult to achieve experimentally. It should be noted that the theoretical basis for the analysis of the experimental data often derives from thin-flame models and that the simulations have no such limitation. Similarly, analysis of the velocity field can go beyond comparisons with two dimensional PIV data, to obtain, within the context of a laboratory sized flow field, a detailed understanding of the interaction of the flame front with the three dimensional strain field.

We also applied PIV to flames stabilized in a low-swirl burner (LSB) to support complimentary CCSE simulation efforts on this flame configuration . Unlike v-flames, LSB does not require a stabilizer and could be a simpler simulation configuration. The conditions chosen for the computation and experiments involve relatively low velocity and turbulence (CH_4/air at $\phi = 0.8$, $U_0 = 5 \text{ m/s}$, $u' = 7\%$, and $v' = 5\%$). However, simulating the LSB flame is non-trivial due to the fact that the flame is stabilized aerodynamically by flow divergence produced when the swirl intensity is below the critical vortex breakdown point. Therefore, to capture this freely propagating and detached flame, it is necessary to capture not only the turbulence produced in the flowfield but also the complex 3D shear interactions between the axial flow of the reactants and the tangential swirl jets. Thus far, the simulation has yet to produce a stable flame. This seems to imply that the swirl interactions may not have been properly captured. To provide the critical velocity data on the swirling flow, we made cross-stream PIV velocity measurements. This was accomplished by turning the PIV laser sheet perpendicular to the burner axis and point the PIV camera down towards the burner throat. To shield the camera from the flame, a quartz window was placed over the flame and its position was optimized so to minimize its influence on the flame flowfield. The swirling velocity measurement were obtained for the non-reacting and the reacting flows. The data from ten different locations downstream clearly shows a non-swirling center core surrounded by an annulus swirling region. A significant weakening of the swirling velocity components downstream of the burner was found in both reacting and non-reacting flows. These data are being analyzed to determine the swirl and divergence rate as function of axial distance for comparison with the simulated results.

Our closely coordinated collaboration with CCSE's computational efforts represents a major advance in the tools available for studying reacting flow. By designing experiments that are well-characterized and specifically designed as companions to such simulations, we can not only provide a much more comprehensive view of a turbulent flame; we can also establish fundamental linkages between turbulent flame experiments and basic combustion chemistry.

4. Summary of Planned Research

Our longer term goal is to develop the experimental capabilities to characterize 3D velocity statistics and flame structures. The tasks for FY 06 – 08 are:

1. Collaborate on the development of computational methods with LBNL-CCSE group on Low Reynolds number AMR simulations of v-flame and LSB flame.
2. Extend PIV to 3D
3. Investigate the role of thermal-diffusive effects on flame/turbulence interactions to determine a possible attenuation of the thermal/diffusive instability with increasing turbulence.
4. Studies of turbulent flames at high initial pressures and/or temperatures
5. Experimental database for premixed turbulent flames

Publications

Bell, J.B., M.S. Day, I.G. Shepherd, M.R. Johnson, R.K. Cheng, V.E. Beckner, M.J. Lijewski, and J.F. Grear, *Numerical Simulation of a Laboratory-Scale Turbulent V-Flame*. Submitted to, Proceedings of the National Academy of Sciences, 2005.

**Dynamics and Energetics of Elementary Combustion Reactions and Transient Species
Grant DE-FG03-98ER14879**

Robert E. Continetti
Department of Chemistry and Biochemistry
University of California San Diego
9500 Gilman Drive
La Jolla, CA 92093-0340
rcontinetti@ucsd.edu

April 11, 2005

Program Scope

This research program focuses on the transition state dynamics of hydroxyl radical reactions and the energetics and dynamics of combustion-relevant oxygenated organic radicals. A unique photoelectron-photofragment coincidence technique is used to create energy selected transient species by photodetachment of the corresponding negative ions, and subsequently follow the dissociation dynamics of the transient neutrals produced in dissociative states. In the case of hydroxyl radical reactions, the stability of OH^- allows the production of a number of precursor anions that allow probing important regions of the corresponding neutral potential energy surfaces. In the past year we have completed a study of the OHF^- anion, and are currently extending our previous studies of the $\text{H} + \text{CO}_2 \rightarrow \text{HOCO}^- \rightarrow \text{OH} + \text{CO}$ potential energy surface by use of lower photon energies in the photodetachment of HOCO^- . Optimization of the ion source conditions and selection of the optimum photon energy for further studies are underway prior to studies of isotope effects in this system using the DOCO^- anion as a precursor. Previous studies in this laboratory of oxygenated radicals have focused on the acetate and formate anions, and will soon be extended to other small carboxylate radicals. Comparison of these results with theoretical predictions should become increasingly feasible in the near future given advances in the calculation of reactive potential energy surfaces and dynamics calculations, providing benchmark data for fundamental combustion reactions.

Recent Progress

Probing the $\text{O} + \text{HF} \rightarrow \text{OH} + \text{F}$ reaction by dissociative photodetachment of OHF^-

The $\text{O} + \text{HF} \rightarrow \text{OH} + \text{F}$ provides a benchmark system for study by dissociative photodetachment of the OHF^- anion, as originally shown by the photoelectron spectroscopy measurements by Neumark and co-workers.¹ Owing to the relative simplicity of this system, wavepacket dynamics studies by Dixon and Tachikawa² on model potential energy surfaces have been supplanted in the last year by new potential energy surface and dynamics calculations by Roncero and co-workers,^{3, 4} focusing on non-adiabatic effects on the reaction dynamics on the neutral potential energy surface. In this laboratory, photoelectron-photofragment coincidence studies of this system have been carried out at a photon energy of 4.8 eV (258 nm), as recently reported in Phys. Chem. Chem. Phys. (DOE publication 3 below).

The photoelectron spectra observed in these experiments are consistent with the earlier studies of Neumark and co-workers, but acquisition of the photoelectron-photofragment coincidence data provides a measurement of the product state distribution, revealing a vibrationally resolved kinetic energy distribution. In addition, the correlation spectrum reveals two different features in the energetically allowed O + HF product channel: (a) diagonal ridges, resulting from direct dissociative photodetachment (DPD) and vibrationally adiabatic dissociation dynamics and (b) areas with higher E_T in the neutral fragments from nonadiabatic dissociation leading to the formation of O + HF($v=1$) from states expected to adiabatically correlate with O + HF($v=2$). The most likely cause for the experimentally observed vibrational nonadiabaticity is found in the recent multi-surface three-dimensional simulations of the DPD of OHF by González-Sánchez *et al.*⁴ They found that in a collinear configuration $^3 \Sigma^-$ and $^3 \Sigma^+$ states correlating with O + HF products have two conical intersections along the reaction coordinate, providing the opportunity for vibronic effects leading to a breakdown of vibrational adiabaticity.

The high (3.3 eV) electron affinity of this system limits these recent experiments to only probing the three lowest vibrational levels of the O + HF(v) products. To extend this study to OH + F exit channel as well will require higher energy photons. We have prepared for future experiments using the 4th harmonic of the 772 nm Ti:Sapphire fundamental, yielding 6.4 eV photons near 193 nm.

Dissociative Photodetachment of the Acetate Anion: Energetics and Stability of the Acetyloxy Radical

In the last year our study of the dissociative photodetachment of the acetate anion was published (DOE publication 2 below). Oxygenated organic radicals such as the carboxyl radicals are important combustion intermediates and also have a significant role in other applications in chemistry. The dissociation of the acetyloxy radical, CH₃CO₂, was studied by photodetachment of the acetate anion at 355, 340 and 258 nm. The experiments showed that at all of these wavelengths 90% of the nascent radicals dissociated to CH₃ + CO₂ radicals, with a large kinetic energy release, peaking at $E_T = 0.65$ eV for 355 nm excitation. The EA of the CH₃CO₂ radical was found to be 3.47 eV, yielding a near-threshold photoelectron spectrum in the 355 nm data with two resolved features. Experiments with CD₃CO₂⁻ yielded a nearly identical photoelectron spectrum, indicating that the observed features do not involve C-H vibrations, and suggesting that these features correspond to two low-lying electronic states of this radical. The 258 nm data revealed evidence for two higher-lying electronic states, consistent with the complicated electronic structure predicted for this free radical. Extension of these studies to other small carboxylate systems, including propanoate and benzoate are planned.

HOCO and DOCO

We are presently returning to our previous studies of the dissociative photodetachment of HOCO⁻ in preparation for a study of the H/D isotope effect in this system using DOCO⁻. In our previous work on this system,⁵ extensive photoelectron-photofragment coincidence studies at 258 nm revealed HOCO, OH + CO and H+CO₂ products from the previously uncharacterized HOCO⁻ anion. These results were supported by theoretical calculations by Prof. J. Francisco on the structure of the anion and the corresponding neutral. Preliminary studies of HOCO⁻ at 388 nm were also carried out, recording only the photoelectron energy and angular distributions. Currently, following the implementation of a new multiparticle detector on our coincidence

spectrometer, we have returned to study this system anew in anticipation of theoretical predictions of the reaction dynamics expected in dissociative photodetachment by Gray, Goldfield and co-workers. At this point, we have completed the coincidence measurements at 388 nm, and are currently going to a lower photon energy (2.33 eV, 532 nm) to acquire higher resolution results near the photodetachment threshold. Once these measurements are completed, we will determine the most useful wavelength to carry out the isotopic studies, which require the use of expensive CD₄ for ion generation.

Future Plans

While the HOCO/DOCO experiments are being carried out, we are currently preparing for a significant change in the pumping system of the apparatus. A new diffusion pump/roots blower system has been acquired and the necessary modifications designed that will allow us to increase the source pumping speed by approximately a factor of five, enabling us to produce colder weakly bound precursor anions at the 1 kHz repetition rate required for these coincidence experiments. We will focus initially on studies of the OH + H₂ and OH + Cl systems, which require H₃O⁻ and OHCl⁻ precursor anions we have found difficult to make with our present ion sources. In addition, the improved source should allow us to try more sophisticated multiple beam synthetic approaches, like those demonstrated by Johnson and co-workers⁶ in their recent study of the OH⁻(CH₃) system. Dissociative photodetachment studies of this species would be of considerable interest, as it represents a complicated radical-radical surface that governs the OH + CH₃ reaction. Following the focus on hydroxyl radical reactions over the coming months, we anticipate extending our previous studies of oxygenated radicals by examining the energetics and stability of larger carboxyl radicals by photodetachment of species including the propanoate (CH₃CH₂CO₂⁻) and benzoate (C₆H₅CO₂⁻) anions.

DOE Publications: 2003 – Present

1. R.E. Continetti and C.C. Hayden, "Coincidence imaging techniques," in Modern Trends in Reaction Dynamics, ed. X. Yang and K. Liu, World Scientific (Singapore), 2004.
2. Z. Lu and R.E. Continetti, "Dynamics of the acetyloxy radical studied by dissociative photodetachment of the acetate anion.", *J. Phys. Chem. A* **108**, 9962-9969 (2004).
3. H.J. Deyerl and R.E. Continetti, "Photoelectron-photofragment coincidence study of OHF⁻: transition state dynamics of the reaction OH + F → O + HF.", *Phys. Chem. / Chem. Phys.* **7**, 855-860 (2005).

Literature Cited

1. S.E. Bradforth, D.W. Arnold, R.B. Metz, A. Weaver and D.M. Neumark, *J. Phys. Chem.* **95**, 8066 (1991).
2. R.N. Dixon and H. Tachikawa, *Mol. Phys.* **97**, 195 (1999).
3. L. González-Sánchez, S. Gómez-Carrasco, A. Aguado, M. Paniagua, M. L. Hernández, J. M. Alvariño and O. Roncero, *J. Chem. Phys.* **121**, 309 (2004). ; S. Gómez-Carrasco, L. González-Sánchez, A. Aguado, O. Roncero, J. M. Alvariño, M. L. Hernández and M. Paniagua, *J. Chem. Phys.* **121**, 4605 (2004).

-
4. L González-Sánchez, S Gomez-Carrasco, A. Aguado, M. Paniagua, M. Luz Hernandez, J. M. Alvarino and O. Roncero, *J. Chem. Phys.* **121**, 9865 (2004).
 5. T. G. Clements, R. E. Continetti and J. S. Francisco, *J. Chem. Phys.* **117**, 6478 (2002).
 6. E.G. Diken, G.H. Weddle, J.M. Headrick, J. M. Weber and M.A. Johnson, *J. Phys. Chem. A*, **108**, 10116 (2004).

Flame Sampling Photoionization Mass Spectrometry

Terrill A. Cool
School of Applied and Engineering Physics
Cornell University, Ithaca, New York 14853
tac13@cornell.edu

Project Scope

Photoionization mass spectrometry (PIMS) using monochromated synchrotron radiation, applied to the selective detection of flame species, is uniquely suited for the development and testing of kinetic models of combustion chemistry. The ability to precisely tune the photon energy over a wide range with good energy resolution often enables selective detection of a single isomer. A primary goal of this project is the determination of the isomeric composition of intermediate flame species important in describing chemical reaction mechanisms with hydrocarbon fuels. A second goal is the quantitative measurement of absolute species concentrations in low-pressure one-dimensional laminar flames of alkanes, alkenes, alkynes, cyclic hydrocarbons, aromatics, and alcohols.

The work described here is part of a collaborative effort between investigators at Cornell, the Sandia Combustion Research Facility, and the University of Massachusetts. Further descriptions of recent achievements of this collaboration appear in the abstracts of Nils Hansen and Craig Taatjes, and Phil Westmoreland.

Recent Progress

A. The identification of isomers of C_3 , C_4 , C_5 , C_6 , and C_7 hydrocarbons

The isomers of C_3H_2 , C_4H_3 , and C_5H_3 exemplify the small unsaturated hydrocarbon free radicals that are critical elements of the gas-phase chemistry that leads ultimately to soot formation in rich flames. Reactions involving these radicals are thought to play a significant role in the growth of higher PAH's (polycyclic aromatic hydrocarbons) in flames. Jim Miller and Stephen Klippenstein are key participants in collaborative research directed toward the characterization of the isomeric composition of these radicals in rich flames. Stephen has shown that our observed ionization thresholds for several of these isomeric species compare favorably with adiabatic ionization energies found with high level QCISD(T) quantum calculations.

C_3H_2 The photoionization efficiency C_3H_2 has been measured between 8.5 eV and 11.0 eV. Franck-Condon factors for photoionization are calculated from B3LYP/6-311++G(d,p) characterizations of the neutral and cation of the two lowest-energy C_3H_2 isomers, triplet propargylene (HCCCH, prop-2-ynylidene) and singlet cyclopropenylidene (cyclo-HCCCH). Comparison of the calculated Franck-Condon envelopes with the experimental photoionization efficiency spectrum determines the adiabatic ionization energy of triplet propargylene to be (8.96 ± 0.04) eV. Ionization energies for cyclopropenylidene, propargylene, and propadienylidene (H_2CCC)

calculated using QCISD(T) with triple- and quadruple- ζ basis sets extrapolated to the infinite basis set limit are in excellent agreement with the present determination of the ionization energy for propargylene and with literature values for cyclopropenylidene and propadienylidene.

C₄H₃ We observe an ionization threshold for C₄H₃ at 8.05(5) eV. This is assigned to the *i*-C₄H₃ radical, the thermodynamically most stable C₄H₃ isomer, based on the excellent agreement with the calculated adiabatic ionization energy of 8.02 eV.

C₅H₃ A Franck-Condon analysis, based on *ab initio* calculations of frequencies and force constants, is used to provide “best-fit” simulations of observed PIE curves, which show the presence of the CH₂CCCCH and CHCCHCCH isomers with respective ionization thresholds of 8.20(5) and 8.31(5) eV. These values are in excellent agreement with respective calculated adiabatic ionization energies of 8.19 and 8.28 eV.

C₅H₄ An observed ionization threshold at 9.20(5) eV is in good agreement with a calculated adiabatic ionization energy of 9.24 eV for the CH₂CCHCCH isomer, which is 5 kcal/mol less stable than the most stable isomer, CH₃C≡CC≡CH (1,3-pentadiyne).

B. Absolute photoionization cross sections for reaction intermediates. Studies of hydrocarbon combustion with synchrotron PIMS have been performed with our apparatus with photon energy spreads ranging from 25 to 60 meV. Quantitative determinations of flame species concentrations require absolute photoionization cross sections of comparable resolution, preferably measured under experimental conditions corresponding to those used in the flame chemistry studies.

Although measurements of near-threshold relative cross sections (photoionization efficiency (PIE) curves), traditionally used for determinations of ionization energies and thermochemical properties, are available for many molecules, reliable measurements of absolute cross sections are less common. The focus of our measurements is on the near-threshold region within about 2 eV of the adiabatic ionization energies. For many hydrocarbons the appearance energies for dissociative ionization are within 1-2 eV of the adiabatic ionization energy of the parent molecule and mass-resolved ion detection is required to distinguish the partial contributions to the total photoionization cross section made by dissociative ionization channels. Indeed, in PIMS studies of flame chemistry, ion fragments of a given mass-to-charge (*m/z*) ratio may interfere with the detection of parent ions with the same *m/z* value. Successful strategies for quantitative measurements of flame species composition often require partial photoionization cross sections for many such dissociative channels.

Absolute cross sections for molecular and dissociative photoionization have been measured for 21 common stable reaction intermediates found in the combustion of many simple hydrocarbons. These measurements contribute to a growing comprehensive data base critically needed for PIMS studies of hydrocarbon flame chemistry. The measurement of absolute photoionization cross sections for radical species presents difficult experimental challenges, although recent encouraging progress has been achieved by Neumark and co-workers with measurements for propargyl, vinyl, and the allyl and 2-propenyl isomers of C₃H₅ radicals [1,2].

C. The detection of enols in hydrocarbon flames

Until the recent discovery of ethenol (vinyl alcohol) in a fuel-rich ethylene flame [3], the C_2H_4O molecules observed in flames were presumed to be acetaldehyde or oxirane. We have recently demonstrated that ethenol occurs in significant concentrations in fourteen prototypical fuels representing a range of compounds present in modern hydrocarbon fuel blends. Moreover, propenols and butenols are also observed for the first time in hydrocarbon flames.

Systematic measurements of photoionization efficiency (PIE) spectra and flame species concentration profiles in low-pressure laminar flames indicate that enol flame chemistry is markedly different from that of aldehyde tautomers. The results suggest that several different reaction mechanisms may contribute to enol formation in flames of alkenes, alkynes, cyclic alkanes, alcohols and aromatics.

Figure 1 shows photoionization efficiency spectra for $C_2H_4O^+$ ions ($m/z=44$) sampled from four of these flames, along with the derived ratio [3] of ethenol to acetaldehyde. Flames of other fuels: propyne, benzene, cyclohexane, 1,3-butadiene, ethanol, propene, allene, cyclopentene and ethene were also found to exhibit significant contributions from ethenol, with peak mole fractions in the range of 10^{-3} - 10^{-4} .

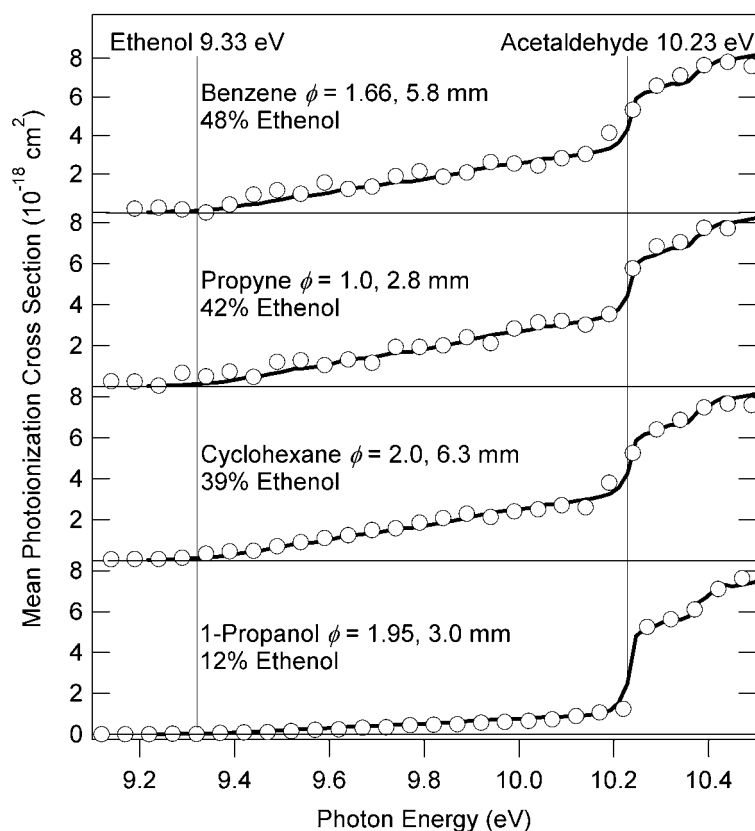


Figure 1. PIE curves taken for $m/z = 44$ ions sampled from four representative flames. Photo-ion signals (circles), taken at the indicated distance from the burner, have been background-corrected and normalized by the measured photon flux. Signals are then scaled to computed mean photoionization cross sections [3] (lines), for hypothetical mixtures of ethenol and acetaldehyde that give best fits to the data. Ionization energies for ethenol ($CH_2=CHOH$) and acetaldehyde (CH_3CHO) are indicated by the thin vertical lines.

Future Directions

Several modifications to our PIMS instrument will be performed in the coming months to improve the accuracy of measurements of absolute species concentrations. Close collaborations with research groups at the University of Bielefeld and the University of Massachusetts enable measurements with other techniques, e.g., electron-impact mass spectrometry (EIMS) and the laser-based LIF and REMPI methods to be combined with our PIMS data for comprehensive analyses of several reaction systems. Work currently in progress includes a comparison of the results for the propene/oxygen, cyclopentene/oxygen, cyclohexane/oxygen, propyne/oxygen and allene/oxygen systems with kinetic modeling calculations. Species mole fraction profiles, temperature profiles and species PIE curves measured for several of the 20 reaction systems studied to date are available for the development and testing of kinetic models. Our growing data base will be archived in the Collaboratory for Multi-Scale Chemical Science in an initiative directed by Larry A. Rahn and David J. Leahy of the Sandia CRF.

Current research priorities include determinations of the isomeric composition of intermediate flame species, the measurement and computation of adiabatic ionization energies for radical intermediates, and continued measurements of absolute photoionization cross sections for many additional stable reaction intermediates.

References

1. J. C. Robinson, N. E. Sveum, and D. M. Neumark, *J. Chem. Phys.* **119**, 5311 (2003).
2. J. C. Robinson, N. E. Sveum, and D. M. Neumark, *Chem. Phys. Lett.* **383**, 601 (2004).
3. T. A. Cool, K. Nakajima, T. A. Mostefaoui, F. Qi, A. McIlroy, P. R. Westmoreland, M. E. Law, L. Poisson, D. S. Peterka, and M. Ahmed, *J. Chem. Phys.*, **119**, (2003) 8356-8365.

DOE Publications

1. T. A. Cool, K. Nakajima, T. A. Mostefaoui, F. Qi, A. McIlroy, P. R. Westmoreland, M. E. Law, L. Poisson, D. S. Peterka, and M. Ahmed, "Selective Detection of Isomers with Photoionization Mass Spectrometry for Studies of Hydrocarbon Flame Chemistry", *J. Chem. Phys.*, **119**, (2003) 8356-8365.
2. C. A. Taatjes, D. L. Osborn, T. A. Cool, and K. Nakajima, "Synchrotron Photoionization Measurements of Combustion Intermediates: The Photoionization Efficiency of HONO", *Chem. Phys. Lett.*, **394**, (2004) 19-24.
3. C. A. Taatjes, S. J. Klippenstein, N. Hansen, J. A. Miller, T. A. Cool, J. Wang, M. E. Law, and P. R. Westmoreland, "Synchrotron Photoionization Measurements of Combustion Intermediates: Photoionization Efficiency of C₃H₂ Isomers", *Phys. Chem. Chem. Phys.* **7**, (2005) 806-813.
4. T. A. Cool, K. Nakajima, C. A. Taatjes, A. McIlroy, P. R. Westmoreland, M. E. Law and A. Morel, "Studies of a fuel-rich propane flame with photoionization mass spectrometry", *Proc. Combust. Inst.*, **30**, 1681 (2004).
5. A. Morel, M. E. Law, P. R. Westmoreland, T. A. Cool, K. Nakajima, T. A. Mostefaoui, F. Qi, A. McIlroy, L. Poisson, D. S. Peterka, M. Ahmed, "Selective detection of isomers using a new photoionization MBMS apparatus." *Chemical and Physical Processes of Combustion*, Pittsburgh: The Combustion Institute, pp. 281-284 (2003).
6. M. E. Law, A. Morel, P. R. Westmoreland, T. A. Cool, C. A. Taatjes. "Selective Detection of C₃H₄ and C₆H₆ Isomers in Flames." *Chemical and Physical Processes of Combustion*, Pittsburgh: The Combustion Institute, pp. 285-288 (2003).
7. M.E. Law, P. R. Westmoreland, T. A. Cool, J. Wang, N. Hansen, C. A. Taatjes, T. Kasper. "Benzene Formation in a Stoichiometric Cyclohexane Flame," *Proceedings of the Fourth Joint Technical Meeting of the U.S. Sections of the Combustion Institute*, The Combustion Institute: Pittsburgh (2005). Accepted.

STATE CONTROLLED PHOTODISSOCIATION OF VIBRATIONALLY EXCITED MOLECULES AND HYDROGEN BONDED DIMERS

F.F. Crim
Department of Chemistry
University of Wisconsin–Madison
Madison, Wisconsin 53706
fcrim@chem.wisc.edu

Our research investigates the chemistry of vibrationally excited molecules. The properties and reactivity of vibrationally energized molecules are central to processes occurring in environments as diverse as combustion, atmospheric reactions, and plasmas and are at the heart of many chemical reactions. The goal of our work is to unravel the behavior of vibrationally excited molecules and to exploit the resulting understanding to determine molecular properties and to control chemical processes. A unifying theme is the preparation of a molecule in a specific vibrational state using one of several excitation techniques and the subsequent photodissociation of that prepared molecule. Because the initial vibrational excitation often alters the photodissociation process, we refer to our double resonance photodissociation scheme as *vibrationally mediated photodissociation*. In the first step, fundamental or overtone excitation prepares a vibrationally excited molecule and a second photon, the photolysis photon, excites the molecule to an electronically excited state. Vibrationally mediated photodissociation provides new vibrational spectroscopy, measures bond strengths with high accuracy, alters dissociation dynamics, and reveals the properties of and couplings among electronically excited states.

Several recent measurements illustrate the scope of the approach and point to new directions. We have completed an extensive study the spectroscopy and non-adiabatic dissociation dynamics of ammonia (NH_3), have published new results on the vibrationally mediated photodissociation of methanol (CH_3OH), and have made our first ion imaging measurements using our new capabilities. In each case, the goals are understanding and exploiting vibrations in the ground electronic state, studying the vibrational structure of the electronically excited molecule, and probing and controlling the dissociation dynamics of the excited state.

Ammonia (NH_3)

Ammonia is a famously well-studied molecule that holds interesting opportunities for vibrationally mediated photodissociation experiments because it has both a nonadiabatic dissociation to yield ground state $\text{NH}_2 + \text{H}$ and an adiabatic dissociation to form excited state $\text{NH}_2^* + \text{H}$. We have used vibrationally mediated photodissociation spectroscopy to observe the symmetric N-H stretching vibration (ν_1), the antisymmetric N-H stretching vibration (ν_3), and the first overtone of the bending vibration ($2\nu_4$), obtaining simplified spectra originating in the lowest few rotational states. In addition, we have observed combination bands with the umbrella vibration (ν_2) for each of these states, ($\nu_1+\nu_2$), ($\nu_2+\nu_3$), and ($\nu_2+2\nu_4$). The action spectra come from observing the production of the excited state NH_2^* from photolysis well above the threshold energy for its formation.

The electronic spectroscopy available through vibrationally mediated photodissociation is particularly informative. Because the initial vibrational excitation of NH_3 molecules cooled in a supersonic expansion selects single rotational states of vibrationally excited molecules, both the Franck-Condon factors and positions of the transitions change from the one-photon spectra. By using this extra dimension, we are able for the first time to identify unambiguously the progression in the excited state bending vibration (ν_4), the combination bands between the bending and excited state umbrella vibration ($\nu_2+\nu_4$), and the origin of the excited state symmetric stretch vibration (ν_1).

Information about the excited state structure makes it possible to investigate the dynamics of the dissociation of electronically excited molecules with different vibrations excited. The experiments use resonant enhanced multiphoton ionization to perform Doppler spectroscopy on the H atom fragment. In agreement with previous measurements, we observe both slow and fast components in the distribution of recoil velocities upon excitation of different excited state umbrella vibrations. The excited state bending vibrations behave similarly with a slightly larger fraction of fast hydrogen atoms. The striking difference is in the stretching vibrations, which we can excite unambiguously for the first time. Dissociation from the state containing one quantum of symmetric stretch (ν_1) produces a distribution with both fast and slow components that are similar to that for the origin. Dissociation from the antisymmetric N-H stretch state (ν_3), however, produces dramatically different results. It forms *only* slow hydrogen atoms, likely reflecting preferential decomposition to make solely the excited state product. New calculations by D. Yarkony (J. Chem. Phys. **121**, 628 (2004)) seem consistent with molecules that have excited asymmetric N-H stretching vibrations preferentially remaining on the excited state surface, apparently avoiding one conical intersection by moving toward another intersection for which the crossing probability is smaller.

Methanol (CH_3OH)

Our first explorations of the vibrationally mediated photodissociation of methanol allowed us to obtain spectra of the second and third overtone of the O-H stretching vibration in the cooled molecules that agreed well with other measurements. We have also obtained similar spectra in the fundamental region of the O-H stretch and made the first measurements of the vibrationally mediated photodissociation dynamics detecting the H-atom product in order to obtain the ultraviolet spectra of the vibrationally excited molecules. The electronic excitation spectrum of vibrationally excited methanol begins about 2600 cm^{-1} lower in total excitation energy than that for ground vibrational state methanol. A simple model using a one-dimensional vibrational wavefunction mapped onto a dissociative excited electronic state surface recovers the qualitative features of the spectrum. Using *ab initio* calculations of portions of the ground and excited potential energy surfaces, we calculate vibrational wavefunctions and simulate the electronic excitation spectra using the overlap integral for the bound and dissociative vibrational wavefunctions on the two surfaces. The qualitative agreement of the calculation with the measurement suggests that, at the energy of the fundamental vibration, the O-H stretch is largely uncoupled from the rest of the molecule during the dissociation.

Ion Imaging

Implementing ion imaging in vibrationally mediated photodissociation experiments has been a focus of our effort during the past year. We have modified our apparatus, tested the system by obtaining velocity mapped images of molecules such as NO and O₂, and made our first measurements on one-photon dissociation of NH₃. Adding vibrational excitation is demanding on both the detection scheme, particularly with regards to spurious background ionization, and on the infrared generation system. Both aspects are working satisfactorially, and we have further improvements planned. Our first efforts to observe images in vibrationally mediated photodissociation are very encouraging.

FUTURE DIRECTIONS

The first near term goal of the project is to study the dissociation of vibrationally excited ammonia using ion imaging. Ion imaging detection will allow a more incisive study of the striking result on vibrational control of the passage through the conical intersection in ammonia. The second goal step is to investigate the photolysis of carboxylic acids and, most important, their dimers using the new capabilities we are proving.

PUBLICATIONS SINCE 2003 ACKNOWLEDGING DOE SUPPORT

Competition between Adiabatic and Nonadiabatic Pathways in the Photodissociation of Vibrationally Excited Ammonia. Andreas Bach, J. Matthew Hutchison, Robert J. Holiday, and F. Fleming Crim, *J. Phys. Chem. A*, **107**, 10490 (2003).

Photodissociation of Vibrationally Excited Ammonia: Rotational Excitation in the NH₂ Product. Andreas Bach, J. Matthew Hutchison, Robert J. Holiday, and F. Fleming Crim, *J. Chem. Phys.* **118**, 7144 (2003).

Action spectroscopy and photodissociation of vibrationally excited methanol. J. Matthew Hutchison, Robert J. Holiday, Andreas Bach, Shizuka Hsieh, and F. Fleming Crim, *J. Phys. Chem. A* **108**, 8115 (2004).

Spectroscopy and Dynamics of Vibrationally Excited Transient Radicals

Hai-Lung Dai

Department of Chemistry, University of Pennsylvania
Philadelphia, PA 19104-6323; dai@sas.upenn.edu

I. Program Scope

The present primary goal of this project is to characterize the previously unknown vibrational modes and structure of transient radicals that are important in combustion processes. The radicals we choose for study at present are small radicals that are known or proposed to play important roles in combustion reactions.

To tackle the vibrational spectroscopy of radicals that can only be generated in small quantities with short life times, we have applied the nanosecond time resolved Fourier Transform IR Emission Spectroscopy (TR-FTIRES) to the study. The transient radical species is produced with high vibrational excitation through UV photolysis of a precursor molecule. IR emission from the highly excited species through its IR active vibrational modes is detected with fast time resolution. Inert buffer gas is used for collision quenching of the radicals so that IR emission observed at later times is from the fundamental levels. A two-dimensional cross-spectra correlation technique has been developed for analyzing the time-resolved FTIR emission spectra. This approach allows the previously unknown vibrational modes be detected as emission transitions with modest resolution. The spectroscopic approach also allows the reactions of the excited radical and the photolysis reaction of the precursor molecules to be characterized.

Within the last several years, using this approach we have detected all nine vibrational modes of the vinyl radical, two vibrational modes and the structure of cyanovinyl, two modes of OCCN, and the vibrational modes of deuterated vinyl and cyanovinyl. Our present focus is the HCCO radical.

At present we are also developing a new thrust within this study: characterizing collision energy transfer of the vibrationally excited radicals. We have demonstrated that by using the TR-FTIRES technique to monitor the vibrational energy content of excited molecules during a collision quenching process, the energy distribution and the amount of energy transferred per collision can be measured. Information on collision energy transfer of highly excited radicals is important to the characterization of combustion processes but little is known on this subject. TR-FTIRES will allow the deduction of the energy content of the IR emitting radicals, once their vibrational structure is well characterized, as a function of time for the measurement of energy distribution and energy transfer quantity of the excited radicals in a collision process.

II. The Ketenyl Radical (HCCO)

HCCO is an important radical in hydrocarbon combustion chemistry. Combustion of several small hydrocarbons such as acetylene involves the HCCO radical as a reaction intermediate. One such reaction in which HCCO is a key product is between acetylene and

O(³P), a dominating reaction in combustion of all fuels. In the presence of molecular oxygen the ketyenyl radical is able to further react through one of the two pathways for prompt CO₂ formation. For its importance, HCCO has been a focus of study by several laboratories (see for example Unfried, Glass, and Curl, *Chem. Phys. Lett.*, 177, 33(1991); Brock, Mischler, and Rohlfing, *J. Chem. Phys.*, 110, 6773(1999); Osborn *et al.*, *J. Chem. Phys.*, 106, 10087(1997) and *J. Phys. Chem. A*, 107, 3728(2003); Krisch, Miller, and Butler, *J. Chem. Phys.*, 119, 176(2003); and Sattelmeyer and Schaefer, *Chem. Phys. Lett.*, 383, 266(2004)).

Our present study of HCCO has resulted in the detection of the ν_1 CH stretch mode and the characterization of the excited quartet state dynamics.

A. The ν_1 CH Stretch Mode

Recently, Butler and coworkers have demonstrated an efficient means to produce the HCCO radical through 193 nm dissociation of ethyl ethynyl ether (EEE). Their Photofragment Translational Energy Spectroscopy study found that the EEE precursor is a clean source of HCCO with a unit photodissociation quantum yield. Based on the bimodal translational energy distributions for the HCCO and C₂H₅ fragments it was suggested that the ketyenyl radical is produced in two different electronic states: 63% in the $\tilde{a}^4(A'')$ state while 37% are in the lower $\tilde{X}(^2A'')/\tilde{A}(^2A')$ states. Up to 97 kcal/mol energy may be available for internal excitation of the products after 193 nm photolysis of EEE.

Selected time-resolved emission spectra from 700 and 4000 cm⁻¹ recorded following 193 nm photodissociation of EEE are shown in Figure 1. The time-resolved spectra contain emission features not only from IR active modes of vibrationally excited HCCO, but also from the other vibrationally excited species that may result from EEE fragmentation and subsequent reactions. Due to effects of anharmonicity, many emission features in the earliest time slices when the emitting species energy is higher shift from the red side toward the fundamental transition frequency.

The emission features in Figure 1, based on the time-dependence of emission intensity and theoretical calculations, can be assigned to the known HCCO CO stretch mode and the other photolysis products and their secondary reaction products. Time behavior of spectral intensity can be used to differentiate the origin with respect to primary vs secondary reactions. Figure 2 is a comparison of the time-dependence of two features. The upper trace is the integration of intensity from 1600 to 1840 cm⁻¹, highlighted by the inset in Figure 5, which is on the lower energy side of the main peak that is assigned to the early time emission of the HCCO CO stretch. The lower trace is integration over the weak feature region from 3100 to 3300 cm⁻¹. The comparison shows that the spectral activity in the higher frequency region is identical to that of the HCCO CO stretch. The center of this feature is identified at 3208 cm⁻¹ and it is assigned to the CH stretch mode of HCCO.

B. The Lowest Quartet State

This work provides the first spectroscopic evidence for the detection of the quartet state of HCCO. According to the Butler and coworkers' study the radical generated through the 193

nm dissociation of EEE exists with majority as $\text{HCCO}(\tilde{a}^4A'')$. IR emission from the CO stretch of the quartet state has been identified. The quartet state has initially sufficient energy for dissociation into CH and CO. Collision with buffer gas causes both internal vibrational relaxation and intersystem crossing to the lower quartet state surface where dissociation may also occur. The rate of collision induced intersystem crossing can be extracted from integrated intensity time-profiles obtained using three different collision partners: He, Ar and Xe. Since helium is a light and fast atom, collision with He is more efficient for vibrational relaxation within the quartet state potential surface and less efficient in inducing the intersystem crossing to the lower doublet state. Collision with He provides effectively a means to trap $\text{HCCO}(\tilde{a}^4A'')$ for a longer period of time than with argon or xenon. Both heavier atoms are efficient at inducing intersystem crossing that allows the ISC rate constants to be extracted from the appearance of diatomic CO in the time-resolved IR emission spectra. This work also allows the determination of the fundamental transition of the ν_2 stretch of $\text{HCCO}(\tilde{a}^4A'')$ at $\sim 1923 \text{ cm}^{-1}$.

III. Plans for Next Year- Collision Energy Transfer from Vibrationally Excited Radicals

In the high temperature environment of a combustion chamber, it is expected that the transient intermediates and reaction products are excited with high internal energies. The internal excitation will have an effect on the reaction rates that need to be characterized for the understanding of combustion reaction mechanisms. The other important factor for understanding the reaction mechanism in a combustion environment is the characterization of the collision energy transfer rates of the excited species. The collision energy transfer rate is deterministic of the thermalization of the reaction exothermicity and gravely affects the amount of energy available in promoting the reactions of the excited species.

We have used time-resolved IR emission from vibrationally excited molecules during collision quenching process to measure the collision energy transfer rates of highly excited stable polyatomic molecules. The IR emission spectrum at a specific time following the excitation laser pulse can be used to reveal the vibrational energy distribution at that time. This information allows the deduction of the average energy of the excited molecules as a function of the number of collisions with the ambient gas after the initial excitation and the determination of the average energy transferred per collision.

To determine the energy distribution from the IR emission bands of vibrationally excited molecules we need to know the vibrational anharmonicity of at least a few modes. This information is available for many stable small/medium size molecules for which detailed spectroscopic studies have been performed. This is in general not the case for radicals. On the other hand, both information- the anharmonicity and the energy distribution- is inherently contained in the IR emission spectra. Previous studies have conformed that a Gaussian function can be effectively used to describe the energy distribution characterized by the average energy and the width. It is also known that the range and behavior of anharmonicity can be approximately modeled for a specific mode. We propose that a model can be set up with the anharmonicity and the Gaussian characteristics as variables to be determined from fitting of the multiple time-resolved spectra for the radicals. Collision energy transfer behavior of radicals can thus be investigated and characterized.

Publications since 2003 acknowledging support from this grant

The ν_1 and ν_2 Vibrational Bands of The OCCN Radical Detected Through Time-Resolved Fourier Transform IR Emission Spectroscopy

Can. J. Chem. [Herzberg Memorial Issue], 82(6), 925-933 (2004) W. McNavage, W. Dailey and H. L. Dai

Two-Dimensional Cross-Spectra Correlation Analysis of Time-Resolved Fourier Transform IR Emission Spectra

J. Chem. Phys. (2005), W. McNavage and H. L. Dai

Time-Resolved FTIR Emission Spectroscopy of Transient Radicals

J. Chinese Chem. Soc. (Taipei), [K. C. Lin issue] (2005), L. T. Letendre, W. McNavage, C. Pibel, D.-K. Liu, and H. L. Dai

Fig. 1

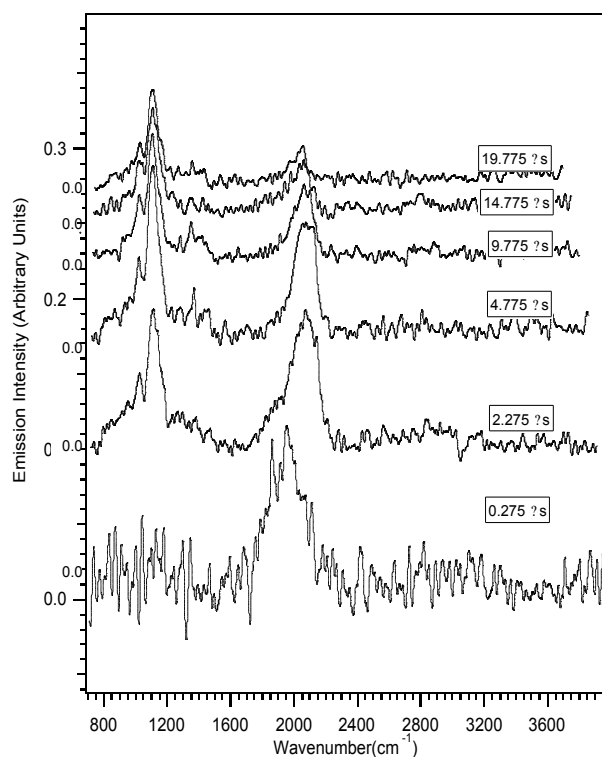
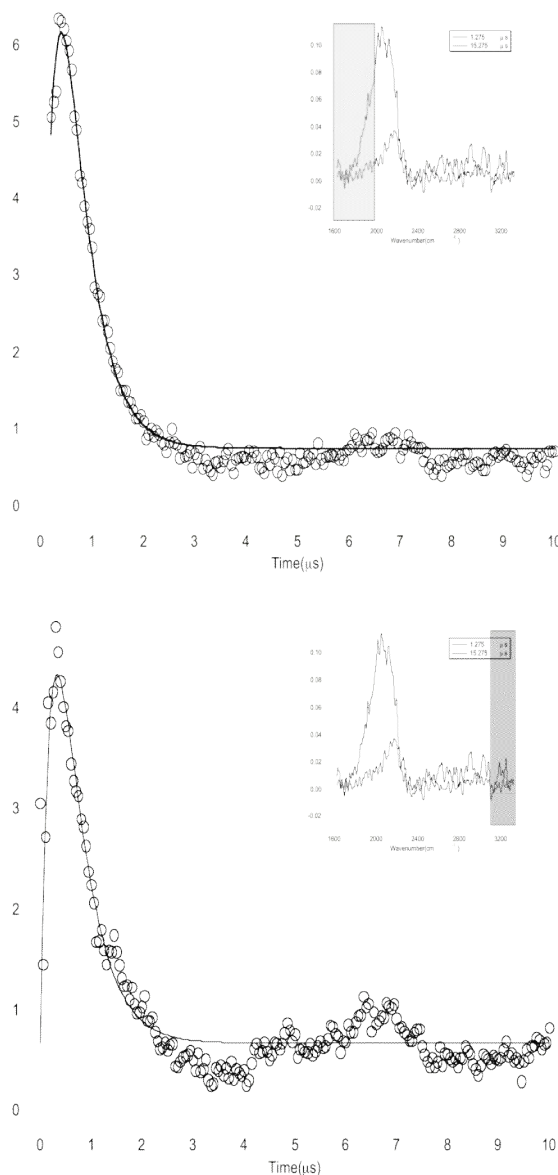


Fig. 2



Bimolecular Dynamics of Combustion Reactions

H. Floyd Davis

Department of Chemistry and Chemical Biology
Baker Laboratory, Cornell University, Ithaca NY 14853-1301

I. Program Scope:

The aim of this project is to better understand the mechanisms and product energy disposal in bimolecular reactions fundamental to combustion chemistry. Using the crossed molecular beams method, a molecular beam containing highly reactive free radicals is crossed at right angles with a second molecular beam. The angular and velocity distributions of the products from single reactive collisions are measured, primarily using the oxygen Rydberg tagging method.¹

II. Recent Progress:

During the second year of this grant, we have primarily focused on studies employing O atom Rydberg time-of-flight (ORTOF) spectroscopy for velocity and angular measurements of ground state oxygen atoms produced by photodissociation and bimolecular reactions.

i. Photodissociation Dynamics of N₂O at 130 nm.

ORTOF spectroscopy was used to study the VUV photodissociation dynamics of N₂O near 130 nm. The O(³P_J) products were tagged by excitation to high-n Rydberg levels and subsequently field ionized at a detector. Formation of O(³P_J) following excitation to the repulsive N₂O D(¹Σ⁺) state correlates with the first two electronically excited states of the N₂ counterfragment, N₂(A ³Σ_u⁺) and N₂(B ³Π_g). The O(³P_J) translational energy distribution reveals that the overall branching ratio between N₂(A ³Σ_u⁺) and N₂(B ³Π_g) formation is approximately 1.0:1.0 for J = 1 and 2, with slightly less N₂(B ³Π_g) produced in coincidence with O(³P₀). The angular distributions were found to be independent of J and highly anisotropic, with β = 1.5 ± 0.2.

Although our earlier study of NO₂ photodissociation¹ demonstrated that the lifetimes of oxygen atom Rydberg states are sufficiently long to facilitate Rydberg tagging TOF studies, the sensitivity of the method relative to the well-characterized HRTOF method was unknown. In particular, the viability of this technique for studies of crossed beams reactions of importance in combustion, such as H + O₂ → OH + O remained uncertain. Thus, the N₂O photodissociation experiments provided a good test system that allowed us to evaluate the sensitivity of ORTOF. Our results on N₂O suggest that the sensitivity is comparable to that for HRTOF. The primary limitation of the ORTOF technique relative to HRTOF is that phase matching at 130 nm is not possible, limiting the VUV intensity.

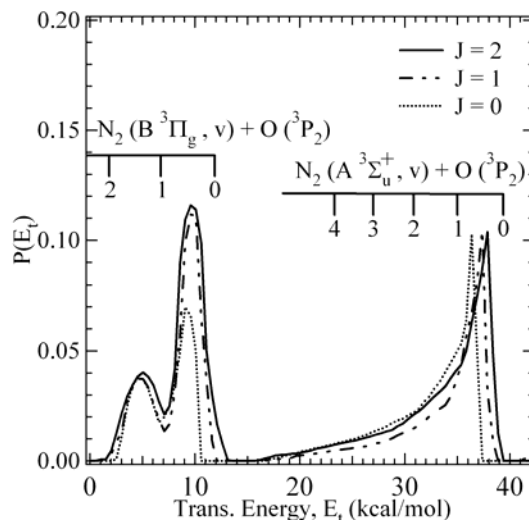


Fig. 1: O atom center-of-mass translational energy distributions for O(³P_{J=2,1,0}) from 130 nm N₂O photodissociation. Maximum energies for N₂(A ³Σ_u⁺, B ³Π_g) in different vibrational levels are indicated for O(³P₂)

ii. Crossed Beams Study of the $\text{CN} + \text{O}_2 \rightarrow \text{NCO} + \text{O}({}^3\text{P})$ Reaction

The $\text{CN} + \text{O}_2$ reaction is one of the simplest 4-atom systems containing “heavy” atoms, and represents a prototypical reaction between two open-shell species. The reaction has therefore been studied in some detail. Dagdigian’s group² has studied the reaction at room temperature in a static gas cell. Their studies indicated that the NCO was produced in a wide range of vibrational energies, with a substantial fraction of the available energy appearing in NCO bending excitation. On the other hand, MacDonald, Liu and coworkers,³ who studied the reaction in crossed pulsed beams, found that NCO was formed vibrationally cold, with most of the excess energy appearing in product translational energy. Thus, the results of two careful experimental studies would at first appear to be mutually inconsistent. It has been suggested, however,^{4,5} that the vibrational energy disposal (particularly the degree of NCO bending excitation) in the $\text{CN} + \text{O}_2$ reaction may depend strongly on the amount of rotational energy in the CN reactant. If this is correct, the $\text{CN} + \text{O}_2$ reaction would be an important prototype system in which reactant rotational energy plays an important role in the reaction dynamics.

We have used ORTOF to carry out a crossed beam study of the $\text{CN} + \text{O}_2$ reaction at collision energies of 3.08 and 4.16 kcal/mol. In the study at 3.08 kcal/mol, the CN beam was produced by 193 nm photodissociation of 10% C_2N_2 in He directly in front of the orifice of a pulsed nozzle with a total gas pressure of 20 PSI. Under these conditions, the CN rotational temperature was found to be 25 K for $J < 10$, with an additional component in the CN rotational distribution extending to higher rotational excitation, up to $J = 45$. In the second experiment, carried out at 4.16 kcal/mol, the photolysis was carried out using a Teflon nozzle extension, which facilitated

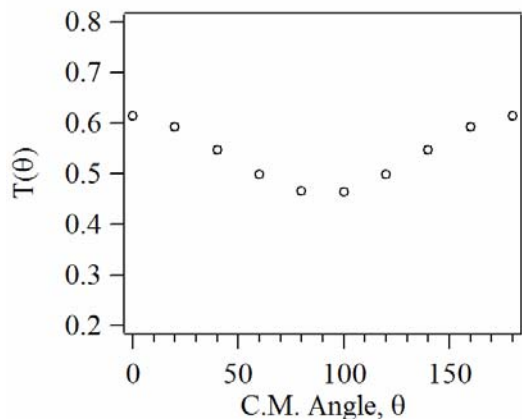


Fig. 3: Center of mass angular distribution for $\text{O}({}^3\text{P}_2)$ atoms from $\text{CN} + \text{O}_2$ reaction.

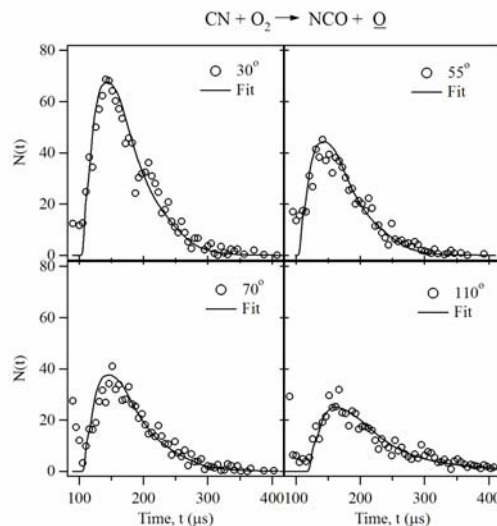


Fig. 2: $\text{O}({}^3\text{P}_2)$ TOF spectra from $\text{CN} + \text{O}_2$ reaction.

much better rotational cooling, thereby eliminating the high rotational component from the CN beam. We found that the NCO + O product distributions were not significantly different in the two experiments. In both cases, the NCO vibrational energy distribution was broad, with a forward-backward symmetric angular distribution. This suggests the participation of long-lived NCOO intermediates with lifetimes long compared to their picosecond rotational timescales. We are presently carrying out further experimentation with the CN radical source conditions in an effort to drastically reduce the CN rotational temperature, in order to better understand how CN rotational energy controls the dynamics of the reaction.

III. Future Plans:

After considerable effort, we have reached the point where we are able to reliably and reproducibly observe reactive scattering from the $\text{CN} + \text{O}_2 \rightarrow \text{NCO} + \text{O}({}^3\text{P})$ reaction. The detection scheme is rather complex, involving the simultaneous overlapping of two molecular beams and two laser beams (one of which is in the VUV, produced by four wave mixing). We have now reached the level of sensitivity and reproducibility where we are able to “tune up” the oxygen Rydberg signal by monitoring the photodissociation of O_2 at 130nm. By careful optimization of the experimental conditions, we have improved the sensitivity of the technique over the past year by at least an order of magnitude. We believe that experimental studies of two key combustion reactions, $\text{H} + \text{O}_2 \rightarrow \text{OH} + \text{O}$ and $\text{C}_2\text{H}_3 + \text{O}_2 \rightarrow \text{C}_2\text{H}_3\text{O} + \text{O}$, are within reach. These will be the focus of our attention during the upcoming year.

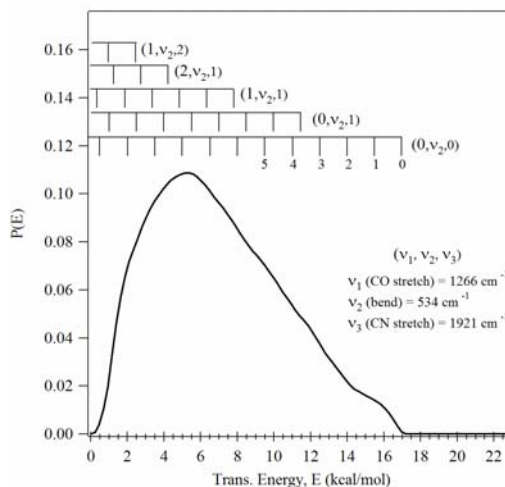


Fig. 4: NCO + O translational energy distribution for for CN + O₂ reaction.

At the meeting last year, we presented preliminary results of an experimental study of reactive quenching of electronically excited OH radicals, $\text{OH}(\text{A}^2\Sigma^+) + \text{D}_2 \rightarrow \text{HOD} + \text{D}$. Now that our sensitivity has been substantially increased through a number of changes to the experimental apparatus, we plan to revisit that system. We are also planning to investigate the H atom channel, $\text{OH}(\text{A}^2\Sigma^+) + \text{D}_2 \rightarrow \text{DOD} + \text{H}$, seen in the previous work by the Lester group.⁶ Following that study, we plan to pursue the study of $\text{OH} + \text{D}_2 (v=1) \rightarrow \text{HOD} + \text{D}$ using stimulated Raman pumping of D_2 molecules.

IV. Publications since 2003:

1. Oxygen Atom Rydberg Time-of-Flight Spectroscopy- ORTOF, C. Lin, M.F. Witinski, and H. Floyd Davis, *J. Chem. Phys.* **119**, 251 (2003).
2. Crossed Beams Study of the Reaction ${}^1\text{CH}_2 + \text{C}_2\text{H}_2 \rightarrow \text{C}_3\text{H}_3 + \text{H}$, H. F. Davis, J. Shu, D.S. Peterka, and M. Ahmed, *J. Chem. Phys.* **121**, 6254 (2004).
3. Photodissociation Dynamics of N_2O at 130 nm: The $\text{N}_2(\text{A } {}^3\Sigma_u^+, \text{B } {}^3\Pi_g) + \text{O}({}^3\text{P}_j)$ Channels, Mark F. Witinski, Mariví Ortiz-Suárez, and H. Floyd Davis, *J. Chem. Phys.*, accepted.

V. References:

1. C. Lin, M.F. Witinski, and H. Floyd Davis, *J. Chem. Phys.* **119**, 251 (2003).
2. D. G. Sauder, D. Patel-Misra, and P.J. Dagdigian, *J. Chem. Phys.* **95**, 1696 (1991).
3. R.G. MacDonald, K. Liu, D.M. Sonnenfroh, and D.-J. Liu, *Can. J. Chem.* **72**, 660 (1994).
4. S.A. Wright, and P.J. Dagdigian, *J. Chem. Phys.* **103**, 6479 (1995).
5. I.W.M. Smith, in *The Chemical Dynamics and Kinetics of Small Radicals, Part I*, K.Liu and A.Wagner, eds., World Scientific, 1995 (page 215-249)
6. M.W. Todd, D.T. Anderson, and M.I. Lester, a) *J. Phys. Chem. A* **105**, 10031 (2001); b) *J. Chem. Phys.* **110**, 11117 (1999).

Multiple–time–scale kinetics

Michael J. Davis

Chemistry Division
Argonne National Laboratory
Argonne, IL 60439
Email: davis@tcg.anl.gov

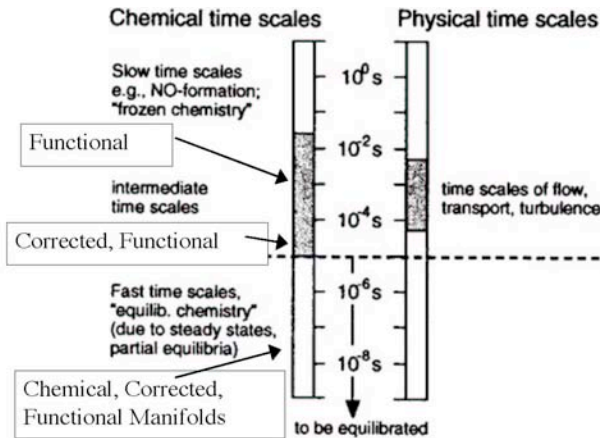
Research in this program focuses on three interconnected areas. The first involves the study of intramolecular dynamics, particularly of highly excited systems. The second area involves the use of nonlinear dynamics as a tool for the study of molecular dynamics and complex kinetics. The third area is the study of the classical/quantum correspondence for highly excited systems, particularly systems exhibiting classical chaos.

Recent Progress

The main focus of the work in the last year has been on the rational reduction of systems of reaction-diffusion equations, with the goal of understanding how the interaction of kinetics and transport affect the reduction. A number of small systems have been studied which include isolated reactions and small reaction mechanism previously studied in the literature: 1) a chain-branching mechanism¹, and 2) the combustion of ozone.²

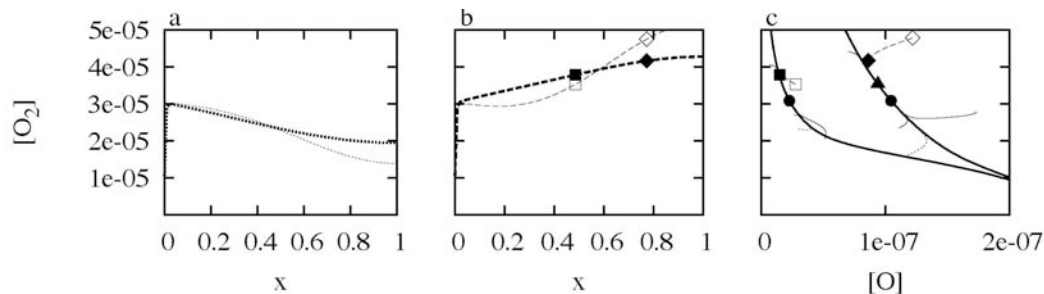
Our work on the reduction of systems of nonlinear partial differential equations can be divided into transient and steady problems, with the main focus of the work so far being transient phenomena. The reduction of the transient problem has two components: 1) species reduction and 2) dimension reduction. Species reduction involves reduction of the number of species that need to be followed accurately over a spatial domain. Dimension reduction is a more complete reduction of computational effort, because it involves not only the reduction of the number of species, but also the number of spatial points (or spectral components). The extent to which either type of reduction can be accomplished depends on the physical process studied and the time range of interest.

Our approach to reduction is geometric and depends on the resolution of low-dimensional manifolds. The species-reduction work is a collaboration with Zagaris and Kaper (Mathematics Department, Boston University). For small systems we have been able to demonstrate how the typical approaches to species reduction can be extended into dynamical regimes not previously anticipated. The chart below is from Ref. 3. The boxes on the left are added to indicate how species reduction can be extended with new approaches to the dynamical definitions of low-dimensional manifolds.



From U.
Maas and S.
B. Pope

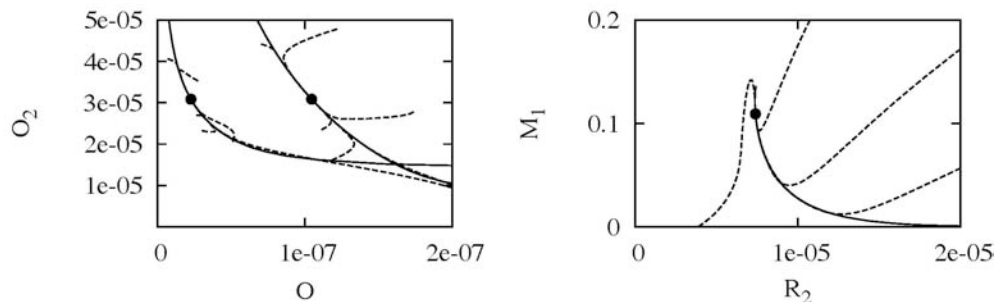
The rest of the abstract discusses the work on dimension reduction. It is motivated by results such as those shown below for ozone combustion. The left two panels show results for O_2 , with (a) showing the concentration profile of O_2 at two times. The thinner dotted line is at $t = 0$ and the thicker dotted line is at $t = 1$ ms. Panel (b) shows results for a different initial distribution at the same two times, with the thin dashed line showing $t = 0$ and the thicker dashed line $t = 1$ ms. The plots in (b) highlight two pairs of points. Points at $x = 0.49$ are plotted as an open square on the $t = 0$ curve and a filled square on the $t = 1$ ms curve. Points at $x = 0.77$ are plotted as an open diamond on the $t = 0$ curve and a filled diamond on the $t = 1$ ms curve.



There are two sets of curves plotted in (c). The left set follows the evolution of the distributions from (a) and (b), plotting $[O_2]$ vs. $[O]$ at the spatial point $x = 0.49$. The solid dot shows the equilibrium value of the distributions at $x = 0.49$. There are four other curves on the left side of (c). Three of these are plotted with thin solid lines and a fourth with a thicker solid line. The three thin-line curves are the time-development of three additional distributions. The left part of (c) demonstrates that all five sets of initial distributions asymptotically approach the thicker solid line. This latter curve is a "low-dimensional manifold". When a system reaches this curve there is a reduction in the number of partial differential equations that need to be followed. The left curve of (c) shows that after ~ 1 ms $[O_2]$ is a function of $[O]$. Plots of O_3 vs. O also show a functional relationship. On the low-dimensional manifold the system of partial differential equations is reduced from three to one, with the value of the other two species described by the functional relationships defined by the low-dimensional manifold.

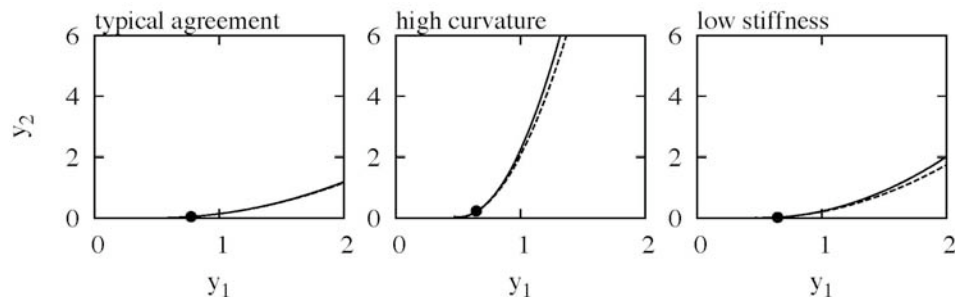
The curves on the left in (c) demonstrate that all initial distributions relax to equilibrium in a similar manner, first approaching a one-dimensional curve in the space of species on the way to equilibrium, a standard result in the study of low-dimensional manifolds for systems of ordinary differential equations approaching equilibrium, and is what is referred to above as “species reduction”. However, the plots on the right side of (c) indicate further reduction, labeled as “dimension reduction” above. This latter set of curves was generated by plotting the value of O_2 versus the concentration of O at *different* spatial points, $x = 0.29$ for O and $x = 0.77$ for O_2 . The figure indicates that this representation also approaches a single curve (thick line), although different than the one on the left of the panel. The dashed and dotted curves on the right correspond to the same pair of initial distributions as on the left set of (c) and the distributions in Figs. (a) and (b). The solid and open diamonds are the points plotted in (b) with the same symbols. The solid dot is the coordinate pair formed from the equilibrium value of O at $x = 0.29$ and O_2 at $x = 0.77$. The solid triangle on the right set of curves is the coordinate pair at $t = 4.6$ ms.

The set of curves on the right in (c) indicates that the system of three partial differential equations is reduced beyond what is implied by the left set of curves. At a time between 1.0 and 4.6 ms the system of partial differential equations has been reduced to a one-dimensional system. At that point it can be described by a single ordinary differential equation and a set of functional relationships between the value of O at a single point and the values of all species (O , O_2 , and O_3), at all other spatial points. The time is set between 1.0 and 4.6 ms because the closed diamond on the right and the closed square on the left are both plotted at the same time. The closed square lies on the manifold that describes the reduction of the number of partial differential equations, and the closed diamond on the right does not lie on the manifold describing the reduction to one ordinary differential equation. The solid triangle on the right does indicate that such a final reduction occurs by 4.6 ms.



The method of Refs. 3 and 4 has been adapted to the calculations of the manifolds in the figure above. It was necessary to extensively modify the algorithm. It was made faster and more stable. This algorithm finds the manifold by investigating only the slow subspace, whereas other algorithms typically divide the space into slow and fast components. Important time-savings in the algorithm arise from the calculation of eigenvector derivatives,⁵ which do not involve finite difference approximations. The figure above shows good agreement between the exact dynamics and the estimates of the manifolds from our modified procedure for the system of Ref. 2 (left) and Ref. 1 (right).

The relatively good results pictured in this figure led us to a detailed study of the ways the algorithm could break down. A nonlinear reaction-diffusion system was studied for which exact manifolds can be calculated. There are two conditions under which the methods of Refs. 3 and 4 breakdown: high curvature and low attractivity. The plot on the left shows a typical case and the next two show situations where a breakdown occurs.



Future Plans

The work will be extended to larger systems, particularly the H_2/O_2 system, and include advection as well as diffusion. It is also anticipated that there will be connections made to other means to reduce computational effort for the equations describing reactive flows, particularly operator-splitting techniques.

References

- ¹M. Hadjinicolaou and D. A. Goussis, *SIAM J. Sci. Comput.* **20**, 781 (1999).
- ²S. Singh, J. M. Powers, S. Paolucci, *J. Chem. Phys.* **117**, 1482 (2002).
- ³U. Maas and S. B. Pope, *Combust. Flame* **88**, 239 (1992).
- ⁴U. Maas, *Comput. Vis. Sci.* **1**, 69 (1998)
- ⁵R. B. Nelson, *AIAA J.* **14**, 1201 (1976).

Publications

- M. J. Davis and J. H. Kiefer, "Modeling of nonlinear vibrational relaxation of large molecules in shock waves with a nonlinear, temperature-varying master equation", *J. Chem. Phys.* **116**, 7814 (2002),
- M. J. Davis, "Dynamics of a nonlinear master equation: Low-dimensional manifolds and the nature of vibrational relaxation:", *J. Chem. Phys.* **116**, 7828 (2002).
- M. J. Davis and S. J. Klippenstein, "Geometric investigation of association/dissociation kinetics with an application to the master equation for $CH_3 + CH_3 \leftrightarrow C_2H_6$ ", *J. Phys. Chem. A* **106**, 5860 (2002)
- M. J. Davis, "Low-dimensional manifolds in reaction-diffusion equations: Fundamental aspects", preprint
- M. J. Davis, "Low-dimensional manifolds in reaction-diffusion equations: Numerical analysis and method development", preprint

COMPREHENSIVE MECHANISMS FOR COMBUSTION CHEMISTRY: EXPERIMENT, MODELING, AND SENSITIVITY ANALYSIS

Frederick L. Dryer

*Department of Mechanical and Aerospace Engineering
Princeton University, Princeton, New Jersey 08544-5263*

fldryer@princeton.edu

Grant No. DE-FG02-86ER-13503

Program Scope

Experiments conducted in a Variable Pressure Flow Reactor (VPFR) at pressures from 0.3 to 20 atm and temperatures from 500 K to 1200 K, with observed reaction times from 0.5×10^{-2} to 2 seconds, and laminar flame speed measurements at atmospheric pressure are combined with literature data and numerical studies to develop and validate chemical kinetic reaction mechanisms and to improve determinations of important elementary rates. Continuing efforts are: (1) utilizing the perturbations of the H_2/O_2 and $\text{CO}/\text{H}_2\text{O}/\text{Oxidant}$ reaction systems by the addition of small amounts of other species to further clarify elementary reaction properties; (2) further elucidating the reaction mechanisms for the pyrolysis and oxidation of hydrocarbons (alkanes, olefins) and oxygenates (aldehydes, alcohols, and ethers).

Recent Progress

This last year we have published and/or presented new comprehensive mechanisms for hydrogen oxidation [1], for oxidation systems involving species containing a single carbon atom, excluding methane [2, 9], and for ethanol decomposition and oxidation [2,3, 15]. We have also described and demonstrated new methodology that identifies the windows of temperature over which temperature dependent properties in flames exhibit strong effects on laminar flame propagation [4, 5, 11, 12]. In addition to the above areas of progress, we recently published laminar flame speed measurements for propane/air [6] and n-decane/air mixtures, with a revised kinetic model for decane oxidation validated against shock tube, flow reactor, and flame experimental data [7, 10]. In the work summarized below, we have also investigated the unimolecular decomposition and mechanisms of high temperature pyrolysis and oxidation of dimethyl ether [4, 13], and the reactions of phenoxy and benzyl radicals with HO_2 [14].

Dimethyl Ether

Since our previous work on the mechanism of dimethyl ether pyrolysis and oxidation (*Int. J. Chem. Kinet.* **32**: 713-740; 741-759, 2000) significant advances in fundamentals (mechanistic issues, thermochemical and kinetic parameters) have occurred particularly for H_2/O_2 and $\text{C}_1\text{-C}_2$ kinetics that are important at high temperatures and pressures. As in ethanol pyrolysis and oxidation [2, 3], the molecular decomposition of dimethyl ether contributes significantly not only to initiation but to substantial, sustained radical pool formation at flow reactor, shock tube and laminar flame conditions. As a result, decomposition and abstraction processes are significantly coupled throughout pyrolysis and oxidation. Only the unimolecular decomposition, $\text{CH}_3\text{OCH}_3 = \text{CH}_3 + \text{CH}_3\text{O}$ (R1) is of significance below 2000 K, and we have theoretically investigated this decomposition using the RRKM/master equation approach. Equilibrium geometries of the reactants and products were optimized by the hybrid density functional B3LYP method with the 6-31G(d) basis set. Vibrational frequencies, calculated using the same method, were scaled by a factor of 0.96, and energies were computed at G3B3 level of theory. Molecular orbital calculations were performed using the Gaussian 98 package (Frisch, M. J., *et. al. Gaussian 98*, Revision A.6, Gaussian, Inc., Pittsburgh PA, 1998). We also compared the calculated energy barriers with those determined using different theoretical methods, as well as with available experimental results. The energy barrier that we obtain matches very well the recent *ab initio* results of Nash and Francisco (*J. Phys. Chem. A*, **102**: 236). Special consideration was given to the two hindered rotations of CH_3 groups to evaluate the rotational potentials and to compute their contributions to the density and sum of states. The microscopic rate coefficient for (R1) was evaluated using the prescribed high-pressure limit for this channel, the molecular properties of reaction products, a calculated high-pressure limit rate constant based upon microscopic reversibility and an estimated rate constant of 2.75×10^{13} $\text{cm}^3/\text{mol}\cdot\text{s}$. The molecular parameters (reaction barriers, moments of inertia, and vibrational frequencies) were used as input for the sum and density-of-states computations, followed by the microscopic rate constant $k(E)$ calculation based upon RRKM theory. With the input information for the collision model, rate constants were calculated after solving the master equation, using an in-house computer program that permits extensive parametric studies without sacrificing accuracy. Variations in energy and temperature dependence of $\langle \Delta E_{\text{down}} \rangle$, a more rigorous treatment of hindered rotations, and evaluation of microscopic rate coefficients for loose transition states from the prescribed high-pressure-limit rate constant were included in the evaluation.

Utilizing a $\langle \Delta E_{\text{down}} \rangle$ of 300 cm^{-1} at 298 K, the rate constant for (R1) in nitrogen calculated for the temperature range 500 - 2500 K at 1 atm (Fig. 1) agrees well with the experimental data of Batt *et al.* (*Proc. Combust. Inst.* **19**: 81-87, 1982). The rate constant at the high-pressure limit is in very good agreement with the measurements of Pacey (*Can. J. Chem.* **53**: 2742-2747, 1975), but is significantly lower than the experimental indirect determinations reported by Aronowitz *et al.* (*Int. J. Chem. Kinet.*, **9**: 471-479, 1977) or Held *et al.* (*Can. J. Chem.* **55**: 4128-4134, 1977). The disparities can be reconciled only if a rate constant of at least $(1-2) \times 10^{14}$ is assigned to the reverse reaction of (R1), which is much higher than rate constants of similar reactions, for example $\text{CH}_3 + \text{CH}_3$ (Cody *et al.*, *J. Phys. Chem. A*, **106**: 6060 - 6067, 2002) or $\text{CH}_3\text{O} + \text{CH}_3\text{O}$ (Barker *et al.*, *U.S. NTIS PB Rep.* 1977). Under all

reasonable conditions, the present analysis results in a rate coefficient for (R1) at 1 atm that is a factor of 3 lower (at 1000 K) and that exhibits a higher degree of falloff than that estimated in our earlier work.

A revised high temperature DME pyrolysis and oxidation model of 263 reversible reactions and 46 species incorporating the above analysis has been developed and evaluated against high temperature shock tube, flow reactor, stirred reactor and laminar premixed flame data. The H₂ [1], and C₁-C₂ sub-model components are those utilized in our recent work on ethanol pyrolysis and oxidation [2, 3]. The DME high temperature subset was based on our earlier work and contains reactions with O₂ as well as the thermal decomposition as initiation steps. The methoxymethyl radical (CH₃OCH₂) is formed by H-atom abstraction from DME and subsequently undergoes thermal decomposition and reactions with O₂, HO₂, O, OH, CH₃, and CH₃O. Among the H atom abstraction reactions, the reaction of fuel with CH₃ is important for describing fuel consumption at flow reactor conditions and for ignition delay at shock tube conditions. A least square modified Arrhenius fit of experimental rate data for this reaction based on the experimental data exhibits very strong curvature, similar to the theoretical work of Wu et al. (*J. Comp. Chem.* **24** (5): 593-600, 2003), but with rates consistently lower by a factor of 3. The correlation is, however, a factor of 1.4 higher (at 1000 K) than that we recommended earlier. The H abstraction from DME by OH is also an important fuel consuming reaction, and the rate correlation for this reaction and abstraction by H atoms were both updated using the recent work of Tranter and Walker (*Phys. Chem. Chem. Phys.*, **3**: 4722-4732, 2001). The former correlation exhibits stronger temperature dependence than that recommended in the earlier model, while the abstraction by H atoms is about a factor of 1.5 higher than the previous recommendation. The termination reaction between formyl and methyl radical HCO + CH₃ = CO + CH₄ (R2), is also an important reaction in the DME oxidation/pyrolysis system, since both HCO and CH₃ radical are in high concentrations. The rate constant in the original mechanism (1.20×10¹⁴ cm³/mol/s) is close to the collision limit, and likely exceeds the high-pressure limit. In the present mechanism, we used the value of 2.65×10¹³ cm³/mol/s, as recommended by Mulencko (*Rev. Roum. Phys.* **32**:173 [43], 1987).

The revised model predicts the VPRF, shock tube ignition delay, and stirred reactor data compared with the prior mechanism in our earlier publications (*Int. J. Chem. Kinet.* **32**: 713-740; 741-759, 2000) with similar fidelity, but predictions of laminar premixed flame data are substantially improved over earlier work ([8]; Kaiser et al., *J. Phys. Chem. A*, **104**: 8194-8206, 2000; McIlroy, et al., *Proc. Combust. Inst.*, **28**: 1647-1653, 2000; Daly et al., *Combust. Flame* **125**: 1329-1340, 2001; Qin and Ju, *Proc Combust Ins.* **30**, 233-240, 2004; Law and Jomass, G. *Personal communication*, 2004). Exemplary comparisons are shown in Figs. 2 and 3.

The disagreement in OH predictions (Fig. 2) results from the use of an earlier OH heat of formation value in calibrating the LIF experimental measurements. The updated heat of formation of OH (Ruscic et al. *J. Phys. Chem. A* **106**: 2727, 2002) is utilized in the present work. Fig. 2 shows generally good agreement between model and experiment for major species, intermediate species, such as C₂H₄ and C₂H₆, and some minor deficiencies for CH₂O and CH₄. Some comparisons with very recent laminar premixed flame speeds at room temperature and different pressure are shown in Fig. 3. Similar to other fuels, the experimental data exhibit significant scatter (~19%). The present model reproduces well the laminar flame speed at atmospheric pressure, with some differences evident at higher pressures. The sensitivity spectrum for DME/air flame speeds is similar for all pressures, and is dominated by the main chain branching reaction, H + O₂ = OH + O, formyl decomposition, HCO + M = CO + H + M, and CO oxidation, CO + OH = CO₂ + H. The only reactions involving DME that contribute noticeably to the laminar flame speed sensitivity spectrum are (R1), and CH₃OCH₃ + H = CH₃OCH₃ + H₂ (R10).

Oxidation of Phenoxy and Benzyl Radicals by HO₂

The mechanism of toluene oxidation at lower (below 1000 K) temperatures has significant practical implications. However, the existing kinetic models of toluene oxidation primarily target high-temperature conditions and generally fail to predict the kinetic behavior observed experimentally at 920 K in the VPRF. One of the potential deficiencies of existing models appears to be the lack of an efficient chain-branching mechanism at low-temperature conditions. Because benzyl and phenoxy are major resonantly stabilized radicals present during toluene oxidation, we conducted a theoretical study of benzyl + HO₂ and phenoxy + HO₂ reaction systems aimed to identify additional reaction pathways leading to chain branching and possible ring opening. All quantum chemical calculations were carried out using the Gaussian 98 code. Geometries were optimized using modified Perdew-Wang 1-parameter for kinetics, MPW1K/6-31G+(d,p), method proposed by Linch and Truhlar (*J. Phys. Chem. A* **106**: 842-846, 2002).

The recombination of phenoxy and benzyl radicals with HO₂ leads to phenoxy-OOH and benzyl-OOH adducts as shown in Fig. 4. These adducts, denoted as A1 and A2, are formed via barrierless adsorption of HO₂ in ortho and para position, respectively. Both reactions are exothermic with reaction energies in the case of the phenoxy-OOH adduct computed to be 27.4 and 26.3 kcal/mol for A1 and A2, respectively. In the case of the benzyl-OOH adduct, reaction energies were computed to be 16.3 and 19.2 kcal/mol for A1 and A2, respectively. Relatively modest reaction energies are due to destabilization of the aromatic ring in A1 and A2 adducts. For comparison, the exothermicity of the addition of HO₂ to the side chain of benzyl radical was computed to be 49.8 kcal/mol. Note that our value falls between the previously reported values of 39 and 78 kcal/mol computed at the B3LYP and MP2 levels of theory, respectively (Davis et al., *J. Chem. Soc. Faraday Trans.* **94**, 2725-2728, 1998).

The mechanisms for subsequent decomposition of phenoxy-OOH and benzyl-OOH adducts with -OOH in ortho position (A1) are shown in Fig. 5. The lowest energy path in both systems proceeds via breaking the O-O bond in hydroperoxy group (G1 in Fig. 5).

The mechanism of decomposition of phenoxy-OOH and benzyl-OOH compounds with -OOH in the para position (A2) was found to be much simpler than the decomposition of A1 due to an absence of interaction between the adsorbed OOH group and the side group. As in the case of A1, the dissociation of the O-O bond in the hydroperoxy group was found to be the most energetically favorable path.

Simple comparison of barriers heights for different reaction channels indicates that benzoquinones and methylene substituted cyclohexadienones will be the dominant intermediate compounds in the studied systems. The activation energy for thermal decomposition of *para*-benzoquinone into cyclopentadienone and CO was estimated previously to be about 60 kcal/mol (Frank et al., *Symp. (Int.) Combust. Proc.* **25**, 833-840, 1994). However, no data are available for *ortho*-benzoquinone or methylene substituted cyclohexadienones. The calculations performed in this study indicate that multi-step decomposition of *ortho*-benzoquinone leading to cyclopentadienone and CO has the highest energy barrier of 48.2 kcal/mol above the reactant. In contrast, 2-methylene-3,5-cyclohexadiene-1-one appears to be more stable with the highest barrier being 80.8 kcal/mol above the reactant.

Preliminary rate estimates based on the present results using VARIFLEX (Klippenstein, et al., *VARIFLEX*, Version 1.0, 1999) suggest that decomposition of phenoxy-OOH and benzyl-OOH adducts may provide additional chain branching pathways needed to explain the trends observed experimentally.

Plans

Reaction systems of present interest over the coming year, include continued efforts on the pyrolyses and oxidations of acetaldehyde, acetone, and toluene, all over a range of pressures and temperatures similar to our previous work.

Publications, 2003 – Present

1. J. Li, Z. Zhao, A. Kazakov, and F.L. Dryer, "An Updated Comprehensive Kinetics Model of H₂ Combustion", *Int. J. Chem. Kin.* 36: 566-575 (2004).
2. "Experimental and Numerical Studies of Ethanol Chemical Kinetics", Juan Li, Ph.D. Thesis, Department of Mechanical and Aerospace Engineering, Princeton University, Princeton, NJ, June 2004. MAE 3122-T.
3. J. Li, A. Kazakov, and F.L. Dryer, "Experimental and Numerical Studies of Ethanol Decomposition Reactions", *J. Phys. Chem. A*, 108: 7671-7680 (2004).
4. Z. Zhao, A. Kazakov, J. Li, and F.L. Dryer, "Temperature-Dependent Feature Sensitivity Analysis for Combustion Modeling", *Int. J. Chem. Kin.* 37: 282-295 (2005).
5. "Experimental and Numerical Studies of Burning Velocities and Kinetic Modeling for Practical and Surrogate Fuels", Zhenwei Zhao, Ph.D. Thesis, Department of Mechanical and Aerospace Engineering, Princeton University, Princeton, NJ, June 2005. MAE 3130-T.
6. Z. Zhao, A. Kazakov, J. Li, and F.L. Dryer, "Initial Temperature and N₂ Dilution Effect on the Laminar Flame Speed of Propane/Air Mixtures", *Combust. Sci. and Tech.* 176: 1705-1723 (2004).
7. Z. Zhao, J. Li, A. Kazakov, S. P. Zeppieri, and F.L. Dryer, "Burning Velocities of N-Decane A High Temperature Skeletal Kinetic Model for N-Decane-Air Mixtures", *Combust. Sci. Tech.* 177: 89-106 (2005).
8. Z. Zhao, A. Kazakov, and F.L. Dryer, "Measurements of DME/Air Mixture Burning Velocities by Using Particle Image Velocimetry", *Combust. Flame* 139: 52-60 (2004).

Pre-prints and Presentations 2004-Present

9. J. Li, Z. Zhao, A. Kazakov, and F.L. Dryer, "Comprehensive Kinetic Mechanisms For C₁ Species Combustion", 30th International Symposium on Combustion, Chicago, IL, July 26-31, 2004. Poster *1F1-04*.
10. Z. Zhao, J. Li, A. Kazakov, F.L. Dryer, and S.P. Zeppieri, "Burning Velocities and a High Temperature Skeletal Kinetic Model for n-Decane Oxidation", 30th International Symposium on Combustion, Chicago, IL, July 26-31, 2004. Poster *416-05*.
11. Z. Zhao, J. Li, A. Kazakov, and F.L. Dryer, "Temperature-Dependent Feature Sensitivity Analysis of Flames", 30th International Symposium on Combustion, Chicago, IL, July 26-31, 2004. Poster *1F2-13*. Z.
12. Zhao, J. Li, A. Kazakov, and F.L. Dryer, "Temperature-Dependent Feature Sensitivity Analysis for Combustion Modeling", Annual National Meeting of the American Chemical Society, Philadelphia, PA, August 22-25, 2004.
13. S. Skokov, A. Kazakov, and F. L. Dryer, "A Theoretical Study of Oxidation of Phenoxy and Benzyl Radicals by HO₂", Joint Meeting of the U.S. Sections of the Combustion Institute, Drexel University, Philadelphia, PA, March 22-24, 2005.
14. Z. Zhao, J. Li, A. Kazakov, and F.L. Dryer, "Thermal Decomposition Reaction and a High Temperature Kinetic Model of Dimethyl Ether", Joint Meeting of the U.S. Sections of the Combustion Institute, Drexel University, Philadelphia, PA, March 22-24, 2005.
15. J. Li, A. Kazakov, and F.L. Dryer, "Chemical Kinetics of Ethanol Oxidation", 2nd European Combustion Meeting, Louvain-la-Neuve, Belgium, April, 3-6, 2005.

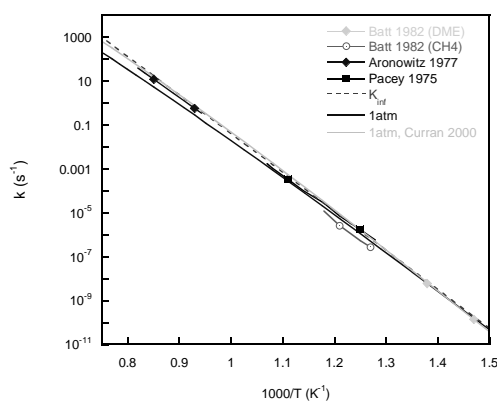


Fig. 1. Rate constant of the reaction $\text{CH}_3\text{OCH}_3 = \text{CH}_3 + \text{CH}_3\text{O}$.

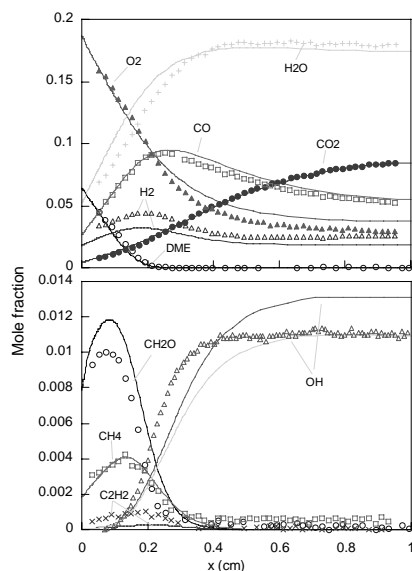


Fig. 2. Comparison of experimental (McIlroy et al., 2000) (symbols) and computed (lines) species profiles in DME- O_2 -Ar burner stabilized flame ($P = 40$ kPa, $\phi = 0.98$).

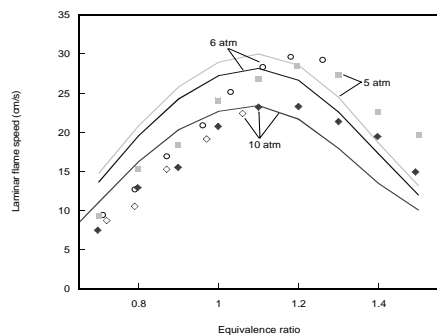


Fig. 3. Laminar flame speed of DME/air mixtures at different pressure (5, 6 and 10 atm). Symbols represent the experimental data (open symbol: Qin & Ju 2004, solid: Law et al. 2004); line: model prediction.

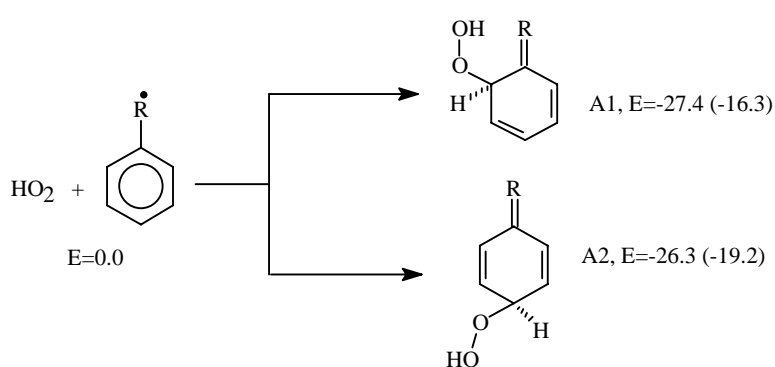


Fig. 4. Recombination of benzyl ($R = \text{CH}_2$) and phenoxy ($R = \text{O}$) radicals with HO_2 radical. Numbers are relative energies in kcal/mol, including ZPE, at the MPW1K/6-31+G(d,p) level of theory for phenoxy + HO_2 reaction. Numbers in parentheses are for benzyl + HO_2 reaction.

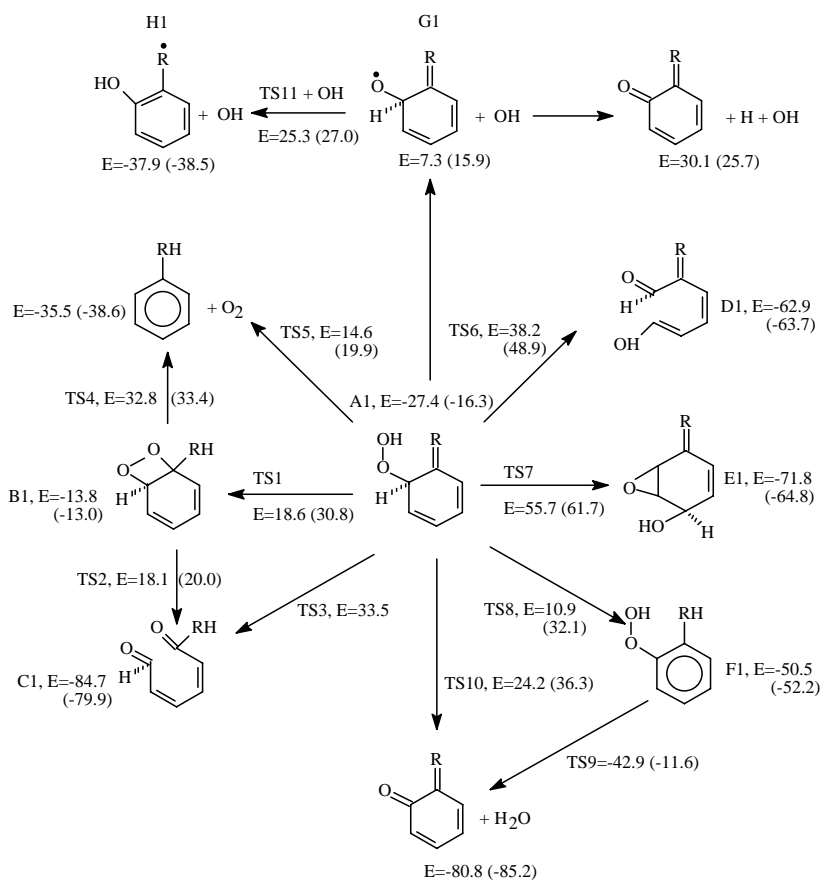


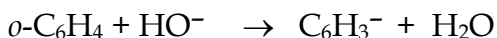
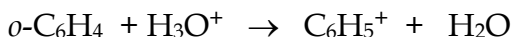
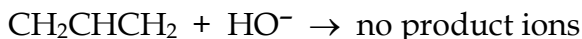
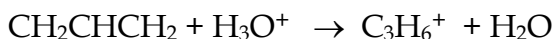
Fig. 5. Reaction mechanism for decomposition of A1 intermediate of benzyl ($R = \text{CH}_2$) and phenoxy ($R = \text{O}$) radicals. Numbers are relative energies in kcal/mol, including ZPE, at the MPW1K/6-31+G(d,p) level of theory for phenoxy- HO_2 adduct. Numbers in parentheses are for benzyl- HO_2 adduct.

LASER PHOTOELECTRON SPECTROSCOPY OF IONS

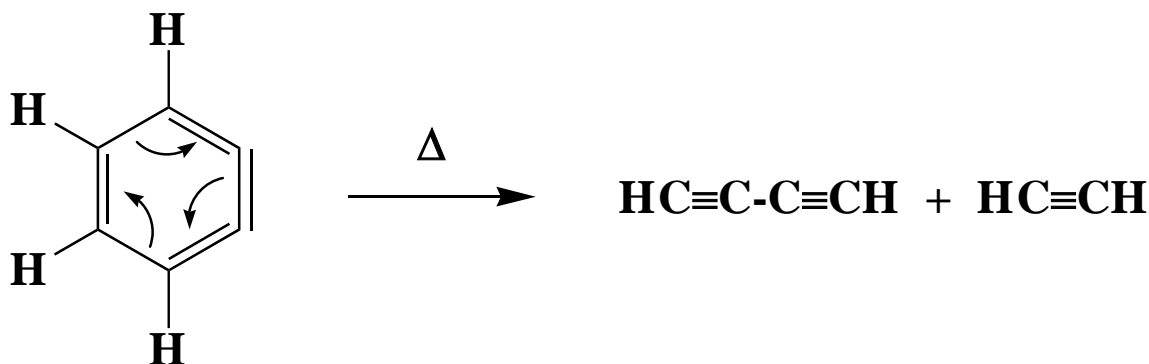
G. Barney Ellison
Department of Chemistry & Biochemistry
University of Colorado
Boulder, CO 80309-0215
Email: barney@JILA.colorado.edu

1. Ion-Radical Reactions

Last year we published a letter¹ and a more complete paper that describes our efforts to study ion-radical reactions.² Clean, intense flows of hydrocarbon radicals/diradicals can be produced by a heated supersonic nozzle and are delivered to a flowing afterglow selected ion flow tube (FA-SIFT) instrument. The reactions of a simple radical, allyl (CH_2CHCH_2), and a diradical, *ortho*-benzyne (*o*- C_6H_4), with hydronium (H_3O^+) and hydroxide (HO^-) ions were studied at thermal energy. We studied the following reactions:



During these ion-radical experiments,² we noticed that the hyperthermal nozzle was producing small signals of $[\text{C}_4\text{H}_2]^+$. We can demonstrate that this is the radical cation of $\text{H-C}\equiv\text{C-C}\equiv\text{C-H}$. Subsequently we used an FTIR, PIMS, and chemical ion mass spectrometry (both negative and positive) to identify both $\text{H-C}\equiv\text{C-H}$ and $\text{H-C}\equiv\text{C-C}\equiv\text{C-H}$ as decomposition products of *o*- C_6H_4 . A possible source could be a retro Diels-Alder fragmentation of the diradical.



2. Propargyl Radical Spectra and Structure

The propargyl³ radical, HCCCH_2 , is one of the simpler conjugated hydrocarbon radicals. In addition to being interesting in its own right, propargyl is believed⁴ to be a

direct precursor of aromatic species in flames; $\text{HCCCH}_2 + \text{HCCCH}_2 \rightarrow \text{C}_6\text{H}_6$ (benzene). We have observed the infrared spectrum of the propargyl radical. Using a heated supersonic or hyperthermal nozzle we are able to prepare matrix isolated propargyl radicals. A Fourier transform infrared (FTIR) spectrometer was used to measure the infrared absorption spectra of these matrix isolated radicals. Polarized 248 nm light from a KrF excimer laser was used to orient the propargyl radicals so we can measure the linear dichroism (LD) spectra of photooriented samples. The LD spectra enable us to establish experimental polarizations of most of the vibrational bands. We have measured the infrared absorption spectra of propargyl radicals and have identified 9 of the 12 fundamental vibrational modes.

To analyze these spectra, we have determined the potential energy and dipole moment surfaces of the $\text{HCCCH}_2 \tilde{X}^2\text{B}_1$ radical with coupled-cluster theory. Coupled-cluster theory,⁵⁻⁸ while more expensive than DFT methods, provides a nearly quantitative treatment of electron correlation in most cases and can therefore provide accuracy beyond that achievable with DFT. Accordingly, we have used another package (ACES III) to calculate the equilibrium geometry, anharmonic force field, and dipole moment function for propargyl using the CCSD(T) method^{9,10} with an atomic natural orbital (ANO) basis set.¹¹ Due to relatively strong spin contamination in the unrestricted Hartree-Fock orbitals, we have used the restricted open-shell (ROHF) approach to provide the orbitals. While analytic first derivatives of ROHF-based CCSD(T) are available,¹² analytic second derivatives have not yet been implemented. Accordingly, the harmonic frequencies and anharmonic force constants needed for estimation of the fundamental, combination and overtone frequencies were calculated using numerical differentiation of analytic gradients using a general approach described elsewhere.¹³ Care was taken to ensure that the numerical precision of the frequencies (harmonic and anharmonic) quoted in Table 2 are precise to roughly 1 cm^{-1} . The core molecular orbitals corresponding to the 1s carbon atomic orbitals were excluded from the correlation treatment.

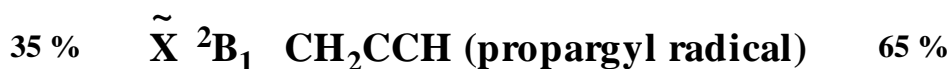
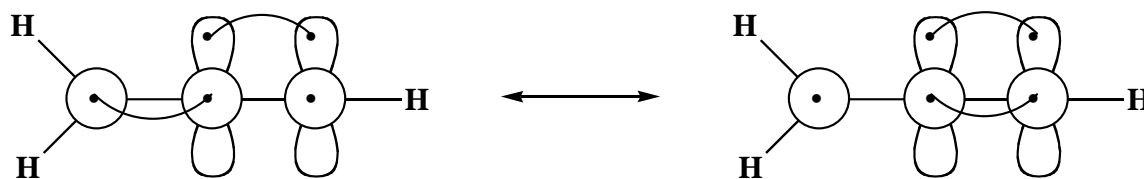
CCSD(T) calculations were employed to analyze the molecular structure, spin density, and electric dipole moment. The combination of the experimental vibrational frequencies, the measured polarizations, and the CCSD(T) anharmonic frequencies, permits a relatively straightforward assignment of the vibrational spectrum of the propargyl radical.

$\text{CH}_2\text{CCH } \tilde{X}^2\text{B}_1$ Vibrational Modes in an Ar Matrix

		Electronic Structure Calc		Exp't'l Frequencies	
		CCSD(T)/ANO		Ar matrix	
	Description	ν/cm^{-1}	$A/\text{km mol}^{-1}$	ν/cm^{-1}	Polarizat'n
a ₁	1 CH ₂ CC-H st	3322	51	3308.5 ± 0.5	negative
	2 sym H ₂ C=CCH st	3037	2	3028.3 ± 0.6	negative

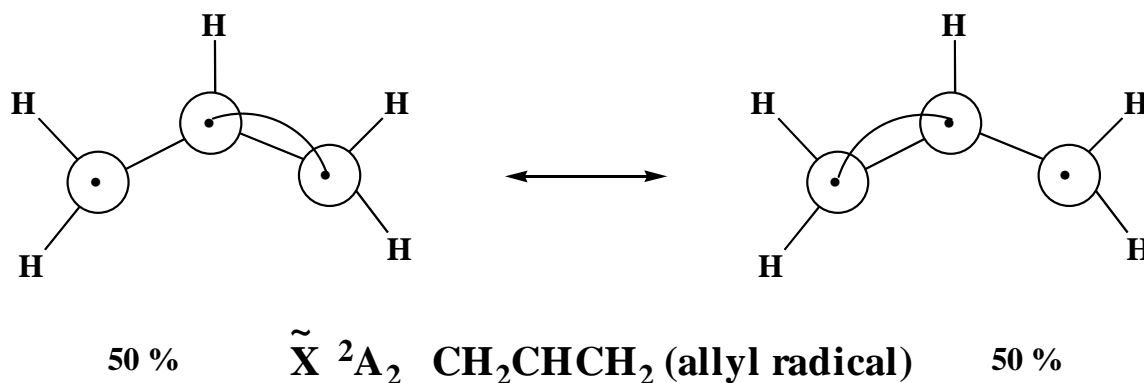
	3	$\text{CH}_2\text{C}=\text{CH} - \text{CH}_2\text{:}\ddot{\text{C}}\text{CH}$ st	1923	6	1935.4 ± 0.4	negative
	4	$\text{H}_2\text{C}\text{:}\ddot{\text{C}}\text{CH}$ scissors	1444	0	1440.4 ± 0.5	not available
	5	$\text{CH}_2\text{C}=\text{CH} \oplus \text{CH}_2\text{:}\ddot{\text{C}}\text{CH}$ st	1055	4	1061.6 ± 0.8	negative
b ₁	6	$\text{H}_2\text{C}\text{:}\ddot{\text{C}}\text{CH}$ umbrella	689	40	686.6 ± 0.4	positive
	7	$\text{CH}_2\text{CC-H}$ out-of-plane-bend	482	51	483.6 ± 0.5	positive
	8	$\text{CH}_2\text{:}\ddot{\text{C}}=\text{CH}$ out-of-plane-bend	398	5	not available	
b ₂	9	asym $\text{H}_2\text{C}\text{:}\ddot{\text{C}}\text{CH}$ st	3116	0	not available	
	10	$\text{H}_2\text{C}\text{:}\ddot{\text{C}}\text{CH} \oplus \text{CH}_2\text{-C}=\text{CH}$ in-plane-bend	1018	2	1016.7 ± 0.4	positive
	11	$\text{CH}_2\text{CC-H}$ in-plane-bend	612	47	620 ± 2	positive
	12	$\text{CH}_2\text{:}\ddot{\text{C}}=\text{CH}$ in-plane-bend	338	5	not available	

We can represent the propargyl radical with the Generalized Valence Bond formula.¹⁴ The coefficients in are based on an atomic partitioning of the CCSD(T)/ANO spin density using Mulliken populations.



The calculated structure of the propargyl radical predicts a hydrocarbon radical with a long CC bond and a short CC bond. The delocalized GVB structure in is supported by the small dipole moment, $\mu_{\text{D}}(\text{HC}=\text{C}\text{:}\ddot{\text{C}}\text{H}_2) = 0.150 \pm 0.005$ D, and by the strongly coupled CC stretching vibrations.

There is a striking resemblance of propargyl, $\text{HC}=\text{C}\text{:}\ddot{\text{C}}\text{H}_2 \tilde{\text{X}} \text{ } ^2\text{B}_1$, to allyl, $\text{CH}_2\text{:}\ddot{\text{C}}\text{H}\text{:}\ddot{\text{C}}\text{H}_2 \tilde{\text{X}} \text{ } ^2\text{A}_2$. Both are strongly delocalized, C_{2v} π radicals as shown by the molecular structures. The resonance energy¹⁵ is roughly 11 kcal mol⁻¹ for each of these hydrocarbons. Both radicals have small electric dipole moments,¹⁶ $\mu_{\text{D}}(\text{HC}=\text{C}\text{:}\ddot{\text{C}}\text{H}_2) = 0.150$ D *vs.* $\mu_{\text{D}}(\text{CH}_2\text{:}\ddot{\text{C}}\text{H}\text{:}\ddot{\text{C}}\text{H}_2) = 0.07$ D. The vibrational modes of both allyl¹⁷ and propargyl are not easily described by local modes but more naturally by a set of vibrations delocalized over the entire molecule. Because of its symmetry, the allyl radical must be described by an equal mixture of two GVB structures. Such is nearly the case for propargyl.



Recommended Gas-Phase Vibrational Frequencies for $\text{HC}\equiv\text{C}\cdots\text{CH}_2$ $\tilde{X} \ ^2B_1$

<u>Mode</u>	<u>ν/cm^{-1}</u>	<u>Method</u>	<u>Reference</u>
a ₁ 1	3322.2929 ± 0.0020	CW color center laser spectroscopy	18,19
2	3028 ± 15	Ar matrix, CCSD(T) calculation	this work
3	1935 ± 15	Ar matrix, CCSD(T) calculation	this work
4	1440 ± 15	Ar matrix, CCSD(T) calculation	this work
5	1061 ± 15	Ar matrix, CCSD(T) calculation	this work
b ₁ 6	687.17603 ± 0.00062	time resolved IR diode laser spectroscopy	20
7	490 ± 10	$\text{CH}_2=\text{C}=\text{CH}^-$ photodetachment	21,22
8	396 ± 15	CCSD(T) calculation	this work
b ₂ 9	3124 ± 15	Ar matrix, CCSD(T) calculation	23
10	1017 ± 15	Ar matrix, CCSD(T) calculation	this work
11	620 ± 30	Ar matrix, CCSD(T) calculation	this work
12	352 ± 15	CCSD(T) calculation	this work

References

- ¹ X. Zhang, V. M. Bierbaum, G. B. Ellison, and S. Kato, *J. Chem. Phys.* **120**, 3531 (2004).
- ² X. Zhang, S. Kato, V. M. Bierbaum, M. R. Nimlos, and G. B. Ellison, *J. Phys. Chem. A* **108**, 9733 (2004).
- ³ W. E. Flood, *The Dictionary of Chemical Names*. (Littlefield, Adams, & Co., Totowa, NJ, 1967).
- ⁴ D. K. Hahn, S. J. Klippenstein, and J. A. Miller, *Faraday Discuss.* **119**, 79 (2001).
- ⁵ T. J. Lee and G. E. Scuseria, in *Quantum Mechanical Electronic Structure Calculations with Chemical Accuracy*, edited by S. R. Langhoff (Kluwer, Dordrecht, 1995).

- ⁶ R. J. Bartlett, in *Modern Electronic Structure Theory, Part II*, edited by D. R. Yarkony (World Scientific, Singapore, 1995).
- ⁷ J. Gauss, in *Encyclopedia of Computational Chemistry*, edited by P. Schleyer (Wiley, New York City, 1998).
- ⁸ T. D. Crawford and H. F. Schaefer III, *Rev. Comp. Chem.* **14**, 36 (1999).
- ⁹ K. Raghavachari, G. W. Trucks, J. A. Pople, and M. Head-Gordon, *Chem. Phys. Lett.* **157**, 479 (1989).
- ¹⁰ K. Raghavachari, G. W. Trucks, J. A. Pople, and E. Replogle, *Chem. Phys. Lett.* **158**, 207 (1989).
- ¹¹ J. Almlof and P. R. Taylor, *J. Chem. Phys.* **86**, 4070 (1987).
- ¹² J. D. Watts, J. Gauss, and R. J. Bartlett, *J. Chem. Phys.* **98**, 8718 (1993).
- ¹³ J. F. Stanton, C. L. Lopreore, and J. Gauss, *J. Chem. Phys.* **108**, 7190 (1998).
- ¹⁴ W. A. Goddard III and L. B. Harding, *Ann. Rev. Phys. Chem.* **29**, 363 (1978).
- ¹⁵ Notice that this makes the resonance stabilization energy of the propargyl radical to be about that of allyl radical; see Ellison *et. al.*, *Int. J. Mass Spectrom. Ion Processes* (1996). Comparing propene [$DH_{298}(\text{CH}_2\text{CHCH}_2\text{-H}) = 88.8 \pm 0.4 \text{ kcal mol}^{-1}$] and methacetylene [$DH_{298}(\text{HCCCH}_2\text{-H}) = 90 \pm 3 \text{ kcal mol}^{-1}$] ethane [$DH_{298}(\text{CH}_3\text{CH}_2\text{-H}) = 101.1 \pm 0.4 \text{ kcal mol}^{-1}$], one finds Resonance Energy(CH_2CHCH_2) = 12 kcal mol⁻¹ and Resonance Energy(HCCCH_2) = 11 kcal mol⁻¹.
- ¹⁶ J. Küpper, J. M. Merritt, and R. E. Miller, *J. Chem. Phys.* **117**, 647 (2002).
- ¹⁷ S. Nandi, P. A. Arnold, B. K. Carpenter, M. R. Nimlos, D. C. Dayton, and G. B. Ellison, *J. Phys. Chem. A* **105**, 7514 (2001).
- ¹⁸ C. L. Morter, C. Domingo, S. K. Farhat, E. Cartwright, G. P. Glass, and R. F. Curl, *Chem. Phys. Lett.* **195**, 316 (1992).
- ¹⁹ L. Yuan, J. DeSain, and R. F. Curl, *J. Mol. Spectrosc.* **187**, 102 (1998).
- ²⁰ K. Tanaka, T. Harada, K. Sakaguchi, K. Harada, and T. Tanaka, *J. Chem. Phys.* **103**, 6450 (1995).
- ²¹ J. M. Oakes and G. B. Ellison, *J. Am. Chem. Soc.* **105**, 2969 (1983).
- ²² M. S. Robinson, M. L. Polak, V. M. Bierbaum, C. H. Depuy, and W. C. Lineberger, *J. Am. Chem. Soc.* **117**, 6766 (1995).
- ²³ F. A. Korolev, A. K. Mal'tsev, and O. M. Nefedov, *Bull. Acad. Sci. USSR Div. Chem. Sci.* **38**, 957 (1989).

DOE Publications

- M. R. Nimlos, S. J. Blanksby, G. B. Ellison, R. J. Evans, , "Enhancement of 1,2-dehydration of alcohols by alkali cations and protons: a model for dehydration of carbohydrates", *J. Anal. Appl. Pyrolysis* **2003**, *66*, 3-27.
- Stephen J. Blanksby and G. Barney Ellison, "Bond Dissociation Energies of Organic Molecules," *Acct. Chem. Res.*, **36**, 255-263 (2003).
- X. Zhang, A. V. Friderichsen, S. Nandi, G. B. Ellison, D. E. David, J. T. McKinnon, T. G. Lindeman, D. C. Dayton, and M. R. Nimlos, "An Intense, Hyperthermal Source of Organic Radicals for Matrix-Isolation Spectroscopy" *Rev. Sci. Instrum.* **74**, 3077-3086 (2003).
- Stephen J. Blanksby, Veronica M. Bierbaum, G. Barney Ellison, and Shuji Kato, "Fragmentations of Deprotonated Alkyl Hydroperoxides (ROO⁻) Upon Collisional Activation: A Combined Experimental and Computational Study, *Aust. J. Chem.*, **56**, 459-472 (2003).
- G. Barney Ellison, "Photoelectron Spectroscopy of Negative Ion Beams: Measurements of Electron Affinities", 390-398. in *The Encyclopedia of Mass Spectroscopy*, **Vol. 1 Theory and Ion Chemistry** Ed. Peter B. Armentrout, Elsevier Amsterdam (2003).
- Xu Zhang, Veronica M. Bierbaum, G. Barney Ellison, and Shuji Kato, "Gas-Phase Reactions of Organic Radicals and Diradicals with Ion", *J. Chem. Phys.*, **120**, 3531-3534 (2004).
- G. Barney Ellison, John M. Herbert and Anne B. McCoy, Péter G. Szalay and John F. Stanton, "Unimolecular Rearrangement of *trans*-FONO to FNO₂. A Possible Model System for Atmospheric Nitrate Formation", *J. Phys. Chem. A*, **108**, 7639-7642 (2004).
- Xu Zhang, Shuji Kato, Veronica M. Bierbaum, Mark R. Nimlos, and G. Barney Ellison, "The Use of a Flowing Afterglow-SIFT Apparatus to Study the Reactions of Ions with Organic Radicals", *J. Phys. Chem. A*, **108**, 9733-9741 (2004).
- Evan B. Jochowitz, Xu Zhang, Mark R. Nimlos, Mychel Elizabeth Varner, John F. Stanton, and G. Barney Ellison, "Propargyl Radical: *ab initio* Anharmonic Modes and the Polarized Infrared Absorption Spectra of Matrix-Isolated HCCCH₂", *J. Phys. Chem. A*, (in press, April, 2005).

Hydrocarbon Radical Thermochemistry: Gas-Phase Ion Chemistry Techniques

Kent M. Ervin
Department of Chemistry/216
University of Nevada, Reno
Reno, Nevada 89557
E-mail: ervin@chem.unr.edu

Project Scope

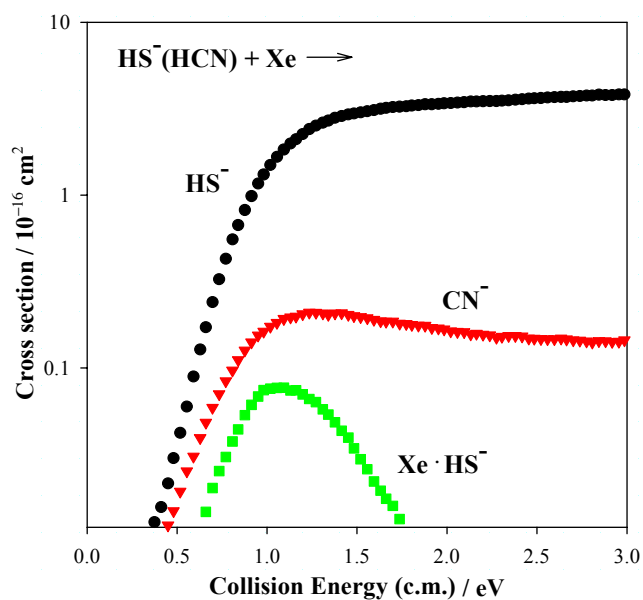
Gas phase negative ion chemistry methods are employed to determine enthalpies of formation of hydrocarbon radicals that are important in combustion processes and to investigate the dynamics of ion–molecule reactions. Guided ion beam tandem mass spectrometry is used to measure the activation of endoergic ion-molecule reactions as a function of kinetic energy. Modeling the measured reaction cross sections using statistical rate theory or empirical reaction models allows extraction of reaction threshold energies. These threshold energies yield relative gas-phase acidities, proton affinities, or hydrogen-atom affinities, which may then be used to derive neutral R–H bond dissociation enthalpies using thermochemical cycles involving established electron affinities or ionization energies. The reactive systems employed in these studies include endoergic bimolecular proton transfer reactions, hydrogen-atom transfer reactions, and collision-induced dissociation of heterodimer complex anions and cations. Electronic structure calculations are used to evaluate the possibility of potential energy barriers or dynamical constrictions along the reaction path, and as input for RRKM and phase space theory calculations.

Recent Progress

Collision-induced dissociation of proton-bound clusters

In recently published work,¹ we used competitive threshold collision-induced dissociation techniques to determine the bond dissociation energy of phenol, $D(\text{C}_6\text{H}_5\text{O}-\text{H})$, for which recent literature determinations are not in complete agreement. We produced proton-bound heterodimers such as $[\text{C}_6\text{H}_5\text{O}\cdots\text{H}\cdots\text{CN}]^-$, which upon collisional activation dissociates into either $\text{C}_6\text{H}_5\text{O}^- + \text{HCN}$ or $\text{C}_6\text{H}_5\text{OH} + \text{CN}^-$. Using statistical rate theories, we quantitatively model the branching ratio between these two product channels as a function of the available energy. Our results yield $D_{298}(\text{C}_6\text{H}_5\text{O}-\text{H}) = 359 \pm 8 \text{ kJ/mol}$, smaller than the values reported from proton transfer energy thresholds by both our group ($\text{Cl}^- + \text{C}_6\text{H}_5\text{OH}$)² and by Anderson and coworkers ($\text{ND}_3 + \text{C}_6\text{H}_5\text{OH}^+$).³

Because phenoxy radical is important in combustion and because the gas-phase acidity scale is deficient in the region of phenol, we are currently extending our experimental work on the phenol system by using additional reference acids besides HCN, namely H_2S and several cresols, to create a local thermochemical network of relative acidities for a more precise



determination. As a first step, we have examined the HCN/H₂S system,⁴ as these two acids have well-established gas-phase acidities and are well characterized spectroscopically. The energy-resolved competitive collision-induced dissociation of the proton-bound complex [HS·H·CN]⁻ is studied in the guided ion beam apparatus. H₂S and HCN have very similar gas-phase acidities. The cross sections for the HS⁻ + HCN and the CN⁻ + H₂S product channels, shown in the figure, therefore exhibit nearly the same threshold energy as expected. However, the HS⁻ + HCN channel has a cross section up to a factor of fifty larger than CN⁻ + H₂S at

higher energies. The cross sections are modeled using RRKM theory and classical phase space theory. Modeling the systems requires a loose transition state for the HS⁻ + HCN channel and a tight transition state for CN⁻ + H₂S. Theoretical calculations show that the proton-transfer potential energy surface has a single minimum and that the hydrogen bonding in the complex is strongly unsymmetrical, with an ion-molecule complex of the form HS⁻··HCN rather than CN⁻··H₂S or an intermediate structure. The requirement for proton transfer before dissociation to CN⁻ + H₂S and curvature along the reaction path impedes that product channel. Although these issues complicate the extraction of energetic information, the relative gas-phase acidity can be obtained with reasonable precision (within ±4 kJ/mol).

Collision-induced dissociation of O₂⁻

The energetics and dynamics of collision-induced dissociation of O₂⁻ with Ar and Xe targets have been studied experimentally using guided ion-beam tandem mass spectrometry and modeled theoretically by classical trajectory calculations.⁵ The collisionally activated dissociation process is surprisingly inefficient. Experimental threshold energies are 2.1 and 1.1 eV in excess of the thermochemical O₂⁻ bond dissociation energy for argon and xenon, respectively. Classical trajectory calculations confirm the observed threshold behaviour and the dependence of cross sections on the relative kinetic energy. Representative trajectories reveal the bond dissociation taking place on a short time scale of about 50 fs in direct collisions. Collision-induced dissociation is found to be remarkably restricted to the perpendicular approach of Ar/Xe to the molecular axis of O₂⁻, while collinear collisions do not result in dissociation.

Kinetic method

The so-called “kinetic method” is a popular technique in the mass spectrometry community for determining ion affinities (e.g., proton affinities or gas-phase acidities).⁶ It involves measuring the branching ratio for the metastable dissociation or collision-induced dissociation of an ion-bound heterodimer, for example, A–M⁺–B_i into AM⁺ + B_i and A + MB_i⁺, where the M⁺-affinity of A is the unknown and those of a series of compounds B_i are used for calibration. A correlation plot is based on the thermodynamic formulation of transition state theory, $\ln(I_A/I_{B_i}) = \Delta\Delta H/RT_{\text{eff}} - \Delta\Delta S/R$, where the I_A and I_{B_i} are the AM⁺ and B_iM⁺ ion

abundances in the mass spectrum, $\Delta\Delta H$ is the enthalpy difference between the two channels (ion affinity difference, assumed to be the same as the transition state energy difference), and T_{eff} is called the “effective temperature” but is just a correlation parameter. Our competitive threshold collision-induced dissociation technique is superficially similar to the kinetic method, but has the advantage of making the competitive dissociation measurements over a very wide range of energies (rather than one or a few energies in the kinetic method) and modeling the branching ratios with a full statistical rate theory analysis (namely, with RRKM theory and including all experimental energy broadening effects). We recently examined the systematic errors inherent in the kinetic method, in particular for systems with large entropic effects, using Monte Carlo simulations.⁷

Photoelectron spectroscopy of phosphorus hydrides

Phosphorus hydride compounds and radicals are of interest because of the role of organophosphorus compounds in catalysis of radical recombination reactions involved in combustion^{8,9} and fundamentally because of the challenge accurate descriptions of multiply-bonded compounds of third-row elements by theoretical methods.^{10,11} Whereas neutral phosphanes have been studied extensively,¹² their radical and anionic fragments are less well characterized. In this work, we apply negative ion photoelectron spectroscopy to a series of phosphorus hydride anions, PH^- , PH_2^- , P_2H^- , P_2H_2^- , and P_2H_3^- . Franck-Condon simulations of the photoelectron spectra are used to analyze the spectra and to identify various P_2H_n^- species. The simulations employ density functional theory calculations of molecular geometries and vibrational frequencies and normal modes, and coupled-cluster theory calculations of electron affinities. The following electron affinities are obtained: $\text{EA}_0(\text{PH}) = 1.027 \pm 0.006$ eV, $\text{EA}_0(\text{PH}_2) = 1.263 \pm 0.006$ eV, and $\text{EA}_0(\text{P}_2\text{H}) = 1.514 \pm 0.010$ eV, $\text{EA}_0(\text{trans-HPPH}) = 1.00 \pm 0.01$ eV, and $\text{EA}_0(\text{cis-HPPH}) = 1.03 \pm 0.01$ eV.

Future Directions

In this project period, we will continue studies to refine the bond dissociation enthalpies of polyynes ($\text{HC}_{2n}-\text{H}$), which are possible intermediates in formation of PAHs (polycyclic aromatic hydrocarbons). We will improve the bond dissociation enthalpy of phenol and determine those of cresols by a local thermochemical network (gas-phase acidity ladder) involving H_2S and HCN as reference acids. Because of the importance of oxygen-containing species in combustion, especially with oxygenated fuels, we will target the O–H bond dissociation enthalpies of unsaturated alcohols, carboxylic acids, and peroxides. We will examine additional ions for their suitability as proton transfer and hydrogen atom transfer reagents. For proton affinity measurements, the experimental apparatus will be modified to allow the positive ion reactions as well as negative ions.

References

- ¹L. A. Angel and K. M. Ervin, *J. Phys. Chem. A* **108**, 8345 (2004).
- ²V. F. DeTuri and K. M. Ervin, *Int. J. Mass Spectrom.* **175**, 123 (1998).
- ³H.-T. Kim, R. J. Green, J. Qian, and S. L. Anderson, *J. Chem. Phys.* **112**, 5717 (2000).
- ⁴F. A. Akin and K. M. Ervin, manuscript in preparation (2005).
- ⁵F. A. Akin, J. Ree, K. M. Ervin, and H. K. Shin, manuscript in preparation, (2005).

- ⁶R. G. Cooks, J. T. Koskinen, and P. D. Thomas, *J. Mass Spectrom.* **34**, 85 (1999).
- ⁷K. M. Ervin and P. B. Armentrout, *J. Mass Spectrom.* **39**, 1004 (2004).
- ⁸O. Korobeinichev, T. Bolshova, V. Shvartsberg, and A. Chernov, *Combust. Flame* **125**, 744 (2001).
- ⁹N. L. Haworth and G. B. Bacskay, *J. Chem. Phys.* **117**, 11175 (2002).
- ¹⁰T. L. Allen, A. C. Scheiner, Y. Yamaguchi, and H. F. Schaefer, III, *J. Am. Chem. Soc.* **108**, 7579 (1986).
- ¹¹T. L. Allen, A. C. Scheiner, and H. F. Schaefer, III, *J. Phys. Chem.* **94**, 7780 (1990).
- ¹²M. Baudler and K. Glinka, *Chem. Rev.* **94**, 1273 (1994).

Publications, 2003–present

“Gas-phase S_N2 and bromine abstraction reactions of chloride ion with bromomethane: Reaction cross sections and energy disposal into products”, L. A. Angel and K. M. Ervin, *J. Am. Chem. Soc.* **125**, 1014-1027 (2003).

“Thermochemistry: Definitions and Tabulations”, Ervin, K. M.; Armentrout, P. B. In *The Encyclopedia of Mass Spectrometry. Volume 1: Theory and Ion Chemistry*, Armentrout, P. B., Ed.; (Elsevier: Amsterdam, 2003) pp. 309-315.

“The only stable state of O_2^- is the $X^2\Pi_g$ ground state and it (still!) has an electron detachment energy of 0.45 eV”, K. M. Ervin, I. Anusiewicz, P. Skurski, J. Simons, and W. C. Lineberger, *J. Phys. Chem. A.*, **107**, 8521-8529 (2003).

“Gas-phase hydrogen abstraction reactions of S^- with H_2 , CH_4 , and C_2H_6 ”, L. A. Angel, M. K. Dogbevia, K. M. Rempala, and K. M. Ervin, *J. Chem. Phys.* **119**, 8996-9007 (2003).

“Systematic and random errors in ion affinities and activation entropies from the extended kinetic method”, K. M. Ervin and P. B. Armentrout, *J. Mass Spectrom.* **39**, 1004-1015 (2004).

“Competitive threshold collision-induced dissociation: Gas-phase acidity and O-H bond dissociation enthalpy of phenol”, L. A. Angel and K. M. Ervin, *J. Phys. Chem. A.* **108**, 8345-8352 (2004).

“Photoelectron spectroscopy of phosphorus hydride anions”, K. M. Ervin and W. C. Lineberger, *J. Chem. Phys.*, in press (2005).

PESCAL, Fortran program for Franck-Condon analysis of photoelectron spectra, K. M. Ervin, (revised 2004).

ODRFIT, Fortran program for analysis of extended kinetic method data using orthogonal distance regression analysis, K. M. Ervin and P. B. Armentrout, (2004).

CRUNCH, Fortran program for analysis of reaction cross sections with RRKM and PST models, K. M. Ervin and P. B. Armentrout, version 5.10 (2005).

Experimental Kinetics and Mechanistic Investigations of Hydrocarbon Radicals Relevant to Combustion Modeling

Askar Fahr

Chemistry Department
American University
Washington, D.C. 20899-8382
fahr@american.edu

PROGRAM SCOPE

The objective of this research program is to determine, experimentally, kinetic parameters the nature and yields of reaction products and mechanistic data for key elementary radical-radical and radical-molecule reactions involving C1 to C3 hydrocarbon radicals. Small hydrocarbon radicals, such as vinyl, propargyl and allyl radicals are believed to play pivotal roles in the formation of aromatic and polyaromatic hydrocarbons and in the inception of soot. There are either very limited or no experimental or computational results on reactions of these radicals.

Methods employed for these studies include, excimer-laser photolysis for generating the radicals, time-resolved UV-absorption spectroscopy for direct kinetic studies, GC/MS methods for identification and quantification of final reaction products as well as for comparative rate determinations. Detailed kinetic modeling is used for data analysis and interpretations. For a better understanding of the reaction mechanisms emphasis is given to determination of the isomeric nature of the products and on examining the effects of pressure and temperature on product channels and on the nature and yields of the reaction products.

RECENT PROGRESS

a) UV-Absorption Spectra of the Radical Transients Generated from the 193-nm Photolysis of Allene, Propyne and 2-Butyne. Allene ($\text{CH}_2=\text{C}=\text{CH}_2$) and propyne ($\text{CH}_3\text{C}\equiv\text{CH}$) have been used as photolytic sources of propargyl radicals. A number of studies have examined the intermediate product(s), subsequent to the 193 nm photolysis of allene and propyne and reported formation of various C_3H_3 and C_3H_2 radical isomers.^{1,2,3} However, recent experimental results⁴ suggest formation of only propargyl radicals, contradicting the earlier results. We have re-examined the 193 nm photochemistry of allene, propyne and 2-butyne ($\text{H}_3\text{C}-\text{C}\equiv\text{C}-\text{CH}_3$) and have surveyed the UV spectral region (220 nm to 350 nm) for detection of transient specie(s) generated subsequent to photolysis of these molecules. An emphasis of the study has been on the examination of possibilities of formation of different C_3H_3 isomeric radicals from the 193 nm photolysis of these molecules. Since these precursors are of current interest, the nature of the optical properties of the transients generated from photolysis of these radical precursors are, similarly, of interest and may provide further evidence for the nature of the primary photolytic processes.

Survey of the ultraviolet spectral region, following the 193 nm photolysis of dilute mixtures of allene/He resulted in detection of a strong absorption band around 230 nm and a weaker band in the 320 nm region with a relative intensity of about 8/1. The time-resolved absorption traces subsequent to the photolysis event show an instantaneous rise, followed by a simple decay. The spectral features, observed in this work, following photolysis of allene are in good agreement with the previously reported⁵ spectrum of H_2CCCH radical in the 240 nm and 320 nm regions and are believed to be originated primarily from propargyl radicals.

In comparison the spectra obtained from the 193 nm photolysis of dilute mixtures of HCCCH_3/He and $\text{CH}_3\text{CCCH}_3/\text{He}$ were nearly identical consisting of two relatively broad bands centered at about 240 nm and 320 nm regions with a relative intensity of about 2/1, respectively. In addition, the time-resolved absorption traces subsequent to photolysis of

propyne and 2-butyne samples, both in the 240 nm and 320 nm regions, indicated an instant rise followed by an additional slower absorption rise. The distinct differences between the results of allene with those of propyne and 2-butyne suggest that the observed absorption features following the 193 nm photolysis of these molecules are likely to be composite with contributions from a number of transient specie(s) in addition to propargyl radicals. Propyne and 2-butyne are structurally similar. The methyl and propynyl radicals are likely to be among the photodissociation products of 2-butyne and similarly propynyl is likely to be a photodissociation product of propyne. GC/MS product analysis of photolyzed 2-butyne/He mixtures does indicate the formation of C_2H_6 (formed from the combination of CH_3 radicals), and a number of C_6H_6 and C_4H_6 isomers formed from self- and cross- reactions of C_3H_3 and CH_3 radicals including 1,5-hexadiyne and 2,4-hexadiyne which potential products of combination reactions of propargyl as well as propynyl radicals.

Considering the structural similarities of various C_3H_3 isomers, particularly propargyl and propynyl, it is not surprising for these species to have similar UV-absorption characteristics. The fine differences in absorption characteristics of these species can be identified by TOF studies and high-resolution UV/IR spectroscopic methods (not currently available in this laboratory). These results suggest that spectral observations provide valuable information that is adjunct to molecular beam experiments and provide data not obtainable by other techniques.

In addition, it is needless to say that theoretical predictions of the energetics and absorption characteristics of various C_3H_3 species would be very valuable and helpful.

b) The Rate Coefficient and Products of the Reaction $CH_3 + C_2H_5$

The reaction kinetics and products of the methyl and ethyl cross-radical reactions have been studied at various temperature (202 K to 300 K) and pressure (1.0 to 250 Torr) conditions employing the discharge flow–mass spectrometric (DF–MS), direct time-resolved UV-absorption spectroscopy and GC/MS quantitative product analysis techniques. An overall, high pressure, rate coefficient of $k = (4.4 \pm 0.8) \times 10^{-11} \text{ cm}^3 \text{ molecule}^{-1} \text{ s}^{-1}$ was determined for the $CH_3 + C_2H_5$ reaction. The k value derived from this work is smaller by a factor of about two than the recently reported⁶ value of $10.0 \times 10^{-11} \text{ cm}^3 \text{ molecule}^{-1} \text{ s}^{-1}$. Using the DF–MS method, rate coefficient values of $(2.1 \pm 0.4) \times 10^{-11} \text{ cm}^3 \text{ molecule}^{-1} \text{ s}^{-1}$ at $P = 1.0 \text{ Torr}$ and $T = 295 \text{ K}$, and $(2.6 \pm 0.6) \times 10^{-11} \text{ cm}^3 \text{ molecule}^{-1} \text{ s}^{-1}$ at $P = 1.0 \text{ Torr}$ and $T = 202 \text{ K}$ were determined. The product studies suggest a combination (k_C) and disproportionation ratio of $k_C / k_D = [n\text{-}C_3H_8]/[CH_4] = 21 \pm 5$.

FUTURE PLANS

We will continue our work on kinetics and product studies of the vinyl, propargyl and allyl radical reactions. We will examine effects of pressure and temperature on kinetics and on product channels of a number of key radical-radical and radical-molecule reaction relevant to combustion/soot formation. As in the past, an emphasis of the studies will be on identifying the nature and quantifying the yields of the final products at various pressure and temperature conditions. Particular attention will be given to see if any of the products will undergo isomerization and/or cyclization.

References:

1. Mebel, A. W., Jackson, W. M., Chang, A. H. H., Lin, S. H., J. Am. Chem. Soc., 1998, 120, 5751
2. Ni, C. K., Huang, J. D., Chen, Y. T., Kung, A. H., Jackson, W. M., J. Chem. Phys., 1999, 110, 3320.
3. Sun, W., Yokayama, K., Robinson, J., Suits, A. G., Neumark, D. M., J. Chem. Phys., 1999, 110, 4363

4. Qadiri, R. H., Feltham, E. J., Nahler, N. H., Garcia, R. P., Ashfold, M. N. R., *J. Chem. Phys.*, 2003, 119, 12842.
5. a) Fahr, A., Hassanzadeh, P., Laszlo, B., Huie, R. E., *Chem. Phys.*, 1997, 215, 59
b) Deyerl, H. J., Fischer, I., Chen, P. J. *Chem. Phys.*, 1997, 111, 3441
6. Knyazev, V. and Slagle, I.R., *J. Phys. Chem.. A*, 2001, 105, 6490.

PUBLICATIONS RESULTING FROM DOE SPONCERED RESEARCH

Howe, P. T. and Fahr, A. "Pressure and Temperature Effects on Product Channels of the Propargyl ($\text{HC}\equiv\text{CCH}_2$) Combination Reaction and the Formation of the "First Ring" " *J. Phys. Chem. A*, **2003**, 107, 9603.

Howe, P. T.; Fahr, A. and Laufer, A. H., "Effect of Water Vapor on the Combination and Disproportionation of Ethyl Radicals in the Gas Phase" *J. Phys. Chem. A*, **2004**, 108, 1639.

Laufer, A. H. and Fahr, A. "Review of Reactions and Kinetics of Unsaturated C_2 Hydrocarbon Radicals" *Chemical Reviews*, **2004**, 104, 2813.

Striebel, F., Jusinski, L. E., Fahr, A., Halpern, J. B., Klippenstein, S. J.' and Taatjes, C. A; "Kinetics of the Reaction of Vinyl Radicals with NO: Ab Initio Theory, Master Equation Predictions, and Laser Absorption Measurements" *Phys. Chem. . Chem. Phys.* **2004**, 6, 2216.

Fahr, A. and Laufer, A. H.; " UV-Absorption Spectra of the Radical Transients Generated from the 193-nm Photolysis of Allene, Propyne and 2-Butyne" *J. Phys. Chem A* , **2005** (in press, web release Feb 16th).

Pimentel, A. S., Payne, W. A., Nesbitt, F. L., Fahr*, A. and Cody* R., "The Rate Coefficient and Products of the Reaction $\text{CH}_3 + \text{C}_2\text{H}_5$ " , *J. Phys. Chem. A*, **2005** (submitted).

Spectroscopic and Dynamical Studies of Highly Energized Small Polyatomic Molecules

Robert W. Field

Massachusetts Institute of Technology

Cambridge, MA 02139

rwfield@mit.edu

Program Definition

Our research program focuses on the development and application of theoretical and experimental methods to examine the dynamics of highly excited combustion species. The primary goal is to extract and understand the dynamical information encoded in the spectra of small molecules at internal energies above the barrier to bond-breaking isomerization. We are currently examining two systems: the $S_0(\tilde{X}^1\Sigma^+)$ state of C_2H_2 near the acetylene \leftrightarrow vinylidene isomerization barrier and the $S_0(\tilde{X}^1\Sigma^+)$ state of HCN near the hydrogen cyanide \leftrightarrow hydrogen isocyanide isomerization barrier.

Recent Progress

Although we are continuing our efforts to selectively populate and conclusively assign vibrational levels in the energetic and configurational vicinity of the acetylene \leftrightarrow vinylidene isomerization transition state, most of our attention has been devoted toward the hydrogen cyanide \leftrightarrow hydrogen isocyanide system. The HCN \leftrightarrow HNC system has received considerable attention experimentally and theoretically as a prototypical isomerization reaction. The reduced density of states at high energy makes reliable experimental assignments possible, and the presence of only three atoms makes this system particularly amenable to high levels of theory. As in acetylene, we seek methods to definitively identify eigenstates that are delocalized over both isomeric minima. Theoretical calculations have shown that the bending vibration of HCN/HNC has a profound effect on the molecular dipole moment: the oppositely signed HCN and HNC dipole moments are essentially averaged out by the delocalization and eventual free rotation of the hydrogen atom around the CN core. On the other hand, comparable excitation of vibrations confined to linearity does not alter the dipole moment significantly from its

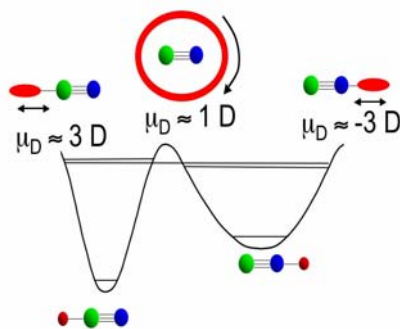


Figure 1. Ground state potential energy surface of HCN/HNC. The character of the nuclear wavefunction, as monitored by the Stark effect, is sensitive to the delocalization across both potential wells.

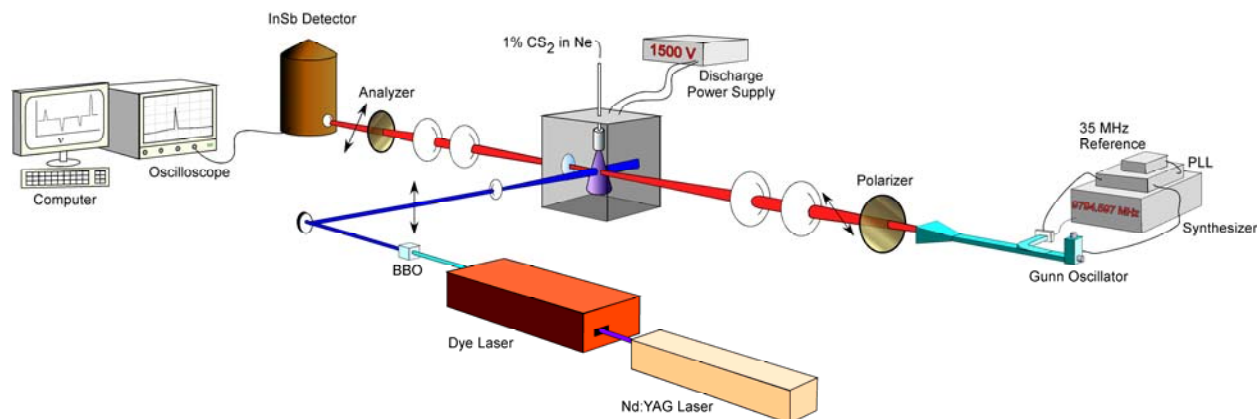


Figure 2. Experimental diagram of newly constructed mm-wave jet spectrometer. The mm-wave source is a Gunn oscillator (73-106 GHz), stabilized by a phase-locked loop (PLL). PFTE lenses are used to collimate and focus the mm-waves into a molecular beam produced from a pulsed DC discharge nozzle. The mm-waves are recollimated and focused with another set of PFTE lenses onto a liquid helium cooled InSb detector.

equilibrium value. Thus, dipole moment measurements of highly vibrational states of HCN/HNC are a sensitive filter for the delocalized states (see Figure 1).

We have recently constructed a millimeter (mm) wave jet spectrometer (see Figure 2) in order to make these measurements with mm-wave Stark spectroscopy. The spectrometer was optimized using CS molecules produced in a pulsed DC discharge. We have demonstrated that the absorption dip of the mm-waves can be used to sensitively detect optical transitions (see Figure 3). In the mm-wave detected mm-wave optical double resonance (mmD-mmODR) technique, we lock the mm-wave frequency to a ground state rotational transition and scan the laser frequency while observing changes in the mm-wave absorption. The spectrum is considerably simplified because only transitions originating from the lower and upper level of the mm-wave transition are observed. Moreover, the sign of the mmD-mmODR signal unambiguously labels the initial state of the molecule. Because the absorption of the mm-waves is proportional to the population difference between the two rotational levels of the transition, the absorption decreases when the laser depopulates the lower level of the mm-wave transition, whereas the absorption increases when the laser depopulates the upper level of the mm-wave transition. This technique is particularly useful in complex environments, such as pulsed discharges, where numerous molecular species are produced.

Although our discharge is run under conditions chosen to optimize its stability, the sensitivity of mmD-mmODR is limited by the large and often fluctuating background of mm-wave absorption. We can remove this molecular source noise by detecting the extent of the mm-wave polarization rotation induced by the optical transition. In the mm-wave polarization detected mm-wave optical double resonance (mmP-mmODR) technique, the mm-waves are placed between two crossed wire-grid polarizers at 45° and 135° (labeled polarizer and analyzer, respectively), such that the mm-waves do not reach the detector in the absence of the laser (see Figure 2). When the vertically polarized laser (0°) is absorbed, it creates an anisotropy in the otherwise isotropic distribution. This anisotropy leads to a differential absorption of the mm-wave perpendicular and parallel components, which causes the mm-wave polarization to rotate and some mm-wave radiation to pass through the analyzer. In theory, the polarization detected experiment can be performed with a background that is limited by the imperfect extinction of the polarizers and any birefringence of the transmission optics. In practice, we find that the signal-

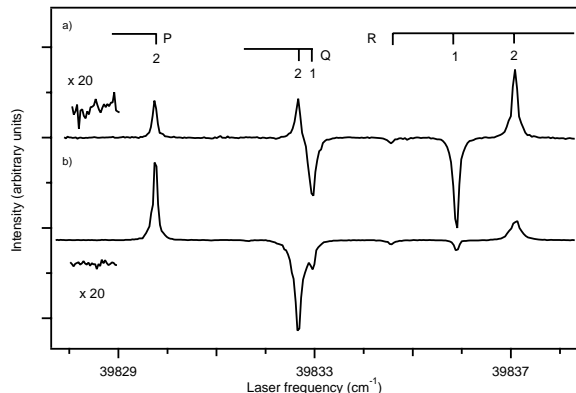


Figure 3. (a) mmD-mmODR and (b) mmP-mmODR spectra of the $A\ ^1\Pi - X\ ^1\Sigma(v = 1 - 0)$ transition of CS. For both spectra, the mm-waves probed the $J=2-1$ rotational transition at 97,980.9533 MHz. In mmD-mmODR spectra, a positive (negative) signal indicates that the optical transition originated from the upper (lower) rotational state. For mmP-mmODR spectra, the sign of the signal is more complicated because it depends on the relative magnitudes of the uncrossing angle and the differential absorption. The insets of (a) and (b) clearly demonstrate the improvement in baseline noise for the mmP-mmODR spectrum.

to-noise is increased when the polarizers are slightly uncrossed to heterodyne the weak polarization-rotation signal with the much stronger non-rotated field. Under these conditions, the mmP-mmODR signal is proportional to $\left[\frac{1}{2}\theta L\Delta\alpha + \left(\frac{1}{2}L\Delta\alpha\right)^2\right]$, where θ is the uncrossing of the polarizers, L is the interaction length, and $\Delta\alpha$ is the differential absorption between the parallel and perpendicular components of the mm-wave. Thus, the signs of mmP-mmODR signals are more complicated than those of mmD-mmODR because, in mmP-mmODR, the signal depends on the relative magnitude of the linear and quadratic terms. We find, however, that mmP-mmODR increases our sensitivity by a factor of >4 . This factor could be much larger if polarizers with extinction coefficients larger than 10^{-3} were used. Polarization spectroscopy is widely used in the visible and infrared regions of the spectrum, but to our knowledge, our work is the first demonstration of the use of mm-wave polarization detection for sensitive detection of optical transitions.

In order to further demonstrate this new technique, we have used mmP-mmODR to detect a pure rotational transition in a CS triplet state, $e\ ^3\Sigma^-(v = 2)$. The $e\ ^3\Sigma^-(v = 2)$ state gets its intensity from the nearby $A\ ^1\Pi(v = 1)$ state and has approximately 18% singlet state character. Here, we lock the laser frequency onto a single rotational line in the $e\ ^3\Sigma^- - X\ ^1\Sigma^+(v = 2 - 0)$ transition and scan the millimeter wave source. The ability to observe pure rotational transitions of vibrational and electronic excited states with mm-waves is a crucial step toward our goal of finding delocalized states in the $\text{HCN} \leftrightarrow \text{HNC}$ system.

Future Plans

We plan to continue our optimization of the mmD-mmODR and mmP-mmODR techniques to explore the $\text{HCN} \leftrightarrow \text{HNC}$ system. Unlike previous experimental investigations, which initiate excitation from the more stable HCN isomer, we intend to start from the HNC geometry because the stabilization of HNC relative to HCN in the \tilde{A} state results in a considerably lower electronic transition frequency. Despite the simplicity of the HNC molecule, the $\tilde{A} \leftrightarrow \tilde{X}$ transition has not previously been observed, in part due to pervasive predissociation of the Franck-Condon accessible \tilde{A} state vibrational levels. In order to access the lowest and least predissociated vibrational levels of the \tilde{A} state, we plan to use an IR-UV double resonance scheme where we exploit an intermediate state with excitation in the bending and CN-stretch vibrational levels. We will use mmD-mmODR and mmP-mmODR to identify the rotational and

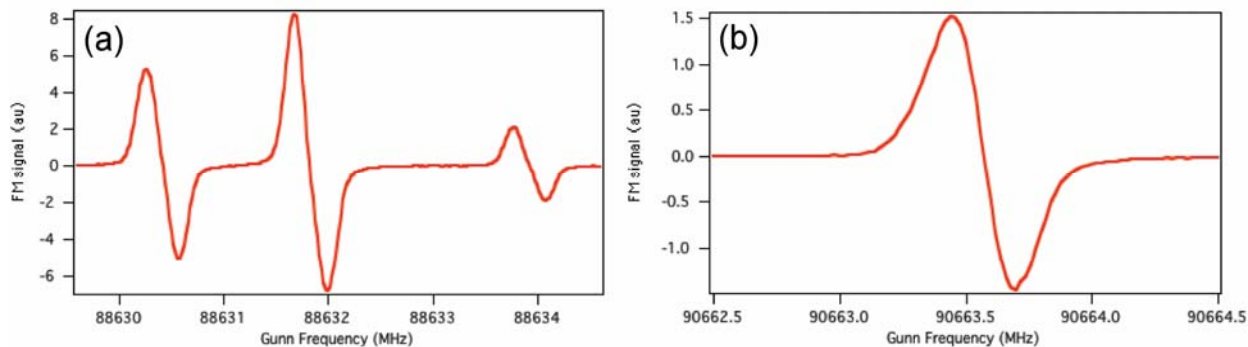


Figure 4. (a) HCN(1-0) and (b) HNC(1-0) rotational spectra obtained in a 1% DC discharge of acrylonitrile in neon. The mm-wave source was frequency modulated and the signal was detected in a phase-sensitive manner. HCN and HNC show dramatic differences in hyperfine structure, which could be exploited to measure the extent of delocalization between the two minima.

vibrational levels of the ground state overtones. Currently, we are using a DC discharge nozzle to produce HNC (see Figure 4), but we are planning to use a pyrolysis jet source in which an organic precursor (formamide or acrylonitrile) is decomposed by passing it rapidly through a resistively heated SiC tube. This method should allow a CN-free source of HNC, which would allow us to electronically excite HNC and detect the CN photofragments in a highly sensitive manner. Ultimately, we plan to record stimulated emission pumping (SEP) spectra via the mmP-mmODR or CN photofragment fluorescence dip method to provide information about highly excited vibrational states of HNC. These experiments will provide complementary information to the known vibrational level structure of HCN and provide a complete picture of the vibrational dynamics of the HCN \leftrightarrow HNC system. Once the vibrational levels in the HNC \tilde{X} state are located, the dipole moments will be measured directly by SEP-mm-wave Stark spectroscopy to identify the delocalized states.

Recent DOE-supported Publications (since 2003)

1. Z. -H. Loh and R. W. Field, "Contrasting origins of the isomerization barriers for vinylidene, fluorovinylidene, and difluorovinylidene," *J. Chem. Phys.* **118**, 4037 (2003).
2. A. J. Merer, N. Yamakita, S. Tsuchiya, J. F. Stanton, Z. Duan, and R. W. Field, "New vibrational assignments in the $\tilde{A}^1A_u \leftarrow \tilde{X}^1\Sigma_g^+$ electronic transition of acetylene, C_2H_2 : the ν_1 frequency," *Mol. Phys.* **101**, 663 (2003).
3. Z. Duan, N. Yamakita, S. Tsuchiya, and R. W. Field, "Differential Temperature Laser Induced Fluorescence Spectroscopy," *Chem. Phys.*, submitted.
4. A. H. Steeves, H. A. Bechtel, S. L. Coy, and R. W. Field, "Millimeter wave polarization detected millimeter wave optical double resonance spectroscopy of CS," in preparation.

Scanning Tunneling Microscopy Studies of Chemical Reactions on Graphite Surfaces

George Flynn, Department of Chemistry, Columbia University
Mail Stop 3109, 3000 Broadway, New York, New York 10027
flynn@chem.columbia.edu

Introduction and Overview

Our Department of Energy sponsored work is now focused on fundamental chemical events taking place on graphite surfaces with the intent of shedding light on the role of these surfaces in mediating the formation of polycyclic aromatic hydrocarbons (PAHs) and the growth of soot particles.¹⁻¹¹ Interest in soot is ultimately driven by the environmental and health implications arising from its formation in combustion reactions (particularly those involving heavier, diesel fuels), which are nearly ubiquitous throughout our society.¹ Of the four phases of soot formation,^{3,4} the work being pursued here is focused on surface reactions that lead to growth and oxidation of these particles.

Our experimental system employs Scanning Tunneling Microscopy and other surface science techniques to study a well defined graphite surface (rather than the more complex soot particle) interacting with vapor phase or adsorbed molecules. This experimental method provides a powerful tool with which to follow the behavior of reaction processes on surfaces and complements gas phase spectroscopic studies of PAH formation.¹⁻¹¹ Scanning Tunneling Microscopy can be used to identify surface defects and step edges, as well as to resolve and probe individual molecules on surfaces. The convenience and importance of being able to probe single molecules and/or single sites on surfaces probably cannot be overemphasized. Graphite itself is largely inert and reactive events are likely to occur when individual molecules are at or near dangling surface bonds typically found only at defect sites or step edges. Because of this, our initial efforts have been focused on the identification of adsorbates on the surface using temperature tunable, ultra-high-vacuum Scanning Tunneling Microscopy. There are basically two ways to do this. For the highest resolution images where STM topographs are dominated by Orbital Mediated Tunneling, the actual shape of the molecular wavefunction can be observed providing clues to molecular identity when size and shape are sufficient to distinguish species on the surface. For example, we have probed the PAH chrysene on graphite using this approach.¹² When the sample is held at a positive voltage, the image of a chrysene molecule is different from that obtained when the sample is negative. The positive sample image shows a tunneling pattern over an individual chrysene molecule that resembles the shape of the chrysene π -LUMO electronic wavefunction while the tunneling pattern with negative sample bias resembles the π -HOMO electronic state wavefunction. This suggests that the tunneling process for electrons moving from tip to surface is predominantly mediated by the empty LUMO state, while tunneling from surface to tip is dominated by the filled HOMO orbital. Both represent cases of high resolution images dominated by Orbital Mediated Tunneling. Though such behavior is somewhat unusual for non-conjugated hydrocarbons on graphite,¹³ it is likely to be typical of highly conjugated systems such as PAH's. Molecules of this type have relatively small HOMO-LUMO gaps and ionization potentials, which taken together, place the HOMO and LUMO levels of the adsorbates near in energy to the surface Fermi level. When this

happens, tunneling into the surface tends to be dominated by the empty LUMO while tunneling out of the surface tends to be dominated by the filled HOMO level.^{13,14}

A second method of identifying individual species on surfaces is to use Scanning Tunneling Spectroscopy. STS employs high resolution electron scattering to identify quantum states of individual adsorbate molecules by measuring current-voltage curves above specific sites. In its most elegant form (achieved with a STM operating at 4 K) the method can resolve vibrational states of single molecules.¹⁵⁻¹⁷ In the absence of adsorbates, STS trivially provides information about whether a surface site is electron donating or accepting by simply measuring I-V curves at a given site as a function of the voltage polarity. This is one of the most important factors in determining the reactivity of different points on a surface. For example, we have shown that electrons can easily tunnel in and out of iron atoms on an Fe₃O₄ terminated iron oxide surface, but can only easily tunnel into O atom sites on the same surface.¹⁸ For reactions mediated by electron attachment, such as the decomposition of organic chlorides, clearly the Fe sites are likely to be the most reactive.

Results:

While chrysene provides a stunning example of a molecule whose orbital shape can be imaged by STM, its STS spectrum is somewhat featureless in the ± 2 eV window typically available in experiments of this type. This observation is consistent with calculations of the HOMO—LUMO gap calculated for this molecule using DFT methods. Naphthalocyanine, which has many geometric factors in common with PAH's, is a molecule with significant electron delocalization in its π states and the calculated HOMO-LUMO gap falls well within the convenient voltage window for STS experiments. Using temperature tunable, ultra-high-vacuum Scanning Tunneling Microscopy we have studied the STM/STS features of naphthalocyanine by depositing it on a graphite surface that was pre-cleaned by heating to >700 K. Because of the low vapor pressure of this species, we have used a vacuum evaporation oven in conjunction with a quartz-crystal microbalance to deposit molecules on the surface at mono-layer or sub-mono-layer coverage. STM topographs of naphthalocyanine on graphite, taken at 50 K, show clear orbital mediated tunneling as the image shape changes when the voltage polarity is reversed (for a tunneling voltage of $|V|=1.83$ volts, $I=83$ pA). Orbital electron distributions are consistent with the known geometry of the molecule.

An average of approximately 50 individual STS I-V curves were also taken above the center of the molecules, and the derivative of this I-V curve was calculated numerically. The spectroscopic data indicates semi-conducting behavior with a gap in both the I-V and dI/dV characteristics, as would be expected for an adsorbate with a gap in its electronic structure. Since there is no current measured in the gap region from $-(0.9\pm 0.1)$ V to $+(0.9\pm 0.1)$ V, a contribution of the substrate states can be excluded for tip-sample distances used in the STS work. The I-V curves are asymmetric with a higher tunneling current measured for positive compared to negative sample bias at the same absolute voltage. This is consistent with an observed height change in constant current mode found upon switching the voltage polarity. The apparent height of the unoccupied states is larger than that of the occupied states. In the I-V curves the current is larger for

positive sample bias and therefore in constant current mode the tip must retract when switching from negative to positive sample bias. Of course, the height difference between occupied and unoccupied sample states is also dependent on the tunneling voltage. The numerically computed derivative curves exhibit clear maxima of the kind expected for resonant tunneling into molecular orbitals.¹⁴ To test the reproducibility of the dI/dV curve, the data set of 50 I-V curves was split into two independent data sets of equal size. The two curves obtained from these sets show very good agreement, even in the apparent fine structure. Most important is that this observed structure in the STS data can be closely associated with the electronic state energies of naphthalocyanine (calculated to reasonable levels of accuracy using DFT methods), thereby providing a fingerprint that can be used to identify single molecules on the surface.

Present and Future Experimental Program

By taking advantage of Orbital Mediated Tunneling and STS data, we plan to identify small and large PAH molecules and their precursors on graphite surfaces. The spectroscopic “signatures”, especially for different conjugated molecules, are expected to be quite distinct, thereby allowing identification of individual molecules on the surface. This will be followed by studies of mixtures of several PAH’s to determine if specific molecules can be located on the surface in a 2-dimensional mixture.

Studies of clean graphite and graphite impregnated with metals (to mimic diesel soot conditions) will also be undertaken. These investigations will be aimed at detecting electron donating surface sites, by using the STM to determine at what energy electrons tunnel from the surface to the tip. Low and high temperature STM images of metal impregnated graphite will also be obtained to see if the metal atoms are mobile on these surfaces.

References

1. J. A. Miller and G. A. Fisk, “Combustion Chemistry”, Chem. & Eng. News, 65 (35), 22-46, August 31, 1987
2. C. S. McEnally, A. G. Robinson, L. D. Pfefferle and T. S. Zwier, “Aromatic Hydrocarbon Formation in Nonpremixed Flames Doped with Diacetylene, Vinylacetylene, and Other Hydrocarbons: Evidence for Pathways Involving C₄ Species”, Combustion and Flame 123, 344-357 (2000)
3. M. Frenklach, “Reaction mechanism of soot formation in flames”, Phys. Chem. Chem. Phys. 4, 2028-2037 (2002)
4. M. Frenklach and H. Wang, “Detailed modeling of soot particle nucleation and growth”, Proc. Combust. Inst. 23, 1559-1566 (1991)
5. H. Richter and J. B. Howard, “Formation of Polycyclic Aromatic Hydrocarbons and their Growth to Soot – A Review of Chemical Reaction Pathways”, Prog. Energy and Combust. Sci. 26, 565-608 (2000)
6. C. F. Melius, M. E. Colvin, N. M. Marinov, W. J. Pitz and S. M. Senkan, “Reaction mechanisms in aromatic hydrocarbon formation involving the C₅H₅ cyclopentadienyl moiety”, Proc. Combust. Inst. 26, 685-692 (1996)
7. P. R. Westmoreland, A. M. Dean, J. B. Howard and J. P. Longwell, “Forming benzene in flames by chemically activated isomerization”, J. Phys. Chem. 93, 8171-8180 (1989)

8. M. Frenklach, N. W. Moriarty and N. J. Brown, "Hydrogen migration in polyaromatic growth", *Proc. Combust. Inst.* **27**, 1655-1661 (1998)
9. M. Frenklach, "On surface growth mechanism of soot particles", *Proc. Combust. Inst.* **26**, 2285-2293 (1996)
10. C. A. Arrington, C. Ramos, A. D. Robinson and T. S. Zwier, "Aromatic ring-forming reactions of metastable diacetylene with 1, 3-butadiene", *J. Phys. Chem. A* **102**, 3315-3322 (1998)
11. N. M. Marinov, W. J. Pitz, C. K. Westbrook, M. J. Castaldi and S. M. Senkan, "Modeling of aromatic and polycyclic aromatic hydrocarbon formation in premixed methane and ethane flames", *Combust. Sci. Technol.* **116**, 211-287 (1996)
12. Gina M. Florio, Tova L. Werblowsky, Thomas Mueller, Bruce J. Berne, and George W. Flynn, "The Self-Assembly of Small Polycyclic Aromatic Hydrocarbons on Graphite: A Combined STM and Theoretical Approach", *J. Phys. Chem. B* (2005) (accepted)
13. Leanna C. Giancarlo and George W. Flynn, "Scanning Tunneling and Atomic Force Microscopy Probes of Self-Assembled, Physisorbed Monolayers: Peeking at the Peaks", *Annu. Rev. Phys. Chem.*, **49**, 297-336 (1998)
14. K.W. Hips, D.E. Barlow, U. Mazur, *J. Phys. Chem. B* **104**, 2444-2447 (2000)
15. J. Gaudioso, H. J. Lee and W. Ho, "Vibrational Analysis of Single Molecule Chemistry: Ethylene Dehydrogenation on Ni(110)", *J. Am. Chem. Soc.*, **121**, 8479-8485 (1999).
16. B. C. Stipe, M. A. Rezaei, and W. Ho, "Single-molecule Vibrational Spectroscopy and Microscopy", *Science*, **280**, 1732-1735 (1998). on NiAl(110)". *J. Chem. Phys.* **119**, 2296-2300 (2003).
17. W. Ho, "Single Molecule Chemistry", *J. Chem. Phys.* **117**, 11033-11061(2002)
18. Kwang Taeg Rim, Jeffrey P. Fitts, Thomas Müller, Kaveh Adib, Nicholas Camillone, III, Richard M. Osgood, S. A. Joyce, and George W. Flynn, "CCl₄ Chemistry on the Reduced Selvege of a α -Fe₂O₃(0001) Surface: A Scanning Tunneling Microscopy Study", *Surf. Sci.* **541**, 59-75, (2003).

DOE Publications: (2003-2005)

1. Natalie Seiser, Kavita Kannappan, George Flynn, "Long Range Collisional Energy Transfer from Highly Vibrationally Excited Pyrazine to CO Bath Molecules: Excitation of the $\nu=1$ CO Vibrational Level", *J. Phys. Chem.*, **107**, 8191-97, (2003)
2. Markus Lackinger, Thomas Müller, T.G. Gopakumar, Falk Müller, Michael Hietschold and George W. Flynn, "Tunneling Voltage Polarity Dependent Submolecular Contrast of Naphthalocyanine on Graphite – a STM Study of Close Packed Monolayers under Ultrahigh-Vacuum Conditions", *J. Phys. Chem.* **108**, 2279-2284 (2004)
3. Gina M. Florio, Tova L. Werblowsky, Thomas Mueller, Bruce J. Berne, and George W. Flynn, "The Self-Assembly of Small Polycyclic Aromatic Hydrocarbons on Graphite: A Combined STM and Theoretical Approach", *J. Phys. Chem. B* (2005) (accepted)

Quantitative Imaging Diagnostics for Reacting Flows

Jonathan H. Frank

Combustion Research Facility
Sandia National Laboratories
P.O. Box 969, MS 9051
Livermore, CA 94551-0969
email: jhfrank@ca.sandia.gov

Program Scope

The primary objective of this project is the development and application of laser-based imaging diagnostics for studying reacting flows. Imaging diagnostics provide temporally and spatially resolved measurements of species, temperature, and velocity distributions over a wide range of length scales. Multi-dimensional measurements are necessary to determine spatial correlations, scalar and velocity gradients, flame orientation, curvature, and connectivity. Current efforts focus on planar laser-induced fluorescence (PLIF) and Rayleigh scattering techniques for probing the detailed structure of both isolated flow-flame interactions and turbulent flames. The investigation of flow-flame interactions is of fundamental importance in understanding the coupling between transport and chemistry in turbulent flames. These studies require the development of a new suite of imaging diagnostics to measure key species in the hydrocarbon-chemistry mechanism as well as to image rates of reaction and scalar dissipation.

Recent Progress

Recent research has continued to emphasize the development and application of diagnostics for probing the detailed structure of reaction zones during flow-flame interactions. Research activities have included the following: i) Mixture fraction and reaction-rate imaging, ii) An investigation of CH LIF as a marker of heat release rate, iii) Laser-induced fragmentation fluorescence as a C2 species diagnostic.

Combined mixture fraction and reaction-rate imaging

Simultaneous imaging of depolarized and polarized Rayleigh scattering combined with OH LIF and two-photon CO LIF provided two-dimensional measurements of mixture fraction (ξ), temperature, scalar dissipation rate (χ), and the forward reaction rate of the reaction $\text{CO} + \text{OH} = \text{CO}_2 + \text{H}$ in turbulent partially premixed flames. Multi-dimensional measurements of mixture fraction are needed to determine the scalar dissipation rate, which is defined as $\chi = 2D(\nabla \xi \cdot \nabla \xi)$, where D is the mass diffusivity. The concept of a three-scalar technique for determining mixture fraction using CO-LIF with depolarized and polarized Rayleigh signals was previously demonstrated in a partially premixed CH_4/air jet flame (Sandia Flame D) [Frank, Kaiser, Long, *Proc. Combust. Inst.* 29 (2002) 2687-2694]. The technique is based on the construction of a conserved scalar from a linear combination of the enthalpy, fuel mass fraction, and CO mass fraction. For an isotropic molecule, such as methane, the fuel concentration can be determined from a combination of depolarized and polarized Rayleigh scattering. Rayleigh scattering from isotropic molecules contains no measurable depolarized component when excited by a polarized laser beam. In contrast, Rayleigh scattering from anisotropic molecules, such as N_2 , O_2 , CO_2 , H_2O , H_2 , and CO , contains both depolarized and polarized components. The

methane concentration can be related to the difference between the polarized and depolarized Rayleigh signals when these signals are normalized to their respective values in air. Fuel mixtures that have no depolarized component provide optimal contrast between the difference Rayleigh signal in the fuel mixture and the air coflow. The use of anisotropic diluent gases, such as nitrogen and oxygen, in the fuel mixture decreases the dynamic range of the difference Rayleigh signal. Partial premixing of methane with air, however, produces more robust flames and significantly reduces broadband fluorescence interference from polycyclic aromatic hydrocarbons. The dynamic range of the difference Rayleigh signal can be significantly improved by replacing the nitrogen in air with a noble gas, which has zero depolarization ratio. Recently, we investigated a partially premixed turbulent jet flame with a fuel-stream mixture that was better suited for the diagnostic technique. The contrast between the depolarized and polarized Rayleigh signals in the fuel and air streams was improved by partially premixing methane with an argon/oxygen mixture that had the same oxygen content as air. The substitution of argon, which has zero depolarization ratio, for the nitrogen in air decreased the depolarized Rayleigh signal in the fuel stream and thereby increased the contrast between the depolarized and polarized Rayleigh signals. Additional improvements in the detection systems significantly increased the signal-to-noise ratios of the depolarized Rayleigh and two-photon CO-LIF signals. The improved diagnostics provided 2-D measurements of mixture fraction and scalar dissipation, which was determined by $\chi = 2D((\partial\xi/\partial r)^2 + (\partial\xi/\partial x)^2)$. Measurements were performed in turbulent jet flames with a range of probabilities of localized extinction. Analysis of the results have thus far focused on flames with a relatively low probability of extinction. The contribution of noise to the scalar dissipation was evaluated from measurements in a laminar flame, and a first-order correction to the noise contribution in turbulent flames was performed. Conditional statistics of scalar dissipation and reaction rate have been evaluated. Further analysis is underway to determine the mixture fraction and scalar dissipation rates in flames with significant localized extinction. A portion of this effort was conducted in collaboration with Marshall Long (Yale).

Adequacy of CH laser-induced fluorescence as a marker of heat release rate

The CH radical is frequently used as a flame marker because it is relatively short lived, is present over a narrow region in flames, and can be measured by LIF. Discontinuities in the CH LIF signal along a flame front are often interpreted as localized extinction of the flame. However, the adequacy of CH LIF as a flame marker is uncertain because of previous evidence that the CH LIF signal does not consistently correlate with heat release rate when highly N₂-diluted premixed methane flames are perturbed by a transient flow. To resolve this issue, we initiated a detailed study of the correlation between CH-LIF signals and heat release rate in steady and unsteady flames. Two-dimensional LIF measurements of CH, OH, and CH₂O were performed simultaneously. The pixel-by-pixel product of the OH and CH₂O LIF measurements were used to determine the forward reaction rate of CH₂O+OH = HCO + H₂O, which is highly correlated with the rate of heat release in premixed methane/air flames. Initial measurements in undiluted steady flames indicate that CH-LIF signals correlate well with heat release rate when the strain rate is varied and the stoichiometry of the reactant mixture remains constant. Unsteady laminar flame calculations indicate that this correlation is better in undiluted flames than in N₂-diluted flames. Both measurements and calculations indicate that CH-LIF signals do not correlate well with heat release rate when the stoichiometry of the reactants is varied from rich to

lean. Further measurements are needed to determine the correlation of CH-LIF signals with heat release rate in unsteady flames with a range of strain rates.

C2-Species diagnostic

We are developing an optical diagnostic for imaging vinyl (C_2H_3) and acetylene (C_2H_2) in premixed flames. When excited at 230 nm, the vinyl radical and acetylene are detected by fluorescence from $C_2(d^3\Pi_g \rightarrow a^3\Pi_u)$ laser-induced fragmentation fluorescence (LIFF). Our previous studies in a room temperature low-pressure cell indicated that vinyl photodissociation creates $C_2(d^3\Pi_g)$ more efficiently than acetylene photodissociation by a factor of 1300-200 depending on the internal excitation of the vinyl radical. The vinyl radical is believed to be an important combustion intermediate and has not previously been measured in flames with optical diagnostics. The use of direct detection by laser-induced fluorescence is precluded by the fact that vinyl has no known fluorescent excited state. Current efforts are focused on determining the temperature dependence of the LIFF process. In the Advanced Imaging Laboratory, LIFF measurements are performed in an atmospheric pressure flow that can be heated to 900 K. Initial results indicate a significant temperature enhancement of the LIFF process in C_2H_2 . This enhancement is consistent with improved Frank-Condon factors in vibrationally excited acetylene. To determine the temperature dependence of the LIFF signals at flame temperatures, a series of low-pressure flames are being investigated. The spatial profiles of acetylene and vinyl in rich premixed ethylene flames were measured with a photoionization mass spectrometer on the Chemical Dynamics Beamline of the Advanced Light Source (ALS) at Lawrence Berkeley National Laboratory in collaboration with David Osborn (Sandia), Craig Taatjes (Sandia), Nils Hansen (Sandia), Terrill Cool (Cornell), and Stephen Leone (Berkeley). The temperature and LIFF profiles in these low-pressure flames were measured in Sandia's Flame Chemistry and Diagnostics Laboratory. We are currently in the process of analyzing the data from the ALS and Sandia to determine the temperature dependence of the LIFF signals in these flames.

Future Plans

The ongoing analysis of our multiscale imaging data is expected to provide measurements of reaction rates and scalar dissipation rates in a series of piloted $CH_4/O_2/Ar$ jet flames with significant levels of localized extinction. We expect that this data set will offer insight into the extinction and re-ignition processes in turbulent partially premixed flames. The analysis will include an examination of the effects of local flame curvature. Our experimental results will be coupled with the highly-resolved large-eddy simulations (LES) that are described in Joseph Oefelein's abstract.

We are in the initial phases of adding a new capability to the Advanced Imaging Laboratory. We plan to construct a tunable picosecond dye laser system for PLIF excitation. This effort builds upon our recent demonstration of interference-free imaging of two-photon O-atom LIF using a picosecond pulsed laser for excitation. O-atom LIF imaging will be available for coupling with the suite of imaging diagnostics that is currently available in the Advanced Imaging Laboratory. Atomic hydrogen is another key radical in combustion chemistry that is challenging to measure without photolytic interference. H-atom LIF detection with ps lasers may provide H-atom measurements without photolytic interference. In two-photon H-atom LIF, ground-state atomic hydrogen is excited at 205 nm via the $3d \ ^2D \leftarrow \leftarrow 1s \ ^2S$ transition, and

fluorescence is detected from the $3d^2D \rightarrow 2p^2P$ transition at 656 nm. Single-photon photodissociation of CH_3 and thermally excited water molecules is a significant source of photolytic interference for 205-nm excitation. Since H-atom LIF excitation is a two-photon process while the photolytic interference is a single-photon process, ps-laser excitation may provide a significant advantage over ns lasers. This effort will be conducted in collaboration with Tom Settersten (Sandia).

Another planned addition to the Advanced Imaging Laboratory is a counterflow burner for repeatable ignition experiments. This facility will be used to conduct detailed measurements of the effects of unsteady flows on ignition kernels. In a recent collaboration with Kal Seshadri (UCSD), we demonstrated that highly repeatable ignition events can be obtained in a nonpremixed hydrogen/air counterflow burner using laser ignition. In the future, we plan to investigate a broader range of conditions for hydrogen ignition and study the edge-flame propagation that occurs as the ignition kernel spreads. We will extend the ignition and edge-flame studies to include other fuels. These experiments will be coupled with direct numerical simulations (DNS) by Jackie Chen (Sandia).

DOE Supported Publications (2003–present)

J.H. Frank, X. Chen, B.D. Patterson, T.B. Settersten, “Comparison of Nanosecond and Picosecond Excitation for Two-Photon LIF Imaging of Atomic Oxygen in Flames,” *Appl. Opt.*, 43:2588 (2004).

J.H. Frank and T.B. Settersten, “Two-photon LIF Imaging of Atomic Oxygen in Flames with Picosecond Excitation,” *Proc. Combust. Inst.* 30:1527-1534 (2004).

C.M. Vagelopoulos and J.H. Frank, “An Experimental and Numerical Study on the Adequacy of CH as a Flame Marker in Premixed Methane Flames,” *Proc. Combust. Inst.* 30:241-249 (2004).

R. Seiser, J.H. Frank, S. Liu, J.H. Chen, R.J. Sigurdsson, and K. Seshadri, “Ignition of Hydrogen in Unsteady Nonpremixed Flows,” *Proc. Combust. Inst.* 30:423-430 (2004).

G. Amantini, J.H. Frank, and A. Gomez, “Experiments on Standing and Traveling Edge Flames around Flame Holes in Both Ignition and Extinction Modes,” *Proc. Combust. Inst.* 30:313-321 (2004).

S. A. Kaiser, J. H. Frank, and M. B. Long, “Use of Rayleigh Imaging and Ray Tracing to Correct for Beam-Steering Effects in Turbulent Flames,” *Applied Optics*, in press (2005).

MECHANISM AND DETAILED MODELING OF SOOT FORMATION

Principal Investigator: Michael Frenklach

Department of Mechanical Engineering

The University of California

Berkeley, CA 94720-1740

Phone: (510) 643-1676; E-mail: myf@me.berkeley.edu

Project Scope: Soot formation is one of the key environmental problems associated with operation of practical combustion devices. Mechanistic understanding of the phenomenon has advanced significantly in recent years, shifting the focus of discussion from conceptual possibilities to specifics of reaction kinetics. However, along with the success of initial models comes the realization of their shortcomings. This project focuses on fundamental aspects of physical and chemical phenomena critical to the development of predictive models of soot formation in the combustion of hydrocarbon fuels, as well as on computational techniques for the development of predictive reaction models and their economical application to CFD simulations. The work includes theoretical and numerical studies of gas-phase chemistry of gaseous soot particle precursors, soot particle surface processes, particle aggregation into fractal objects, and development of economical numerical approaches to reaction kinetics.

Recent Progress:

Developing models for representing combustion chemistry at varying levels of complexity to use with models for laminar and turbulent flow fields to describe combustion processes (with J. C. Lee and H. N. Najm)

The ongoing collaborative project with the Sandia group of Habib Najm is aimed at combining Piecewise Reusable Implementation of Solution Mapping (PRISM) and Computational Singular Perturbation (CSP) techniques for ultra-economic modeling of reactive flows with realistic chemistry. During the past year, we demonstrated a new strategy for construction of an adaptive chemistry model. The technique is based on a slow manifold projection scheme derived from CSP combined with PRISM. PRISM is used to tabulate the response surfaces of the CSP tensors. We examined the effectiveness of this scheme by considering a model problem with variable stiffness. We found that, while the degradation in accuracy is minimal, the CPU cost of the CSP projection method can potentially be reduced substantially using this tabulation strategy, which bypasses the CPU-intensive CSP analysis. Furthermore, we found that the size of the hypercubes used to build the PRISM tabulation can be very large and their dimensionality can be reduced. The dimensionality reduction is achieved by collapsing the dimensions corresponding to the CSP radicals. This reduction in the hypercubes dimensionality is a key aspect of the new strategy.

Particle Aggregation with Simultaneous Surface Growth: Time-Dependent Monte Carlo Simulations of a Particle Ensemble (with M. Balthasar and M. Kraft)

During the past several years we completed theoretical development and numerical analysis of a single aggregate particle colliding with surrounding spherical particles and simultaneous surface growth, and of aggregate-aggregate collisions treated in a lumped manner. During the past year, in collaboration with Markus Kraft (Cambridge University) and Michael Balthasar (Volvo), we

initiated analysis at a detailed level by performing Monte Carlo simulations with aggregate-aggregate collisions resolved explicitly.

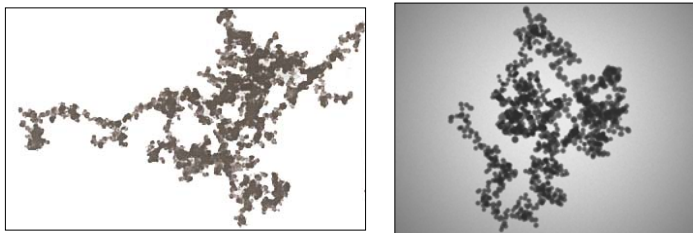
The dynamics of a soot particle ensemble was modeled by the Smoluchowski master equations with additional source terms included for nucleation and surface reactions. The geometric structure of each particle was considered explicitly. The incepting particles were assumed to be spherical. A detailed physical model of aggregate-aggregate collisions was employed, treating individual constituent particles as hard spheres upon collision. Surface growth was modeled as a uniform increase in the diameters of constituent particles comprising the aggregates. The population balance was solved by an efficient stochastic algorithm, built on the concept of majorant kernels.

First, the model was tested at conditions of coalescent coagulation. A monodispersed size distribution of spherical particles was used at outset and the temperature was kept constant. The results of the stochastic simulations were compared to the solution of the master equations obtained with a deterministic ODE solver. A close agreement between the two was obtained. Aggregation phenomena and aggregate properties formed by collision of mono-dispersed particles have been investigated extensively in the past. Hence, the second test of the model was performed at conditions of aggregation of mono-dispersed particles. The resulting fractal dimension of 1.9 obtained in our Monte-Carlo simulations compared well with the literature report of 1.91 ± 0.03 .

After the above validations tests, several series of Monte Carlo simulations were performed. In one such series, we started with nucleation without surface reactions for the initial time interval. In the following time interval, for reaction times greater than 0.5 ms, nucleation rate was decreased and surface growth increased linearly in time. This case was constructed mainly to generate large particles (in terms of particle volume) within a small simulation time and to test the Monte-Carlo sampling of particle properties: radius of gyration, R_g , surface area, S , and volume, V . After a coagulation event, surface area and volume were calculated directly by adding the surface areas and volumes of the two colliding particles. After each surface growth numerical step, the Monte-Carlo sampling was used to calculate R_g , S , and V of each particle.

The next series of Monte-Carlo runs aimed at closely mirroring soot formation processes in a laminar premixed flame but on a shorter time scale. In the beginning of the simulation, a strong peak in nucleation was constructed with a surface growth being small but non-zero. Shortly after the decline in the nucleation rate, surface growth was increased and peaked. Surface growth then was decreased again and at the end only coagulation was active. It was observed that the evolution of the computed particle number densities and volume fraction closely resemble those

TEM image of a soot aggregate (left), and two-dimensional TEM-style projection of a sample particle generated in the numerical simulations (right).



usually found in experimental studies of premixed flames. The particle mean collision diameter and particle shape descriptor obtained from the simulated distributions were very similar to those found in the simulations with the method of moments. Finally, we performed numerical simulations with the present model for the condition of a 10-bar laminar premixed ethylene-air flame, at $C/O = 0.673$. Two-dimensional TEM-style projections of sample particles generated in

these numerical simulations show features similar to the typical TEM images of soot particle collected in experimental flame studies, as shown in the above figure.

Pre-nucleation Soot Chemistry (with W. A. Lester, Jr.)

Collaboration with Professor William Lester and his group has continued in the area of theoretical studies using Quantum Monte Carlo (QMC) and a series of other ab initio as well as density functional theory (DFT) calculations with the objective of predicting enthalpies of formation of chemical species and transition state for reactions of interest to the growth of aromatic precursors to soot. As the debate surrounding the energy difference between *n*-C₄H₃ and *i*-C₄H₃ isomers has intensified, we performed a quantum Monte Carlo (QMC) benchmark study of heats of formation at 298K, bond dissociation energies (BDEs), and atomization energies of 22 small hydrocarbons. Diffusion Monte Carlo (DMC) results, obtained using a simple product trial wave functions consisting of a single determinant and correlation function, were compared to experiment and to other theory including a version of complete basis set theory (CBS-Q) and DFT with the B3LYP functional.

For heats of formation, the findings are a mean absolute deviation from experiment of 1.2 kcal/mol for CBS-Q, 2.0 kcal/mol for B3LYP, and 2.2 kcal/mol for DMC. The mean absolute deviation of 31 BDEs was 2.0 kcal/mol for CBSQ, 4.2 kcal/mol for B3LYP, and 2.5 kcal/mol for DMC. These findings were for 17 BDEs of closed-shell molecules that have mean absolute deviations from experiment of 1.7 kcal/mol (CBS-Q), 4.0 kcal/mol (B3LYP), and 2.2 kcal/mol (DMC). The corresponding results for the 14 BDEs of open-shell molecules studied were 2.4 kcal/mol (CBS-Q), 4.3 kcal/mol (B3LYP), and 2.9 kcal/mol (DMC). For atomization energies, comparison of the DMC results to experiment yielded a mean absolute deviation of 1.9 kcal/mol, which is comparable to that of the B3LYP/cc-pVQZ (1.7 kcal/mol) level of theory, but less accurate than that of CBS-Q (1.1 kcal/mol). DMC performed similarly for both closed-shell and open-shell molecules with mean absolute deviations of 2.1 kcal/mol for the former and 1.7 kcal/mol for the latter systems. The use of experimental zero point energies (ZPEs), rather than scaled B3LYP ZPEs, was found to have negligible effect on DMC atomization energies. The DMC results provide a baseline from which improvement using multi-determinant trial functions can be measured.

Future Plans

Developing Models for Representing Combustion Chemistry at Varying Levels of Complexity to Use with Models for Laminar and Turbulent Flow Fields to Describe Combustion Processes: In collaboration with the Sandia group of Habib Najm, we have demonstrated that the combination of the CSP-slow-manifold projection method and PRISM offers a new way to construct an adaptive reduced-order model for a stiff dynamical system. CSP allows not only a reduction in dimensionality, but also the use of larger hypercubes. By constructing tabulations for the CSP tensors, we have an efficient explicit time integration construction. The test performed on a stiff model demonstrated the feasibility of this novel model construction method. It showed that high level of accuracy is readily achievable. Future work will concentrate on the construction of such an adaptive model for chemical kinetic systems that are of relevance to the area of combustion.

Soot Particle Aggregation: We will continue collaboration with Markus Kraft (Cambridge University, UK) and Michael Balthasar (Volvo, Sweden) on Monte Carlo simulations of aggregate-aggregate collisions. Having completed these simulations, we will use the data

obtained to further refine the method of moments and incorporate the developed algorithm into the soot modeling software.

Pre-nucleation Chemistry: The collaboration with William Lester's group we will continue on quantum ab initio and Quantum Monte Carlo (QMC) analysis of reactions that are critical to the development of kinetic models of aromatic growth. Now, with the uncertainties of QMC documented, we will repeat the QMC analysis for the C₄ and C₅ hydrocarbon species.

Soot Particle Surface Reactions: We have speculated on a possible role of the "collision" between the cyclopenta groups migrating along the graphene edge. We will explore this and other related reactions of graphene layer growth using quantum chemical methods (ab initio, DFT, and QMC) in collaboration with Professor William Lester and his group, and then determine the reaction rates through solution of master equations. The rate coefficients determined in this manner will serve as input to the kinetic Monte Carlo simulations with a new, three-dimensional code.

Graphene Structure Growth: Our objective is to complete the development of the new, three-dimensional kinetic Monte Carlo code and, after the code is completed and validated, to perform a series of KMC calculations with the new reactions and their kinetics included, focusing on the development of the curvature in the evolving aromatic structures.

Homogeneous Nucleation of Carbon Nanoparticles: We will continue molecular dynamics simulations with on-the-fly quantum forces. Our current objective is to complete the ongoing investigation of the external rotational energy of the incoming PAH molecules and, when accomplished, to examine the formation and behavior of PAH clusters larger than dimers.

Publications

1. "Computational Economy Improvements in PRISM," S. R. Tonse, N. W. Moriarty, M. Frenklach, and N. J. Brown, *Int. J. Chem. Kinet.* **35**, 438–452 (2003).
2. "Particle Aggregation with Simultaneous Surface Growth," P. Mitchell and M. Frenklach, *Phys. Rev. E* **67**, 061407 (2003).
3. "Geometry Optimization in Quantum Monte Carlo with Solution Mapping: Application to Formaldehyde," C. A. Schuetz, M. Frenklach, A. C. Kollias, and W. A. Lester, Jr., *J. Chem. Phys.* **119**, 9386–9392 (2003).
4. "On the Role of Surface Migration in Growth and Structure of Graphene Layers," M. Frenklach and J. Ping, *Carbon '03, International Conference on Carbon*, 2003, ISBN 84-607-8305-7.
5. "Coupling Reaction Chemistry with Fluid Dynamics: Methods and Applications," M. Frenklach, *19th International Colloquium on the Dynamics of Explosions and Reactive Systems*, 2003, ISBN4-9901744-1-0.
6. "On the Role of Surface Migration in the Growth and Structure of Graphene Layers," M. Frenklach and J. Ping, *Carbon* **42**, 1209–1211 (2004).
7. "Detailed Kinetic Modeling of Soot Aggregate Formation in Laminar Premixed Flames," M. Balthasar and M. Frenklach, *Combust. Flame* **140**, 130–145 (2005).
8. "Migration Mechanism of Aromatic-edge Growth," M. Frenklach, C. A. Schuetz, and J. Ping, *Proc. Combust. Inst.* **30**, 1389–1396 (2005).
9. "Monte-Carlo Simulation of Soot Particle Coagulation and Aggregation: The Effect of a Realistic Size Distribution," M. Balthasar and M. Frenklach, *Proc. Combust. Inst.* **30**, 1467–1475 (2005).
10. "Kinetic Monte Carlo Simulations of Soot Particle Aggregation," M. Balthasar, M. Kraft, and M. Frenklach, *Prepr. Pap.-Am. Chem. Soc., Div. Fuel Chem.* 50(1), 2005, pp. 135–136.
11. "Quantum Monte Carlo Study of Heats of Formation and Bond Dissociation Energies of Small Hydrocarbons," A. C. Kollias, D. Domin, G. Hill, M. Frenklach, D. M. Golden, and W. A. Lester, Jr., *Int. J. Chem. Kinet.*, accepted for publication.

CHEMICAL DYNAMICS IN THE GAS PHASE: QUANTUM MECHANICS OF CHEMICAL REACTIONS

Stephen K. Gray

Chemistry Division
Argonne National Laboratory
Argonne, IL 60439

Email: gray@tcg.anl.gov

PROGRAM SCOPE

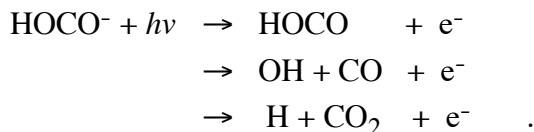
This program is in the area of theoretical chemical reaction dynamics, It centers around accurate quantum mechanical studies of the spectroscopy and dynamics of experimentally relevant and combustion important gas phase systems. Rigorous time-dependent quantum methods (wave packets) and iterative time-independent quantum methods are used, or developed as necessary, for such purposes. The results obtained allow one to gauge the quality of potential energy surfaces, and to infer the validity of more approximate theoretical methods such as quasiclassical trajectories and transition state theory. The results also can provide mechanistic insights into the dynamics.

RECENT PROGRESS

Building on our previous work on the decay of reactant channel $\text{OH}\cdots\text{CO}$ complexes with two vibrational quanta in OH, but zero-point energy in the remaining degrees of freedom [1], we first determined a variety of the higher energy metastable states, and then began to propagate a number of these states with the real wave packet method [2] in order to look at their decay dynamics. These states are interesting because of the increased chance of forming HOCO complexes and thus $\text{H} + \text{CO}_2$ products. This work was motivated by the interesting experimental results Lester and her co-workers [3,4], and their conjecture that some of these complexes may decay not only back to reactants, $\text{OH} + \text{CO}$ but to the $\text{H} + \text{CO}_2$ product channel. We also have available a global potential energy surface that includes high-quality *ab initio* information on the relevant reactant channel well region [5]. While we do find an increased probability of formation of $\text{H} + \text{CO}_2$ in some cases relative to the original calculations, more than 95% of the decay is still to the reactant channel. It is likely that higher states not yet examined will have more interesting dynamics and this project continues. This work, and indeed most of the current four-atom quantum dynamics work being carried out in this research program, has been greatly facilitated by the development of an efficient, massively parallel version of the four-atom wave packet code [6].

In collaboration with Goldfield at Wayne State University, work was initiated on another aspect of the $\text{OH} + \text{CO}$ system, of relevance to the negative ion dissociative photodetachment experiments of

Continetti and his co-workers [7]. In these experiments, the photodetachment of the negative ion can lead to several product channels:



The structures of the possible negative ions accessed in the experiments are such that immediately after photodetachment, one has effectively created energized neutral HOCO molecules (and some bound HOCO molecules) on the ground state potential surface. The experimental product branching ratios were found to be quite different from statistical (RRKM) theory predictions. Our study, among other things, should shed light on the origins of this discrepancy and further test the quality of the potential energy surface. We have completed the development of the basic code, which involves transformation from a normal mode ground state wavefunction for HOCO⁻ to the diatom-diatom Jacobi coordinates employed in the wave packet code and flux analysis for the product states. We have also determined, with the iterative Lanczos method, the bound states of HOCO which will be used in the analysis.

The quantum reaction dynamics of $\text{CH} + \text{H}_2 \rightarrow \text{CH}_2 + \text{H}$, its reverse are important in combustion because they lead to the equilibration of CH and CH₂, and there are interesting experimental results available for comparison [8-11]. Among the fundamental questions quantum dynamics can answer include the nature of the formation and breakup of methyl radical, CH₃[·] complexes. My colleague Harding has recently developed a global high-level potential energy surface for studying this important four-atom system, based on high-level multi-reference configuration interaction calculations. The initial phase of our quantum dynamics work on this reaction system was completed [12]. In this first phase we tested the quality of the potential energy surface by determining the vibrational states of the methyl and triplet methylene radicals with an implementation of Lanczos method similar to our earlier work on resonances in H₂O [13], and compared these results with available experimental and related theoretical data. It is found, for example, that there is a large “negative anharmonicity” effect regarding the out-of-plane umbrella motion, in agreement with the earlier results. Excellent results for many vibrational levels of both the methyl and (triplet) methylene radicals were obtained. We conclude that the surface should provide an excellent, global description of the CH + H₂ system.

FUTURE PLANS

The four-atom quantum dynamics studies initiated above, involving the unimolecular reactions of OH[·]·CO and HOCO⁻, and the bimolecular $\text{CH} + \text{H}_2 \rightarrow \text{CH}_2 + \text{H}$ reaction, will be completed. In collaboration with Goldfield, and enabled by our parallel wave packet code [6], we will revisit the bimolecular reaction dynamics of $\text{OH} + \text{CO} \rightarrow \text{CO}_2 + \text{H}$ [14], this time allowing for non-zero total angular momentum and reactant excitations. In this system, as in the case of CH + H₂, particular focus will be placed on the role of intermediate complexes on the reaction dynamics.

The current four-atom real wave packet code will be extended to allow for ABC + D reactants. The code will be tested with studies of several triatom-atom systems, including H₂O + H and HCN + H. I also plan to extend the four-atom dynamics work to electronically non-adiabatic processes. For example, one new and interesting problem it should then be possible to tackle is the conversion of singlet to triplet methylene, $^1\text{CH}_2 + \text{H} \rightarrow ^3\text{CH}_2 + \text{H}$, for which Harding will provide the relevant electronic structure information.

References

- [1] Y. He, E. M. Goldfield, and S. K. Gray, *J. Chem. Phys.* **121**, 823 (2004).
- [2] S. K. Gray and G. G. Balint-Kurti, *J. Chem. Phys.* **108**, 950 (1998).
- [3] M. D. Marshall, B. V. Pond, and M. I. Lester, *J. Chem. Phys.* **118**, 1196 (2003).
- [4] B. V. Pond and M. I. Lester, *J. Chem. Phys.* **118**, 2223 (2003).
- [5] M. J. Lakin, D. Troya, G. C. Schatz, and L. B. Harding, *J. Chem. Phys.* **119**, 5848 (2003).
- [6] D. M. Medvedev, E. M. Goldfield, and S. K. Gray, *Comp. Phys. Comm.* **166**, 94 (2005). This work was funded by DOE's Scientific Discovery through Advanced Computing, or SciDAC, program.
- [7] T. G. Clements, R. E. Continetti, and J. S. Francisco, *J. Chem. Phys.* **117**, 6478 (2002).
- [8] R. G. Macdonald and K. Liu, *J. Chem. Phys.* **89**, 4443 (1988).
- [9] A. McIlroy and F. P. Tully, *J. Chem. Phys.* **99**, 3597 (1993).
- [10] R. A. Brownsword, A. Canosa, B. R. Rowe, I. R. Sims, I. W. M. Smith, D. W. A. Stewart, A. C. Symonds and D. Travers, *J. Chem. Phys.* **106**, 7662 (1997).
- [11] R. A. Eng, G. E. Goos, H. Hippler, and C. Kachiani, *Phys. Chem. Chem. Phys.* **3**, 2258 (2001).
- [12] D. M. Medvedev, S. K. Gray, and L. B. Harding, *Mol. Phys. (Mark Child Issue)*, *submitted* (2005).
- [13] S. K. Gray and E. M. Goldfield, *J. Phys. Chem. A* **105**, 2634 (2001).
- [14] D. M. Medvedev, S. K. Gray, E. M. Goldfield, M. J. Lakin, D. Troya, and G. C. Schatz, *J. Chem. Phys.* **120**, 1231-1238(2004).

DOE COMBUSTION PROGRAM SUPPORTED PUBLICATIONS (2003-2005)

1. I. Miquel, M. Gonzalez, R. Sayos, G. G. Balint-Kurti, S. K. Gray, and E. M. Goldfield, Quantum reactive scattering calculations of cross sections and rate constants for the $\text{N}(^2\text{D}) + \text{O}_2(\text{X}) \rightarrow \text{O}(^3\text{P}) + \text{NO}(\text{X})$ reaction, *J. Chem. Phys.* **118**, 3111-3123 (2003).
2. M. Hankel, G. G. Balint-Kurti, and S. K. Gray, Sinc wavepackets: A new form of wavepacket for time-dependent quantum mechanical reactive scattering calculations, *Int. J. Quant. Chem.* **92**, 205-211 (2003).
3. P. Defazio and S. K. Gray, Quantum dynamics study of the $\text{D}_2 + \text{OH} \rightarrow \text{DOH} + \text{D}$ reaction on the

- WSLFH potential energy function, *J. Phys. Chem. A* **107**, 7132-7137 (2003).
4. T. Lu, E. M. Goldfield, and S. K. Gray, The equilibrium constants for molecular hydrogen adsorption in carbon nanotubes based on iteratively determined nano-confined bound states *J. Theor. Comp. Chem.* **2**, 621-626 (2003).
 5. T. Lu, E. M. Goldfield, and S. K. Gray, Quantum states of molecular hydrogen and its isotopes in single-walled carbon nanotubes, *J. Phys. Chem. B*, **107**, 12989-12995 (2003).
 6. D. M. Medvedev and S. K. Gray, A new expression for the direct quantum mechanical evaluation of the thermal rate constant, *J. Chem. Phys.* **120**, 9060-9070 (2004).
 7. D. M. Medvedev, S. K. Gray, E. M. Goldfield, M. J. Lakin, D. Troya, and G. C. Schatz, Quantum wave packet and quasiclassical trajectory studies of OH + CO: Influence of the reactant channel well on thermal rate constants, *J. Chem. Phys.* **120**, 1231-1238(2004).
 8. Y. He, E. M. Goldfield, and S. K. Gray, Quantum dynamics of vibrationally activated OH-CO reactant complexes, *J. Chem. Phys.* **121**, 823-828 (2004).

SKG was supported by the Office of Basic Energy Sciences, Division of Chemical Sciences, Geosciences, and Biosciences, U.S. Department of Energy under Contract No. W-31-109-ENG-38.

Computer-Aided Construction of Chemical Kinetic Models

William H. Green, Jr., MIT Department of Chemical Engineering,
77 Massachusetts Ave., Cambridge, MA 02139. email: whgreen@mit.edu

Project Scope

The combustion chemistry of even simple fuels can be extremely complex, involving hundreds or thousands of kinetically significant species. The most reasonable way to deal with this complexity is to use a computer not only to numerically solve the kinetic model, but also to construct the kinetic model in the first place. We are developing the methods needed to make computer-construction of accurate combustion models practical, as well as tools to make it feasible to handle and solve the resulting large kinetic models with rigorous error control, even in CFD reacting flow situations. Many of the parameters in the models are derived from quantum chemistry, and the models are compared with experimental data measured by our collaborators or in our lab.

Recent Progress

We have applied the new tools we have developed to several technological problems, including pyrolysis and oxidative chemistry of molecules with 5 or 6 carbons, and (with additional support from DOE's Transportation Technologies division) to predict the performance of homogeneous charge compression-ignition (HCCI) engines. We also have begun to address the serious human-interface issues: developing methods to document the large mechanisms constructed using computer-aided modeling software, and to make it feasible for humans to see (and so be able to check) the assumptions underlying the kinetic simulation. We have focused considerable effort on data models and software architecture, to make it practical for other scientists to easily and correctly extend the software and databases to address new systems. (The computer-science-oriented aspects of this effort are financially supported primarily by DOE's MICS division and by NSF; the combustion)

The research necessarily spans the range from quantum chemical calculations on individual molecules and elementary-step reactions, through the development of improved rate/thermo estimation procedures based on generalizations, to the creation of algorithms and software for constructing and solving the simulations.

Notable accomplishments during this grant period include:

- 1) Development of the first automated reaction-mechanism generation software that is easily extensible to incorporate new chemistry knowledge. We are beginning to distribute this software, along with extensive documentation and databases.
- 2) Use of the above software to construct models for the hexane pyrolysis data measured in Marin's lab, and for the neo-pentane oxidation experiments conducted in Taatjes's lab. In both cases the accurate detailed models reveal features of the chemistry that were unexpected and difficult to infer from the experimental data alone.
- 3) Development of general-purpose software for going beyond the Pitzer-Gwinn approach to hindered rotors, to more accurately calculate reaction rates and thermochemistry. The Pitzer-Gwinn approximations

were found to be quite accurate when the hindered rotor is a symmetric top (e.g. methyl groups),[19] but significant errors arise for heavy asymmetric rotors or when the rotor mode is strongly coupled to a low-frequency vibrational mode. We will publicly distribute software that automatically computes the most important corrections.

- 4) Development of the first rigorous method for controlling the error associated with use of reduced chemistry models in CFD reacting-flow simulations.[18] The complete description of this method has been submitted to *Combustion & Flame*.
- 5) Demonstration (in collaboration with Paul Barton) of several new global optimization algorithms and applications of interval analysis, e.g. [8,17,18]. Most importantly, we recently demonstrated the first algorithm guaranteed to find the best-fit to the nonlinear least-squares problems that arise in kinetics (paper submitted to *J. Phys. Chem.*)

Future Plans

We are now preparing a public version of our kinetic modeling software, and a corresponding rate and thermo estimation parameter database, suitable for wide distribution among the combustion chemistry community. In addition to speeding the construction of chemistry models needed for different applications, we believe that the transparency of the assumptions in our approach will facilitate high quality peer reviews, and so improve the quality of large combustion chemistry models. (With existing software and approaches, it is very difficult to check the large models.) We are currently adding the capability to compute uncertainty estimates to the model predictions, make it much easier to sensibly test the models vs. data. The uncertainty estimates are critical so users will know how much credence to give the model predictions in cases where there are no data available.

We will apply our new high-accuracy method (*J. Am. Chem. Soc.* 2004) for predicting PAH thermochemistry to develop a thermodynamically-consistent soot formation model. (Most existing soot-formation models include some irreversible steps. Many of the steps in soot formation are partially equilibrated, so the thermochemistry is crucial.)

We will also compute the thermochemistry and rates for reactions important in combustion of organic nitrogen and organic phosphorus compounds. Our published predictions of the high temperature oxidation of methyl phosphonic acid (*Phys. Chem. Chem. Phys.* 2004), are in very encouraging agreement with experiment.

Publications Resulting from DOE Sponsorship (Since 2003)

1. D.M. Matheu, W.H. Green, and J.M. Grenda, "Capturing Pressure-Dependence in Automated Mechanism Generation: Reactions Through Cycloalkyl Intermediates", *Int. J. Chem. Kinet.* **35**, 95-119 (2003).
2. J.M. Grenda, I.P. Androulakis, A.M. Dean, and W.H. Green, "Application of Computational Kinetic Mechanism Generation to Model the Autocatalytic Pyrolysis of Methane", *Ind. Eng. Chem. Res.* **42**, 1000-1010 (2003).
3. D.A. Schwer, P. Lu, & W.H. Green, "An Adaptive Chemistry approach to modeling Complex Kinetics in Reacting Flows", *Combust. Flame* **133**, 451-465 (2003).

4. B. Bhattacharjee, D.A. Schwer, P.I. Barton, & W.H. Green, "Optimally-Reduced Kinetic Models: Reaction Elimination in Large-Scale Kinetic Mechanisms", *Combust. Flame* **135**, 191-208 (2003).
5. C.D. Wijaya, R. Sumathi, and W.H. Green, "Cyclic Ether Formation from Hydroperoxyalkyl Radicals (QOOH)", *J. Phys. Chem. A* **107**, 4908-4920 (2003).
6. B. Wong, D.M. Matheu, and W.H. Green, "The Temperature and Molecular Size Dependence of the High-Pressure Limit", *J. Phys. Chem. A* **107**, 6206-6211 (2003).
7. D.A. Schwer, P. Lu, W. H. Green, and V. Semiao, "A Consistent-Splitting Approach to Computing Stiff Steady-State Reacting Flows with Adaptive Chemistry", *Combust. Theory & Modelling* **7**, 383-399 (2003).
8. P. Lu, B. Bhattacharjee, P.I. Barton & W.H. Green, "Reduced Models for Adaptive Chemistry Simulation of Reacting Flows", in *Computational Fluid & Solid Mechanics*, ed. by K.J. Bathe (Elsevier, 2003).
9. D.M. Matheu, J.M. Grenda, M. Saeys, & W.H. Green, "New, computer-discovered pathways for methane and ethane pyrolysis", *Preprints of the ACS Division of Fuel Chemistry* (2003). [awarded Glenn prize by ACS Fuels Division]
10. D.M. Matheu, A.M. Dean, J.M. Grenda, and W.H. Green, "Mechanism Generation with Integrated Pressure-Dependence: A New Model for Methane Pyrolysis", *J. Phys. Chem. A* **107**, 8552-8565 (2003).
11. R. Sumathi and W.H. Green, "Oxygenate, Oxyalkyl, and Alkoxy-carbonyl Thermochemistry and Rates for Hydrogen Abstraction from Oxygenates", *Phys. Chem. Chem. Phys.* **5**, 3402-3417 (2003).
12. P.E. Yelvington, M. Bernat i Rollo, S. Liput, J. Yang, J.W. Tester, & W.H. Green, "Predicting Performance Maps for HCCI Engines", *Combust. Sci. & Tech.* **176**, 1243-1282 (2004).
13. W.H. Green, C.D. Wijaya, P.E. Yelvington, & R. Sumathi, "Predicting Chemical Kinetics with Computational Chemistry: Is QOOH = HOQO Important in Fuel Ignition?", *Mol. Phys.* **102**, 371-380 (2004).
14. H. Richter, S. Granata, W.H. Green, & J.B. Howard, "Detailed Modeling of PAH and Soot Formation in a Laminar Premixed Benzene/Oxygen/Argon Low-Pressure Flame", *Proc. Combust. Inst.* (2004).
15. H. Ismail, J. Park, B.M. Wong, W.H. Green, & M.C. Lin, "A Theoretical and Experimental Kinetic Study of Phenyl Radical Addition to Butadiene", *Proc. Combust. Inst.* (2004).
16. J.W. Taylor, G. Ehlker, H.-H. Carstensen, L. Ruslen, R.W. Field, & W.H. Green, "Direct Measurement of the Fast Reversible Addition of Oxygen to Cyclohexadienyl Radicals in Nonpolar Solvents", *J. Phys. Chem. A* **108**, 7193-7203 (2004).
17. B. Bhattacharjee, P. Lemonidis, W.H. Green and P.I. Barton "Global Solution of Semi-infinite Programs", *Mathematical Programming (Series A)* (2005, in press).
18. O.O. Oluwole and W.H. Green, "Rigorous Error Control in Reacting Flow Simulations Using Reduced Chemistry Models", *Computational Fluid and Solid Mechanics: Proceedings of the Third MIT Conference on Computational Fluid & Solid Mechanics*, ed. by K.J. Bathe (Elsevier, 2005, in press).

19. B.M. Wong & W.H. Green, "Effects of Large-Amplitude Torsions on Partition Functions: Beyond the Conventional Separability Assumption", *Mol. Phys.* **103**, 1027-1034 (2005).

HIGH-RESOLUTION SPECTROSCOPIC PROBES OF CHEMICAL DYNAMICS*

Gregory E. Hall (gehall@bnl.gov)

Chemistry Department, Brookhaven National Laboratory, Upton, NY 11973-5000

PROGRAM SCOPE

This research is carried out as part of the Gas Phase Molecular Dynamics group program in the Chemistry Department at Brookhaven National Laboratory. High-resolution spectroscopic tools are developed and applied to problems in chemical dynamics. Recent topics have included the state-resolved studies of collision-induced electronic energy transfer, dynamics of barrierless unimolecular reactions, and the kinetics and spectroscopy of transient species.

RECENT PROGRESS

Collision-induced singlet-triplet transitions in CH₂

Last year, we reported detailed kinetic and spectroscopic studies on collision-induced intersystem crossing in CH₂. We have observed state-resolved relaxation of velocity distributions and rotational distributions of CH₂ during the thermalization following ketene photolysis at 308 nm. Seeking a signature of mixed-state kinetics, we compared transient kinetics for both members of two different mixed state pairs. In the photolysis, the dominant singlet and triplet components of these mixed states are initially formed in proportion to their singlet character, but the triplet grows and the singlet decays, converging to a common time dependence even faster than translational thermalization. On timescales longer than required for translational and rotational thermalization of singlet CH₂, we observed biexponential kinetics, indicative of reversible singlet-triplet conversion occurring faster than vibrational relaxation of the triplet. The two nuclear spin modifications of singlet CH₂ show distinct kinetic differences, most significantly in the ratio of fast to slow decay amplitudes. The vibrational energy of the triplet members of the dominant mixed states of *ortho* or *para* nuclear spin is evidently the controlling factor. Simplified master equation models can account for the observations; equilibrium kinetics cannot. We have extended this work along several lines described below.

Temperature dependence of intersystem crossing in CH₂

An approximate mixed-state model¹ of collision-induced ISC in CH₂ gives the rate as

$$k_{isc} \approx \sum_i \beta_i^2 (1 - \beta_i^2) f_i k_{rot}$$

a sum over mixed states i , with β^2 the fractional triplet character of

the dominant singlet component of each mixed state pair i , f_i the rotational Boltzmann fraction and k_{rot} the total rotationally inelastic energy transfer rate constant. Chance differences between the energies and mixing coefficients of the mixed states of *ortho* and *para* symmetry lead to previously untested differences in the temperature dependence of intersystem crossing rates between the two nuclear spin symmetry modifications. Low-energy, weakly coupled *para* states and higher energy, more strongly coupled *ortho* states have significantly different predicted temperature-dependent rates of intersystem crossing that coincidentally cross near room temperature. Previous temperature-dependent studies had not compared *ortho* and *para* states, although they are known to be similar at room temperature. Between 300K and 500K, we find only slight temperature dependence, and no significant differences between *ortho* and *para* states in the rare-gas dependence of the initial loss rate of CH₂ populations. We do, however, see a significant increase with temperature in the relative amplitude of the slow component of the bi-exponential decay for *ortho* states, and an even more dramatic increase in the slower components of the decay for *para* states, requiring more than double-exponential forms for accurate fitting. Clearly, the reverse flux from excited triplet back to singlet is enhanced at elevated temperatures, but we do not yet have a fully consistent interpretation of these observations.

Double-resonance studies of energy transfer in CH₂

Because of the close connection between collision-induced intersystem crossing and rotational energy transfer in the sparse mixed-state limit, we have initiated a double resonance study of collisional energy transfer in CH₂. In these new experiments, individual CH₂ rotational levels are bleached by a tunable ns dye laser operating in the 590 nm region, while monitoring the populations of the same or nearby rotational levels with near-infrared transient FM spectroscopy. Saturation recovery and saturation transfer have been characterized using this technique for “normal” and mixed rotational levels. Figure 1 shows a saturation recovery signal for a

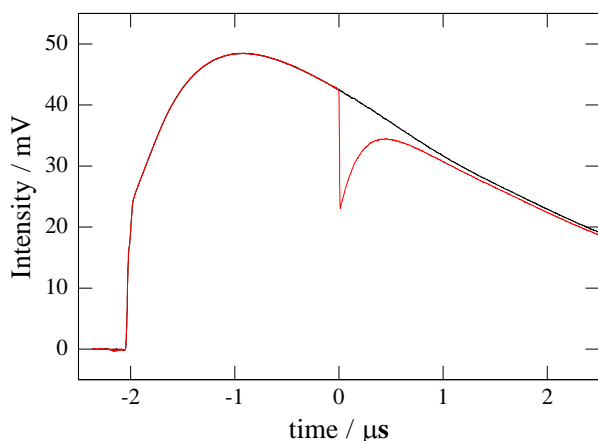


Figure 1. Saturation and recovery of CH₂ absorption signal. Ketene photolysis at $t = -2 \mu\text{s}$ creates CH₂ sample, which is rotationally thermalized by $t = 0$. Probe CH₂ a state (0,0,0) 4_{14} with near-infrared FM spectroscopy; bleach same level with ns yellow dye laser at $t = 0$.

“normal” singlet rotational level, with and without the saturation laser. The probe laser frequency is fixed at the peak of the room-temperature FM absorption line, and a few mJ from the ns dye laser is sufficient to saturate the full Doppler line. The fractional depletion recovers from ~45% to a final value nearly equal to the initial depletion ratio times the Boltzmann fraction of the bleached state at 300K. These observations are consistent with simple rotational thermalization of the hole in the a state rotational distribution, *i.e.*, no significant repopulation of the a state (0,0,0) levels from the optically saturated b state level, and no interconversion of *ortho* and *para* CH₂ on this timescale. The kinetics of saturation transfer to other rotational states have also been investigated.

Growth rates vary with the choice of saturated and probed rotational levels, and final values are also consistent with rotational thermalization of the hole. Relatively efficient coupling between nearby levels, such as 2_{12} and 4_{14} , is revealed by rapid saturation transfer and small overshoot above the final value of depletion. Transfer between more distant, less directly coupled levels proceeds more slowly and does not overshoot. Particularly interesting is the behavior following saturation of single components of a mixed-state pair. We find evidence for extremely strong collisional coupling between the two components of the singlet-triplet mixed-state pair sharing a state (0,0,0) 8_{18} character. Saturation transfer between these states is very rapid, and leads to a more dramatic overshoot above the thermalized saturation value than we have observed for any other pair of states. The rotationally thermalized final values of depletion are furthermore significantly less than that observed for comparable unmixed states, which we tentatively attribute to the deviations from Boltzmann populations of the mixed states at a time when other states are in rotational equilibrium. The double resonance experiments, combined with modeling of the nonequilibrium kinetics of the multi-state relaxation can provide a uniquely detailed test of the mixed-state model for surface crossing in the small molecule limit.

Correlated photochemistry: CH₂CO

In collaboration with Arthur Suits, time sliced, velocity-mapped images of CO photofragments from ketene dissociation have been measured to characterize the correlated product distributions of this benchmark unimolecular dissociation. Despite the relatively low and nearly continuous distribution of recoil velocities for the CO fragments, multiple rings in the CO images can be

observed, corresponding to the irregular density of CH₂ rotational states. An effective velocity resolution on the order of 10 m/s for fragments with no more than 800 m/s of recoil velocity allows for a detailed analysis of the product correlations, to compare with theory and previous work in the laboratories of Wodtke² (UCSB) and Hall³ (BNL). We find the correlated product distributions can be accurately described by a single constraint, in the spirit of a linear surprisal, representing an exponential bias toward low energy CH₂ states with respect to a phase-space theory reference distribution of CH₂ states. Similar patterns were obtained in the direct dynamics study of this unimolecular reaction in collaboration with Klippenstein and Gray.⁴ Previous measurements in the Wodtke lab and at BNL were inconsistent with both the calculations and with these new experimental results, and different types of non-statistical effects were considered to explain the earlier experiments. We think we understand the source of the problems with at least the previous BNL results. The observed deviations from the statistical product distributions are consistent with exit channel coupling beyond a statistically sampled variational transition state.

Polarization quantum beats in photofragments

We have recently completed the analysis of Doppler-resolved transient frequency modulation absorption spectroscopy of low rotational states of CN X ²Σ⁺ photofragments produced in the ultraviolet photodissociation of ICN. We have measured both alignment and orientation quantum beats arising from nuclear hyperfine depolarization of the initially polarized sample. Under our conditions of fully resolved fine-structure and completely unresolved hyperfine structure, the observed time evolution is insensitive to the rapid depolarization of angular momentum **N** that would be observed if the fine-structure components were not resolved. Nonstatistical spin-rotation populations of CN photofragments, previously observed only for high rotational states, are now observed even for the lowest rotational states, indicating that the electron cannot be considered a spectator spin in either the photodissociation or the depolarization. Further work continues on the interpretation of Doppler-resolved circular dichroism of CN photofragments. Particularly for low angular momentum states, for which semiclassical stereodynamical arguments are inadequate, analysis of polarized Doppler lineshapes will be sensitive to phase-dependent properties of the multiple-surface paths. Correct treatment of hyperfine depolarization is then essential to extract the nascent photofragment polarization properties.

FUTURE WORK

Nonequilibrium kinetics of singlet CH₂

Following clarification of the intersystem crossing kinetics with rare gases, similar measurements in the presence of reactive gases such as H₂O, O₂ and H₂ will be performed. Compared to the rare gases, we will look for differences in the evolution of the state distribution and total singlet survival probability as the nascent CH₂ ensemble thermalizes, reacts, and interconverts with triplet. Recent work from the laboratories of Hancock⁵ (Oxford) and Pilling⁶ (Leeds) on the ¹CH₂ + O₂ reaction indicating that quenching to ³CH₂ is the only significant channel implies that mixed states have little to do with this much more efficient intersystem crossing process. Our preliminary measurements with O₂ show strongly curved semi-logarithmic decays, and require open-minded interpretation. We have the tools in hand to explore these interesting questions.

Double-resonance studies in CH₂

The same experiment used for energy transfer studies in CH₂ has very recently provided confirmation of a theoretical assignment⁷ of some sharp lines observed but never assigned by

Herzberg in the near-ultraviolet *c-a* system. With a visible dye laser tuned to a known transition in the *b-a* spectrum, the near-ir FM laser is scanned in the region of the predicted *c-b* transition, seeking an *increase* in the probe absorption on resonance. The method shows good discrimination against background *a-b* transitions observed with the probe laser alone, and shared *a* state double-resonance signals, which have the opposite sign. Several of the tentative assignments of Bunker and co-workers have been confirmed in preliminary studies, to be continued in close collaboration with Trevor Sears.

Cited References

1. U. Bley and F. Temps, *J. Chem. Phys.*, 1993, **98**, 1058.
2. G. C. Morgan, M. Drabbels, and A. M. Wodtke, *J. Chem. Phys.*, 1996, **104**, 7460.
3. M. L. Costen, H. Katayanagi, and G. E. Hall, *J. Phys. Chem. A*, 2000, **104**, 10 247.
4. K. M. Forsythe, S. K. Gray, S. J. Klippenstein, and G. E. Hall, *J. Chem. Phys.*, 2001, **115**, 2134.
5. G. Hancock and V. Haverd, *Chem. Phys. Lett.*, 2003, **372**, 288.
6. M. A. Blitz, K. W. McKee, M. J. Pilling, and P. W. Seakins, *Chem. Phys. Lett.*, 2003, **372**, 295.
7. S. N. Yurchenko, P. Jensen, Y. Li, R. J. Buenker, and P. R. Bunker, *J. Mol. Spectrosc.*, 2001, **208**, 136.

DOE SPONSORED PUBLICATIONS SINCE 2002

Hyperfine quantum beats from photolytic orientation and alignment

M. L. Costen and G. E. Hall

Phys. Chem. Chem. Phys., **7** 1408-13 (2005)

Doppler-resolved spectroscopy as an assignment tool in the spectrum of singlet methylene

G. E. Hall, A. Komissarov and T. J. Sears

J. Phys. Chem. A, **108** 7922-27 (2004)

The photodissociation of bromoform at 248 nm: Single and multiphoton processes

P. Zou, J. Shu, T. J. Sears, G. E. Hall and S. W. North

J. Phys. Chem. A, **108**, 1482-8 (2004)

Superexcited state dynamics probed with an extreme-ultraviolet free electron laser

W. Li, R. Lucchese, A. Doyuran, Z. Wu, H. Loos, G. E. Hall and A. G. Suits

Phys. Rev. Lett., **92**, 083002 (2004)

Imaging O (³P) + alkane reactions in crossed beams: vertical vs. adiabatic H abstraction dynamics

X. Liu, R. L. Gross, G. E. Hall, J. T. Muckerman and A. G. Suits

J. Chem. Phys. **117**, 7947-59 (2002)

Axis-Switching and Coriolis coupling in the A (010) - X (000) transitions of DCCl and HCCl

A. Lin, K. Kobayashi, H-G Yu, G. E. Hall, J. T. Muckerman, T. J. Sears and A. J. Merer

J. Mol. Spectr. **214**, 216-24 (2002)

The E ³Π – X ³Δ transition of jet-cooled TiO observed in absorption

K. Kobayashi, G. E. Hall, J. T. Muckerman, T. J. Sears and A. J. Merer

J. Mol. Spectr. **212**, 133-41 (2002)

* This work was performed at Brookhaven National Laboratory under Contract No. DE_AC02_98CH10886 with the U.S. Department of Energy and supported by its Division of Chemical Sciences.

Flame Chemistry and Diagnostics

Nils Hansen

Combustion Research Facility, Sandia National Laboratories, Livermore, CA 94551-0969

Email: nhansen@sandia.gov

SCOPE OF THE PROGRAM

The goal of this program is to provide a rigorous basis for the elucidation of chemical mechanisms of combustion, combining experimental measurements employing state of the art combustion diagnostics with detailed kinetic modeling. The experimental program concentrates on the development and application of combustion diagnostics for measurements of key chemical species concentrations. These measurements are carried out in low-pressure, one-dimensional laminar flames and are designed to serve as benchmarks for the validation of combustion chemistry models. Comparison of experimental data to models employing detailed chemical kinetics is critical to determining important chemical pathways in combustion and in pollutant formation in combustion systems. As turbulent combustion models become increasingly sophisticated, accurate chemical mechanisms will play a larger role in computations of realistic combustion systems. Verification of detailed chemistry models against a range of precise measurements under thoroughly-characterized steady conditions is necessary before such flame models can be applied with confidence in turbulent combustion calculations.

PROGRESS REPORT

Molecular Beam Mass Spectrometry at the Advanced Light Source

In collaboration with Terrill A. Cool of Cornell University and Phillip R. Westmoreland of the University of Massachusetts, great progress has been made measuring low pressure flames using molecular beam mass spectrometry with synchrotron photoionization at the Advanced Light Source at Lawrence Berkeley National Laboratory. The molecular-beam photoionization mass spectrometer (PIMS) is now in full operation. In the past year, different flames over a wide range of stoichiometry using the following fuels have been characterized, and the data is currently being reduced for comparison to detailed models: allene, benzene, cyclohexane, cyclopentene, ethanol, ethylene, methane, propane, propene, and propyne.

Enols are common combustion intermediates: With its intense, finely tunable VUV photons, the ALS flame experiment allows discrimination of many isomeric species by their photoionization thresholds. This feature led to the discovery of ethenol (vinyl alcohol) in a rich ($\phi = 1.9$) ethene flame. Now, a systematic search for enols has been undertaken among different flames of prototypical single fuels representing the major classes of chemicals appearing in modern fuel blends: alkanes, alkenes, alkynes, cyclic hydrocarbons, aromatics, and alcohols. Ethenol has been identified unmistakably in flames fueled by propyne ($\phi = 1.8$), benzene ($\phi = 1.0$), cyclohexane ($\phi = 2.0$), 1,3-butadiene ($\phi = 1.46$), ethanol ($\phi = 1.97$, $\phi = 1.0$), propene ($\phi = 2.3$, $\phi = 1.68$), allene ($\phi = 1.8$ and $\phi = 1.0$), cyclopentene ($\phi = 2.0$), and ethene ($\phi = 2.1$ to $\phi = 1.2$). Interestingly, ethenol is below the present detection limit in ethane, methane, propane and 2-propanol flames.

In fact, a rich and previously unsuspected enol chemistry occurs in a wide range of flames. The photoionization efficiency curves for $m/z = 58$ sampled from a stoichiometric ($\phi = 1.0$) cyclohexane flame and a rich ($\phi = 1.44$) ethanol flame show significant contribution with a threshold near 8.7 eV, which is assigned to ionization of either propen-1-ol or propen-2-ol. This is the first observation of propenol in any hydrocarbon flame, and it demonstrates that the chemistry of larger enols must be included in flame modeling.

Photoionization Spectra of Flame Species: The identification of chemical species in a flame with VUV PIMS involves measurement of the photoionization efficiency spectra. It is thereby sometimes possible to provide new ionization potential data from flame-sampled MBMS experiments. These determinations do not approach state-of-the-art precision, but are useful in cases where no other experimental measurements are yet available. Especially, flames may be used to acquire information about short-lived species that are hard to obtain in other ways.

We applied photoionization mass spectrometry to the study of C_3H_2 sampled from a rich cyclopentene flame. The photoionization efficiency has been measured between 8.5 eV and 11.0 eV. Franck-Condon factors for photoionization are derived from calculated geometries and force constants of the cation and neutral of the two-lowest-energy C_3H_2 isomers (triplet propargylene – HCCCH, prop-2-ynylidene) and singlet cyclopropenylidene (cyclo-HCCCH). Comparison of the calculated Franck-Condon envelopes with the experimental photoionization

efficiency spectrum determines the adiabatic ionization energy of triplet propargylene to be 8.96(4) eV.

In collaboration with S. J. Klippenstein, several C₄/C₅ species have been identified in fuel rich allene, propyne, and cyclopentene flames. For example the i-C₄H₃ radical (CH₂CCCH) was identified in those flames and the adiabatic ionization energy is determined to 8.02 eV. The two most stable linear isomers of C₅H₃ contribute to the m/z = 63 signal. A detailed Franck-Condon analysis yields adiabatic ionization energies of 8.19 eV (CH₂CCCCH) and 8.28 eV (CHCCHCCH). A possible contribution of the most stable five-membered ring isomer is not conclusive at this point.

C₂-Species diagnostics: In collaboration with J. H. Frank we are developing a laser-induced fragmentation fluorescence (LIFF) technique for probing vinyl (C₂H₃) and acetylene (C₂H₂) in premixed laminar low-pressure flames. As part of the development, we will conduct a series of low-pressure flame experiments to quantify the temperature dependence of the LIFF signal by combining LIFF measurements with photoionization mass spectrometry in a low-pressure flame at the ALS. The mass spectrometer will provide quantitative measurements of the vinyl and acetylene profiles in the flames which will then be compared with the LIFF signal profiles.

FUTURE DIRECTIONS

In recent work, different C₆H₆ isomers have been identified in fuel-rich allene and propyne flames. Besides benzene, fulvene is clearly identified by its ionization energy of 8.3 eV. The limitations on identifying more isomers appear to be uncertainties about the shapes of their PIE curves. It is planned to measure those during the next beam cycle.

To improve the resolution of the time-of-flight mass spectrometer used in the described ALS experiments a reflectron will be installed. Early calculations predict an improvement of the resolution by one order of magnitude. This will help to separate accidentally overlapped species like ketene and propene and to separate isotopic contributions to the target signal.

One key immediate task is the analysis of the large body of ALS data accumulated in the past year, which may compel further or confirmatory measurements during subsequent beam cycles. However, several new areas of investigation are planned for the ALS flame experiments. Studies of oxygenated fuel chemistry will continue with investigations of aldehydes (ethanal,

propanal) and ketones. In addition, esters, as contents in biodiesel, are of considerable interest. Doping these fuels in a well-characterized H₂/O₂ flame may be an attractive alternative or complement to pure-fuel studies. For cyclic aliphatic fuels (e.g. cyclohexane, cyclopentene), dehydrogenation of the cycloalkanes will compete with fragmentation and ring-opening; the isomeric selectivity of the ALS photoionization will have a large impact in unraveling chemical pathways.

In collaboration with L. A. Rahn and D. J. Leahy we will incorporate the ALS flame data into the web based “Collaboratory for Multi-Scale Chemical Science – CMCS” (<http://cmcs.org>). This will make the data widely available for the interested scientific community – especially theorists will be able to compare their flame models with the data.

PUBLICATIONS ACKNOWLEDGING BES SUPPORT 2003-PRESENT

1. P. Wilcox, E. t. H. Chrysostom, A. McIlroy, J.W. Daily, I. M. Kennedy, “Measurement of CrO in flames by cavity ringdown spectroscopy,” *Appl. Phys. B* **77**, 535-540 (2003).
2. T. A. Cool, K. Nakajima, T. A. Mostefaoui, F. Qi, A. McIlroy, P. R. Westmoreland, M. E. Law, L. Poisson, D. S. Peterka, M. Ahmed, “Selective detection of isomers with photoionization mass spectrometry for studies of hydrocarbon flame chemistry,” *J. Chem. Phys.* **119**, 8356-8365 (2003).
3. J. Bood, A. McIlroy, and D. L. Osborn, “Cavity-enhanced frequency modulation absorption spectroscopy of the sixth overtone band of nitric oxide,” *Proc. SPIE* **4962**, 89-100 (2003).
4. M. Kamphus, N.-N. Liu, B. Atakan, F. Qi and A. McIlroy, “REMPI Temperature measurement in molecular beams sampled from low-pressure flames,” *Proc. Combust. Inst.* **29**, 2627-2633 (2003).
5. T. A. Cool, K. Nakajima, C. A. Taatjes, A. McIlroy, P. R. Westmoreland, M. E. Law and A. Morel, “Studies of a Fuel-Rich Propane Flame with Photoionization Mass Spectrometry,” *Proc. Combust. Inst.* **30**, 1631-1638 (2004).
6. C. A. Taatjes, D. L. Osborn, T. A. Cool, K. Nakajima, “Synchrotron Photoionization of Combustion Intermediates: The Photoionization Efficiency of HONO,” *Chem. Phys Lett.* **394**, 19-24 (2004).
7. A. McIlroy, A. H. Steeves and J. W. Thoman, Jr. “Chemical Intermediates in Low-Pressure Dimethyl Ether/Oxygen/Argon Flames,” *Combustion and Flame*, accepted.
8. A. McIlroy and F. Qi, “Identifying Combustion Intermediates via Tunable Vacuum Ultraviolet Photoionization Mass Spectrometry,” *Combust. Sci. Technol.*, in press.
9. C. A. Taatjes, S. J. Klippenstein, N. Hansen, J. A. Miller, T. A. Cool, J. Wang, M. E. Law, and P. R. Westmoreland, “Synchrotron Photoionization Measurements of Combustion Intermediates: Photoionization Efficiency of C₃H₂ Isomers,” *Phys. Chem. Chem. Phys.* **7**, 806-813 (2005).
10. C. A. Taatjes, N. Hansen, A. McIlroy, J. A. Miller, J. P. Senosiain, S. J. Klippenstein, F. Qi, L. Sheng, Y. Zhang, T. A. Cool, J. Wang, P. R. Westmoreland, M. E. Law, T. Kasper, and K. Kohse-Höinghaus, “Enols are Common Intermediates in Hydrocarbon Oxidation,” submitted to *Science* (2005).
11. M. E. Law, P. R. Westmoreland, T. A. Cool, J. Wang, C. A. Taatjes, N. Hansen, T. Kasper, “Benzene Formation in a Stoichiometric Cyclohexane Flame,” *Proc. Fourth Joint Meeting US Sections Comb. Inst.* accepted.

SPECTROSCOPY AND KINETICS OF COMBUSTION GASES AT HIGH TEMPERATURES

Ronald K. Hanson and Craig T. Bowman
Department of Mechanical Engineering
Stanford University, Stanford, CA 94305-3032
hanson@me.stanford.edu,ctbowman@.stanford.edu

Program Scope:

This program involves two complementary activities: (1) development and application of cw laser absorption methods for the measurement of concentration time-histories and fundamental spectroscopic parameters for species of interest in combustion; and (2) shock tube studies of reaction kinetics relevant to combustion. Species investigated in the spectroscopic portion of the research include OH, CH₃ and NCN using narrow-linewidth ring dye laser absorption. Reactions of interest in the shock tube kinetics portion of the research include: OH + toluene → products; OH + acetone → products; CH₃ + O₂ → Products; C₂H₆ → 2CH₃; C₃H₈ → CH₃ + C₂H₅; and CH+N₂ → NCN +H.

Recent Progress: Shock Tube Chemical Kinetics

OH Measurements The reaction of hydroxyl [OH] radicals with toluene [C₆H₅CH₃] was studied at temperatures between 911 and 1389 K behind reflected shock waves at pressures of ~2.25 atm. OH radicals were generated by shock heating tert-butyl hydroperoxide [(CH₃)₃-CO-OH], and monitored by narrow-line ring dye laser absorption of the R₁(5) line of the OH A-X (0, 0) band near 306.7 nm. A comprehensive toluene oxidation mechanism was used to model the OH concentration time histories. Rate coefficient data for the reaction of C₆H₅CH₃ with OH were extracted by matching modeled and measured OH concentration time histories behind reflected shocks. The current high temperature data were fit with the lower temperature measurements of Tully et al. (1981) in a two-parameter form, applicable over 570 - 1389 K (see Fig. 1): $k(\text{toluene}+\text{OH}) = 1.62 \times 10^{13} \exp(-1394/T [\text{K}]) [\text{cm}^3/\text{mol}/\text{s}]$.

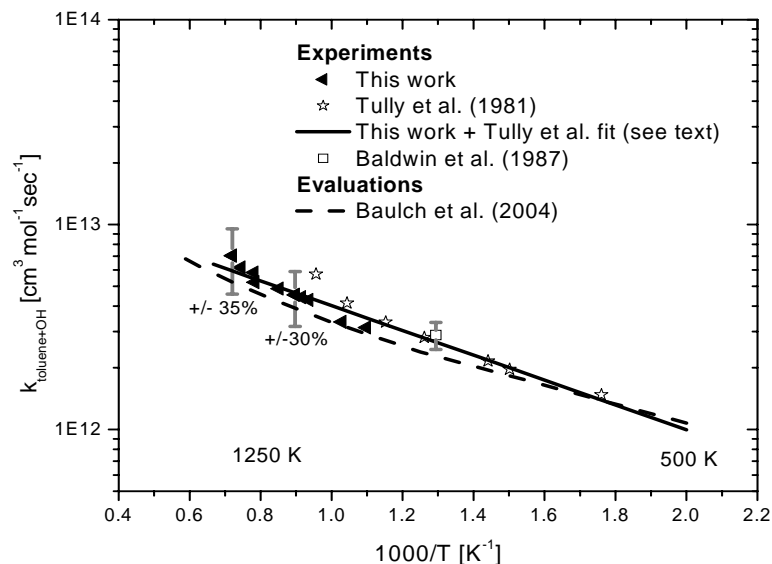


Fig. 1. Arrhenius plot C₆H₅CH₃ + OH → product.

The reaction between OH radicals and acetone [CH₃COCH₃], one of the secondary reactions encountered in the toluene + OH experiments, was measured at temperatures ranging from 982 to 1300 K in reflected shock wave experiments at an average total pressure of 1.65 atm. A multi-parameter fit of the current data with existing lower room temperature measurements yields the following rate expression (see Fig. 2): $k(\text{acetone}+\text{OH}) = 8.0 \times 10^{10} + (6.08 \times 10^8) T^{1.41} \exp(-1289 / T \text{ [K]}) \text{ [cm}^3/\text{mol/s}]$.

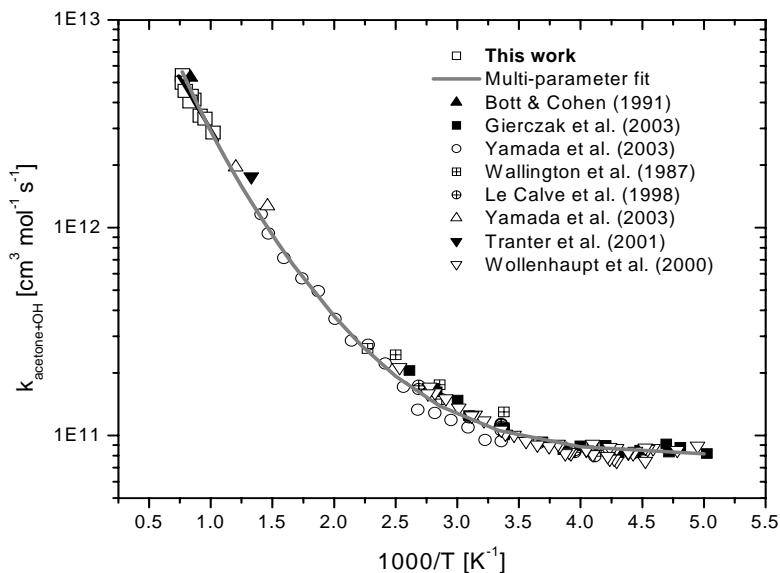


Fig. 2. Arrhenius plot CH₃COCH₃ + OH → products.

CH₃ + O₂ → Products: We have completed a shock tube investigation of the reaction of CH₃ with O₂ from 1600 to 2700 K. The two well-known bimolecular product channels are the dominant reaction pathways at combustion temperatures:



The overall reaction rate coefficient, $k_1 = k_{1a} + k_{1b}$, and individual rate coefficients for the two high-temperature product channels were determined in ultra-lean mixtures of CH₃I and O₂ in Ar/He. Narrow-linewidth UV laser absorption at 306.7 nm was used to measure normalized OH rise times that were sensitive to the overall rate coefficient k_1 but relatively insensitive to the branching ratio. Atomic resonance absorption spectroscopy measurements of O-atoms were used for a direct measurement of channel (1a). Through the combination of measurements using the two different diagnostics, rate coefficient expressions for both channels were determined. Over the temperature range 1600 to 2400 K, $k_{1a} = 6.1 \times 10^7 T^{1.5} \exp(-14200/T) \text{ cm}^3 \text{ mol}^{-1} \text{ s}^{-1}$ and $k_{1b} = 69 T^{2.9} \exp(-4900/T) \text{ cm}^3 \text{ mol}^{-1} \text{ s}^{-1}$.

Ethane and Propane Decomposition: We have completed a shock tube investigation of the decomposition rates of ethane and propane in the fall-off regime at high temperatures using UV narrow-line laser absorption of CH₃ at 216.6 nm. The alkane decomposition reactions are important initiation steps in the detailed reaction mechanisms describing alkane oxidation and in describing global combustion phenomena such as ignition times. Experimental conditions ranged from 1350 to 2050 K and 0.13 to 8.4 atm with mixtures varying in concentration from 100 to 400 ppm of ethane or propane dilute in argon. Decomposition rate coefficients were determined by monitoring the formation rate of CH₃ immediately behind shock waves and modeling the CH₃ formation with a detailed kinetic model.

Recent Progress: Spectroscopy

CH₃ Absorption Coefficient: We have completed measurements of the absorption coefficient (k_v) of CH₃ near 216 nm using external-frequency-doubled laser radiation. The increased power and reduced noise available with this technique, over the previous internal-frequency-doubling technique, has permitted a substantially more accurate measurement of k_v . Three precursors were used as sources of methyl radicals: azomethane CH₃N=NCH₃ which was used at the lowest temperatures, down to 1200 K, methyl iodide CH₃I which was used at intermediate temperatures between 1600 and 2000 K, and ethane C₂H₆ which was used at the highest temperatures up to 2500 K. Excellent agreement in the measured absorption coefficients was found among the different precursors in the overlapping temperature regions. Measurements of the absorption coefficient over a range of wavelengths 210 to 220 nm were also made and compared to those predicted from a symmetric top model. Accurate expressions for the variation of this absorption coefficient with wavelength and temperature are critical to making accurate, quantitative measurements of CH₃ species concentration in our ongoing studies of hydrocarbon kinetics. The least-squares-fit expression for the CH₃ absorption coefficient at 216.62 nm over the temperature range 1200 to 2500 K is (see Fig. 3): $k_{v,CH_3} = 1.475 \times 10^4 T^{-1.004} \exp(2109 \text{ K}/T) \text{ atm}^{-1} \text{ cm}^{-1} (\pm 5\%)$.

NCN and CH Measurements: Current work is focused on developing a continuous wavelength laser absorption system for the NCN radical. This diagnostic is to be used to study the reaction: CH (²Π) + N₂ → Products, in particular H + NCN (³Σ). This reaction, with these products, has been hypothesized to be the major pathway to prompt-NO at high temperatures, rather than the previously considered reaction with the spin-forbidden products HCN + N (4S). There have been no quantitative measurements of NCN concentration time histories performed to date - this study would help substantiate the above hypothesis, and establish the product channels of this key reaction.

A detailed literature survey of NCN spectroscopy has been carried out and the A³Π - X³Σ transition near 329 nm has been identified as a feature that is well suited to monitoring the NCN radical. To the best of our knowledge, a quantitative analysis of this transition has not been carried out. An extensive literature survey was performed to identify strategies to quantitatively calibrate the NCN laser absorption diagnostic. A kinetic calibration scheme using the reaction between CN and N₂O shows promise. This reaction occurs via two pathways that form NCN+NO and NCO+N₂ respectively. Low temperature measurements by Williams et al. indicate that the NCN product pathway is predominant (with a branching ratio of ~1) in the 400-900K temperature range; there have, however, been no prior studies of this reaction system at combustion temperatures. Preliminary theoretical calculations indicate that the NCN pathway continues to be the dominant channel even at elevated temperatures. Geometries were optimized using the B3LYP method and the 6-31++g** basis set, and single point energy calculations were performed on these optimized geometries using the CCSD(T) method and the cc-pVDZ basis set. Rate coefficients for the two channels were evaluated using transition state theory and master equation analysis.

We are, concurrently, trying to identify sources for the CH radical. CH is to be detected using a cw laser absorption diagnostic at 431 nm that has been developed in our laboratory. Light at 431 nm will be generated by pumping a tunable, Coherent 699 ring-dye laser cavity, with an all-line UV beam produced by an Ar⁺ laser. Various CH generation schemes, such as ketene pyrolysis and strategies that involve a combination of pyrolysis and photolysis, have been identified and will be investigated.

Carbon Dioxide-Based Temperature Measurements: One of the most critical problems facing shock tube research is the accurate determination of temperature at long test times. Improvements in this area will extend the useable range of shock tube conditions, particularly at lower temperature where current investigations are demanding longer, and more accurately known, test conditions. We have developed a diagnostic for microsecond time-resolved temperature measurements behind shock waves, based on the ultraviolet laser absorption of vibrationally hot carbon dioxide. Continuous wave laser radiation at 244 and 266 nm is employed to probe the spectrally smooth high-temperature CO₂ ultraviolet absorption and an absorbance ratio technique was used to determine temperature. Measurements behind shock waves in both non-reacting and reacting (ignition) systems and comparisons between isentropic and constant volume calculations have been made.

Future Plans:

1) Continue development of external-cavity frequency-doubling methods for the generation of laser radiation in the deep ultraviolet. Apply these frequency-doubling methods to wavelengths of interest including the detection of CH₃ at 216 nm, the detection of NCN at 329 nm, and the detection of HCO at 230 and 258 nm. 2) Develop multi-pass techniques to improve the sensitivity of current OH laser absorption measurements. 3) Develop experimental approaches to measure the overall rate and product branching ratio of the reaction $\text{CH} + \text{N}_2 \rightarrow \text{NCN} + \text{H}$ using laser absorption. 4) Begin to apply the CO₂-based temperature measurement scheme in shock tube reaction rate measurement experiments.

Recent Publications of DOE Sponsored Research: 2003-2005

1. M. A. Oehlschlaeger, D. F. Davidson and R. K. Hanson, "Temperature Measurements behind Shock Waves Using Ultraviolet Laser Absorption of Carbon Dioxide," submitted to Applied Optics, January (2005).
2. V. Vasudevan, D. F. Davidson and R. K. Hanson, "High Temperature Measurements of the Reaction of OH with Toluene and Acetone," Journal of Physical Chemistry A, in press.
3. V. Vasudevan, D. F. Davidson and R. K. Hanson, "High Temperature Measurements of OH Radical Reactions," Joint Meeting of the US Sections of the Combustion Institute Philadelphia, March (2005).
4. M. A. Oehlschlaeger, D. F. Davidson and R. K. Hanson, "High Temperature UV Absorption of Methyl Radicals behind Shock Waves," Journal of Quantitative Spectroscopy and Radiative Transfer, 92: 393-402 (2005).
5. J. T. Herbon, R. K. Hanson, C. T. Bowman, and D. M. Golden, "The Reaction of CH₃+O₂: Experimental Determination of the Rate Coefficients for the Product Channels at High Temperatures," Proceedings of the Combustion Institute 30: 955-963 (2004).
6. M. A. Oehlschlaeger, D. F. Davidson, and R. K. Hanson, "High Temperature Ethane and Propane Decomposition," Proceedings of the Combustion Institute 30: 1119-1127 (2004); also presented as Paper 03F-56, Western States Section/Combustion Institute Fall Meeting UCLA, October (2003).
7. S. Song, D. M. Golden, R. K. Hanson, C. T. Bowman, J. P. Senosiain, C. B. Musgrave, and G. Friedrichs, "A Shock Tube Study of the Reaction $\text{NH}_2 + \text{CH}_4 = \text{NH}_3 + \text{CH}_3$ and Comparison with Transition State Theory," International Journal of Chemical Kinetics **35**, 304-309 (2003).

Theoretical Studies of Potential Energy Surfaces*

Lawrence B. Harding
Chemistry Division
Argonne National Laboratory
Argonne, IL 60439
harding@anl.gov

Program Scope

The goal of this program is to calculate accurate potential energy surfaces for both reactive and non-reactive systems. Our approach is to use state-of-the-art electronic structure methods (CASPT2, MR-CI, CCSD(T), etc.) to characterize multi-dimensional potential energy surfaces. Depending on the nature of the problem, the calculations may focus on local regions of a potential surface (for example, the vicinity of a minimum or transition state), or may cover the surface globally. A second aspect of this program is the development of techniques to fit multi-dimensional potential surfaces to convenient, global, analytic functions that can then be used in dynamics calculations. Finally a third part of this program involves the use of direct dynamics for high dimensional problems to by-pass the need for surface fitting.

Recent Results

Radical-Radical Association Reactions

Last year, in a collaborative effort with Stephen Klippenstein, we developed a new approach that allows us to accurately calculate radical-radical association rates for systems with 10-15 heavy atoms. The key to this approach came from comparisons of radical-radical interaction potentials from inexpensive CASPT2/cc-pvdz with potentials from more accurate (and expensive) CAS+1+2/aug-cc-pvtz calculations. These comparisons showed that although the CASPT2/cc-pvdz potentials are not as attractive as they should be, addition of a simple one dimensional, R-dependent but orientation independent correction yields potentials that are in very good agreement with the more accurate calculations. Variable reaction coordinate, transition state theory (VRC-TST) calculations on both the corrected CASPT2/cc-pvdz and CAS+1+2/aug-cc-pvtz potentials yield very similar association rates (within ~10% of each other) for a number of smaller systems (H+CH₃, H+C₂H₅, H+C₂H₃, H+CCH, and CH₃+CH₃). We have now used this approach to calculate association rates for a series of H+alkyl radical associations (H+methyl to H+tert-butyl) and a series of alkyl radical+alkyl radical associations (methyl+methyl to tert-butyl+tert-butyl). In both cases we find that each additional methyl substituent, adjacent to a radical site lowers the association rate by approximately a factor of two. The H+alkyl radical associations are all predicted to have modest positive temperature dependences while the alkyl+alkyl rates are all predicted to have fairly strong negative temperature dependences.

To test whether or not the same method gives good results for reactions involving resonance stabilized radicals we have done calculations on the H+propargylene (HCCCH) and methyl+propargyl associations. For H+propargylene we compare the rate calculated with the new approach to the rate calculated on a more accurate CAS+1+2/aug-cc-pvtz potential surface and find the two to be in satisfactory agreement (within 10%). For methyl+propargyl we

compare both the calculated rate and the calculated head-tail branching ratio with the measurements of Fahr¹ and Knyazev². These comparisons are shown in Figures 1 and 2.

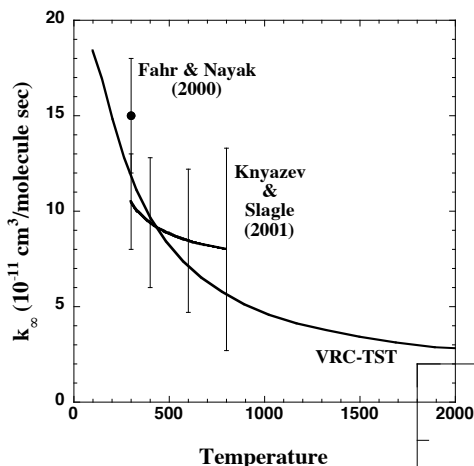


Figure 1. High pressure limit rate constants for the $\text{CH}_3+\text{H}_2\text{CCCH}$ association reaction.

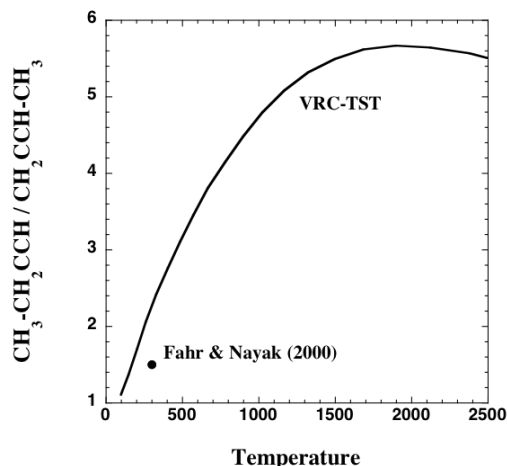
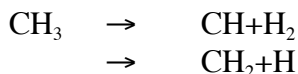


Figure 2. High pressure limit branching ratios for the $\text{CH}_3+\text{H}_2\text{CCCH}$ association reaction.

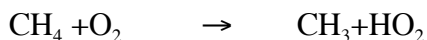
Again very good agreement is found. The calculations predict a strong temperature dependence to the branching ratio, increasingly favoring addition at the CH_2 end at higher temperatures.

CH_3 : We have completed a new analytic surface for CH_3 which gives a realistic description of the two lowest decomposition pathways,



Over 75,000 ab initio (CAS+1+2/aug-cc-pvtz) calculations were done. The fit consists of four full 6th order direct product, multinomials in Morse variables connected by switching functions. One of the multinomials is fit to the full set of ab initio points the other three are more localized fits to points in the vicinity of the CH_3 minimum, the CH_2+H asymptotic region and the $\text{CH}+\text{H}_2$ asymptotic region. Stephen Gray has now used this surface to calculate the lower vibrational levels of CH_3 . It is planned to use this surface in the near future to study the decomposition of CH_3 and the reactions of $\text{CH}+\text{H}_2$ and CH_2+H .

CH_4+O_2 : Joe Michael has recently suggested that the reaction,



may be an important initiation reaction under fuel lean conditions. In collaboration with Stephen Klippenstein, we have begun a theoretical study of this reaction to complement Michael's ongoing experimental study. CCSD(T)/aug-cc-pvtz // CCSD(T)/aug-cc-pvdz calculations predict the existence of a shallow, van der Waals complex between CH_3 and HO_2 separated by a small barrier from CH_4+O_2 . The barrier is predicted to lie below the CH_3+HO_2 asymptote, i.e. there is no net barrier for the reverse reaction. IRC's have been followed using both B3LYP/6-311++G** and MP2/aug-cc-pvdz calculations. Interestingly, CCSD(T) calculations using the geometries from the B3LYP-IRC predict a small net barrier to the reverse reaction while

CCSD(T) calculations using the MP2-IRC geometries predict no net barrier, in agreement with the CCSD(T) transition state optimization. Figure 3 shows a plot of the CH_3+HO_2 interaction potential, including the long-range minimum. Figure 4 shows the results of a variational TST calculation of the CH_4+O_2 rate along with a comparison to Michael's recent measurements,

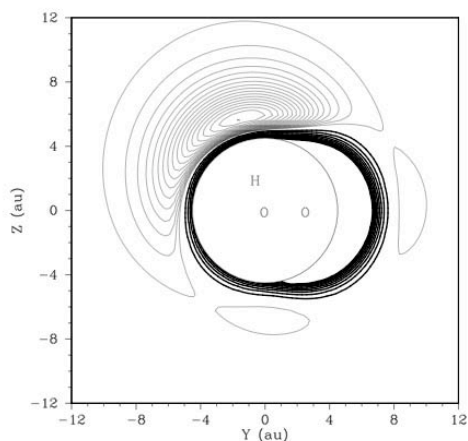


Figure 3. CCSD(T)/aug-cc-pvdz potential for CH_3+HO_2 . Heavy contours are positive (increment=1.0 kcal/mole), light contours are negative (increment=0.1 kcal/mole).

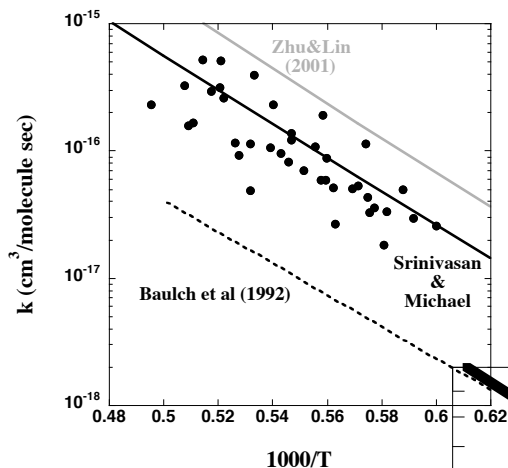


Figure 4. Comparison of the present calculated rate for the reaction $\text{CH}_4 + \text{O}_2 \rightarrow \text{CH}_3 + \text{HO}_2$ (heavy solid line) with new measurements by Michael (dots) and two previous estimates.

the Baulch evaluation and an earlier calculation by Lin³. The calculated rate, Michael's new measurements and Lin's previous calculations are all in good agreement, all being significantly higher than the Baulch evaluation.

Future Work: We intend to continue our studies of radical-radical reactions focusing on two areas, (1) reactions involving resonance stabilized radicals, such as propargyl+propargyl and H+benzyl, and (2) disproportionation channels. For both of these classes of reactions one needs to consider the effects of geometry relaxation, especially at higher temperatures. This can be done using IRC's as we have demonstrated in our calculations on CH_3+HO_2 described above.

We also plan to fit global surfaces for both the lowest doublet and quartet states of H_2NO . These surfaces will allow us to then calculate rates for the reactions,



The reaction of OH with NH has been cited as an important reaction in combustion systems although no experimental data is yet available.

References:

- (1) A. Fahr and A. Nayak, *International J. Chem. Kinetics* **32**, 118 (2000)
- (2) V. D. Knyazev and I. R. Slagle, *J. Phys. Chem.* **105**, 3196 (2001)
- (3) R. Zhu and M. C. Lin, *J. Phys. Chem. A* **105**, 6243 (2001)
- (4) K. J. Hughes, A. S. Tomlin, E. Hampartsoumian, W. Nimmo, I. G. Zsely, M. Ujvari, T. Turanyi, A. R. Clague and M. J. Pilling, *Comb. and Flame* **124**, 573 (2001).

Acknowledgement: This work was performed under the auspices of the Office of Basic Energy Sciences, Division of Chemical Sciences, Geosciences and Biosciences, U.S. Department of Energy, under Contract W-31-109-Eng-38.

PUBLICATIONS (2003 - Present):

Implementation of a Fast Analytic Ground State Potential Energy Surface for the $N(^2D)+H_2$ Reaction

T.-S. Ho, H. Rabitz, F. J. Aoiz, L. Banares, S. A. Vazquez, and L. B. Harding
J. Chem. Phys. **119**, 3063-3070 (2003)

A Quasiclassical Trajectory Study of the Reaction $OH + CO \rightarrow H + CO$

M. J. Lakin, D. Troya, G. C. Schatz and L. B. Harding
J. Chem. Phys. **119**, 5848-5849(2003)

Rate Constants for $D + C_2H_2 \rightarrow C_2HD + H$ at High Temperature: Implications to the High Pressure Rate Constant for $H + C_2H_2 \rightarrow C_2H_3$

J. V. Michael, M.-C. Su, J. W. Sutherland, L. B. Harding, and A. F Wagner
J. Phys Chem A **107**, 10533-10543(2003)

Speciation of C_6H_6 Isomers by GC-Matrix Isolation FTIR-MS

K.B. Anderson, R.S. Trantor, W. Tang, K. Brezinsky and L.B. Harding
J. Phys. Chem. A **108**,3403-3405 2004)

A Global Analytic Potential Surface for Formaldehyde

X. Zhang, S. Zou, L.B. Harding and J.M. Bowman, *J. Phys. Chem A* **108**, 8980-8986 (2004)

The Roaming Atom: Straying from the Reaction Path in Formaldehyde Decomposition

D. Townsend, S.A. Lahankar, S.K. Lee, S.D. Chambreau, A.G. Suits, X. Zhang, J. Rheinecker, L.B. Harding, and J.M. Bowman, *Science* **306**, 1158 (2004)

Reaction of Oxygen Atoms with Hydrocarbon Radicals: A Priori Kinetic Predictions for the CH_3+O , C_2H_5+O and C_2H_3+O Reactions

L.B. Harding, S.J. Klippenstein and Y. Georgievskii
Proc. Combust. Inst. **30**, 985-993 (2005)

Rate Constants for the $D+C_2H_4 \rightarrow C_2H_3D+H$ at High Temperature: Implications to the High Pressure Rate Constant for $H+C_2H_4 \rightarrow C_2H_5$

J.V. Michael, M.-C. Su, J.W. Sutherland, L.B. Harding and A.F. Wagner
Proc. Combust. Inst. **30**, 965-973 (2005)

Predictive Theory for Hydrogen Atom – Hydrocarbon Radical Association Kinetics

L. B. Harding, Y. Georgievskii and S. J. Klippenstein, *J. Phys. Chem. A* (in press)

CHEMICAL ACCURACY FROM AB INITIO MOLECULAR ORBITAL CALCULATIONS

Martin Head-Gordon

Department of Chemistry, University of California, Berkeley, and,
Chemical Sciences Division, Lawrence Berkeley National Laboratory,
Berkeley, CA 94720.
mhg@cchem.berkeley.edu

1. Scope of Project.

Short-lived reactive radicals and intermediate reaction complexes are believed to play central roles in combustion, interstellar and atmospheric chemistry. Due to their transient nature, such molecules are challenging to study experimentally, and our knowledge of their structure, properties and reactivity is consequently quite limited. To expand this knowledge, we develop new theoretical methods for reliable computer-based prediction of the properties of such species. We apply our methods, as well as existing theoretical approaches, to study prototype radical reactions, often in collaboration with experimental efforts. These studies help to deepen understanding of the role of reactive intermediates in diverse areas of chemistry. They also sometimes reveal frontiers where new theoretical developments are needed in order to permit better calculations in the future.

2. Summary of Recent Major Accomplishments.

2.1 *Time-dependent density functional theory calculations.*

Time-dependent density functional theory (TDDFT) is an in-principle exact framework for calculating excitation energies. We have extended TDDFT [1] to treat diradicals with good accuracy starting from a triplet ground state and flipping a spin.

We have applied TDDFT to excited states of polycyclic aromatic hydrocarbon (PAH) cations, which are known intermediates in sooting flames, and also occur in the interstellar medium, as a likely source of the diffuse interstellar bands (DIB's). Accuracy of about 0.3 eV or better for excited states of PAH cations is attainable via TDDFT [9]. On this basis we have contributed to several studies of PAH species [2,3,5,24], where the main features of the experimental electronic spectra have been assigned by TDDFT. Such calculations are feasible on systems up to about 100 non-hydrogen atoms on PC's.

We have also applied TDDFT to study excited states in biological systems [7,11,13,14,21,28]. Perhaps the most interesting results were on excited states of models of chlorophyll and associated carotenoids that are found in the photosynthetic light-harvesting complex [11,13,14]. Our calculations [11,14] are relevant to the mechanism of non-photochemical quenching (NPQ); the process by which excited chlorophyll molecules are directly relaxed under high-light conditions to prevent damage to the reaction center. We showed that both direct singlet-singlet excitation energy transfer, and also a novel electron transfer reaction are energetically feasible. If the latter process is operative, we suggested that it may be experimentally probed by seeking the spectral

signature of the corotenoid radical cation under high-light conditions. Such detection has subsequently just been accomplished in Graham Fleming's group at LBNL.

2.2 *Failure of TDDFT for charge-transfer excited states.*

While TDDFT calculations are clearly often useful, they are far from perfect. For instance various reports suggest poor results for charge-transfer excited states. We have examined the charge-transfer problem in considerable [12,19], and, for the first time clarified both the nature of the problem, and its origin. The long-range Coulomb attraction between donor and acceptor is *entirely absent* in TDDFT using local and gradient corrected functionals. A correct description requires 100% non-local exact exchange. Thus the popular B3LYP functional, which includes 20% exact exchange, has 20% of the correct Coulomb attraction! We also suggested a simple work-around which uses a hybrid of single excitation CI (CIS) (which has 100% exact exchange) for charge-transfer excited states, and regular TDDFT for the localized excitations. Finding more satisfactory solutions to this fundamental problem is now an important issue in DFT.

2.3 *Electron correlations in molecules.*

For molecular ground states, the highest levels of accuracy currently possible come from wavefunction-based calculations, such as CCSD(T) (which are dramatically more expensive than DFT). Yet for radicals, CCSD(T) quite often performs more poorly than for closed shell molecules. In addition to new (more expensive) alternatives [10], we have found that the poor CCSD(T) can be greatly improved by using different orbitals [8]. The Kohn-Sham orbitals are more resistant to symmetry breaking [16], and are the simplest alternative that greatly improves on Hartree-Fock orbitals. We have also addressed the problem of identifying and visualizing the most important correlations from the CCSD doubles amplitudes [22], using a singular value decomposition.

2.4 *Characterizing unpaired electrons in radicals.*

We have proposed a new definition of the unpaired electrons in molecules [4,17], which has a formal advantage over the "distribution of unpaired electrons" that has been explored in recent years. In particular, the latter can in principle yield more unpaired electrons than there are electrons in the molecule, while our new definition does not. This definition involves only single particle information, which makes it particularly simple to use. A novel alternative to characterizing radical, diradical and polyradical character in molecules is to manipulate the wavefunction itself to find the orbitals which have the highest probability of single occupancy (for radical character) or simultaneous single occupancy (for diradical character, and higher) [26]. These methods [4,26] may be useful in helping to qualitatively characterize complex wavefunctions.

2.5 *Application to radicals and radical-radical coupling reactions.*

Radicals such as the neutral PAH, C₁₃H₉ (phenalenyl), and the TCNE anion are known experimentally to form stable pi dimers, characterized by stacking distances of about 3

Angstroms; too short for van der Waal complexes, and yet far too long for a conventional chemical bond. We have recently attempted to understand the nature of this fascinating bonding [20,24], which we find to be a dispersion-assisted diradicaloid bond. Weak bonding interactions between the monomers together with dispersion-driven attraction are sufficient to overcome Pauli repulsions between filled levels and permit approach inside the usual van der Waals radius. Upon ionization of the phenalenyl dimer, there are significant electrostatic perturbations that, remarkably, cause the “1-electron bond” to be stronger than the “2-electron bond”.

3. Summary of Research Plans.

- Exploration of ways to solve the charge-transfer problem in TDDFT
- Development and testing of simplified coupled cluster methods for radicals
- Studies of the properties of reactive radicals and radical reactions

4. Publications from DOE Sponsored Work, 2003-present.

- [1] “The spin-flip approach within time-dependent density functional theory: theory and application to diradicals”, Y. Shao, M. Head-Gordon, and A.I. Krylov, *J. Chem. Phys.* 118, 4807-4818 (2003).
- [2] “Time Dependent Density Functional Theory Calculations of Large Compact PAH Cations: Implications for the Diffuse Interstellar Bands” J.L. Weisman, T.J. Lee, F. Salama, and M. Head-Gordon, *Astrophys. J.* 587, 256-261 (2003).
- [3] “Vibrational and electronic spectroscopy of acenaphthylene and its cation”, J. Banisaukas, J. Szczepanski, J. Eyler, M. Vala, S. Hirata, M. Head-Gordon, J. Oomens, G. Meijer and G. von Helden, *J. Phys. Chem A* 107, 782-793 (2003)
- [4] “Characterizing unpaired electrons from the one-particle density matrix”, M. Head-Gordon, *Chem. Phys. Lett.* 372, 508-511 (2003).
- [5] “Electronic Absorption Spectra of Neutral Perylene ($C_{20}H_{12}$), Terrylene ($C_{30}H_{16}$), and Quaterrylene ($C_{40}H_{20}$) and their Positive and Negative Ions: Ne Matrix-Isolation Spectroscopy and Time Dependent Density Functional Theory Calculations”, T.M. Halasinski, J.L. Weisman, R. Ruitkamp, T.J. Lee, F. Salama, and M. Head-Gordon, *J. Phys. Chem. A* 107, 3660-3669 (2003).
- [6] “Local Correlation Models”, M. Head-Gordon, T. Van Voorhis, G. Beran and B. Dunietz, in “Computational Science: ICCS 2003”, Part IV, Lecture Notes in Computer Science, Vol. 2660, pp. 96-102 (2003).
- [7] “Initial steps of the photodissociation of the CO-ligated heme group”, B.D. Dunietz, A. Dreuw, and M. Head-Gordon, *J. Phys. Chem B* 107, 5623-5629 (2003).
- [8] “Approaching closed-shell accuracy for radicals using coupled cluster theory with perturbative triple substitutions”, G.J.O. Beran, S.R. Gwaltney, and M. Head-Gordon, *Phys. Chem. Chem. Phys.* 5, 2488-2493 (2003).
- [9] “Time-dependent density functional study of the electronic excited states of polycyclic aromatic hydrocarbon radical ions”, S. Hirata, M. Head-Gordon, J. Szczepanski and M. Vala *J. Phys. Chem. A* 107, 4940-4951 (2003).
- [10] “Partitioning Techniques in Coupled Cluster Theory”, S.R. Gwaltney, G.J.O. Beran, and M. Head-Gordon, in “Fundamental World of Quantum Chemistry: A Tribute to the memory of Per-Olov Lowdin”, edited by E. Kryachko & E. Brandas, Kluwer (2003), Vol. I pp. 433-458.

- [11] “Charge-transfer state as possible signature of a zeaxanthin-chlorophyll dimer in the non-photochemical quenching process in green plants”, A. Dreuw, G.R. Fleming and M. Head-Gordon, *J. Phys. Chem. B* 107, 6500-6503 (2003).
- [12] “Long-range charge-transfer excited states in time-dependent density functional theory require non-local exchange”, A. Dreuw, J.L. Weisman, and M. Head-Gordon, *J. Chem. Phys.* 119, 2943-2946 (2003).
- [13] “Quantum chemical evidence of an intramolecular charge transfer state in the carotenoid peridinin of peridinin-chlorophyll-protein”, H.M. Vaswani, C.-P. Hsu, M. Head-Gordon and G.R. Fleming, *J. Phys. Chem. B* 107, 7940-7946 (2003).
- [14] “Chlorophyll fluorescence quenching by xanthophylls”, A. Dreuw, G.R. Fleming, and M. Head-Gordon, *Phys. Chem. Chem. Phys.* 5, 3247-3256 (2003).
- [15] “Electro-oxidation of CO on Pt-based electrodes simulated by electronic structure calculations”, C. Saravanan, B.D. Dunietz, N.M. Markovic, G.A. Somorjai, M. Head-Gordon and P.N. Ross, *J. Electroanal. Chem.* 554-555, 459-465 (2003)
- [16] “Manifestations of symmetry-breaking in self-consistent field calculations”, B.D. Dunietz and M. Head-Gordon, *J. Phys. Chem A* 107, 9160-9167 (2003).
- [17] “Reply to comment on characterizing unpaired electrons in molecules”, M. Head-Gordon, *Chem. Phys. Lett.* 380, 488-489 (2003).
- [18] “Are both symmetric and buckled dimers on Si(100) minima? Density functional and multireference perturbation theory calculations”, Y. Jung, Y. Shao, M.S. Gordon, D.J. Doren and M. Head-Gordon, *J. Chem. Phys* 119, 10917-10923 (2003).
- [19] “Failure of time-dependent density functional theory for long-range charge-transfer excited states: the zincbacteriochlorin-bacteriochlorin and bacteriochlorophyll-spheroidene complexes”, A. Dreuw and M. Head-Gordon, *J. Am. Chem. Soc.* 126, 4007-4016 (2004).
- [20] “What is the nature of the long bond in the $(\text{TCNE})_2^{(2-)} \pi$ dimer?”, Y. Jung and M. Head-Gordon, *Phys. Chem. Chem. Phys.* 6, 2008-2011 (2004).
- [21] “The spatial size of Fe(II) spin states and the spin-dependence of the structure of Fe(II)-porphyrins”, J.M. Ugalde, B. Dunietz, A. Dreuw, M. Head-Gordon and R.J. Boyd, *J. Phys. Chem. B* 108, 4653-4657 (2004)
- [22] “Extracting dominant pair correlations from many-body wavefunctions”, G.J.O. Beran and M. Head-Gordon, *J. Chem. Phys.* 121, 78-88 (2004).
- [23] “Initiation of electro-oxidation of CO on Pt-based electrodes at full coverage conditions simulated by ab initio electronic structure calculations”, B.D. Dunietz, N. Markovic, G. Somorjai, P.N. Ross and M. Head-Gordon, *J. Phys. Chem B* 108, 9888-9892 (2004).
- [24] “Intermolecular π -to- π bindings between stacked aromatic dyads. Experimental and theoretical binding energies and NIR optical transitions for phenalenyl radical/radical versus radical/cation dimerization”, D. Small, Vladimir Zaitsev, Yousung Jung, Sergiy V. Rosokha, Martin Head-Gordon and Jay K. Kochi, *J. Am. Chem. Soc.* 126, 13850-13858 (2004).
- [25] “An efficient method for calculating maxima of homogeneous functions of orthogonal matrices: Applications to localized occupied orbitals”, J.E. Subotnik, Y. Shao, W. Liang and M. Head-Gordon, *J. Chem. Phys.* 121, 9220-9229 (2004).
- [26] “An orbital-based definition of radical and multi-radical character”, A.D. Dutoi, Y. Jung, and M. Head-Gordon, *J. Phys. Chem. A* 108, 10270-10279 (2004).
- [27] “Scaled opposite spin second order correlation energy: An economical electronic structure method”, Y. Jung, R. Lochan, A.D. Dutoi, and M. Head-Gordon, *J. Chem. Phys.* 121, 9793-9802 (2004).
- [28] “Ultra-fast photo-initiated long-range electron transfer in cyclophane-bridged zincporphyrin-quinone complexes via conical intersections”, A. Dreuw, G.A. Worth, M. Head-Gordon, and L.S. Cederbaum, *J. Phys. Chem. B* 108, 19049-19055 (2004)
- [29] “A localized basis that allows fast and accurate second order Moller-Plesset calculations”, J.E. Subotnik and M. Head-Gordon, *J. Chem. Phys.* 122, 034109 (2005) (9 pages).

Laser Studies of Combustion Chemistry

John F. Hershberger

Department of Chemistry
North Dakota State University
Fargo, ND 58105
john.hershberger@ndsu.edu

Time-resolved infrared absorption and laser-induced fluorescence spectroscopy are used in our laboratory to study the kinetics and product channel dynamics of chemical reactions of importance in the gas-phase combustion chemistry of nitrogen-containing radicals. This program is aimed at improving the kinetic database of reactions crucial to the modeling of NO_x control strategies such as Thermal de-NO_x, RAPRENO_x, and NO-reburning. The data obtained is also useful in the modeling of propellant chemistry. The emphasis in our study is the quantitative measurement of both total rate constants and product branching ratios.

HCCO+NO₂ Reaction

While the HCCO+NO reaction has been extensively studied in several laboratories, relatively little literature data exist on HCCO+NO₂, with only a couple of previous reports of total rate constants,¹⁻² and no information on product channels.

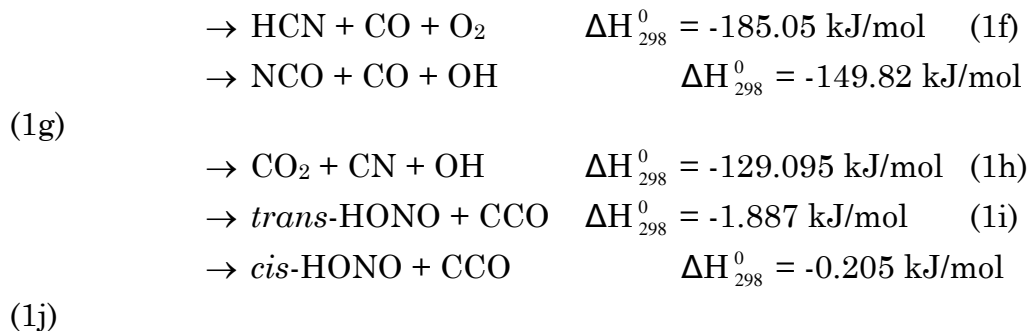
We have used transient infrared absorption spectroscopy to measure the total rate constant over the temperature range 298-423 K as well as the product branching ratios at 296 K. Similar to our previous study of HCCO+NO, we use ethyl ethynyl ether, C₂H₅OCCH, as our HCCO radical precursor.



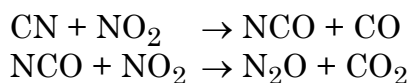
Reaction with NO₂ has many possible exothermic product channels:



(1e)



We have detected CO, CO₂, and HCNO products by infrared absorption spectroscopy. We also looked for HNCO and N₂O, but failed to detect these molecules. The lack of N₂O formation is particularly significant, because of secondary chemistry such as



We can therefore eliminate channels (1a), (1d), (1g), and (1h) from consideration. We also looked for HNO by transient absorption, and HCN by static FTIR analysis (we can't do the transient experiment because laser diodes are not available at 3300 cm⁻¹). Neither molecule was detected. In summary, we find that only channels (1b) and (1e) are significant. Although we did not directly detect HCO, we expect CO and CO₂ formation via secondary chemistry:³



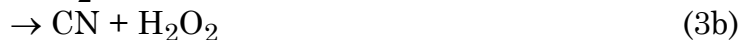
After analysis of product yields including consideration of reaction (2), we obtain $\phi_{1b} = 0.40 \pm 0.05$, and $\phi_{1e} = 0.60 \pm 0.05$ at 298 K.

We are also characterizing the PES of this reaction by ab initio quantum chemistry calculations. At the CCSD(T)/6-31G(d,p)//CCSD(T)/6-311++G(2d,p) level of theory, we find energetically feasible pathways to both channels (1b) and (1e), in agreement with our experimental results.

HCNO Kinetics

There is virtually no literature data available on the kinetics of the fulminic acid molecule. After recent work in our laboratory to synthesize pure HCNO for infrared absorption coefficient calibration purposes, we are in a position to examine reaction kinetics of this species. The HCNO synthesis is slow and inefficient, but our reaction cell geometry is ideally suited to dealing with reagents that are only available in small quantities. We are currently

measuring the rate constant of the OH+HCNO reaction, which plays an important role in NO-reburning mechanisms:⁴



To produce OH, we use 193 nm photolysis of N₂O to produce O(¹D), followed by reaction with H₂O. We have verified that the small amount of H₂O does not significantly increase the rate of HCNO decomposition. OH is then detected by LIF at 307.966 nm. At this point, we have a preliminary value of $k_3 = 1.22 \times 10^{-11} \text{ cm}^3 \text{ molecule}^{-1} \text{ s}^{-1}$ at 296 K. This is the first experimental measurement reported on this reaction, and is in fair agreement with an estimate of $3.32 \times 10^{-11} \text{ cm}^3 \text{ molecule}^{-1} \text{ s}^{-1}$ computed from an ab initio PES.⁴ Product yield studies are planned in the near future.

We have also begun work on the CN + HCNO reaction:



Our initial effort is to measure the total rate constants, with product yield studies to follow later. CN is produced by photolysis of ICN or C₂N₂, and detected by infrared absorption spectroscopy. At present, we have a preliminary 296 K rate constant of $k_4 = 3.1 \times 10^{-11} \text{ cm}^3 \text{ molecule}^{-1} \text{ s}^{-1}$.

Future plans include kinetic measurements of other radical species reacting with HCNO, including NCO+HCNO, etc.

NCCO + NO_x Reactions

We have spent considerable effort in an attempt to detect the NCCO radical by infrared diode laser absorption spectroscopy. Two 193-nm precursors, methyl cyanofornate and acetyl cyanide have been tried. Methyl cyanofornate is believed to produce NCCO, based on mass spectrum experiments.⁵ A low resolution FTIR study of methyl cyanofornate dissociation found emission at 2093 cm⁻¹ which was attributed to the NCCO radical.⁶ Unfortunately, we have been unable to find any transient signals in this wavelength region which can be definitely assigned to this species. We do find signals for CN radicals, as well as signals due to hot band transitions of vibrationally excited CO in this region. We

postulate that most of the signal observed in ref. 6 was actually due to emission by vibrationally hot CO.

As a result of our failure to directly detect NCCO, we have been unable so far to measure total rate constants of NCCO reactions. We have, however, detected N₂O and CO₂ products upon photolysis of an methyl cyanoformate/NO/buffer gas mixture:



We observe N₂O + CO₂ in roughly equal yields, which is consistent with formation from the secondary reaction (6). We therefore tentatively conclude that (5a) is the major product channel of reaction (5).

References

1. S.A. Carl, Q. Sun, L. Teugels, and J. Peeters, *Phys. Chem. Chem Phys.* **5**, 5424 (2003).
2. F. Temps, H.G. Wanger, M. Wolf, *Zeit. Physik. Chem.* **176**, 27 (1992).
3. K.T. Rim and J.F. Hershberger, *J. Phys. Chem. A* **102**, 5898 (1998).
4. J.A. Miller, S.J. Kilppenstein, and P. Glarborg, *Comb. Flame* **135**, 357 (2003).
5. A. Furlan, H. A. Scheld, and J. Robert Huber, *J. Phys. Chem. A* **104**, 1920 (2000).
6. W. McNavage, W. Dailey, and H.-L. Dai, *Can. J. Chem.* **82**, 925 (2004).

Publications acknowledging DOE support (2003present)

“Kinetics of the SiH₃+O₂ and SiH₃+H₂O₂ Reactions”, J.P. Meyer and J.F. Hershberger, *J. Phys. Chem. A* **107**, 3963 (2003).

“Kinetics of the CCO+NO and CCO+NO₂ Reactions”, W.D. Thweatt, M.A. Erickson, and J.F. Hershberger, *J. Phys. Chem. A* **108**, 74 (2004).

“Product Channels of the HCCO+NO Reaction”, J.P. Meyer and J. F. Hersberger, *J. Phys. Chem. A*, accepted for publication.

“Kinetics of the HCCO+NO₂ Reaction”, J.P. Meyer and J.F. Hersberger, *J. Phys. Chem. A*, submitted.

“Theoretical Characterization of the HCCO+NO₂ Potential Energy Surface”, J.P. Meyer and J.F. Hersberger, manuscript in preparation.

Product Imaging of Molecular Dynamics Relevant to Combustion

P. L. Houston

Department of Chemistry

Cornell University

Ithaca, NY 14853-1301

plh2@cornell.edu

Program Scope

Reaction dynamics important to a fundamental understanding of combustion will be investigated using the technique of product imaging. The imaging technique produces a "snapshot" of the three-dimensional velocity distribution of a state-selected reaction product. In favorable cases, these measurements uncover reaction mechanisms, determine more accurate heats of formation, and provide information about the excited states of combustion species and the couplings between them. They also improve our knowledge of intramolecular potentials and provide important tests of *ab initio* calculations. We are investigating two classes of reaction: 1) bimolecular reactions pertinent to combustion and 2) photodissociation of combustion radicals. In the first class, we will study the reactions of O(¹D) with N₂O, of O(³P) with C₂H₂ and C₂H₄, and of CN with O₂. In the second class, we will investigate the photodissociation dynamics of the allyl and methyl radicals.

Recent Progress

Photodissociation of N₂O near 130 nm

Nitrous oxide is an important component of Earth's natural atmosphere produced primarily by biological processes in soils and oceans but also as a by-product of combustion. Mostly inert in the troposphere, it is transported to the stratosphere where it is destroyed both by photodissociation (at $\lambda \approx 200$ nm),



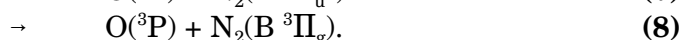
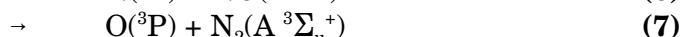
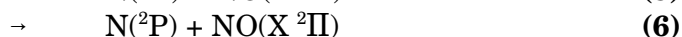
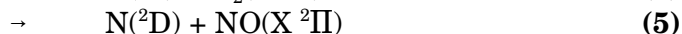
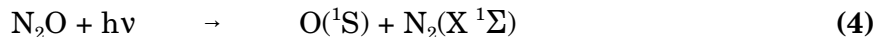
and by reaction with O(¹D) produced either in (1) or from the dissociation of ozone,



NO produced in (3) is the primary catalytic agent destroying stratospheric ozone in the natural atmosphere, as noted by Crutzen.¹

At shorter wavelengths, N₂O can be excited to the C(¹Π) state near 145 nm or to the D(¹Σ⁺) state near 130 nm. The absorption coefficient for the latter transition is high,²⁻⁴ about 80 Mb (1 Mb = 10⁻¹⁸ cm²). Although dissociation process (1) near 200 nm has been extensively studied,⁵⁻¹³ that at shorter wavelengths is both more complex and less well understood.¹⁴⁻¹⁷

At 130 nm, the following channels are thought to be important:



We have investigated channels (4) - (8) by using product imaging to detect the angular distributions for the five channels as well as the kinetic energy release for each of the product atoms or diatoms. The atomic products were probed by resonant ($1 + 1'$) ionization using ultraviolet excitation for the first step, while the diatomic products were probed by non-resonant ionization. Our work is part of a larger effort at Cornell to characterize this photodissociation process. Witinski, Ortiz-Suárez, and Davis, whose work is also supported by DOE, have used oxygen Rydberg time-of-flight spectroscopy to study channels (7) and (8), with results that are in reasonable agreement with ours.¹⁸

Figure 1 shows the total kinetic energy release for the $O + N_2$ products based on measurements of the $O(^1S)$, $O(^3P_0)$, $O(^3P_2)$, and N_2 products. In each case, conservation of momentum is assumed to determine the total kinetic energy release. The good match for the N_2 and $O(^3P)$ peaks in the lower panel shows that these are indeed momentum matched. Figure 2 shows similar data for the $N + NO$ channel, where $N(^2D)$, $N(^2P)$, and NO were probed. In each of these figures, the energy release data provides information about the vibrational distribution of the diatomic fragment.

Information about the branching ratio between various channels has also been obtained. The ratio of O^+ and NO^+ can be converted to a branching ratio between the dissociation channels leading to $O(^3P) + N_2$ vs. $N + NO$ by calibrating against the O^+ and NO^+ peaks obtained from the dissociation of NO_2 at 355 nm, assuming that the vibrational distributions for NO in the NO_2 dissociation and the $N + NO$ products are not too different. The reaction appears to favor the $O(^3P) + N_2$ channel by a ratio of 1.4 ± 0.5 . Vacuum ultraviolet line strengths for $O(^3P)$ and $O(^1S)$ are known, so that correcting for laser power variations and assuming similar ionization efficiencies, we find that the $O(^1S) + N_2(X)$ channel has about 10 ± 1.5 times the quantum yield of the $O(^3P) + N_2(A,B)$ channel. Spin-orbit distributions have also been obtained for all atomic products, and the ratio of quantum yields for the $N(^2D) + NO$ vs. $N(^2P) + NO$ channels is about 3.

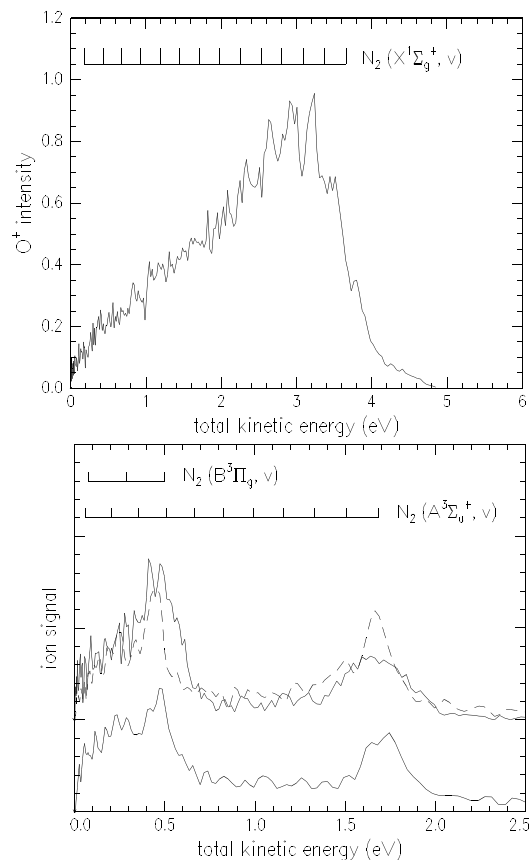


Fig. 1 Total kinetic energy released for $O + N_2$ products from the dissociation of N_2O at 130.2 nm: a) $O(^1S)$; b) $O(^3P_{2})$ top solid curve; $O(^3P_0)$ top dashed curve; N_2^+ bottom curve.

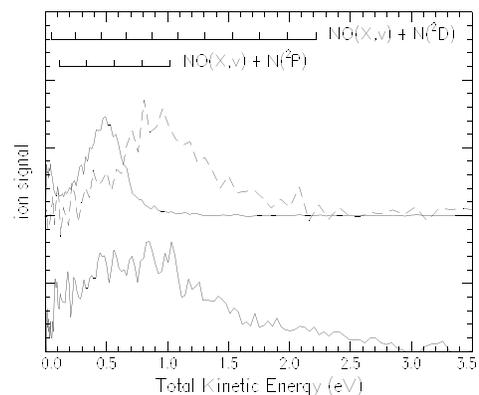


Fig. 2 Total kinetic energy released for $N+NO$ products from the dissociation of N_2O at 130.2 nm: $N(^2P_{3/2})$ top solid curve (at 131.054 nm); $N(^2D_{5/2})$ top dashed curve; NO^+ bottom curve.

Current Projects and Future Plans

The $O(^1D) + N_2O$ Reaction

A schematic diagram of the crossed beam adaptation to the imaging apparatus is shown in Fig. 3. Two molecular beams are brought within 1 cm of one another in the repeller region of the time-of-flight mass spectrometer. The precursor beam is dissociated at point A with a pulsed, polarized laser to produce a reactant atom or radical. Although the atoms fly in all directions, the intensity of those traveling vertically toward the reactant beam at point B can be maximized by choice of the polarization direction of the dissociation laser. After reaction occurs at point B, products of the reaction are ionized and imaged using velocity mapping. The time delay between the pulsed dissociation and ionization lasers (and to some extent, the laboratory velocity of the reactant beam) defines the relative collision velocity. The velocity map of the product can be analyzed to provide the differential cross section for the reaction.

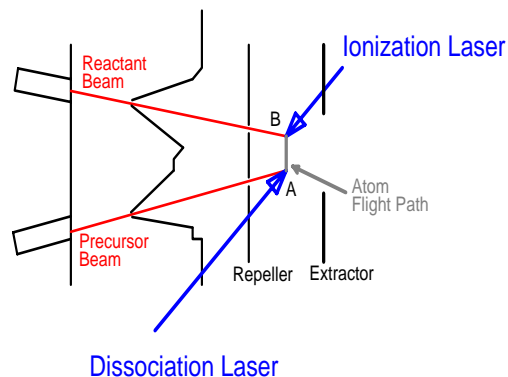


Fig. 3 Schematic diagram of crossed beam adaptation to imaging apparatus. The flight tube and microchannel plate detector, not shown, are to the right of the diagram.

We are using this apparatus to investigate the reaction of $O(^1D)$ with N_2O . Several preliminary experiments have been performed:

Ozone beam, $O(^1D)$ reactant characterization. Ozone in one beam was dissociated at 266 nm and the resulting $O(^1D)$ was detected by (2+1) REMPI at 203.7 nm. The probe laser beam was moved in order to detect the $O(^1D)$ atoms which fly toward the N_2O molecular beam. The position of this second beam was determined by expanding 100% N_2O through the nozzle, also with a backing pressure of ~ 1 atm, and first detecting the $O(^1D)$ atoms produced by the 203.7 nm dissociation. With a separation of 1 cm between the O_3/He and the N_2O molecular beams and between the positions of the 266 nm dissociation and the 203.7 nm probe laser beams, the expected time delay is 4.3 μs , in good agreement with the measured of 4.5 μs .

Single beam experiments. Co-expansion of O_3/He and N_2O through the lower nozzle, dissociation at 266 nm, and probing NO at $NO(v=4)$ was accomplished. The rotational distribution is quite hot. Rough comparison with simulations using the LIFbase program indicates a rotational temperature near 1900 K. A portion of the $NO(v=4)$ spectrum is shown in Fig. 4.

In addition to exploration of the reaction via the double beam scheme, we are also investigating an imaging experiment using a two-dimensional version of the photoloc experiment. Co-expansion of O_3/He and N_2O through one of the nozzles produces NO that can be detected by 1+1' ionization. The image of this NO, however, is in the ozone COM frame rather than in the COM frame of the $O(^1D)+N_2O$ system. The results are a two-dimensional version of the Doppler scan results obtained, for example, by Brouard and Simons.^{19,20}

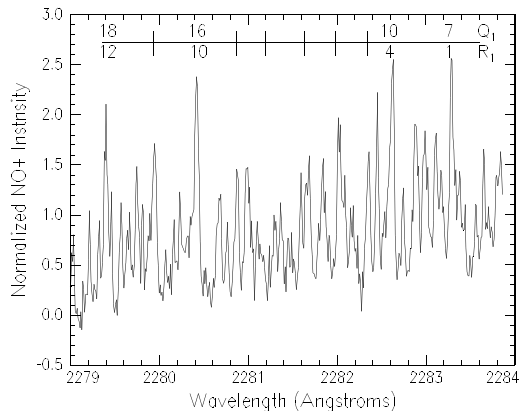


Fig. 4 Spectrum containing $NO(v=4)$ rotational transitions.

References

1. P. J. Crutzen, Q. J. R. Meterol. Soc. **96**, 320-325 (1970); P. J. Crutzen, J. Geophys. Res. **76**, 7311-7327 (1971).
2. J. B. Nee, J. C. Yang, P. C. Lee, X. Y Wang, and C. T. Juo, Chinese J. Phys. **37**, 172 (1999).
3. L. C. Lee and M. Suto, J. Chem. Phys. **80**, 4718-4726 (1984).
4. M. Zelikoff, K. Watanabe, and E. C. Y. Inn, J. Chem. Phys. **21**, 1643-1647 (1953).
5. P. Felder, B.-M. Haas, and J. R. Huber, Chem. Phys. Lett. **186**, 177 (1991).
6. N. Shafer, K. Tonokura, Y. Matsumi, S. Tasaki, and M. Kawasaki, J. Chem. Phys. **95**, 6218 (1991).
7. L. L. Springsteen, S. Satyapal, Y. Matsumi, L. M. Dobeck, and P. L. Houston, J. Chem. Phys. **97**, 7239-7241 (1993).
8. T. F. Hanisco and A. C. Kummel, J. Phys. Chem. **97**, 7242-7246 (1993).
9. T. Suzuki, H. Katayanagi, Y. Mo, and K. Tonokura, Chem. Phys. Lett. **256**, 90 (1996).
10. D. W. Neyer, A. J. R. Heck, and D. W. Chandler, J. Chem. Phys. **110**, 3411-3417 (1999).
11. D. W. Neyer, A. J. R. Heck, D. W. Chandler, J. M. Teule, and M. H. M. Janssen, J. Phys. Chem. A **103**, 10388-10397 (1999).
12. A. Brown, P. Jimeno, and G. G. Balint-Kurti, J. Phys. Chem. A **103**, 11089 (1996).
13. S. Nishida, K. Takahashi, Y. Matsumi, N. Taniguchi, and S. Hayashida, J. Phys. Chem. A. **108**, 2451 (2004).
14. G. Black, R. L. Sharpless, T. G. Slanger, and D. C. Lorents, J. Chem. Phys. **62**, 4266-73 (1975).
15. R. Gilpin and K. H. Welge, J. Chem. Phys. **55**, 975-978 (1971).
16. E. J. Stone, G. M. Lawrence, and C. E. Fairchild, J. Chem. Phys. **65**, 5083-5092 (1976).
17. D. G. Hopper, J. Chem. Phys. **80**, 4290-316 (1984).
18. M. F. Witinski, M. Ortiz-Suárez, and H. F. Davis, submitted.
19. M. Brouard, S. P. Duxon, P. A. Enriquez, R. Sayos, and J. P. Simons, J. Phys. Chem. **95**, (1991) 8169-74.
20. M. Brouard, S. P. Duxon, P. A. Enriquez, and J. P. Simons, Journal of Chemical Physics **97**, (1992) 7414- 22.

Publications Prepared with DOE Support, 2003 - present

P. L. Houston, "Charged Particle Imaging in Chemical Dynamics: An Historical Perspective," in *Imaging in Molecular Dynamics: Technology and Applications*, B. Whitaker, ed. (Cambridge University Press, Cambridge, 2003).

Amitavikram A. Dixit, Yuxiu Lei, Keon Woo Lee, Edwin Quiñones, and Paul L. Houston, "Dissociation of sulphur dioxide by ultraviolet multiphoton absorption between 224 and 232 nm," J. Phys. Chem. A **109**, 1770-1775 (2005).

H. M. Lambert, A. A. Dixit, E. W. Davis and P. L. Houston, "Quantum Yields for Product Formation in the 120-130 nm Photodissociation of O₂," J. Chem. Phys. **121**, 10437-10446 (2004).

M. Lambert, E. W. Davis, O. Tokel, A. A. Dixit, and P. L. Houston, "Photodissociation Channels for N₂O near 130 nm Studied by Product Imaging," J. Chem. Phys., accepted.

These publications may be accessed at

<http://people.ccmr.cornell.edu/~plh2/group/PLHPublicat.htm>

Terascale High-Fidelity Simulations of Turbulent Combustion with Detailed Chemistry <http://scidac.psc.edu/>

SciDAC: Computational Chemistry
(DOE Office of Science, BES: Chemical Sciences, Program Manager: R. Hilderbrandt)
Work-in-Progress Report – *Period from 04/01/04 to 03/31/05*

List of Principal Investigators

- Hong G. Im (University of Michigan, UMI, hgim@umich.edu)
- Arnaud Trouvé (University of Maryland, UMD, atrouve@eng.umd.edu)
- Christopher J. Rutland (University of Wisconsin, UW, rutland@engr.wisc.edu)
- Jacqueline Chen (Sandia National Laboratories, SNL, jhchen@ca.sandia.gov)

Project Summary

The TSTC project is a multi-university collaborative effort to develop a high-fidelity turbulent reacting flow simulation capability utilizing terascale, massively parallel computer technology. The main paradigm of our approach is direct numerical simulation (DNS) featuring highest temporal and spatial accuracy, allowing quantitative observations of the fine-scale physics found in turbulent reacting flows as well as providing a useful vehicle towards description of sub-models needed in device-level simulations. The new S3D software is enhanced with new numerical algorithms and physical models to provide predictive capabilities for spray dynamics, combustion, and pollutant formation processes.

Program Scope

The primary goal of the SciDAC TSTC project for FY04-07 is to extend the S3D code with new physical and algorithmic modules. The ultimate demonstration of the task will be simulations of partially premixed turbulent flames with liquid spray description, thereby achieving the full potential of the state-of-the-art DNS capability as a companion of detailed experimental studies. The specific objectives of this project include:

- To develop and complete the high-fidelity numerical algorithms under the component-based and parallel computing platform. This includes high-order, implicit/explicit (IMEX) stiff time integrators based on additive Runge-Kutta, and the immersed boundary method (IBM) for solid body representation associated with high-order interpolation schemes.
- To expand and upgrade the physical submodels to describe the underlying mechanisms with great details. The existing modules of radiation, soot, and spray evaporation model will be further enhanced to allow direct comparisons against experimental studies. In particular, detailed soot formation model using the method of moments will be developed and improved spray models will be added to represent direct injection and droplet distortion effects.
- To demonstrate the capability of the terascale DNS code in investigating fundamental science issues by several pilot simulations of canonical flames observed in turbulent combustion. The pilot configurations proposed for TSTC Phase II include partially-premixed turbulent counterflow and jet flames, and turbulent spray jet evaporation and ignition problems. The S3D DNS code will further allow access to various post-processing functionalities for effective data-mining and visualization that are being developed under BES Chemical Sciences core program.

Recent Progress

We present here a summary of progress made during the past 12 months work period of this project extending from 04/01/04 to 03/31/05.

Software design developments:

- As a completion to the collaboration with Pittsburgh Supercomputing Center under TSTC Phase I, S3D has been modified to fit into GrACE (grid adaptive computational engine) and componentized into the CCA (common component architecture) framework (PSC/Raghurama Reddy).
- S3D has been ported to the CrayX1 architecture and optimized by rewriting key modules, i.e. chemistry and thermodynamics, to facilitate vectorization (SNL).
- Performed test simulations of S3D to identify optimal physical and numerical parameters for INCITE goal (SNL).
- As part of 2005 Joule Software Effectiveness Study, benchmark test simulations were performed to identify the code efficiencies with radiation/soot models (UMI/UMD) and spray vaporization models (UWI) on two supercomputing facilities at NERSC and ORNL CCS.

Numerical developments:

- New improved characteristic boundary conditions have been formulated to properly account for multi-dimensional flow effects in nonreflecting inflow and outflow conditions. Applications to various counterflow configurations demonstrate accurate and robust solutions over a wide range of flow and scalar variables, allowing high fidelity in detailed numerical studies of turbulent counterflow flames. This work has been submitted for publication in *Combustion Theory and Modelling* (UMI/UMD).

Physical model developments:

- Two alternative radiative heat transfer models, discrete ordinate method (DOM) and discrete transfer method (DTM) have been established and validated. Their overall performance was tested under the Joule Software Effectiveness Study (UMI/UMD).
- The spray module has been improved to efficiently handle a large number of fuel droplets. The code effectiveness has been tested under the Joule Software Effectiveness Study (UWI).

New combustion science:

- The S3D solver has been applied to study the interaction of turbulent ethylene-air jet diffusion flame and a solid wall. The simulations feature flame extinction events resulting from excessive wall cooling, and convective heat transfer up to 100 kW/m². The structure of the simulated wall flames is studied in terms of a classical fuel-air-based mixture fraction and an excess enthalpy variable. Preliminary results have been submitted for publication in *Combustion and Flame* (UMD).
- Various cases of fuel spray ignition with different initial droplet sizes and velocities were simulated to investigate the impact on turbulent mixing, auto-ignition and initial combustion of n-heptane fuel spray using detailed chemistry (UWI).

- Using the developed radiation and soot models, the interaction of counter-rotating vortices and laminar nonpremixed flame and their impact on the soot formation characteristics have been studied (UMI/UMD).

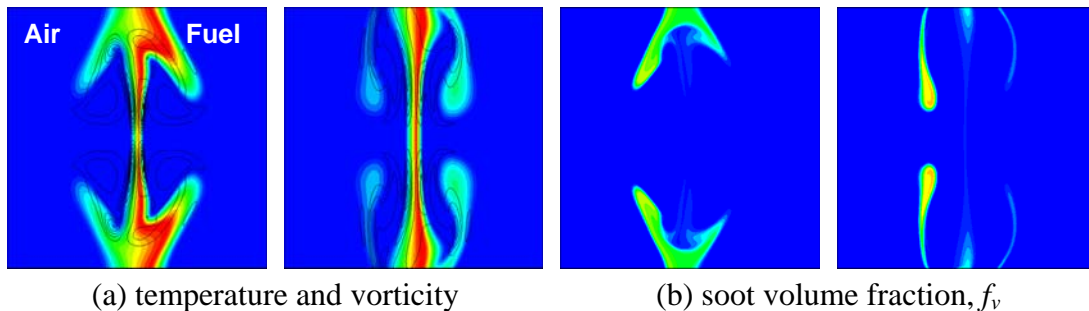


Figure 1. Temporal variations of (a) temperature (flood) and vorticity (black lines), and (b) soot volume fraction, f_v , during the interaction of an ethylene nonpremixed flame and counter-rotating vortices, exhibiting highly transient nature of the soot formation process during flame extinction.

Future Plans

- Develop new method for turbulence injection for wall-bounded flows to improve the accuracy and realism of turbulent fluctuations that are equilibrated with the mean flow, and to reduce the length of the turbulence development section in spatially-evolving flows (SNL)
- Immersed boundary method for solid body representation (UMD).
- Advanced soot models based on the method of moments (UMI)
- Continuation of studies on the radiation/soot interaction in counterflow (UMD/UMI)
- Three dimensional simulations of n-heptane fuel spray injections to investigate autoignition of fuel spray in realistic turbulent flow and mixing fields (UWI).

Publications

Journals

- [1] Wang, Y. and Trouvé, A. (2004), "Artificial acoustic stiffness reduction in fully compressible, direct numerical simulation of combustion," *Combust. Theory Modelling*, **8**:633-660.
- [2] Wang, Y. and Rutland, C. J. (2004), "Effects of temperature and equivalence ratio on the ignition of n-heptane fuel droplets in turbulent flow," *Proc. Combust. Inst.*, **30**:893-900.
- [3] Yoo, C. S. and Im, H. G. (2004), "Transient dynamics of edge flames in a laminar nonpremixed hydrogen-air counterflow," *Proc. Combust. Inst.*, **30**:349-356.
- [4] Sankaran, R., Im, H. G., Hawkes, E. R. and Chen, J. H. (2004), "The effects of nonuniform temperature distribution on the ignition of a lean homogeneous hydrogen-air mixture," *Proc. Combust. Inst.*, **30**:875-882.
- [5] Chen, J. H., Hawkes, E., Sankaran, R., Mason, S. D., and Im, H. G. (2005), "Direct numerical simulation of ignition front propagation in a constant volume with temperature inhomogeneities, Part I: Fundamental analysis and diagnostics," *Combustion and Flame*, submitted.
- [6] Hawkes, E., Sankaran, R., Pébay, P. P., and Chen, J. H. (2005), "Direct numerical simulation of ignition front propagation in a constant volume with temperature inhomogeneities, Part II: Parametric Study," *Combustion and Flame*, submitted.
- [7] Yoo, C. S., Wang, Y., Trouvé A. and Im, H. G. (2005), "Characteristic boundary conditions for direct simulations of turbulent counterflow flames", *Combust. Theory Modelling*, submitted.

- [8] Wang, Y. and Trouvé A. (2005), "Direct numerical simulation of non-premixed flame-wall interactions", *Combustion and Flame*, submitted.

Communications

- [1] Trouvé, A., (2002), "Artificial removal of the acoustic penalty in fully compressible, direct numerical simulations of combustion," *9th SIAM Intl. Conf. on Numerical Combustion*, Sorrento, Italy.
- [2] Wang, Y. and Rutland, C. J. (2003), "On the combustion of normal heptane fuel droplets in isotropic turbulence with DNS," *3rd Joint Meeting of the US Sections of the Combustion Institute*, Chicago, IL.
- [3] Wang, Y. and Trouvé, A. (2003), "Artificial acoustic stiffness reduction in fully compressible, direct numerical simulation of combustion", *3rd Joint Meeting of the US Sections of the Combustion Institute*, Chicago, IL.
- [4] Yoo, C. and Im, H. G. (2003), "A computational study on the dynamics of counterflow hydrogen-air edge flames," *3rd Joint Meeting of the US Sections of the Combustion Institute*, Chicago, IL.
- [5] Chen, J. H., Mason, S. D., and Hewson, J. C. (2003), "The effect of temperature inhomogeneity on low-temperature autoignition of fuel-lean premixed hydrogen/air mixtures", *3rd Joint Meeting of the US Sections of the Combustion Institute*, Chicago, IL.
- [6] Hawkes, E. R. and Chen, J. H. (2003) "Turbulent stretch effects on hydrogen enriched lean premixed methane-air flames," *3rd Joint Meeting of the US Sections of the Combustion Institute*, Chicago, IL.
- [7] Liu, S. and Chen, J. H. (2003), "The effect of product gas enrichment on the chemical response of premixed diluted methane/air flames," *3rd Joint Meeting of the US Sections of the Combustion Institute*, Chicago, IL.
- [8] Sutherland, J. C., Smith, P. J., and Chen, J. H. (2003), "DNS of a nonpremixed CO-H₂ jet using detailed chemistry – toward improved LES models," *3rd Joint Meeting of the US Sections of the Combustion Institute*, Chicago, IL.
- [9] Wang, Y. and Rutland, C. J. (2003), "Direct numerical simulation of turbulent droplets flow with evaporation," *The 41st AIAA Aerospace Sciences Meeting and Exhibit*, AIAA Paper 2003-1281, 6-9 January 2003, Reno, Nevada, USA.
- [10] Trouvé A., Wang Y., Im H. G., Yoo C. S., Rutland C. J., Wang Y., Chen J. H., Sutherland J. C., and Mason S. D. (2004), "Direct numerical simulation of turbulent combustion using a fully compressible flow formulation," *Tenth SIAM International Conference on Numerical Combustion*, May 9-12, Sedona, AZ.
- [11] Yoo, C. S., Im, H. G. Trouvé, A., and Wang, Y. (2004), "Direct numerical simulation of turbulent nonpremixed counterflow ethylene-air flame with soot and radiation models," *Tenth SIAM International Conference on Numerical Combustion*, May 9-12, Sedona, AZ.
- [12] Yoo, C. S. and Im, H. G. (2004), "Soft inflow boundary conditions for direct numerical simulations of compressible reacting flows," *Tenth SIAM International Conference on Numerical Combustion*, May 9-12, Sedona, AZ.
- [13] Wang, Y. and Rutland, C. J., "Effects of droplet velocity and size on the ignition of n-heptane fuel spray in turbulent flow using DNS." *Tenth SIAM International Conference on Numerical Combustion*, May 9-12, Sedona, AZ.
- [14] Yoo, C. S. and Im, H. G. (2004), "Transient dynamics of edge flames in a laminar nonpremixed hydrogen-air counterflow," *30th International Symposium on Combustion*, July 25-30, Chicago, IL.
- [15] Wang, Y. and Rutland, C. J. (2004), "Effects of temperature and equivalence ratio on the ignition of n-heptane fuel droplets in turbulent flow," *30th International Symposium on Combustion*, July 25-30, Chicago, IL.
- [16] Sankaran, R., Im, H. G., Hawkes, E. R. and Chen, J. H. (2004), "The effects of nonuniform temperature distribution on the ignition of a lean homogeneous hydrogen-air mixture," *30th International Symposium on Combustion*, July 25-30, Chicago, IL.
- [17] Wang, Y. and Rutland, C. J. (2004), "DNS study of the ignition of n-heptane fuel spray under HCCI condition," the 57th APS Annual Meeting of the Division of Fluid Dynamics, Seattle, WA, November.
- [18] Yoo, C. S., Wang, Y., Trouvé A. and Im, H. G. (2005) "Characteristic boundary conditions for direct simulations of turbulent counterflow flames", *Joint Meeting US Sections of Combustion Institute*, March 20-23, Philadelphia, PA.
- [19] Wang, Y. and Trouvé, A. (2005) "Direct numerical simulation of non-premixed flame-wall interactions", *Joint Meeting US Sections of Combustion Institute*, March 20-23, Philadelphia, PA.
- [20] Yoo, C. S., Im, H. G., Wang, Y. and Trouvé A. (2005) "Improved Navier-Stokes characteristic boundary conditions for direct simulations of compressible reacting flows", *3rd MIT Conf. Computational Fluid and Solid Mech.*, Cambridge, MA.

IONIZATION PROBES OF MOLECULAR STRUCTURE AND CHEMISTRY

Philip M. Johnson
Department of Chemistry
Stony Brook University, Stony Brook, NY 11794
Philip.Johnson@sunysb.edu

PROGRAM SCOPE

Photoionization processes provide very sensitive probes for the detection and understanding of molecules and chemical pathways relevant to combustion processes. Laser based ionization processes can be species-selective by using resonances in the excitation of the neutral molecule under study or by exploiting the fact that different molecules have different sets of ionization potentials. Therefore the structure and dynamics of individual molecules can be studied, or species monitored, even in a mixed sample. We are continuing to develop methods for the selective spectroscopic detection of molecules by ionization, to use these spectra for the greater understanding of molecular structure, and to use these methods for the study of some molecules of interest to combustion science.

RECENT PROGRESS

The exploitation of Rydberg molecules has enabled orders-of-magnitude increases in the resolution available for recording the spectra of molecular ions. These spectra provide information equivalent to photoelectron spectra, but contain much more information by virtue of that resolution and the versatility of laser preparation of the states involved.

To provide high resolution spectra of the various electronic states of ions, we primarily use techniques developed in our laboratory called mass analyzed threshold ionization spectroscopy (MATI) and photoinduced Rydberg ionization spectroscopy (PIRI). MATI and PIRI are multilaser techniques using Rydberg states, which produce cationic spectra. The multiresonant nature of the overall processes are of great use in sorting out the vibrational structure of some ionic states.

We are currently involved in a project that probes the limits of resolution for PIRI. The development of a new method for measuring spectra of larger cations with rotational resolution would give a valuable new tool to be used for the precision measurement of molecular parameters.

PIRI spectroscopy involves the optical core excitation of a high- n Rydberg state, producing an autoionization which provides a marker that a transition has taken place. If n and l of a Rydberg orbital are large enough, the electron is effectively decoupled from the ion core and the properties of that core are essentially those of the bare cation. It therefore follows that the spectroscopy of a high- n,l Rydberg molecule and the spectroscopy of the equivalent cation are identical.

The Rydberg states in PIRI are created by either one or two photon excitation from the neutral ground state of a molecule, with stray electric fields from the chamber and local ions perturbing the Rydberg orbits in such a way that the angular momentum goes from an initial low- l value to high- l . The decrease in core-electron interaction produces a long lifetime for the state. In PIRI an additional laser excites the ion core and this excitation increases the autoionization

rate of the Rydberg molecule, creating ions that are markers for the core excitation. A spectrum is produced by scanning the core excitation laser while measuring the number of optically induced autoionization events.

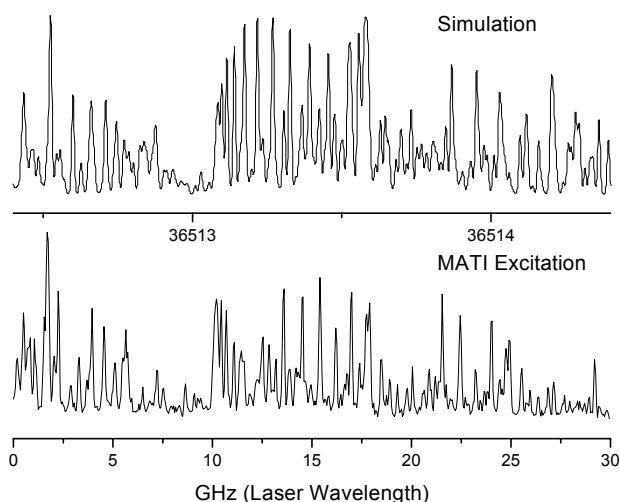
In terms of resolution, the key point is that in PIRI there is no field ionization, which limits the resolution in MATI and ZEKE. Therefore from a given Rydberg state the optical resolution should be limited only by the linewidth of the laser and the natural linewidth of the transition. Of course, due to the high density of states in the high-Rydberg region, it is unlikely that only a single Rydberg state will be excited and the question arises; *how does the resolution of the PIRI spectrum depend on the resolution of the lasers preparing the Rydberg states?*

Fortunately, there are arguments that say the linewidths of the Rydberg-preparation lasers are not very important, since the principle quantum numbers and the quantum defects of a Rydberg electron do not change significantly during a core excitation. This is an untested hypothesis, however.

To find out whether rotational resolution is possible in PIRI for a larger molecule, benzonitrile is being studied. This molecule has a dense rotational structure, absorbs in the proper spectral regions, and is in the family of molecules with which we have the most experience, so is an ideal candidate. In order to proceed, however, we need to understand the cation vibronic spectroscopy and the Rydberg dynamics for benzonitrile (cyanobenzene).

Spectroscopy and Rydberg dynamics of benzonitrile cation

We have previously studied the spectra of the $\tilde{B}-\tilde{X}$ cation transitions in benzene and various substituted benzenes, and established the symmetry of the B state from analysis of the vibrational structure. The ordering of the electronic states is very sensitive to the substitution in the spectral region of the \tilde{B} state, and symmetries cannot be easily determined without a detailed analysis. Vibrational assignments are verified by acquiring multistep MATI and PIRI spectra



through various vibrations of the S1 state and the ground cation state, after correcting some previous assignments in the latter. It is found that the \tilde{B} state of benzonitrile has 2B_2 symmetry, which makes it forbidden optically from the 2B_1 ground state. The dominant inducing modes in the PIRI spectrum from the ground state origin are a_2 symmetry, coupling to the nearby 2B_1 \tilde{C} state. The half-filled molecular orbital for the \tilde{B} state of benzonitrile is a 2p sigma orbital, similar to benzene and phenol, but different than fluoro- and chlorobenzene where the \tilde{B} states have half-filled pi orbitals.

Using a newly constructed pulse-amplified CW dye laser system, we have recorded MATI excitation spectra, scanning through the origin band of the S1 state with this high resolution laser while making Rydbergs with a normal pulsed dye laser. Comparing the rotational structure with simulations from the known rotational constants, it is seen that the high

J values are attenuated, and certain rotational branches are more prominent than expected. This can be attributed to rotational effects on the Rydberg state lifetimes, and is vital information for selecting excitation wavelengths. By exciting a single rotational line in S1, rotational structure is apparent in the MATI spectra of benzonitrile, since congestion is eliminated.

FUTURE PLANS

We are now in a position where high resolution PIRI can be attempted while controlling the relevant parameters, and this will be taking place shortly. Other future projects include examinations of the spectroscopy of cyclopentadienyl, and benzyne cations.

DOE PUBLICATIONS

Andrew Burrill, Jia Zhou and Philip Johnson, "The Mass Analyzed Threshold Ionization Spectra of $C_6H_6^+$ and $C_6D_6^+$ obtained via the $^3B_{1u}$ Triplet State," J. Phys. Chem. A, **107**, 4601-4606 (2003).

James Lightstone, Heather Mann, Ming Wu, Philip Johnson and Michael White, "Gas-phase production of molybdenum carbide, nitride, and sulfide clusters and nanocrystallites," J. Phys. Chem. B, **107**, 10359-10366 (2003).

Andrew. B. Burrill, You K. Chung, Heather. A. Mann, and Philip M. Johnson, "The Jahn-Teller effect in the lower electronic states of benzene cation: Part III The ground state vibrations of $C_6H_6^+$ and $C_6D_6^+$," J. Chem. Phys. **120**, 8587-8599 (2004).

Investigating the chemical dynamics of bimolecular reactions of dicarbon and tricarbon molecules with hydrocarbons in combustion flames

Ralf I. Kaiser
Department of Chemistry
University of Hawai'i at Manoa
Honolulu, HI 96822
kaiser@gold.chem.hawaii.edu

1. Program Scope

The goal of this project is to untangle experimentally the energetics and the dynamics of reactions of dicarbon, $C_2(X^1\Sigma_g^+/a^3\Pi_u)$, and tricarbon molecules, $C_3(X^1\Sigma_g^+)$, with unsaturated hydrocarbons acetylene ($C_2H_2(X^1\Sigma_g^+)$), ethylene ($C_2H_4(X^1A_g)$), methylacetylene ($CH_3CCH(X^1A_1)$), allene ($H_2CCCH_2(X^1A_1)$), and benzene ($C_6H_6(X^1A_{1g})$) on the most fundamental, microscopic level. These reactions are of crucial importance to understand the formation of carbonaceous nanostructures as well as of polycyclic aromatic hydrocarbons and their hydrogen deficient precursors in combustion flames. The closed shell hydrocarbons serve as prototype reaction partners with triple (acetylene), double (ethylene), and aromatic (benzene) bonds; methylacetylene and allene are chosen as the simplest representatives of closed shell hydrocarbon species to investigate how the reaction dynamics change from one structural isomer to the other. The experiments are carried out under single collision conditions utilizing a crossed molecular beams machine at The University of Hawai'i. Projected results of these studies are an identification of the reaction products and the determination of the energetics and entrance barriers of the reaction, the intermediates involved, and of the branching ratios - data which are very much required by the combustion chemistry community. The experiments are pooled together with electronic structure calculations to verify the elucidated reaction mechanisms theoretically. All findings are then incorporated into chemical reaction networks to examine the influence of dicarbon and tricarbon molecules on the growth of carbonaceous nanostructures and of polycyclic aromatic hydrocarbons together with their hydrogen deficient precursors in combustion flames.

2. Recent Progress

In year one of this project, we designed and constructed a new crossed molecular beams machine with universal, mass spectrometric detector. In year two, we have incorporated the detection system and calibrated the machine (ionizer with the mass spectrometric detector, primary and secondary sources (continuous and pulsed), ion flight constants, neutral flight lengths, photodiode dead times, laser ablation source, pulsed valve electronics) (June 2004 – December 2004). To demonstrate that the machine actually works (i.e. that the beams cross), we also carried out scattering experiments (elastic, inelastic, and reactive scattering) to compare the signal of these systems with previous studies (neon – argon; carbon – neon; carbon – methylacetylene) (January 2005 – present). Most important, the scattering experiments show that the absolute signal and signal-to-noise ratios are improved by a factor of 20-30 (elastic and inelastic scattering) and about 20 (reactive scattering) compared to competing 'universal' crossed beams machine. Additionally, the enhanced sensitivity of the mass spectrometer allows a detection of trace amounts of residual species of about two orders of magnitude lower than previously accomplished. Based on these data, we will be able to conduct the proposed reactive scattering experiments of dicarbon and tricarbon.

2.1. Upgrade of the crossed molecular beams machine

The main chamber of the crossed beams machine consists of a 2300 liter 304 stainless steel box (machining accuracy: ± 0.03 mm) and is evacuated by three 2000 ls^{-1} magnetically suspended turbo molecular pumps (Osaka Vacuum; TG 2003) backed by a single scroll pump (Edwards XD35; 10 ls^{-1}) to the low 10^{-8} torr region. To reduce the background from straight-through molecules into the detector, the machine is also

equipped with a cold shield located between the skimmer and chopper wheel (primary source) and downstream the skimmer (secondary source). This oxygen free high conductivity (OFHC) copper shield is interfaced to the first stage (10 K) of a CTI CP-1020 cold head (4500 ls^{-1} (water); 1500 ls^{-1} (nitrogen/oxygen) and improves the vacuum in the main chamber to 4×10^{-9} torr. During an actual experiment, this arrangement keeps the pressure in the main chamber to 10^{-7} torr (continuous sources) and 5×10^{-8} torr (pulsed sources). Two source chambers are located inside the main chamber; in its current geometry, both beams cross perpendicularly. Each source chamber is pumped by a 2000 ls^{-1} and a 430 ls^{-1} maglev pump (Osaka Vacuum; TG2003 and TG430) to the low 10^{-8} torr region; operating pulsed and continuous sources increases the pressure to about 10^{-5} torr and 10^{-4} torr, respectively. A dry roots pump (Leybold WS505; 140 ls^{-1}) roughed by two oil-free EcoDry M30 pumps (Leybold; 16 ls^{-1}) backs the turbo pumps of each source chamber. Note that all critical components associated with the detector of the machine (these parts are under ultra high vacuum) are hooked up to a single UPS system so that in case of extended power outages (longer than 5 hours battery backup time) the detector can be operated with a dedicated fuel generator.

2.2. Optimization and calibration of mass spectrometric detector

Compared to the year 1 abstract, we re-optimized the potentials of the Brink type ionizer nested inside a triply differentially pumped, rotatable mass spectrometric detector. These are: extractor: -55 V, focus lens, 0V; electron energy: 200 eV, ion energy, 32 eV and added to the $\frac{3}{4}$ " quadrupole rod system the following items: i) a grounded quadrupole housing, ii) quad pre- and post filters (0 – -2 V), and iii) entrance and exit lens (- 4V). This improved the sensitivity of our system by a factor of about 30–40 (residual gas analyzer mode). In addition, we incorporated a four lead circuit, i.e. feeding two instead of one wire to the anode and cathode of the thoriated iridium filament. This circuit eliminates the resistance of the leads to the filament and hence minimizes voltage drops. The reduced voltage drop in turn minimized the heat released from the filament to typically 6.3 VA (1.8 V and 3.5 A for 1 mA emission current) and 9 VA (2 V and 4.5 A for 10 mA emission current). Table 1 lists those species observable in the residual gas analyzer mode operated in the low 10^{-11} torr range. Also, we incorporated an air cooled design of the photomultiplier tube cluster-based resistance/capacitor chain which eliminates the water cooling; this ensures safer operation conditions in case of water line ruptures. We would like to stress that we also run tests with an operating cold head; since the ion gauges do not measure accurately below 10^{-11} torr, the actual pressure has to be calculated via matrix interval algebra; this is currently in progress. Qualitatively, it should be noted that the signal of the carbon dioxide does not decrease in time suggesting that signal at $m/e = 44$ actually arises from carbon dioxide formed in the ion molecule reaction of neutral carbon monoxide with singly ionized carbon monoxide to form carbon dioxide and singly ionized carbon ($m/e = 12$). Also, the signal at $m/e = 18$ and 17, which arises from water traces, is completely absent.

2.3. Scattering experiments

To demonstrate that the beams of the primary and secondary sources cross in the interaction region, we carried out four sets of scattering experiments:

i) scattering experiments of neon with argon utilizing continuous sources (Fig. 1) [the distance of the sources from the skimmer was optimized to be 6.0 mm; data were accumulated for 50 s utilizing the following parameters: $p(\text{Ne}) = 276$ torr; $p(\text{Ar}) = 400$ torr); MCS dwell time = 2.56 μs ; 10240 TOFs; 10 mA ionizer current; 1600 V PMT voltage; 100 Hz chopper wheel; comparing the elastic scattering signal of the present machine with previous measurements suggests an enhanced scattering signal by a factor of 20-30].

ii) scattering experiments of neon with argon utilizing pulsed sources (Fig. 2) [the distance of the sources from the skimmer was optimized to be 18.0 mm; signal was also accumulated for 50 s. The following para-

meters have been used: p(neon) = 4 atm, p(argon) = 1 atm, pulsed valve opening time: 80 μ s; 10240 TOFs; 10 mA ionizer current; 1250 V PMT voltage; 120 Hz chopper wheel]

iii) scattering experiment of helium seeded tricarbon with neon utilizing pulsed sources [data were collected for 30 s with p(helium) = 4 atm, p(neon) = 4 atm, dwell time = 5.12 μ s, 5120 TOFs, 10 mA ionizer current, 1400 V PMT voltage].

iv) reactive scattering experiments of carbon atoms with methylacetylene [to show that the new machine can produce reactive scattering data, we repeated the reactive scattering experiment of carbon atoms with methylacetylene and detected the n-C₄H₃ reaction product at m/e = 50. To compare this system and the intensity of the signal in particular with a previous study, the experiment was carried out with a continuous methylacetylene beam. Data were collected for 10 min with p(helium) = 4 atm, p(methylacetylene) = 400 torr, dwell time = 5.12 μ s, 10 mA ionizer current, 1500 V PMT voltage. These data suggest an enhanced intensity by a factor of about 20].

Table 1: Mass-to-charge (m/e) values and assignment of species observed in the residual gas analyzer mode of our Extrel mass spectrometer. Data were taken with the 1.2 MHz oscillator (1-500 amu). Species at m/e values larger than 44 contribute less than 5 counts compared to 3,000 counts for m/e = 28. Thorium and iridium bearing species originate from the filament, copper from the heated copper leads to the ionizer, iron/nickel/ chromium from the heated stainless steel electrodes

m/e	assignment	m/e	assignment	m/e	assignment	m/e	assignment
1	¹ H ⁺	17	¹⁶ O ¹ H ⁺ / ¹⁷ O ⁺	50	⁵⁰ Cr ⁺	64.3	¹⁹³ Ir ³⁺
2	¹ H ₂ ⁺	18	¹ H ₂ ¹⁶ O ⁺ / ¹⁸ O ⁺	52	⁵² Cr ⁺	65	⁶⁵ Cu ⁺
3	¹² C ⁴⁺	20	⁴⁰ Ar ²⁺	53	⁵³ Cr ⁺	77.3	²³² Th ³⁺
4	¹² C ³⁺	28	¹² C ¹⁶ O ⁺ / ¹⁴ N ₂ ⁺ / ⁵⁶ Fe ²⁺	54	⁵⁴ Cr ⁺ / ⁵⁴ Fe ⁺	95.5	¹⁹¹ Ir ²⁺
6	¹² C ²⁺	29	¹³ C ¹⁶ O ⁺ / ¹⁵ N ¹⁴ N ⁺	56	⁵⁶ Fe ⁺	96.5	¹⁹³ Ir ²⁺
7	¹⁴ N ²⁺	30	¹² C ¹⁸ O ⁺	57	⁵⁷ Fe ⁺	116	²³² Th ²⁺
8	¹⁶ O ²⁺	32	¹⁶ O ₂ ⁺	58	²³² Th ⁴⁺ / ⁵⁸ Ni ⁺	124	²³² Th ¹⁶ O ²⁺
12	¹² C ⁺	40	⁴⁰ Ar ⁺	60	⁶⁰ Ni ⁺	191	¹⁹¹ Ir ⁺
13	¹³ C ⁺ / ¹² CH ⁺	44	¹² C ¹⁶ O ₂ ⁺	61	⁶¹ Ni ⁺	193	¹⁹¹ Ir ⁺
14	¹⁴ N ⁺ / ¹² CH ₂ ⁺	45	¹³ C ¹⁶ O ₂ ⁺	62	⁶² Ni ⁺	232	²³² Th ⁺
15	¹⁵ N ⁺ / ¹² CH ₃ ⁺	47.8	¹⁹¹ Ir ³⁺	63	⁶³ Cu ⁺	248	²³² Th ¹⁶ O ⁺
16	¹⁶ O ⁺ / ¹² CH ₄ ⁺	48.6	¹⁹³ Ir ³⁺	63.7	¹⁹¹ Ir ³⁺	264	²³² Th ¹⁶ O ₂ ⁺

3. Future Plans

The crossed beams machine is now operational. Test experiments (neon-argon, tricarbon-neon, carbon-methylacetylene) verified that the absolute signal and signal-to-noise ratios are improved by a factor of 20-30 (elastic and inelastic scattering) and about 20 (reactive scattering) compared to previous experiments utilizing 'universal' crossed beams machine. From April 2005 on, the scattering experiments of dicarbon and tricarbon will be carried out.

4. Acknowledgements

This work was supported by US Department of Energy (Basic Energy Sciences).

5. Publications

X. Gu, Y. Guo, E. Kawamura, R.I. Kaiser, *Design and performance of a high repetition rate, dual pulse shaper to operate pulsed, piezo electric valves*. Rev. Sci. Instr. (submitted 2005).

X. Gu, Y., Guo, H. Chang, E. Kawamura, R.I. Kaiser, *Design and characteristics of a high precision chopper wheel motor driver to operate ultrahigh vacuum compatible laser ablation sources with nanosecond time accuracy*. Rev. Sci. Instr. (submitted 2005).

X. Gu, Y. Guo, E. Kawamura, R.I. Kaiser, *Design of a compact, air-cooled, cluster-based resistor chain for photomultiplier tubes*. Rev. Sci. Instr. (in progress 2005).

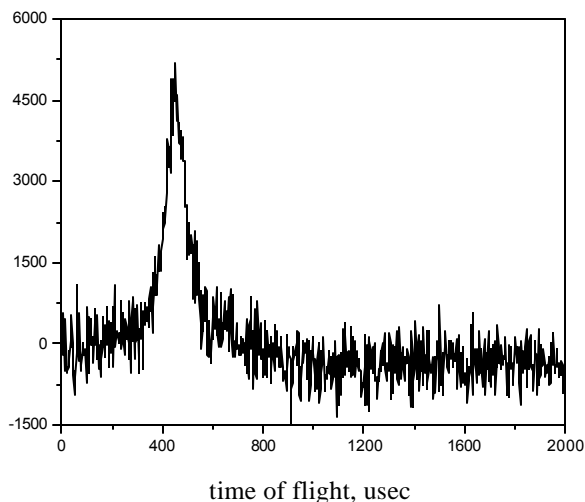


Fig. 1: Neon (1° source) - argon (2° source) elastic scattering signal taken at $m/e = 20$ and at 10° .

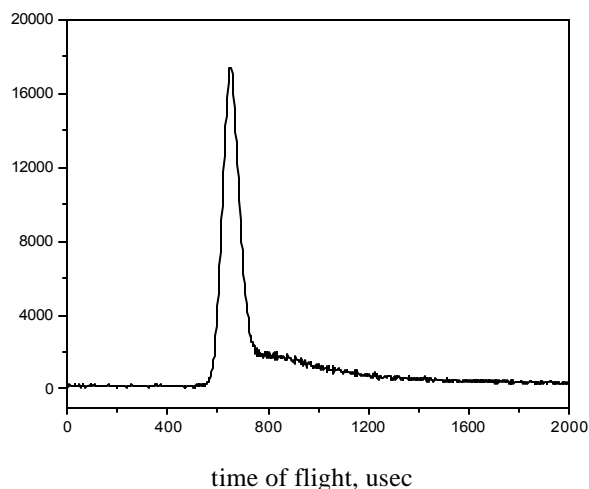


Fig. 2: Neon (source 1) - argon (source 2) elastic scattering signal taken at $m/e = 20$ and 10° .

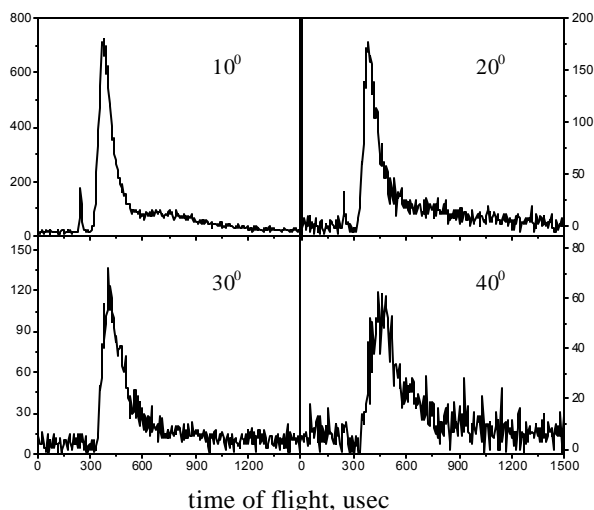


Fig. 3: C_3 -Ne scattering signal taken at $m/e = 36$ at four laboratory angles. The sharp peak at around $250 \mu s$ arises from meta stable species generated in the ablation process. This underscores the necessity of a chopper wheel

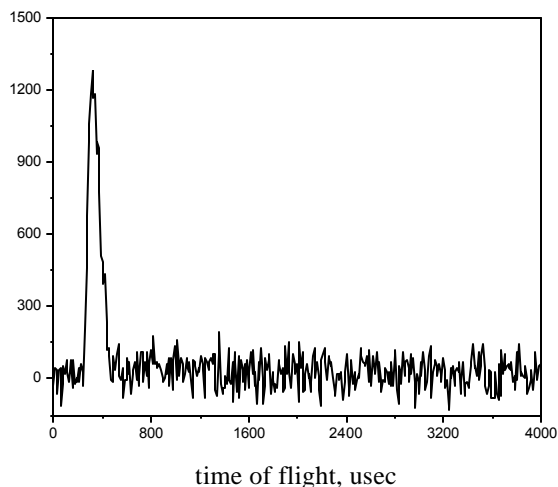


Fig. 4: Reactive scattering signal recorded at $m/e = 50$ of the reaction of carbon atoms with methylacetylene. Data were taken at a laboratory angle of 40° .

DYNAMICAL ANALYSIS OF HIGHLY EXCITED MOLECULAR SPECTRA

Michael E. Kellman

Department of Chemistry, University of Oregon, Eugene, OR 97403

kellman@oregon.uoregon.edu

PROGRAM SCOPE:

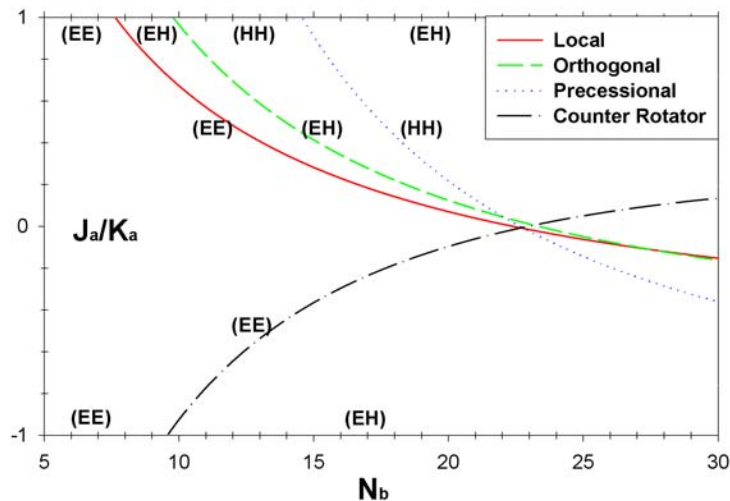
Spectra and internal dynamics of highly excited molecules are essential to understanding processes of fundamental importance for combustion, including intramolecular energy transfer and isomerization reactions. The goal of our program is to develop new theoretical tools to unravel information about intramolecular dynamics encoded in highly excited experimental spectra. We want to understand the formation of "new vibrational modes" when the ordinary normal modes picture breaks down in highly excited vibrations. For this we use bifurcation analysis of semiclassical versions of the effective Hamiltonians used by spectroscopists to fit complex experimental spectra.

The acetylene/vinylidene system is of great importance in combustion, acetylene as an intermediate, and the vinylidene isomer as precursor of the radical pool formed by reaction with O₂. We are nearing completion of an effort to gain a systematic understanding of the bending dynamics of the acetylene system. We have made progress on the difficult but crucial problem of treating the full stretch-bend degrees of freedom. We have begun to make progress in incorporating multiple potentials and above-barrier dynamics, with the goal of extending our methods to encompass isomerization phenomena.

In the near future, the goals are (1) to fully develop and apply our bifurcation methods to systems of greater number of degrees of freedom, in particular, the full stretch-bend dynamics of acetylene; and (2) to develop effective Hamiltonians for analysis of real isomerizing systems.

RECENT PROGRESS: DYNAMICS FROM SPECTRA OF HIGHLY EXCITED ACETYLENE APPROACHING ISOMERIZATION.

Bifurcation analysis: Branchings of the normal modes into new anharmonic modes. Our approach to highly excited vibrational spectra uses bifurcation analysis of the classical version of the effective Hamiltonian used to fit spectra. We have applied this to a bifurcation analysis of the bend degrees of freedom of acetylene. The results are summarized in the bifurcation diagram of Fig. 1. We now understand the number and character of the new modes. We have found that there is a unique "evolutionary tree" of new modes, born in bifurcations of the normal modes. This is in contrast to earlier work on HCP, where multiple bifurcation trees were observed.



Visualization of complex molecular dynamics. One of our primary goals is to translate the abstract dynamical knowledge of the bifurcation analysis into a directly visualizable representation. For this, we are using computer techniques to make animations of the anharmonic modes born in bifurcations. Examples of our animations can be found on a web-site at [http://darkwing.uoregon.edu/~sim\\$meklab/](http://darkwing.uoregon.edu/~sim$meklab/), which the interested reader is invited to access.

Higher 1-vibrational angular momentum states of acetylene. The bifurcation analysis of the pure bends system described above is for spectra with vibrational angular momentum $\mathbf{l} = 0$ in the fitting Hamiltonian. Obviously, it is of great interest to extend the analysis to systems with $\mathbf{l} > 0$, which constitutes a second polyad number, with the complications discussed above. We have performed the bifurcation analysis for $\mathbf{l} = 2, 6, 10$. The results are shown in bifurcation diagrams in Fig 2. Three points are worthy of notice. Fig. 2 starts out similar to Fig. 1, but with added structure (a second panel, right-hand member of each column), because of the added freedom which $\mathbf{l} > 0$ constitutes. The task before us is to understand the qualitative nature and dynamical implications, classical and quantum, of these new bifurcations. Finally, an eventual issue is to include rotation degrees of freedom when we have sufficient mastery of the full vibrational problem; this point is clearly approaching with our progress on the $\mathbf{l} > 0$ system.)

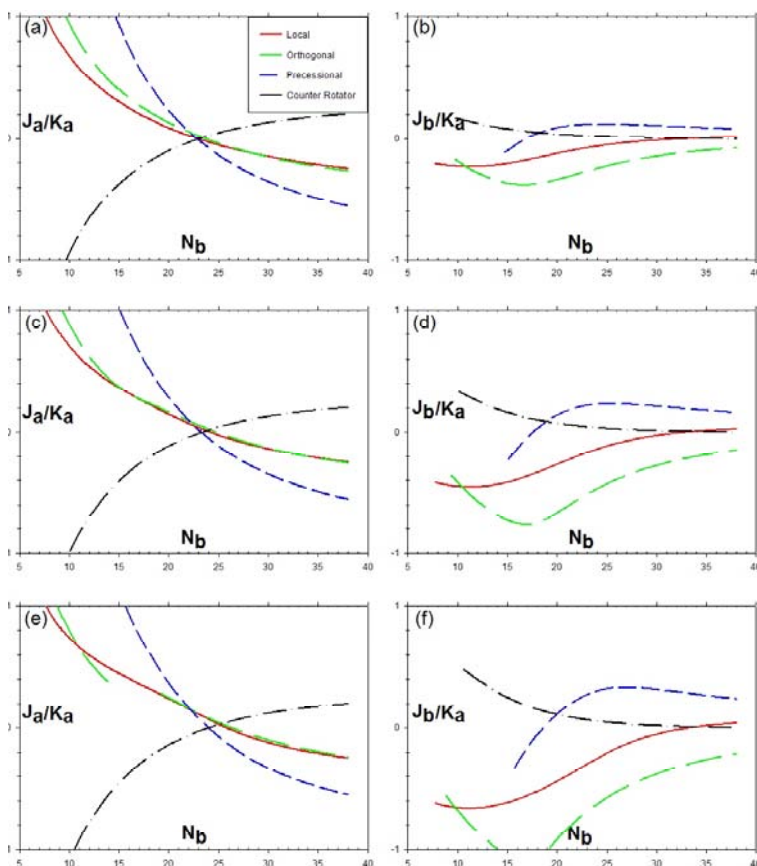


Fig. 2. Critical points with $\mathbf{l} = 2, 6, 10$ (top, middle, and bottom). The left panel for each \mathbf{l} is analogous to Fig. 1 for $\mathbf{l} = 0$; the right panel for each \mathbf{l} is new phase space behavior with $\mathbf{l} > 0$.

FUTURE PLANS: FULL STRETCH-BEND DYNAMICS, ABOVE BARRIER MOTION AND ISOMERIZATION DYNAMICS.

The bifurcation analysis completed so far is for pure bends spectra. It is of great interest to extend this to systems with combinations of stretch and bend excitation, for which fitting Hamiltonians of existing experimental spectra are available. Another major goal is to extend the bifurcation approach to isomerizing systems. We have made a start with the study on model isomerizing systems in Ref. 2. The challenge, however, is to extend the bifurcation analysis of real spectroscopic Hamiltonian to multiple potential wells, and very large-amplitude motion above two or more wells.

The challenge of higher dimensions: Analytically scalable bifurcation analysis.

Existing spectra of the acetylene system access states in which the stretches and bends are coupled in a highly complex way. As the dimensionality of the problem becomes larger, one of the challenges is whether our analysis can be performed, in a way that is still understandable and useful.

The key to making tractable larger systems such as the full stretch-bend degrees of freedom is use of the polyad quantum number, which is an integral part of the standard spectroscopic fitting Hamiltonian. A fact that has been rarely utilized outside our group is that the polyad Hamiltonian makes possible determination of the mode bifurcation structure by *analytic* means, i.e. by solution of simple algebraic equations related to the Hamiltonian function, rather than numerical solution of the equations of motion. Specifically, in our approach we seek the critical points or “flat spots” of the polyad Hamiltonian. Because the critical points are obtained analytically, it is not necessary to perform numerical integration of Hamilton's equations and analysis of surfaces of section. This is expected to become extremely advantageous as the number of degrees of freedom and phase space dimensions increase, as in the full stretch-bend system.

“Reaction modes” from bifurcation analysis. Another issue has to do with the relation of modes born in bifurcations to molecular reaction dynamics, in particular molecular rearrangements. Intuitively, it seems that certain of the new modes born in bifurcations should be implicated when a system undergoes a rearrangement. A reaction mode would be a vibrational mode that follows closely a reaction path i.e. minimum energy path on the molecular potential surface. In acetylene, the natural candidate for the acetylene/vinylidene isomerization reaction mode is the local bend. More generally, it is desirable to explore “reaction modes” born in bifurcations as a general concept in polyatomic rearrangements

Spectroscopic Hamiltonians for multiple wells and above barrier spectroscopy. The basic problem is to build an effective spectroscopic Hamiltonian. Nobody has yet done this, but developments in experiment and theory make the time ripe to face this challenge. The familiar spectroscopic Hamiltonian consists of two parts: a zero-order part which is diagonal in the zero-order quantum numbers; and a coupling part consisting of a sum of resonance coupling operators.

For systems with multiple wells and above-barrier motion, there are two problems in building an effective resonance Hamiltonian. The first is to define separate zero-order quantum numbers for each of the well regions and for the above-barrier region. The second is to define coupling operators that couple the zero-order states. Most challenging of all is to devise cross-barrier couplings that act above and below the barrier, and between wells.

Recent publications (in print or in press since 2003) related to DOE supported research:

1. S. Yang, V. Tyng, and M.E. Kellman, “Spectral Patterns of Isomerizing Systems”, *J. Phys. Chem. A.* 107, 8345-8354 (2003).
2. M.E. Kellman, M.W. Dow, and Vivian Tyng, "Dressed Basis for Highly Excited Vibrational Spectra", *J. Chem. Phys.* 118, 9519-9527 (2003).

High Energy Processes

Alan R. Kerstein
Combustion Research Facility
Sandia National Laboratories
Livermore, CA 94551-0969
Email: arkerst@sandia.gov

PROJECT SCOPE

This project focuses on the development and application of a novel mathematical representation of the random nature of advection in turbulent flows. The conventional representation of random advection in turbulence involves time advancement of equations governing statistical properties of an ensemble of flow realizations. This Fokker-Planck type of treatment can be associated (non-uniquely) with a representation of fluid-element trajectories in individual flow realizations based on Langevin-type stochastic differential equations.

This treatment has enjoyed considerable success in diverse applications, but is subject to limitations that are severe in some situations. Applications to date capture, at best, two-point correlations of flow properties, and therefore provide only a partial representation of the coherence and non-negligible spatial extent of individual eddy motions within turbulence. Turbulent combustion is prominent among scientific problems requiring a relatively detailed representation of flow structure. Details of chemical-kinetic evolution that determine flame ignition, extinction, radiative emission, and pollutant formation are coupled to turbulent motion in a manner that in some instances is not adequately captured within the Langevin-Fokker-Planck framework. Another example that is relevant to combustion and also to a variety of other technological and environmental flows is the collision and coagulation of small particles or droplets.

The modeling framework introduced in this project can be described as event-based advection. Consider a series of snapshots of a turbulent flow. If one does not model the continuous time advancement from one snapshot to the next, but rather models the motion as sudden displacement of all fluid elements from their original positions (first snapshot) to their final positions (second snapshot), implemented at the instant of the second snapshot, then a discrete-event representation of continuous-in-time fluid motion is obtained. This in fact is the strategy generally adopted for numerical advancement of the exact governing equations, where the numerical time step corresponds to the time interval between snapshots.

However, the concept of event-based advection can be extended from a near-exact but costly (hence limited in scope) numerical solution of the exact equations to a model-based flow representation that compromises fidelity to reduce computational cost. The benefit of this strategy depends on the trade-off between the cost reduction that is achieved and the loss of fidelity that is incurred. Work during this project has provided many demonstrations of the advantages of this strategy.

Conceptually, the benefit of this approach, in the context of random advection, is that the modeled advection event is a mapping of the entire flow onto a new spatial arrangement of all fluid elements (though not all fluid is necessarily displaced during each event). The model is formulated so that the sequence of events captures the random nature of fluid-element trajectories, while individual events capture the coherent nature of the displacement of extended regions of the flow.

Two model formulations of this type have been shown to be beneficial in this regard. One involves the introduction of event-based models of reduced dimensionality, with emphasis on implementation in one spatial dimension in a formulation denoted one-dimensional turbulence (ODT). This reduction of dimensionality enables considerable cost reduction while capturing relevant flow phenomenology with minimal empiricism. [4,7-9]. An alternative strategy being pursued in current work involves advection based on 3D mappings. The intended application of this strategy, and its benefit in that context, is discussed in the last section.

A current research direction that is described in the next section is the coupling of arrays of event-based simulations, each implemented in 1D, so as to obtain a 3D flow simulation with advantageous cost-benefit characteristics. Success of this effort would introduce a new form of flow simulation, with some features in common with spatially filtered large-eddy simulation (LES), but unique in that it can affordably provide the spatial resolution of near-exact direct numerical simulation (DNS) for some flows of interest that cannot be affordably simulated using DNS.

RECENT PROGRESS

In earlier work [2], arrays of wall-normal ODT domains were imbedded in LES of channel flow in order to provide sub-filter-scale wall-normal spatial refinement in the vicinity of the walls. This work demonstrated that ODT can improve the fidelity of under-resolved turbulent flow simulations through selective spatial refinement in 1D.

To broaden the applicability of ODT as an economical spatial refinement method, an initial test of a turbulent flow simulation based on coupled arrays of ODT domains in all three coordinate directions has recently been performed [A]. In this context, ODT is not just a subgrid-scale closure. Rather, it is an all-scale model in 1D, with cross-directional domain couplings that capture the 3D character of the flow at scales larger than the separation of adjacent ODT domains, which is orders of magnitude larger than the 1D spatial refinement within each ODT domain. This does not mean that 3D flow characteristics are entirely absent at scales smaller than the domain separation. They are represented, albeit in an idealized manner, by means of the ODT stochastic event-based advection model [4,7-9].

Within this framework, ODT is an all-scale model in both a physical and an operational sense. Its all-scale physical character is highlighted by the time evolution of velocity power spectra during simulated evolution of homogeneous, isotropic decaying turbulence. The power spectra evaluated on ODT domains resemble measured power spectra at all scales resolved on the 1D domains [A]. Operationally, this ODT-based 3D turbulence simulation is different from conventional LES subgrid closure in that there is no time advancement of the momentum equation on a 3D LES mesh. Momentum advancement is wholly represented by ODT processes, with the caveat that an LES-scale 3D pressure projection is performed in order to enforce continuity within the present incompressible formulation. In future work (next section), a compressible formulation will be implemented that will eliminate the need for pressure projection and thus enable fully autonomous ODT-based 3D turbulent flow simulation.

Despite the gain in efficiency resulting from resolution of the smallest scales in 1D rather than 3D, this methodology cannot affordably resolve all relevant flow and molecular-transport scales for all flows of interest. Therefore a conventional eddy-viscosity-type closure that is suitable for implementation within ODT has been developed [B]. Its derivation involves an adaptation of the

theoretical basis of conventional LES subgrid closure to ODT. An interesting outcome of this effort is that the eddy-viscosity closure derived in this manner is found to have significant performance advantages for closure of conventional LES relative to closures that are commonly used. The newly developed closure has been used both in a single-domain ODT geophysical-flow application [9,10] and in the 3D ODT-based simulation of decaying turbulence [A].

FUTURE WORK

The 3D ODT-based simulation method will be reformulated as a compressible-flow simulation. For low-speed flows, it will be implemented as a pseudo-compressible simulation (using an artificially low sound speed to increase acoustic time scales). This will eliminate the need for a pressure-projection step to enforce continuity, rendering the 1D advancement truly autonomous (i.e., not requiring any inherently 3D solution steps). Resulting simplification of the enforcement of conservation laws will establish transparent relationships between this method and conventional LES and DNS, allowing straightforward comparison of the advantages of each for application to a given problem. The new formulation will be validated through application to a suite of canonical flows within the following flow categories: homogeneous flows, free shear flows, wall-bounded flows, buoyant stratified flows. For application to multi-physics problems, established ODT representations of variable-density effects [7], buoyancy effects [4,8], and multi-phase flow phenomena [C] will be incorporated. In conjunction with the recently developed subgrid closure method for under-resolved ODT [B], this development effort will produce a versatile, cost-effective multi-scale multi-physics turbulence simulation tool.

The discussion of project scope mentions a 3D implementation of event-based advection. As in 1D, 3D event-based advection processes can be defined that capture the correlated-though-stochastic nature of turbulent fluid motions. There is no obvious advantage to applying event-based stochastic advection on a spatially resolved 3D mesh because the cost of molecular-transport implementation remains high.

However, there is a class of problems for which mesh-free Lagrangian advancement is feasible. Notably, the motions, collisions, and coalescence of a dispersed phase (particles or droplets) in turbulence can be treated in this manner.

In fact, event-based evolution is familiar in this context. Gillespie [D] developed an efficient stochastic event-based method for selecting droplet pairs that are combined during a numerical simulation of coalescence. This Monte Carlo simulation based on the master equation governing state transitions captures important fluctuation effects omitted from the ensemble-mean (Smoluchowski-type) evolution equation governing this process.

This approach lacks any representation of the spatial distribution of droplets, and therefore neglects effects of droplet spatial clustering, whose existence and importance were recognized after this approach was developed [E]. Accordingly, a Monte Carlo method will be implemented that evolves droplet trajectories explicitly yet retains the efficiency of Gillespie's event-based sampling. This involves linked-list algorithmic representation of droplet spatial locations, time advancement of droplet locations by advection events incorporating the combined effects of fluid motion and droplet inertia, and a collision-detection protocol. A preliminary mathematical analysis has identified a suitable class of 3D event-based advection processes that reproduce salient spatial characteristics and parameter dependencies of droplet clustering that were previously identified through theoretical and computational study.

Other research efforts not described here are being pursued through collaborations addressing problems in turbulent combustion, stellar convection, cloud dynamics, and the turbulent flow of multiple immiscible fluid phases. These efforts will continue. Another ongoing effort is the development of improved models of the time advancement of ensemble-average flow statistics by means of probabilistic analysis of stochastic event-based advection. Finally, an initiative is planned on mathematical analysis of front propagation through random media (e.g., heterogeneous propellant combustion) and stirred fluids (e.g., turbulent combustion) in order to develop a well-founded theory of these processes.

REFERENCES

- A. R. C. Schmidt, R. McDermott, and A. R. Kerstein, "ODTLES: A Model for 3D Turbulent Flow Based on One-dimensional Turbulence Modeling Concepts," Sandia National Laboratories Report SAND2005-0206 (2005).
- B. R. J. McDermott, A. R. Kerstein, R. C. Schmidt, and P. J. Smith, "Ensemble Mean Closure for Large-Eddy Simulation based on 'One-Dimensional Turbulence' Modeling Concepts," submitted to *J. Turbulence* (2005).
- C. J. R. Schmidt, J.O.L. Wendt, and A. R. Kerstein, "Prediction of Particle-Laden Turbulent Channel Flow Using One Dimensional Turbulence," submitted for publication in *Proc. IUTAM Sympos. on Computational Approaches to Disperse Multiphase Flow*, Kluwer (2005).
- D. D. T. Gillespie, "An Exact Method for Numerically Simulating the Stochastic Coalescence Process in a Cloud," *J. Atmos. Sci.* **32**, 1977 (1975).
- E. W. C. Reade and L. R. Collins, "Effect of Preferential Concentration on Turbulent Collision Rates," *Phys. Fluids* **12**, 2530 (2000).

PUBLICATIONS SINCE 2003

1. Wm. T. Ashurst, A. R. Kerstein, L. M. Pickett, and J. B. Ghandhi, "Passive Scalar Mixing in a Spatially Developing Shear Layer: Comparison of ODT Simulations with Experimental Results," *Phys. Fluids* **15**, 579 (2003).
2. R. C. Schmidt, A. R. Kerstein, S. Wunsch, and V. Nilsen, "Near-Wall LES Closure Based on One-Dimensional Turbulence Modeling," *J. Comput. Phys.* **186**, 317 (2003).
3. A. R. Kerstein, "Turbulence in Combustion Processes: Modeling Challenges," *Proc. Combust. Inst.* **29**, 1763 (2003).
4. S. Wunsch, "Stochastic Simulations of Buoyancy-Reversal Experiments," *Phys. Fluids* **15**, 1442 (2003).
5. S.E. Woosley, S. Wunsch, and M. Kuhlen, "Carbon Ignition in Type Ia Supernovae: An Analytic Model," *Astrophys. J.* **607**, 921 (2004).
6. S. Wunsch and S.E. Woosley, "Convection and Off-Center Ignition in Type Ia Supernovae," *Astrophys. J.* **616**, 1102 (2004).
7. Wm. T. Ashurst and A. R. Kerstein, "One-Dimensional Turbulence: Variable-Density Formulation and Application to Mixing Layers," *Phys. Fluids* **17**, 025107 (2005).
8. S. Wunsch and A. R. Kerstein, "A Stochastic Model for High Rayleigh Number Convection," *J. Fluid Mech.* **528**, 173 (2005).
9. A. R. Kerstein and S. Wunsch, "Simulation of a stably stratified atmospheric boundary layer using One-Dimensional Turbulence," *Bound. Layer Meteorol.*, in press (2005).
10. J. Cuxart, A. A. M. Holtslag, A. R. Kerstein, S. Wunsch, *et al.*, "Single-column model intercomparison for a stably stratified atmospheric boundary layer," *Bound. Layer Meteorol.*, in press (2005).

KINETICS OF COMBUSTION-RELATED PROCESSES AT HIGH TEMPERATURES

J. H. Kiefer

Department of Chemical Engineering

University of Illinois at Chicago
Chicago, IL 60607
(kiefer@uic.edu)

Program Scope

This program involves the use of the shock tube with laser-schlieren, dump-tank GC/MS analysis, and time-of-flight mass spectrometry as diagnostics for the exploration of reaction rates and energy relaxation processes over an extremely wide range of temperatures and pressures. We are interested primarily in energy transfer and the kinetics of unimolecular reactions at combustion temperatures, in particular the phenomena of unimolecular incubation and falloff. Over the past year we have managed to obtain some new results on all of these.

Relaxation

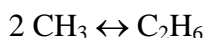
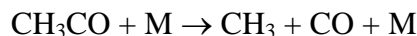
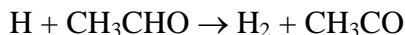
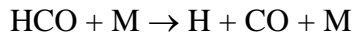
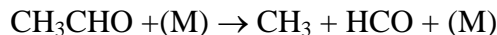
In an effort to further understand our earlier observation of non-RRKM dissociation in 1,1,1-trifluoroethane [pub.#4, below], we have begun a study of relaxation and dissociation in the related 1,1-difluoroethane. This project is not complete, and the dissociation presents several difficulties that may well be insurmountable (see below), but we have been able to establish that the relaxation is not double as it is in the trifluoro compound. We also have investigated relaxation in the product vinyl fluoride where it has been possible to fully establish accurate rates for both molecule and rare gas diluent, and to accurately extrapolate to the room-T ultrasonic pure-molecule relaxation time. This molecule has peculiarly optimal rates for such a complete characterization. We plan to publish this after some minor additional analysis. We have also measured relaxation in pyrazine, a popular donor species for pump/probe studies of energy transfer [1]. Not surprisingly, these experiments show that relaxation in pyrazine is non-exponential as it is in benzene [2]. Nonetheless, relaxation times can be extracted and low-energy $\langle \Delta E \rangle_{\text{down}}$ values extracted for comparison with higher-energy results.

Dissociation

As mentioned above we have carried out a large number of experiments on the HF elimination from 1,1-difluoroethane in an effort to characterize falloff in this molecule. Unfortunately, this reaction again has a rather small ΔH_{298}° (27 kcal/mol), leading to small gradients, and dissociation of the product vinyl fluoride also now interferes. To deal with this problem, we have done a very complete study of the product dissociation, and this study is now almost complete. It still seems we will be able to produce reasonably accurate rates for the difluoroethane dissociation, and we are continuing to work on the matter.

Some time ago we began a very extensive examination of the acetaldehyde decomposition. As has been known for a very long time, in mixtures not extremely dilute,

this is a fast chain reaction initiated by C-C fission, and carried by both H and CH₃. The most important reactions are well known to be



The recent and convincing presentation of a reduced rate for the HCO dissociation [3] has increased the late exothermicity in the calculations (mainly from the last step) to the point where we are finally able to produce a near quantitative modeling of the entire observed gradient. Examples of this are shown in Fig. 1. Here both the initial positive gradients (dissociation of the parent) and both the onset and magnitude of the subsequent chain exothermicity are all beautifully reproduced, and this is true for a very large number of such experiments. The majority of these are actually similar to the upper right example, where the long initial positive gradient allows extraction of an unambiguous dissociation rate. Here the reproduction of the exothermic gradients is a strong indication that the entire chain is essentially correct and certainly its contribution to the dissociation gradients is properly accounted for. As with ethane (Pub. # 5), when the secondary chemistry is solid, it is possible to produce a very complete description of LS gradients. We plan to extend these determinations to lower pressures to complete the examination of falloff in this molecule.

Regarding the origin of non-RRKM behavior in 1,1,1-trifluoroethane

We would still suggest that both the non-RRKM behavior of the four-center fission of this molecule and our observation of a double relaxation (pub. #4, below) are a consequence of slow IVR from the low-frequency torsion. The notion is that this mode is thermally excited by rapid T,R-V but its symmetry is such that it does not easily transfer this energy to the other modes; hence the double relaxation. Unlike other dissociation reactions, here excitation of this mode does not assist reaction, in fact it is likely to impede it. At the four-center TS for HF elimination there is a large torsional barrier (see Fig. 2) and adiabatic motion to this TS is actually impeded by significant torsional excitation. For dissociation energies, more than 90% of the states have torsional energy. It is then not clear whether preferential excitation of the torsion is actually necessary for the observed reduction in rate, considering that in falloff with slow IVR the other modes will be relatively depleted by reaction. So even thermal activation of the torsion might lead to the anomalously low rate observed for this reaction. This torsional interpretation

seems fairly convincing, but remains qualitative, and it would be very difficult to make anything quantitative of it. We now have some indirect experimental support for this model in that relaxation of the unsymmetrical difluoroethane is not double (as above), and the dissociation of ethane, long known to show such a double relaxation, is solidly RRKM [Pub. #5, below]. Here, of course, the reaction is a C-C fission, and is thus unimpeded by torsional excitation.

Time-of-flight mass spectrometer construction

Please see the abstract of R.S. Tranter for this.

Future work

Our intentions for the forthcoming year include the extended use of our simple method for the extraction of $\langle \Delta E \rangle_{\text{down}}(\alpha)$ from the extensive array of Pt data generated by us and many others. We plan to use our combined TOF/LS facility to reinvestigate the decomposition of toluene, now properly dealing with the chemical activation step: $\text{H} + \text{C}_7\text{H}_7 \rightarrow \text{C}_7\text{H}_8^* \rightarrow \text{CH}_3 + \text{C}_6\text{H}_5$ by combining variflex calculations with the recent results of L. B. Harding for the recombinations. Longer-range plans include the examination of falloff in the dissociation of pyrrole and perhaps cyclohexane, all to involve the TOF and again selected in part for their practical importance.

References

1. C. A. Michaels, A. S. Mullin, and G.W. Flynn, J. Chem. Phys. **102**, 6682 (1995); A. S. Mullin, C. A. Michaels and G.W. Flynn, J. Chem. Phys. **102**, 6032 (1995).
2. J. H. Kiefer, L. L. Buzyna, A. Dib, And S. Sundaram, J. Chem. Phys. **113**, 48 (2000).
3. L. N. Krasnaperov, E. N. Chesokov, H. Stark, and A. R. Ravshankara, J. Phys. Chem. **108**, 11526 (2004).

Publications

1. "Dissociation, Relaxation, and Incubation in the Pyrolysis of Neopentane: Heat of Formation for *tert*-butyl Radical", N. K. Srinivasan, J. H. Kiefer, and R.S. Tranter, J. Phys. Chem. **107**, 1532 (2003).
2. "A Shock-Tube, Laser-Schlieren Study of the Pyrolysis of Isobutene: Relaxation, Incubation, and Dissociation Rates", S. Santhanam, J. H. Kiefer, R.S. Tranter and N. K. Srinivasan, Int. J. Chem. Kinet. **35**, 381 (2003).
3. "Vibrational Relaxation in Methyl Hydrocarbons at High Temperatures: Propane, Isobutene, Isobutane, Neopentane and Toluene", J. H. Kiefer, G. C. Sahukar, S. Santhanam, N. K. Srinivasan., and R.S. Tranter, J. Chem. Phys., **120**, 918 (2004).
4. "A Shock-Tube, Laser-Schlieren Study of the Dissociation of 1, 1, 1-Trifluoroethane: An Intrinsic non-RRKM Process", J. H. Kiefer, C. Katopodis, S. Santhanam, N. K. Srinivasan, and R. S. Tranter, J. Phys. Chem. **108**, 2443 (2004).
5. "Dissociation, Relaxation, and Incubation in the High-Temperature Pyrolysis of Ethane, and a Successful RRKM Modeling", J. H. Kiefer, S. Santhanam, N. K. Srinivasan, R.S. Tranter, and S. J. Klippenstein, Proc. Combust. Inst. **30**, 1129 (2005).

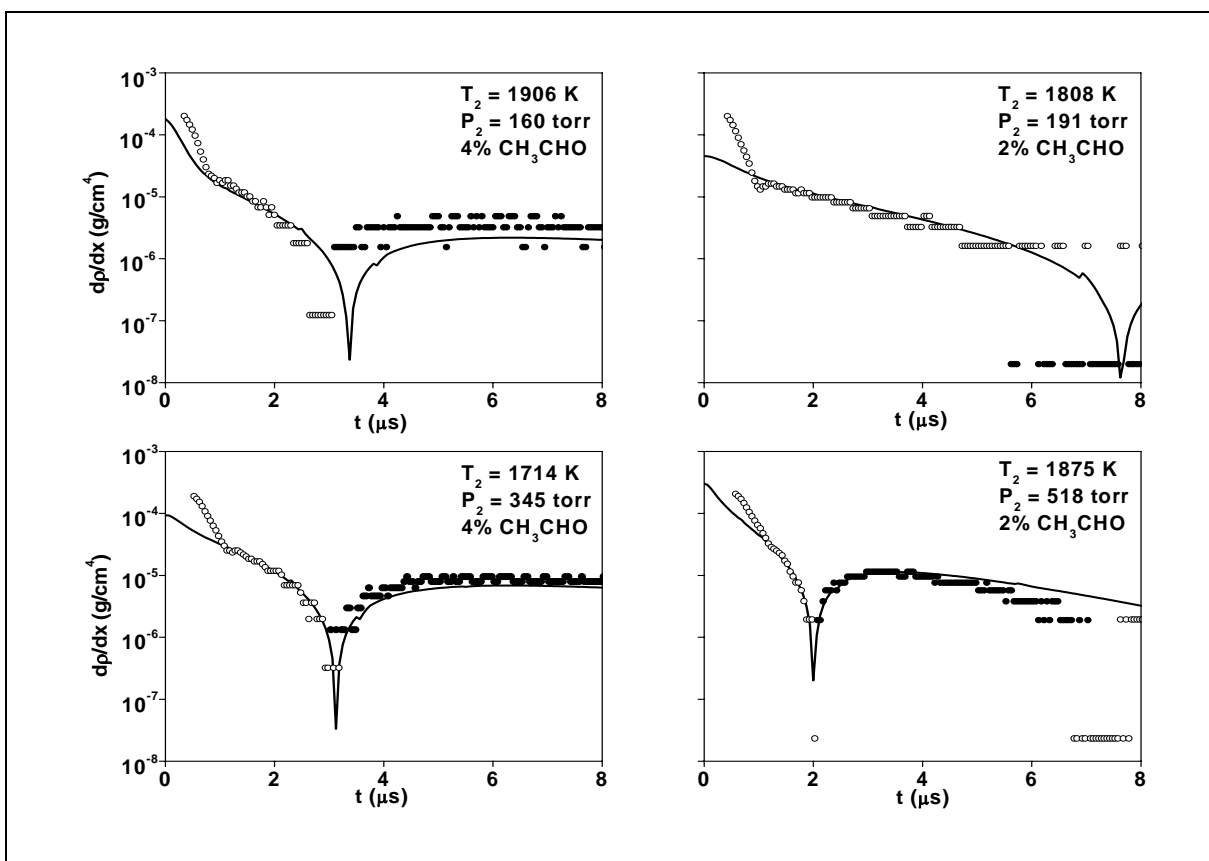
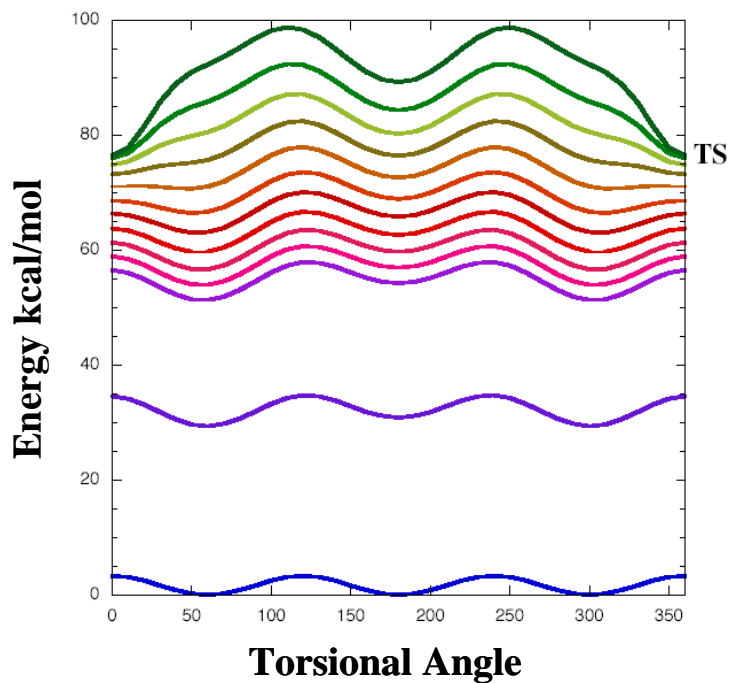


Fig. 1. Acetaldehyde pyrolysis gradients (absolute values). Measured gradients as circles, empty positive, filled negative. The solid lines show simulations.

Fig. 2. Torsion potentials for CH_3CF_3 following the reaction path from the TS down in energy, by Larry Harding, at B3LYP/6-31G*.

The bottom curve is the minimum energy (here at the TS for internal rotation). The top curve is at the TS for HF elimination. Here the torsion barrier has increased to over 20 kcal/mol.



THEORETICAL CHEMICAL KINETICS

Stephen J. Klippenstein
Combustion Research Facility
Sandia National Laboratories
Livermore, CA, 94551-0969
E-mail: sjklipp@sandia.gov

Program Scope

The focus of this program is the theoretical estimation of the kinetics of elementary reaction steps of importance in combustion chemistry. The research involves a combination of *ab initio* quantum chemistry, variational transition state theory, direct dynamics, and master equation simulations. The emphasis of our current applications is on (i) reactions of importance in soot formation, (ii) radical oxidation reactions, and (iii) NO_x chemistry. We are also interested in a detailed understanding of the limits of validity of and, where feasible, improvements in the accuracy of specific implementations of transition state theory. Detailed comparisons with experiments, and with other theoretical methods are used to explore and improve the predictive properties of the transition state theory models. Direct dynamics simulations are being performed as a means for testing the statistical assumptions, for exploring reaction mechanisms, and for generating theoretical estimates where statistical predictions are clearly inadequate. Master equation simulations are used to study the pressure dependence of the kinetics and to obtain phenomenological rate coefficients for use in kinetic modeling.

Recent Progress

Radical-Radical Associations (in collaboration with Larry Harding)

We have developed and applied an efficient and quantitatively accurate method for predicting the kinetics of radical-radical association reactions. The approach is based on CASPT2/cc-pvdz evaluations of the orientation dependent interaction energies within variable reaction coordinate transition state theory (VRC-TST). One-dimensional corrections to the interaction energies are estimated from CAS+1+2/aug-cc-pvtz evaluations for a simple reference system. Our first application of this approach was to the association of H atoms with hydrocarbon radicals. The corrected CASPT2 approach yielded results that are within 10% of those obtained with the full CAS+1+2/aug-cc-pvtz potential for the H + CH₃, H + C₂H₅, H + C₂H₃, and H + C₂H reactions. New predictions were made for the H + *iso*-C₃H₇, H + *tert*-C₄H₉, H + C₆H₅, and H + C₁₀H₇ reactions. For the H + CH₃ and H + C₂H₃ reactions, where the experimental values appear to be the most well determined, theory and experiment essentially agree to within their error bars. For the other reactions the agreement is reasonably satisfactory given the often large dispersion in the experimental results. For the reactions with saturated alkyl radicals, the theory predicts that each additional CH₃ group increases the steric factor by approximately a factor of two. In contrast, for the unsaturated radicals, the H + C₆H₅ and H + C₁₀H₇ high pressure association rate coefficients are nearly identical to that for H + C₂H₃.

As the next application of this approach we have considered the association kinetics of two alkyl radicals using the CH₃ + CH₃ addition for the development of the one-dimensional correction to the potential. For this reaction the corrected CASPT2/cc-pvdz and CAS+1+2/aug-cc-pvtz results were again found to be in good agreement. Predictions were made for the methyl, ethyl, *iso*-propyl and *tert*-butyl radical recombinations and for their cross reactions. Detailed

comparisons with experiment suggest that the present approach provides quantitatively accurate predictions. Each additional methyl group is again found to reduce the addition rate by about a factor of two. In each instance, the rates are predicted to decrease quite substantially with increasing temperature, with the more sterically hindered reactants having a more rapid decrease. The simple geometric mean rule, relating the rates for the cross reactions to those for the self reaction, is in reasonable agreement with the more detailed predictions. For $\text{CH}_3 + \text{CH}_3$, direct trajectory simulations, performed at the B3LYP/6-31g* level, indicate that there is again little local recrossing of the optimal variable reaction coordinate transition state dividing surface.

Two Transition States Models

In collaboration with Simon North we have applied a two transition state model to the addition kinetics of hydroxyl radical to ethylene. This reaction serves as a prototypical example of a radical-molecule reaction with a negative activation energy in the high pressure limit. The model incorporates variational treatments of both inner and outer transition states. The outer transition state is treated with our recently derived long-range transition state theory approach focusing on the longest ranged term in the potential. High level quantum chemical estimates are incorporated in a variational transition state theory treatment of the inner transition state. Anharmonic effects in the inner transition state region are explored with direct phase space integration. A two dimensional master equation is employed in treating the pressure dependence of the addition process. An accurate treatment of the two separate transition state regions at the energy and angular momentum resolved level is found to be essential to the prediction of the global temperature dependence of the addition rate. The transition from a dominant outer transition state to a dominant inner transition state is predicted to occur at about 130 K, with significant effects from both transition states over the 10 to 400 K temperature range. Modest adjustment in the ab initio predicted inner saddle point energy yields theoretical predictions which are in quantitative agreement with the available experimental observations.

In collaboration with Mitsuo Koshi we have applied a related two transition state model to the kinetics on the Si_2H_6 potential energy surface (PES). These calculations confirm that the dissociation of Si_2H_6 to $\text{H}_3\text{SiSiH} + \text{H}_2$ is negligible under conditions relevant to the thermal chemical vapor deposition (CVD) processes. Predictions for the temperature and pressure dependent chemical activation rate coefficients ($\text{SiH}_2 + \text{SiH}_4 \rightarrow \text{Si}_2\text{H}_6$ and $\text{SiH}_2 + \text{SiH}_4 \rightarrow \text{H}_3\text{SiSiH} + \text{H}_2$), indicate that the latter reaction is the dominant channel for low pressures and high temperatures; i.e., below 100 Torr for temperatures above 1100 K. In the words of a reviewer this work “ties together many of the findings and discrepancies of the last 20 years of the modern era of silicon hydride kinetics”.

Radical Oxidation

In collaboration with Jim Miller, we have calculated the PES for the reaction between OH and acetylene using the RQCISD(T) method extrapolated to the complete basis-set limit. Rate coefficients were determined for a wide range of temperatures and pressures, based on this surface and the solution of the 1-d and 2-d master equations. With a small adjustment to the association energy barrier (1.1 kcal/mol), agreement with experiments is good. The rate for direct hydrogen abstraction is significantly smaller than that commonly employed in combustion models. Also in contrast to previous models, ketene is found to be the main product at normal combustion conditions.

In collaboration with Craig Taatjes we have developed a kinetic model, on the basis of ab initio based time-resolved master equation results, for the formation of HO₂ in the reactions of C₂H₅, *n*-C₃H₇ and *i*-C₃H₇ radicals with O₂. The radicals for this study were generated by the 266 nm photolysis of alkyl iodides. The isomer-specificity of the experimental results enabled refinement of the model for *i*-C₃H₇ + O₂ and improved the agreement with experimental measurements of HO₂ production in propane oxidation.

Soot Formation (in collaboration with Jim Miller)

We have completed a systematic exploration of the PES for the *n*-C₄H₃ + C₂H₂ reaction. Starting from the initial entrance adducts, additional wells were successively added on the basis of their predicted contribution to the flux in the collisionless limit. Incorporating all channels that contribute at least 10% of the flux for some temperature in the range from 300 to 2000 K leads to a 19 well PES. The process is clearly more complex than described in the earlier works of Lin and coworkers, of Walch, and of Frenklach and coworkers. This PES is now being incorporated in master equation simulations of the association rate coefficients. Further calculations will implement this PES, with appropriate extensions, to the treatment of the C₆H₅ dissociation, the *i*-C₄H₃ + C₂H₂ addition, and the additions of H to various linear and cyclic C₆H₄ species.

In other partially completed work on the formation of the first aromatic ring we have calculated the addition rate for the reaction of C₃H₃ + C₃H₄. We have also coupled our detailed PES for the C₃H₃ + C₃H₃ reaction with Mebel's results for other channels on the C₆H₆ PES to obtain kinetic predictions for a number of other reactions on the C₆H₆ PES. We have also shown that the implementation of an association rate for C₃H₃ + C₃H₃ that decreases with temperature according to the expectations from our radical-radical addition studies yields improved agreement with the experimental measurements of Hippler and of Knyazev.

Future Directions

We will continue our studies of radical-radical reactions in collaboration with Larry Harding. These studies will consider the C₃H₃ + C₃H₃ reaction, reactions on the C₇H₈ surface, abstraction reactions, comparisons with simpler harmonic oscillator based predictions, and estimates for the effect of geometric relaxation. We are continuing our exploration of the reactions leading to the formation of the first aromatic ring, including a collaboration with Wes Allen on the C₃H₃ + C₃H₅ reaction. In collaboration with Alexander Mebel, we intend to provide kinetic predictions for a number of the key steps in the HACA and Bittner-Howard mechanisms for the formation of naphthalene. Our work on radical oxidation reactions is continuing with current studies in progress on the C₂H₄ + OH reaction (with Jim Miller), and on the modeling of deuterium isotope effects (with Craig Taatjes).

DOE Supported Publications, 2003-Present

1. John D. DeSain, Stephen J. Klippenstein, Craig A. Taatjes, Michael D. Hurley, and Timothy J. Wallington, *Product Formation in the Cl-Initiated Oxidation of Cyclopropane*, J. Phys. Chem. A, **107**, 1992-2002 (2003).
2. Yuri Georgievskii and Stephen J. Klippenstein, *Variable Reaction Coordinate Transition State Theory: Analytic Results and Application to the C₂H₃ + H → C₂H₄ Reaction*, J. Chem. Phys., **118**, 5442-5455 (2003).
3. John D. DeSain, Stephen J. Klippenstein, and Craig A. Taatjes, *Time-Resolved Measurements of OH and HO₂ Product Formation in Pulsed-Photolytic Chlorine-Atom Initiated Oxidation of Neopentane*, Phys. Chem. Chem. Phys., **5**, 1584-1592 (2003).
4. James A. Miller and Stephen J. Klippenstein, *From the Multiple-Well Master Equation to Phenomenological Rate Coefficients: Reactions on a C₃H₄ Potential Energy Surface*, J. Phys. Chem. A, **107**, 2687-2692, (2003).

5. John D. DeSain, Stephen J. Klippenstein, James A. Miller, and Craig A. Taatjes, *Measurements, Theory, and Modeling of OH Formation in Ethyl + O₂ and Propyl + O₂ Reactions*, J. Phys. Chem. A, **107**, 4415-4427 (2003).
6. James A. Miller and Stephen J. Klippenstein, *The Recombination of Propargyl Radicals and Other Reactions on a C₆H₆ Potential*, J. Phys. Chem. A, **107**, 7783-7799 (2003).
7. Samuel M. Clegg, Bradley F. Parsons, Stephen J. Klippenstein, and David L. Osborn, *Photodissociation dynamics of Dicyclopropyl Ketone at 193 nm: Isomerization of the Cyclopropyl Ligand*, J. Chem. Phys. **119**, 7222-7236 (2003).
8. Yuri Georgievskii and Stephen J. Klippenstein, *Transition State Theory for Multichannel Addition Reactions: Multifaceted Dividing Surfaces*, J. Phys. Chem. A, **107**, 9776-9781 (2003).
9. James A. Miller, Stephen J. Klippenstein, and Peter Glarborg, *A Kinetic Issue in Reburning: The Fate of HCNO*, Comb. Flame, **135**, 357-362 (2003).
10. Stephen J. Klippenstein, *RRKM Theory and Its Implementation*, in Comprehensive Chemical Kinetics, v. 39, xxx, (2003).
11. James A. Miller and Stephen J. Klippenstein, *The H + C₂H₂ (+M) ↔ C₂H₃ (+M) and H + C₂H₄ (+M) ↔ C₂H₅ (+M) Reactions: Electronic Structure, Variational Transition State Theory, and Solutions to a Two-Dimensional Master Equation*, Phys. Chem. Chem. Phys., **6**, 1192-1202 (2004).
12. Frank Striebel, Leonard E. Jusinski, Askar Fahr, Joshua B. Halpern, Stephen J. Klippenstein, and Craig A. Taatjes, *Kinetics of the Reaction of Vinyl Radicals with NO: Ab Initio Theory, Master Equation Predictions, and Laser Absorption Measurements*, Phys. Chem. Chem. Phys., **6**, 2216-2223 (2004).
13. Juan P. Senosiain, Stephen J. Klippenstein and James A. Miller, *A Complete Statistical Analysis of the Reaction of OH with CO*, Proc. Comb. Inst., **30**, 943-950 (2004).
14. Lawrence B. Harding, Stephen J. Klippenstein, and Yuri Georgievskii, *Reaction of Oxygen Atoms with Hydrocarbon Radicals: A Priori Predictions for the CH₃ + O, C₂H₅ + O, and C₂H₃ + O Reactions*, Proc. Comb. Inst., **30**, 985-993 (2004).
15. J. H. Kiefer, S. Santhanam, N. K. Srinivasan, R. S. Tranter, S. J. Klippenstein, and M. A. Oehlschlaeger, *Dissociation, Relaxation, and Incubation in the High-Temperature Pyrolysis of Ethane, and a Successful RRKM Modeling*, Proc. Comb. Inst. **30**, in press (2004).
16. James A. Miller and Stephen J. Klippenstein, *Some Observations Concerning Detailed Balance in Association/Dissociation Reactions*, J. Phys. Chem. A, **108**, 8296-8306 (2004).
17. T. D. Jaeger, D. van Heijnsbergen, S. J. Klippenstein, G. von Helden, G. Meijer, and M. A. Duncan, *Vibrational Spectroscopy and Density Functional Theory of Transition Metal Ion-Benzene and Di-benzene Complexes in the Gas Phase*, J. Am. Chem. Soc., **126**, 10981-10991 (2004).
18. Craig A. Taatjes, Stephen J. Klippenstein, Nils Hansen, James A. Miller, Terrill A. Cool, Juan Wang, Matthew E. Law, and Phillip R. Westmoreland, *Synchrotron Photoionization Measurements of Combustion Intermediates: Photoionization Efficiency of C₃H₂ Isomers*, Phys. Chem. Chem. Phys., **7**, 806-813, (2005).
19. Edgar G. Estupinan, Stephen J. Klippenstein, and Craig A. Taatjes, *Measurements and Modeling of HO₂ Formation in the Reactions of n-C₃H₇ and i-C₃H₇ Radicals with O₂*, J. Phys. Chem. A, in press (2004).
20. Donald G. Truhlar, James A. Miller, Stephen J. Klippenstein, and Antonio Fernandez Ramos, *Bimolecular Reactions*, Comprehensive Chemical Kinetics, in press (2005).
21. Keiji Matsumoto, Stephen J. Klippenstein, Kenichi Tonokura, and Mitsuo Koshi, *Channel Specific Rate Constants Relevant to Thermal Decomposition of Disilane*, J. Phys. Chem. A, in press (2005).
22. Yuri Georgievskii and Stephen J. Klippenstein, *Transition State Theory for Long-Range Potentials*, J. Chem. Phys., in press (2005).
23. Stephen J. Klippenstein and James A. Miller, *The Addition of Hydrogen Atoms to Diacetylene and the Heats of Formation of i-C₄H₃ and n-C₄H₃*, J. Phys. Chem. A, in press (2005).
24. Erin E. Greenwald, Simon W. North, Yuri Georgievskii, and Stephen J. Klippenstein, *A Two Transition State Model for Barrierless Radical-Molecule Reactions: A Case Study of the Addition of OH to C₂H₄*, J. Phys. Chem. A, in press (2005).
25. Peng Zou, Stephen J. Klippenstein, and David L. Osborn, *The Vinyl + NO Reaction: Determining the Products with Time-Resolved Fourier Transform Spectroscopy*, J. Phys. Chem. A, in press (2005).
26. Larry B. Harding, Yuri Georgievskii, and Stephen J. Klippenstein, *Predictive Theory for Hydrogen Atom – Hydrocarbon Radical Association Kinetics*, J. Phys. Chem. A, feature article, in press (2005).
27. Juan P. Senosiain, Stephen J. Klippenstein and James A. Miller, *The Reaction of Acetylene with Hydroxyl Radicals*, J. Phys. Chem. A, in press (2005).

TIME-RESOLVED FTIR EMISSION AND ADVANCED LIGHT SOURCE STUDIES OF PHOTOFRAGMENTATION, RADICAL REACTIONS, AND AEROSOL CHEMISTRY

Stephen R. Leone
Departments of Chemistry and Physics
and Lawrence Berkeley National Laboratory
University of California
Berkeley, California 94720
(510) 643-5467 srl@berkeley.edu

Scope of the Project

Combustion is a complex process involving short-lived radical species, highly excited states, kinetics, transport processes, heterogeneous chemistry and aerosols such as soot, fluid dynamics, and energy transfer. Detailed measurements of microscopic reaction pathways, rate coefficients, vibrational and rotational product state distributions, and thermochemistry have resulted in considerable information to aid in the understanding of combustion processes. Infrared emission is used to explore laser-initiated radical reactions, radical-radical reactions, photofragmentation events, energy transfer processes. Vibrationally excited and low-lying visible electronically excited species generated in chemical dynamics processes are probed by time-resolved Fourier transform emission spectroscopy. The current research involves the study a variety of important radical reactions (e.g. $C_2H + O$, $HCCO + O$, $C_2H + SO_2$, $O + C_2H_2$) to determine the nascent product species and states and the mechanisms and kinetic pathways. The vacuum ultraviolet light at the Chemical Dynamics Beamline of the Advanced Light Source provides a tool to measure the energetics and photoionization spectroscopy of important combustion species. At the Chemical Dynamics Beamline there are efforts to study photoionization spectroscopy of radical species, such as CH_3 (with Branko Ruscic), propargyl (postdoctoral fellow at the beamline Christophe Nicolas), and $CICO$ (with Cheuk Ng). Ongoing work at the Chemical Dynamics Beamline also involves interactions with Terry Cool, Craig Taatjes (Combustion Research Facility), and Phil Westmoreland in their pursuit of the study of flame chemistry. We are working with Taatjes and David Osborn (Combustion Research Facility) on a new kinetics apparatus that uses single photon VUV ionization detection, and we have initiated a new theme to study aerosol formation, light scattering, and aerosol chemistry. The latter effort will explore aerosol species and their roles and production in combustion, and the resulting soot species from combustion. Molecular beam photofragmentation studies were completed by a postdoctoral fellow at the beamline, Jinian Shu, on the dissociation of crotonaldehyde ($CH_3CHCHCHO$), and this type of study is being extended to velocity map imaging using synchrotron radiation for detection. A new laser ablation apparatus has been developed at the beamline with Musa Ahmed to produce and study C_1 , through C_5 species in photoionization. The same source has also been applied to biomolecules by M. Ahmed and to metal oxide species with Ricardo Metz.

$C_2H + O$ Radical-Radical Reaction

The reaction of C_2H with O proceeds with a rate coefficient of $5.6 \times 10^{-11} \text{ cm}^3 \text{ molecule}^{-1} \text{ s}^{-1}$ and produces primarily $CO + CH$; the CH can be formed in the ground $X^2\Pi$ state or excited $A^2\Delta$ state. This reaction was investigated to determine the $CO(v)$ vibrational distribution of the two branching pathways, to reveal information about the ratio of the $CH(X)$ and $CH(A)$ state products and details of the reaction mechanism. Three other reactions, $HCCO + O$, $C_2H + SO_2$,

and $O + C_2H_2$ contribute significantly to the observed $CO(v)$ signals and were also studied. The absolute rate coefficient for $C_2H + SO_2$ was measured in this work to model the product signals. The rate coefficient at room temperature is $(1.1 \pm 0.3) \times 10^{-11} \text{ cm}^3 \text{ molecule}^{-1} \text{ s}^{-1}$. The vibrational distribution of the CO product from $C_2H + O$ extends to $CO(v=12)$ and is strongly bimodal, suggesting two different distributions that correspond to the $CH(X)$ and $CH(A)$ states. In this work, the $CO(v)$ products corresponding to both $CH(X)$ and $CH(A)$ channels are close to statistical, suggesting a long-lived $HCCO$ intermediate; however, the pathway that forms the $CH(X)$ state has a somewhat hotter vibrational distribution, suggesting a possible more direct mechanism for that channel. In addition, the pathway to form $CH(A)$ has a remarkable prominence. New studies have been initiated to quantify the state distributions of the $CH(A^2\Delta)$ species formed in the reaction of C_2H with O . In addition, single photon dissociation at the Advanced Light Source, as well as multiphoton dissociation with short pulse fs lasers is being explored to examine the state resolved dynamics for multiple-body dissociation of molecules, such as bromoform, $CHBr_3$.

O + C₂H₂ and HCCO Reactions

A detailed study was performed on the reactions of the $C_2H_2 + O(^3P)$ and $HCCO + O(^3P)$ using Fourier transform infrared spectroscopy (FTIR). The $C_2H_2 + O$ reaction results in CO , $CH_2(^3B)$ and $HCCO$ products that subsequently react with O atoms producing additional CO and CO_2 products. The analysis of the vibrational states of the vibrationally excited $CO(v)$ reveals the multiple reactions that contribute to the nascent vibrational distribution of the $CO(v)$. By varying the experimental conditions, the nascent vibrational distributions for the $CO(v)$ channels of the $C_2H_2 + O(^3P)$ and the $HCCO + O(^3P)$ reactions are extracted. The nascent vibrational distribution of the $HCCO + O(^3P)$ reaction is obtained for the first time using two separate precursors. In this reaction, two $CO(v)$ product molecules plus an H atom are produced in each reaction. The nascent vibrational distribution of CO from both the $C_2H_2 + O(^3P)$ and $HCCO + O(^3P)$ reactions show noninverted behavior, which is consistent with an intermediate complex mechanism.

Photoionization Measurements

At the Advanced Light Source, a novel laser vaporization source has been developed to produce carbon cluster species for photoionization spectral studies. Such investigations provide basic thermodynamic and structural information for these fundamental species. The cluster source was used to produce C_1 , C_2 , C_3 , C_4 , and C_5 by vaporization of a graphite rod, and the ionization potentials for each of these species have now been measured. The detailed photoionization efficiency data for species such as C_3 , coupled with CAS-SCF calculations on the resulting C_3^+ ion states, performed by our collaborator M. Hochlaf, suggest that additional intensity maxima in the photoionization efficiency versus energy data can be attributed to identifiable electronically excited states of C_3^+ . Work is in progress to revise this information and to determine the implications for the basic thermodynamics and structure correlations of carbon cluster species.

Aerosol Chemistry

Using a newly constructed aerosol machine at the Chemical Dynamics Beamline, we have undertaken fundamental studies of the optical properties of aerosol particles using VUV radiation. Silica particles, chemically synthesized online, are size-selected by a differential mobility analyzer, and introduced into vacuum through a set of aerodynamic lenses. The angular

distributions of scattered photons originating from 70, 100, 200 nm diameter silica particles are measured with 145.9 and 118.1 nm synchrotron radiation. As predicted by Mie Theory, these angular distributions show strong forward scattering. Using Mie theory to analyze the experimental results, the refractive indices of these chemically synthesized silica particles are determined to be $2.6 + 1.1i$ and $1.6 + 0.0001i$ for 118.1 nm and 145.9 nm wavelengths, respectively. A careful comparison of scattered fluxes at visible and VUV wavelengths clearly shows enhanced size sensitivity at shorter wavelengths. The smallest particle size detected with this apparatus using visible illumination was 250 nm. Conversely, the VUV studies exhibited at a small size detection limit of 70 nm, which is limited by the particle transmission efficiency our aerosol endstation. As anticipated, VUV scattering is a more sensitive probe for ultrafine particles and their optical properties.

A collaborative effort with Prof. Eckart Ruhl (University of Würzburg) studied the fundamental electronic properties of nanoparticles for the first time using velocity map imaging (VMI) of the ejected photoelectrons. A pronounced asymmetry in the photoelectron angular distributions was observed and correlated with particle size. The asymmetry is most pronounced for 500 nm diameter particles and decreases with particle size down to 45 nm, suggesting that for insulating particles the light is absorbed on the illuminated surface and the electrons ejected from that surface. However, the magnitude of this asymmetry with particle size is dependent upon the electronic properties. Gold particles, which are conducting, show very little asymmetry compared to an insulator like NaCl. This is presumably due to differences in low energy (1 eV) electron dynamics and the field interactions with a conductor vs. an insulator. Efforts are currently underway to develop a quantitative model of this photoelectron asymmetry.

The capability to study aerosol composition and chemistry using VUV photoionization was also initiated. This “soft” ionization technique has been shown to yield near “fragment free” mass spectra of a variety of organic molecules. Aerosol particles are flash vaporized (50-500°C) and the resulting molecules are photoionized near threshold and then analyzed using time of flight (TOF) mass spectrometry. In this way, the chemical composition of aerosol particles can be monitored in the course of a chemical reaction. The first studies of aerosol chemistry using this technique were conducted in collaboration with Prof. Tom Baer (University of North Carolina). Oleic acid aerosol particles are generated in urban areas as a by-product of meat grilling in the fast food industry. Oleic acid particles were generated in situ and the resulting mass spectrum (at 9 eV photon energy) after the oleic acid aerosol was vaporized contains a single parent peak at 284 amu. In contrast, electron impact ionization results in extensive fragmentation that prohibits the detailed investigation of more complex aerosol chemistry due to interference between reactant and product fragmentation peaks in the electron impact mass spectrum. Oleic acid aerosols were also reacted with O₃ (a ubiquitous atmospheric oxidant). The VUV photoionization mass spectrum showed a decrease of the parent ion with O₃ addition as well as an increase in the particle phase products located at lower masses.

We also constructed a 130 L aerosol reaction chamber to be used in conjunction with the aerosol endstation and the commercial particle sizing instruments currently operational at the Chemical

Dynamics Beamline. The reaction chamber is ideal for measuring the kinetics of secondary aerosol formation. Initial experiments were conducted in collaboration with T. Baer (UNC). The goal of these experiments was to examine both the size and chemical evolution of particles generated by the gas phase reaction of alpha pinene with ozone. We were able to follow in real time both the particle size evolution as well as the chemistry. As expected from the oleic acid experiments, VUV photoionization allowed detection in real time, with less fragmentation, of how the particle composition evolves as a function of reaction time. We have observed the real time evolution of pinonic acid in the particle phase.

Future Plans

New studies will explore radical reactions such as $C_2H + SO_2$, $C_2H + NO$, $CH_3 + N$, and kinetic energy enhanced OH reactions with hydrocarbons. Experiments are also being considered to use the time-resolved FTIR method to examine heterogeneous processes with aerosol or surface reactions. Other investigations are ongoing to explore the CH(A) state formed by photodissociation of bromoform with vacuum ultraviolet light at the Advanced Light Source. Upon absorption of a VUV photon in the 10-14 eV regime, a single photon causes the bromoform to undergo a multibody dissociation: $CHBr_3 \rightarrow CH(A) + 3Br$. This reaction can take place as a concerted or as a sequential process. Major studies will exploit the aerosol generation and detection described above, and the new kinetics machine being constructed with Sandia National Laboratory will be tested in the upcoming year.

Recent Publications Citing DOE Support

V. Chikan, B. Nizamov and S. R. Leone, "Product state distributions of vibrationally excited CO(v) for the CH(X²Π) and C(A²Δ) channels of the C₂H+O(³P) reaction," *J. Phys. Chem. A* **108**, 10770 (2004).

V. Chikan and S. R. Leone, "Vibrational distributions of the CO(v) products of the C₂H₂ + O(³P) and HCCO + O(³P) reactions studied by FTIR emission," *J. Phys. Chem. A* (in press).

J. Shu, D. S. Peterka, S. R. Leone, and M. Ahmed, Tunable synchrotron vacuum ultraviolet ionization, time-of-flight investigation of the photodissociation of trans-crotonaldehyde at 193 nm," *J. Phys. Chem. A* **108**, 7895 (2004).

B. Nizamov and S. R. Leone, "Rate coefficients and kinetic isotope effect for the C₂H reactions with NH₃ and ND₃ in the 104 K – 294 K temperature range," *J. Phys. Chem. A* **108**, 3766 (2004).*

B. Nizamov and S. R. Leone, "Kinetics of C₂H reactions with hydrocarbons and nitriles in the 104 K – 296 K temperature range," *J. Phys. Chem. A* **108**, 1746 (2004).*

J. Shu, K. R. Wilson, A. N. Arrowsmith, M. Ahmed, and S. R. Leone, "Light scattering of ultrafine particles by VUV synchrotron radiation, *Nanoletters* (in preparation).

*Work primarily supported by NASA, but the apparatus for this NASA project was used for the C₂H + SO₂ investigations reported on here and DOE provided support for laboratory renovations, which was acknowledged in these two papers.

INTERMOLECULAR INTERACTIONS OF HYDROXYL RADICALS ON REACTIVE POTENTIAL ENERGY SURFACES

Marsha I. Lester
Department of Chemistry
University of Pennsylvania
Philadelphia, PA 19104-6323
milester@sas.upenn.edu

PROGRAM SCOPE

The primary objective of the DOE-sponsored research in this laboratory is to examine the interaction potentials and reaction dynamics of the hydroxyl radical (OH) with molecular partners of combustion relevance, most recently acetylene and ethylene. For these partners, molecular associations of OH radicals have already been predicted to play a critical role in the reaction mechanism. A hydrogen-bonded complex between OH and the π -bond of C_2H_4 has been suggested as an important precursor in the addition reaction of OH radicals to the double bond of ethylene, and an analogous T-shaped complex has been predicted on the reaction path for OH addition to acetylene (C_2H_2). This laboratory has obtained the first experimental evidence of such a hydrogen-bonded complex between the OH and C_2H_2 reactants in the entrance channel to reaction. Infrared action spectra of the OH- C_2H_2 reactant complex have been acquired in the regions of the OH overtone stretch and asymmetric CH stretch fundamental of acetylene, which reveal the structure and stability of the complex. New spectral analysis procedures have been developed to account for partial quenching of the electronic orbital angular momentum of the OH radical in the T-shaped complex and gain more insight on the nature of the molecular association between the partners. The results of these experiments provide new information on the electronic transformations that occur along the reaction pathway as the system evolves from reactants to products.

RECENT PROGRESS

The stationary points along the addition and abstraction reaction pathways, shown in Fig. 1, have been identified through previous *ab initio* calculations. The initial calculations indicated that the reactant complex has a T-shaped structure with the H atom of OH pointing toward the midpoint of the acetylene triple bond. This structure closely resembles that of its closed shell analogs FH- and ClH- C_2H_2 . We have carried out *ab initio* calculations at the RCCSD(T) level with extrapolation to the complete basis set limit, which complement our

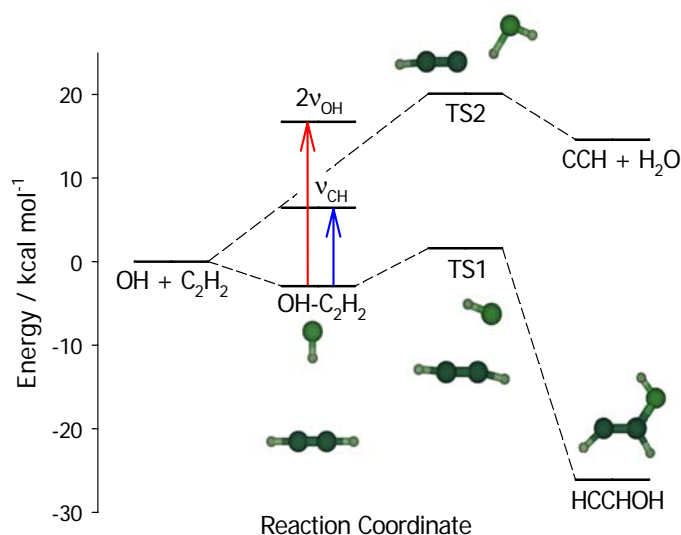


Fig. 1 Reaction coordinate for OH addition to acetylene, showing IR excitation of reactant complex in the OH overtone stretch and asymmetric CH stretch fundamental regions.

experimental investigation of the OH-acetylene complex. These calculations enable us to predict the minimum energy structure, the binding energy of the complex, and most importantly the separation between the two low-lying adiabatic surfaces, $^2A'$ and $^2A''$, in nonlinear configurations. These two adiabatic potentials differ in whether the half-filled $p\pi$ orbital of the OH radical lies within or perpendicular to the plane of the complex. The difference potential, $\rho = E(^2A') - E(^2A'')$, reaches a significant magnitude of $\sim 140 \text{ cm}^{-1}$ at the equilibrium T-shaped geometry, and results in a partial quenching of the electronic orbital angular momentum in the complex.

We have recently stabilized a hydrogen-bonded complex between the OH and C_2H_2 reactants in the entrance channel well leading to the addition reaction. The OH- C_2H_2 complexes are generated by photolyzing HNO_3 at 193 nm to produce OH radicals, which are entrained in a premixed 5-10% C_2H_2 / Ar gas mixture at a total pressure of 60 psi. We have used infrared action spectroscopy to obtain infrared spectra of the OH- C_2H_2 reactant complex in the regions of the $2\nu_{\text{OH}}$ OH overtone stretch and the ν_3 asymmetric stretch fundamental of acetylene using a KTP-based OPO to generate tunable infrared radiation at 1.4 or 3.0 μm . In addition, we have identified the principal OH (ν, j_{OH}) product channels that are populated following dissociation of the complex by utilizing UV laser-induced fluorescence on various OH A-X transitions to detect the OH fragments.

The infrared action spectrum of OH-acetylene in the OH overtone region is centered at $6885.53(1) \text{ cm}^{-1}$, shifted $85.81(1) \text{ cm}^{-1}$ to lower energy of the OH monomer transition. The rotational band structure is characteristic of a parallel (*a*-type) transition of a near prolate asymmetric top. The transition type indicates that the OH subunit lies along the *a*-inertial axis, as expected for a T-shaped complex in which OH is hydrogen-bonded to the π -cloud of acetylene. The large spectral shift indicates that the OH subunit is significantly perturbed upon forming a hydrogen bond with the H-side of OH interacting with acetylene.

The lines in the *P*- and *R*-branches are uniformly spaced by $(B+C)$, but at *odd* multiples of $(B+C)/2$ relative to the *Q*-branch (Fig. 2, lower trace), rather than the *even* multiples (Fig. 2, upper trace) seen for other acetylene-HX complexes. The line positions are fit to obtain the band origin and rotational constants, from which we determine a $3.327(5) \text{ \AA}$ separation between the centers-of-mass of the monomer constituents. The *odd* multiples indicate that there is sufficient OH orbital angular momentum to keep the electron spin coupled to the *a*-inertial axis. However, the inhomogeneous broadening evident in the spectrum shows that the situation is

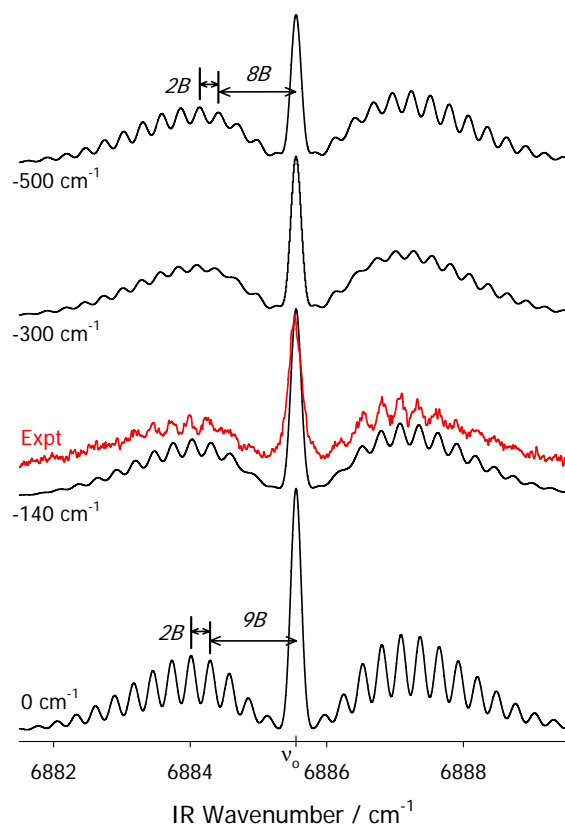


Fig. 2 Rotationally resolved infrared action spectrum of the OH overtone band of OH-acetylene (Expt.) and simulations of the *a*-type band with observed spectroscopic constants and four different values of the difference potential.

actually intermediate between the two limits shown in Fig. 2.

By contrast, the infrared spectrum in the asymmetric CH stretch region of acetylene is centered at $3278.64(1) \text{ cm}^{-1}$, indicating a much smaller spectral red shift of $9.75(1) \text{ cm}^{-1}$. The relatively small spectral shift confirms that the asymmetric acetylenic stretch is remote from the hydrogen bond. This perpendicular (*b*-type) transition exhibits much more complicated rotational band structure consisting of seven peaks of various intensities and widths (Fig. 3, Expt. trace). This spectrum is very different from those previously reported for similar HF/HCl-acetylene complexes, which is what one would expect if the orbital angular momentum of the OH radical were fully quenched (Fig. 3, upper trace). However, neither does this *b*-type band have the *Q*-branch pattern that would be expected if the electronic angular momentum were completely unquenched (Fig. 3, lower trace). We have developed a theoretical model to examine the origin of this unexpected result as well as more subtle effects seen in the *a*-type band. We attribute the partial quenching of the OH orbital angular momentum in the complex to the difference potential.

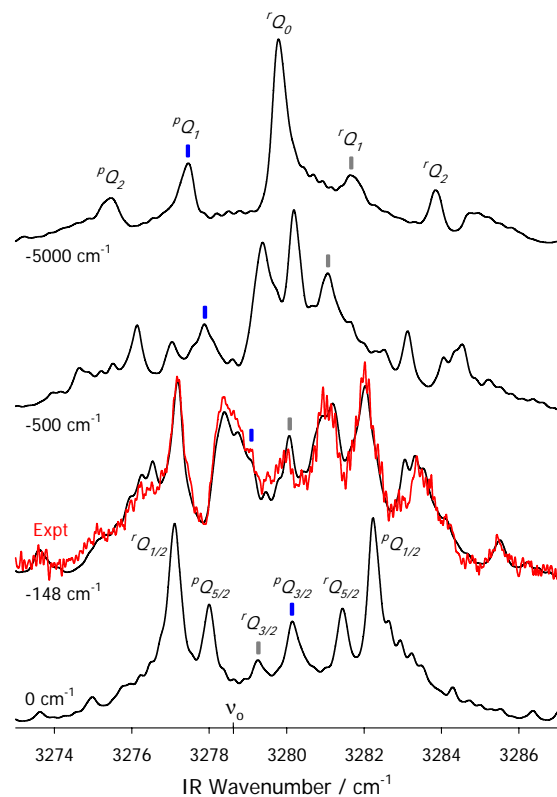


Fig. 3 Experimental infrared spectrum and simulations of the asymmetric CH stretching fundamental band of OH-acetylene for four different values of the difference potential.

The simulated vibration-rotational spectra are found to be quite sensitive to the magnitude of the difference potential, particularly for *b*-type transitions. The simulations shown in Figs. 2 and 3 result from model calculations with four different values of the difference potential and other spectroscopic parameters derived from the experimental data. In the analysis of the observed asymmetric CH stretch band, we were able to obtain an experimental determination of the difference potential (-148.1 cm^{-1}) that is in excellent accord with the *ab initio* prediction.

The spectroscopy of the OH-acetylene complex provides evidence of the lifting of the OH orbital degeneracy and partial quenching of its electronic orbital angular momentum. This demonstrates that the electronic changes accompanying the evolution of reactants into products have begun to occur in the reactant complex. The partial quenching of orbital angular momentum is expected to be a general phenomenon in OH complexes with strongly interacting partners.

We have also examined the principal OH (ν, j_{OH}) product channels populated following dissociation of the complex. This provides information on the stability of the OH-acetylene complex and the mechanism for inelastic decay. Following OH overtone excitation, the highest energy product state in the $\Delta\nu = -1$ channel, $j_{\text{OH}}=21/2$, $\omega=1/2$ with 2361 cm^{-1} of internal excitation, sets an upper limit for the ground state binding energy of $D_0 \leq 956 \text{ cm}^{-1}$.

FUTURE PLANS

We have recently extended this work by predicting the rotational band structure associated with microwave and infrared transitions of the OH-water complex. The OH monomer orbital angular momentum is predicted to be partially quenched in the OH-water complex, resulting from a significant splitting of the OH monomer orbital degeneracy into ${}^2A'$ and ${}^2A''$ electronic states. This orbital angular momentum quenching and associated decoupling of the electron spin from the a inertial axis are shown to have dramatic effects on the rotational band structure of microwave and infrared transitions of the OH-water complex. At the *ab initio* values for the splitting between the ${}^2A'$ and ${}^2A''$ surfaces, simulated spectra of a - and b -type bands, such as those expected for the OH radical stretch and water asymmetric stretch, are predicted to have a noticeably different appearance than the well established limiting cases associated with fully quenched or completely unquenched orbital angular momentum. Spectral identification of the OH-water complex in the gas-phase will require explicit consideration of this quenching phenomenon. In the next grant period, our primary focus will be experimental studies of the binary OH-water complex and OH embedded in small water clusters. Our goal is to understand the solvation structures, energetics, dynamics, and reactions of OH radicals in aqueous systems.

DOE SUPPORTED PUBLICATIONS 2003-2005

1. J. B. Davey, M. E. Greenslade, M. D. Marshall, M. I. Lester, and M. D. Wheeler, "Infrared Spectrum and Stability of a π -type Hydrogen-Bonded Complex between the OH and C_2H_2 Reactants", *J. Chem. Phys.* **121**, 3009-3018 (2004).
2. M. D. Marshall and M. I. Lester, "Spectroscopic Implications of the Coupling of Unquenched Angular Momentum to Rotation in OH-Containing Complexes", *J. Chem. Phys.* **121**, 3019-3029 (2004).
3. M. D. Marshall, J. B. Davey, M. E. Greenslade, M. I. Lester, "Evidence for Partial Quenching of Orbital Angular Momentum upon Complex Formation in the Infrared Spectrum of OH-Acetylene", *J. Chem. Phys.* **121**, 5845-5851 (2004).
4. M. D. Marshall and M. I. Lester, "Spectroscopic Implications of Partially Quenched Orbital Angular Momentum in the OH-Water Complex", *J. Phys. Chem. B*, in press (2005). (G. W. Flynn Special Issue)

Theoretical Studies of Molecular Systems

William A. Lester, Jr.
Chemical Sciences Division,
Ernest Orlando Lawrence Berkeley National Laboratory and
Kenneth S. Pitzer Center for Theoretical Chemistry,
Department of Chemistry, University of California, Berkeley
Berkeley, California 94720-1460
walester@lbl.gov

Program Scope

This research program is directed at extending fundamental knowledge of atoms and molecules. The approach combines the use of ab initio basis set methods and the quantum Monte Carlo (QMC) method to describe the electronic structure and energetics of systems of primarily combustion interest.

Recent Progress

ZORI Code Development (with A. Aspuru-Guzik, R. Salomon-Ferrer, B. Austin, R. Perusquia-Flores, M. A. Griffin, R. A. Oliva, D. Skinner, and D. Domin)

ZORI is a new computer code developed in this laboratory for the study of the electronic structure of atoms and molecules using quantum Monte Carlo (QMC) methods. The design goal for the code is to provide a research platform for developing and testing new QMC approaches as well as a robust computational environment for the user. The development model is based on the GNU General Public License (GNU/GPL) that encourages users to become co-developers of the tool as well as to submit suggestions for code improvement. ZORI continues to be augmented with new capabilities focused on large chemical systems. An online community of ZORI developers and users provide documentation, forums and mailing lists, and can be found at <http://www.zori-code.com>.

QMC Forces (with A. C. Kollias; collaborative effort with M. Caffarel and R. Assaraf, CNRS, France)

The goal of this project is the development of the capability to compute forces ($3N$ coordinates, for N atoms) at no additional expense in central processor unit (cpu) cost in the presence of effective core potentials (ECPs). This is an essential step to enable the computation of QMC optimized geometries and to carry out dynamics studies using QMC forces. Unlike the all-electron case in which the computation of the derivative of the potential is trivial to evaluate, the ECP case is quite different. Although one can, in principle, develop an improved estimator with a small variance that is inexpensive in cpu time, it is, however, a major effort to implement this direction. The basic reason, is that one has to compute efficiently the derivatives of the ECP energy with respect to all atom coordinates.

Future Plans

Future work will continue in the direction of establishing fundamental understanding of mechanisms leading to soot formation as well as other molecular species of combustion interest and associated computer code development.

DOE Supported Publications 2003-2005

1. O. El Akramine, W. A. Lester, Jr., X. Krokidis, C. A. Taft, T. C. Guimaraes, A. C. Pavao, and R. Zhu, "Quantum Monte Carlo Study of the CO Interaction with a Model Surface for Cr(110)" *Mol. Phys.* **101**, 277 (2003).
2. J. A. W. Harkless, J. H. Rodriguez, L. Mitas, and W. A. Lester, Jr., "Quantum Monte Carlo and Density Functional Theory Study of Peroxynitrite Anion," *J. Chem. Phys.* **118**, 4987 (2003).
3. A. C. Kollias and W. A. Lester, Jr., "Quantum Monte Carlo Study and Electron Localization Function of CO_2^+ ," *J. Mol. Struct. Theochem* **634**, 1 (2003).
4. A. Aspuru-Guzik and W. A. Lester, Jr., "Quantum Monte Carlo for the Solution of the Schrodinger Equation for Molecular Systems", in Special Volume Computational Chemistry, C. Le Bris, ed., of Handbook of Numerical Analysis, P. G. Ciarlet, ed., Elsevier, 2003, p. 485.
5. O. El Akramine, A. C. Kollias, and W. A. Lester, Jr., "Quantum Monte Carlo Study of the Singlet-Triplet Transition in Ethylene", *J. Chem. Phys.* **119**, 1483 (2003).
6. C. A. Schuetz, M. Frenklach, A. C. Kollias, and W. A. Lester, Jr., "Response Surface Approach to Geometry Optimization in Quantum Monte Carlo: Application to Formaldehyde," *J. Chem. Phys.* **119**, 9386 (2003).
7. O. El Akramine, A. Aspuru-Guzik, J. C. Grossman, and W. A. Lester, Jr., "Quantum Monte Carlo Study of the Electronic Structure of Free Base Porphyrin," *J. Chem. Phys.* **120**, 3049 (2004).
8. A. C. Kollias, O. Couronne, and W. A. Lester, Jr., "Quantum Monte Carlo Study of the Reaction: $\text{Cl} + \text{CH}_3\text{OH} \rightarrow \text{CH}_2\text{OH} + \text{HCl}$," *J. Chem. Phys.* **121**, 1357 (2004).
9. A. Aspuru-Guzik and W. A. Lester, Jr., "Quantum Monte Carlo: Theory and Application to Molecular Systems," Proceedings of the International Conference on Computational and Mathematical Methods in Science and Engineering, CMMSE-2004, Uppsala, June 4-8, 2004, pp. 100-115.
10. W. A. Lester, Jr., Commentary on "Quantum Monte Carlo Studies on Be and LiH," in *Molecular Quantum Mechanics, Selected papers of N. C. Handy*, D. C. Clary, S. M. Colwell, and H. F. Schaefer III, eds, 2004, p. 145.
11. A. Aspuru-Guzik, A. C. Kollias, R. Salomon-Ferrer, and W. A. Lester, Jr. "Quantum Monte Carlo: Theory and Applications to Atomic, Molecular and Nano Systems," to appear in the Handbook of Theoretical and Computational Nanotechnology, eds. M. Rieth and W. Schommers.
12. A. C. Kollias, D. Domin, G. Hill, M. Frenklach, D. M. Golden, and W. A. Lester, Jr., "Quantum Monte Carlo Study of Heats of Formation and Bond Dissociation Energies of Small Hydrocarbons," to appear in *Int. J. Chem. Kinetics*.
13. A. Aspuru-Guzik, R. Salomon-Ferrer, and W. A. Lester, Jr., "A Sparse Algorithm for the Evaluation of the Local Energy in Quantum Monte Carlo," to appear in *J. Comp. Chem.*
14. A. Aspuru-Guzik and W. A. Lester, Jr., "Quantum Monte Carlo: Theory and Application to Molecular Systems," to appear in *Adv. Quant. Chem.*

15. A. C. Kollias, D. Domin, G. Hill, M. Frenklach, and W. A. Lester, Jr., "Quantum Monte Carlo Study of Small Hydrocarbon Atomization Energies," to appear in Mol. Phys.

Quantum Dynamics of Fast Chemical Reactions

DE-FG02-87ER13679

Progress Report 3/2003 - 3/2004

John C. Light

The James Franck Institute and Department of Chemistry

The University of Chicago

5640 S Ellis, Chicago, Illinois 60637

email: j-light@uchicago.edu

The aims of this research are to develop a theoretical understanding and predictive ability for a variety of processes occurring in the gas phase. These include bimolecular chemical exchange reactions, photodissociation, predissociation resonances, unimolecular reactions and recombination reactions. Our focus on accurate quantum dynamics of small system is important for many reactions related to combustion and atmospheric chemistry involving light atom transfer reactions and, for example, resonances in dissociation and recombination reactions.

A major impediment to extension of these techniques to large or heavier molecular systems is the poor scaling of quantum methods with number of atoms treated accurately quantum mechanically and with the number of vibrational basis functions per degree of freedom. The scaling for straightforward quantum solutions is between n^{3d} and n^d where $d = 3N - 6$, N is the number of atoms, and "n" the number of points or basis functions required to describe the motions in *each* dimension accurately – perhaps 10 to 100. For heavier atoms (e.g. O atoms in ozone) as many as 250 per degree of freedom are required.

We focus on developing substantially improved approaches and applying them to larger systems of interest. The techniques developed and used are primarily quantum mechanical (sometimes combined with classical mechanics) which permits us to focus on the effects of the internal states of reactants on reactions, and the internal state distributions, isotopic ratios, and branching ratios for products.

I. RECENT PROGRESS

During the past two years we have refined computational methods to make the calculation of states of four atom systems more feasible and routine and have applied them to molecular systems relevant to combustion such as CO₂ dimer and hydrogen peroxide, H₂CO, water and ozone. The latter two were investigated near the dissociation limit for bound states and some resonances.

Our theoretical approach to the quantum dynamics of such "floppy" molecules has utilized three recent important innovations: the generation and use of reduced dimensionality *minimum* PES's to define the basis functions for each subset of the coordinates [1–3]; the combination of these reduced dimensional basis functions to form an *energy selected* non-direct product basis [2–4]; and the use of an iterative (IRLM) solution method for determining eigenvalues, eigenfunctions of the molecule [1,3,4]. Optimized grids for each of the degrees of freedom may also be used [5]. These

improvements are synergistic, with the minimum potentials assuring appropriate coordinate ranges for the bases, the energy selected basis reducing both the basis size and, perhaps more important, the spectral range, and the iterative (IRLM) solution providing excellent scaling as well as eigenfunction evaluation. Last year we reported an improved grid approach for problems with several angular degrees of freedom as well as applications to important tetra-atomic and triatomic systems [5].

A. Tetra-atomic systems with Energy Selected Bases:

Many tetra-atomic systems are important for combustion such as CH_3 , HOCO , H_2CO , HOOH , etc. We have looked at the high energy vibrational dynamics of some of these systems using the above methods. The application to highly excited HOOH was relatively straightforward while the application to the formaldehyde/vinyl system (H_2CO) was more difficult [3]. Some 730 A_1 states (up to $13,600 \text{ cm}^{-1}$) were calculated. This reaches, but does not exceed the barrier to isomerization to vinylidene.

B. Triatomic molecules near dissociation: Water and Ozone

Although these are triatomic molecules and therefore inherently easier to treat than formaldehyde or hydrogen peroxide, the very highly excited vibrational levels of these systems are of interest for photodissociation and recombination particularly in the atmosphere. In addition the highly excited vibrations and resonance states of ozone for the (^{16}O) $_3$ and ($^{16}\text{O}_2$ ^{18}O) isotopomers are probably responsible for the observed "isotopic anomaly" of atmospheric ozone in which the isotopic ratios are not in the expected chemical equilibrium.

The vibrational levels of H_2O were computed using the ESB method for the PJT2 potential energy surface of Mussa and Tennyson [6]. Some 1000 even and 800 odd vibrational states were calculated, extending well above the dissociation limit. The identity of the resonance states was determined by examining the stability with respect to the distance parameters of the calculation [3].

In the ozone calculation we determined all the bound states, including the long range van der Waals states, of $^{48}\text{O}_3$ and $^{50}\text{O}_3$ [7]. The accurate PES of Babikov [8] was used. This calculation resolved a discrepancy between the calculations of Grebenshchikov et al. and Babikov, *J. Chem. Phys.* **119**, 6512 and 6564 (2003) respectively. Since the high lying vdW states are likely to be strongly involved in the anomalous isotope effect in the ozone recombination process, resolution of the discrepancy was important. Our results agreed extremely well with a subset of the results (corresponding to the proper A_2 vibrational symmetry) of Grebenshchikov (within about 0.04 cm^{-1}) [3].

II. CONTINUING PROJECTS: REACTIONS OF OZONE AND OF $\text{H}_3^+ + \text{H}_2$

Both the recombination of $\text{O}_2 + \text{O}$ in the atmosphere and the low energy reactions of H_3^+ and H_2 proceed via complexes which have deep attractive wells. In both cases

quantum effects will be important, via resonances, tunneling, and nuclear symmetry effects. The understanding of ozone recombination is important for atmospheric chemistry whereas the understanding of the ortho-para exchange processes and rotational relaxation in the low energy H_3^+ collision system is important for interstellar chemistry.

A. Ozone Recombination reactions:

Ozone recombination in the atmosphere occurs by $\text{O} + \text{O}_2$ collisions to form a metastable resonance state followed by collision with an atmospheric molecule to de-excite the system to a stable O_3 molecule. The apparent kinetic preference (over and above thermodynamic equilibrium) for ^{18}O enhanced ozone [9,10] presumably is a result of selective enhancement by resonances.

We are continuing calculations on the ozone system in two stages, first to determine the resonance states which might participate in the three body association process; then to calculate the thermal collisional relaxation rates from each resonance state and then the final relaxation to stable ozone via a master equation. This will require the determination of the state specific energy transfer and dissociation rates for collisions of O_3^* with atmospheric gases. This will be a mixed quantum-classical calculation similar to our $\text{Ar} + \text{HCO}$ calculation done some time ago [11].

This requires determining not only the eigenvalues of ozone but the wave functions of the stable states and lifetimes and eigenfunctions of metastable states. We have started this process using "Ozone Lite", where the masses are reduced by a factor of 4 from real ozone. This permits the techniques for the above calculations to be evaluated and the approach to be made efficient *before* the very large final calculations are started. It appears that the most efficient approach is to use large 1-D bases with minimum marginal potentials to generate PODVR's and an energy selected basis. Solution using the iterative "IRLM" algorithm provides both (real) eigenvalues and eigenfunctions for bound and resonance states. Scattering wave functions and resonance lifetimes can then be found using the "artificial boundary inhomogeneity" method [12,13] or by iterative means [14].

B. $\text{H}_3^+ + \text{H}_2$ reaction:

The low energy $\text{H}_3^+ + \text{H}_2$ ion-molecule reaction is one of the only relaxation mechanisms for ortho-para exchange in interstellar space. We will first look at the cross sections from a relatively simple statistical theory approach (Ref [15,16], then look at the long range quantum dynamical effects such as tunneling and anisotropic collision effects on barrier crossing [17]. This five nucleus system is difficult because of the nuclear symmetry and large quantum effects but is fascinating for the same reasons. This calculation also will be a precursor to the more combustion oriented system CH_5^+ which shares the fermion symmetry of the five H nuclei.

PUBLICATIONS supported by this DOE Grant, 2004-2005: References 2,3,and 7 below.

REFERENCES

- [1] H. S. Lee and J. C. Light. Molecular vibrations: Iterative solution with energy selected bases. *J. Chem. Phys.*, 118:3458, 2003.
- [2] Hee-Seung Lee and J. C. Light. Iterative solutions with energy selected bases for highly excited vibrations of tetra-atomic molecules. *J. Chem. Phys.*, 120:4626, 2004.
- [3] J. C. Light and H. S. Lee. *Molecular dynamics: energy selected bases*. Kluwer Academic Publishers, 2004.
- [4] X.G. Wang and T.C. Carrington, Jr. The utility of constraining basis function indices when using the lanczos algorithm to calculate vibrational energy levels. *J. Phys. Chem. A*, 105:2575, 2001.
- [5] Hua Chen H. S. Lee and J. C. Light. Symmetry adapted direct product discrete variable representation for the coupled angular momentum operator: Application to the vibrations of $(\text{CO}_2)_2$. *J. Chem. Phys.*, 119:4187, 2003.
- [6] H. Y. Mussa and J. Tennyson. Calculation of the rotation-vibration states of water up to dissociation. *J. Chem. Phys.*, 109:10885, 1998.
- [7] Hee-Seung Lee and J. C. Light. Vibrational energy levels of ozone up to dissociation revisited. *J. Chem. Phys.*, 120:5862, 2004. Communication.
- [8] D. Babikov, B. K. Kendrick, R. B. Walker, R. T. Pack P. Fleurat-Lesard and R. Schinke. *J. Chem. Phys.*, 118:6298, 2003.
- [9] Y. Q. Gao and R. A. Marcus. Strange and unconventional isotope effects in ozone formation. *Science*, 293:259–263, 2001.
- [10] C. Jansssen, J. Guenther, D. Krankowsky, and K. Mauersberger. Relative formation rates of $^{50}\text{O}_3$ and $^{52}\text{O}_3$ in ^{16}O - ^{18}O mixtures. *J. Chem. Phys.*, 111:7179–7182, 1999.
- [11] G. S. Whittier and J. C. Light. Quantum/classical time-dependent self-consistent field treatment of Ar-HCO. *J. Chem. Phys.*, 110:4280, 1999.
- [12] Hyo Weon Jang and J. C. Light. Finite range scattering wave function method for scattering and resonance lifetime. *J. Chem. Phys.*, 99:1057, 1993.
- [13] G. S. Whittier and J. C. Light. Calculation of resonances of HCO by the artificial boundary inhomogeneity method. *J. Chem. Phys.*, 107:1816, 1997.
- [14] H. Zhang and S. C. Smith. Calculation of product state distributions from resonance decay via Lanczos subspace filter diagonalization: Application to HO_2 . *J. Chem. Phys.*, 115:5751–5758, 2001.
- [15] P. Pechukas and J. C. Light. On detailed balancing and statistical theories of chemical kinetics. *J. Chem. Phys.*, 42:3281, 1965.
- [16] J. C. Light. Statistical theory of bimolecular exchange reactions. *Discuss. Faraday Soc.*, 44:14, 1967.
- [17] E. J. Rackham, T. Gonzalez-Lezana, and D. E. Manolopoulos. A rigorous test of the statistical model for atom-diatom insertion reactions. *J. Chem. Phys.*, 119:12895, 2003.

Kinetics of Elementary Processes Relevant to Incipient Soot Formation

PI: M. C. Lin

Department of Chemistry

Emory University, Atlanta, GA 30322

chemmcl@emory.edu

I. Program Scope

Soot formation and abatement processes are some of the most important and challenging problems in hydrocarbon combustion. The key reactions involved in the formation of polycyclic aromatic hydrocarbons (PAH's), the precursors to soot, remain elusive. Small aromatic species such as C_5H_5 , C_6H_6 and their derivatives are believed to play a pivotal role in incipient soot formation.

The goal of this project is to establish a kinetic database for elementary reactions relevant to soot formation in its incipient stages. In the past year, our major focus has been placed on the experimental studies on the reactions of C_6H_5 with allene and propyne; their mechanisms have been elucidated computationally by quantum-chemical calculations. A similar study on the effects of temperature and pressure on the reaction of $C_6H_5C_2H_2$ with O_2 has been studied for the first time. In addition, several reactions involving CH_3 , C_2H_5 , and HCO radicals have been calculated at the G2M level of theory.¹

II. Recent Progress

A. Aromatic Radical Reaction Kinetics and Mechanisms

1. Kinetics of the $C_6H_5C_2H_2 + O_2$ reaction (ref. 2)

The effects of temperature and pressure on the formation and decomposition of $C_6H_5C_2H_2O_2$ in the $C_6H_5C_2H_2 + O_2$ reaction have been investigated at temperatures from 298 – 358 K by monitoring radical in the visible region with CRDS.³ The rate of $C_6H_5C_2H_2 + O_2$ association and the rate of fragmentation of $C_6H_5C_2H_2O_2$ were found to be, respectively, $k_1 = 2.84 \times 10^{12} \exp(+780/T) \text{ cm}^3 \text{ mol}^{-1} \text{ s}^{-1}$ $k_2 = (1.68 \pm 0.10) \times 10^4 \text{ s}^{-1}$. k_1 was found to be weakly dependent on pressure in the range of 40 – 120 Torr Ar, where as k_2 was found to be independent of pressure. The mechanism for this very fast reaction has been elucidated quantum-chemically by B3LYP/6-31G(d,p) calculations. The result of the calculations indicated that the reaction effectively occur by two competitive association paths giving 3- and 4-member-ring peroxide intermediates which fragment rapidly to $C_6H_5CHO + CHO$ with a predicted 382 kJ/mol exothermicity.³ A full RRKM calculation on the system is underway.

2. Computational Study of $C_6H_5 + C_2H_4$, $C_2H_3 + C_6H_6$ and $H + C_6H_5C_2H_3$ (ref. 4):

Reactions of phenyl radicals with ethylene (R1), vinyl radicals with benzene (R2) and H atoms with styrene (R3) are important prototype processes pertinent to the formation and degradation of aromatic hydrocarbons in high-temperature environments. Detailed mechanisms for these reactions are elucidated with the help of quantum-chemical calculations at the G2M level of theory. Reactions R1-R3 initially produce chemically activated intermediates interconnected by isomerization pathways on the extended $[C_8H_9]$ potential energy surface.⁴ All kinetically important transformations of these isomeric C_8H_9 radicals are explicitly characterized and utilized in the construction of multichannel kinetic models for reactions R1-R3. Accurate thermochemistry is evaluated for the key intermediates from detailed conformational and isodesmic analyses. An examination of the G2M energetic parameters for reactions R1-R3 and for briefly revisited $C_6H_5 + C_2H_2$, and $C_6H_6 + H$ addition reactions reveals common theoretical deficiencies and suggests that the quality of theoretical predictions can be improved by small systematic corrections. Theoretical molecular and adjusted energetic parameters are used in a consistent way to calculate the total rate constants and product branching for reactions R1-R3 by weak collision master equation/RRKM analysis (addition channels) and transition state theory with Eckart tunneling corrections (abstraction channels). The available experimental kinetic data for reactions R1 and R2 is surveyed and found in good agreement with the best theoretical estimates.

3. $C_6H_5 + HNO$ vs $CH_3 + HNO$ (ref 5):

Kinetics and mechanisms for the reactions of HNO with CH₃ and C₆H₅ have been investigated by ab initio molecular orbital and transition-state theory and/or RRKM/ME calculations. The G2M(RCC, MP2)//B3LYP/6-31G(d) method was employed to evaluate the energetics for construction of their potential energy surfaces and prediction of reaction rate constants. The reactions R + HNO (R = CH₃ and C₆H₅) were found to proceed by two key product channels giving (1) RH + NO and (2) RNO + H, primarily by direct abstraction and indirect association/decomposition mechanisms, respectively. As both reactions initially occur barrierlessly, their rate constants were evaluated with a canonical variational approach in our TST and RRKM/ME calculations. For practical applications, the rate constants evaluated for the atmospheric-pressure condition are represented by modified Arrhenius equations in units of cm³ mol⁻¹ s⁻¹ for the temperature range 298 – 2500 K: $k_{1A} = 1.47 \times 10^{11} T^{0.76} \exp[-175/T]$, $k_{2A} = 8.06 \times 10^3 T^{2.40} \exp[-3100/T]$, $k_{1B} = 3.78 \times 10^5 T^{2.28} \exp[230/T]$, and $k_{2B} = 3.79 \times 10^9 T^{1.19} \exp[-4800/T]$; where A and B represent CH₃ and C₆H₅ reactions, respectively. Based on the predicted rate constant at 1 atm pressure for R + HNO → RNO + H, we estimated their reverse rate constants for R + HNO production from H + RNO in units of cm³ mol⁻¹ s⁻¹: $k_{2A'} = 7.01 \times 10^{10} T^{0.84} \exp[120/T]$ and $k_{2B'} = 2.22 \times 10^{19} T^{-1.01} \exp[-9700/T]$. The heats of formation at 0 K for CH₃NO, CH₃N(H)O, CH₃NOH, C₆H₅N(H)O, and C₆H₅NOH have been estimated to be 18.6, 18.1, 22.5, 47.2, and 50.7 kcal mol⁻¹ with an estimated ± 1 kcal mol⁻¹ error.

4. Computational study of the C₆H₅ + O₂ reaction (ref. 6):

The C₆H₅ + O₂ reaction is one of the most important reaction which affects the formation of soot in its incipient stages. It competes with C₆H₅ + C₂H₂ which ultimately leads to the formation of PAHs. Ab initio G2M calculations have been performed to investigate the potential energy surface for the reaction of phenyl radical with molecular oxygen. The reaction is shown to start with an exothermic barrierless addition of O₂ to the radical site of C₆H₅ to produce phenylperoxy (**1**) and, possibly, 1,2-dioxaspiro[2.5]octadienyl (dioxiranyl, **8**) radicals. Next, **1** loses the terminal oxygen atom to yield the phenoxy + O products (**3**) or rearranges to **8**. The dioxiranyl can further isomerize to a seven-member ring 2-oxepinyloxy radical (**10**), which can give rise to various products including C₅H₅ + CO₂, pyranil + CO, *o*-benzoquinone + H, and 2-oxo-2,3-dihydrofuran-4-yl + C₂H₂. Once **10** is produced, it is unlikely to go back to **8** and **1**, because the barriers separating **10** from the products are much lower than the reverse barrier from **10** to **8**. Thus, the branching ratio of C₆H₅O + O against the other products is mostly controlled by the critical transition states between **1** and **3**, **1** and **8**, and **8** and **10**. According to the calculated barriers, the most favorable product channel for the decomposition of **10** is C₅H₅ + CO₂, followed by pyranil + CO and *o*-benzoquinone + H. Since C₆H₅O + O and C₅H₅ + CO₂ are expected to be the major primary products of the C₆H₅ + O₂ reaction and thermal decomposition of C₆H₅O leads to C₅H₅ + CO, cyclopentadienyl radicals should be the dominant product of oxidation of phenyl radicals by O₂; the oxidation results in degradation of the six-member aromatic ring to cyclopentadienyl ring.

5. Computational Studies of C₆H₅ + NO₂ and C₆H₅O + NO and the Unimolecular Decomposition of C₆H₅NO₂ (ref. 7):

The kinetics and mechanisms for the unimolecular dissociation of nitrobenzene and related association reactions C₆H₅ + NO₂ and C₆H₅O + NO have been studied computationally at the G2M(RCC, MP2) level of theory in conjunction with rate constant prediction with multi-channel RRKM calculations. Formation of C₆H₅ + NO₂ was found to be dominant above 850 K with its branching ratio > 0.78, whereas the formation of C₆H₅O + NO via the C₆H₅ONO intermediate was found to be competitive at lower temperatures, with its branching ratio increasing from 0.22 at 850 K to 0.97 at 500 K. The third energetically accessible channel producing C₆H₄ + HONO was found to be uncompetitive throughout the temperature range investigated, 500 – 2000 K. The predicted rate constants for C₆H₅NO₂ → C₆H₅ + NO₂ and C₆H₅O + NO → C₆H₅ONO under varying experimental conditions were found to be in good agreement with all existing experimental data. For C₆H₅ + NO₂, the combination processes producing C₆H₅ONO and C₆H₅NO₂ are dominant at low temperature and high pressure, while the disproportionation

process giving $C_6H_5O + NO$ via C_6H_5ONO becomes competitive at low pressure and dominant at temperatures above 1000 K.

7. Photolytic and thermal decomposition of C_6H_5NO (ref. 8):

In collaboration with Y. T. Lee and coworkers of the Institute of Atomic and Molecular Sciences in Taiwan, we have investigated the photodissociation of nitrosobenzene, the most convenient photolytic and thermal source of the C_6H_5 radical, in a molecular beam using multimass ion imaging techniques. Photodissociation at 248 nm shows that there is only one dissociation channel, i.e., $C_6H_5NO \rightarrow C_6H_5 + NO$, regardless of the fact that the other channel $C_6H_5NO \rightarrow C_6H_4 + HNO$ is energetically accessible in agreement with theoretically predicted result. Photodissociation at 193 nm also shows the same dissociation channel. However, about 10% of the C_6H_5 radicals produced at this wavelength further decomposed into benzyne and H atom, and the dissociation rates of phenyl radical as a function of internal energies were measured. The averaged photofragment translational energies released from the dissociation of nitrosobenzene at 193 nm and 248 nm are 10.2 and 6.9 kcal/mol, respectively, and fragment distributions are almost isotropic at both wavelengths. In addition, the thermal rate constant for dissociation of C_6H_5NO has been computed on the basis of the PES evaluated at G2M(RCC, MP2)//B3LYP/6-31+G(d) and compared with experimental data; the agreement between theory and experiment is excellent, confirming the most recently reported unusually high A-factor ($k^\infty = (1.42 \pm 0.13) \times 10^{17} \exp[-(55060 \pm 1080)/RT] \text{ s}^{-1}$).

B. Experimental and Computational Studies of Small Radical Reactions Relevant to Combustion

1. $O + CH_3OH$ (ref. 9):

In collaboration with Y-P Lee's group at National Chiao Tung University in Taiwan, we have investigated the kinetics of the $O + CH_3OH$ reaction in a shock tube. Rate coefficients of the reaction in the temperature range 835–1777 K were determined using a diaphragmless shock tube. O atoms were generated by photolysis of SO_2 with a KrF excimer laser at 248 nm or an ArF excimer laser at 193 nm; their concentrations were monitored via atomic resonance absorption excited by emission from a microwave-discharged mixture of O_2 and He. Rate coefficients determined for the temperature range can be represented by the Arrhenius equation: $k(T) = (2.29 \pm 0.18) \times 10^{-10} \exp[-(4210 \pm 100)/T] \text{ cm}^3 \text{ molecule}^{-1} \text{ s}^{-1}$; unless otherwise noted, all listed errors represent one standard deviation in fitting. Combination of these and previous data at lower temperature shows a non-Arrhenius behavior described as the three-parameter equation $k(T) = (2.74 \pm 0.07) \times 10^{-18} T^{2.25 \pm 0.13} \exp[-(1500 \pm 90)/T] \text{ cm}^3 \text{ molecule}^{-1} \text{ s}^{-1}$. Theoretical calculations at the B3LYP/6-311+G(3df, 2p) level locate three transition states. Based on the energies computed with CCSD(T)/6-311+G(3df, 2p)//B3LYP/6-311+G(3df, 2p), rate coefficients predicted with canonical variational transition state theory with small curvature tunneling corrections agree satisfactorily with experimental observations. The branching ratios of two accessible reaction channels forming $CH_2OH + OH$ (1a) and $CH_3O + OH$ (1b) are predicted to vary strongly with temperature. At 300 K, reaction (1a) dominates, whereas reaction (1b) becomes more important than reaction (1a) above 1700 K.

2. $CH_3 + C_2H_5$ (ref. 10):

We have reported the first quantitative *ab initio* prediction of the disproportionation/ combination ratio of alkyl + alkyl reactions using $CH_3 + C_2H_5$ as an example. The reaction has been investigated by the modified Gaussian-2 (G2M) method with variational TST/RRKM calculations for several channels producing (1) $CH_4 + {}^1,3CH_2CH_2$, (2) C_3H_8 , (3) $CH_4 + {}^1,3CH_3CH$, (4) $H_2 + CH_3CHCH_2$, (5) $H_2 + CH_3CCH_3$ and (6) $C_2H_6 + {}^1,3CH_2$ by H-abstraction and association/decomposition mechanisms through singlet and triplet potential energy paths. Significantly, the disproportionation reaction (1) producing $CH_4 + C_2H_4$ was found to occur primarily by the lowest energy path via a loose hydrogen-bonding singlet molecular complex, $H_3C \cdots HC_2H_4$, with a 3.5 kcal/mol binding energy and a small decomposition barrier (1.9 kcal/mol), instead of a direct H-abstraction process. Bimolecular reaction rate constants for the formation of the above products have been calculated in the temperature range 300–3000 K. At 1 atm,

formation of C₃H₈ is dominant below 1200 K. Over 1200 K, the disproportionation reaction becomes competitive. The sum of products (3) – (6) accounts for less than 0.3% below 1500 K and it reaches around 1 ~ 4% above 2000 K. The predicted rate constant for the disproportionation reaction with multiple reflections above the complex well, $k_1 = 5.04 \times T^{0.41} \exp(429/T)$ at 200 - 600 K and $k_1 = 1.96 \times 10^{-20} T^{2.45} \exp(1470/T) \text{ cm}^3 \text{ molecule}^{-1} \text{ s}^{-1}$ at 700 -3000 K, agrees closely with experimental values. Similarly, the predicted high-pressure rate constants for the combination reaction forming C₃H₈ and its reverse dissociation reaction in the temperature range 300 - 3000 K, $k_2^\infty = 2.41 \times 10^{-10} T^{-0.34} \exp(259/T) \text{ cm}^3 \text{ molecule}^{-1} \text{ s}^{-1}$ and $k_{-2}^\infty = 8.89 \times 10^{22} T^{-1.67} \exp(-46037/T) \text{ s}^{-1}$, respectively, are also in good agreement with available experimental data.

III. Future Plans

Currently, we continue the acquisition of kinetic data for C₆H₅ reactions by CRDS and PLP/MS techniques to determine the total rate constants and product branching probabilities in the C₆H₅ reactions with CH₃OH and C₂H₅OH. Computationally, we will carry out high-level *ab initio* MO calculations to improve our predictive capability for the rate constant and product branching ratios of C₆H₅ and C₆H₅C₂H₂ reactions with O₂ and other combustion species. We hope to wrap up most key C₆H₅ reactions with combustion species or fuel molecules by the end of the current funding cycle. Future works will be focused on phenylvinyl and naphthyl radical reactions.

IV. References (DOE publications, 2003 - present, denoted by *)

1. A. M. Mebel, K. Morokuma and M. C. Lin, *J. Chem. Phys.*, **103**, 7414 (1995).
- *2. J. Park, L. Y. M. Choi and M. C. Lin, *ChemPhysChem*, to be submitted.
- *3. Y. M. Choi, J. Park, Liming Wang, and M. C. Lin, *ChemPhysChem*, **5**, 1231-34 (2004).
- *4. I. V. Tokmakov and M. C. Lin, *J. Phys. Chem., A*, **108**, 9697-714 (2004).
- *5. Y. M. Choi and M. C. Lin, *Int. J. Chem. Kinet.*, **37**, 261 (2005).
- *6. I.V. Tokmakov, G.-S. Kim, V. V. Kislov, A. M. Mebel and M. C. Lin, *J. Phys. Chem. A*, submitted.
- *7. Shucheng Xu and M. C. Lin, *J. Phys. Chem., A*, in press.
- *8. Cheng-Ming Tzeng, Y. M. Choi, Cheng-Liang Huang, Chi-Kung Ni, Yuan T. Lee, and M. C. Lin, *J. Phys. Chem., A*, **108**, 7928-35, (2004).
- *9. Chi-Wei Lu and Shen-Long Chou, Yuan-Pern Lee, Shucheng Xu, Z. F. Xu and M. C. Lin, *J. Chem. Phys.*, in press.
- *10. R. S. Zhu, Z. F. Xu and M. C. Lin, *J. Chem. Phys.*, **120**, 6566 (2004).

Other DOE Publications Not Cited in the Text:

1. I. V. Tokmakov, L. V. Moskaleva and M. C. Lin, *J. Phys. Chem., A*, **107**, 1066 (2003).
2. I. V. Tokmakov, L. V. Moskaleva, D. V. Paschenko and M. C. Lin, *J. Phys. Chem., A*, **107**, 1066 (2003).
3. Y. M. Choi and M. C. Lin, *J. Phys. Chem., A*, **107**, 7755 (2003).
4. I. V. Tokmakov and M. C. Lin, *J. Am. Chem. Soc.*, **125**, 11397 (2003).
5. J. Park, Z. F. Xu and M. C. Lin, *J. Chem., Phys.*, **118**, 9990-96 (2003).
6. Y. M. Choi and M. C. Lin, *J. Phys. Chem., A*, **107**(39), 7755-61 (2003).
7. Chih-Wei Lu, Yu-Jong Wu, Yuan-Pern Lee, R. S. Zhu and M. C. Lin, *J. Phys. Chem., A*, **107**, 11020-11029 (2003).
8. J. Park, Liming Wang and M. C. Lin, *Int. J. Chem. Kinet.*, **36**, 49-56 (2004).
9. I. V. Tokmakov, L. V. Moskaleva, and M. C. Lin, *Int. J. Chem. Kinet.*, **36**, 139-51 (2004).
10. Y. M. Choi and M. C. Lin, *ChemPhysChem.*, **5**, 225-32 (2004).
11. Y. M. Choi and M. C. Lin, *ChemPhysChem.*, **5**, 661-68 (2004).
12. Z. F. Xu, J. Park and M. C. Lin, *J. Chem. Phys.*, **120**, 6593 – 99 (2004).
13. Huzeifa Ismail, Joonbum Park, Bryan M. Wong, W. H. Green, Jr. and M. C. Lin, *Proc. Combust. Inst.*, xxx (2004).

INVESTIGATION OF POLARIZATION SPECTROSCOPY AND DEGENERATE FOUR-WAVE MIXING FOR QUANTITATIVE CONCENTRATION MEASUREMENTS

Principal Investigator: Robert P. Lucht
School of Mechanical Engineering, Purdue University, West Lafayette, IN 47907-2088
(Lucht@purdue.edu)

I. PROGRAM SCOPE

Nonlinear optical techniques such as laser-induced polarization spectroscopy (LIPS) and degenerate four-wave mixing (DFWM) are techniques that show great promise for sensitive measurements of transient gas-phase species, and diagnostic applications of these techniques are being pursued actively at laboratories throughout the world. Over the last few two years we have also begun to explore the use of three-laser electronic-resonance-enhanced (ERE) coherent anti-Stokes Raman scattering (CARS) as a minor species detection method with enhanced selectivity.

The objective of this research program is to develop and test strategies for quantitative concentration measurements using these nonlinear optical techniques in flames and plasmas. We are investigating the physics of these processes by direct numerical integration (DNI) of the time-dependent density matrix equations for the resonant interaction. Significantly fewer restrictive assumptions are required using this DNI approach compared with the assumptions required to obtain analytical solutions. Inclusion of the Zeeman state structure of degenerate levels has enabled us to investigate the physics of LIPS and of polarization effects in DFWM. We have incorporated the effects of hyperfine structure in our numerical calculations of LIPS signal generation. We are concentrating on the accurate simulation of two-photon processes, including Raman transitions, where numerous intermediate electronic levels are included.

During the last year we have characterized and significantly optimized the performance of our injection-seeded, high-resolution optical parametric (OP) laser sources. The pulsed laser radiation produced by these OP systems is single-frequency-mode and tunable, and the system is an ideal laser source for nonlinear optical diagnostic techniques such as LIPS and ERE CARS. Experimental measurements are performed in well-characterized flames or gas cells for comparison with our theoretical calculations.

II. RECENT PROGRESS

A. *Development of Tunable, Injection-Seeded Optical Parametric Sources*

We have developed a pulsed OP system that is injection-seeded with near-infrared distributed feedback (DFB) diode lasers. The first stage of the OP system is injection-seeded at the near-infrared idler wavelength of without the use of a resonant cavity at the idler wavelength, eliminating problems associated with the stabilization of the cavity and simplifying greatly the wavelength tuning of the system. The wavelength of the system can be tuned by varying the current and/or the temperature of the DFB laser. Two beta barium borate (β -BBO) crystals are used in the first stage and are pumped by the third harmonic 355-nm output of an injection-seeded Nd:YAG laser. We have operated the first stage with no cavity mirrors; we refer to this as an optical parametric generator (OPG). We have also operated the first stage with a cavity formed by mirrors at the signal wavelength, referred to as the optical parametric oscillator (OPO). The transverse spatial profile of the OPG output is near-Gaussian, and when a concave mirror is used as an output coupler we can obtain near-Gaussian spatial profiles from the OPO as well.

The OPG or OPO output is then amplified using an additional four-crystal optical parametric amplifier (OPA) stage. The OPO/OPA system is shown in Fig. 1. A pulse energy of over 30 mJ at signal wavelengths around 450 nm has been demonstrated with the system shown in Fig. 1. The frequency spectrum and stability of the OPG/OPA system was monitored using a spectrum analyzer with a 2 GHz free

spectral range and a finesse of 200, and the measured spectral width of the signal and idler outputs from the OPO/OPA or OPG/OPA system was approximately 220 MHz. The OP systems are described in detail in an Applied Physics B article which is currently available online [1].

B. *High-Resolution Spectroscopy of Nitric Oxide*

As an initial demonstration of the use of our OPG/OPA system, we have performed two-photon-excited fluorescence of the NO molecule for both a single-beam configuration and a two-beam counterpropagating configuration. Following two-photon excitation of transitions within the (0,0) band of the $A^2\Sigma^+ - X^2\Pi$ electronic transition, ultraviolet fluorescence is monitored from this same band. The fluorescence signal following two-photon excitation of the ${}^5S_{11}(6)$ and ${}^5R_{21}(6)$ transitions is shown in Fig. 2 for the counter-propagating configuration for two different laser powers. The measurements were performed in a room-temperature gas cell at a pressure of 0.8 kPa for a mixture of 3000 ppm NO in N_2 buffer gas. In the single-beam configuration, the two lines were not resolved and a single line with a width of 1.5 GHz is observed, corresponding to the expected Doppler width of 3 GHz in the ultraviolet. For the counter-propagating configuration, the two-photon absorption process is Doppler-free when a single-photon is absorbed from each of the pump beams, and the two transitions are resolved clearly with the expected peak separation of approximately 200 MHz. This separation is due to spin splitting of the $N' = 6, v' = 0$ level in the $A^2\Sigma^+$ electronic level, and is in good agreement with literature values for the expected splitting. The measurements shown in Fig. 2 were performed with the 452-nm beam down-collimated to a diameter of 1 mm. Saturation and Stark shifting of the transitions starts to become apparent when the pulse energy is increased to 25 mJ. As discussed in the next section, we are currently developing the computer code for numerical simulation of this process and will investigate the saturation and Stark shifting of the two-photon line shape in detail.

C. *Numerical Modeling of the Two-Photon Absorption and the Femtosecond CARS Process*

The physics of the two-photon absorption process was investigated for a model three-state system [2]. The density-matrix equations for the two-photon interaction were solved in the steady-state limit for a monochromatic pump laser. Collisional broadening, saturation and Stark shifting of the two-photon resonance were investigated in detail by numerical solution of the steady-state density-matrix equations. Analytical expressions for the saturation intensity and the Stark shift were derived for the case where the single-photon transitions between the intermediate state and the initial and final states are far from resonance with the pump laser. For this case, it was found that the direction of the Stark shift is dependent on the relative magnitudes of the dipole-moment matrix elements for the single-photon transitions that couple the intermediate state with the initial and final states. For the three-state system shown in Fig. 3, the calculated two-photon line shapes are shown in Fig. 4.

We have continued to develop and refine over the last year a computer code for the numerical simulation of two-photon absorption and Raman processes. Because of our interest in LIPS, two-photon LIF, and ERE CARS measurements of NO, we have concentrated on developing a realistic model of these processes for the NO molecule. The two-photon absorption and Raman processes both proceed through intermediate levels that are single-photon-coupled with both the initial and final transition levels. The intermediate levels that are by far the most important in this process lie in excited electronic levels such as the $B^2\Pi$, $C^2\Pi$, $D^2\Sigma^+$, and $E^2\Sigma^+$ levels. We have presently included all of these electronic levels in our DNI computer code. Modeling the two-photon process in this manner is necessary in order to obtain accurate values of the two-photon cross sections and to calculate accurate polarization properties for the transitions. For ERE CARS, the resonance enhancements cannot be calculated without including the $A^2\Sigma^+$ level. Using this code, we have begun to simulate the ERE CARS process for the NO molecule.

We have also started to model the fsec CARS process. Because of the two-photon difference-frequency nature of the Raman excitation process, significant excitation of the Raman transition can be

obtained even though the spectral bandwidth of the laser radiation is three orders of magnitude greater than typical Raman line widths for gas-phase transitions. Our DNI methods are ideally suited for the time-dependent simulation of the femtosecond CARS process, provided that the pulses are on the order of 100 fsec long. For pulses much shorter than this, the rotating wave approximation would not be valid.

III. FUTURE WORK

Our investigation of the physics of two-photon, two-color LIPS will continue. We will continue to explore the physics of this process using our direct numerical integration (DNI) code. We will use the OP system for LIPS measurements of the NO molecule. We will also develop a second OP system. We plan to use this system to investigate two-photon, two-color LIPS technique for measurements of the O-atom and of the C-atom. The single-mode output, narrow line width, and smooth temporal pulse shape from the OP system will allow rigorous comparison of theory and experiment. The OP system will also be used to explore further the potential of infrared LIPS for species measurements. Further collaborative picosecond LIPS experiments with Tom Settersten at Sandia are planned for the summer of 2005.

We will further develop and characterize the injection-seeded OP systems. In particular, the simultaneous operation of two OP systems for two-color, high-resolution experiments is a major goal for next year. Simultaneous operation of two OP systems will be demonstrated and the system will be applied for two-color LIPS and/or three-laser CARS. The performance of both the first stage OPO/OPG and the second OPA stage will be further optimized, especially in terms of the transverse spatial profile. We view the optimization of the spatial profile as a key factor in increasing the signal-to-noise ratios in nonlinear optical processes. This OP source technology will enhance greatly the potential for quantitative application of pulsed cavity ring-down spectroscopy and nonlinear techniques such as LIPS, DFWM, dual-pump CARS, and ERE CARS spectroscopy.

We plan to pursue further theoretical and experimental investigations of the ERE CARS process for NO and C₂H₂, especially at higher cell pressures where collisional narrowing may result in significant improvement in the detection limits. The DNI code for ERE CARS has been developed and will be used to explore the physics of the ERE CARS process.

IV. REFERENCES

1. W. D. Kulatilaka, T. N. Anderson, T. L. Bougher, and R. P. Lucht, "Development of an Injection-Seeded, Pulsed Optical Parametric Generator for High-Resolution Spectroscopy," *Applied Physics B*, in press (2005).
2. R. P. Lucht, S. Roy, and J. R. Gord, *J. Chem. Phys.* **121**, 9820-9829 (2004).

V. BES-SUPPORTED PUBLICATIONS 2003-2005

1. R. P. Lucht, S. Roy, and T. A. Reichardt, "Calculation of Radiative Transition Rates for Polarized Laser Radiation," *Progress in Energy and Combustion Science* **29**, 115-137 (2003).
2. S. F. Hanna, W. D. Kulatilaka, Z. Arp, T. Opatrný, M. O. Scully, J. P. Kuehner, and R. P. Lucht, "Electronic-Resonance-Enhanced (ERE) Coherent Anti-Stokes Raman Scattering (CARS) Spectroscopy of Nitric Oxide," *Applied Physics Letters* **83**, 1887-1889 (2003).
3. W. D. Kulatilaka, R. P. Lucht, S. F. Hanna, and V. R. Katta, "Two-Color, Two-Photon Laser-Induced Polarization Spectroscopy Measurements of Atomic Hydrogen in Near-Adiabatic, Atmospheric Pressure Hydrogen/Air Flames," *Combustion and Flame*, **137**, 523-537 (2004).
4. R. P. Lucht, S. Roy, and J. R. Gord, "Nonperturbative Modeling of Two-Photon Absorption in a Three-State System," *Journal of Chemical Physics* **121**, 9820-9829 (2004).
5. W. D. Kulatilaka, T. N. Anderson, T. L. Bougher, and R. P. Lucht "Development of an Injection-Seeded, Pulsed Optical Parametric Generator for High-Resolution Spectroscopy," *Applied Physics B*, in press (2005).

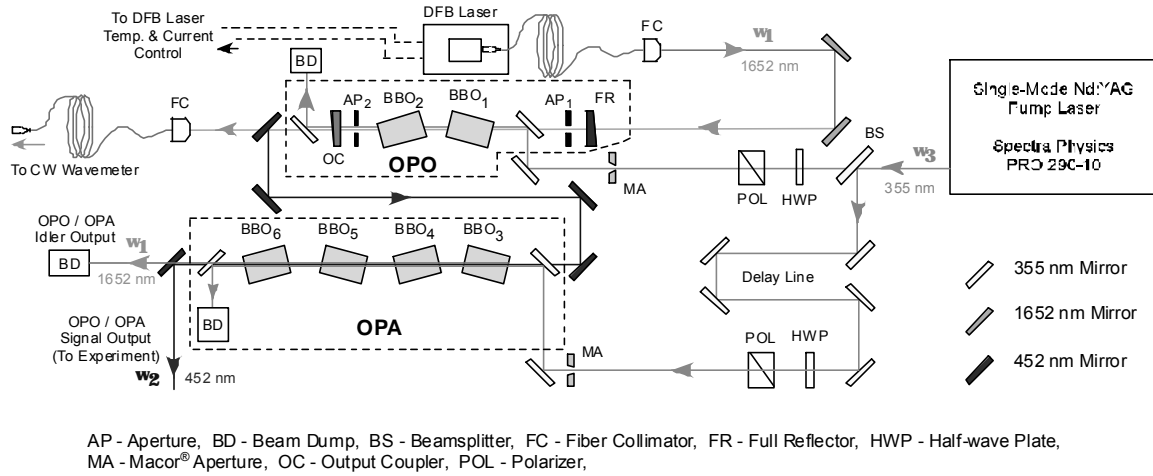


Fig. 1. Schematic diagram of the injection-seeded OPO/OPA system operating at a signal wavelength of 452 nm.

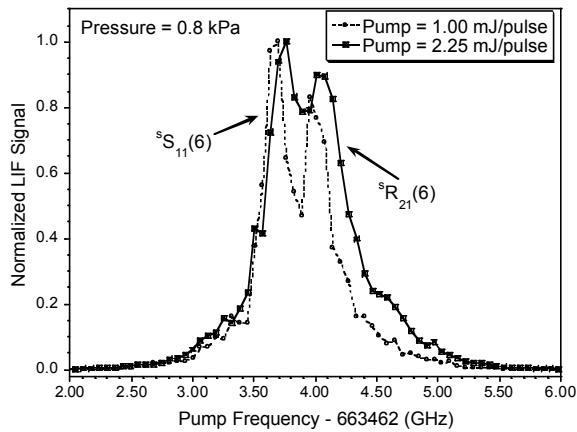


Fig. 2. Line shapes for two-photon excited NO LIF from two-beam counterpropagating excitation.

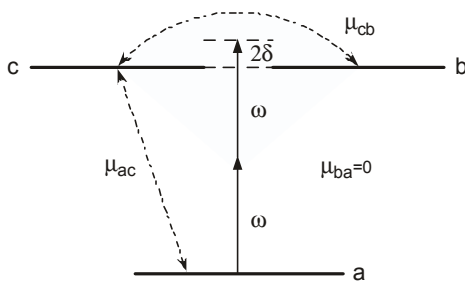


Fig. 3. Three-state system for two-photon absorption calculations.

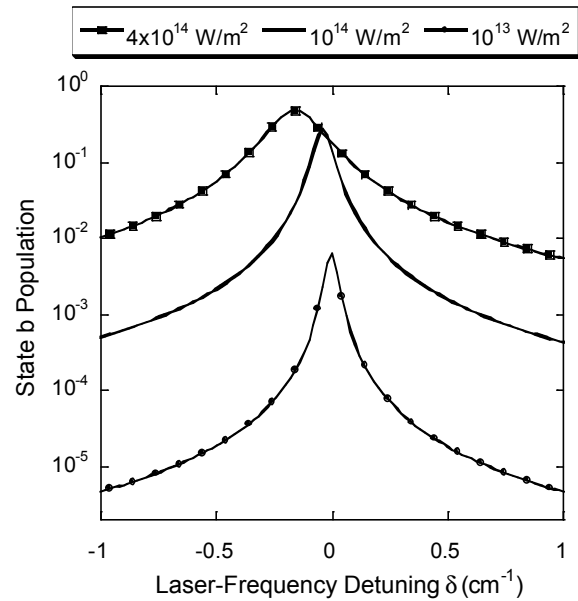


Fig. 4. Final state population r_{bb} versus laser-frequency detuning d for $m_{ac} = ea_0/4$ and $m_{cb} = ea_0$. Line shapes are shown for three different laser intensities. The direction of the Stark shift depends on the ratio of m_{ac} and m_{cb} . For these calculations $w_{ba}/2pc = 80,000 \text{ cm}^{-1}$, $w_{cb} = 0 \text{ cm}^{-1}$, $g_{cb} = g_{ac} = g_{ba} = 10^{10} \text{ s}^{-1}$, and $\Gamma_{ca} = \Gamma_{ba} = 5 \times 10^5 \text{ s}^{-1}$.

Time-Resolved Infrared Absorption Studies of the Dynamics of Radical Reactions

R. G. Macdonald
Chemistry Division
Argonne National Laboratory
Argonne, IL 60439
Email: macdonald@anlchm.chm.anl.gov

Background

There is very little information available about the dynamics of radical-radical reactions. These processes are important in combustion being chain termination steps as well as processes leading to new molecular species. For almost all radical-radical reactions, multiple product channels are possible, and the determination of product channels will be a central focus of this experimental effort. Two approaches will be taken to study radical-radical reactions. In the first, one of the species of interest will be produced in a microwave discharge flow system with a constant known concentration and the second by pulsed-laser photolysis of a suitable photolyte. The rate constant will be determined under pseudo-first order conditions. In the second approach, both transient species will be produced by the same photolysis laser pulse, and both followed simultaneously using two different continuous-wave laser sources. This approach allows for the direct determination of the second-order rate constant under any concentration conditions if the appropriate absorption cross sections have been measured. In both approaches, the time dependence of individual ro-vibrational states of the reactants and/or products will be followed by frequency- and time-resolved absorption spectroscopy. In order to determine branching ratios and second-order rate constants, it is necessary to measure state-specific absorption coefficients and transition moments of radicals and these measurements will play an important role in this experimental study.

Recent Results

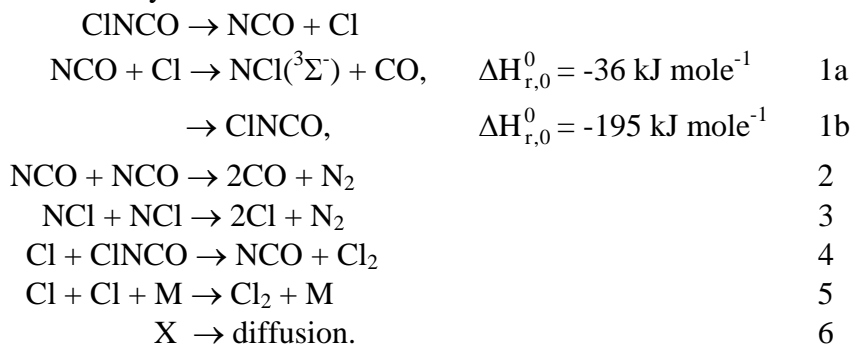
In the current work, the above difficulty was dealt with by either monitoring the concentration of the two reacting radical species using time-resolved infrared absorption spectroscopy or by monitoring one of the reacting species and inferring the concentration of the other from a stoichiometric relationship between the two species. These experiments also illustrate the utility of the time-resolved absorption technique, and the power of infrared spectroscopy to probe a variety of molecular and/or transient species at the individual ro-vibration state level of detail.

The current series of systems under study were initiated to investigate the chemistry between NCO($X^2\Pi$) and simple alkyl radicals. The NCO radical is an important intermediate in the chemistry of NO_x generation and several NO_x abatement strategies, such as the RAPRENOX and NOXOUT processes. In general, the chemistry of the NCO radical has not been extensively explored, and in particular, there are few studies of the interaction between NCO and other open shell species. In many cases, the NCO radical appears to behave as a pseudohalogen abstracting an H atom from hydrogen donors.

The NCO and alkyl (R) radicals were generated by the 248 nm photolysis of CINCO and the subsequent reaction of Cl with RH, where RH was H₂, CH₄ or C₂H₆. In each system NCO and HCl were monitored along with C₂H₆, HCN, HNC, HNCO, CH₃, and NH, depending on the system under study.

(a) NCO(²Π) + Cl(²P)

Work has been completed on the study of the NCO + Cl reaction. It was necessary to understand the NCO + Cl system as a prerequisite to use the photodissociation of CINCO as a generator of the alkyl radicals, H, CH₃, and C₂H₅. The following reaction scheme describes the system:



The rate constants for reactions 1 and 4 have not been previously measured, and were measured in this work. For future kinetic studies, an important question is the products of reaction 1. The dominant reaction channel was taken as 1a. Wategaonkar and Sester^(a) studied the similar reaction F + NCO, and concluded that the formation of the NF(X³Σ⁻) + CO channel was the major product channel. An estimate of k₁ using the low pressure recombination rate constant formulation of Troe^(b) indicated that k_{1b} was 50 times smaller than the measured value of k₁. This calculation was based on an estimate of the Cl-NCO bond energy provided by bond energy and bond order correlations and theoretical DFT B3-LYP 6-311G** calculations.

The temporal dependence of the NCO concentration was monitored using time-resolved infrared absorption spectroscopy with rotation transitions of the (10¹1) ← (00¹0) vibrational band. The absorption coefficients for these transitions have been measured in separate experiments. The rate constants k₁ and k₄ were determined by minimizing the sum of the squares of the residuals between the calculated and experimental NCO profiles. The rate constants were measured with either Ar or CF₄ as a bath gas and a pressure range of 2 to 6 Torr. No dependence of k₁ on the bath gas or pressure was found. The measurements were carried out at 293 K and 345 K. The rate of reaction 1a was found to be (6.9 ± 3.8) × 10⁻¹¹ and (4.0 ± 3.8) × 10⁻¹¹ cm³ molecule⁻¹s⁻¹ at 293 and 345 K, respectively. The rate of reaction k₄ was found to be (2.4 ± 1.6) × 10⁻¹³ and (1.9 ± 1.2) × 10⁻¹³ at 293 and 345 K, respectively. The error bars are an estimate of the total experimental uncertainty based on experimental scatter, uncertainty in the absorption cross section determination, and an estimate of the errors in the rate constants in the model used to fit the experimental NCO profiles.

^(a) S. Wategaonkar and D. W. Setser, *J. Phys. Chem.* **97**, 10028 (1993).

^(b) J. Troe, *J. Chem. Phys.* **66**, 4758 (1977).

(b) $\text{NCO}(X^2\Pi) + \text{CH}_3(X^2A_2)$

Work has been completed on the study of the $\text{NCO} + \text{CH}_3$ reaction. In most experiments, the temporal concentration profiles for NCO , CH_3 , HCl , C_2H_6 , HNC , and HCN were recorded while in a few others HNCO and NH were also detected. Each species was monitored in its ground vibrational level using time-resolved infrared absorption spectroscopy. The recombination of CH_3 radicals was directly monitored by following the formation of C_2H_6 . The absorption coefficients for C_2H_6 and HNCO were measured in separate experiments. A model system consisting of 12 chemical reactions and diffusion was used to determine calculated temporal concentration profiles for the detected species. Appropriate rate constants were determined using a χ^2 minimization procedure. The high signal-to-noise of the NCO , CH_3 , HCl , and C_2H_6 profiles limited the range over which various unknown rate constants could vary. The total reaction rate constant for the $\text{NCO} + \text{CH}_3$ reaction was determined by fitting the NCO profile, and was found to be $(2.1 \pm 0.37) \times 10^{-10} \text{ cm}^3 \text{ molecule}^{-1} \text{ s}^{-1}$, at 293 K, where the uncertainty is $\pm 1\sigma$ from the average. These measurements were carried out over an initial radical concentration ranging from 7.3×10^{12} to $3.0 \times 10^{13} \text{ molecules cm}^{-3}$. It appeared that HCN and HNC were minor products of the $\text{NCO} + \text{CH}_3$ reaction. The branching fractions were $(0.39 \pm 0.24) \%$ and $(0.22 \pm 0.09) \%$ for HCN and HNC , respectively. The co-product for each channel was assumed to be H_2CO .

Comparing the model and experimental CH_3 profiles indicated that some chemistry was missing from the model. Furthermore, the model predictions consistently under predicted the observed C_2H_6 concentration by 1.38 ± 0.14 . This difference of 40% was considerably outside the estimated uncertainty in the C_2H_6 absorption coefficient of $\pm 4 \%$ and again indicated that some chemistry was missing from the basic model. The CH_3 radical recombination accounted for about 20% of the loss of CH_3 . Four different reaction models were investigated to explore the types of processes that might lead to the observed behavior and their influence on the determination of the $\text{NCO} + \text{CH}_3$ reaction rate constant. Generally, the missing chemistry accounted for about 10% of the CH_3 flux lost through reaction with NCO but increased the rate constant by about 20%.

(c) $\text{NCO}(^2\Pi) + \text{C}_2\text{H}_5(^2A')$

The temporal concentration profiles of NCO , HCl , HNCO , C_2H_4 and HCN were monitored for this system. Unfortunately, the spectral region where the C_2H_5 radical is known to absorb is strongly overlapped by C_2H_6 absorption features, preventing the direct detection of C_2H_5 . However, both HNCO and C_2H_4 were observed to be direct products of the $\text{NCO} + \text{C}_2\text{H}_5$ reaction so that these two species provide a connection to the C_2H_5 radical temporal dependence. The secondary chemistry is complicated by the reaction of C_2H_5 with ClNO giving at least HCl and likely HNCO as products.

Preliminary results indicate that the rate constant for the $\text{NCO} + \text{C}_2\text{H}_5$ reaction is $2 \times 10^{-10} \text{ cm}^3 \text{ molecule}^{-1} \text{ s}^{-1}$, similar to that for the other systems. About 50 % of the reaction proceeds through the $\text{C}_2\text{H}_4 + \text{HNCO}$ product channel.

(d) $\text{NCO}(^2\Pi) + \text{H}(^2S)$

Preliminary work has been completed on this reaction. The temporal concentration profiles NCO , $\text{NH}(^3\Sigma^-)(v=0,1,2)$, and HCl were recorded. Other species probed but not detected were HCN , HNC , NH_2 and HNCO . The model simulations of

the NH concentration profiles consistently over predicted the NH concentration. Much better agreement could be obtained if the NH + CO channel only accounted for 50 % of the products. This implies that the recombination reaction forming HNCO accounts for the other 50% of the products, as no other product channels are possible. The initial attempts to detect HNCO used a rotational transition with a small absorption coefficient and these experiments will be reinvestigated using a more sensitive transition. This system is complicated by the large uncertainty in NH chemistry and the rather small reaction rate constant between Cl and H₂. The usefulness of state-to-state detection is illustrated by the observation of vibrationally excited NH. The production of NH(v=1) was found to account for 6.5% of the NH reaction product. The preliminary measurements give the reaction rate constant to be $2.1 \times 10^{-10} \text{ cm}^3 \text{ molecule}^{-1} \text{ s}^{-1}$. This a factor of 10 greater than the only previous measurement for this rate constant^(a)

^(a) K. H. Becker, R. Kurtenbach, F. Schmidt, and P. Wiesen, *Combustion and Flame*, **120**, 570, (2000).

Future Work

Work will also begin on the investigation of the $\text{CH}_3(^2\text{A}_2'') + \text{OH}(^2\Pi)$, radical – radical reaction. As in the CN + OH work, both species will be interrogated on the same photolysis laser pulse using different laser sources. The product branching ratio into the $^1\text{CH}_2 + \text{H}_2\text{O}$ channel will be probed using time-resolved absorption spectroscopy of $^1\text{CH}_2$ using the vibronic transitions of the $^1\text{CH}_2$ ($b \ ^1\text{B}_1$) \leftarrow ($a \ ^1\text{A}_2$) transition in the near infrared. The formation of other product channels will be probed using infrared vibrational spectroscopy.

Publications 2003-2005.

Determination of the rate constant for the $\text{NCO}(X^2\Pi) + \text{O}(^3\text{P})$ reaction at 292 K.

-Y. Gao and R. G. Macdonald

J. Phys. Chem. 107A, 4625-4635 (2003).

Determination of the rate constant for the radical-radical reaction $\text{CN}(X^2\Sigma) + \text{OH}(^2\Pi)$ at 292 K.

-B. K. Decker and R. G. Macdonald

J. Phys. Chem. 107A, 9137-9146 (2003).

Determination of the rate constants for the $\text{NCO}(X^2\Pi) + \text{Cl}(^2\text{P})$ and $\text{Cl}(^2\text{P}) + \text{ClNCO}(X^2\text{A}')$ reactions at 293 and 345 K.

-Y. Gao and R. G. Macdonald

J. Phys. Chem. 109A, accepted (2005).

Quantum chemical studies of chemical reactions related to the formation of polyaromatic hydrocarbons and of spectroscopic properties of their key intermediates

Alexander M. Mebel

Department of Chemistry and Biochemistry, Florida International University
Miami, Florida 33199. E-mail: mebela@fiu.edu

Program Scope. The goal of this project is to theoretically investigate the formation reactions of polyaromatic hydrocarbons (PAHs) from smaller ring and chain hydrocarbons, some key reactions of PAH oxidation, and the reactions of dicarbon and tricarbon molecules with simplest unsaturated hydrocarbons leading to hydrogen-deficient hydrocarbon radicals relevant to the PAH growth. To achieve this goal, we employ chemically accurate *ab initio* calculations of potential energy surfaces and statistical calculations of absolute reaction rate constants and product branching ratios. Another important objective is to predict the spectroscopic properties of the most important intermediates and products through calculations of their excited potential energy surfaces and vibronic spectra. This is helpful for experimental spectroscopic identification and monitoring the key species involved in the PAH formation and growth. Our studies help to untangle elementary mechanisms for the complex reactions and to predict rate constants and relative product yields in a broad range of reaction conditions. The results to be produced can be directly applied in kinetic modeling of reaction networks for PAH formation and growth. The computed energies and molecular and spectroscopic properties also contribute to the creation of a comprehensive database for a variety of hydrocarbon radicals relevant to the soot formation processes in combustion.

Recent Progress

1. Detailed *ab initio* study of hydrogen abstraction acetylene addition and Diels-Alder mechanisms of PAH formation

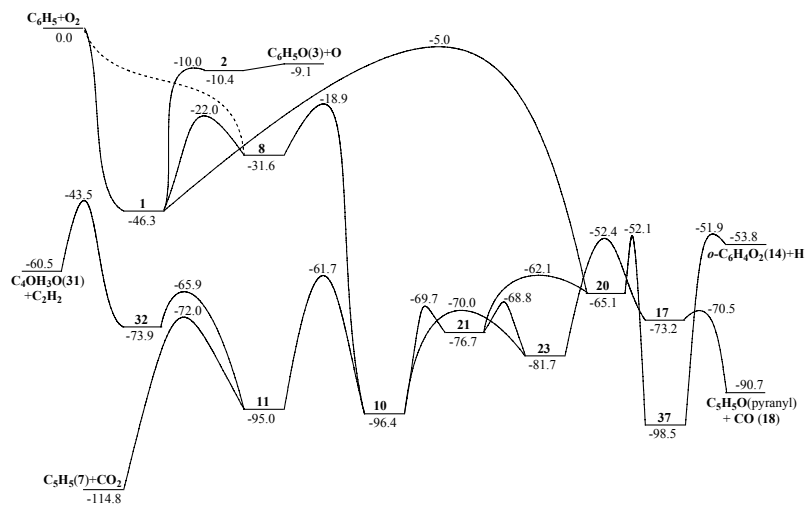
Extensive *ab initio* G3 calculations of potential energy surfaces (PES), which are expected to be accurate within 1-2 kcal/mol, combined with TST calculations of high-pressure-limit reaction rate constants have been applied to study various possible pathways in the hydrogen abstraction acetylene addition (HACA) mechanism of naphthalene and acenaphthalene formation as well as Diels-Alder pathways to acenaphthalene, phenanthrene, and pyrene. The barrier heights, reaction energies, and molecular parameters of the reactants, products, intermediates, and transition states have been generated for all types of reactions involved in the HACA and Diels-Alder mechanisms, including H abstraction from various aromatic intermediates, acetylene addition to radical sites, ring closures leading to the formation of additional aromatic rings, elimination of hydrogen atoms, H disproportionation, C₂H₂ cycloaddition, and H₂ loss. The reactions participating in various HACA sequences (e.g., Frenklach's, alternative Frenklach's, and Bittner and Howard's routes) are demonstrated to have relatively low barriers and high rate constants under combustion conditions. A comparison of the significance of different HACA mechanisms in PAH growth can be made in the future using PES and molecular parameters obtained in the present work. The results show that the Diels-Alder mechanism cannot compete with the HACA pathways even at high combustion temperatures, because of high barriers and consequently low

reaction rate constants. The calculated energetic parameters and rate constants have been compared with experimental and theoretical data available in the literature.

2. G2M study of the potential energy surface for the reaction of phenyl radical with molecular oxygen

In collaboration with M. C. Lin (Emory University), we have performed *ab initio* G2M calculations to investigate the potential energy surface for the reaction of phenyl radical oxidation, $C_6H_5 + O_2$, which competes with reactions leading to PAH growth. As seen on the PES diagram below (relative energies are given in kcal/mol), the reaction starts with an exothermic barrierless addition of O_2 to the radical site of C_6H_5 to produce phenylperoxy (**1**) and, possibly, 1,2-dioxaspiro[2.5]octadienyl (dioxiranyl, **8**) radicals.

Next, **1** loses the terminal oxygen atom to yield the phenoxy + O products (**3**) or rearranges to **8**. The dioxiranyl can further isomerize to a seven-member ring 2-oxepinyloxy radical (**10**), which can give rise to various products including $C_5H_5 + CO_2$, pyranlyl + CO, *o*-benzoquinone + H, and 2-oxo-2,3-dihydrofuran-4-yl + C_2H_2 .



The branching ratio of $C_6H_5O + O$ against the other products is mostly controlled by the critical transition states between **1** and **3**, **1** and **8**, and **8** and **10**. In terms of calculated enthalpies of transition states, the most favorable product channel for the decomposition of **10** is $C_5H_5 + CO_2$, followed by pyranlyl + CO and *o*-benzoquinone + H. Since $C_6H_5O + O$ and $C_5H_5 + CO_2$ are expected to be the major primary products of the $C_6H_5 + O_2$ reaction and thermal decomposition of C_6H_5O leads to $C_5H_5 + CO$, cyclopentadienyl radicals are likely to be the major product of phenyl radical oxidation, and so it results in degradation of the six-member aromatic ring to the five-member cyclopentadienyl ring. Future multichannel RRKM calculations of rate constants are required to support these conclusions and to quantify the product branching ratios at various conditions.

3. Theoretical study of possible reaction mechanisms for the formation of indene

Indene is a prototype molecule and a major precursor of the broad class of cyclopentafused PAHs and fullerenes. We apply extensive *ab initio* G3 calculations combined with statistical theory computations of reaction rate constants to map out various reaction pathways leading to the formation of indene. All major pathways, including C_7/C_2 (toluene + C_2H_2), C_6/C_3 (benzene, fulvene + C_3H_3), C_5/C_2 (cyclopentadienyl + $2C_2H_2$), C_5/C_4 (cyclopentadienyl + vinylacetylene), and naphthalene + O_2 reactions are considered in our study. Several important radical recombination reactions such as $C_6H_5 + CH_3$, $C_6H_5 + CH_2$, and naphthalene + O_2 , are investigated using variational transition state theory (VTST). According to the calculated PESs, the HACA pathway leading from benzene to toluene and then to indene via C_2H_2 addition to toluene

followed by the ring closure, is found to be the most energetically favorable and is likely to be dominant at typical combustion conditions. The other considered pathways normally involve several hydrogen migration steps with relatively high barriers or formation of unfavorable biradical structures. However, those pathways may contribute to the PAH growth at certain conditions, e.g., at higher temperatures, and/or at low acetylene concentrations. Calculated molecular structural parameters and rate constant can be utilized in subsequent kinetic modeling of complex combustion systems.

4. Theoretical study of the reaction mechanism of $C_2 + CH_3CCH$

We have studied PES of the $C_2(^1\Sigma_g^+) + \text{methylacetylene}$ reaction at the G2M level of theory. The calculations show that the singlet C_2 molecule can add to CH_3CCH without a barrier producing a three-member or a four-member ring intermediate, which can rapidly rearrange to the most stable $H_3CCCCCH$ isomer on the C_5H_4 singlet surface. This isomer then can lose a hydrogen atom or H_2 from the CH_3 group with the formation of $H_2CCCCCH$ and $HCCCCCH$, respectively. Alternatively, H atom migrations and three-member-ring closure rearrangements followed by H and H_2 losses can lead to other isomers of the C_5H_3 and C_5H_2 species. According to the calculated energetics, the $C_2(^1\Sigma_g^+) + CH_3CCH$ reaction is likely to be a major source of the C_5H_3 radicals (in particular, the most stable $H_2CCCCCH$ and $HCCCHCCH$ isomers, which are relevant to the formation of benzene through the reactions with CH_3). Among heavy-fragment product channels, only $c\text{-}C_3H_2 + C_2H_2$ may compete with $C_5H_3 + H$ and $C_5H_2 + H_2$. RRKM calculations of reaction rate constants depending on the reactive collision energy are now underway to predict product branching ratios to be compared with experiments carried out in crossed molecular beams by R. I. Kaiser at the University of Hawaii.

5. Ab initio/RRKM study of PES and product branching ratios for $F(^2P) + CH_3$

When studying combustion reaction, one often encounters situations where a rate constant needs to be evaluated for a single bond cleavage process occurring without an exit barrier. The VTST approach can be then applied but this requires a scan of PES along the breaking bond length serving as the reaction coordinate. The ab initio method, which is often used to carry out this scan, as it can be applied to reaction systems of a rather large size, is CCSD(T)//B3LYP. However, since the wave function can have a strong multireference character in the area of PES where a single bond is being cleaved, questions remain how well the single-reference CCSD(T)//B3LYP approach can describe the energetic and molecular parameters, and ultimately the variational rate constant. To address this issue, we have chosen a small system, $F + CH_3$, for which multireference full-valence-active-space MRCI//CASSCF are feasible, and compared four different procedures for ab initio/RRKM and TST calculations of energy-dependent and thermal reaction rate constants and product branching ratios, MRCI//CASSCF, CCSD(T)//B3LYP, CCSD(T)//QCISD, and CCSD(T)//MP2. The CCSD(T)//B3LYP calculations gave 2-3 kcal/mol lower relative energies for the microcanonical VTSTs of the $CH_2F + H$ channel but 3-6 kcal/mol higher energies for those of $CH_3 + F$. As a result, at the CCSD(T)//B3LYP level of theory, the $CH_2F + H$ rate constant increases by factors of 2.2-3.9 as compared to the MRCI//CASSCF results, while the $CH_3 + F$ rate constant decreases by factors of 1.3-1.6. The CCSD(T)//MP2 approach significantly overestimates rate constants for both $CH_2F + H$ and $CH_3 + F$ channels, but the CCSD(T)//B3LYP and CCSD(T)//QCISD values are in general similar. CCSD(T)//B3LYP and CCSD(T)//QCISD appeared to be much better alternatives than CCSD(T)//MP2 and, in

terms of the cost efficiency, the CCSD(T)//B3LYP method seems to be the best choice for larger systems, for which multireference calculations are not feasible. One has to keep in mind however that MRCI//CASSCF and CCSD(T)//B3LYP rate constants for barrierless bond cleavage channels may disagree by as much as a factor of 4, which may result in deviations of branching ratios of up to $\sim 10\%$. For thermal rate constants, the agreement of CCSD(T)//B3LYP and CCSD(T)//QCISD results with MRCI//CASSCF is also within factors of 2-3 and the CCSD(T)//MP2 values are clearly inferior.

Future Plans

We will continue theoretical studies of various routes of the HACA mechanism for the formation of naphthalene and acenaphthalene focusing on additional reaction channels, which can play a significant role if the reactions occur at pressures below the high-pressure limit. Then, in collaboration with S. J. Klippenstein, temperature- and pressure-dependent rate constants will be computed for various channels using VTST, RRKM, and master equation simulations. We will start to investigate other potentially important channels of naphthalene formation in combustion, such as the $C_5H_5 + C_5H_5$, $C_6H_5 + C_4H_4$, and $C_7H_7 + C_3H_3$ reactions. The study of the formation pathways of indene will be continued with more accurate G3 calculations of the PES followed by RRKM and TST computations of rate constants. We will also carry on our collaboration with M. C. Lin on the studies of the phenyl radical oxidation. Now, when the PES has been mapped out and most important reaction channels have been identified, multichannel RRKM calculations and master equation simulations will be performed to predict temperature- and pressure-dependent rate constants and product branching ratios. An important issue to address here is the accuracy of single-reference ab initio methods for the $C_6H_5O_2$ species. In this view, we are currently recalculating the $C_2H_3O_2$ system, which is a smaller prototype of $C_6H_5O_2$, using multireference CASPT2 and MRCI methods with large and flexible active spaces. The goal is to follow the convergence of energetics with respect to the active space size and the basis set and to evaluate the accuracy of CCSD(T) and G2M results as compared to the most accurate MRCI data. Some benchmarking multireference calculations will also be carried out for critical species on the $C_6H_5 + O_2$ PES. We will continue to investigate the C_5H_4 singlet and triplet PESs in order to understand the mechanisms and to predict collision energy dependent product branching ratios for reactions related to these surfaces, in particular, $C_2(^1\Sigma_g^+)/C_2(^3\Pi) +$ methylacetylene/allene. These studies will be performed in parallel with experimental crossed molecular beam measurements in R. I. Kaiser's group at the University of Hawaii. Finally, we will carry out calculations of electronic/vibrational spectra for the most stable isomers of the C_4H_3 radical, an important intermediate in combustion.

DOE/BES sponsored publications (since 08/2004)

1. L. Wang, V. V. Kislov, A. M. Mebel, X. Yang, X. Wang, "Potential energy surface and product branching ratios for the reaction of $F(^2P)$ with the methyl radical: An ab initio/RRKM study," *Chem. Phys. Lett.* 406, 60 (2005).
2. V. V. Kislov, N. I. Islamova, A. M. Kolker, S. H. Lin, A. M. Mebel, "Hydrogen abstraction acetylene addition and Diels-Alder mechanisms of PAH formation: A detailed study using first principles calculations," *J. Chem. Theory and Comput.*, submitted.
3. I. V. Tokmakov, G.-S. Kim, V. V. Kislov, A. M. Mebel, M. C. Lin, "The reaction of phenyl radical with molecular oxygen: A G2M study of the potential energy surface," *J. Phys. Chem. A*, submitted.

FLASH PHOTOLYSIS-SHOCK TUBE STUDIES

Joe V. Michael

Gas Phase Chemical Dynamics Group, Chemistry Division
Argonne National Laboratory, Argonne, IL 60439
e-mail: jmichael@anl.gov

The scope of the program is to measure high-temperature thermal rate constants with shock tube techniques for use in high-temperature combustion. During the past year, we have used a multi-pass optical system for detecting OH-radicals.¹ The new configuration is similar to that described previously.²⁻⁴ We have measured rate constants for several bimolecular reactions in shock wave experiments.

The reflected shock tube technique with multi-pass absorption spectrometric detection of OH-radicals at 308 nm, corresponding to a total path length of ~2.8 m, has been used to study the reaction



We have reanalyzed our earlier O-atom ARAS measurements⁵ for the atomic channel



and have compared both these results with earlier studies⁶⁻¹⁰ to derive an evaluation in Arrhenius form. The evaluated rate coefficient expressions, in units of $\text{cm}^3 \text{ molecule}^{-1} \text{ s}^{-1}$, are

$$k_1 = 3.11 \times 10^{-13} \exp(-4953 \text{ K}/T) \text{ over the T- range } 1237\text{-}2430 \text{ K}, \quad (3)$$

and

$$k_2 = 1.253 \times 10^{-11} \exp(-14241 \text{ K}/T) \text{ over the T- range } 1250\text{-}2430 \text{ K}. \quad (4)$$

Since CH_2O is a major product in both these reactions, reliable rates for the reaction



could be derived from $[\text{OH}]_t$ and $[\text{O}]_t$ experiments over the T- range 1587-2109 K. The combined linear least squares fit result is

$$k_5 = 1.34 \times 10^{-8} \exp(-26883 \text{ K}/T) \text{ cm}^3 \text{ molecule}^{-1} \text{ s}^{-1}. \quad (6)$$

Eqn. (6) can be compared with a recent VTST calculation¹¹ where there is clearly overlap within the uncertainties in both studies. Finally, high sensitivity for the reaction, $\text{OH} + \text{O}_2 \rightarrow \text{HO}_2 + \text{O}$, was noted at high temperature in the O-atom data set simulations. The values obtained by fitting the O-atom data sets at later times (~1.2ms) follow the

Arrhenius form, $k = 2.56 \times 10^{-10} \exp(-24145 \text{ K/T}) \text{ cm}^3 \text{ molecule}^{-1} \text{ s}^{-1}$, over the T- range 1950-2100 K.

Using the same reflected shock tube technique with multi-pass absorption spectrometric detection of OH-radicals at 308 nm, the reaction



has been studied over the temperature range, 840-2025 K¹. The rate constants can be represented by the Arrhenius expression

$$k_7 = (9.52 \pm 1.62) \times 10^{-11} \exp(-4134 \pm 222 \text{ K/T}) \text{ cm}^3 \text{ molecule}^{-1} \text{ s}^{-1}. \quad (8)$$

Since this reaction is important in both combustion and atmospheric chemistry, there have been many prior investigations with a variety of techniques. The present results extend the temperature range by 500 K and have been combined with the most accurate earlier studies to derive an evaluation over the extended temperature range, 195-2025 K. A three parameter expression describes the rate behavior over this temperature range

$$k_7 = 8.73 \times 10^{-19} T^{2.265} \exp(-1183 \text{ K/T}) \text{ cm}^3 \text{ molecule}^{-1} \text{ s}^{-1}. \quad (9)$$

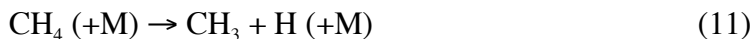
Previous theoretical studies are discussed, and the present evaluation is compared to earlier theoretical estimates.

With the same OH-radical detection method, experiments have been carried out in order to measure rate constants for the initiation reaction



This reaction has been suggested to have importance in the lean oxidation of CH₄ at high temperatures.

Using three mixtures (73 ppm CH₄, 14.7% O₂; 95 ppm CH₄, 10.0% O₂; and 95 ppm CH₄, 12.1% O₂, all in Kr diluent) at ~450 Torr and 1667-2018 K, initial OH profiles were measured and fitted with a chemical simulation consisting of 42 reactions. In the initial stages of reaction, several reactions showed some sensitivity with reaction (10) and



being by far of most importance. Under the present conditions, reaction (11) is well known,¹² and all other reactions that contribute are also well characterized. Hence, the values obtained by profile fitting require only rate constant adjustment for reaction (10). The results are shown in Fig. 1. The data can be described in Arrhenius form by

$$k_{10} = 2.861 \times 10^{-10} \exp(-27190 \text{ K/T}) \text{ cm}^3 \text{ molecule}^{-1} \text{ s}^{-1}. \quad (12)$$

The line calculated from (12) is also shown in Fig. 1. The expression recommended by Baulch et al.¹³ is also shown in the figure where the latter is seen to be low by about a factor of eight.

Harding and Klippenstein have carried out electronic structure and flexible transition state calculations to theoretically predict rate constants for (10). Without any energy scaling, the agreement between the data shown in Fig. 1 and theory is excellent. This comparison is explicitly shown in Harding's report in this volume.

Additional atom and radical with molecule reaction studies (e. g. Cl + hydrocarbons, OH + hydrocarbons, CF₂ + O₂, etc.) and, also, thermal decomposition investigations (e. g. C₂H₅, C₂H₃, etc.) are in the planning stage at the present time.

This work was supported by the U. S. Department of Energy, Office of Basic Energy Sciences, Division of Chemical Sciences, Geosciences and Biosciences, under Contract No. W-31-109-ENG-38.

References

1. N. K. Srinivasan, M.-C. Su, J. W. Sutherland, and J. V. Michael, *J. Phys. Chem. A* **109**, 1857 (2005).
2. M.-C. Su, S. S. Kumaran, K. P. Lim, and J. V. Michael, *Rev. Sci. Instr.* **66**, 4649 (1995).
3. M.-C. Su, S. S. Kumaran, K. P. Lim, J. V. Michael, A. F. Wagner, D. A. Dixon, J. H. Kiefer, and J. DiFelice, *J. Phys. Chem.* **100**, 15827 (1996).
4. M.-C. Su, S. S. Kumaran, K. P. Lim, J. V. Michael, A. F. Wagner, L. B. Harding, and D.-C. Fang, *J. Phys. Chem. A* **106**, 8261 (2002).
5. J. V. Michael and S. S. Kumaran, *J. Phys. Chem. A* **103**, 5942 (1999).
6. C.-L. Yu, C. Wang, and M. Frenklach, *J. Phys. Chem.* **99**, 14377 (1995).
7. S. M. Hwang, S.-O. Ryu, K. J. DeWitt, and M. J. Rabinowitz, *J. Phys. Chem. A* **103**, 5949 (1999).
8. J. P. Hessler, *18th Combustion Research Conference*, Chemical Sciences Division, Office of Basic Energy Sciences, U. S. DOE, Tahoe City, CA, May, 1996, pp. 134-137. J. P. Hessler, H. Du, A. F. Wagner, and P. J. Ogren, private communication, 2004.
9. J. T. Herbon, R. K. Hanson, C. T. Bowman, and D. M. Golden, *Proc. Combust. Inst.* **30**, 955 (2004).
10. (a) M. Braun-Unkhoff, C. Naumann, and P. Frank, *Proceedings of the 19th International Symposium on Shock Waves*; R. Brun and L. Z. Dumitrescu, Eds.; Springer-Verlag: Berlin, 1995; Vol. 2, pp. 203-208; (b) C. Naumann, in *Reaktionen von Methyl mit Sauerstoff und Stickstoffmonoxid und die O₂ Vibrationsrelaxation bei Verbrennungsrelevanten Temperaturen*, Ph. D. Dissertation, Universität Stuttgart, 1998, Göttingen: Cuvillier, 1999; with (b) apparently superseding (a).
11. J. V. Michael, M.-C. Su, J. W. Sutherland, D.-C. Fang, L. B. Harding, A. F. Wagner, D. K. Maity, D. Lin, M. Tirtowidjojo, and T. N. Truong, *J. Phys. Chem. A*, in preparation.
12. J. W. Sutherland, M.-C. Su, and J. V. Michael, *Int. J. Chem. Kinet.* **33**, 669 (2001).
13. D. L. Baulch, C. J. Cobos, R. A. Cox, C. Esser, P. Frank, Th. Just, J. A. Kerr, M. J. Pilling, J. Troe, R. W. Walker, and J. Warnatz, *J. Phys. Chem. Ref. Data* **21**, 411 (1992).

PUBLICATIONS FROM DOE SPONSORED WORK FROM 2003-2005

- *H + H₂ Thermal Reaction: A Convergence of Theory and Experiment*, S. L. Mielke, K. A. Peterson, D. W. Schwenke, B. C. Garrett, D. G. Truhlar, J. V. Michael, M.-C. Su, and J. W. Sutherland, *Phys. Rev. Lett.* **91**, 063201 (2003).
- *Rate Constants for D + C₂H₂ → C₂HD + H at High Temperature: Implications to the High Pressure Rate Constant for H + C₂H₂*, J. V. Michael, M.-C. Su, J. W. Sutherland, L. B. Harding, and A. F. Wagner, *J. Phys. Chem. A* **107**, 10533 (2003).
- *New Rate Constants for D + H₂ and H + D₂ between ~1150 and 2100 K*, J. V. Michael, M.-C. Su, and J. W. Sutherland, *J. Phys. Chem. A* **108**, 432 (2004).
- *Shock Tube Studies Using a Novel Multi-pass Absorption Cell: Rate Constant Results for OH + H₂, and OH + C₂H₆*, L. N. Kransnoperov and J. V. Michael, *J. Phys. Chem. A* **108**, 5643 (2004).

- *High Temperature Shock Tube Studies Using Multi-pass Absorption: Rate Constant Results for OH + CH₃, OH + CH₂, and the Dissociation of CH₃OH*, L. N. Kransoperov and J. V. Michael, *J. Phys. Chem. A* **108**, 8317 (2004).
- *Rate Constants for D + C₂H₄ → C₂H₃D + H at High Temperature: Implications to the High Pressure Rate Constant for H + C₂H₄ → C₂H₅*, J. V. Michael, M.-C. Su, J. W. Sutherland, L. B. Harding, and A. F. Wagner, *Proc. Combust. Inst.* **30**, 965 (2005).
- *Reflected Shock Tube Studies of High-Temperature Rate Constants for OH + CH₄ → CH₃ + H₂O and CH₃ + NO₂ → CH₃O + NO*, N. K. Srinivasan, M.-C. Su, J. W. Sutherland, and J. V. Michael, *J. Phys. Chem. A* **109**, 1857 (2005).

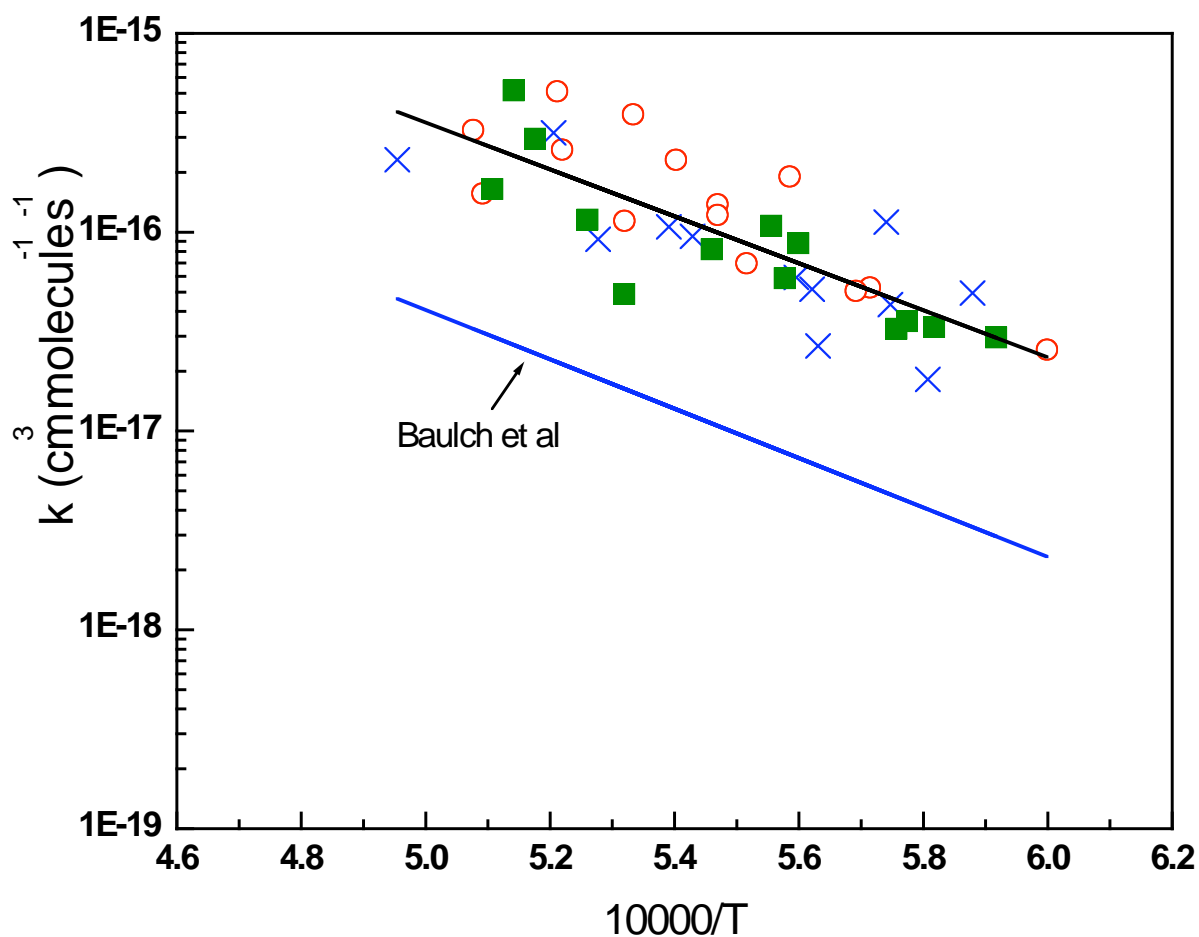


Fig. 1

Particle Diagnostics Development

H. A. Michelsen

Sandia National Labs, MS 9055, P. O. Box 969, Livermore, CA 94551

hamiche@ca.sandia.gov

1. Program Scope

Small (sub-micron) particulates are believed to pose a greater health risk than larger soot particles¹ and are expected to have a significant impact on the Earth's climate.² A growing concern about adverse health and environmental effects of small particles has prompted strict regulations of fine particulate emissions and has intensified research on the formation and impact of combustion-generated particles.³ Studies of particle formation and evolution, however, are hindered by a lack of sensitive, accurate, noninvasive measurements of their physical characteristics. The research program described here focuses on the development of optical diagnostics for particles, primarily soot particles, in combustion environments and combustion exhaust plumes. The goal of this work is in situ measurements of volume fraction, size, composition, and morphology of such particles with fast time response and high sensitivity.

2. Recent Progress

Our work has focused on developing a detailed understanding of the chemical and physical mechanisms that influence the applicability of Laser-Induced Incandescence (LII) for soot detection under a wide range of conditions. In order to understand these mechanisms, we have coupled experimental studies with the development of a model that predicts the temporal behavior of LII from soot on a nanosecond time scale. The model accounts for particle heating by laser absorption, oxidation, and annealing and cooling by sublimation, conduction, and radiation. The model also includes mechanisms for convective heat and mass transfer, melting, and nonthermal photodesorption of carbon clusters.⁴ Initial experimental results used in the development of the model were collected in a coflow diffusion flame with fresh, mature, dry soot as the sample.

Current work builds on these results and extends to combustion-generated particles with inorganic and organic coatings representative of particles found in exhaust plumes. Coatings investigated to date have been selected for diagnostic development for diesel exhaust and include sulfuric acid, heptamethylnonane, and oleic acid. In order to simulate exhaust-plume particulates, we have constructed a flow-tube system that allows controlled deposition of a coating with low volatility on flame-generated soot. The thickness of the coating can be varied, and the resulting particle electric mobility diameter is measured with a Scanning Mobility Particle Sizer (SMPS).

Using this new apparatus, we have studied (1) the effects of laser radiation on the morphology of dry and coated soot aggregates, (2) the effects of particle coating on LII signal and sensitivity, and (3) the applicability of a new technique (Laser-Induced Desorption/Elastic Laser Scattering or LIDELS) for determining coating volume fraction. Based on these experimental studies, we are adding the effects of coatings to our laser-particle interaction model.

2.1. The effects of laser radiation on the morphology of dry and coated soot aggregates.

Soot is composed of dendritic aggregates of small (30-50 nm diameter) carbon spheroids called primary particles. Previous work has suggested that, during laser heating, these aggregates are reduced in size, possibly because of fragmentation.⁵ Transmission Electron Microscopy (TEM) images of laser-heated soot, however, have demonstrated substantial changes to particle morphology without the appearance of small fragments.^{6,7} This result suggests that either mass loss occurred via laser-induced sublimation of carbon clusters or that any fragments were not retained on the grids.

In collaboration with Prof. Peter Buseck and his group at Arizona State University, we have used particle electric mobility sizing and TEM techniques to investigate the physical changes induced in dry

and coated soot aggregates exposed to laser radiation at 532 nm. In these experiments, soot particles were measured with an SMPS and were concurrently collected on TEM grids prior to and following exposure to laser radiation over a wide range of laser fluences (0-0.8 J/cm²).

2.1.1. The effects of laser radiation on dry soot.

The initial soot particles produced by the flame during these experiments were polydisperse and followed a log-normal size distribution with a median electric mobility diameter of ~100 nm. TEM images of these particles revealed typical fractal-like branched-chain aggregates consisting of approximately 50 spherical primary particles. The average geometric diameter of the primary particles was 25 nm, and that of the aggregates was 110 nm, as inferred from TEM images. The aggregate fractal dimension was $d_f = 1.7$.

No change in particle electric mobility diameter was observed when the particles were exposed to laser radiation at 532 nm at low fluences (<~0.2 J/cm²). At higher fluences, a new size mode (centered at 10 – 40 nm in electric mobility diameter) was observed. These smaller particles became apparent at a laser fluence of ~0.2 J/cm² and grew in size and particle number density with increasing fluence. Our experimental results and TEM images of laser-heated and unexposed soot indicate that the small particle mode resulted from fragmentation of soot aggregates from laser irradiation. The onset of soot fragmentation at 0.2 J/cm² is consistent with energetic requirements for carbon sublimation observed experimentally and predicted by the LII model.⁴ TEM images of soot subjected to 532-nm radiation at high fluences (0.9 J/cm²) revealed no primary particle structure but appeared to be conglomerates of very thin sheets of amorphous carbon. Some of the particles contained banded or ribbon-like graphitic structures. The average geometric diameter of the fragments was 30 nm.

2.1.2. The effects of laser radiation on coated soot.

Laser fragmentation experiments were also performed with soot coated with sulfuric acid. The thickness of the deposited coating was varied between 10 and 70 nm (as estimated from the change in electric mobility diameter relative to dry soot).

Similarly to dry soot, formation of a small particle mode (10 – 40 nm electric mobility diameter) was detected upon heating coated aerosols with 532-nm laser radiation. In this case, however, small particles began to form at much lower fluences (~0.02 J/cm²) than for dry soot, indicating that laser-induced desorption of particle coatings occurs at lower fluences than carbon sublimation (~0.2 J/cm²). These results suggest that a low-fluence laser pulse (0.02 to 0.2 J/cm² at 532 nm) can be used to remove coatings from soot particles. The measured coating vaporization threshold (0.02 J/cm²) is consistent with model results of laser absorption, particle heating, and coating loss. Furthermore, these coating vaporization results are consistent with laser-induced desorption/elastic laser scattering (LIDELS) results presented in Section 2.3.

2.2. The effects of particle coatings on LII signal and sensitivity.

The LII signal is generally assumed to be linearly dependent on black carbon aerosol volume fraction. Quantitative applications of this technique for soot volume fraction measurements, however, require an understanding of the validity of this assumption under a wide range of conditions. Even if this assumption were valid for dry soot particles in flames, for example, it may not be valid when measuring soot particles coated with unburned fuel in exhaust plumes or soot aerosols incorporated in larger droplets in the atmosphere.

We performed laboratory experiments to study the effects of particle coatings on LII signal and sensitivity. In these experiments, sulfuric-acid-coated soot particles were sampled with an SMPS and detected with LII to yield the sensitivity of LII to black carbon as a function of SMPS-estimated coating thickness. Sulfuric acid coatings were 10 – 200 nm thick (based on mobility diameter measurements). The sensitivity of our LII setup was estimated at 10 pptv for dry soot. For coated soot particles sensitivity dropped significantly at low laser fluences for which the energy required for coating desorption constitutes a significant fraction of the total energy absorbed by a particle. Thus,

for example, a 200-nm coating reduced LII sensitivity by a factor of ~ 10 at a fluence of 0.1 J/cm^2 . At 0.7 J/cm^2 , however, the LII sensitivity to coated particles was reduced by $\sim 20\%$. These observations are consistent with modeling results that also predict a severe sensitivity loss at fluences below 0.2 J/cm^2 .

2.3. The effects of particle coatings on LII signal and sensitivity.

In collaboration with Dr. Peter Witze from the Engine Combustion Department at Sandia, we have been investigating the applicability of double-pulse laser-induced desorption / elastic laser scattering (LIDELS), a real-time soot diagnostic technique developed recently at Sandia.⁸ This technique uses two laser pulses of comparable energy and separated in time by $\sim 100 \text{ ns}$ to measure the volume fraction of non-refractory soot coatings. The elastic scatter from the first laser pulse yields information about the aggregate size of the coated particle and also deposits the energy to desorb the volatile coatings. Scatter from the second pulse gives the size of the remaining (black carbon) portion of the particle. The ratio of the scatter from the second pulse relative to that from the first provides a measure of the solid (black carbon)-to-total volume fraction.

To validate the LIDELS technique, uncoated ceramic microspheres suspended in air were flowed through the instrument, yielding a solid volume fraction (SVF) measurement of $\text{SVF} = 1.00 \pm 0.02$ independent of laser fluence (in the range 0 to 0.9 J/cm^2), as expected. Subsequent experiments were performed to measure SVF of soot particles generated in a flame with and without coatings of sulfuric and oleic acid. In agreement with laser-induced desorption results described in Section 2.1.2, no material desorption was observed at low laser fluences ($<0.02 \text{ J/cm}^2$). At intermediate laser fluences, between 0.05 and 0.15 J/cm^2 , the energy of the first laser pulse was sufficient to drive off particle coatings, and SVF measurements in this region were independent of laser fluence. We interpret the SVF values obtained at intermediate fluence as the true solid volume fraction measurement for coated particles. At high laser fluences ($>0.15 \text{ J/cm}^2$), interactions of the particles with both laser pulses resulted in carbon desorption.

3. Future plans

We are performing experiments designed to isolate fast (picosecond timescale) laser-particle mechanisms from processes that are expected to evolve over longer (nanosecond) timescales. Fast processes, such as laser absorption and photolytic desorption, can have an influence on LII and ELS. These experiments are being performed using a regeneratively amplified modelocked Nd:YAG laser with a pulse duration at 532 nm of $\sim 65 \text{ ps}$ and a streak camera with a temporal resolution of $\sim 15 \text{ ps}$. These measurements will be compared with those made using a YAG laser with a 7-ns pulse duration to heat the particles. The results will be used to revise and refine the LII model and our understanding of the mechanisms involved in LII detection.

Annealing is another mechanism with large uncertainties. In addition to uncertainties in the rates of annealing, there are large uncertainties associated with the change in optical properties as the particles anneal. Studies of the optical properties of carbon onions (with 10^4 times the number of carbon atoms of C_{60}) have been limited by the inability to generate significant numbers of particles to study. Following a recently published procedure,⁹ we have set up an apparatus to generate carbon onions in sufficiently large quantities to measure their optical properties for comparison with those of soot. TEM images of the particles generated indicate a mixture of onion-type structures and large amorphous globs up to 10 times larger than the pseudo-onion particles ($\sim 40 \text{ nm}$). The technique used to generate these onions thus requires refinement before we can measure their optical properties.

Most of the carbon atoms in mature soot are thought to be included in flat graphite crystallites with sp^2 hybridization. As the particles anneal, defects form, allowing the surfaces to curve. Annealing of fullerenes by formation of 7-member rings leads to greater sp^3 hybridization.¹⁰ Investigations are underway in collaboration with Dr. Mary Gilles at the Advanced Light Source at the Lawrence

Berkeley National Laboratory using Near-Edge X-ray Absorption Fine Structure (NEXAFS) spectroscopy to study the change in character of the carbon-bond hybridization when the particles are annealed.

We will perform experiments on laser-induced aggregate fragmentation at 1064 nm for better comparison with published studies. We will also expand our studies of the effects of coatings on LII to include coatings of large organic species representative of coatings found on diesel particulates. For these experiments we currently do not have a way of monitoring the mass loading of particle coatings. Developing an understanding of the cause and magnitude of the effects of coatings will require characterization of the particle coatings. Coating the particles increases the mean aggregate size as measured by the SMPS, but measurements of electric mobility diameter provided by the SMPS do not provide a quantitative measure of the volatile coating fraction either by volume or by mass. In order to measure the volatile fraction, we will build a chamber that includes a temperature-controlled oscillating quartz microbalance on which we can deposit the particles. Heating the particles will force vaporization of the volatile component and enable us to determine its mass relative to that of the nonvolatile portion. This chamber will also be equipped with a residual gas analyzer for additional coating characterization through mass spectrometric speciation and temperature programmed desorption measurements.

4. References

- (1) Horvath, H. *J. Environ. Radioact.* **2000**, *51*, 5.
- (2) IPCC *Climate Change 2001: The Scientific Basis. Contribution of Working Group I to the Third Assessment Report of the Intergovernmental Panel on Climate Change*; Cambridge University Press: Cambridge, UK and New York, NY, 2001.
- (3) NRC *Research Priorities for Airborne Particulate Matter: IV. Continuing Research Progress*; National Academy Press: Washington, DC, 2004.
- (4) Michelsen, H. A. *J. Chem. Phys.* **2003**, *118*, 7012.
- (5) Filippov, A. V.; Markus, M. W.; Roth, P. J. *Aerosol Sci.* **1999**, *30*, 71.
- (6) Vander Wal, R. L.; Ticich, T. M.; Stephens, A. B. *Appl. Phys. B: Lasers Opt.* **1998**, *67*, 115.
- (7) Vander Wal, R. L.; Choi, M. Y. *Carbon* **1999**, *37*, 231.
- (8) Witze, P. O. *Proc. SAE* **2002**, SAE Paper no. 2002.
- (9) Sano, N.; Wang, H.; Chhowalla, M.; Alexandrou, I.; Amaratunga, G. A. J. *Nature* **2001**, *414*, 506.
- (10) Murry, R. L.; Strout, D. L.; Odom, G. K.; Scuseria, G. E. *Nature* **1993**, *366*, 665.

5. BES peer-reviewed publications

H. A. Michelsen, P. O. Witze, D. Kayes, and S. Hochgreb, "Time-resolved laser-induced incandescence of soot: The influence of experimental factors and microphysical mechanisms", *Appl. Opt.* **42**, 5577-5590 (2003).

H. A. Michelsen, "Understanding and predicting the temporal response of laser-induced incandescence from carbonaceous particles", *J. Chem. Phys.* **118**, 7012-7045 (2003).

6. Collaborators

Dr. Peter Witze and Dr. Michael Gershenson, Sandia National Labs

Dr. Mary Gilles, Advanced Light Source, Lawrence Berkeley National Lab

Prof. Peter Buseck and Dr. Laura van Poppel, Arizona State University

Chemical Kinetics and Combustion Modeling

James A. Miller

Combustion Research Facility, Sandia National Laboratories

MS 9055, Livermore, CA, 94551-0969

email: jamille@sandia.gov

Program Scope

The goal of this project is to gain qualitative insight into how pollutants are formed in combustion systems and to develop quantitative mathematical models to predict their formation and destruction rates. The approach is an integrated one, combining theory, modeling, and collaboration with experimentalists to gain as clear a picture as possible of the processes in question. My efforts and those of my collaborators are focused on problems involved with the nitrogen chemistry of combustion systems and the formation of soot and PAH in flames, as well as on general problems in hydrocarbon combustion. Current emphasis is on determining phenomenological rate coefficients from the time-dependent, multiple-well master equation for reactions involved in the pre-cyclization and cyclization chemistry of flames burning aliphatic fuels.

Recent Results

The Reactions of OH with Acetylene and Ethylene (with Juan Senosiain and Stephen Klippenstein)

The reactions of hydroxyl radicals with ethylene and acetylene are important in combustion processes and in the chemistry of terrestrial and planetary atmospheres. The doublet potential energy surfaces for the reactions of C_2H_2 and C_2H_4 with OH were calculated with the RHF-RQCISD(T) method and extrapolated to the complete basis set limit. To investigate the reaction kinetics on these complex potential energy surfaces we employed an RRKM/master-equation approach, treating some transition states variationally. Corrections for tunneling were done on an asymmetric Eckart potential, and the effect of conserving total angular momentum was investigated in the zero-pressure limit. Rate coefficients for the different channels were obtained as a function of temperature and pressure and compared to existing experimental data. The agreement between theory and experiment is generally excellent. At low temperature and/or high pressure, the reactions proceed by stabilization of the initial addition complexes. At higher temperatures isomerization and decomposition of the energized adducts compete with direct hydrogen abstraction for dominance. In the reaction of acetylene with OH, the decomposition to ketene and H is the main channel at intermediate temperatures and low pressures, while hydrogen abstraction and formation of $HCCOH+H$ become dominant above 2000 K. In the case of ethylene, direct hydrogen abstraction plays the dominant role above 600 K, contrary to some previous reports. Production of vinyl alcohol increases with temperature and is the second most important channel for this reaction.

The Addition of Hydrogen Atoms to Diacetylene and the Heats of Formation of $i-C_4H_3$ and $n-C_4H_3$ (with Stephen Klippenstein)

In this work, we investigated in detail the addition of hydrogen atoms to diacetylene and the reverse dissociation reactions,



The theory utilizes high-level electronic-structure methodology to characterize the potential energy surface, RRKM theory to calculate microcanonical/J-resolved rate coefficients, and a two-dimensional master-equation approach to extract phenomenological (thermal) rate coefficients. With a minor adjustment of the barrier to addition of both reactions, we obtain almost perfect agreement with the limited experimental data available. The rate coefficients $k_1(T,p)$ and $k_2(T,p)$ were cast in forms that can be used in chemical kinetic modeling. In addition, we have predicted values of the heats of formation of *i*-C₄H₃ and *n*-C₄H₃ and investigated their importance in flame chemistry. Our basis-set extrapolated QCISD(T) predictions of these heats of formation at 298 K are 130.8 kcal/mole for *n*-C₄H₃ and 119.3 kcal/mole for the *i*-isomer; multi-reference, configuration-interaction calculations with a 9-electron, 9-orbital CAS wavefunction give just slightly larger values for these parameters. Our results are in good agreement with the recent focal-point analysis of Wheeler, et al. (*J. Chem. Phys.* **004**, 121, 8800-8813), but they differ substantially for $\int H^0_{298}(n-C_4H_3)$ with the earlier diffusion Monte Carlo predictions of Krokidis, et al. (*Int. J. Chem. Kinet.* **2001**, 33 808-820).

The Reaction of n-C₄H₃ with Acetylene and the Dissociation of the Phenyl Radical (with Stephen Klippenstein)

Using electronic-structure methods similar to those described above, we have mapped out the features of the C₆H₅ potential important for understanding the reactions of interest. As many as 19 potential wells were identified as potentially significant. However, preliminary master-equation calculations indicate that the reactions of interest, under combustion conditions, are simpler than this number would indicate. Our results for the product distribution of *n*-C₄H₃+C₂H₂ are qualitatively similar to those obtained previously by others using simpler methods:

1. At lower temperatures and high pressure, stabilization to form phenyl is dominant.
2. At high temperatures and lower pressures, L-C₆H₄+H are the dominant products, where L-C₆H₄ is the simple exchange product of the reaction.
3. The ortho-benzyne + H channel is important only at low pressure and intermediate temperatures. For example, at 20 Torr it is dominant between 900 and 1100 K.
4. Our results also indicate that the equilibrium of the reaction *n*-C₄H₃+C₂H₂ ⇌ phenyl shifts to favor the *reactants* at a temperature somewhere between 1300K and 1600K, depending on the particular flame condition. This appears to be a general result for reactions of the *radical + molecule* ⇌ *radical* type, one that may have important implications for mechanisms of higher-hydrocarbon growth in flames.

At low pressures, phenyl dissociates thermally almost exclusively to *o*-benzyne + H, but as the pressure is increased, other product channels come into play. At 10 atm, dissociation to *n*-C₄H₃+C₂H₂ and L-C₆H₄ + H are as important as the *o*-benzyne + H channel at combustion temperatures. At higher pressures, other product channels may contribute as well.

Future Directions

We shall continue our work on the chemical kinetics of rich flames of aliphatic fuels, particularly that concerned with the formation of the first aromatics containing one or two rings. Currently, we are finishing up our work on *n*-C₄H₃+C₂H₂ and phenyl dissociation and plan to initiate more work on reactions of propargyl (C₃H₃(+M)→C₃H₂+H(+M), C₃H₃ + allene, and C₃H₃ + propyne). However, our next major project will be the propargyl + allyl reaction, which could be almost as important as C₃H₃+C₃H₃ as a cyclization step in some flames. This work is being pursued in collaboration with Wesley Allen and co-workers at the University of Georgia. We shall also continue to maintain our interest in the nitrogen chemistry of combustion, particularly that concerned with NO_x control technologies such as reburning, Thermal De-NO_x, and RAPRENO_x.

Publications of James A. Miller 2003-present

- J.A. Miller and S.J. Klippenstein, "Some Observations Concerning Detailed Balance in Association /Dissociation Reactions", *J. Phys. Chem. A* **108**, 8296-8306 (2004)
- J.A. Miller, M.J. Pilling, and J. Troe, "Unravelling Combustion Mechanisms Through a Quantitative Understanding of Elementary Reactions", *Proc. Combust. Inst.* **30**, 43-88 (2005)
- J.P. Senosiain, S.J. Klippenstein, and J.A. Miller, "The Reaction of Acetylene with Hydroxyl Radicals", *J. Phys. Chem. A*, in press(2005)
- C.A. Taatjes, N. Hansen, A. McIlroy, J.A. Miller, J.P. Senosiain, S.J. Klippenstein, F. Qi, L. Sheng, Y. Zhang, T.A. Cool, J. Wang, P.R. Westmoreland, M.E. Law, T. Kasper, and K. Köhse-Hoeninghaus, "Enols are Common Combustion Intermediates in Hydrocarbon Oxidation", *Science*, submitted (2005)
- C. A. Taatjes, S. J. Klippenstein, N. Hansen, J. A. Miller, T. A. Cool, J. Wang, M.E. Law, and P. R. Westmoreland, "Synchrotron Photoionization Measurements of Combustion Intermediates: Photoionization Efficiency and Identification of C₃H₂ Isomers", *Phys. Chem. Chem. Phys.* **7**, 806-813 (2005)
- S.J. Klippenstein and J.A. Miller, "The Addition of Hydrogen Atoms to Diacetylene and the Heats of Formation of i-C₄H₃ and n-C₄H₃", *J. Phys. Chem. A*, in press(2005)
- J.P. Senosiain, S.J. Klippenstein, and J.A. Miller, "A Complete Statistical Analysis of the Reaction Between OH and CO," *Proc. Combust. Inst.* **30**, 943-950 (2005)
- A.Fernandez-Ramos, J.A.Miller, S.J.Klippenstein, and D.G.Truhlar, "Bimolecular Reactions," Chapter 3 of upcoming volume of *Comprehensive Chemical Kinetics* (Ed. R.W. Carr and M.R. Zachariah), Elsevier Publishing Company, 2005 (in press)
- J.A.Miller and S.J. Klippenstein, "The H+C₂H₂(+M)↔C₂H₃(+M) and H+C₂H₄(+M)↔C₂H₅(+M) Reactions: Electronic Structure, Variational Transition-State Theory, and Solutions to a Two-Dimensional Master Equation", *Physical Chemistry Chemical Physics* **6**, 1192-1202 (2004).
- J.A. Miller and S.J. Klippenstein, "The Recombination of Propargyl Radicals and Other Reactions on a C₆H₆ Potential," *J. Phys. Chem. A* **107**, 7783-7799 (2003).
- J.A. Miller and S.J. Klippenstein, "From the Multiple-Well Master Equation to Phenomenological Rate Coefficients: Reactions Occurring on a C₃H₄ Potential Energy Surface," *J. Phys. Chem. A* **107**, 2680-2692 (2003).
- J.A. Miller, S.J. Klippenstein, and P. Glarborg, "A Kinetic Issue in Reburning: The Fate of HCNO", *Combustion and Flame* **135**, 357-362 (2003).
- J.D. DeSain, S.J. Klippenstein, J.A. Miller, and C.A. Taatjes, "Measurements, Theory, and Modeling of OH Formation in Ethyl + O₂ and Propyl + O₂ Reactions", *J. Phys. Chem. A* **107**, 4415-4427 (2003).

Detection and Characterization of Free Radicals Relevant to Combustion Processes

Terry A. Miller

Laser Spectroscopy Facility, Department of Chemistry
The Ohio State University, Columbus OH 43210, email: tamiller+@osu.edu

1 Program Scope

The chemistry of combustion is well-known to be extremely complex. Modern computer codes are now available that employ hundreds of reaction steps and a comparable number of chemical intermediates. Nonetheless the predictions of such models can be no better than the fundamental dynamical and mechanistic data that are their inputs. Spectroscopic identifications and diagnostics for the chemical intermediates in the reaction mechanisms constitute an important experimental verification of the models. Such spectroscopic investigations also provide experimental “gold standards” against which quantum chemistry computations of molecular properties may be judged.

Our spectroscopic work has centered upon two families of reactive radical intermediates that are of key importance in (low temperature) combustion processes. These families are the organic peroxy radicals, RO₂, and the corresponding alkoxy radicals, RO.

2 Recent Progress

2.1 Alkoxy radicals

In past work we have identified and characterized the laser induced fluorescence (LIF) $\tilde{A} - \tilde{X}$ electronic spectra of the open-chain, jet-cooled alkoxy radicals, C_nH_{2n+1}O, for $n = 2 - 10$. Work on primary alkoxies is essentially complete with the various bands in the electronic spectrum being assigned to the origins of the electronic transitions of particular conformers of the 1-C_nH_{2n+1}O isomers and the corresponding transitions to excited vibrational levels of the \tilde{A} state.

Table 1: Experimental and calculated $\tilde{A} - \tilde{X}$ energy separation (in cm⁻¹) of a number of open-chain alkoxy radicals. Both the calculated and experimental values (except where otherwise noted) are from our work. Calculated values are at the B3LYP/6-31+G* level of theory, except for those included in brackets which were calculated by the EOM-EE-CCSD/CC-pVDZ method.

Alkoxies	$\tilde{A} - \tilde{X}$ Separation	
	Calculated	Experimental
Ethoxy (² A')	314 [380]	370, ^a 355(10) ^b
1-Propoxy, <i>T</i> (² A'')	225 [369]	321(5)
1-Propoxy, <i>G</i> (² A)	[8]	N.A.
2-Propoxy (² A')	101	68(5), 1225(65) ^b
1-Butoxy, <i>T</i> ₁ <i>G</i> ₂ (² A)	-	271(5)
1-Butoxy, <i>T</i> ₁ <i>T</i> ₂ (² A'')	162	292(5)
1-Butoxy, <i>G</i> ₁ <i>T</i> ₂ (² A)	-	129(5)?
2-Butoxy, <i>G</i> ₊ (² A)	-	55(5)
2-Butoxy, <i>G</i> ₋ (² A)	-	125(5)
Cyclohexoxy (² A'?)	101	62

a. X. Zhu, M. M. Kamal, and P. Misra, *Pure Appl. Opt.* **5**, 1021 (1996). We have re-assigned the spectrum.

b. T. M. Ramond, G. E. Davico, R. L. Schwartz, and W. C. Lineberger, *J. Chem. Phys.* **112**, 1158 (2000).

Work is presently continuing on the secondary and tertiary isomers of the same radicals as well as cyclohexoxy, an intermediate in the oxidation of cyclohexane which is a constituent of automotive fuel, as are many of the open chain alkanes. The goal is of course to provide similarly well-understood spectra as are presently available for the primary alkoxy radicals. Such spectra lead to second and third generation spectroscopic, kinetic and dynamics experiments.

An example of such a second-generation experiment is the laser excited, dispersed fluorescence (LEDf) spectroscopy, on an isomer and conformer specific basis, of jet-cooled alkoxy radicals. These experiments provide detailed information about the vibrational structure of the ground \tilde{X} state. However, most importantly they provide a precise determination of the excitation energies of the \tilde{A} state. This is particularly important information because the \tilde{A} state is sufficiently low-lying to be a major contributor to thermal kinetics. In addition we have also carried out quantum chemistry calculations for these species; however, locating the \tilde{A} state is still a major challenge for such calculations. Our experimental and computed results are summarized in Table 1 for a total of 10 species.

A number of interesting trends concerning the \tilde{A} state excitation energy can be gleaned from Table 1. First the excitation energies are all sufficiently small so that the \tilde{A} state will be very significantly populated under even low temperature (<1000K) combustion conditions. Interestingly as the chain length grows there is a gradual decrease in $\tilde{A} - \tilde{X}$ separation. For a given chemical species the $\tilde{A} - \tilde{X}$ separation seems to be significantly larger for primary alkoxy radicals as compared to secondary alkoxy radicals (including cyclohexoxy). Finally for a given isomer, conformers that are *trans* in the O-C-C-C bond linkage have larger excitation energies than those that are *gauche*.

By comparing our experimental and computational results it appears that the $\tilde{A} - \tilde{X}$ separation can be rather accurately predicted by EOM-EE-CCSD/CC-pVDZ level calculations, but these are still prohibitively time-consuming except for the smallest radicals. Such calculations appear significantly better than B3LYP/6-31+G* calculations, which in addition only yield $\tilde{A} - \tilde{X}$ separations if the states are of different symmetry, which is increasingly rare for the larger species.

2.2 Peroxy Radicals

While our work on alkoxy radicals has involved LIF and LEDf studies of jet-cooled radicals, our efforts for peroxy radicals have utilized the cavity ringdown spectroscopy (CRDS) technique to study their weak $\tilde{A} - \tilde{X}$ electronic transition in the near infrared (NIR) at near room temperature. Using NIR CRDS we approach the sensitivity of peroxy radical detection that has been achieved on the much stronger, and widely utilized, ultra-violet (UV) $\tilde{B} - \tilde{X}$ transition. However the UV transition is broad and unstructured making it extremely difficult to discriminate among peroxy radicals, while the NIR transition is intrinsically sharp and its position quite sensitive to chemical species, making it an excellent diagnostic to distinguish among various organic peroxy radicals, and thereby follow their reactions and dynamics individually.

We have recently obtained for the first time the NIR spectra of all the isomers of the alkyl peroxy radicals, $C_nH_{2n+1}O_2$ for $n = 3$ and 4. Examples of CRDS spectra of propyl peroxy radicals are shown in Fig. 1, which compares the spectra obtained from three different methods of radical production. In the top trace, a strong propyl peroxy spectrum is obtained from reaction of O_2 with propyl radicals produced by H atom extraction from propane using Cl atoms produced by excimer laser photolysis of $(COCl)_2$. This is a non-isomer specific production method with the yield of both 1- and 2-propyl peroxy radicals being significant. In trace B, the 2-propyl radical is produced from 2-bromopropane yielding, after O_2 reaction, isomerically

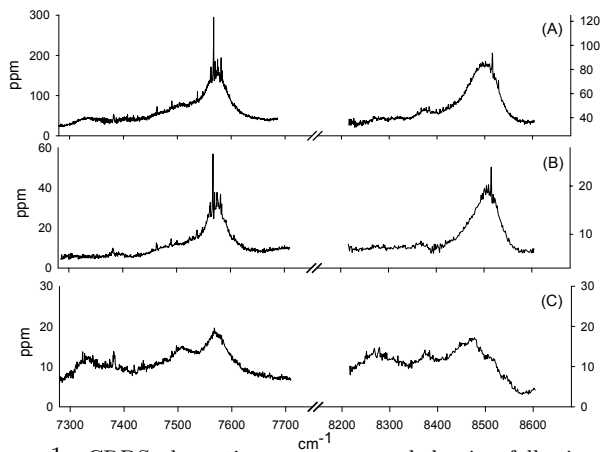


Figure 1: CRDS absorption spectra recorded using following production mechanisms: (A) hydrogen-atom abstraction (B) 2-bromopropane photolysis (C) 1-bromopropane photolysis. The delay time between the excimer laser and CRDS probe is $10\mu s$.

Table 2: Calculated and experimental relative $\tilde{A}-\tilde{X}$ origin transition frequencies, O–O stretching vibrations (both in cm^{-1}), and relative populations/intensities at 25°C of the different conformers of the 1 and 2-propyl peroxy radicals.

$\text{C}_3\text{H}_7\text{O}_2$ Conformer	Calculated				Experimental ^a			
	$\tilde{A}-\tilde{X}$ blue shift ^b	O–O stretch ^c	ΔG^d	Relative population ^e	Band	$\tilde{A}-\tilde{X}$ blue shift ^b	O–O stretch	Relative intensity
T_1T_2	0	918	104	0.30	A ^f	0	941	0.7
T_1G_2	12	919	90	0.65				
G_1G_2	67	862	0	1.00	B	176	872	1.0
G_1T_2	166	913	27	0.88	C ^f	237	950	1.5
$\text{G}_1\text{G}'_2$	213	873	147	0.49				
T	73	899	149	0.24	B'(?)	125	938	0.1
G	0	927	0	1.00	A'	0	948	1.0

a. Relative $\tilde{A}-\tilde{X}$ origin transition frequencies and O–O stretching vibrations are listed with $\pm 10 \text{ cm}^{-1}$ uncertainty.

b. $\tilde{A}-\tilde{X}$ origin transition frequencies relative to corresponding value of the conformer with the smallest $\tilde{A}-\tilde{X}$ excitation energy, i.e. T_1T_2 (as observed at 7332 cm^{-1}) and G (as observed at 7567 cm^{-1}) for 1-propyl and 2-propyl peroxy conformers, respectively.

c. Scaled EOMIP-CCSD/6-31G* frequencies.

d. G2 Gibbs free energies (in cm^{-1}) at 25°C relative to that of the G_1G_2 or G conformer.

e. Calculated from the G2 Gibbs free energies at 25°C.

f. Bands A and C are assumed to arise from pairs of unresolved conformers, respectively T_1T_2 and T_1G_2 , and G_1T_2 and $\text{G}_1\text{G}'_2$. See Fig 2.

pure 2-propyl peroxy radical. In trace C, isomerically pure 1-propyl peroxy radical is similarly produced from 1-bromopropane.

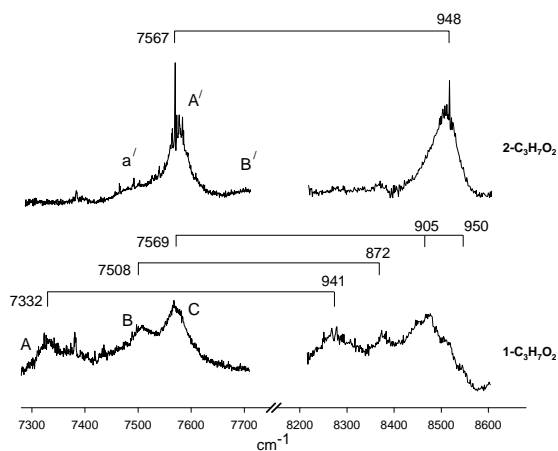


Figure 2: Cavity ringdown absorption spectra of 1-propyl and 2-propyl peroxy radicals. The frequencies are given in cm^{-1} for the assigned origin bands and the separation of the O–O stretching bands.

Fig. 2 shows the isomerically pure spectra with several features assigned to various conformers of the isomers. Since rotational structure is clearly not resolved in these spectra, the only way to assign the bands to a given conformer is to turn to quantum chemistry calculations for each conformer (see Fig. 3) of the band origins, O–O stretch frequencies, and conformer populations, which are key for determining band strengths.

Our calculations have utilized both the BLY/6-31+G* and EOMIP/3-31G* methods. In Table 2 we summarize the results of the calculations and experimental measurements. As the table shows comparison of the two allow very probable assignments of the observed bands. Completely definitive results would require rotationally resolved spectra, which we are hopeful of obtaining in the future.

3 Future Plans

The combustion of fossil fuels necessarily involves complicated reaction mechanisms containing numerous reactive intermediates, some of which are relatively large and complex. As the size of organic molecules increase, their structural diversity in terms of isomers and conformers rapidly grows. The complications this diversity presents for spectroscopic diagnostics and/or reaction kinetics and dynamics are largely unexplored. We intend both to expand our spectroscopic techniques for probing these intermediates and to explore new classes of intermediates. Once the spectroscopy is well understood, precise dynamic and kinetic studies can be carried out.

A particularly useful area to explore spectroscopically are unsaturated peroxy radicals. Both aromatic species, e.g., phenyl peroxy, benzoyl peroxy, etc. and non-aromatic ones, e.g., vinyl peroxy, propargyl peroxy, etc. are important intermediates in combustion for which generally not much is known spectroscopically. Recently we have observed for the first time via CRDS the NIR $\tilde{A} - \tilde{X}$ electronic transition of phenyl peroxy, and are presently investigating it. It will be particularly interesting to compare the $\tilde{A} - \tilde{X}$ transition with the $\tilde{B} - \tilde{X}$ transition of this radical which was previously reported (T. Yu and M. C. Lin, *J. Am. Chem. Soc.*, **116**, 9571 (1994)).

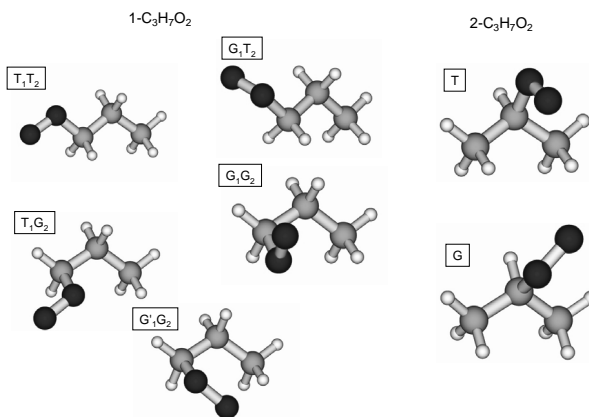


Figure 3: Schematic representations of the structures of the unique conformers of the 1-propyl and 2-propyl peroxy radicals.

List of Publications Supported by DOE

- [1] "Rotationally Resolved Electronic Spectra of the $\tilde{B} - \tilde{X}$ Transition in Multiple Conformers of 1-Butoxy and 1-Pentoxy Radicals," S. Gopalakrishnan, L. Zu, and T. A. Miller, *J. Phys. Chem. A*, **107**, 5189 (2003).
- [2] "Theoretical Prediction of Spectroscopic Constants of 1-Alkoxy Radicals," G. Tarczay, S. Gopalakrishnan, and T. A. Miller, *J. Mol. Spectros.*, **220**, 276 (2003).
- [3] "Radiative and Non-Radiative Decay of Selected Vibronic Levels of the \tilde{B} State of Alkoxy," S. Gopalakrishnan, L. Zu, and T. A. Miller, *Chem. Phys. Lett.*, **380**, 749 (2003).
- [4] "Jet-Cooled LIF Spectra of Cyclohexoxy Radical," L. Zu, J. Liu, and T. A. Miller, *J. Chem. Phys.* **120**, 10579 (2004).
- [5] "Dispersed Fluorescence Spectroscopy of Primary and Secondary Alkoxy Radicals," J. Jin, I. Sioutis, G. Tarczay, S. Gopalakrishnan, A. Bezant, and T. A. Miller, *J. Chem. Phys.* **121**, 11780 (2004).
- [6] "Conformational Analysis of the 1- and 2-Propyl Peroxy Radicals," G. Tarczay, S. Zalyubovsky, and T. A. Miller, *Chem. Phys. Lett.*, *accepted*.

Reaction Dynamics in Polyatomic Molecular Systems

William H. Miller

Department of Chemistry, University of California, and
Chemical Sciences Division, Lawrence Berkeley National Laboratory
Berkeley, California 94720-1460
millerwh@berkeley.edu

Program Scope or Definition

The goal of this program is the development of theoretical methods and models for describing the dynamics of chemical reactions, with specific interest for application to polyatomic molecular systems of special interest and relevance. There is interest in developing the most rigorous possible theoretical approaches and also in more approximate treatments that are more readily applicable to complex systems.

Recent Progress

There are only a few computational methodologies that are available for treating molecular systems with *many degrees of freedom*, primarily methods based on integrating the classical equations of motion (i.e., classical trajectory calculations \equiv molecular dynamics simulations), and those based on evaluating Feynman path integrals (by Monte Carlo or other statistical sampling methods) for the Boltzmann operator, $\exp(-\beta\hat{H})$. This research program has been focusing in recent years on developing theoretical approaches to chemical dynamics that leverage these two computational methodologies.

The most general (and mature) theoretical approach is the semiclassical (SC) initial value representation (IVR), which provides a SC approximation to the quantum mechanical time evolution operator, $\exp(-i\hat{H}t/\hbar)$. It requires classical trajectories for its implementation and is thus effectively a way for adding quantum effects (within the SC approximation) to classical molecular dynamics simulations; it has been applied by a number of research groups to a wide variety of phenomena. Paper 1 (on the 2003-2005 publication list) is one of our recent applications, to the evaluation of the reactive flux correlation function,

$$C_{fs}(t) = \text{tr} \left[e^{-\beta\hat{H}/2} \hat{F} e^{-\beta\hat{H}/2} e^{i\hat{H}t/\hbar} h(f(\mathbf{q})) e^{-i\hat{H}t/\hbar} \right] \quad (1a)$$

for the $\text{D} + \text{H}_2 \rightarrow \text{HD} + \text{H}$ reaction; the long time limit of this correlation function gives the thermal rate constant $k(T)$,

$$k(T) = Q_r^{-1} \lim_{t \rightarrow \infty} C_{fs}(t), \quad (1b)$$

where Q_r is the reactant partition function (per unit volume). The Boltzmann operators in Eq. (1) were evaluated by Feynman path integration and the time evolution operators by the SC-IVR. Since this benchmark calculation was done to serve as a demonstration of the general approach,

the calculation was carried out in 3d Cartesian coordinates (i.e., total angular momentum conservation was not explicitly invoked, and thus no sum over total angular momentum quantum numbers is involved in the calculation — this is all implicitly incorporated in evaluation of the trace), since this is certainly what one would do in treating a many-atom reaction. The agreement of these calculations with the results given by quantum reactive scattering (with appropriate thermal averages over initial and final states) is quantitative.

The SC-IVR approach, since it provides an approximation for the time evolution operator, allows one to describe *any* dynamical phenomena (within the SC approximation). For the specific application to calculating thermal reaction rates, however, one can make useful approximations that are simpler to evaluate because the long time limit of the flux correlation function of Eq. (1) is often reached in relatively short time. Thus short time approximations to $C_{ff}(t)$, which are essentially quantum generalizations of the transition state approximation of classical mechanics, are often useful (and much simpler to evaluate than the fully dynamical rate expression of Eq. (1)).

One of the most successful of these short-time approximate theories is the *quantum instanton* (QI) model that we have recently developed (paper 2) and which has been the focus of most of our efforts over the last year or two. The name is due to the relation to a much older SC approximation¹ for thermal rates that came to be known as the instanton model. The SC instanton model has many qualitatively correct features and insights, but the SC approximation to the Boltzmann operator that is inherent to it was not sufficiently quantitative in early test calculations. The present QI model incorporates the physical ideas of the SC instanton model but is expressed wholly in terms of the *quantum* Boltzmann operator, thus alleviating most of the quantitative deficiencies of the SC version. Its evaluation thus involves (Monte Carlo) evaluation of the path integral expression for the Boltzmann operator, but no real time dynamics. The basic result for the thermal reaction rate is

$$k(T) = Q_r^{-1} \frac{\hbar\sqrt{\pi/2}}{\Delta H(T)} C_{ff}(0) , \quad (2a)$$

where $C_{ff}(0)$ is the zero time flux-flux autocorrelation function

$$C_{ff}(0) = \text{tr} \left[e^{-\beta\hat{H}/2} \hat{F} e^{-\beta\hat{H}/2} \hat{F} \right] , \quad (2b)$$

and $\Delta H(T)$ is a particular kind of energy variance (also expressed wholly in terms of the Boltzmann operator). Most of the papers in the 2003-2005 list below have to do with technical developments related to evaluating the QI rate expression and to its applications to various test reactions.

QI calculations of thermal rate constants for the $\text{H/D} + \text{H}_2 \rightarrow \text{H}_2/\text{HD} + \text{H}$ reactions (collinear and 3d), for the $\text{H} + \text{CH}_4 \rightarrow \text{H}_2 + \text{CH}_3$ reaction (3d), and most recently to a model of proton transfer in a polar solvent, $\text{AH} + \text{B} \rightarrow \text{A}^- + \text{H}^+\text{B}$ solvated by 255 methyl chloride molecules (the Azzouz-Borgis model²). All of these calculations were carried out in the full Cartesian coordinates of all the atoms, again the desire to make the approach as 'generic' as possible. Comparison with the

(known) rate constants for the simple atom-diatom reactions is in general quite good (10% or better) over a wide temperature range, from deep in the tunneling regime (i.e., low temperature) to high temperature where over-barrier dynamics dominates. (The primary exception to this good agreement is for the collinear atom-diatom reactions at high temperature, where 're-crossing' dynamics becomes significant, invalidating the transition state assumption of no re-crossing dynamics; re-crossing effects are greatly diminished in the 3d version of these atom-diatom reactions and more complex reactions in general). There is no way to know how accurate our QI results are for the Azzouz-Borgis problem, but the indications are that they are probably the most accurate results yet obtained for it. But the final word is not in on this non-trivial example that lies beyond the possibility of a brute-force 'exact' calculation.

A particularly attractive feature of the QI methodology (described in paper 8, on the Azzouz-Borgis problem) is the ability of use the free-energy perturbation methods of Monte Carlo technology to calculate *isotope effects* much more efficiently than the calculation of the absolute rate constant for each isotope individually.

Future Plans

Perhaps the most outstanding problem remaining for the quantum instanton (QI) model for reaction rates is the choice of the 'dividing surface' (which defines the flux operators). A poor choice for it causes the assumption of 'no re-crossing dynamics' to be poor. If, however, one evaluates the full dynamical rate expression ala Eq (1), then the location of the dividing surface is immaterial (since the real time dynamics takes any re-crossing effects into account). A particularly powerful approach, therefore, would be to combine the QI model with the SC-IVR approach for including real time dynamics. This would thus eliminate any error caused by not having the 'best' dividing surface.

References

1. W. H. Miller, J. Chem. Phys. **62**, 1899-1906 (1975).
2. H. Azzouz and D. Borgis, J. Chem. Phys. **98**, 7361 (1993); J. Mol. Liq. **61**, 17 (1994); **63**, 89 (1995).

2003 - 2005 (to date) DOE Publications

1. T. Yamamoto and W. H. Miller, "Semiclassical Calculation of Thermal Rate Constants in Full Cartesian Space: The Benchmark Reaction for $D + H_2 \rightarrow DH + H$ ", J. Chem. Phys. **118**, 2135-2152 (2003). LBNL-51587.
2. W. H. Miller, Y. Zhao, M. Ceotto and S. Yang, "Quantum Instanton Approximation for Thermal Rate Constants of Chemical Reactions", J. Chem. Phys. **119**, 1329-1342 (2003). LBNL-52311.
3. C. Venkataraman and W. H. Miller, "The Quantum Instanton (QI) Model for Chemical Reaction Rates: the 'Simplest' QI with One Dividing Surface", J. Phys. Chem. A **108**, 3035-3039 (2004). LBNL-53815.

4. T. Yamamoto and W. H. Miller, "On the Efficient Path Integral Evaluation of Thermal Rate Constants within the Quantum Instanton Approximation", *J. Chem. Phys.* **120**, 3086-3099 (2004). LBNL-53821.
5. Y. Zhao, T. Yamamoto and W. H. Miller, "Path Integral Calculation of Thermal Rate Constants within the Quantum Instanton Approximation: Application to the $\text{H}+\text{CH}_4 \rightarrow \text{H}_2+\text{CH}_3$ Hydrogen Abstraction Reaction in Full Cartesian Space," *J. Chem. Phys.* **120**, 3100-3107 (2004). LBNL-53881.
6. M. Ceotto and W. H. Miller, "Test of the Quantum Instanton Approximation for Thermal Rate Constants for Some Collinear Reactions", *J. Chem. Phys.* **120**, 6356-6362 (2004). LBNL-54170.
7. Y. Li and W. H. Miller, "Different Time Slices for Different Degrees of Freedom in Feynman Path Integration", *Molec. Phys.* **103**, 203-208 (2005). LBNL-56194.
8. T. Yamamoto and W. H. Miller, "Path Integral Evaluation of the Quantum Instanton Rate Constant for Proton Transfer in a Polar Solvent", *J. Chem. Phys.* **122**, 044106.1-13 (2005). LBNL-56319.
9. M. Ceotto, S. Yang and W. H. Miller, "Quantum Reaction Rate from Higher Derivatives of the Thermal Flux-Flux Autocorrelation Function at Time Zero", *J. Chem. Phys.* **122**, 044109.1-7 (2005). LBNL-56546.
10. C. Predescu and W. H. Miller, "Optimal Choice of Dividing Surface for the Computation of Quantum Reaction Rates", *J. Phys. Chem.* (accepted). LBNL-56195.
11. W. H. Miller, "Quantum Dynamics of Complex Molecular Systems", *Proceedings of the National Academy of Sciences* (accepted). LBNL-56664.

GAS-PHASE MOLECULAR DYNAMICS: THEORETICAL STUDIES OF COMBUSTION-RELATED CHEMICAL REACTIONS

James T. Muckerman
Chemistry Department, Brookhaven National Laboratory
Upton, NY 11973-5000
muckerma@bnl.gov

Program Scope

This project explores the energetics, dynamics and kinetics of chemical reactions resulting from molecular collisions in the gas phase. The goal of this work is a fundamental understanding of chemical processes related to combustion. We are interested in the microscopic factors affecting the structure, dynamics and reactivity of short-lived intermediates such as free radicals in gas-phase reactions. There is a very strong coupling between the theoretical and experimental efforts in all of the group's work. From the phenomenon of axis-switching in halocarbenes, dynamical aspects of the rovibronic spectrum of methylene to the spectroscopy of coordinatively unsaturated transition-metal-containing species, the interplay between state of the art theory and experiment has provided deep new insights. The theoretical work in spectroscopy seeks to generate extremely accurate benchmark calculations of the electronic structure of systems at the small end of the size scale of interest for comparison with (and as a guide to) high-resolution experimental studies carried out in this program. There is also a strong focus in the theoretical work on the direct dynamics of the reactions of polyatomic molecules involving species being studied in the experimental part of the program.

Recent Progress

Theoretical study of the CH₃OH potential energy surface and direct dynamics of the O(¹D) + CH₄ reaction

The stationary point geometries and frequencies on the lowest singlet potential energy surface for the CH₃OH system have been calculated using the CASSCF method with an active space consisting of ten electrons and ten orbitals. The energetics were refined using a restricted internally contracted MRCI (RMRCI) in which configurations with more than two electrons in active space orbitals not populated in the principal configuration are excluded from the CAS reference function. These energies were extrapolated to the complete basis set (CBS) limit using the scheme of Halkier *et al.* with two large basis sets: aug-cc-pVDZ and aug-cc-pVTZ. The implications of our calculated results concerning the O(¹D) + CH₄ and OH + CH₃ reactions were explored. In addition, the O(¹D) + CH₄ reaction at a collision energy of 6.8 kcal/mol is investigated using a variant of the "scaling all correlation" (SAC) method of Truhlar *et al.* and the coupled-cluster double excitation (CCD) method in a direct dynamics study with a D95(d,p) basis set. The results show that the O(¹D) + CH₄ → OH + CH₃ reaction occurs both *via* direct and long-lived intermediate mechanisms. The differential cross section for the direct reaction to form OH is forward peaked with a nearly isotropic background. Finally, the branching fractions for OH, H, H₂, and H₂O are predicted to be 0.725:0.186:0.025:0.064.

Exploring the multiple reaction pathways for the H + cyc-C₃H₆ reaction

Reaction pathways for the hydrogen atom plus cyclopropane (cyc-C₃H₆) reaction are studied using an extrapolated coupled-cluster/complete basis set (CBS) method based on the cc-pVDZ, cc-pVTZ and cc-pVQZ basis sets. For this activated reaction, results reveal two reaction mechanisms, a direct H-abstraction and a H-addition/ring-opening. The hydrogen abstraction reaction yields the H₂ and

cyclopropyl (cyc-C₃H₅) radical products. The vibrationally adiabatic ground-state (VAG) barrier height is predicted to be 13.03 kcal/mole. The isomerization barrier height from the product cyclopropyl to allyl radical is 21.98 kcal/mole *via* a cyc-C₃H₅ ring-opening process. In addition, the H-addition and ring-opening mechanism will lead to an n-C₃H₇ radical, which can result in a variety of products such as CH₃ + C₂H₄, H + CH₃CHCH₂ and H₂ + C₃H₅, *etc.* The VAG barrier height of the H-addition reaction is 16.49 kcal/mole, which is slightly higher than that of the direct H-abstraction reaction. Although the H + cyc-C₃H₆ → CH₄ + CH₂CH reaction is exoergic by 11.90 kcal/mol, this reaction is unlikely due to a high barrier of 43.05 kcal/mole along the minimum energy path. These results may explain the mysterious behavior observed by Valentini *et al.* [J. Phys. Chem. A **107**, 8380 (2003)] in the Doppler-resolved REMPI experiment.

Experimental (TOFMS) and theoretical (VARIFLEX and MULTIWELL) studies of the CH₃ + OH reaction

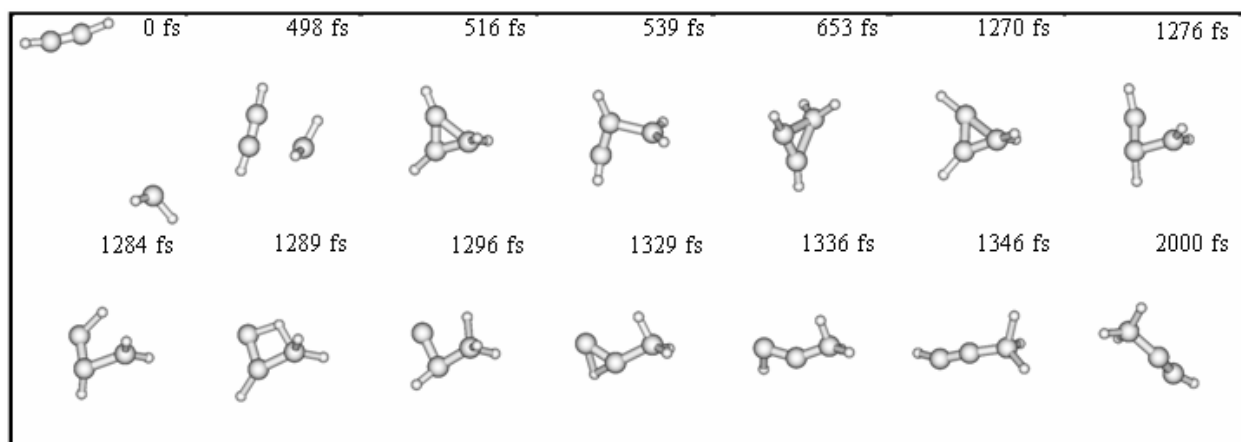
The CH₃ + OH reaction has been investigated both experimentally and theoretically. Isotopic substitution (¹²C → ¹³C and H → D) facilitated a clean distinction between the main product species in the experimental system: formaldehyde isomers, methanol, and ethane. While the analysis of the experimental data at 300 K and 4 Torr remains inconclusive, the observations indicate that ¹CH₂ + H₂O is the main product channel and stabilization to methanol is of minor importance. At 612 K and 8 Torr the data show that three channels (¹CH₂ + H₂O, CH₂O/HCOH + H₂, CH₃OH) are operating with similar yields, with the direct formation of formaldehyde being more efficient than the production of HCOH.

Two different types of RRKM methods (VARIFLEX and MULTIWELL) have been applied to calculate the product distribution of this reaction using different sets of theoretically and experimentally obtained energies of the potential energy surface. In the pressure range of interest (1 to 10 Torr) the yield of the methanol channel is rapidly varying, and, as shown by comparison of the MULTIWELL and VARIFLEX results, is sensitive to the parameters of the RRKM calculation and the implementation of the master equation (ME) solution. In addition, the product yields show a high sensitivity toward the relative position of the transition states in each set.

Despite these sensitivities to unknown parameters, general trends of pressure and temperature dependence of the product distribution can be captured theoretically. At 300 K, qualitative agreement between the present calculations and experimental results was obtained with our *ab initio* energy values leading to ¹CH₂ + H₂O as the dominant products, with methanol being of lesser importance. At 612 K, isomers of formaldehyde, ¹CH₂ + H₂O and methanol are all important channels in the calculated results when the experimental dissociation energies for CH₃ + OH (R1) and ¹CH₂ + H₂O (R2) were chosen. While the yield of isomers of formaldehyde calculated with the experimental dissociation energies for R1 and R2 at 612 K is in excellent agreement with experiment, the calculated yield of formaldehyde *per se* falls well below that observed. It appears that the energy of the transition state to CH₂O would have to be significantly lower than the energy of the entrance channel, CH₃ + OH, or the ¹CH₂ + H₂O product channel, and it is unlikely that errors in our *ab initio* calculations could be large enough to justify such an assertion. Choosing a constant value for <ΔE_{down}> could not explain the curious observation that the methanol yield at pressures below 10 Torr increases with temperature. This strongly suggests that a temperature-dependent energy transfer parameter has to be considered for this reaction.

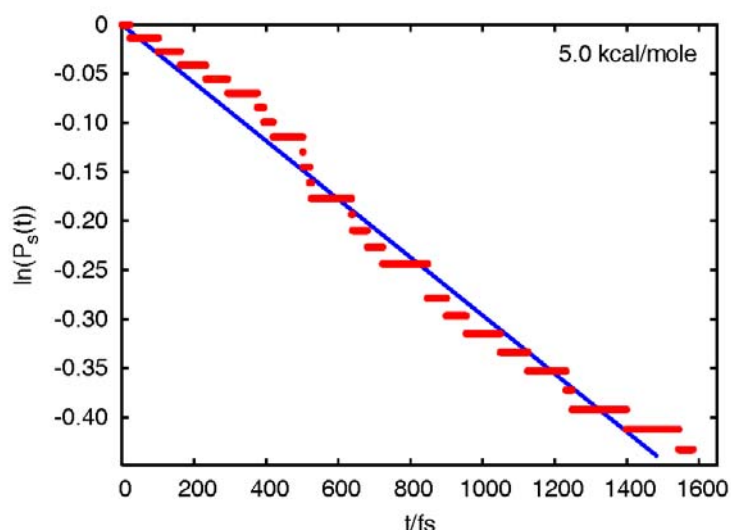
A direct *ab initio* dynamics study of the ¹CH₂ + C₂H₂ reaction

Our *ab initio* direct dynamics studies of radical-radical and chemical activation reactions have been extended to two new systems, namely the ¹CH₂ + C₂H₂ and OH + HOCO reactions. The ¹CH₂ + C₂H₂ reaction is one of important combustion reactions because the product propargyl radical (C₃H₃) is



Snapshots during a typical trajectory for singlet CH₂ reacting with C₂H₂ via an addition/ring-opening mechanism, forming a cyc-propene intermediate which undergoes ring opening, a 1,3 hydrogen shift, and finally a 1,2 hydrogen shift to yield propyne.

believed to be the precursor of soot in hydrocarbon combustion. We have carried out a direct *ab initio* molecular dynamics simulation of the reaction using a dual-level SAC approach. The scaling factor was determined by using accurate extrapolated coupled-cluster/complete basis set (CBS) results. We have also devised a convenient way to monitor the geometry (connectivity) of the system along each trajectory without storing the coordinates for subsequent visualization. We used graph theory to recognize the structure and fragments of the collision system at each time increment, and we stored that information as a single integer. In that way, the reactants, products, and the complex intermediates could be traced as a function of time. In particular, the lifetime (3 ps) of the cyclopropene complex was calculated from the decay of its survival probability using a statistical method. We also were able to determine the branching of the decay of the cyclopropene complex into allene and propyne.



A logarithm plot of the survival probability, $P_s(t)$, of the cyclopropene complex in $^1\text{CH}_2 + \text{C}_2\text{H}_2$ collisions as a function of time at a collision energy of 5.0 kcal/mol. Graph theory was used to calculate the lifetime of the complex in each trajectory.

Future Plans

Energetics and dynamics of the reaction of OH with HOCO

In another application of our *ab initio* direct dynamics approach, in collaboration with J. Francisco (Purdue Univ.), we plan to map out the properties (energies, geometries, vibrational frequencies) of the stationary points on the ground-state singlet potential energy surface for the reaction of OH and HOCO using high-level *ab initio* electronic structure methods. This potential surface includes the product channel $\text{H}_2\text{O} + \text{CO}_2$. Then, in a manner similar to our treatment of the singlet methanol potential surface, we will calibrate the SAC method (probably the SAC/MP2 variant for efficiency in view of the four heavy atoms in the system) to achieve the best fit to the high-level stationary-point calculations. We will then carry out

direct dynamics studies of the reaction to elucidate the reaction pathways. The temperature dependence of the thermal rate constant as well as the reaction mechanism will be the main questions we will address.

Theoretical dynamics of $^1\text{CH}_2/^3\text{CH}_2$ mixed-state collisions with He

High-level *ab initio* calculations of the potential energy surfaces of singlet and triplet methylene and the spin-orbit coupling between them will be carried out, and the rovibrational levels of the coupled potential energy surfaces will be computed. We will then identify various rovibrational states that have mixed singlet and triplet character for a subsequent study of their collision dynamics with a He atom. The objective of this work is to elucidate how a quantum mechanical description of the mixed-state dynamics correlates with the perturbative semiclassical approach involving collisions of unmixed states.

Acknowledgment

This work was performed at Brookhaven National Laboratory under Contract DE-AC02-98CH10886 with the U.S. Department of Energy and supported by its Division of Chemical Sciences, Office of Basic Energy Sciences.

Publications since 2003

- H.-G. Yu and J. T. Muckerman, *Theoretical determination of rovibrational energies and the anomalous isotope effect of the weakly bound cluster HXeOH*. J. Theor. Comput. Chem. **2**, 573 (2003).
- B. Wang, H. Hou, L. Yoder, J. T. Muckerman and C. Fockenberg, *Experimental and theoretical investigations on the methyl-methyl recombination reaction*. J. Phys. Chem. A **107**, 11414 (2003).
- H.-G. Yu and J.T. Muckerman, *MRCI calculations of the lowest potential energy surface for CH_3OH and direct *ab initio* dynamics calculations of the $\text{O}(^1\text{D}) + \text{CH}_4$ and $\text{OH} + \text{CH}_3$ reactions*, J. Phys. Chem. A **108**, 8615 (2004).
- E. Fujita and J. T. Muckerman, *Why is Re-Re bond formation/cleavage in $[\text{Re}(\text{bpy})(\text{CO})_3]_2$ different from that in $[\text{Re}(\text{CO})_5]_2$? Experimental and theoretical studies on the dimmers and fragments*, Inorg. Chem. **43**, 7636 (2004).
- H.-G. Yu and J.T. Muckerman, *Exploring the multiple reaction pathways for the $\text{H} + \text{cyc-C}_3\text{H}_6$ reaction*, J. Phys. Chem. A **108**, 10844 (2004).
- H.-G. Yu and J.T. Muckerman, *Ab initio and direct dynamics studies of the reaction of singlet methylene with acetylene, and the lifetime of the cyclopropene complex*, J. Phys. Chem. A **109**, 1890 (2005).
- C. Fockenberg, R.A. Weston, Jr. and J.T. Muckerman, *Product Study of the Reaction of CH_3 with OH Radicals at Low Pressures and Temperatures*, J. Phys. Chem. B, (in press, 2005).
- S. Chaudhuri and J. T. Muckerman, *First-principles study of Ti-catalyzed hydrogen chemisorption on an Al surface: A critical first step for reversible hydrogen storage in NaAlH_4* , J. Phys. Chem. B, (in press, 2005).
- H.-G. Yu, J.T. Muckerman and J.S. Francisco, *Direct Ab initio Dynamics Study of the $\text{OH} + \text{HOCO}$ Reaction*, J. Phys. Chem. A (submitted, 2005).
- H. Hou and J. T. Muckerman, *Ab initio Studies of the Metcar Building Blocks TiC_2 and MoC_2* . J. Chem. Phys. (submitted, 2005).

Dynamics of Activated Molecules, DE-FG02-03ER15429

Amy S. Mullin, Department of Chemistry & Biochemistry
University of Maryland, College Park, MD, 20742-4454, mullin@bu.edu

Program Scope

The research activities of my group are designed to investigate the collisional behavior of highly excited molecules that play key roles in activated chemical processes and in the chemistry of high temperature environments. We utilize pulsed UV lasers to generate highly excited molecules with well defined amounts of energy between $E=30,000$ to $40,000\text{ cm}^{-1}$, corresponding to vibrational temperatures of 2000-4000 K. We monitor energy loss processes from the activated molecules using transient high resolution infrared absorption spectroscopy of the collision products. By focusing on energy gain in collision partners at short times relative to the time between collisions, we are able to extract information about energy transfer following single encounters of activated molecules, despite the large energy and high state density of the activated molecules. The remarkable resolution of our IR lasers (0.0003 cm^{-1}) allows us to monitor all degrees of freedom in the energy accepting collision partner, thus providing insight into the mechanisms that control collisional relaxation and compete with unimolecular decomposition reactions.

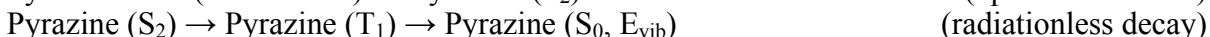
Recent Progress

Much of our research efforts over the past funding cycle have focused on supercollision relaxation wherein large amounts of internal energy are lost from activated molecules in single collisions with small bath molecules. We have used high resolution transient IR probing to measure state resolved energy gain distributions for a number of donor/acceptor pairs. Classical trajectory calculations have also been performed to extend our understanding of how the activated donor molecules influence supercollision energy transfer. We have observed that in the relaxation of highly excited azabenzene molecules with a series of small bath molecules, some collisions lead to very large releases of energy with ΔE as large as $10,000\text{ cm}^{-1}$. While such supercollision events are rare, they play a significant role in pressure dependent reactive environments and provide insight into the properties of molecules with internal energy near the dissociation limit. The signature for supercollision relaxation of highly vibrationally excited molecules is vibration to rotation/translation energy transfer ($V\rightarrow RT$). This type of energy transfer is the source of the high energy tail in the energy transfer distribution function. To measure supercollision energy transfer, we target the appearance of population in high rotational states of bath molecules following pulsed UV excitation of the hot donor molecule. Time resolved population and Doppler-broadened linewidth measurements yield information about the extent of rotational and translational excitation following single collisions between the hot donor and the energy accepting bath molecule. Our efforts to date that have been supported by the Department of Energy have focused on a number of outstanding questions regarding highly excited molecules, which are described below.

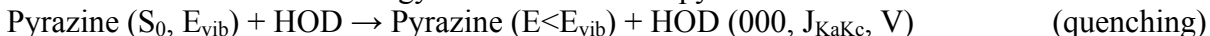
1) Supercollision relaxation of pyrazine (E_{vib}) with deuterated water HOD

One of our research goals is to identify how molecular properties such as shape, mass, polarity, and internal degrees of freedom influence the ability of bath molecules to accept large amounts of energy from activated donor molecules. We have already measured supercollision energy gain in CO_2 , H_2O , and DCI following collisions with hot pyrazine and found that for these three bath species, large ΔE values are observed, but the partitioning of that energy is species-dependent. In recent experiments, we have investigated how deuterated water HOD quenches vibrationally hot pyrazine ($E_{\text{vib}}=38000\text{ cm}^{-1}$) via strong collisions. In these studies, highly vibrationally excited pyrazine molecules are prepared by pulsed 266 nm excitation followed by

radiationless decay to high vibrational levels of the ground electronic state. Radiationless decay to S_0 occurs in ~ 50 ns with near unity quantum yield and leaves pyrazine with $E_{\text{vib}}=37,900 \text{ cm}^{-1}$.



Collisions with HOD remove energy from the activated pyrazine molecules.



The appearance of population in individual quantum states of HOD is monitored by transient IR absorption spectroscopy using a single mode tunable F-center laser and the ν_3 OH stretching transition near 3700 cm^{-1} .



Here, 000 indicates the ground vibrationless state of HOD, J is the angular momentum quantum number, K_a and K_c are projections of the angular momentum along the molecular axes and V is the velocity vector along the IR probe axis. Fig. 1 shows the transient IR absorption of energy gain in HOD ($000, 12_{2,10}$) following collisions with pyrazine(E_{vib}).

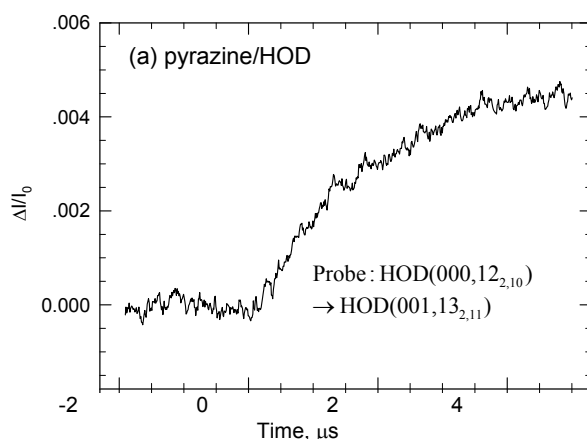


Fig. 1. Transient IR absorption of scattered HOD following collisions with activated pyrazine. The ($000, 12_{2,10}$) state has a rotational energy of 1331.2 cm^{-1} .

Nascent populations and Doppler-broadened linewidths were measured for a number of HOD rotational states with energies between 960 and 1400 cm^{-1} . The distribution of rotational states is characterized by a relatively low temperature of $T_{\text{rot}}=460 \text{ K}$ and the center of mass frame translational energy distributions for individual HOD states are $T_{\text{trans}}\sim 700 \text{ K}$. Taken together with previous results for other bath molecules, our results for energy partitioning in HOD highlight the importance of angular momentum constraints in supercollision relaxation. Angular momentum conservation requires that the combined changes in rotational angular momentum be equal in magnitude to the change in orbital angular momentum. The change in orbital angular momentum is $\Delta L = \mu \Delta v_{\text{rel}} b$, where μ is the reduced mass, Δv_{rel} is the change in relative velocity and b is the impact parameter. A comparison of ΔJ_{bath} with Δv_{rel} is shown in Fig.2 for HOD, H_2O , CO_2 and DCI . We find that the energy partitioning in HOD is consistent with our earlier observation that translational energy changes are larger for bath molecules with larger moments of inertia. Thus, for comparable amounts of energy that are transferred into rotation of the bath, molecules with larger spacing between rotational states have smaller changes in rotational quantum numbers relative to molecules with a denser manifold of rotational states. This in turn results in smaller amounts of translational energy released to the scattered molecules. While our measurements do not provide information about ΔJ_{donor} , other studies indicate that for impulsive collisions ΔJ_{bath} and ΔJ_{donor} add constructively.

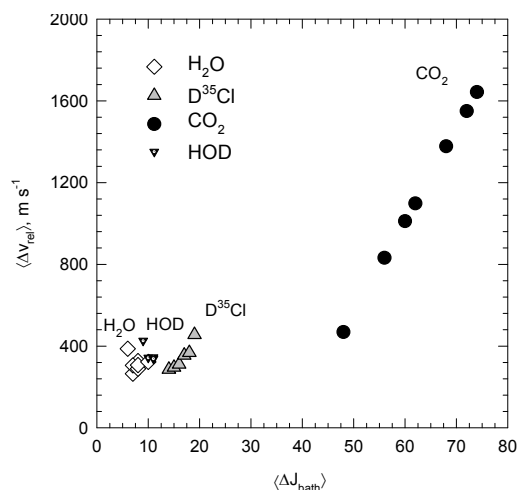


Fig. 2. Changes in relative velocity as a function of changes in bath rotation.

2) Supercollision quenching of substituted pyridines with HOD

Another goal of our studies is to identify how supercollision relaxation is influenced by the identity of the activated molecule. In this funding cycle we have investigated supercollision relaxation for a series of highly excited azabenzene molecules of increasing complexity: pyridine C_5H_5N , picoline (2-methyl pyridine) and lutidine (2,6-dimethyl pyridine). In these studies the donors are prepared with $E_{vib} \sim 38300 \text{ cm}^{-1}$ using 266 nm excitation and quenched in the presence of HOD. While the $V \rightarrow RT$ energy gain pathway is observed for these donor/acceptor pairs, the HOD rotational energy distributions decrease as the donor complexity increases. The translational energy distributions are all near $T_{trans} \sim 700 \text{ K}$ and do not change for the different donor molecules. For these studies, the shape of the high energy component of the energy transfer distribution function for each donor/HOD pairs is well described a single exponential decay with $P(\Delta E) = \alpha_{obs} \exp(-\Delta E/kT_{rot})$. We find that the curvature in the high energy tail correlates extremely well with the energy dependence of the state density $\rho(E-\Delta E)$ for the highly excited donor molecule. This correlation is illustrated in Fig. 3 for HOD and H_2O . We have observed a similar correlation for relaxation with CO_2 . Such a correlation has important predictive capabilities for supercollision relaxation.

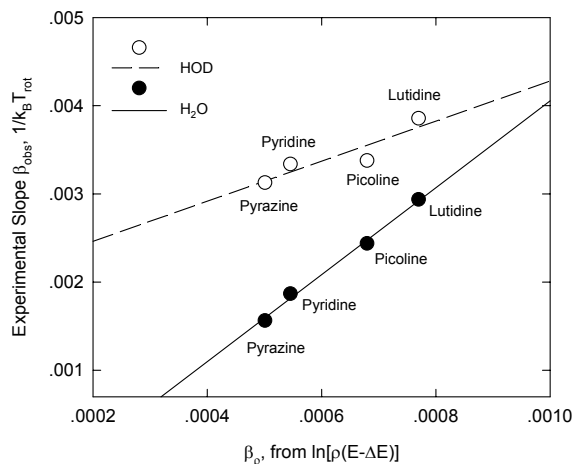


Fig. 3. Correlation of supercollision $P(\Delta E)$ distribution function with changes in vibrational state density for activated donor molecule.

3) Supercollision relaxation of picoline isomers with CO₂

In related studies, we have further explored the role of state density in supercollision relaxation by measuring the supercollision relaxation profiles of the picoline isomers (2-methyl pyridine, 3-methyl pyridine and 4-methyl pyridine) with CO₂. In these studies, 266 nm light is used to prepare the activated picoline isomers and energy gain in CO₂ is detected by transient IR absorption using a single mode diode laser. Similarities in vibrational frequencies lead to nearly identical state density functions $\rho(E-\Delta E)$ while moving the methyl group in picoline changes the dipole moment considerably. These studies find that the rotational and translational energy gain profiles for CO₂ are essentially the same for the three different donor species. Absolute rate constant measurements also show little difference among the three donors. These results are further evidence that state density is a controlling factor in the shape of the energy transfer distribution function and that for comparable donor/acceptor pairs, polarity has little effect.

4) Modeling supercollision relaxation with classical trajectory calculations

We have performed classical trajectory calculations, in collaboration with Prof. David Coker, a theoretical chemist at Boston University, to gain further insight in the dynamics of supercollision relaxation. Our most extensive calculations on the pyrazine(E_{vib})/CO₂ system confirm experimental observations that the largest ΔE values result from an impulsive mechanism for energy transfer. We have successfully reproduced the qualitative features of energy partitioning in the scattered CO₂ molecules. In some cases the calculations indicate that the largest energy transfer events result from multiple encounters of the donor-acceptor pair, as illustrated in Fig. 4 where changes in the intermolecular energy are shown for two different collisions. Both trajectories have multiple points of contact between donor and acceptor, but supercollision energy exchange results here from highly impulsive encounters. Donor rotation is nearly always involved in supercollision exchange. We have also used trajectory calculations to explore how mass effects and moments of inertia influence the energy partitioning in the scattered molecules.

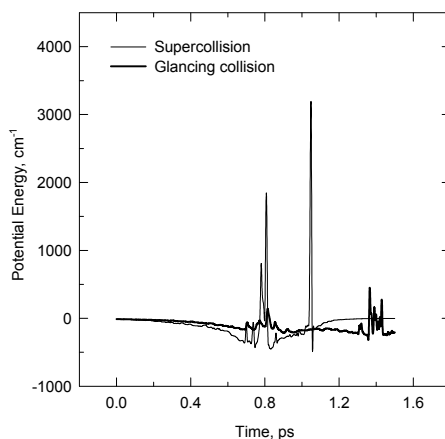


Fig. 4. Intermolecular potential energy as function of time for two trajectories.

Future Directions

In the upcoming funding cycle, we plan to further investigate angular momentum and state density effects in supercollisions. We also plan to investigate the role of polarity on long-range vibrational energy transfer from vibrationally hot molecules and the role of electronic vs vibrational energy in supercollision relaxation.

Publications

Two manuscripts have been submitted for publication and four more are in preparation.

Reacting Flow Modeling with Detailed Chemical Kinetics

Habib N. Najm

Sandia National Laboratories
7011 East Ave, MS 9051, Livermore, CA 94550
hnajm@sandia.gov

1 Program Scope

The purpose of this research program is to understand the transient behavior of flames in reacting flow, thereby improving the state of the art in predictive modeling of combustion. The work involves: (1) Using advanced computations to investigate the structure and dynamical behaviour of flames in unsteady vortical laboratory-scale flows; (2) Conducting detailed studies with matched experimental-numerical comparisons to improve understanding of transient flame-flow interaction; (3) Developing advanced techniques for the analysis of, and extraction of information from, multidimensional reacting flow computations; (4) Developing improved numerical methods for discretizing large scale reacting flow systems of equations with detailed kinetics and transport; and (5) Developing efficient massively parallel programming approaches for computing large scale reacting flow with detailed kinetics.

2 Recent Progress

2.1 Flame Computations with CSP-Reduced Chemistry

We used Computational Singular Perturbation (CSP) theory for simplification of chemical mechanisms. We developed a CSP-based kinetic mechanism simplification algorithm employing a CSP database, constructed by analyzing detailed mechanism solutions, in order to discard reactions that are deemed unimportant for a user-specified set of species. The degree of simplification is also user-specified through a threshold tolerance value on CSP Importance indices. Comprehensive simplified mechanisms are achievable by cross-referencing several CSP databases. The simplified mechanisms were tested for three prototypical methane combustion problems: spatially homogeneous constant-pressure autoignition, premixed and counterflow diffusion flames. Model reduction is achieved when species, and the reactions involving them, are eliminated from the detailed mechanism. A CPU run-time analysis revealed a maximum speed-up factor of ~ 3 before errors, w.r.t. the detailed mechanism, become unacceptable. Computations of premixed flame-vortex interactions with CSP-reduced methane mechanisms over a range of stoichiometry are in progress. This work is in collaboration with M.Valorani, Univ. of Rome, and D.Goussis, Greece.

2.2 Flame Computations with In-Situ Adaptive Tabulation (ISAT)

We investigated the use of ISAT in low Mach number premixed methane-air reacting flow computations, with detailed chemistry and temperature-dependent transport properties, to examine resulting accuracy and computational speedup. With suitable modifications, ISAT was included in the original operator-split time integration scheme. The construction was initially applied to one-dimensional laminar premixed methane-air flames. We examined the impact of the ISAT error tolerance on solution accuracy, and demonstrated solution error control by changing the ISAT tolerance. We found that with GRIMech3.0, after an initial ISAT table build-up, the use of ISAT speeds-up the reaction sub-steps of the computations by roughly a factor of 13 and the overall scheme achieves a speed-up of approximately 7.5. We also demonstrated the use of ISAT in the context of the simulation of a two-dimensional unsteady reacting flow with detailed chemistry: a premixed methane-air flame-vortex interaction. ISAT performance was examined and compared to that of the original DVODE-based scheme. Here it was found that ISAT provides a reaction sub-step speed-up of approximately 2–4 and an overall code speed-up of 1.75–3. This work is in collaboration with S.Pope, Cornell.

2.3 Uncertainty Quantification (UQ) in Reacting Flow

We have demonstrated the use of multiwavelets (MW) for UQ in isothermal ignition of chemical systems. The construction uses an adaptive domain decomposition approach, with a local MW construction in each local do-

main. Instabilities encountered with the hitherto-used global polynomial chaos construction are avoided, allowing computations with realistic uncertainties in chemical rate constants. Work is in progress on the extension of the construction to ignition with heat release, and one-dimensional flames. This work is in collaboration with O.Le Maître, Univ. d'Evry, France.

2.4 Bayesian Methods for Stochastic Inverse Problems

We have implemented Bayesian statistics for the solution of stochastic inverse problems. Such problems arise naturally in the context of model inference from observations in the presence of noise and uncertainty. The Bayesian approach enables model construction with specified stochastic uncertainties in inferred model parameters. We demonstrated the construction in the context of source inversion from observations of a diffusive field quantity. We also identified means of using Polynomial Chaos constructions to achieve potentially dramatic acceleration of the evaluation of Bayes integrals, a key computational bottleneck in Bayesian inversion. The implementation and demonstration of this PC-Bayes construction is work in progress.

2.5 High-Order Structured Adaptive Mesh Refinement (SAMR)

We have demonstrated distributed-parallel high-order SAMR computations of scalar field transport and chemistry in multiple dimensions, using the Common Component Architecture framework. The construction uses requisite high order interpolant and filtering strategies. In pursuit of load balanced scalable parallel computations, we opted to use a hybrid SAMR/fixed-mesh construction, where scalar fields are computed on the adaptive mesh while the velocity field is computed on the fixed mesh. We have demonstrated a second-order (in-time) operator-split coupled construction that brings the two mesh solutions together.

2.6 CSP/PRISM Adaptive Chemistry

We developed an adaptive chemistry model based on PRISM-tabulation of CSP basis vectors and a slow-manifold-projection stabilized explicit scheme. We evaluated this construction using hydrogen and n-heptane fuels. The numerical experiments revealed the following: (1) The CSP-slow-manifold projector allows the use of time step sizes equal to that of the fastest active modes in all explicit schemes tested. (2) The use of an approximated CSP-slow-manifold (such as a linear-interpolation based tabulation) has a negligible effect on the accuracy of the system but can improve computational efficiency; (3) The performance of the new scheme using a fourth-order explicit integrator and tabulation of the CSP-slow-manifold are very encouraging; (4) The performance gain with tabulation of the CSP-manifold is expected to be more significant with larger kinetic mechanisms; (5) Being an explicit algorithm, there is an additional benefit in the ease of load balancing in a distributed memory computing environment. We found that the technique of tabulating the CSP-slow-manifold holds much promise for the construction of an adaptive chemistry model in a multi-dimensional operator-split reacting flow simulation. We also demonstrated the potential of using the CSP-slow-manifold projection to avoid the operator-split construction all together, since the same explicit time integration strategy can be effectively used for both transport and CSP-slow-manifold-projected chemical source terms. This work is in collaboration with M.Valorani, Univ. of Rome, D. Goussis, Greece, and M.Frenklach, UC Berkeley.

2.7 Premixed Flame Eigenmode Structure

We performed both homogeneous and 1D reacting flow computations with CSP analysis to investigate the classical theories of chain branching and thermal-run-away that lead to the rapid oxidation of fuels. Mathematically, both theories infer the existence of eigenvalues with positive real parts i.e. explosive modes. We found in studies of homogeneous hydrogen-air and the methane-air mixtures that, when ignition is initiated by a sufficiently high initial temperature, the transient response of the system exhibits two stages. The first is characterized by the existence of explosive modes. The ensuing second stage consists of fast exponential decay modes that bring the system to its equilibrium point. On the other hand, we demonstrated with two 1D-flame examples (hydrogen-air and methane-air) that the existence of explosive modes is not a necessary condition for the existence of a premixed flame. Homogeneous ignition calculations for mixtures with an initial concentration of radical species suggest that the diffusive transport of radical species is probably responsible for the lack of explosive modes in premixed flames.

3 Future Plans

3.1 Flame Computations with CSP-Reduced Chemistry

We will investigate transient flame response in premixed flame-vortex reacting flow, with a range of strain-rate and curvature disturbances, using different CSP-reduced chemical mechanisms. This will be done under a range of stoichiometry conditions, and a variety of hydrocarbon fuels, e.g. methane, propane, n-heptane. The goal is to evaluate the accuracy and efficiency of different degrees of CSP-reduced chemical models, as compared to detailed mechanisms, under multidimensional flow conditions including transient strain-rate and curvature disturbances. Covering a wide range of stoichiometry will serve to evaluate the comprehensiveness of reduced models and their robustness over ranges of operating conditions.

3.2 Uncertainty Quantification (UQ) in Reacting Flow

We plan to apply the multiwavelet (MW) UQ construction in the context of homogeneous ignition with heat release. The local nature of the MW construction is crucial for enabling robust implementation of the pseudo-spectral intrusive UQ formulation for exponential Arrhenius rate terms with temperature uncertainties. With the successful extension of the methodology to this problem, a clear path will be open to application of the intrusive MW approach in one-dimensional premixed flame UQ computations. We also plan to investigate global Polynomial Chaos UQ constructions using higher-numbers of degrees of freedom, in order to improve the utility of these constructions for representing general stochastic quantities, and for UQ in PDE systems with strong nonlinearities.

3.3 Bayesian Methods for Stochastic Inverse Problems

We are focusing on Bayesian methods in order to provide means for rational construction of chemical models, with embedded stochastic specification of parametric uncertainties, given sparse noisy experimental data. The fundamental bottleneck in such Bayesian inference computations is the evaluation of integrals over the model space. We plan to implement intrusive Polynomial Chaos UQ techniques to accelerate the forward-problem evaluations, which are the dominant cost in the computation of Bayes integrals. These techniques enable the use of a single direct pseudo-spectral UQ solution of the forward problem to provide a complete parameterization of the data in terms of the model parameters. Substituting this parameterization in place of the model solution for each sample point in the Bayes integral computations will provide the sought-after computational speed-up.

3.4 High-Order Structured Adaptive Mesh Refinement (SAMR)

We are in the process of coupling time integration of high-order SAMR scalar field solutions with velocity field solutions on an underlying fixed mesh. This will enable the integration of SAMR and fixed-mesh computations of scalar and momentum conservation equations respectively. We will be building the fixed mesh low Mach number momentum solver to fit in this construction. The resulting scheme should have optimal parallel scalability, as long as suitable load balancing is pursued for the chemical source terms. We will investigate different options for load balancing the chemistry integration cost when the chemical source terms are integrated implicitly. This chemistry load balancing will not be necessary when the chemical source terms are integrated explicitly, using the CSP/PRISM adaptive chemistry approach.

3.5 CSP/PRISM Adaptive Chemistry

We will develop a general implementation of CSP and PRISM-tabulation for enabling reacting flow computations with adaptive chemical reduction. We have had a positive experience with the coupling of CSP and tabulation using PRISM using various model problems. We will now extend this construction to general kinetic mechanisms of chemical systems. This will involve development of general methodologies for construction of response-surface representations of CSP vectors in a given hypercube in the chemical phase space, and suitable table search and retrieval algorithms. The overall construction will be demonstrated and evaluated in comparison with direct computations with detailed chemical models.

4 DOE/BES-Supported Published/In-Press Publications [2003-2005]

- [1] Valorani, M., Goussis, D.A., Creta, F., and Najm, H.N., Higher Order Corrections in the Approximation of Low Dimensional Manifolds and the Construction of Simplified Problems with the CSP Method, *J. Comput. Phys.* (2005) in press.
- [2] Lefantzi, S., Ray, J., Kennedy, C.A., and Najm, H.N., A Component-based Toolkit for Reacting Flows with Higher Order Spatial Discretizations on Structured Adaptively Refined Meshes, *Progress in Computational Fluid Mechanics* (2005) in press.
- [3] Goussis, D.A., Valorani, M., Creta, F., and Najm, H.N., Reactive and Reactive/Diffusive Time Scales in Stiff Reaction-Diffusion Systems, *Progress in Computational Fluid Mechanics* (2005) in press.
- [4] Najm, H.N., and Knio, O.M., Modeling Low Mach Number Reacting Flow with Detailed Chemistry and Transport, *J. Sci. Comp.* (2005) in press.
- [5] Reagan, M.T., Najm, H.N., Pébay, P.P., Knio, O.M., and Ghanem, R.G., Quantifying Uncertainty in Chemical Systems Modeling, *Int. J. Chem. Kin.* (2005) in press.
- [6] Reagan, M.T., Najm, H.N., Debusschere, B.J., Maître, O.P. Le, Knio, O.M., and Ghanem, R.G., Spectral Stochastic Uncertainty Quantification in Chemical Systems, *Combustion Theory & Modeling*, 8:607–632 (2004).
- [7] Pébay, P.P., Najm, H.N., and Pousin, J., A Non-Split Projection Strategy for Low Mach Number Reacting Flows, *Int. J. Multiscale Computational Eng.*, 2(3):445–460 (2004).
- [8] Debusschere, B.J., Najm, H.N., Pébay, P.P., Knio, O.M., Ghanem, R.G., and Le Maître, O.P., Numerical Challenges in the Use of Polynomial Chaos Representations for Stochastic Processes, *SIAM Journal of Scientific Computing*, 26(2):698–719 (2004).
- [9] Le Maître, O.P., Ghanem, R.G., Knio, O.M., and Najm, H.N., Uncertainty Propagation using Wiener-Haar Expansions, *Journal of Computational Physics*, 197(1):28–57 (2004).
- [10] Le Maître, O.P., Reagan, M.T., Debusschere, B.D., Najm, H.N., Ghanem, R.G., and Knio, O.M., Natural Convection in a Closed Cavity under Stochastic, Non-Boussinesq conditions, *SIAM J. Scientific Computing*, 26(2):375–394 (2004).
- [11] Le Maître, O.P., Najm, H.N., Ghanem, R.G., and Knio, O.M., Multi-Resolution Analysis of Wiener-type Uncertainty Propagation Schemes, *J. Comp. Phys.*, 197:502–531 (2004).
- [12] Matta, A., Knio, O.M., Ghanem, R.G., Chen, C.-H., Santiago, J.G., Debusschere, B., and Najm, H.N., Computational Study of Band Crossing Reactions, *J. MEMS*, 13(2):310–322 (2004).
- [13] Reagan, M.T., Najm, H.N., Ghanem, R.G., and Knio, O.M., Uncertainty Quantification in Reacting Flow Simulations Through Non-Intrusive Spectral Projection, *Combustion and Flame*, 132:545–555 (2003).
- [14] Reagan, M.T., Najm, H.N., Ghanem, R.G., and Knio, O.M., Analysis of Parametric Uncertainty Propagation in Detailed Combustion Chemistry, in *Computational Fluid and Solid Mechanics* (K. Bathe, Ed.), volume 2, Cambridge, MA, (2003), Elsevier Science, , pp. 1501–1505.
- [15] Valorani, M., Najm, H.N., and Goussis, D., CSP Analysis of a Transient Flame-Vortex Interaction: Time Scales and Manifolds, *Combustion and Flame*, 134(1-2):35–53 (2003).
- [16] Debusschere, B.J., Najm, H.N., Matta, A., Knio, O.M., Ghanem, R.G., and Le Maître, O.P., Protein Labeling Reactions in Electrochemical Microchannel Flow: Numerical Simulation and Uncertainty Propagation, *Physics of Fluids*, 15(8):2238–2250 (2003).
- [17] Debusschere, B.J., Najm, H.N., Matta, A., Knio, O.M., Ghanem, R.G., and Le Maître, O.P., Protein Labeling Reactions in Electrochemical Microchannel Flow: Numerical Simulation and Uncertainty Propagation, *Virtual Journal of Biological Physics Research*, 6(1) (2003) <http://ojps.aip.org/dbt/dbt.jsp?KEY=VIRT02&Volume=6&Issue=1#MAJOR16>.
- [18] Goussis, D.A., Valorani, M., Creta, F., and Najm, H., Inertial Manifolds with CSP, in *Computational Fluid and Solid Mechanics 2003* (K. Bathe, Ed.), volume 2, Cambridge, MA, (2003), Elsevier Science, , pp. 1951–1954.
- [19] Le Maître, O.P., Knio, O.M., Debusschere, B.J., Najm, H.N., and Ghanem, R.G., A Multigrid Solver for Two-Dimensional Stochastic Diffusion Equations, *Comp. Meth. App. Mech. and Eng.*, 192:4723–4744 (2003).
- [20] Marzouk, Y.M., Ghoniem, A.F., and Najm, H.N., Toward a Flame Embedding Model for Turbulent Combustion Simulation, *AIAA J.*, 41(4):641–652 (2003).

Photodissociation and Photoionization of Radicals and Closed-shell Hydrocarbons

Daniel Neumark
Chemical Sciences Division
Lawrence Berkeley National Laboratory
Berkeley, CA 94720

This research program is aimed at elucidating the photodissociation dynamics and bimolecular chemistry of free radicals and hydrocarbons, with particular emphasis on species that play a role in combustion chemistry. Our experiments yield primary chemistry and photochemistry, bond dissociation energies, heats of formation, photoionization cross sections, and excited state dynamics. This fundamental information is vital for the development of accurate models of reaction mechanisms in combustion

Although much time and effort has been invested in modeling combustion chemistry, the accuracy of these models depends on the primary chemistry of the reactions in the models and the thermochemistry of the species involved in these reactions. Our program is focused on fundamental studies of species and reactions relevant to combustion chemistry. We have developed a state-of-the-art fast beam dissociation instrument for studying the photodissociation dynamics of free radicals and negative ions. Recent installation of a photofragment coincident imaging detection system enables the study of three-body photodissociation events. A crossed molecular/laser beam instrument is used to investigate the primary chemistry and photochemistry of both closed-shell hydrocarbons and hydrocarbon radicals, and these measurements. A similar instrument (Endstation 1) on the Chemical Dynamics Beamline at the Advanced Light Source, in which scattered products are ionized with tunable synchrotron radiation, is used to look at hydrocarbon photodissociation in more detail and to measure absolute photoionization cross sections for free radicals.

Motivated by our previous studies of the vinoxy radical, the photodissociation spectroscopy and dynamics of CH_2CHO resulting from excitation of the $\tilde{B}^2A'' \leftarrow \tilde{X}^2A''$ transition were investigated using fast beam photofragment translational spectroscopy. The photofragment yield spectrum revealed vibrationally resolved structure between 29 870 cm^{-1} and 38 800 cm^{-1} , extending $\sim 6000 \text{ cm}^{-1}$ higher in energy than previously reported in a laser-induced fluorescence excitation spectrum. At all photon energies investigated, only the $\text{CH}_2\text{F} + \text{CO}$ and $\text{HCCO} + \text{HF}$ fragment channels are observed. Both product channels yield photofragment translational energy distributions that are characteristic of a decay mechanism with a barrier to dissociation. We have also re-investigated the photodissociation of the ethoxy radical at excitation energies from 5-6 eV, finding the primary dissociation channels to be $\text{OH} + \text{C}_2\text{H}_4$, $\text{CH}_3 + \text{CH}_2\text{O}$, and $\text{H} + \text{CH}_3\text{CHO}$. Experiments with the mixed isotopomer, $\text{CH}_3\text{CD}_2\text{O}$, show that there is no isotopic scrambling and that the hydrogen atom in the OH channel comes from the CH_3 group.

We are also using the new capabilities of the fast beam instrument to investigate three-body dissociation, a phenomenon much less well understood than two-body dissociation. The competition between two-body and three-body decay of I_3^- were studied from 390-290 nm (3.18-4.28 eV). At photon energies ≤ 3.87 eV, two-body dissociation that generates $\Gamma + I_2$ ($A^3\Pi_{1u}$) and vibrationally excited I_2^- ($X^2\Sigma_u^+$) + I ($^2P_{3/2}$) is observed, while at energies ≥ 3.87 eV, I^* ($^2P_{1/2}$) + I_2^- ($X^2\Sigma_u^+$) is the primary two-body dissociation channel. Three-body dissociation yielding $\Gamma + 2I$ ($^2P_{3/2}$) photofragments is seen throughout the energy range probed; this is the dominant channel at all but the lowest photon energy. Analysis of the three-body dissociation events indicates that this channel results primarily from a synchronous concerted decay mechanism.

The dissociation dynamics of allene, propyne, and propyne- d_3 at 193 nm were investigated with photofragment translational spectroscopy. Products were either photoionized using tunable VUV synchrotron radiation or ionized with electron impact. Product time-of-flight data were obtained to determine center-of-mass translational energy ($P(E_T)$) distributions, and photoionization efficiency (PIE) curves were measured for the hydrocarbon products. The two major product channels evident from this study are atomic and molecular hydrogen loss, with a H:H₂ branching ratio of 90:10, regardless of precursor. The $P(E_T)$ distribution for each channel is also largely independent of precursor. Both channels appear to occur following internal conversion to the ground electronic state. The propyne- d_3 results show that there is extensive isotopic scrambling prior to H(D) atom loss, and that the H:D product ratio is approximately unity. The PIE curves for H(D) atom loss from allene, propyne, and propyne- d_3 indicate that the dominant corresponding C_3H_3 product is the propargyl radical in all cases. There is some evidence from the PIE curves that the dominant C_3H_2 products from allene and propyne are propadienylidene ($H_2CCC:$) and propargylene ($HCCCH$), respectively.

Photoionization cross sections were measured for the C_6H_5 radical through photodissociation of C_6H_5Cl at 248 and 193 nm followed by detection via photoionization of the momentum-matched Cl and C_6H_5 fragments. Studies at the two wavelengths were performed in order to test the effect of internal excitation of the radical on the measured cross sections. These effects were found to lie within the error bars of the experiment ($\sim 25\%$). Measurements of this type are highly complementary to experiments at the Chemical Dynamics Beamline in which photoionization is used to investigate flame chemistry, because photoionization cross sections are needed to infer radical concentrations from ionization signals.

In future experiments, radical photoionization cross section measurements on Endstation 1 will continue, with particular emphasis on measuring cross sections for CH_3 from the photodissociation at 193 nm of CH_3Cl . In these experiments, tunable VUV synchrotron radiation is used to photoionize both photofragments, and if the photoionization cross section of one is known, the cross section for the other can be determined by momentum-matching considerations. Once the CH_3 cross section is determined, we plan to measure the HCO cross section via photodissociation of CH_3CHO at 308 nm.

Fast beam photodissociation measurements will focus on radicals such as HCNN which undergo two-body decay; results for this species will be of interest in light of past work in our group on HNCN photodissociation. We will also investigate more model systems that undergo three-body dissociation, as this phenomenon is not nearly as well understood as two-body dissociation. The $I_2 \cdot Ar$ van der Waals complex, which we can generate in our instrument from $I_2^- \cdot Ar$, is a particularly attractive target in which the competition between two-body ($I_2 + Ar$) and three-body dissociation can be determined.

Finally, radical photodissociation experiments will be carried out on our molecular beam photofragment translational spectroscopy instrument using electron impact ionization of the scattered products. The radicals are generated by photolysis of suitable precursors. This experiment is particularly sensitive to photodissociation channels in which the mass ratio between fragments is large, and as such will complement the fast beam instrument.

Publications:

J. C. Robinson, S. A. Harris, W. Sun, D. M. Neumark, "Photofragment translational spectroscopy of 1,3-butadiene and 1,3-butadiene-1,1,4,4- d_4 at 193nm," *Journal of American Chemical Society* 124, 10211, (2002).

A. A. Hoops, J. R. Gascooke, A. E. Faulhaber, K. E. Kautzman, and D. M. Neumark, "Fast beam studies of I_2^- and $I_2^- \cdot Ar$ photodissociation," *Chem. Phys. Lett.* 374, 235 (2003).

J. C. Robinson, N. E. Sveum, and D. M. Neumark "Determination of absolute photoionization cross sections for vinyl and propargyl radicals," *J. Chem. Phys.* 119, 5311 (2003).

J. C. Robinson, N. E. Sveum, and D. M. Neumark, "Determination of absolute photoionization cross sections for isomers of C_3H_3 : Allyl and 2-propenyl radicals," *Chem Phys Lett.* 383, 601 (2004).

A. A. Hoops, J. R. Gascooke, A. E. Faulhaber, K. E. Kautzman, and D. M. Neumark, "Two- and three-body photodissociation of gas phase I_3^- ," *J. Chem Phys.* 120, 7901 (2004).

A. A. Hoops, J. R. Gascooke, K. E. Kautzman, and D. M. Neumark, "Photodissociation spectroscopy and dynamics of the CH_2CFO radical," *J. Chem. Phys.* 120, 8494 (2004).

J. C. Robinson, N. E. Sveum, S. J. Goncher and D. M. Neumark, "Photofragment translational spectroscopy of allene, propyne, and propyne- d_3 at 193 nm" (accepted to *Molecular Physics*).

Determination of Accurate Energetic Database for Combustion Chemistry by High-Resolution Photoionization and Photoelectron Methods

C. Y. Ng

Department of Chemistry, University of California, Davis
One Shields Avenue, Davis, California 95616
E-mail Address: cyng@chem.ucdavis.edu

Program Scope:

The main goal of this project is to obtain accurate thermochemical data, such as ionization energies (IEs), dissociative photoionization thresholds, bond dissociation energies, and 0 K heats of formation (ΔH°_{f0} 's) for small and medium sizes molecular species and their ions of relevance to combustion chemistry. Accurate thermochemical data determined by high-resolution photoionization and photoelectron studies for selected polyatomic neutrals and their ions are also useful for benchmarking the next generation of *ab initio* quantum computational procedures.

Recent Progress:

1 X. M. Qian, K. C. Lau, and C.Y. Ng, "A High-Resolution Pulsed Field Ionization-Photoelectron-Photoion Coincidence Study of Vinyl Bromide", *J. Chem. Phys.* **120**, 11031-11041 (2004).

By employing the high-resolution pulsed field ionization-photoelectron (PFI-PE)-photoion coincidence method, we have examined the unimolecular dissociation reaction of energy-selected $C_2H_3Br^+$ to form $C_2H_3^+ + Br$ near its threshold. The analysis of the breakdown curves for $C_2H_3Br^+$ and $C_2H_3^+$ yields a value of 11.9010 ± 0.0015 eV for the 0 K dissociative photoionization threshold or appearance energy (AE) for $C_2H_3^+$ from C_2H_3Br . This $AE(C_2H_3^+)$ value, together with the IE for C_2H_3Br (9.8200 ± 0.0015 eV) obtained by PFI-PE and threshold photoelectron (TPE) measurements, has allowed the determination of the 0 K dissociation energy (D_0) for the $C_2H_3^+-Br$ bond to be 2.081 ± 0.002 eV. The 0 K $AE(C_2H_3^+)$ from C_2H_3Br obtained in this study corresponds to $\Delta H^\circ_{f0}(C_2H_3^+) = 1123.7 \pm 1.9$ kJ/mol. Combining the latter value and the known $\Delta H^\circ_{f0}(C_2H_3) = 306.7 \pm 2.1$ kJ/mol, we calculated a value of 8.468 ± 0.029 eV for the $IE(C_2H_3)$, which is in accord with the result obtained in the previous photoionization efficiency (PIE) study. We have also carried out high-level *ab initio* calculations for the $IE(C_2H_3)$ at the Gaussian-3 and the CCSD(T, full)/CBS level of theory. The CCSD(T, full)/CBS prediction of 8.487 eV for the $IE(C_2H_3 \rightarrow \text{bridged-}C_2H_3^+)$ is in good agreement with the $IE(C_2H_3)$ value derived in the present experiment. Combining the 0 K $AE(C_2H_3^+) = 11.9010 \pm 0.0015$ eV and the $IE(C_2H_3) = 8.468 \pm 0.029$ eV yields the value of 3.433 ± 0.029 eV for $D_0(C_2H_3-Br)$. We have also recorded the TPE spectrum of C_2H_3Br in the energy range of 9.80–12.20 eV. Members ($n=5-14$) of four autoionizing Rydberg series converging to the $C_2H_3Br^+(\tilde{A}^2A')$ state are observed in the TPE spectrum. The analysis of the converging limit of these Rydberg series and the vibrational TPE bands for $C_2H_3Br^+(\tilde{A}^2A')$ has provided more precise values for the ν_6^+ (1217 ± 10 cm^{-1}) and ν_8^+ (478 ± 8 cm^{-1}) modes and the IE (10.9156 ± 0.0010 eV) for the formation of $C_2H_3Br^+(\tilde{A}^2A')$ from C_2H_3Br .

2. H. K. Woo, P. Wang, K.-C. Lau, X. Xing, and C. Y. Ng, "VUV pulsed field ionization-photoelectron and VUV-IR-photo-induced Rydberg study of *trans*-ClCH=CHCl", *J. Phys. Chem. A*, **108**, 9637 (2004).

The VUV-PFI-PE spectrum for *trans*-dichloroethene (*trans*-ClCH=CHCl) has been measured in the energy range of 77,600 – 79,200 cm^{-1} . On the basis of the spectral simulation of the origin VUV-PFI-PE vibrational band, we have determined the $IE(\textit{trans}\text{-ClCH=CHCl})$ to be $77,678.4 \pm 2.0$ cm^{-1} (9.63097 ± 0.00025 eV). The vibrational bands resolved in the VUV-PFI-PE spectrum of *trans*-ClCH=CHCl are

assigned based on *ab initio* vibrational frequencies and calculated Franck-Condon factors for the ionization transitions, yielding eight vibrational frequencies $\nu_1^+ = 163 \text{ cm}^{-1}$, $\nu_3^+ = 367 \text{ cm}^{-1}$, $\nu_4^+ = 871 \text{ cm}^{-1}$, $\nu_5^+ = 915 \text{ cm}^{-1}$, $\nu_6^+ = 944 \text{ cm}^{-1}$, $\nu_8^+ = 1235 \text{ cm}^{-1}$, $\nu_9^+ = 1258 \text{ cm}^{-1}$, $\nu_{10}^+ = 1452 \text{ cm}^{-1}$. The distinct feature of the VUV-PFI-PE spectrum is the strong vibrational progression of the ν_3^+ (C-Cl stretching) mode of *trans*-ClCH=CHCl⁺, which is consistent with the theoretical geometry calculation, predicting a significant change in the C-Cl bond distance upon photoionization of *trans*-ClCH=CHCl. We have also determined the frequency (3068 cm⁻¹) for the ν_{11}^+ (C-H stretching) vibrational mode of *trans*-ClCH=CHCl⁺ by employing the VUV-IR-photo-induced Rydberg ionization (VUV-IR-PIRI) method. The VUV-IR-PIRI spectra for *trans*-ClCH=CHCl prepared in the effective principal quantum numbers, $n^*=14$ and 36, are found to be identical, supporting the previous conclusion that the Rydberg electron behaves as a spectator, i.e., the Rydberg electron orbital is conserved during the IR excitation of the ion core.

3. H. K. Woo, K.-C. Lau, and C. Y. Ng, "Vibrational spectroscopy of trichloroethene cation by vacuum ultraviolet pulsed field ionization-photoelectron method", *Chinese J. Chem. Phys.*(invited article) **17**, 292 (2004).

The VUV-PFI-PE spectrum for trichloroethene (ClCH=CCl₂) has been measured in the energy range of 76 400 – 79 650 cm⁻¹. The vibrational bands resolved in the VUV-PFI-PE spectrum are assigned based on *ab initio* vibrational frequencies and calculated Franck-Condon factors for the ionization transitions, yielding eleven vibrational frequencies for ClCH=CCl₂⁺: $\nu_1^+ = 148 \text{ cm}^{-1}$, $\nu_2^+ = 180 \text{ cm}^{-1}$, $\nu_3^+ = 286 \text{ cm}^{-1}$, $\nu_4^+ = 402 \text{ cm}^{-1}$, $\nu_5^+ = 472 \text{ cm}^{-1}$, $\nu_6^+ = 660 \text{ cm}^{-1}$, $\nu_7^+ = 875 \text{ cm}^{-1}$, $\nu_8^+ = 990 \text{ cm}^{-1}$, $\nu_9^+ = 1038 \text{ cm}^{-1}$, $\nu_{10}^+ = 1267 \text{ cm}^{-1}$, and $\nu_{11}^+ = 1408 \text{ cm}^{-1}$. These measurements along with the frequency $\nu_{12}^+ = 3073 \text{ cm}^{-1}$ determined in the recent VUV-infrared photo-induced ionization study have provided the complete set of twelve experimental vibrational frequencies for ClCH=CCl₂⁺ in its ground electronic state. On the basis of the spectral simulation of the origin VUV-PFI-PE vibrational band, we have determined the IE(ClCH=CCl₂) to be $76\,441.7 \pm 2.0 \text{ cm}^{-1}$ ($9.4776 \pm 0.0002 \text{ eV}$).

4. Jie Yang, Yuxiang Mo, K. C. Lau, Y. Song, X. M. Qian, and C. Y. Ng, "A combined vacuum ultraviolet laser and synchrotron pulsed field ionization study of BCl₃", *Chem. Phys. and Phys. Chem.* (Special issue for the 85th International Bunsen Discussion Meeting on Chemical Processes of Ions-Transport and Reactivity), Web published Jan. 25, 2005.

The PFI-PE spectrum of boron trichloride (BCl₃) in the region of 93590-95640 cm⁻¹ has been measured using VUV laser. At energies 0-1100 cm⁻¹ above the adiabatic IE of BCl₃, the bending vibration progression of BCl₃⁺ is clearly resolved in the PFI-PE spectrum, whereas the spectrum at energies 1200-1900 cm⁻¹ above the IE(BCl₃) is found to exhibit dense vibrational structure. This observation unambiguously shows that BCl₃⁺ in its ground state has C_{2v} symmetry. *Ab initio* calculations performed at the CCSD(T)/CBS level with high-level corrections are consistent with this observation, indicating that the BCl₃⁺(\tilde{X}^2B_2) ground state has two long and one short B-Cl bonds. Furthermore, the CCSD(T)/CBS calculations predict the existence of two BCl₃⁺ transitional structures with D_{3h} and C_{2v} symmetries lying ≈ 800 and 1300 cm^{-1} , respectively, above the BCl₃⁺(\tilde{X}^2B_2) ground state. This prediction is also consistent with the dense features observed in the PFI-PE spectrum in the region of 1200-1900 cm⁻¹ above the IE(BCl₃). The assignment of the PFI-PE vibrational bands gives the IE(BCl₃) = $93891 \pm 2 \text{ cm}^{-1}$ ($11.6410 \pm 0.0003 \text{ eV}$) and the bending frequencies for BCl₃⁺(\tilde{X}^2B_2), $\nu_1^+(b_2) = 194 \text{ cm}^{-1}$ and $\nu_1^+(a_1) = 209 \text{ cm}^{-1}$. We have also examined the dissociative photoionization process BCl₃ + hν → BCl₂⁺ + Cl + e⁻ using the synchrotron based PFI-PE-photoion coincidence method, yielding the 0 K threshold or appearance energy (AE) for this process to be $12.495 \pm 0.002 \text{ eV}$. Combining this 0 K AE value and the IE(BCl₃), we have determined the 0 K bond dissociation energy (D₀) for Cl₂B⁺-Cl as $0.854 \pm 0.002 \text{ eV}$. This experimental and theoretical study indicates that the CCSD(T, Full)/CBS calculations with high-level corrections are highly reliable for the predictions of IE(BCl₃), AE(BCl₂⁺), and

$D_0(\text{Cl}_2\text{B}^+-\text{Cl})$ with error limits less than 35 meV. However, the CCSD(T, Full)/CBS predictions for $\Delta H_{f0}^\circ(\text{BCl}_3)$, $\Delta H_{f0}^\circ(\text{BCl}_2^+)$, and $\Delta H_{f0}^\circ(\text{BCl}_3^+)$ are less reliable with discrepancies up to 0.1 eV as compared to the experimental determinations.

Future Plans:

Recently, we have significantly improved the sensitivity of PFI-PEPICO measurements using the newly developed PFI-PEPICO quadrupole mass spectrometer (QMS). We have also established a state-of-the-art VUV laser photoion-photoelectron apparatus in our laboratory and have recently demonstrated sensitive PFI-PE, PFI-photoion (PFI-PI), and two-color laser infrared (IR)-VUV and VUV-IR photoion-photoelectron measurements. We have begun to perform high-resolution PIE, PFI-PE, VUV synchrotron based PFI-PEPICO, and VUV laser based PFI-PI measurements of hydrocarbon radicals, including methylene (CH_2), methyl (CH_3), ethynyl (C_2H), vinyl (C_2H_3), ethyl (C_2H_5), propargyl (C_3H_3), allyl (C_3H_5), propyl (C_3H_7), butyl (C_4H_7), and phenyl (C_6H_5) radicals, along with halogenated methyl and methylene radicals. These PFI experiments, particularly the determination of 0 K thresholds and product channels for dissociative photoionization reactions of radicals by PIE and PFI-PEPICO QMS and VUV laser PFI-PI methods, are expected to yield highly precise ΔH_{f0}° 's for many radicals with errors similar to those for the most accurate ΔH_{f0}° 's for CH_3 , CH_4 , and C_2H_2 etc. The PFI-PEPICO and PFI-PI measurements of radicals will also yield IEs and D_0 's for many radicals with errors limited only by the precision of the PFI measurements, and will allow the measurement of PFI-PE spectra covering not only the first IE, but also higher IEs of radicals without PFI-PE background interferences from impurities. We also plan to explore the application of the IR-VUV and VUV-IR schemes for PIE and PFI-PE studies of radicals.

Publications of DOE sponsored research (2003-present)

1. Y.-S. Cheung, C. Y. Ng, S.-W. Chiu, and W.-K. Li, "Application of Three-Center-Four-Electron Bonding for Structural and Stability Predictions of Main Group Hypervalent Molecules: The Fulfillment of Octet Shell Rule", *J. Mol. Struct., Theochem.* **623**, 1-10 (2003).
2. J. Liu, W. Chen, M. Hochlaf, X.-M. Qian, C. Chang, and C. Y. Ng, "Unimolecular Decay Pathways of State-Selected CO_2^+ in the Internal Energy Range of 5.2-6.2 eV: An Experimental and Theoretical Study", *J. Chem. Phys.* **118**, 149 (2003).
3. X. M. Qian, T. Zhang, Y. Chiu, D. J. Levandier, J. S. Miller, R. A. Dressler, and C. Y. Ng., "Rovibrational State-Selected Study of $\text{H}_2^+(X, v^+=0-17, N^+=1)+\text{Ar}$ Using the Pulsed Field Ionization-Photoelectron-Secondary Ion Coincidence Scheme", *J. Chem. Phys. (communication)*, **118**, 2455 (2003).
4. J. Liu, M. Hochlaf, and C. Y. Ng, "Pulsed Field Ionization-Photoelectron Bands for CS_2^+ in the Energy Range of 13.2 –17.6 eV: An Experimental and Theoretical Study", *J. Chem. Phys.* **118**, 4487 (2003).
5. Wenwu Chen, Jianbo Liu, and C. Y. Ng, "Vacuum Ultraviolet Pulsed Field Ionization-Photoelectron Study for N_2O^+ in the Energy Range of 16.3-21.0 eV", *J. Phys. Chem. A* **107**, 8086-8091 (2003).
6. X.M. Qian, T. Zhang, C. Y. Ng, A. H. Kung, and M. Ahmed, "Two-Color Photoionization Spectroscopy Using Vacuum Ultraviolet Synchrotron Radiation and Infrared Optical Parametric Oscillator Laser Source", *Rev. Sci. Instrum.* **74**, 2784-2890 (2003).
7. X.-M. Qian, T. Zhang, C. Chang, P. Wang, C. Y. Ng, Y.-H. Chiu, D. J. Levandier, J. S. Miller, R. A. Dressler, T. Baer, and D. S. Peterka, "High-Resolution State-Selected Ion-Molecule Reaction Studies Using Pulsed Field Ionization Photoelectron-Secondary Ion Coincidence Method", *Rev. Sci. Instrum.* **74**, 4096-4109 (2003).
8. H. K. Woo, K.-C. Lau, J.-P. Zhan, C. Y. Ng, Y.-S. Cheung, and W. K. Li, and P. M. Johnson, "Vacuum Ultraviolet Laser Pulsed Field Ionization-Photoelectron Study of *trans*-Butene", *J. Chem. Phys.* **119**, 7789 (2003).

9. X.-M. Qian, A. H. Kung, T. Zhang, K. C. Lau, and C. Y. Ng, "Rovibrational-state selected photoionization of acetylene by the two-color IR + VUV scheme: observation of rotationally resolved Rydberg transitions", *Phys. Rev. Lett.* **91**, 233001 (2003).
10. X.-M. Qian, T. Zhang, X. N. Tang, C. Y. Ng, Y. Chiu, D. J. Levandier, J. S. Miller, and R. A. Dressler, "A state-selected study of the $H_2^+(X, v^+=0-17) + Ne$ proton transfer reaction using the pulsed field ionization-photoelectron-secondary ion coincidence scheme", *J. Chem. Phys.* **119**, 10175-10184 (2003).
11. H. K. Woo, P. Wang, K.-C. Lau, X. Xing, C. Chang, and C. Y. Ng, "State-selected and State-to-State Photoionization Study of trichloroethene Using the two-Color Infrared-Vacuum Ultraviolet Scheme", *J. Chem. Phys. (communication)*, **119**, 9333-9336 (2003).
12. H. K. Woo, P. Wang, K. C. Lau, X. Xing, and C. Y. Ng, "Vacuum Ultraviolet-Infrared Photo-Induced Rydberg Ionization Spectroscopy: C-H stretching frequencies for trans-2-butene and trichloroethene cations", *J. Chem. Phys.* **120**, 1756 (2004).
13. M. Hochlaf, K.-M. Weitzel, and C. Y. Ng, "Vacuum ultraviolet pulsed field ionization-photoelectron studies of H_2S in the range of 10-16 eV", *J. Chem. Phys.* **120**, 6944 (2004).
14. X.-M. Qian, K.-C. Lau, G.-Z. He, and C. Y. Ng, "Accurate Thermochemistry of the ND_2/ND_2^+ and ND_3/ND_3^+ Systems", *J. Chem. Phys.* **120**, 8476 (2004).
15. H. K. Woo, P. Wang, K.-C. Lau, X. Xing, and C. Y. Ng, "Single-photon vacuum ultraviolet laser pulsed field ionization-photoelectron studies of *trans*- and *cis*-bromopropenes", *J. Chem. Phys.* **120**, 9561 (2004).
16. X. M. Qian, K. C. Lau, and C.Y. Ng, "A High-Resolution Pulsed Field Ionization-Photoelectron-Photoion Coincidence Study of Vinyl Bromide", *J. Chem. Phys.* **120**, 11031-11041 (2004).
17. H. K. Woo, K.-C. Lau, and C. Y. Ng, "Vibrational spectroscopy of trichloroethene cation by vacuum ultraviolet pulsed field ionization-photoelectron method", *Chinese J. Chem. Phys.*(invited article) **17**, 292 (2004).
18. H. K. Woo, P. Wang, K.-C. Lau, X. Xing, and C. Y. Ng, "VUV pulsed field ionization-photoelectron and VUV-IR-photo-induced Rydberg study of *trans*- $ClCH=CHCl$ ", *J. Phys. Chem. A*, **108**, 9637 (2004).
19. P. Wang, X. Xing, K.-C. Lau, H. K. Woo, and C. Y. Ng, "Rovibrational-state-selected pulsed field ionization-photoelectron study of methyl iodide using two-color infrared-vacuum ultraviolet lasers", *J. Chem. Phys. (Communication)*, **121**, 7049 (2004).
20. P. Wang, X. Xing, S. J. Baek, and C. Y. Ng, "Rovibrationally selected and resolved pulsed field ionization-photoelectron study of ethylene", *J. Phys. Chem. A (Communication)*, **108**, 10035 (2004).
21. C. Y. Ng, "Two-color photoionization and photoelectron studies by combining infrared and vacuum ultraviolet", *J. Electron Spectroscopy & Related Phenomena* (Invited Review), **142**, 179-192 (2005).
22. Jie Yang, Yuxiang Mo, K. C. Lau, Y. Song, X. M. Qian, and C. Y. Ng, "A combined vacuum ultraviolet laser and synchrotron pulsed field ionization study of BCl_3 ", *J. Chem. Phys. and Phys. Chem.* (Special issue for the 85th International Bunsen Discussion Meeting on Chemical Processes of Ions-Transport and Reactivity), Web published Jan. 25, 2005.
23. X. N. Tang, H. F. Xu, T. Zhang, Y. Hou, C. Chang, C. Y. Ng, Y. Chiu, R. A. Dressler, D. J. Levandier, "A pulsed field ionization photoelectron secondary ion coincidence study of the $H_2^+(X, v^+=0-15, N^+=1) + He$ proton transfer reaction", *J. Chem. Phys.*, accepted.
24. Adam Brooks, Kai-Chung Lau, C.Y. Ng, and Tomas Baer, "The $C_3H_7^+$ Appearance Energy from 2-Iodopropane and 2-Chloropropane Studied by Threshold Photoelectron Photoion Coincidence", *European Journal of Mass Spectrometry on Gas Phase Ion Chemistry and Thermochemistry*, accepted.
25. K. C. Lau and C. Y. Ng, "Accurate *ab initio* predictions of ionization energies of hydrocarbon radicals: CH_2 , CH_3 , C_2H , C_2H_3 , C_2H_5 , C_3H_3 and C_3H_5 ", *J. Am. Chem. Soc.*, submitted.

Large Eddy Simulation of Turbulence-Chemistry Interactions in Reacting Flows

Joseph C. Oefelein
Combustion Research Facility
Sandia National Laboratories, MS 9051
Livermore, California 94551
oefelei@sandia.gov

Program Scope

This program is directed toward combining a unique simulation capability based on the Large Eddy Simulation (LES) technique with a select set of advanced experiments currently under investigation at the CRF. The joint numerical-experimental research is focused primarily on the fundamental issues of turbulence-chemistry interactions in nonpremixed and partially-premixed flames. We have also established preliminary activities focused on premixed flames. The approach involves four key components: 1) application of unique software capabilities and high-performance computational resources, 2) implementation of a sophisticated set of subgrid-scale models aimed at direct closure of the chemical source terms, 3) rigorous model validation using data acquired from select target experiments, and 4) detailed characterization of complex turbulent combustion processes through joint-analysis of respective data. Once validated against experiments, high-fidelity simulations offer a wealth of information that cannot be measured directly. Information from the simulations, combined with detailed laser-based experiments, provide new opportunities to understand the central physics of turbulence-chemistry interactions and the related development of accurate predictive models.

Recent Progress

Development and rigorous validation of predictive science-based models for turbulent combustion is broadly considered an important priority in combustion research. LES is commonly viewed as an engineering tool of the future, holding promise to yield useful predictions of combustion in complex practical geometries. A less appreciated fact is that high-fidelity LES can serve as a powerful method for fundamental scientific inquiry into the structure and dynamics of turbulent flames. The application of LES provides the formal ability to treat the full range of multidimensional time and length scales that exist in turbulent reacting flows in a computationally feasible manner and thus provides a direct link to key experimental studies of relevant combustion phenomena. Treating the full range of scales is a critical requirement since phenomenological processes are inherently coupled through a cascade of nonlinear interactions. Our most recent results can be found in Refs. 1–3.

The current research has been enabled through a unique theoretical-numerical framework developed over the last decade. This framework solves the fully coupled conservation equations of mass, momentum, total-energy and species for complex chemically reacting flows (gas or liquid), in complex geometries. The numerical formulation treats the fully-coupled compressible form of the conservation equations, but can be evaluated in the incompressible limit. Thus, incompressibility is treated as a limiting extreme. The theoretical framework handles both multicomponent and mixture-averaged systems, with a generalized treatment of the equation of state, thermodynamics, and transport processes. It can accommodate high-pressure real-

gas/liquid phenomena, multiple-scalar mixing processes, finite-rate chemical kinetics and multiphase phenomena (or respective simplifications and modeled approximations) in a fully coupled manner. For LES applications, the instantaneous conservation equations are filtered and models are applied to account for the subgrid-scale (SGS) mass, momentum and energy transport processes. The baseline SGS closure used in the current formulation is obtained using the mixed dynamic Smagorinsky model by combining the models of Erlebacher et al. [4] and Speziale [5] with the dynamic modeling procedure [6-8] and the Smagorinsky eddy viscosity model [9]. There are no tuned constants employed anywhere in the closure. The property evaluation scheme is based on the extended corresponding states model [10, 11] and designed to handle full multicomponent systems. This scheme has been optimized to account for thermodynamic nonidealities and transport anomalies over a wide range of pressures and temperatures [12-19].

The baseline numerical framework provides a fully-implicit all-Mach-number time-advancement using a fully explicit multistage scheme in pseudo-time. A unique dual-time multistage scheme is employed with a generalized (pseudo-time) preconditioning methodology that treats convective, diffusive, geometric, and source term anomalies in an optimal and unified manner. The implicit formulation is A-stable, which allows one to set the physical-time step based solely on accuracy considerations. The spatial differencing scheme is optimized for LES using a staggered grid arrangement in generalized curvilinear coordinates. This provides non-dissipative spectrally clean damping characteristics and discrete conservation of mass, momentum and total-energy. The differencing methodology includes appropriate switches to handle shocks, detonations, flame-fronts, and contact discontinuities. The scheme can handle arbitrary geometric features, which inherently dominate the evolution of turbulence. A Lagrangian-Eulerian formulation is employed to accommodate particulates, sprays, or Lagrangian based combustion models, with full coupling applied between the two systems. The numerical algorithm has been designed using a consistent and generalized treatment for boundary conditions based on the method of characteristics. The algorithm is massively-parallel and has been optimized to provide excellent parallel scalability attributes using a distributed multiblock domain decomposition with a generalized connectivity scheme. Distributed-memory message-passing is performed using MPI and the Single-Program—Multiple-Data (SPMD) model. Sustained parallel efficiencies above 90-percent have been achieved with jobs as large as 1600 processors on the BES NERSC platform (Seaborg).

Results presented in Refs. 1–3 highlight some of the more unique capabilities of the theoretical-numerical framework and demonstrate the merits of conducting joint numerical-experimental research in the manner described above. Activities to date have focused on validation of the theoretical-numerical framework with two mutually dependent objectives. The first was to develop a unified model base suitable for performing high-fidelity LES of the complex phenomena associated with contemporary energy and propulsion systems. The second was to develop a high-performance massively-parallel software platform to support the implementation of large-scale simulations. The combined package provides a unique capability that incorporates the stringent algorithmic requirements of LES within a unified framework designed to optimally treat intricately coupled reacting flow phenomena at practical conditions. Key phenomena include wall-bounded three-dimensional flow, unsteady multiphase fluid dynamics, acoustics, transient broadband turbulence, scalar mixing of dense near-critical and supercritical fluid mixtures, high-pressure mixed-mode combustion dynamics, and breakup (or

disintegration) of hydrocarbon or cryogenic propellants over a wide Mach operating range (subsonic through supersonic).

Our combustion modeling approach facilitates direct treatment of turbulence-chemistry interactions and multiple-scalar mixing processes without the use of tuned model constants. The systematic development and validation of this approach is currently the main focal point. Unlike conventional models, chemistry is treated directly within the LES formalism. The filtered energy and chemical source terms are closed by selecting an appropriate chemical kinetics mechanism and employing a moment-based reconstruction methodology that provides a modeled representation of the local instantaneous scalar field. Model coefficients are evaluated locally in closed form as a function of time and space using the dynamic modeling procedure. The only adjustable parameters in the calculations are the grid and integration time-step. In the limit as the grid resolution and time-step approach DNS scales, contributions from the subgrid-scale models approach zero and the limit of a Direct Numerical Simulation (DNS) is achieved. This type of limiting behavior is highly desirable and offers a systematic method to approach a true DNS of a given target experiment without having to make oversimplified canonical geometric and phenomenological approximations.

Future Plans

Our current research efforts are a direct extension of joint activities currently being pursued in the Turbulent Combustion Laboratory and the International Workshop on Measurement and Computation of Turbulent Nonpremixed Flames (TNF) [20]. These activities involve significant domestic and international collaborations. We are currently performing a detailed calculation of the CH₄/air jet flame (Sandia flame D [21-25]), with emphasis placed on 1) investigating the fine-scale structure of mixture fraction and scalar dissipation fields in turbulent flames, 2) studying the instantaneous three-dimensional flame dynamics and orientation, and 3) investigating the influence of scalar dissipation on species mass fractions and temperature. The simulation incorporates the entire experimental test section and burner geometry using grids on the order of 5-10 million cells. These grids provide a level of spatial resolution that approaches and in some cases exceeds that of the experimental data.

The initial simulation of piloted flame D uses the four-step reduced chemical mechanism developed by Seshadri and Peters [26]. The objective is to establish an initial benchmark using the multi-scalar mixing and reaction model described above. In addition to comparison of measured and calculated profiles of velocity and selected scalars, the LES results will be analyzed using methods consistent with those applied to our experimental data in order to extract statistics on 1D (radial), 2D, and 3D scalar dissipation, scalar variance, length scales, and flame orientation. Once a level of confidence is established, the high-fidelity LES results will present opportunities to examine the structure and dynamics of turbulent flames in ways that cannot be measured but are vitally important to our fundamental understanding of combustion. For example, the dynamic coupling of large-scale fluid motion with scalar dissipation rates and reaction rates at the smallest resolved-scales can be followed in both time and full three-dimensional space.

The four-step mechanism is not expected to accurately capture strong effects of turbulence-chemistry interactions. Accordingly, a subsequent calculation will address flame-E, which exhibits strong extinction and re-ignition phenomena, using the Augmented-Reduced-Mechanism (ARM) developed by J.-Y. Chen and coworkers [27]. This mechanism has been

applied in PDF calculations of the piloted flame series by Pope and coworkers [28] and shown to provide an accurate representation of the relevant chemical processes. We will attempt to reproduce numerically the results from multiscale measurements in the piloted D and E flames, including doubly conditional statistics of reactive scalars. We will reconstruct the mixture fraction and scalar-dissipation fields and compare their local dynamic behavior to the corresponding multicomponent constituents, which are carried in the LES. As part of this exercise, we will quantify the degree to which preferential diffusion influences local characteristics of the reacting flow. We will examine the time history of extinction and the reforming of connected reaction zones, and we will analyze the relative contributions of convective, diffusion, and chemical reactions in these processes.

References

1. J. C. Oefelein, "Thermophysical Characteristics of Shear-Coaxial LOX-H₂ Flames at Supercritical Pressure," *Proc. Combust. Inst.*, **30**, 2929-2937, 2005.
2. J. C. Oefelein, R. W. Schefer, and R. S. Barlow, "Toward Validation of LES for Turbulent Combustion," *AIAA J*, Accepted 2005.
3. J. C. Segura, J. K. Eaton and J. C. Oefelein, "Predictive Capabilities of Particle-Laden Large Eddy Simulation," Report No. TSD-156, Mechanical Engineering Department, Stanford University, Sept 2004.
4. G. Erlebacher, M. Y. Hussaini, C. G. Speziale, and T. A. Zang. Toward the large eddy simulation of compressible turbulent flows. *Journal of Fluid Mechanics*, 238: 155-185, 1992.
5. C. G. Speziale. Galilean invariance of subgrid-scale stress models in the large eddy simulation of turbulence. *Journal of Fluid Mechanics*, 156: 55-62, 1985.
6. M. Germano, U. Piomelli, P. Moin, and W. H. Cabot. A dynamic subgrid-scale eddy viscosity model. *Physics of Fluids*, 3(7): 1760-1765, 1991.
7. P. Moin, K. Squires, W. Cabot, and S. Lee. A dynamic subgrid-scale model for compressible turbulence and scalar transport. *Physics of Fluids*, 3(11): 2746-2757, 1991.
8. D. K. Lilly. A proposed modification of the germano subgrid-scale closure method. *Physics of Fluids*, 3(11): 633-635, 1992.
9. J. Smagorinsky. General circulation experiments with the primitive equations. I. The basic experiment. *Monthly Weather Review*, 91: 99-164, 1963.
10. T. W. Leland and P. S. Chappellear. The corresponding states principle. A review of current theory and practice. *Industrial and Engineering Chemistry Fundamentals*, 60(7): 15-43, 1968.
11. J. S. Rowlinson and I. D. Watson. The prediction of the thermodynamic properties of fluids and fluid mixtures-I. The principle of corresponding states and its extensions. *Chemical Engineering Science*, 24(8): 1565-1574, 1969.
12. R. B. Bird, W. E. Stewart, and E. N. Lightfoot. *Transport Phenomena*. John Wiley and Sons, New York, 1960.
13. J. O. Hirschfelder, C. F. Curtiss, and R. B. Bird. *Molecular Theory of Gases and Liquids*. John Wiley and Sons, New York, 2nd edition, 1964.
14. S. Gordon and B. J. McBride. Computer program for calculation of complex chemical equilibrium compositions, rocket performance, incident and reflected shocks and Chapman-Jouguet detonations. Technical Report NASA SP-273, 1971.
15. S. Takahashi. Preparation of a generalized chart for the diffusion coefficients of gases at high pressures. *Journal of Chemical Engineering of Japan*, 7(6): 417-420, 1974.
16. R. C. Reid, J. M. Prausnitz, and B. E. Polling. *The Properties of Liquids and Gases*. McGraw-Hill, New York, 4th edition, 1987.
17. J. F. Ely and H. J. M. Hanley. Prediction of transport properties. 1. Viscosity of fluids and mixtures. *Industrial and Engineering Chemistry Fundamentals*, 20(4): 323-332, 1981.
18. J. F. Ely and H. J. M. Hanley. Prediction of transport properties. 2. Thermal conductivity of pure fluids and mixtures. *Industrial and Engineering Chemistry Fundamentals*, 22(1): 90-97, 1981.
19. R. J. Kee, F. M. Rupley, and J. A. Miller. Chemkin thermodynamic data base. Technical Report SAND87-8215B, Sandia National Laboratories, 1990. Supersedes SAND87-8215 dated April 1987.
20. *Proceedings of the International Workshop on Measurement and Computation of Turbulent Nonpremixed Flames*, R. S. Barlow, ed., Sandia National Laboratories, Combustion Research Facility, <http://www.ca.sandia.gov/TNF>, 2004.
21. A. N. Karpetsis and R. S. Barlow, "Measurements of Scalar Dissipation in a Turbulent Piloted Methane/Air Jet Flame," *Proc. Comb. Inst.*, **29**, 1929-1936, 2002.
22. R. S. Barlow and A. N. Karpetsis, "Measurements of Scalar Variance, Scalar Dissipation, and Length Scales in Turbulent Piloted Methane/Air Jet Flames," *Flow Turb. Combust.*, (special edition on the theme of scalars in turbulence, Bilger and Sreenivasan, Eds., to appear).
23. R. S. Barlow and A. N. Karpetsis, "Scalar Length Scales and Spatial Averaging Effects in Turbulent Piloted Methane/Air Jet Flames," *Proc. Combust. Inst.*, **30**, 673-680, 2005.
24. A. N. Karpetsis, T. B. Stettersten, R. W. Schefer, and R. S. Barlow, "Line Measurements in Turbulent Flames using Raman/Rayleigh/LIF Techniques," *Optics Let.*, (in press).
25. A. N. Karpetsis and R. S. Barlow, "Measurements of Flame Orientation and Scalar Dissipation in Turbulent Partially Premixed Methane Flames," *Proc. Combust. Inst.*, **30**, 665-672, 2005.
26. K. Seshadri and N. Peters, "The Inner Structure of Methane-Air Flames," *Combust. Flame*, **81**, 96-118, 1990.
27. C. J. Sung, C. K. Law, and J.-Y. Chen, "Augmented Reduced Mechanisms for NO Emission in Methane Oxidation," *Combust. Flame*, **125**, 906-919, 2001.
28. Q. Tang, J. Xu and S.B. Pope, "PDF Calculations of Local Extinction and NO Production in Piloted-Jet Turbulent Methane/Air Flames," *Proc. Combust. Inst.*, **28**, 133-139, 2000.

KINETICS AND DYNAMICS OF COMBUSTION CHEMISTRY

David L. Osborn

Combustion Research Facility, Mail Stop 9055

Sandia National Laboratories

Livermore, CA 94551-0969

Telephone: (925) 294-4622

Email: dlosbor@sandia.gov

PROGRAM SCOPE

The goal of this program is to elucidate mechanisms of elementary combustion reactions through the use of optical spectroscopy and mass spectrometry. Several techniques are employed. First, time-resolved Fourier transform spectroscopy (TR-FTS) is used to probe multiple reactants and products with broad spectral coverage ($> 1000 \text{ cm}^{-1}$), moderate spectral resolution (0.1 cm^{-1}) and a wide range of temporal resolution (ns – ms). The inherently multiplexed nature of TR-FTS makes it possible to simultaneously measure product branching ratios, internal energy distributions, energy transfer, and spectroscopy of radical intermediates. Together with total rate coefficients, this additional information provides further constraints upon and insights into the potential energy surfaces that control chemical reactivity. Because of its broadband nature, the TR-FTS technique provides a global view of chemical reactions and energy transfer processes that would be difficult to achieve with narrow-band laser-based detection techniques.

Second, cavity-enhanced frequency modulation spectroscopy (a.k.a. NICE-OHMS) is used to provide an ultrasensitive, differential absorption spectroscopic probe. We have detected a time-resolved, transient absorption spectrum of the NH_2 radical using this technique, which opens the door to measurements of chemical kinetics in flow cells and monitoring of species in flames. This cavity-enhanced FM spectroscopy technique provides very high sensitivity, the generality of absorption spectroscopy, and insensitivity to background absorptions that vary slowly with frequency. These advantages allow the suppression of secondary chemistry by increased dilution of reactive species while still retaining sufficient detection sensitivity.

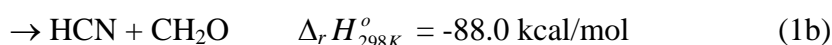
Finally, photoionization mass spectrometry is used to sensitively and selectively probe unimolecular and bimolecular reactions. In the past year, we have constructed a new apparatus, the Multiplexed Chemical Kinetics Photoionization Mass Spectrometer. This apparatus utilizes tunable vacuum ultraviolet light from the Advanced Light Source synchrotron at Lawrence Berkeley National Laboratory for sensitive, isomer specific ionization of reactant and product molecules in chemical reactions.

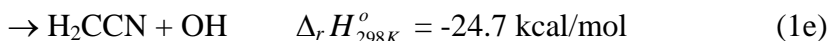
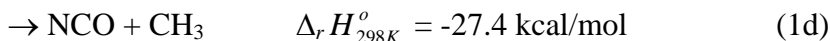
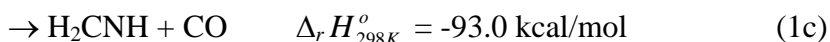
RECENT PROGRESS

The $\text{C}_2\text{H}_3 + \text{NO}$ reaction

The vinyl radical (C_2H_3) is among the simplest unsaturated hydrocarbon free radicals and is an important intermediate in the combustion of aliphatic fuels. Its reaction with NO is important in the fuel reburning processes that can reduce NO_x emissions in combustion. We have studied the vinyl + NO reaction using time-resolved Fourier transform emission spectroscopy, complemented by electronic structure and microcanonical RRKM rate coefficient calculations. In order to unambiguously determine the reaction products, three precursors are used to produce the vinyl radical by laser photolysis: vinyl bromide, methyl vinyl ketone, and vinyl iodide.

There are several reaction pathways of $\text{C}_2\text{H}_3 + \text{NO}$ that are thermodynamically accessible at room temperature (1a – 1f).





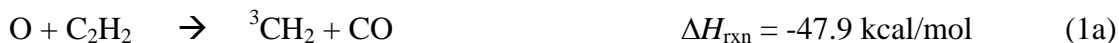
Two experimental reports in the literature yield conflicting conclusions regarding the active product channels at room temperature.^{1,2} A recent theoretical paper³ concluded that bimolecular products could not be formed at all due to a barrier well above reactants on the potential energy surface (PES).

Our emission spectra and theoretical calculations indicate that $\text{HCN} + \text{CH}_2\text{O}$ is formed, and is the only significant reaction channel for the $\text{C}_2\text{H}_3 + \text{NO}$ reaction near room temperature. Furthermore, we observe vibrationally excited NO molecules that form promptly in our reaction chamber. This observation implies a covalent interaction between NO and vinyl in the nitrosoethylene adduct that significantly facilitates energy transfer, allowing prompt production of NO $\nu = 2$.

Our results confirm the reaction mechanism first proposed by Striebel *et al.*,⁴ and suggest that the temperature dependence of the product branching ratio is less sensitive to temperature than one might expect because the low energy portion of the Boltzmann distribution contributes disproportionately to the reactive flux.

The mechanism of the $\text{HCCO} + \text{O}_2$ reaction: Probing multiple pathways to a single product channel

Acetylene is a ubiquitous species present in the combustion of aliphatic and aromatic hydrocarbons.⁵ Acetylene is oxidized in flames exclusively by oxygen atoms:



where reaction (1b), producing HCCO, is the dominant product channel. In lean flames, the ketenyl radical (HCCO) reacts primarily with O_2 , leading to the following possible channels:



Previously, we applied emission-based TR-FTS to measure the branching ratio and state distributions of reaction (3). These experiments demonstrated that channel (3a), yielding $\text{H} + \text{CO} + \text{CO}_2$, represents at least 90% of the products at 300K, in agreement with theoretical predictions.⁶ This work provides experimental evidence that the genesis of prompt CO_2 ⁷ lies in the single reaction $\text{HCCO} + \text{O}_2$. Recently we have delved further into this reaction's mechanism.

In a chemical reaction, each product branching ratio is typically interpreted as a measurement of the flux through one exit channel of that reaction. However, it is possible that two energetically feasible paths on the potential energy surface lead to a single product channel. The PES for $\text{HCCO} + \text{O}_2$ provides several distinct, energetically feasible pathways leading to $\text{H} + \text{CO} + \text{CO}_2$. Following the addition of O_2 to ketenyl at the methylidyne carbon, formation of a 4-membered or 3-membered ring intermediate is possible. The direct dynamics classical trajectory calculations of Klippenstein, Miller, and Harding predict flux through both pathways. Experimentally, it is not easy to make such a determination, since the products are $\text{H} + \text{CO} + \text{CO}_2$ in either case. We have used isotopic labeling combined with state-specific product detection to answer this question.

In the $\text{HCC}^{16}\text{O} + {}^{18}\text{O}_2$ reaction, all the possible isotopomers of the products are distinguishable using rotationally resolved infrared spectroscopy. The dominant isotopic products are C^{18}O and

$^{16}\text{O}^{18}\text{O}$. Combined with data from the corresponding reaction in natural isotopic abundance, these results show that at least 85% of the reactive flux passes through the four-membered OCCO ring intermediate. The three-membered COO ring intermediate represents less than 15% of the total reactive flux. Furthermore, H atom transfer during decomposition of the four-membered ring intermediate is at most a minor process. These results call into question the common assumption that each observed product channel in a reaction arises from a single pathway on the potential energy surface.

Time-resolved, ultrasensitive cavity-enhanced frequency modulation spectroscopy

We have built an ultra-sensitive laser absorption spectrometer based on the Noise Immune Cavity Enhanced Optical Heterodyne Molecular Spectroscopy technique (NICE-OHMS) developed by Ye, Hall and coworkers.⁸ This technique utilizes frequency modulation (FM) spectroscopy to reduce sources of technical noise, coupled with a high-finesse sample cavity to provide long absorption pathlengths. We have made the first observation of the extremely weak ($7 \leftarrow 0$) vibrational overtone of NO near 796 nm. Although NICE-OHMS is a differential technique, we can calibrate the spectrometer response to enable measurement of absolute absorption cross sections. For this overtone we measure a transition dipole moment $|\mu_{70}| = 4.5 \times 10^{-6}$ Debye and the associated Herman-Wallis factor. The minimum detectable absorption is currently $8 \times 10^{-11} \text{ cm}^{-1} \text{ Hz}^{-1/2}$.

We have recently observed a time-resolved, transient absorption of the NH_2 radical on the $\tilde{X} (^2\text{B}_1)$ ($170 \leftarrow 000$) overtone. NH_2 is produced from photolysis of NH_3 . While the results are preliminary, this experiment shows that the abrupt change in optical path length caused by photolysis does not disturb the lock between the laser and the high-finesse cavity. The robustness of this lock loop is critical to the study of chemical kinetics using this technique.

The multiplexed chemical kinetics photoionization mass spectrometer

We have recently completed the first experiments on a new photoionization mass spectrometer at the Chemical Dynamics Beamline of the Advanced Light Source (ALS) of LBNL. The chemical reactor is based on the Gutman design,⁹ which allows the study of photodissociation and bimolecular reactions at pressures of $\sim 3 - 10$ Torr and temperatures up to 1000 K.

While the study of chemical kinetics using PIMS is well-established, this apparatus has two unique features that make it especially powerful for chemical kinetics. First, the widely tunable, intense VUV radiation from the ALS enables isomer specific ionization of product species. For example, the ability to distinguish allene from propyne (C_3H_4 isomers) and vinyl alcohol from acetaldehyde ($\text{C}_2\text{H}_4\text{O}$ isomers) has already been demonstrated in the ALS low-pressure flame chamber.¹⁰

The second unusual feature of this experiment is the mass spectrometer. We employ a small magnetic sector instrument coupled to a time- and position-sensitive single-ion counting detector. This approach creates a mass spectrometer with 100% duty cycle (like a quadrupole instrument) and the multiplex advantage of measuring a broad range of masses simultaneously (as in time-of-flight

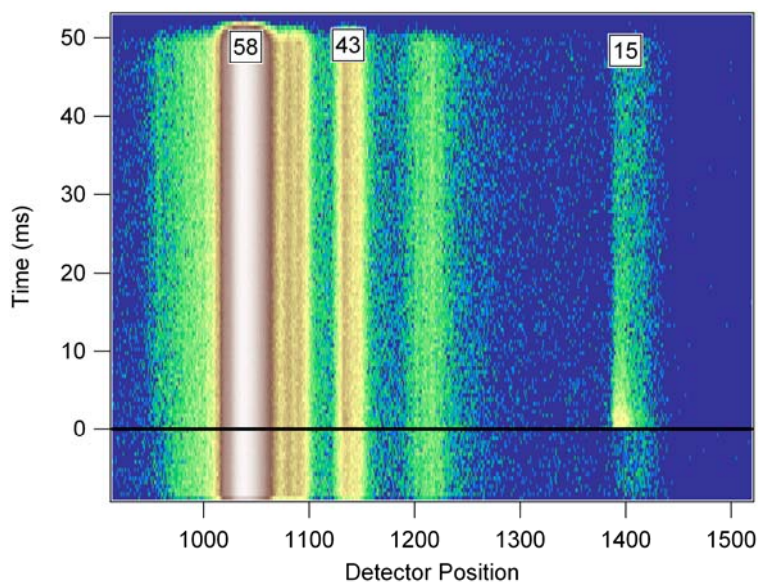


Figure 1: Time-resolved mass spectra of the $\text{CH}_3 + \text{O}_2$ reaction

spectrometry). This detector also measures the time dependence of each observed reactant and product molecule, which provides kinetic information on the reaction.

Our initial experiments investigated the $\text{CH}_3 + \text{O}_2$ and $\text{C}_2\text{H}_5 + \text{O}_2$ reactions. Figure 1 shows a series of time-resolved mass spectra from the former reaction. We succeeded in photoionizing the CH_3O_2 radical, and have made the first measurement of its photoionization efficiency. Our rate coefficient for the $\text{CH}_3 + \text{O}_2$ reaction agrees with the literature value.

Future Directions

Using TR-FTS, we will investigate reactions of the vinyl (C_2H_3) and propargyl (C_3H_3) radicals to determine product channel identities and energy disposal. We will continue development of transient NICE-OHMS measurements for chemical kinetics. In addition, we hope to apply this cavity enhanced FM technique to measurements in low-pressure flames, which display low-level, broad background absorption of ~ 1 ppm. Because NICE-OHMS is a differential technique, it will be insensitive to absorptions that change negligibly on the scale of the modulation frequency.

One interesting problem to explore using the multiplexed chemical kinetics mass spectrometer apparatus instrument is the reaction $\text{C}_3\text{H}_3 + \text{C}_2\text{H}_2$. Previous work by Knyazev and Slagle¹¹ has shown that the initial product (C_5H_5) can react with excess acetylene to form C_7H_7 . This process continues to form C_9H_8 and perhaps larger species. Measuring the isomeric forms of these products will provide information critical to the reaction mechanism for this molecular weight growth process.

BES sponsored publications, 2003 - present

- “The vinyl + NO reaction: determining the products with time-resolved Fourier transform spectroscopy,” Peng Zou, Stephen J. Klippenstein, and David L. Osborn, *Journal of Physical Chemistry A*, (accepted).
- “Synchrotron photoionization measurements of combustion intermediates: the photoionization efficiency of HONO” C. A. Taatjes, D. L. Osborn, T. A. Cool, and K. Nakajima, *Chemical Physics Letters* **394**, 19 (2004)..
- “On the mechanism of the $\text{HCCO} + \text{O}_2$ reaction: Probing multiple pathways to a single product channel” P. Zou and D. L. Osborn, *Physical Chemistry Chemical Physics* **6**, 1697 (2004).
- “Photodissociation dynamics of dicyclopropyl ketone at 193 nm: isomerization of the cyclopropyl ligand” S. M. Clegg, B. F. Parsons, S. J. Klippenstein, and D. L. Osborn, *Journal of Chemical Physics* **119**, 7222 (2003).
- “Cavity-enhanced Frequency Modulation Absorption Spectroscopy of the Sixth Overtone Band of Nitric Oxide.” J. Bood, A. McIlroy, and D. L. Osborn, *Proc. SPIE* **4962**, 89 (2003).
- “The reaction of $\text{HCCO} + \text{O}_2$: experimental evidence of prompt CO_2 by time-resolved Fourier transform spectroscopy” D. L. Osborn, *Journal of Physical Chemistry A* **107**, 3728 (2003).

References

- ¹ Sherwood, A. G.; Gunning, H. E. *J. Am. Chem. Soc.* **1963**, 85, 3506.
- ² Feng, W.; Wang, B.; Wang, H.; Kong, F. *Acta Physico-Chimica Sinica*. **2000**, 16, 776.
- ³ Sumathi, R.; Nguyen, H. M. T.; Nguyen, M. T.; Peeters, J. J. *Phys. Chem. A*. **2000**, 104, 1905.
- ⁴ Striebel, F.; Jusinski, L. E.; Fahr, A.; Halpern, J. B.; Klippenstein, S. J.; Taatjes, C. A. *Phys. Chem. Chem. Phys.* **2004**, 6, 2216.
- ⁵ H. Gg. Wagner, *Proc. Comb. Inst.* **17**, 3 (1979).
- ⁶ S. J. Klippenstein, J. A. Miller, and L. B. Harding, *Proc. Comb. Inst.* **29**, 1209 (2002).
- ⁷ G.P. Glass, G.B. Kistiakowsky, J.V. Michael and H. Niki, *Proc. Combust. Inst.* **10**, 513 (1964).
- ⁸ J. Ye, L. S. Ma, and J. L. Hall, *J. Opt. Soc. Am. B* **15**, 6 (1998).
- ⁹ I. R. Slagle and D. Gutman, *J. Am. Chem. Soc.* **107**, 5342 (1985).
- ¹⁰ T. A. Cool, K. Nakajima, T. A. Mostefaoui, F. Qi, A. McIlroy, P. R. Westmoreland, M. E. Law, L. Poisson, D. S. Peterka, and M. Ahmed *J. Chem. Phys.* **22**, 8356 (2003).
- ¹¹ V. D. Knyazev and I. R. Slagle, *J. Phys. Chem. A* **106**, 5613 (2002).

Large Amplitude Motion as a Generator of Intramolecular Energy Transfer

David S. Perry, Principal Investigator
Department of Chemistry, University of Akron,
Akron OH 44325-3601
DPerry@UAkron.edu

Introduction

In the presence of large amplitude motion, a molecular system no longer remains close to a well-defined reference geometry, which challenges the concepts of the traditional theory of molecular vibrations. Among the challenged concepts are normal modes and point group symmetry. The large amplitude coordinate may take on the character of a reaction coordinate along which one must continuously redefine the remaining “normal” coordinates. The consequences are that large amplitude motion can result in novel energy level structures and it can promote coupling between vibrations and hence accelerate IVR. In the sections below, we show, in three different contexts, how large amplitude motion acts as a generator of intramolecular vibrational energy transfer (IVR).

In this project, we examine the vibrational level structure and dynamics of molecules with a single internal rotor including methanol, nitromethane, and methylamine. Vibrational fundamental and overtone spectra of the jet-cooled molecules are examined by cavity ringdown, FTIR spectroscopy, and photofragment spectroscopy (IRLAPS). The ringdown experiments are done in our lab in Akron; the jet-FTIR is done in collaboration with Robert Sams at Pacific Northwest Labs (PNNL); the IRLAPS experiments are done in Thomas Rizzo’s lab at the EPFL in Switzerland. To understand the level structures and vibrational mode coupling taking place, we analyze high resolution spectra, develop quantum mechanical models of the nuclear motion, and probe the potential surface with *ab initio* calculations.

A. IVR as a Non-adiabatic Effect in the CH Stretch – Torsion Manifold of Methanol.

In previous work under this project,¹ we discovered the inverted torsional tunneling splitting in the asymmetric CH stretch vibrational states ($v_2=1$ and $v_9=1$). These results were successfully explained by our 4-dimensional model calculation that included the three CH stretch coordinates and the torsion.² Torsional motion interchanges the identities of the CH bonds *anti* and *gauche* to the OH, and the CH bonds in these positions have different force constants. A single lowest-order coupling term with the required symmetry (A_1 in G_6) was sufficient to reproduce the observed torsional structure. The inverted torsional structure is a general phenomenon that derives from molecular symmetry and the single coupling term results in a many mixed vibrational states throughout the CH stretch-torsion manifold. Subsequent spectroscopic reports³ of other asymmetric vibrations have confirmed the generality of the effect, and a number of theoretical studies⁴ have contributed to our understanding.

Fehrensen, Luckhaus, Quack, Willeke, and Rizzo⁵ have used *ab initio* calculations, an adiabatic (Born-Oppenheimer-like) separation of the torsion from the other vibrations, and the concept of geometric phase to account for the torsional structure of excited methanol vibrational states. This insightful treatment gives an appealing conceptual unity with electronic spectroscopy and provides a criterion for when such inverted torsional structure should be expected. We have been able to use our fully-coupled 4-D model to test the limits of applicability of the adiabatic approximation and to explore the non-adiabatic effects.

In this adiabatic approximation, the CH stretches are the “fast” degrees of freedom solved at each torsional angle, and the “slow” degree of freedom is torsion motion in the effective potential defined by the CH stretch vibrations. By definition, such an approximation does not allow exchange of energy between the torsion and the CH stretch vibrations. Such energy transfer (IVR) is therefore a non-adiabatic effect. Even though our model contains only a single coupling term in the local-mode – free-rotor basis, the same Hamiltonian, when expressed in the adiabatic basis, contains a myriad of off-diagonal IVR coupling matrix elements. The scaling behavior of these coupling matrix elements with coupling order is shown in Fig. 1. Clearly, the average coupling matrix element is smaller for higher coupling orders where many vibrational quanta must be created or destroyed.

The “ a ” parameter is the factor by which the average coupling matrix element declines for each higher order of coupling. Madsen and Gruebele⁶ found that for rigid molecules $a = 0.05 - 0.2$, that is the average coupling strength is an order of magnitude weaker at each higher order. However, for torsional molecules Pearman and Gruebele⁷ found that a is in the range $0.3 - 0.5$, that is a much slower fall-off of coupling strength at higher orders. Our present results (Fig. 1) support their prediction.

The hundreds of IVR matrix elements represented in Fig. 1 result from the transformation from the local-mode – free-rotor basis and hence the scaling behavior of the matrix elements results from the scaling properties of the coefficients needed to express each adiabatic function as a linear combination of these basis functions. The primary effect here is that even in the vibrational ground state, the torsional potential couples many free-rotor basis states to form each torsional eigenfunction. Thus, we have the insight that the scaling properties of IVR derive from the nature of the adiabatic functions themselves. The origin of all the couplings is a single physical interaction, which may be simply expressed in an appropriate basis. A more sophisticated model of the CH-stretch – torsion coupling might include additional (probably weaker) interactions, but by the same argument, one would expect their contributions to scale in a similar fashion.

At high energies, for example at high torsional excitation, at high CH stretch excitation, or both, the adiabatic basis derived at low energies is not very good. It would seem that in these regions we need qualitatively different zeroth order pictures. Extension of our model calculations indicates that there is a systematic pattern of near-degeneracies in each region, but that the pattern in each region is different. Characterization of these high energy regions and determination of the boundaries between them remains a challenge for the future.

B. Torsional Structure and IVR in the Asymmetric NO Stretch Band of Nitromethane

Nitromethane (CH_3NO_2) is an internal rotor molecule with one more atom than methanol, which increases the molecular symmetry group from G_6 to G_{12} . The planarity of the heavy atoms results in a very low (2 cm^{-1}) 6-fold torsional barrier. Thus, we have the opportunity to extend the stretch-torsion model discussed above to this new situation.

The slit-jet FTIR spectra from PNNL have enabled detailed rotational assignments of the lowest 4 internal-rotation states of the asymmetric NO stretch. The comparison of the observed pattern of the

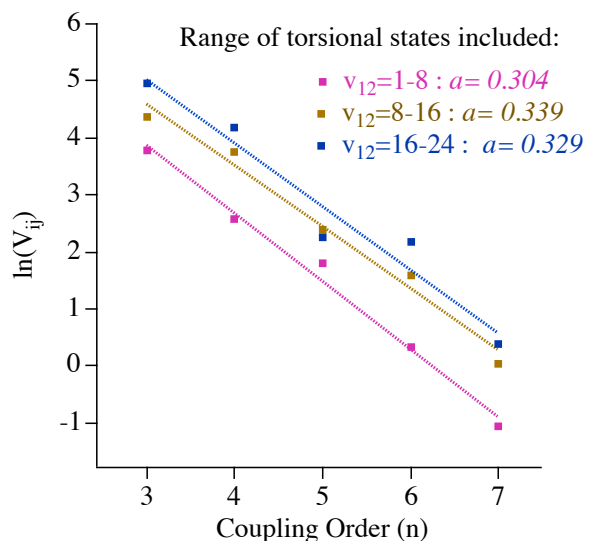


Fig. 1. The scaling with coupling order of average matrix elements coupling the torsion (v_{12}) and the CH stretches in methanol.

torsional levels with our model calculation indicates that the torsion-vibration coupling parameter in nitromethane is much smaller than in methanol. We also find that the rotational lines of lowest torsional state ($m=0$) are each fragmented into clumps of 3 – 6 transitions. These clump structures are the spectroscopic signature of IVR.

There are two unique characteristics of the nitromethane IVR clumps. First, IVR clumps with relatively large splittings (a few cm^{-1}) are observed at a lower total energy (1580 cm^{-1}) than most previous work, which has been in the CH fundamental region (3000 cm^{-1}) or at higher energies. Second, because nitromethane is an asymmetric rotor, only slightly closer to the oblate limit than to the prolate limit, we are able to follow the interactions as a function of J , K_a , and K_c . This enables us to assign each interaction as anharmonic or Coriolis type a , b , or c . The dominant interactions in this nitromethane band are Coriolis interactions involving rotation about the prolate (a) axis, which is coincident with the internal rotation axis. Internal rotation and overall rotation about this axis are strongly coupled for kinematic reasons. Together these characteristics point to the low-barrier internal rotation as the generator of the IVR couplings.

C. Conformational Dependence of IVR in Methanol

In methanol, molecules with one quantum of torsional excitation have a significant probability of being at or near the eclipsed conformation (Fig. 2), whereas molecules without torsional excitation have geometries near the minimum energy (staggered) conformation. In recent work,⁸ we have recorded and assigned spectra representing the direct excitation of torsionally excited states in the OH manifold. This new capability offers the opportunity to study the conformational dependence of IVR in the OH overtone manifold of methanol.

The energy level scheme for these experiments is shown in Fig. 3. Our previous work on the $5\nu_1$ region of methanol, which did not involve torsionally excited intermediate states, revealed three IVR timescales. The new spectra of “eclipsed” methanol also reveal three IVR timescales, but each timescale has changed. Systematic spectra as a function of J' and symmetry have been obtained and are being analyzed.

Plans for the Next Year

Slit-Jet cavity-ringdown spectra of the OH (ν_1) + CH (ν_3) stretch combination band of methanol between 6510 and 6550 cm^{-1} have been recorded at sub-Doppler resolution [5]. In the coming grant period, our continuous-wave cavity ringdown technique (CW-CRDS) will be extended to the CH overtone region ($2\nu_{\text{CH}}$) to test the concepts, presented in section A. above, at a higher level of CH stretch excitation. These

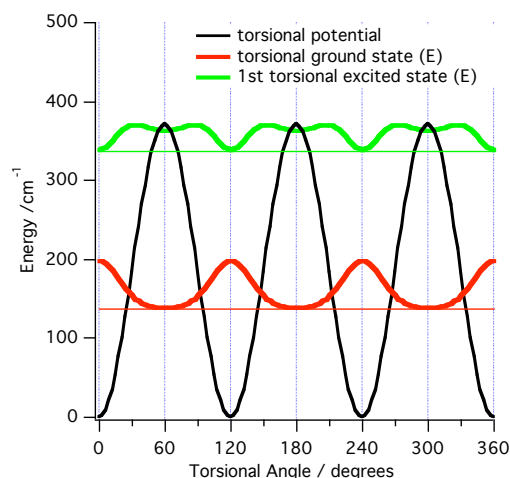


Fig. 2. Torsional angle distribution of the lowest two torsional states in methanol.

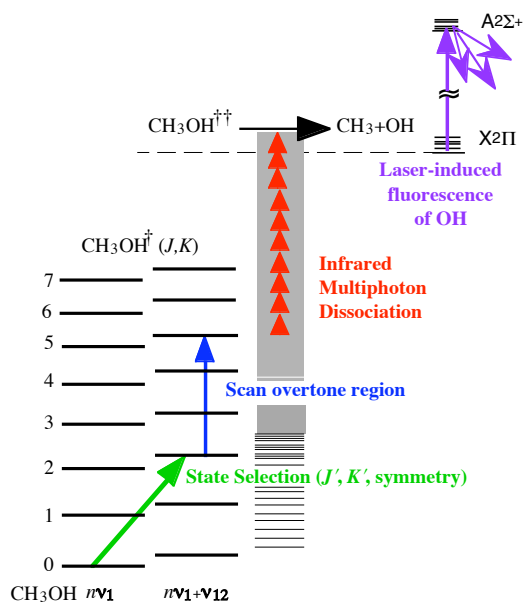


Fig. 3. Energy level scheme for IRLAPS experiments using intermediate states with one quantum of torsion (ν_{12}).

experiments, which will use a new laser source (a CW PPLN OPO) and a CW slit jet, will involve substantial experimental development.

Measurement of pure rotational (FAAAST) spectra of highly excited bending states of acetonitrile oxide will also begin.

Analysis of the data outlined in the sections above will continue and manuscripts will be prepared for publication.

Cited References

- ¹ L.-H. Xu, X. Wang, T. J. Cronin, D. S. Perry, G. T. Fraser, and A. S. Pine, *J. Mol. Spectrosc.* **185**, 158 (1997).
- ² X. Wang and D. S. Perry, *J. Chem. Phys.* **109**, 10795 (1998).
- ³ R. M. Lees and L.-H. Xu, *Phys. Rev. Lett.* **84**, 3815 (2000).
- ⁴ J. T. Hougen, *J. Mol. Spectrosc.* **181**, 287 (1997); J. T. Hougen, *J. Mol. Spectrosc.* **207**, 60 (2001); M. A. Temsamani, L.-H. Xu, and D. S. Perry, *Can. J. Phys.* **79**, 467 (2001).
- ⁵ B. Fehrensen, D. Luckhaus, M. Quack, M. Willeke, and T. R. Rizzo, *J. Chem. Phys.* **119**, 5534 (2003).
- ⁶ D. Madsen, R. Pearman, and M. Gruebele, *J. Chem. Phys.* **106** (14), 5874 (1997).
- ⁷ R. Pearman and M. Gruebele, *Z. Phys. Chem. (Muenchen)* **214** (11), 1439 (2000).
- ⁸ D. Rueda, O. V. Boyarkin, T. R. Rizzo, I. Mukhopadhyay, and D. S. Perry, *J. Chem. Phys.* **116** (1), 91 (2002).

Publications from this Project, 2003-2005

- [1] L. Wang, Y.-B. Duan, R. Wang, G. Duan, I. Mukhopadhyay, D.S. Perry, K. Takagi, Determination of reduced Hamiltonian parameters for the CD₃OH isotopomers of methanol, *Chem. Phys.*, **292**, 23-29, (2003).
- [2] Shucheng Xu, Jeffrey J. Kay, and David S. Perry, Doppler-limited CW infrared cavity ringdown spectroscopy of the $\nu_1+\nu_3$ OH+CH stretch combination band of jet-cooled methanol, *J. Mol. Spectrosc.* **225**, 162-173 (2004).
- [3] David Rueda, Oleg V. Boyarkin, Thomas R. Rizzo, Andrei Chirokolava and David S. Perry, Vibrational overtone spectroscopy of jet-cooled methanol from 5,000 to 14,000 cm⁻¹, *J. Chem. Phys.*, **122**, 044314 (2005).

INVESTIGATION OF NON-PREMIXED TURBULENT COMBUSTION

Grant: DE-FG02-90ER14128

Stephen B. Pope
Sibley School of Mechanical & Aerospace Engineering
Cornell University
Ithaca, NY 14853
pope@mae.cornell.edu

Scope of the Research Program

The focus of the current work is on the development of computational approaches which allow our detailed knowledge of the chemical kinetics of combustion to be applied to the modeling and simulation of combustion devices. Several approaches are being pursued which can be used in combination and which are described in more detail in the following section. These approaches are: dimension reduction of the kinetic mechanism; storage/retrieval algorithms for the computationally-efficient implementation of combustion chemistry; and probability density function (PDF) methods for modeling turbulent combustion.

1 Recent Progress

The principal research results are described in the publications listed in the final section.

1.1 Dimension Reduction of Combustion Chemistry

To a large extent, detailed kinetic mechanisms encapsulate our best current quantitative knowledge of the chemistry of the oxidation of different fuels and of the formation of pollutants. These mechanisms involve of order 10 species for hydrogen, 50 species for methane, and upward of 1,000 species for higher hydrocarbons. Typically, the computational cost of using a chemical mechanism increases as a power of the number of species, n_s , for example as n_s^2 or n_s^3 . Consequently, the direct use of large mechanisms in combustion simulation is usually prohibitive.

For over a century, dimension reduction techniques have been used to reduce the number of degrees of freedom in such mechanisms. The earliest and most widely used technique is based on the quasi-steady state assumption (QSSA). Other techniques have the acronyms ILDM, TGLDM, FGM, RCCE, etc.

We take a geometric and dynamical-systems view of the problem. In the work of Ren & Pope (2005a), the geometry of reaction trajectories in composition space is explored. An infinitesimal ball of initial conditions evolves in time to an ellipsoid. It is shown that, after a short time, most of the principle axes shrink to less than a small fraction (e.g., 10^{-3}) of their

initial size, giving direct evidence of dimension reduction. These and other observations are valuable in providing insights into approaches to dimension reduction.

Two complementary views of dimension reduction are *species reconstruction* and *attracting manifolds*. In species reconstruction, the problem considered is: given the thermodynamic state and the mass fractions of specified “major” species, estimate the mass fractions of the remaining “minor” species. From the attracting manifolds perspective, the task is to identify the attracting low-dimensional manifolds in the composition space close to which all composition that occur lie. If this manifold is parameterized by the major species, then identifying the manifold is identical to species reconstruction.

In Ren & Pope (2005b) we develop a dimension reduction scheme based on species reconstruction. The simple idea on which this method is based is that reaction trajectories are naturally attracted to the attracting manifold. Given values of the major species, we seek “pre-image” points in the composition space. By definition, a trajectory from a pre-image point, after some time, has the given values of the major species: and the values on the trajectory of the minor species provide the species reconstruction. The method developed provides a means of identifying appropriate pre-image points. When applied to a methane/air autoignition test case, with 6 degrees of freedom it yields comparable accuracy to a QSSA scheme with 12 degrees of freedom.

1.2 Storage/Retrieval Algorithms

In the numerical implementation of PDF methods for turbulent combustion, a particle method is used, and reaction is treated in a fractional step. Thus, the computational task (for each particle and on each time step) is: given the thermochemical composition at the beginning of the step, determine the composition at the end of the time step Δt resulting from adiabatic, isobaric reaction. The direct method is to integrate the stiff set of ordinary differential equations arising from the chemical kinetics. But huge efficiency gains can be realized if, instead, storage retrieval methods such as ISAT or PRISM are used. In these techniques, the final composition is stored as a function of the initial composition.

Liu & Pope (2005) studied the numerical errors involved in the *in situ* adaptive tabulation (ISAT) algorithm. The errors resulting from interpolating in the ISAT table are controlled by a specified error tolerance ε_{tol} . A series of PDF calculations of the Barlow & Frank flame D are made using ISAT with different values of ε_{tol} . It is found that conditional means around stoichiometric are most sensitive to numerical errors; and it is shown that the observed errors in these conditional means vary linearly with ε_{tol} (as predicted by theory). Hence, the errors can be satisfactorily controlled through a suitable specification of ε_{tol} .

The use of ISAT in direct numerical simulations (DNS) of laminar and turbulent flames is more difficult because the coupling between reaction and other processes is much stronger. In collaboration with Dr. Habib Najm (Sandia), we have developed a splitting method that enables ISAT to be used in the DNS code of Najm & Knio (see Singer & Pope 2004, Singer, Pope & Najm 2005). The results show that the second-order spatial and temporal accuracy of the scheme is maintained, and that a speedup of around 4 is achieved. This is clearly worthwhile, though much less than the speed-up of 100-1,000 typically observed in PDF calculations.

1.3 PDF Calculations of Turbulent Flames

We continue to perform PDF calculations of the turbulent non-premixed flames studied experimentally at Sandia, with the objective of understanding the behavior and capabilities of different turbulent mixing models and chemical mechanisms. These studies include: the Barlow & Frank piloted jet flames (Cao & Pope 2005); the bluff-body jet flames (Muradoglu et al. 2003, Liu et al. 2005b); and an investigation of mixing models applied to partially-stirred reactors (Ren & Pope 2004).

The work of Cao & Pope (2005) illustrates the current state of the art in PDF calculations. The performance of six different methane mechanisms—ranging from a 5-step reduced mechanism to the 53-species GRI 3.0 mechanism—is investigated in the Barlow & Frank flames *E* and *F*. It is found that the GRI mechanisms (GRI 2.11 and 3.0) and also the 12-step reduced mechanism obtained from GRI 2.11 all perform well (with the exception of GRI 3.0 over-predicting NO_x). However, simpler mechanisms, e.g., the 5-step mechanism and 16-species skeletal mechanisms, have deficiencies.

2 Future Plans

An immediate objective of future work is to provide more understanding of local extinction and re-ignition in non-premixed turbulent combustion. While our recent work has contributed to characterizing these phenomena (e.g., the degree of local extinction predicted by different models in different circumstances) we still do not have a mechanistic understanding of the critical processes. The results of PDF calculations will be appropriately interrogated and compared to existing and emerging experimental data to shed light on this issue.

3 Publications from DOE Research 2003-2005

1. R.W. Bilger, S.B. Pope, K.N.C. Bray and J.F. Driscoll (2005) “Paradigms in turbulent combustion research,” Proceedings of the Combustion Institute, **30**, 21-42. (Plenary lecture at the Thirtieth International Symposium on Combustion.)
2. R. Cao and S.B. Pope (2003) “Numerical integration of stochastic differential equations: weak second-order mid-point scheme for applications in the composition PDF method,” J. Comput. Phys., **185**, 194–212.
3. R. Cao and S.B. Pope, (2005) “The influence of chemical mechanisms on PDF calculations of non-premixed piloted jet flames”, Combustion and Flame (submitted).
4. B.J.D. Liu and S.B. Pope (2005) “The performance of *in situ* adaptive tabulation in computations of turbulent flames,” Combustion Theory & Modelling (to be published).
5. K. Liu, S.B. Pope and D.A. Caughey (2005) “Calculations of bluff-body stabilized flames using a joint PDF model with detailed chemistry,” Combustion and Flame **141**, 89-117.

6. M. Muradoglu, K. Liu and S.B. Pope (2003) "PDF modeling of a bluff-body stabilized turbulent flame," *Combustion and Flame*, **132**, 115–137.
7. S. B. Pope (2004) "Accessed compositions in turbulent reactive flows," *Flow, Turbulence and Combustion*, **72**, 219–243.
8. S.B. Pope (2004) "Gibbs function continuation for the stable computation of chemical equilibrium," *Combustion and Flame*, **139**, 222–226.
9. S.B. Pope (2004) "Advances in PDF methods for turbulent reactive flows," in *Advances in Turbulence X*, H.I. Andersson and P.-A. Krogstad (Eds.), CIMNE, pp. 529–536.
10. S.B. Pope (2005) "Computational modeling of turbulent flames," in *Computing the Future* (to be published).
11. Z. Ren and S.B. Pope (2004) "An investigation of the performance of turbulent mixing models." *Combustion and Flame*, **136**, 208–216.
12. Z. Ren and S.B. Pope (2004) "Entropy production and element conservation in the quasi-steady-state approximation." *Combustion and Flame*, **137**, 251–254.
13. Z. Ren and S.B. Pope (2005a) "The geometry of reaction trajectories and attracting manifolds in composition space," *Combustion Theory and Modeling* (submitted).
14. Z. Ren and S.B. Pope (2005b) "Species reconstruction using pre-image curves" *Proceeding of the Combustion Institute*, **30**, 1293-1300.
15. M.A. Singer and S.B. Pope (2004) "Exploiting ISAT to solve the equations of reacting flow," *Combustion Theory and Modeling*, **8**, 361–383.
16. M.A. Singer, S.B. Pope and H.N. Najm (2005). "Operator-splitting with ISAT to model reacting flow with detailed chemistry," *Combustion, Theory & Modeling* (submitted).

OPTICAL PROBES OF ATOMIC AND MOLECULAR DECAY PROCESSES

S.T. Pratt
Building 200, B-125
Argonne National Laboratory
9700 South Cass Avenue
Argonne, Illinois 60439

Telephone: (630) 252-4199

E-mail: stpratt@anl.gov

PROJECT SCOPE

Molecular photoionization and photodissociation dynamics can provide considerable insight into how energy and angular momentum flow among the electronic, vibrational, and rotational degrees of freedom in isolated, highly energized molecules. This project involves the study of these dynamics in small polyatomic molecules, with an emphasis on understanding the mechanisms of intramolecular energy flow and determining how these mechanisms influence decay rates and product branching ratios. The experimental approach combines double-resonance laser techniques, which are used to prepare selected highly excited species, with mass spectrometry, ion-imaging, and high-resolution photoelectron spectroscopy, which are used to characterize the decay of the selected species. Imaging studies of photodissociation fragments are also being performed using vacuum ultraviolet photoionization to characterize the effects of internal energy on the relative photoionization cross sections of selected hydrocarbon radicals.

RECENT PROGRESS

As discussed last year, we have been using a combination of ion imaging and vacuum ultraviolet (vuv) photoionization to characterize the effect of internal energy on the relative photoionization cross sections of free radicals. In our initial work, CH_3I and CF_3I were photodissociated and the photofragments were ionized by using 118 nm light produced by frequency tripling in Xe. In the images obtained by monitoring the I^+ , the features corresponding to the $\text{I}(^2\text{P}_{3/2})$ and $\text{I}^*(^2\text{P}_{1/2})$ channels were clearly resolved. Within each feature, sub-structure could be resolved that corresponded to the population of different vibrational levels of the molecular radical. The relative intensities of this sub-structure yields the vibrational branching fractions within the I and I^* channels. In the corresponding CH_3 and CF_3 images, similar vibrational structure could be observed. Here, however, the intensities are determined by the product of the vibrational branching fractions and the vibrationally dependent cross section. Thus, by comparing the iodine images with the CH_3 and CF_3 images, the vibrational dependence of the relative photoionization cross sections could be determined.

In CH_3I , photodissociation results in the excitation of the umbrella vibration of CH_3 . The ground states of both CH_3 and CH_3^+ are planar and the geometries are quite similar. As a result, photoionization is expected to favor the vertical transition, that is, the transition that preserves the vibrational quantum number of the neutral. Thus, the Franck-Condon envelopes are expected to be narrow and, at the photon energy employed (~ 0.6 eV above threshold), the photoionization cross section should depend only weakly on the vibrational energy of the ion. This is indeed observed in the experiments. In contrast, the ground state of CF_3 is pyramidal and that of CF_3^+ is planar. In this case, the Franck-Condon envelope is expected to be extremely broad with respect to the umbrella vibration. Photodissociation of CF_3I leads to the

excitation of a regular progression of vibrational levels spaced by $\sim 700\text{ cm}^{-1}$. This progression was originally thought to correspond to the umbrella vibration. However, earlier work by Clary¹ and more recent work by Bowman et al.² has shown that this progression corresponds instead to the CF symmetric stretch. Excitation of this mode is expected to have little effect on the relative photoionization cross section, and indeed, the analysis of the images shows only a weak dependence. By using different precursors and photodissociation wavelengths, it should be possible to modify the vibrational distributions within the radicals and to study the relative cross sections for different vibrational modes.

The experiments on the internal energy dependence of photoionization cross sections have been extended to the C_2H_5 , $n\text{-C}_3\text{H}_7$, $i\text{-C}_3\text{H}_7$, and C_3H_3 (propargyl) radicals. In each case, a suitable precursor was photodissociated and images of the molecular radical were recorded following single-photon ionization. In these experiments, difference-frequency mixing in Kr was used to generate tunable light between 9 and 10 eV. In some cases, single-photon ionization was also used to record the image of the other fragment, but for most of these species, resonant multiphoton ionization will be used to record the image of the radical partner. This will be particularly useful for cases in which the partner can be produced in two or more levels that cannot be resolved in the images. For example, in the photodissociation of $i\text{-C}_3\text{H}_7\text{I}$, the translational energy distributions in the I and I* channels are overlapped, making it difficult to sort out their relative contributions. This separation should be straightforward using resonant multiphoton ionization. It is also possible to use single-photon ionization to selectively detect I* by tuning below the I ionization threshold, and this has been done for some samples.

In larger radicals, the vibrational distribution within the radicals may not be always be resolved in the images. However, as shown by Gross et al.³ for the t-butyl radical, important information on the internal energy dependence of the relative photoionization cross sections can still be obtained. At sufficiently high internal energy (which need not be substantial in larger molecules) intramolecular vibrational energy redistribution (IVR) will be fast, and the energy will be effectively randomized among the vibrational degrees of freedom of the molecule. In this case, the transition between excitation of one or a few modes to complete energy randomization could appear as a significant change in the photoionization cross section vs. internal energy. While several quanta in a single vibration could result in a significant effect on the relative photoionization cross section, complete randomization will make the average population in any one vibrational mode relatively small, and thus the effect on the relative cross sections may also be small. In this case, it may be possible to use this approach to observe the onset of IVR as a change in the relative photoionization cross sections.

In collaboration with Butler's group at the University of Chicago, we have performed an additional study of the photodissociation of propargyl chloride at 193 nm. The translational energy distributions in the $\text{C}_3\text{H}_3 + \text{Cl}(^2\text{P}_{3/2})$ and $\text{C}_3\text{H}_3 + \text{Cl}^*(^2\text{P}_{1/2})$ channels were determined by using ion-imaging and two-photon resonant, three-photon ionization to detect the Cl and Cl* selectively. These distributions both contain a dominant fast peak that appears at essentially the same energy in both channels. In addition, the Cl distribution also contains a small feature at low translational energy. This feature was previously assigned to the HCl elimination channel, but the new experiments demonstrate conclusively that it comes from C-Cl bond fission. The translational energy distribution was also obtained for the sum of the Cl and Cl* channels by using translational spectroscopy and electron-impact ionization of the Cl and Cl* atoms. The relative weights of the separate Cl and Cl* translational energy distributions from the imaging experiments were then varied to provide the best fit to the summed distribution of the translational spectroscopy experiments. This procedure allows the extraction of the Cl and Cl* branching fractions

that could not be determined by either experiment alone, and the resulting values are 0.30 ± 0.05 and 0.70 ± 0.05 for the Cl and Cl* channels, respectively. Translational spectroscopy was also used to determine the translational energy distribution in the HCl elimination channel. We are currently investigating the use of single-photon ionization to record the corresponding C_3H_3 image, as this will provide an alternative method to determine the sum of the Cl and Cl* channels.

FUTURE PLANS

Our imaging studies of the internal-energy dependence of the relative photoionization cross sections of selected free radicals will continue into the coming year. Initial studies of the ethyl, n-propyl, i-propyl, and propargyl radicals will be completed, and a greater emphasis will be placed on mapping out the wavelength dependence of the relative photoionization cross sections of these and other radicals as a function of internal energy. A monochromator for separating the vuv light from the generating beams in the four-wave mixing schemes was delivered this past month. It is planned to incorporate this instrument into a flexible system that can be used with either the imaging apparatus or the magnetic bottle electron spectrometer. Use of this monochromator will eliminate interference from processes produced by the beams used to generate the vuv light, and will considerably reduce the background. As is known from our previous studies, this capability will be particularly important for achieving good resolution and reliable calibrations in vuv studies with the electron spectrometer. This capability will allow us to perform new vuv-visible double-resonance studies of vibrational and electronic autoionization that complement our earlier work in molecules such as NO_2 , H_2O , and NH_3 .

I will continue to collaborate with Christian Jungen (Laboratoire Aime Cotton) on theoretical models of vibrational autoionization in polyatomic molecules. In the past year, our work focused on linear triatomic molecules such as NO_2 and HCO. We worked to draw the connection between the quantum defect parameters, which are necessary to describe the structure and dynamics of high Rydberg states, and the Renner-Teller parameters, which can be extracted from spectroscopic analysis of low-lying Rydberg states. Ultimately, it is our goal to develop a general framework for understanding the role of vibronic interactions (including the Renner-Teller and Jahn-Teller interactions) in the decay dynamics in high Rydberg states.

REFERENCES

1. D. C. Clary, *J. Chem. Phys.* **84**, 4288 (1986).
2. J. M. Bowman, X. Huang, L. B. Harding, and S. Carter, Submitted to *Mol. Phys.*
3. R. L. Gross, X. Liu, and A. G. Suits, *Chem. Phys. Lett.* **362**, 229 (2002).

This work was supported by the U.S. Department of Energy, Office of Science, Office of Basic Energy Sciences, Division of Chemical Sciences, Geosciences, and Biosciences, under Contract W-31-109-Eng-38.

DOE-SPONSORED PUBLICATIONS SINCE 2003

1. F. Aguirre and S. T. Pratt
VELOCITY MAP IMAGING OF THE PHOTODISSOCIATION OF CF_3I : VIBRATIONAL ENERGY DEPENDENCE OF THE RECOIL ANISOTROPY
J. Chem. Phys., 118, 1175-1183 (2003).
2. F. Aguirre and S. T. Pratt
ION-IMAGING OF THE PHOTODISSOCIATION OF CF_3I^+
J. Chem. Phys., 118, 6318-6326 (2003).
3. P. Bell, F. Aguirre, E. R. Grant, and S. T. Pratt
MODE-DEPENDENT VIBRATIONAL AUTOIONIZATION OF NO_2
J. Chem. Phys., 119, 10146-10157 (2003).
4. F. Aguirre and S. T. Pratt
VELOCITY MAP IMAGING OF THE PHOTODISSOCIATION OF CF_3I^+ IN THE $\text{A} \leftarrow \text{X}$ BAND
J. Chem. Phys., 119, 9476-9486 (2003).
5. S. T. Pratt
PHOTOIONIZATION OF EXCITED STATES OF MOLECULES
Radiation Physics and Chemistry, 70, 435-352 (2004).
6. P. Bell, F. Aguirre, E. R. Grant, and S. T. Pratt
MODE-DEPENDENT VIBRATIONAL AUTOIONIZATION OF RYDBERG STATES OF NO_2 . II. COMPARING THE SYMMETRIC STRETCHING AND BENDING VIBRATIONS
J. Chem. Phys. 120, 2667-2676 (2004).
7. Patrice Bell, F. Aguirre, E. R. Grant, S. T. Pratt
STATE-SELECTIVE PRODUCTION OF VIBRATIONALLY EXCITED NO_2^+ BY DOUBLE-RESONANT PHOTOIONIZATION
J. Phys. Chem. A, 108, 9645-9651 (2004).
8. W. L. Glab and S. T. Pratt
ION ROTATIONAL DISTRIBUTIONS FOLLOWING VIBRATIONAL AUTOIONIZATION OF RYDBERG STATES OF WATER
J. Chem. Phys., 120, 8555-8566 (2004).
9. F. Aguirre and S. T. Pratt
PHOTOIONIZATION AND PHOTODISSOCIATION DYNAMICS OF THE $\text{B } ^1\Sigma_u^+$ AND $\text{C } ^1\Pi_u$ STATES OF H_2 AND D_2
J. Chem. Phys., 121, 9855-9864 (2004).
10. S. T. Pratt
VIBRATIONAL AUTOIONIZATION IN POLYATOMIC MOLECULES
Annual Rev. Phys. Chem., in press (2005).

Photoinitiated Reactions of Radicals and Diradicals in Molecular Beams

Hanna Reisler

Department of Chemistry, University of Southern California

Los Angeles, CA 90089-0482

reisler@usc.edu

Program Scope

Open shell species such as radicals and diradicals are central to reactive processes in combustion and environmental chemistry. Hydroxyalkyl radicals and carbenes are important, because cleavage of C-H and O-H bonds is implicated in reactions of atoms and radicals with alcohols and alkanes. For the alkoxy \leftrightarrow hydroxyalkyl and hydroxycarbene \leftrightarrow aldehyde structural isomers, competition between isomerization and dissociation on the ground potential energy surface (PES) may be significant. Our long-term goal is to investigate the dynamics of predissociation of free radicals for which multiple pathways, including molecular rearrangements, compete. The chosen systems are amenable to treatment by high-level theory. The detailed measurements on simple systems will serve as benchmarks that will be extended to larger systems in a homologous series.

Vibrational Spectroscopy and Dynamics of CH₂OH on the Ground and 3p_z States

The hydroxymethyl radical (CH₂OH) and its isomer, the methoxy radical (CH₃O), are important intermediates in hydrocarbon combustion and atmospheric processes.¹ According to *ab initio* calculations, CH₂OH requires $\sim 16,000$ cm⁻¹ to surmount the barrier to H + CH₂O(¹A₁) on the ground state, whereas the barrier to CH₃O decomposition has been determined experimentally to be only $\sim 11,000$ cm⁻¹ relative to the energy of CH₂OH. The height of the isomerization barrier (calculated at $\sim 14,000$ cm⁻¹) and vibrational energy flow will dictate whether CH₂OH can decompose via the isomerization route. Another intriguing question is how the low barriers to isomerization and dissociation affect anharmonicity and promote IVR.

Knowledge of the vibrational spectroscopy of the radical is prerequisite to understanding the competition between CH₂OH/CH₃O isomerization and direct O-H bond fission on the ground and excited PES's. Below we describe our continuing studies on the OH-stretch overtone spectroscopy of CH₂OH in its ground and Rydberg 3p_z states. We report preliminary results on predissociation on the ground PES, achieved by pumping directly the reaction coordinate – the OH stretch. The tight TS's for dissociation and isomerization bear on the subtle issue of the feasibility of high-overtone excitation when the O-H stretch is the reaction coordinate. We hypothesize that dynamical barriers would lend sufficient "molecular eigenstate" character to high overtone wave functions near the equilibrium geometry of CH₂OH.

The experiments are carried out in a differentially pumped chamber with time-of-flight mass selection, core-sampling for kinetic energy determination, and REMPI for detection of excited molecules and products. Three techniques are used in the spectroscopic studies: (i) depletion; (ii) double-resonance ionization; and (iii) photofragment spectroscopy. Depletion spectroscopy is exploited to locate vibrational transitions, with the origin band of the 2²A''(3p_z) \leftarrow 1²A' transition serving as the REMPI probe.² The population of the ground state is depleted whenever IR absorption to a vibrationally excited state takes place, thereby attenuating the CH₂OH⁺ ion signal. In double resonance ionization detected IR (DRID-IR) spectroscopy, the UV frequency is adjusted to excite CH₂OH in a selected rovibrational state to a Franck-Condon favorable vibronic level in the 3p_z Rydberg state and then further ionize it. Rovibrational spectra in the ground electronic state are recorded by tuning simultaneously the IR and UV laser frequencies and fixing their total energy at the peak of the probe transition in 3p_z. This scheme takes

advantage of the broad, homogeneous linewidth of rotational lines of the transition to the $3p_z$ state (>10 cm^{-1}). The major advantages of DRID-IR are its sensitivity and background-free nature. A prerequisite for its application is the existence of a vibronic resonance in the $3p_z$ Rydberg state. In cases when the excited radical dissociates, H-fragment photofragment detection by REMPI is used. Radiation at 121.6 nm, obtained in a tripling cell, excites the H fragment, and 365 nm radiation ionizes the excited atoms.

We also carried out vibrationally-mediated REMPI experiments in which the IR excitation is fixed at the transition peak and the UV laser wavelength is scanned. This allowed us to find the best resonances for DRID-IR spectroscopy, and also to identify vibronic levels in $3p_z$ and determine their lifetimes.

Overtone excitation and dissociation of CH_2OH in the ground PES

Although it is quite difficult to carry out overtone spectroscopy of reactive radicals in molecular beams, we were able to demonstrate good S/N in our previous studies on the fundamental and first overtone of the OH stretch of CH_2OH .³ Our results showed that IVR is not extensive when pumping $2\nu_1$. Excitation of $3\nu_1$ was first detected by depletion. Although the depletion depth was small ($\sim 10\%$ maximum), it served to identify the spectral position of the transition. In order to carry out DRID-IR spectroscopy, the 1_3^3 band of the $2^2A''(3p_z) \leftarrow 1^2A''$ transition was used as probe, because of the large enhancement it exhibited upon exciting $3\nu_1$ (Fig. 2). By scanning the pump laser while keeping the probe laser fixed at the 2+2 REMPI frequency of the 1_3^3 band, the overtone spectrum shown in Fig. 1(a) was obtained. The simulated spectrum is shown in Fig. 1(b).

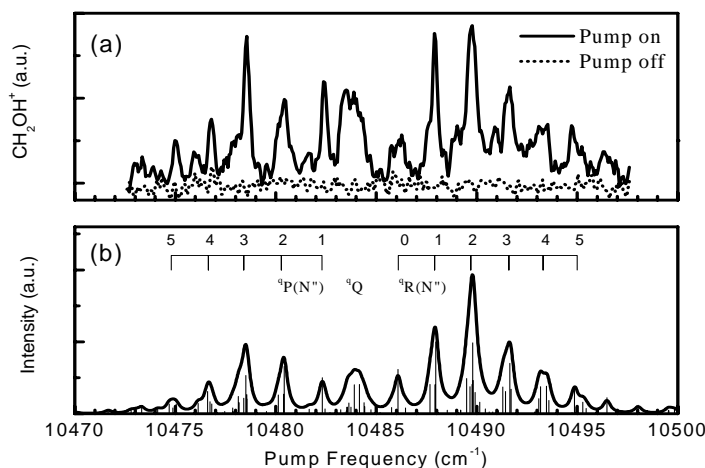


Fig. 1. (a) $3\nu_1$ overtone excitation spectrum of CH_2OH obtained by DRID-IR spectroscopy. (b) Simulation.

CH_2OH is a near-prolate symmetric top. The overtone transition spectra were simulated by using ground-state rotational constants derived from the equilibrium structure predicted by ab initio calculations, and varying the upper state constants A' , B' , and C' . The spectral lines were convoluted with a Voigt profile. The Lorentzian component of the Voigt profile, Γ_L , was optimized at 0.4 cm^{-1} , while the Gaussian component was fixed at the 0.1 cm^{-1} laser bandwidth. Note that the 0.4 ± 0.1 cm^{-1} linewidth is smaller than that for $2\nu_1$ (0.8 ± 0.1 cm^{-1}), indicating that IVR is not dominant, even at $\sim 10,000$ cm^{-1} .

The $3\nu_1$ transition is well described by an a -type band, similar to the fundamental and the first overtone transitions. The P, Q, and R branches are well resolved, while the fine rotational structures due to different quantum numbers of K_a and K_c are not resolvable.

Neither a depletion signal nor a DRID-IR spectrum could be detected in the region of the $4\nu_1$ transition above the noise level. However, an H-atom fragment signal is obtained when the pump laser is scanned in the same region, with the tripled probe laser fixed at the H-fragment 121.6 nm transition (Fig. 3). A

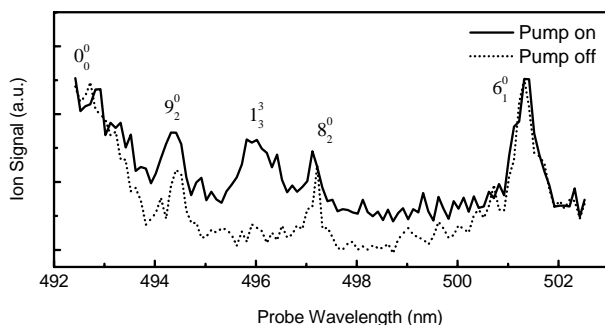


Fig. 2. Vibronic transitions to the $3p_z$ Rydberg state of CH_2OH obtained by double-resonance ionization.

similar spectrum, slightly blue shifted, is observed when using CD_2OH . Both spectra are well simulated as a -type bands. We scanned the pump laser frequency over the region between $3\nu_1$ and $4\nu_1$ but only $4\nu_1$ produced H-atom signals. The Lorentzian linewidths of the bands are 1.3 cm^{-1} , a width consistent with tunneling through the barrier and direct O-H bond fission. It is noteworthy that no D-fragments are observed, indicating that isomerization is not important. The characterization of the dissociation is in progress; preliminary results indicate that the maximum kinetic energy release of the H fragment is in agreement with one-photon dissociation at about $13,600\text{ cm}^{-1}$. The linewidth agrees qualitatively with tunneling through a barrier of $16,000\text{--}17,000\text{ cm}^{-1}$ height, although some contribution from IVR to the linewidth cannot be ruled out.

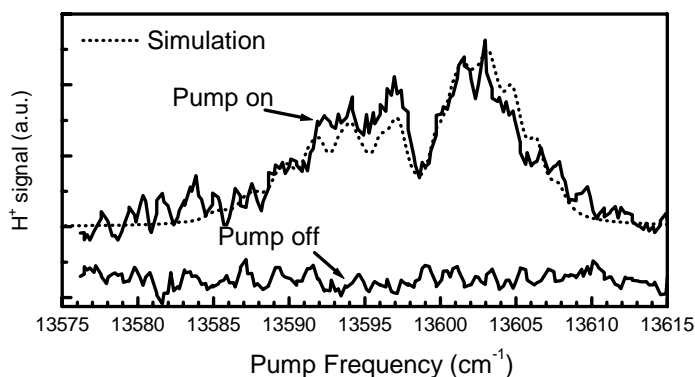


Fig. 3. Hydrogen fragment yield spectrum of CH_2OH obtained following $4\nu_1$ excitation.

Two additional observations are noteworthy. First, the frequency of $4\nu_1$ fits well on a Birge-Sponer plot describing the OH-stretch overtone excitation. The anharmonicity parameter is 91.4 cm^{-1} , not too different from that in methanol and hydroxylamine. Second, while the A rotational constants of the $1\nu_1$ - $3\nu_1$ levels are fairly constant at about 6.4 cm^{-1} , the corresponding value for $4\nu_1$ is smaller, 5.8 cm^{-1} , reflecting the longer bond length in the higher OH-stretch overtone. A summary is given in Table 1.

Table 1: Energies and linewidths of OH-stretch levels of the hydroxymethyl radical

Band		Energy (cm^{-1})	Linewidth (cm^{-1})
CH_2OH	$1\nu_1$	3674.8	< 0.4
	$2\nu_1$	7158.0	0.8
	$3\nu_1$	10484.2	0.4
	$4\nu_1$	13597.9	1.3
CD_2OH	$4\nu_1$	13616.6	1.3

Vibrationally Mediated Spectroscopy of the CH₂OH 2²A''(3p_z) ← 1²A'' transition

No vibronic bands involving the ν_1 - ν_3 modes were observed in the REMPI spectrum of CH₂OH via the 2²A''(3p_z) ← 1²A'' transition. This can be understood from the geometries of the radical in the ground and 3p_z states. The main geometry change in going from the neutral to the Rydberg state involves a 0.12 Å decrease in CO bond distance, consistent with a progression in the CO stretch (ν_6) observed in the REMPI spectrum. The OH and CH bond distances change by only 0.02 and 0.01 Å, respectively. Vibrational levels of these modes in the 3p_z Rydberg state can be accessed, however, by prior vibrational excitation in the ground state. Using vibrationally mediated ionization or photodissociation followed by H-fragment detection, we identified several bands: the 1₁¹ and 1₂² and 1₃³ bands, as well as the 3₁⁰, 2₁⁰, 6₀², 4₁², 6₁⁰, 8₂⁰ and 9₂⁰ bands. The 1₂² and 1₃³ bands, at 6639 and 10,040 cm⁻¹, respectively, are considerably broader than the others, with homogenous widths of >50 cm⁻¹ compared to ~ 10 cm⁻¹ for the lower-lying bands (an example is shown in Fig. 2). This increase in predissociation rate is most likely a consequence of increasing coupling matrix elements to lower lying electronic states. Note that several "hot bands" are evident in Fig. 2,¹ but only the 1₃³ band requires prior IR excitation. The others are hot bands of low frequency levels that persist even in the molecular beam. From the distinct vibronic structures observed up to 3ν₁ of 3p_z, we deduce that 3p_z is bound by at least 10,000 cm⁻¹.

Dissociation from different vibronic levels in the 3p_z state of CH₂OD was also examined.⁴ We did not detect state-specific effects, reinforcing our conclusion that the evolution of the excited 3p_z state towards dissociation proceeds through sequential surface crossings to lower-lying states. We found, however, broad D-fragment kinetic energy distributions, implying that the CH₂O fragments are internally "hot". In fact, when CH₂O has sufficient energy, slow H atoms from H + HCO appear in the kinetic energy distributions. The same is true for HCOD, which gives rise to slow D and H products via direct dissociation and/or isomerization to CHDO. The high internal excitation of the products may be related to the out-of-plane motions required to couple the 2²A''(3p_z) state to lower Rydberg states of A' symmetry.

Future Work

Experimental work is in progress on the predissociation of CH₂OH following OH-stretch overtone excitation, to explore direct dissociation and/or isomerization pathways. We also plan to extend this work to the electronic and vibrational spectroscopy of higher hydroxyalkyl radicals.

References

1. Johnson, R. D.; Hudgens, J. W. *J. Phys. Chem.*, **100**, 19874 (1996)
2. Aristov, V.; Conroy, D.; Reisler, H. *Chem. Phys. Lett.*, **318**, 393 (2000).
3. Lin Feng, Jie Wei, and Hanna Reisler, *J. Phys. Chem. A*, **108**, 7903 (2004).
4. L. Feng and H. Reisler, *J. Phys. Chem. A.*, **108** (45): 9847-9852 (2004).

Publications, 2003-2005

- O-D bond dissociation from the 3s state of deuterated hydroxymethyl radical (CH₂OD), L. Feng, A.V. Demyanenko, and H. Reisler, *J. Chem. Phys.* **118**(21), 9623-9628 (2003).
- Competitive C-H and O-D bond fission channels in the UV photodissociation of the deuterated hydroxymethyl radical (CH₂OD), L. Feng, A. V. Demyanenko, and H. Reisler, *J. Chem. Phys.* **120**, 6524-6530 (2004).
- Rotationally resolved infrared spectroscopy of the hydroxymethyl radical (CH₂OH), L. Feng, J. Wei, and H. Reisler, *J. Phys. Chem. A*, **108**, 7903 (2004).
- Photodissociation of the 3p_z state of the hydroxymethyl radical (CH₂OH): CH₂O and HCOH products, L. Feng and H. Reisler, *J. Phys. Chem. A.*, **108** (45): 9847-9852 (2004).

High Accuracy Calculation of Electronic Structure, Molecular Bonding and Potential Energy Surfaces

Klaus Ruedenberg and Mark S. Gordon

Ames Laboratory USDOE, Iowa State University, Ames, Iowa, 50011
ruedenberg@iastate.edu

Scope

Theoretical predictions of reaction and activation energies with chemical accuracy (~ 1 kcal/mol) require the inclusion of a high degree of dynamic correlation in electronic wavefunctions. This has not been possible for configuration interaction (CI) calculations so far, since the needed computational resources greatly exceeded existing capabilities. Only during the last decade, have coupled-cluster strategies been refined to achieve this goal for molecules in their equilibrium conformations. But this has not yet been possible for systems with strongly multi-configurational zeroth-order reference wavefunction, as is the case, e.g., at kinetically important transition states of many combustion reactions. The CI developments reported here open a new avenue to overcome this difficulty.

Some Recent Results

Assume an appropriate set of ordered molecular orbitals for a given system (e.g. natural orbitals from a SD-CI calculation) and an expression of the wavefunction as the sum of successive excitations from a (single- or multi-determinant) reference function into correlating molecular orbitals. Denote the *incremental* contribution from the set of x -tuple excitations to the correlation energy by $\Delta E(x)$. A sequence of CI calculations is now performed, *each of which using only a limited number, say m , of the total number M of correlating orbitals*. Denote the incremental correlation energy contribution of the x -tuple excitations for such a calculation as $\Delta E(x|m)$. Figure 1 illustrates how the $\Delta E(x|m)$ converge to $\Delta E(x)$ as $m \rightarrow M$, in the case of a triple-zeta calculation for water. The analysis of many systems has shown that, considering $\Delta E(x|m)$ as a function of m for fixed x , linear relationships of the type $\Delta E(x|m) = a_x \Delta E(x-2|m) + b_x$ are valid with great accuracy when $x > 3$. Figure 2 illustrates such relations in the case of water. On this basis, an extrapolation procedure has been developed by means of which full CI energies can be accurately obtained with a greatly reduced computational effort.

Application of the method to C_2 , N_2 , O_2 , F_2 , for double-, triple- and quadruple basis sets, complemented by complete basis set extrapolations as well as relativistic corrections, has yielded binding energies for these molecules that agree with the experimental values within chemical accuracy, as exhibited in the following table:

Calculated and experimental binding energies for C_2 , N_2 , O_2 , F_2

Energies in kcal/mol	$2C \rightarrow C_2$	$2N \rightarrow N_2$	$2O \rightarrow O_2$	$2F \rightarrow F_2$
Experiment	-145.4	-224.9	-117.9	-36.95
Theory	-144.3	-224.9	-117.1	-36.6
Actual max # det's	6.4×10^7	3.2×10^7	2×10^8	1.1×10^8
# det's in full CI	4×10^{12}	2×10^{15}	2×10^{17}	4×10^{19}

The table also lists the number of determinants that would be required in the full configuration space as well as the maximum number of determinants that were needed for the largest CI calculation that had to be actually performed to get the FCI energies.

The method also works for systems with multi-determinantal zeroth-order reference functions. We were therefore able to calculate the first accurate theoretical potential energy curve for the dissociation of F_2 . Figure 3 exhibits the curves obtained with double-zeta, triple-zeta and quadruple-zeta basis sets as well as for the complete basis limit. Figure 4, shows the curve for the triple-zeta basis together with the curve that is obtained by coupled-cluster calculations of the CCSD(T) type for the same basis.

Future Work

The vibrational levels of F_2 will be calculated and compared with the fully known experimental spectrum of 22 lines. The method will be applied to the determination and study of the reaction paths of other dissociations and reactions.

Publications in 2003, 2004, 2005

A MCSCF Method for Ground and Excited States Based on Full Optimizations of Successive Jacobi Rotations

J. Ivanic and K. Ruedenberg

J. Computational Chemistry **24**, 1250-1262 (2003)

Split-Localized Orbitals Can Yield Stronger Configuration Interaction Convergence than Natural Orbitals.

L. Bytautas, J. Ivanic, K. Ruedenberg

J. Chem. Phys. **119**, 8217 (2003)

Molecule Intrinsic Minimal Basis Sets. I. Exact Resolution of Ab-Initio Optimized Molecular Orbitals in terms of Deformed Atomic Minimal-Basis Orbitals.

W.C. Lu, C.Z. Wang, M.W. Schmidt, L. Bytautas, K.M. Ho, K. Ruedenberg

J. Chem. Phys. **120**, 2629-2637 (2004)

Molecule Intrinsic Minimal Basis Sets. II. Bonding Analyses for Si_4H_6 and Si_2 to Si_{10} .

W. C. Lu, C. Z. Wang, M. W. Schmidt, L. Bytautas, K. M. Ho, K. Ruedenberg

J. Chem. Phys. **120**, 2638-2651 (2004)

Exact Representation of Electronic Structures in Crystals in Terms of Highly Localized Quasiatomic Minimal Basis Orbitals.

W. C. Lu, C. Z. Wang, T. L. Chan, K. Ruedenberg, and K. M. Ho

Phys. Rev. B **70**, 04110(R) (2004)

Correlation Energy Extrapolation Through Intrinsic Scaling. I. Method.

L. Bytautas and K. Ruedenberg

J. Chem. Phys. **121**, 10905 (2004)

Correlation Energy Extrapolation Through Intrinsic Scaling II. Nitrogen and Water.

L. Bytautas and K. Ruedenberg

J. Chem. Phys., **121**, 10919 (2004)

Correlation Energy Extrapolation Through Intrinsic Scaling III. Compact Wavefunctions.

L. Bytautas and K. Ruedenberg

J. Chem. Phys. **121**, 10852 (2004)

Correlation Energy Extrapolation Through Intrinsic Scaling. IV. Accurate Binding Energies of the Homonuclear Diatomic Molecules C_2 , N_2 , O_2 and F_2 .

L. Bytautas and K. Ruedenberg

J. Chem. Phys. **122**, 154110 (2005)

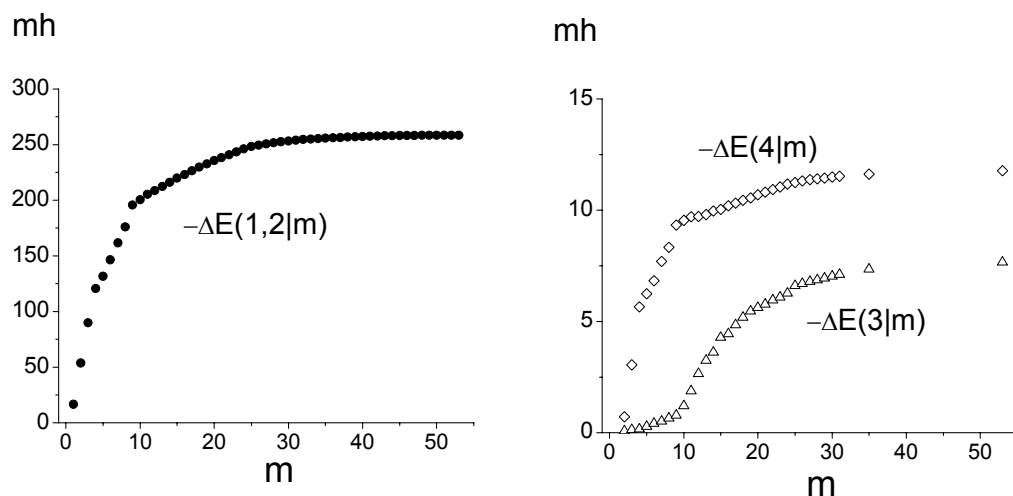


Figure 1. Convergence of the incremental correlation energy contributions $\Delta E(x|m)$ to their full values $\Delta E(x)=\Delta E(x|M)$ for $x=2,3,4$ in the water molecule (cc-pVTZ basis, $M=53$).

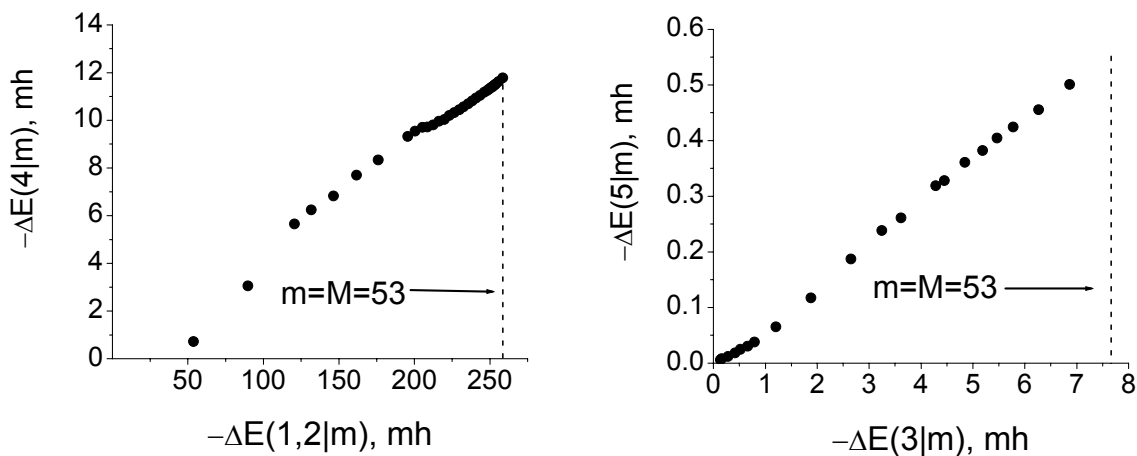


Figure 2. Illustration of the linear relationships $\Delta E(x|m)=a_x \Delta E(x-2|m)+b_x$ for the contributions of the excitations $x=4,5$ in the water molecule (cc-pVTZ basis).

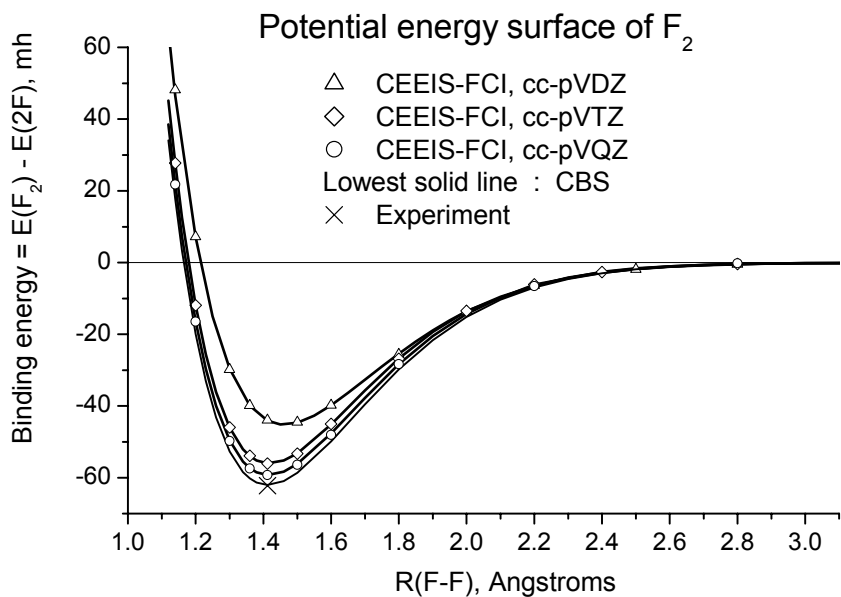


Figure 3. The theoretically calculated accurate dissociation curve of F_2 . CEEIS=Correlation energy extrapolation by intrinsic scaling = present method.

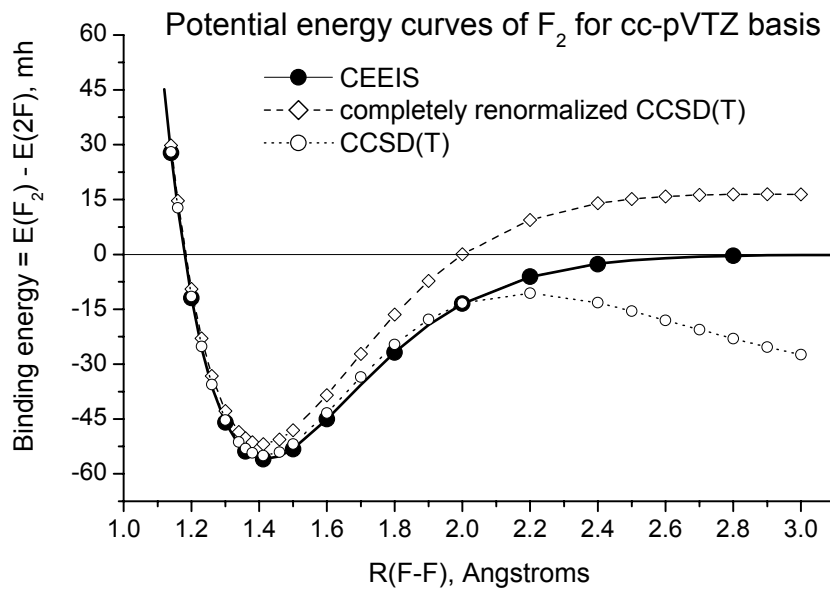


Figure 4. Comparison of the potential energy curve obtained by coupled-cluster calculations of F_2 with the actual curve.

Active Thermochemical Tables – Thermochemistry for the 21st Century

Branko Ruscic

Chemistry Division, Argonne National Laboratory, 9700 South Cass Avenue, Argonne, IL 60439
ruscic@anl.gov

Program Scope

The *spiritus movens* of this program is the need to provide the chemical community with accurate and reliable thermochemical, spectroscopic and structural information on chemical species that are relevant in energy-producing processes, such as combustion, or play prominent roles in the associated post-combustion environmental chemistry, thus contributing to the global comprehension of the underlying chemical reactions and/or providing benchmark values for test and development of advanced theoretical approaches. The program has recently developed a novel approach that aims to optimally extract the knowledge content from thermochemically relevant measurements and hence produce not only *the best currently available* thermochemical values for the target species, but also provide *critical tests of new experimental or theoretical data*, as well as develop *pointers to future determinations that will most efficiently improve the thermochemical knowledge base*. The experimental portion of this program uses photoionization mass spectrometry and related methods to study ephemeral species that are produced *in situ* using various suitable techniques. The effort of this program is coordinated with related experimental and theoretical efforts within the Argonne Chemical Dynamics Group to provide a broad perspective of this area of science.

Recent Progress

Development of Active Thermochemical Tables and the Core (Argonne) Thermochemical Network

Active Thermochemical Tables (ATcT) are a new paradigm of how to derive accurate, reliable, and internally consistent thermochemical values, and are rapidly becoming the archetypal approach to thermochemistry for the 21st century. The current development of ATcT has several related components: The conceptual advances in the underlying approach to thermochemistry, and the construction and evaluation of the Core (Argonne) Thermochemical Network together with the resulting delivery of new thermochemistry for stable and ephemeral species are a direct product of this project (funded by DOE BES), while the accompanying software development involved in bringing to life a practical instance of ATcT as a web-service was highly leveraged by an additional funding source (DOE MICS).

The underpinning philosophy and the pertinent details of the ATcT approach have been given elsewhere and hence will not be repeated here [see, for example, last year's abstract for the DOE/BES Combustion Research Meeting; for a more detailed description please consult Ruscic et al., *J. Phys. Chem. A*, **108**, 9979, (2004); for a succinct description see B. Ruscic, *Active Thermochemical Tables*, in: *2004 Yearbook of Science and Technology*, McGraw-Hill, 2004, pp 3-7].

Though we have a substantial list of additional capabilities and features that we would like to implement in ATcT in the foreseeable future, the current version (1.25.16) contains all the essential elements needed to manipulate and solve Thermochemical Networks (TNs). Hence, during the past year, our focus has gradually shifted on building and enlarging the essential TN that aims to produce new thermochemistry for species of interest in combustion and post-combustion processes. Establishing a good basic *ab ovo* (i.e. non-localized) TN that defines and properly pedigrees the cornerstone chemical species (which act as network hubs in the grand scheme implied by the manifold of inherent thermochemical dependencies) is an important step, which then subsequently allows convenient insertion of additional species that may be considered somewhat more exotic (i.e. less well studied) but nevertheless play crucial roles in the intricate chemical mechanisms describing complex environments, such as flames or the atmosphere, and are needed for their predictive modeling. As a result of the intensified effort over the last year, the number of species currently treated by ATcT has doubled, while the number of determinations that are considered in the TN has tripled. The central TN, a.k.a. Core (Argonne) Thermochemical Network, currently (as of ver. 1.049) encompasses nearly 2500 thermochemically-relevant determinations, defining roughly 500 thermochemically distinct chemical species and producing definitive thermochemistry for many of these moieties. At least from the perspective of future modeling combustion and post-combustion atmospheric processes, this is a very significant leap forward.

The construction and progressive expansion of the Core TN has also offered the much needed opportunity to extensively test and evaluate the response and behavior of ATcT and – in particular – to critically evaluate the soundness of the underlying strategies that are currently used in the statistical analysis of the TN (and hence isolation and treatment of “optimistic” uncertainties). The scope of these ATcT tests was additionally expanded by implementing the capability of performing an independent check of the resulting uncertainties (via a Monte Carlo analysis, including a Latin Hypercube-based strategy). To our complete delight, in every case checked so far, the Monte Carlo analysis has always completely corroborated the computed ATcT uncertainties, hence confirming that the significantly tighter uncertainties associated with the newly derived ATcT thermochemical values are correct. Though the Latin Hypercube strategy is quite efficient, the Monte Carlo analysis is rather CPU-intensive for a TN as large as the present one. Hence, we are now carrying out this type of additional check only occasionally, rather than routinely.

We have also implemented in ATcT the capability to perform a sensitivity analysis, an essential ingredient in the discovery of pointers to “best” new experiments/computations. Besides helping to identify pointers, inspection of the sensitivity matrix offers very interesting (and occasionally rather unexpected) insights into the intricate and subtle nature of thermochemical interdependencies. To mention just one example of such an unexpected detail: The primary contributors to the derived enthalpy of formation of liquid and gas H₂O are, as one would fully expect, the various calorimetric determinations of the combustion of H₂. However, proceeding down the hierarchy of importance, one is surprised to find that an inherent (though admittedly quite small) contributor to the value and uncertainty of the enthalpy of formation of H₂O is the calorimetric determination of the combustion of graphite leading to the enthalpy of formation of CO₂! The dependency goes the other way as well, and the calorimetric determination of H₂O contributes ever so slightly to the final value for CO₂. With a further analysis, the underlying reasons eventually become more transparent: Calorimetric determinations of hydrocarbons (and their derivatives) via combustion produce (and hence relate to) both H₂O and CO₂. The relevant hydrocarbon species are cross-correlated by other determinations, e.g. hydrogenation reactions leading from ethylene to ethane, etc. Thus, the TN inherently contains various thermochemical cycles that proceed through two (or more) hydrocarbon moieties, and the net overall chemical reactions described by such roundabout cycles are tantamount to additional indirect calorimetric determinations of H₂O and/or CO₂. Given the cumulative experimental uncertainties involved in these cycles, none of them are producing *per se* an identifiable impact either on the enthalpy of formation of H₂O or CO₂. However, once the number of these cycles reaches a critical mass within the TN, the interdependence of H₂O and CO₂ rises above the numerical noise level and becomes identifiable both in the sensitivity matrix and in the variance-covariance matrix.

Another novel aspect of ATcT is that the TN can happily commingle experimental and theoretical determinations. This ability is gaining importance as very high quality electronic structure methods are becoming more common. We are now routinely performing G3-type computations for every new species inserted in the TN, and are including other (even higher) level computations, such as *Wn*, FPA, etc., if available. However, successful incorporation of theoretical data in the TN critically depends on the assignment of *realistic uncertainty estimates*. Unfortunately, these are explicitly available only in a precious few cases. In most instances, the computations are published either with no uncertainties or imply and/or explicitly quote MAD (Mean Absolute Deviation) as the uncertainty for the theoretical enthalpies. While MAD, as determined for a given computational method using a test set of benchmark values is a popular (and indeed useful) measure of fidelity of theoretical computations, equating it with the expected uncertainty for the computed enthalpies becomes an altogether different proposition. In fact, in most (but not all!) papers where MAD is first evaluated for a particular method, no such claims are made. However, subsequent papers (sometimes by the same authors) tend to proliferate MAD as *the* uncertainty of the method, while, in fact, it *underestimates by a factor of at least 2 – 3* the normally expected uncertainty in thermochemistry, which should provide the best estimate of *the 95% confidence interval*. Using the 95% confidence interval as the uncertainty, after including random and all conceivable systematic errors, is the *de facto standard in thermochemistry*, introduced originally by Rossini [*J. Res. NBS* **6**, 1 (1931)] and followed by virtually all thermochemical compilation, including CODATA, JANAF, Gurvich et al., etc. The argument for the mentioned underestimation factors of MAD can be made very simple: For an infinite sample, the 95% confidence interval is twice the standard deviation. MAD is typically moderately to significantly smaller than the standard deviation. If, in fact, the mean happens to be close to the median of the absolute deviations, the statistical factor for an infinite sample is

essentially 3. These factors only grow larger as the size and/or representability of the test set decreases. While one can, in a pinch, simply use MAD amplified by the appropriate factor as a rough guide, literature unfortunately abounds with biased comparisons of theoretical and experimental enthalpies that use MAD as the uncertainty for the former and the conventional 95% confidence interval for the latter!

The Core (Argonne) TN has now produced a significant number of new and/or substantially improved thermochemical values, providing in many cases definitive values that are unlikely to significantly change anytime soon. Since the dominant portion of the current TN is close to the thermochemical basis (the present strategy being focused on establishing the important network “hubs”), most of the affected species are of quite fundamental importance. A subset of these species that now have new and/or significantly revised values belongs to the even more select category of “key” species (as defined by CODATA). The ability to have a significant say in this arena is an accomplishment that we are particularly proud of, since CODATA “key” values are notorious for being impossible to improve on. A small sample of such values has been published as a convincing illustration of the power of the TN approach in the introductory paper on ATcT [J. Phys. Chem. A, **108**, 9979, (2004)]. In most cases the uncertainties for the “key” values have been lowered by a significant (and sometimes by a spectacular) factor and the values accordingly refined, thus helping to substantially improve other dependent values across the TN. In many cases (“key” or otherwise) the traditional value is outside the uncertainty of the new ATcT value (though the ATcT value is often contained within the larger uncertainty of the traditional value). In one quite important “key” species (C in gas phase, used by all electronic structure calculations that develop enthalpies of formation via atomization energies), the new value and the accepted CODATA value currently just barely overlap within the combined uncertainties.

We are currently in the process of writing up several sequel papers that will report the newly derived ATcT thermochemistry for various species (grouped in convenient sets amenable to congruent and correlated scientific discussion). In the interim, the latest unpublished thermochemical values for any species currently contained in the Core (Argonne) TN (together with referencing instructions that provide links to archived sets of values) are available (and quotable) as private communication(s) by contacting the PI via e-mail.

Other progress

As part of the IUPAC Task Group on Thermochemistry of Radicals (where the Argonne effort is central to the success of the project), we are in the process of performing critical and meticulous evaluations of the thermochemistry of a number of small radicals important in combustion and atmospheric chemistry. The resulting “IUPAC recommended values” are being published in a series of papers. We have an ongoing collaboration with C.-Y. Ng (U. C. Davis) and T. Baer (UNC Chapel Hill) to perform a number of thermochemically relevant photoionization measurements at the Chemical Dynamics Beamline at ALS Berkeley, which are driven by deficiencies or inconsistencies in some basic thermochemical quantities that are being uncovered as we are building the Core (Argonne) Thermochemical Network. We started a collaboration with K. Ervin (UN Reno) targeting the implementation of gas-phase acidity measurements in the Core TN. We have also an ongoing collaboration with the group of T. Turany (Eötvös U. Budapest) on extending the ATcT approach to Monte Carlo analysis of reaction mechanisms, and with A. Csaszar (Eötvös U. Budapest) and J. Stanton and J. Boggs (U. Texas Austin) on computing critical thermochemistry for small radicals via state-of-the-art theory (where the selection of targets is via ATcT).

Future Plans

Future plans of this program pivot around further developments and use of Active Thermochemical Tables, coupled to laboratory experimental investigation of radicals and transient species that are intimately related to combustion processes, such as those that potentially define the initial attack of O₂ on hydrocarbon moieties during combustion, as well as other ephemeral species that are implicated in subsequent atmospheric chemistry (particularly hydrocarbon moieties that contain oxygen and/or nitrogen). In collaboration with theorists in the Argonne Chemical Dynamics Group, we plan on determining in quantitative ways the effects of hindered rotations and soft and/or coupled internal modes on thermochemical quantities of both transient and stable species. We also intend to further enhance our fitting methods for accurate determination of fragment appearance energies from photoionization measurements.

This work is supported by the U.S. Department of Energy, Office of Basic Energy Sciences, Division of Chemical Sciences, Geosciences, and Biosciences, under Contract W-31-109-ENG-38. The software development of Active Tables was partly supported by the Office of Advanced Scientific Computing Research, Division of Mathematical, Information and Computational Sciences, under the same Contract.

Publications resulting from DOE sponsored research (2002 -)

- *Theoretical Investigation of the Transition States Leading to HCl Elimination in 2-Chloropropene*, B. Parsons, L. Butler, and B. Ruscic, *Mol. Phys.* **100**, 865-874 (2002)
- *On the Enthalpy of Formation of Hydroxyl Radical and Gas-Phase Bond-Dissociation Energies of Water and Hydroxyl*, B. Ruscic, A. F. Wagner, L. B. Harding, R. L. Asher, D. Feller, D. A. Dixon, K. A. Peterson, Y. Song, X. Qian, C. Y. Ng, J. Liu, W. Chen, and D. W. Schwenke, *J. Phys. Chem. A* **106**, 2727-2747 (2002).
- *Toward Hartree-Fock and Density Functional Complete Basis-Set-Predicted NMR Parameters*, T. Kupka, B. Ruscic, and R. E. Botto, *J. Phys. Chem. A* **106**, 10396-10407 (2002)
- *A Grid Service-Based Active Thermochemical Table Framework*, G. von Laszewski, B. Ruscic, P. Wagstrom, S. Krishnan, K. Amin, S. Nijsure, S. Bittner, R. Pinzon, J. C. Hewson, M. L. Morton, M. Minkoff, and A. F. Wagner, *Lecture Notes in Computer Science* **2536**, Springer, Berlin-Heidelberg (2002), pp 25-38
- *Hartree-Fock and Density Functional Complete Basis Set (CBS) Predicted Nuclear Shielding Anisotropy and Shielding Tensor Components*, T. Kupka, B. Ruscic, and R. E. Botto, *Solid State Nucl. Mag. Res.* **23**, 145-167 (2003)
- *A Framework for Building Scientific Knowledge Grids Applied to Thermochemical Tables*, G. von Laszewski, B. Ruscic, K. Amin, P. Wagstrom, S. Krishnan, and S. Nijsure, *Int. J. High Perform. Comp. Applicat.* **17**, 431-447 (2003)
- *A Divertimento in Thermochemistry: From Photoionization Spectroscopy of Radicals to Active Tables*, B. Ruscic, *Abstr. Pap. 225th ACS National Meeting*, March 23-27, 2003, New Orleans, LA, PHYS-058 (2003)
- *Radical Photoionization Studies with VUV Synchrotron Radiation*, C. Nicolas, M. L. Morton, D. S. Peterka, M. Ahmed, L. Poisson, B. Ruscic, C.-Y. Ng, X. Tang, and T. Zhang, *Abstr. Pap. 225th ACS National Meeting*, March 23-27, 2003, New Orleans, LA, PHYS-269 (2003)
- *Further Refinements of the Bond Dissociation Energy in Water and Hydroxyl Radical Using the Active Thermochemical Table Approach*, B. Ruscic, R. E. Pinzon, M. L. Morton, B. Wang, A. F. Wagner, G. von Laszewski, S. G. Nijsure, K. A. Amin, S. J. Bittner, and M. Minkoff, *Proc. 58th Int. Symp. Mol. Spectrosc.*, June 16-20, 2003, Columbus, OH (2003)
- *Metadata in the Collaboratory for Multi-Scale Chemical Science*, C. Pancerella, J. D. Myers, T. C. Allison, K. Amin, S. Bittner, B. Didier, M. Frenklach, W. H. Green, Jr., Y.-L. Ho, J. Hewson, W. Koegler, C. Lansing, D. Leahy, M. Lee, R. McCoy, M. Minkoff, S. Nijsure, G. von Laszewski, D. Montoya, R. Pinzon, W. Pitz, L. Rahn, B. Ruscic, K. Schuchardt, E. Stephan, A. Wagner, B. Wang, T. Windus, L. Xu, C. Yang (full peer reviewed paper for Dublin Core Conf. DC-2003, Sept 28 - Oct. 2, Seattle, WA, published electronically at http://www.siderean.com/dc2003/401_Paper67.pdf)
- *Refinements of the Bond Dissociation Energy of Carbon Monoxide and of the Enthalpy of Formation of Carbon Atom in Gas Phase Using the Active Thermochemical Tables Approach*, B. Ruscic, R. E. Pinzon, M. L. Morton, A. G. Csaszar, J. F. Stanton, M. Kallay, and G. von Laszewski, *Proc. 59th Int. Symp. Mol. Spectrosc.*, June 21-25, 2004, Columbus, OH (2004)
- *From Theoretical Calculations to Experimental Assignment of NMR Spectra*, T. J. Kupka, B. Ruscic, R. E. Botto, L. Curtiss, G. Pasterna, P. Lodowski, and W. Szeja, *Proc. 36th Great Lakes Regional Meeting Amer. Chem. Soc.*, October 17-20, 2004, Peoria, IL
- *Active Thermochemical Tables*, B. Ruscic, in: *2005 Yearbook of Science and Technology* (yearly update to *Encyclopedia of Science and Technology*), McGraw-Hill, New York (2004), pp 3-7
- *Introduction to Active Thermochemical Tables: Several "Key" Enthalpies of Formation Revisited*, B. Ruscic, R. E. Pinzon, M. L. Morton, G. von Laszewski, S. J. Bittner, S. G. Nijsure, K. A. Amin, M. Minkoff, and A. F. Wagner, *J. Phys. Chem. A* **108**, 9979 (2004).
- *IUPAC Critical Evaluation of Thermochemical Properties of Selected Radicals: Part I*, B. Ruscic, J. E. Boggs, A. Burcat, A. G. Csaszar, J. Demaison, R. Janoschek, J. M. L. Martin, M. L. Morton, M. J. Rossi, J. F. Stanton, P. G. Szalay, P. R. Westmoreland, F. Zabel, and T. Berces, *J. Phys. Chem. Ref. Data* (in press)

Theoretical Studies of Elementary Hydrocarbon Species and their Reactions

Henry F. Schaefer III

Center for Computational Chemistry, University of Georgia

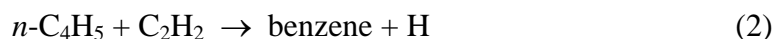
Athens, GA, 30602-2525

Email: hfs@uga.edu

(706)542-2067

Unraveling the complex processes involved in the pyrolysis of aliphatic fuels and the formation of soot is imperative for the development of more efficient internal combustion technologies and the reduction of harmful emissions. The elucidation of the mechanism and associated kinetics of the formation of soot, and more specifically polycyclic aromatic hydrocarbon (PAH) intermediates, has been a primary focus of combustion research in recent years. Some PAHs have been shown to be mutagenic and carcinogenic, elevating the need to minimize their emission into the environment. Vital to the understanding of PAH formation is the mechanism for formation of the first aromatic ring, commonly believed to be the rate-limiting step in the production of larger aromatics.

There has been much debate regarding even-carbon-atom reactions for assembling the first aromatic ring, with particular focus on the addition of acetylene to n -C₄H₃ and n -C₄H₅ radicals:



We have approached several critical aspects of the C₄H₃/C₄H₅ problem using state-of-the-art theoretical methods. Accurate isomeric energy differences and standard enthalpies of formation for disputed intermediates in soot formation, C₄H₃ and C₄H₅, have been determined through systematic extrapolations of *ab initio* energies. Electron correlation has been included through second-order Z-averaged perturbation theory (ZAPT2), and spin-restricted, open-shell coupled cluster methods through triple excitations [ROCCSD, ROCCSD(T), and ROCCSDT] utilizing the correlation-consistent hierarchy of basis sets, cc-pVXZ ($X = \text{D, T, Q, 5, and 6}$), followed by extrapolations to the complete basis set limit via the focal point method of Allen and co-workers. Reference geometries were fully optimized at the ROCCSD(T) level with a TZ(2d1f,2p1d) basis set.

Our analysis finds that the resonance-stabilized *i*-C₄H₃ and *i*-C₄H₅ isomers lie 11.8 and 10.7 kcal mol⁻¹ below *E-n*-C₄H₃ and *E-n*-C₄H₅, respectively, several kcal mol⁻¹ (more, less) than reported in recent (diffusion Monte Carlo, B3LYP density-functional) studies. Moreover, in these systems Gaussian-3 (G3) theory suffers from large spin contamination in electronic wavefunctions, poor reference geometries, and anomalous vibrational frequencies, but fortuitous cancellation of these sizable errors leads to isomerization energies apparently accurate to 1 kcal mol⁻¹. Using focal-point extrapolations for isodesmic reactions, we determine the enthalpies of formation ($\Delta_f H_0^\circ$) for *i*-C₄H₃, *Z-n*-C₄H₃, *E-n*-C₄H₃, *i*-C₄H₅, *Z-n*-C₄H₅, and *E-n*-C₄H₅ to be 119.0, 130.8, 130.8, 78.4, 89.7, and 89.1 kcal mol⁻¹, respectively. These definitive values remove any remaining uncertainty surrounding the thermochemistry of these isomers in combustion models, allowing for better assessment of whether even-carbon pathways contribute to soot formation.

Many studies have shown the importance of propargyl radical reaction routes in the formation of large PAHs and soot. We have recently completed a long-term effort to obtain a definitive quartic force field for high-resolution rovibrational spectroscopy of the propargyl radical. Via extrapolation of both cc-pVXZ and aug-cc-pVXZ series ($X = T, Q, 5$), as well as comparison with results from corresponding atomic natural orbital (ANO) computations, we have converged upon the complete basis set (CBS) limit quadratic force field at the highly-correlated CCSD(T) level. The full quartic force field in internal coordinates has also been computed with CCSD(T) theory and basis sets of aug-cc-pVTZ or greater quality. The linear bending modes of propargyl were found to have a pronounced and insidious basis set dependence. Our results generally support the very recent matrix-isolation/theoretical work on the vibrational spectrum of propargyl by Ellison, Stanton, and co-workers, but reveal aspects of the previous *ab initio* force fields that were not converged.

We have investigated the *trans*- and *cis*-HOCO radical, anion, and cation with unmatched *ab initio* rigor, particularly focal-point extrapolations based on correlation treatments through the CCSDT level and basis sets of the form aug-cc-p(C)VXZ ($X = 2-6$). Zero-point vibrational anharmonicity, core-correlation effects, special relativity, and non-Born-Oppenheimer corrections were explicitly incorporated in pursuit of subchemical accuracy (*ca.* 0.1 kcal mol⁻¹). The final proposals for the adiabatic electron affinity and ionization potential of the *trans*-HOCO radical are 1.371 eV and 8.108 eV, respectively.

A wide-ranging exploratory investigation of the propargyl + allyl reaction surface is being undertaken with DZP B3LYP theory, with the goal of discovering all the salient features warranting subsequent coupled-cluster and/or CASSCF-MR CISD computations. Conjoined with existing, detailed studies of the propargyl self-reaction, characterization of the propargyl +

allyl system promises to more fully elucidate the production of the first benzene ring in soot formation. Our study of the complicated, multistate processes on the propargyl + allyl surface includes mapping the paths for formation of 1,2,5-hexatriene, 1,3,5-hexatriene, 1-hexene-5-yne, fulvene + H₂, benzene, 3-methylene-4-methylcyclobutene, 3- and 4-methylenecyclopentene, and H + 3-methylcyclopentene-4- or -5-yl .

Finally, we are exploring the fascinating fragmentation of *o*-benzyne to acetylene + diacetylene. The concerted, C_{2v} fragmentation is formally allowed by conservation of orbital symmetry, but extensive orbital transformations must simultaneously occur to yield the products. In the transition state region located with RCCSD(T) theory, there is artifactual symmetry breaking in the reference Hartree-Fock wavefunction and essentially zero curvature for distortions along a *b*₂ vibrational mode. Accordingly, there appears to be a competitive path for nonconcerted fragmentation that first opens the ring by homolytic C-C bond cleavage and then breaks a C-C bond in the resulting six-carbon chain to give the products. Careful CASSCF studies will be required to gain final answers for this problem.

Publications Supported by DOE: 2003, 2004, 2005

1. R. I. Kaiser, I. Hahndorf, O. Asvany, Y. T. Lee, L. Vereecken, J. Peeters, H. F. Bettinger, P. R. Schleyer, and H. F. Schaefer, "Neutral-Neutral Reactions in the Interstellar Medium: Elementary Reactions of C₆H₅ and C₆H₆," *Astronomy and Astrophysics*, **406**, 385 (2003).
2. P. R. Schreiner, A. A. Fokin, P. R. Schleyer, and H. F. Schaefer, "Model Studies on the Electrophilic Substitution of Methane with Various Electrophiles E (E = NO₂⁺, F⁺, Cl⁺, Cl₃⁺, HBr₂⁺, HCO⁺, OH⁺, H₂O-OH⁺, and Li⁺)," *Fundamental World of Quantum Chemistry; A Tribute Volume to the Memory of Per-Olov Löwdin*, Editors E. J. Brändas and E. S. Kryachko (Kluwar, Dordrecht, Holland, 2003), Volume 2, pages 359-386.
3. J. P. Kenny, W. D. Allen, and H. F. Schaefer, "Complete Basis Set Limit Studies of Conventional and R12 Correlation Methods: The Silicon Dicarbide (SiC₂) Barrier to Linearity", *J. Chem. Phys.* **118**, 7353 (2003).
4. A. A. Fokin, P. R. Schreiner, S. I. Kozhushkov, K. Sattelmeyer, H. F. Schaefer, and A. de Meijere, "Delocalization in Sigma Radical Cations: The Intriguing Structures of Ionized [n] Rotanes", *Organic Letters* **5**, 697 (2003).
5. E. F. Valeev, W. D. Allen, R. Hernandez, C. D. Sherrill, and H. F. Schaefer, "On the Accuracy of Atomic Orbital Expansion Methods: Explicit Effects of k Functions on Atomic and Molecular Energies", *J. Chem. Phys.* **118**, 8594 (2003).

6. B. Papas, S. Wang, N. DeYonker, and H. F. Schaefer, "The Naphthalenyl, Anthracenyl, Tetracenyl, and Pentacenyl Radicals, and their Anions", *J. Phys. Chem. A* **107**, 6311 (2003).
7. K. Sattelmeyer, H. F. Schaefer, and J. F. Stanton, "Use of 2h and 3h-p- like Coupled-Cluster Tamm-Dancoff Approaches for the Equilibrium Properties of Ozone", *Chem. Phys. Lett.* **378**, 42 (2003).
8. N. R. Brinkmann, G. S. Tschumper, G. Yan, and H. F. Schaefer, "An Alternate Mechanism for the Dimerization of Formic Acid", *J. Phys. Chem.* **107**, 10208 (2003).
9. K. W. Sattelmeyer, Y. Yamaguchi, and H. F. Schaefer, "Energetics of the Low-Lying Isomers of HCCO", *Chem. Phys. Lett.* **383**, 266 (2004).
10. L. D. Speakman, B. N. Papas, H. L. Woodcock, and H. F. Schaefer, "A Reinterpretation of Microwave and Infrared Spectroscopic Studies of Benzaldehyde", *J. Chem. Phys.* **120**, 4247 (2004).
11. R. D. DeKock, M. J. McGuire, P. Piecuch, W. D. Allen, H. F. Schaefer, K. Kowalski, S. A. Spronk, D. B. Lawson, and S. L. Laursen, "The Electronic Structure and Vibrational Spectrum of *trans*-HNOO", *J. Phys. Chem. A* **108**, 2893 (2004).
12. M. Schuurman, S. Muir, W. D. Allen, and H. F. Schaefer, "Toward Subchemical Accuracy in Computational Thermochemistry: Focal Point Analysis of the Heat of Formation of NCO and [H, N, C, O] Isomers", *J. Chem. Phys.* **120**, 11586 (2004).
13. Y. Yamaguchi and H. F. Schaefer, "The Diazocarbene (CNN) Molecule: Characterization of the $\tilde{X}^3\Sigma^-$ and $\tilde{A}^3\Pi$ Electronic States", *J. Chem. Phys.* **120**, 9536 (2004).
14. S. E. Wheeler, W. D. Allen, and H. F. Schaefer, "Thermochemistry of C₄H₃ and C₄H₅ Soot Formation Intermediates", *J. Chem. Phys.* **121**, 8800 (2004).
15. R. K. Sreeruttun, P. Ramasami, G. Yan, C. S. Wannere, P.v. R. Schleyer, and H. F. Schaefer, "The Alkylethynyl Radicals, $\bullet\text{C}\equiv\text{C}-\text{C}_n\text{H}_{2n-1}$ (n=1-4), and their Anions", William L. Hase Special Issue, *Int. J. Mass Spec.* **241**, 295 (2005).
16. W. D. Allen, M. S. Schuurman, and H. F. Schaefer, "On G₀ Anharmonicity in Polyatomic Zero Point Vibrational Energies", *J. Chem. Phys.*
17. M. S. Schuurman, W. D. Allen, and H. F. Schaefer, "The Highly Anharmonic BH₅ Potential Energy Surface Characterized in the *Ab Initio* Limit", *J. Chem. Phys.*
18. M. Schuurman, W. D. Allen, and H. F. Schaefer, "The *Ab Initio* Limit Quartic Force Field of BH₃", *J. Comput. Chem.*
19. B. N. Papas and H. F. Schaefer, "Concerning the Precision of Standard Density Functional Programs: GAUSSIAN, MOLPRO, NWCHEM, and Q-CHEM", *J. Chem. Theory and Comput.*

Spectroscopy and Dynamics of Transient Species

Trevor J. Sears, *Department of Chemistry, Brookhaven National Laboratory, Upton, NY 11973-5000*
(sears@bnl.gov)

Program Scope

High resolution spectroscopy, augmented by theoretical and computational methods, is used to investigate the structure and reactivity of chemical intermediates in the elementary gas phase reactions involved in combustion chemistry and in chemical processes occurring at or near surfaces of heterogeneous catalysts. Techniques to improve the sensitivity of laser absorption spectroscopy are developed as are models of intra-and inter-molecular interactions in molecular free radicals and other reactive species. The results lead to improved understanding and modeling of processes involving these species and are applicable to a wide variety of practical problems.

Recent Progress

Overtone transitions in the near-IR spectrum of methylene

In collaboration with Prof. K. Kobayashi (Toyama U. and Tokyo Tech. U.) we have recorded new bands in the $\tilde{b}^1B_1 \leftarrow \tilde{a}^1A_1$ spectrum of methylene at wavelengths near 1.37 microns using a home-built diode laser constructed in Tokyo. These transitions terminate in levels lying extremely close to the barrier to linearity shared by the two states involved. Levels in this region show of the most severe consequences of the Renner-Teller effect in the radical and provide extreme tests of our understanding of the RTE in light hydride molecules. Most interestingly, transitions were observed to levels whose dominant character is of a high bending overtone of the lower state. These include the $\tilde{a}(070)^1 - \tilde{a}(010)^{0,2}$ and $\tilde{a}(0,10,0)^2 - \tilde{a}(000)^{1,3}$ as well as the expected $\tilde{b}(000)^2 - \tilde{a}(010)^{1,3}$ transitions. Due to the RTE, the axial projection number, K, dependence of some \tilde{a} state energies in this region is predicted to be inverted, while others are expected to show severe perturbations due to the proximity of \tilde{b} state levels of the same symmetry. The spectra show examples of both types of behavior, yet are relatively simple compared to those observed at shorter wavelengths, due to the reduced density of background levels at the lower final state energies involved. In addition, the data provide more and better estimates of the rotational energy levels in the $\tilde{a}(010)$ level than were previously available. Comparison of these energies with computed triplet state levels in the same energy region should permit an improved estimate of the relative energies of the triplet and singlet levels at the energy of the first excited bending level of the lower singlet state.

Collision-induced intersystem crossing and recrossing in CH₂

The chemistry of methylene depends dramatically on its electronic spin state, and most realistic combustion models treat singlet and triplet CH₂ as separate chemical species. They have different formation and loss reactions, but also a surprisingly efficient collision-induced interconversion process that can be fast enough to compete with gas kinetic reactive channels. A sparse set of rovibrational levels of "mixed state" character occur in CH₂ via spin-orbit coupling, when singlet and triplet levels of the same symmetry are nearly degenerate. It has been hypothesized that these special mixed states act as doorways through which population can transfer from singlet to triplet manifolds by means of collisions that resemble pure rotational energy transfer collisions, and do not require any additional spin mixing during the collision. Our approach is to use transient FM spectroscopy to record the time-resolved Doppler absorption spectra of a selection of rotational states of CH₂, starting with nascent photofragments from the well-characterized ketene dissociation at 308 nm, and following the subsequent collisional evolution of populations and Doppler profiles. The observations characterize the translational and rotational thermalization process in competition with reactive and non-reactive quenching, preceding and blending into the time regime of conventionally studied steady-state kinetics. Our measurements show that there are indeed marked differences in relaxation rates between the known mixed state levels and others with purely singlet character. A surprise observation is that the two components of several observed pairs of mixed triplet and singlet levels appear to be kinetically coupled more strongly to one another than to nearby levels of pure singlet or triplet character. Work on this problem is continuing and

we have recently completed some pump-probe experiments in which a pulsed dye laser operating at a visible wavelength saturates a transition involving the same or a connected level to that probed using a NIR transition in the usual FM transient absorption experiment. By following the transient population bleaching, these experiments provide direct information on the collision-induced rotational energy transfer processes that are intimately connected to the efficient CI-ISC. Other population transfer and energy redistribution experiments with other collision partners are also planned. More details are given in G. Hall's abstract.

Hot band transitions in HCCl

In order to measure and characterize the fundamental vibrational intervals in the ground state of the HCCl radical, we have recorded bands to the red of the band origin of the $\tilde{A}^1A'' \leftarrow \tilde{X}^1A'$ spectrum. Surprisingly, only the ν_3 (C-Cl stretching) vibration in HCCl has previously been measured at high resolution. We have recorded and have analyzed the $(000) - (010)$, $(000) - (011)$, and (part of) the $(020) - (012)$ bands at longer wavelengths. The low J , $K = 1$ region of the \tilde{A} (000) level is perturbed and spectra terminating in these levels had proved impossible to analyze previously, and in the present, ambient temperature, hot band data. We therefore recorded part of the strongest $(000) - (010)$ band in absorption in a slit jet expansion where the radical was rotationally cold, but vibrationally still warm, and were able to identify a very strong local perturbation at $J = 3, K = 1$ of the zero point level in the \tilde{A} state. The identity of the perturbing level is not known at present. We have also extended our previous *ab initio* calculations to calculate the position of the low-lying triplet excited state and spin-orbit coupling between it and singlet state levels. Transitions from the triplet state to known levels of the upper singlet are predicted to occur in the same region as the hot band lines recently recorded. They could not be identified in the, congested, ambient temperature spectra, but we plan to search for them in the jet-cooled environment.

Axis-switching in floppy molecules

Axis-switching is a phenomenon that occurs in electronic spectra of polyatomic molecules when there is a large difference between the equilibrium geometries of the connected states. It leads to the appearance of new rotational sub-bands in the spectrum, and modifies the rotational line intensities in the normal sub-bands. We recorded have spectra of both HCCl and HCBBr in which the upper states exhibits large amplitude bending motion (LAM). The standard spectroscopic model, which we have successfully used to interpret the observed structure in other bands in the spectra of these species, underestimates the effect compared to what is observed. This was not unexpected since this model is based on the concepts of small, harmonic, displacements from a rigid equilibrium structure. We developed an extension of our K-dependent adiabatic model for the rovibronic levels of this type of radical, but its predictions also depart from the observations for the observed levels exhibiting LAM. Further work directed towards understanding this problem and resolving the remaining disagreements between experiment and theory is planned.

Pulse amplified c.w. dye laser for ionization studies

Together with Prof. P. Johnson (Stony Brook University), a very high resolution dye laser system based on a c.w. ring dye laser which is used as the seed beam for a three stage pulse amplifier chain pumped by a doubled single mode Nd:YAG laser has been constructed. The pulsed output beam in the yellow is doubled using a standard KDP crystal resulting in more than 1 mJ/pulse of uv light with a measured line width of less than 120 MHz, which is close to the expected Fourier transform limit. The new laser system has been used to record the rotationally resolved S1-S0 spectrum of jet-cooled benzonitrile, BzN, C_6H_5CN , using field ionization of high Rydberg states generated in a resonant 1+1 scheme. The second photon comes from a standard nsec pulsed dye laser operating at a frequency set to excite the S1 state to a level just below the IP. This experiment is a necessary precursor to the spectroscopic study of BzN^+ using the PIRI technique to study the rotationally resolved spectrum of the ion.

Future Plans

In addition to ongoing work in most of the projects described above, the following new projects are planned.

Coordinatively unsaturated metal-containing species

In collaboration with Prof. T. Steimle (Arizona State), we are planning experiments to investigate the low-lying excited electronic states of small transition metal-containing radicals and clusters. These will use experimental chambers at both BNL, where we plan to combine a new OPO/OPA laser system with the capability to tune continuously to 4.2 microns with the existing laser ablation-ionization/LIF chamber, and ASU. The large numbers of low-lying electronic configurations resulting from incompletely-filled *d*-shells in even the simplest species results in novel and potentially useful chemical behavior in the area of catalysis, for example. In the first experiment, we plan to investigate near-IR LIF spectra of FeH at ASU using the BNL near-IR photomultiplier during April 2005. Subsequently, experiments at BNL, and possibly SBU, will target carbide clusters using a combination of LIF and ion-detected spectroscopy.

New near-IR dispersed laser induced fluorescence experiment

In order to extend our experimental capabilities, and improve the detection efficiency of the LIF experiment at BNL, we propose to combine a 1 meter monochromator with a recently acquired near-IR phototube. In this way, dispersed laser fluorescence may be collected following excitation using pulsed red or near-IR dye, OPO/OPA, or our Ti:sapphire ring lasers. Preliminary experiments involving calibration of the efficiency of the PMT using weak rare gas emission lines at wavelengths as long as 1.7 microns were successful and the first LIF experiments planned are an attempt to detect LIF from Ti:sapphire laser excitation of jet-cooled HCCl radicals.

Clusters and molecules in pulsed laser deposition plumes

Pulsed laser deposition (PLD) has moved from a laboratory method to the point where it is now possible to buy a complete PLD machine designed for commercial fabrication of thin-film materials suitable for device development. PLD uses a mildly focused *u.v.* laser to ablate material from a target. The ablated plasma material in the form of an expanding plume is intercepted by a heated substrate, normally held about 5 cm from the target. Empirical work has established rules of thumb for the successful deposition of high quality films, but very few measurements of the plasma composition have been made. We propose to adapt a commercial PLD target assembly to permit spectroscopic study of the ablation plumes formed from commonly used target materials, such as the mixed metal oxides used for superconducting film growth. These experiments will be done in collaboration with Dr Weidong Si (BNL, Physics Department) who uses a commercial PLD apparatus for thin film synthesis for condensed matter physics research. We will also focus on the spectroscopic study of mixed clusters of transition metals and semiconductor elements, such as gallium, to investigate the electronic properties of mixtures of different stoichiometry. Films of semiconductor-doped metals and metal oxides show promise for a new generation of devices in which ferromagnetic or ferroelectric properties may be switched on or off using modest applied voltages. There is currently no spectroscopic information available for even binary compounds of transition metals and semiconductors.

Cold radical source for a measurement of the electric dipole moment of the electron

An international collaboration is being assembled to use polarization quantum beat spectroscopy on cold, trapped PbF ($^2\Pi_{1/2}$) with the aim of measuring the electric dipole moment of the electron, e-EDM, if it exceeds 1×10^{-31} e-cm, some four orders of magnitude below the current experimental limit. Several variants of supersymmetry theory beyond the standard model of particle physics predict specific values of e-EDM within reach of this experiment. The experiment makes use of a blend of chemical physics techniques and particle physics theory and proposes to measure a minute Stark splitting in violation of time-reversal symmetry. Our expertise in cold radical generation, molecular beam spectroscopy and polarization quantum beats, together with experts at BNL in other aspects of the proposal makes

Brookhaven a plausible site for the experiment. Following a planning workshop held at BNL in February, it was decided to attempt some preliminary source development experiments during summer, 2005. These will make use of an existing low-temperature, liquid helium temperature collisional-cooling chamber constructed in our group some years ago.

Publications 2002-

A K-dependent adiabatic approximation to the Renner-Teller effect for triatomic molecules

H. -G. Yu, J. T. Muckerman, and T. J. Sears, *J. Chem. Phys.* **116**, 1435-1442 (2002).

Rovibronic energies of CH_3^+

H. -G. Yu and T. J. Sears, *J. Chem. Phys.* **117**, 666-669 (2002).

The E-X spectrum of jet-cooled TiO observed in absorption

K. Kobayashi, G. E. Hall, J. T. Muckerman, T. J. Sears, and A. J. Merer, *J. Molec. Spectrosc.* **212**, 133-141 (2002).

Axis-switching and Coriolis coupling in the A (010)-X (000) transitions of HCCl and DCCl

A. Lin, K. Kobayashi, H.-G. Yu, G. E. Hall, J. T. Muckerman, T. J. Sears, and A. J. Merer, *J. Molec. Spectrosc.* **214**, 216-224 (2002).

Hot bands in the A-X spectrum of HCB_r

B. -C. Chang, J. Guss and T. J. Sears, *J. Molec. Spectrosc.* **219**, 136-144 (2003).

The photodissociation of bromoform at 248 nm: Single and multiphoton processes

P. Zou, J. Shu, T. J. Sears, G. E. Hall and S. W. North, *J. Phys. Chem A* **108**, 1482-1488 (2004).

Doppler-resolved spectroscopy as an assignment tool in the spectrum of singlet methylene

G. E. Hall, A. Komissarov and T. J. Sears, *J. Phys Chem A.* **108** 7922-7927 (2004).

The vibrational dependence of axis-switching in triatomic spectra

H. G. Yu, G. E. Hall, J. T. Muckerman and T. J. Sears, *Molec. Phys.* (Submitted, 2005)

Picosecond Nonlinear Optical Diagnostics

Thomas B. Settersten
Combustion Research Facility, Sandia National Laboratories
P.O. Box 969, MS 9056
Livermore, CA 94551-0969
tbsette@sandia.gov

Program Scope

This program focuses on the development of innovative laser-based detection strategies for important combustion radicals and the investigation of the fundamental physical and chemical processes that directly affect quantitative application of these techniques. These investigations include the study of fundamental spectroscopy, energy transfer, and photochemical processes. This aspect of the research is essential to the correct interpretation of diagnostic signals, enabling reliable comparisons of experimental data and detailed combustion models. Many of these investigations use custom-built tunable picosecond (ps) lasers, which enable efficient nonlinear excitation, provide high temporal resolution for pump/probe studies of collisional processes, and are amenable to detailed physical models of laser-molecule interactions.

Recent Progress

Hydroxyl ground-state population dynamics. We investigated OH ground-state population dynamics using two-color resonant four-wave mixing spectroscopy (TC-RFWM). Single-mode laser pulses of approximately 50-ps duration provided adequate temporal resolution for time-domain studies of rotational energy transfer (RET) and sufficient spectral resolution for state-resolved excitation in an atmospheric-pressure flame. An infrared pulse excited individual rovibrational P-branch transitions in the OH vibrational fundamental, generating non-equilibrium population and angular momentum distribution in OH $X^2\Pi_{3/2}(v'=1, N')$. Collisions occurring after the IR laser interaction depopulated the excited level and randomized the induced anisotropy. In an isotropic system, the multipole moments (population, alignment, and orientation) of a particular rotational level decay at independent rates, which depend on the collisional conditions. The decays of the first three multipole moments were observed directly by using a time-delayed ultraviolet pulse, which probed the intermediate level via $A^2\Sigma^+(v^*=1, N^*) \leftarrow X^2\Pi_{3/2}(v'=1, N')$. By tuning the probe laser to transitions originating from collisionally populated levels, we were also able to observe rates of population, alignment, and orientation transfer in the RET process.

This study extended our previous investigations using picosecond two-color polarization spectroscopy (TC-PS) [1]. While TC-PS unambiguously detected alignment and orientation in the ground state, it can not be used to measure population directly. The grating spectroscopy geometry used for the current investigation permitted control of the polarization of each of the four fields that took part in the four-wave mixing process, enabling nearly independent measurement of population, alignment, and orientation. Using the spherical tensor formalism to describe the wave-mixing process, we created a symbolic Mathematica program to model the geometrical dependence of the

signal on the four field polarizations and the pump and probe spectroscopic transition branches (P, Q and R). We cataloged polarization schemes that isolate signals arising solely from alignment or orientation gratings in the ground state. Furthermore, we identified other polarization schemes that give rise to signals that are primarily (>98%) due to population gratings in the ground state.

Measurements were conducted in the post-flame gases of an atmospheric-pressure methane/air flame. Measurements of orientation and alignment destruction rates for $1 \leq N' \leq 12$ indicated significant decrease in the decay rate with increasing N' , in excellent agreement with our earlier measurements [1] of these rates using two-color polarization spectroscopy. Population decay rates were only marginally slower than anisotropy destruction rates and also decreased with increasing N' . This result indicates that the anisotropy (alignment and orientation) relaxation in this flame is due primarily to inelastic collisions (presumably with H_2O). The decrease in relaxation rate with increasing N' is consistent with the energy-corrected sudden scaling law, which predicts total RET removal rates that decrease with increasing rotation. We also observed state-to-state population transfer and anisotropy preservation in these collisions by probing collisionally populated levels. Measurable signals were observed $\Delta N'$ up to 3, and we are currently developing a model that will take into account RET among all the relevant levels to simulate these experimental results.

Nitric oxide ground-state population dynamics. Laser-induced fluorescence is commonly used for measurement of nitric oxide in combustion systems. For high-pressure applications, it is not clear whether population cycling is important. Population cycling refers to the process by which a molecule is excited multiple times by the same laser pulse. This can occur if collisions rapidly quench laser-excited molecules to the ground state and subsequent rapid RET refills the laser-pumped level during a saturating laser pulse. Because vibrational energy transfer rates are extremely slow for the lowest vibrational levels in $\text{NO } X^2\Pi$, we assume that the only effective quenching pathway that can lead to significant population cycling is direct quenching from the laser-excited states to $X^2\Pi(v''=0)$. In collaborative experiments (Volker Sick, U. Mich.; John Daily, U. Colorado; Helmut Kronemayer and Christof Schulz, U. Heidelberg) we measured room-temperature branching ratios for direct quenching to $X^2\Pi(v''=0)$ for O_2 , CO_2 , H_2O , and CO . A rate-equation-based model [2] was developed and used to identify operating conditions for the experiment and to evaluate experimental measurements. NO diluted in N_2 flowed through a fluorescence cell. For all experiments, the NO and N_2 partial pressures in the cell were maintained at 6 mTorr and 600 Torr, respectively. Strong quenchers (O_2 , CO_2 , H_2O , or CO) were added to the gas stream to rapidly quench $\text{NO } A(v''=0)$ molecules that were excited by an intense ns laser. The decay of the the excited-state population was directly measured using time-resolved fluorescence detection in the $A-X(0,0)$ band at 235 nm. The ground-state population was measured using LIF from a weak ps probe pulse, which was tuned to transitions in the $\text{NO } A-X(1,0)$ band. Recovery of the ground-state population was determined by scanning the pump-probe delay. The ground-state population recovery rate was the same as the excited-state decay rate for all quenchers, and the degree of recovery was related to quenching branching ratios. Experimental results indicated that CO_2 quenches a significant fraction of the $\text{NO } A$ molecules directly to $v''=0$, with a branching ratio of approximately 0.6. We also observed ground-state refilling due to quenching by O_2 , H_2O , and CO , but to a lesser degree than observed for CO_2 . Although further analysis is necessary, the preliminary results indicate that population cycling via CO_2 quenching may be an important consideration in the analysis of high-pressure saturated LIF measurements of NO . We are currently considering measurements in atmospheric-pressure flames to investigate refilling at combustion temperatures.

Future Plans

Detection of atomic hydrogen and investigation population dynamics in $n=2$. We previously demonstrated the detection of atomic hydrogen in flames using ps TC-PS in collaboration with Suresh Roy (Innovative Scientific Solutions, Inc.) and Robert Lucht (Purdue). In this collaboration, DNI-based calculations were used to develop an understanding of the effects of collisions, saturation, and Doppler broadening on ps TC-PS. The calculations treated the two-photon excitation step to H-2S nonperturbatively and include pathways through bound nP intermediate states. The modeling results indicated that while two-photon excitation to H-2S is very effective, it produces negligible anisotropy in the angular momentum distribution. Because the TC-PS signal arises from the anisotropy, we expect significant improvements in atomic hydrogen detection sensitivity by using two-color wave-mixing spectroscopy in the grating geometry, configured so that it is sensitive to the population. A simple modification of the polarization optics will enable measurement of the signal that is sensitive to the anisotropy. In collaboration with Robert Lucht and Waruna Kulatilaka (Purdue), we will directly compare signals arising from anisotropy and population gratings. Furthermore, we will investigate population dynamics in $n=2$ by scanning the pump-probe delay. Experimental validation of the model results will be used to ensure the important physics is correctly implemented.

Electronic spectroscopy of propargyl. In collaboration with Craig Taatjes and Jeff Gray (Ohio Northern University), we will investigate the electronic spectroscopy of propargyl (C_3H_3) using coherent IR-UV double-resonance spectroscopy. We previously used coherent IR-UV double-resonance spectroscopy (TC-PS and TC-RFWM) to detect photolytically produced CH_3 radicals [3]. In that work, an infrared laser pumped individual lines in the ν_3 fundamental of the $X^2\tilde{A}_2''$ state, and an ultraviolet laser probed the pumped levels via electronic transitions to the predissociated $B^2\tilde{A}_1'$ state. In direct absorption, the CH_3 $B-X$ band lacks rotational structure. The IR-UV double-resonance techniques, however, enabled for the first time the observation of fully rotationally resolved spectra. Using measured spectra we determined the $B-X$ band origin with unprecedented precision [3]. We propose to carry out similar spectroscopic investigations on propargyl. We will use IR excitation in the well-characterized ν_1 band at $3\ \mu m$ [4] and UV probing around 332 nm and 242 nm. The UV absorption bands of propargyl lie between 300 and 340 nm [5], and recent claims attribute UV absorption features around 240 nm to propargyl [6]. There is, however, some contention surrounding the assignment of the 240-nm feature [7], and we will unambiguously confirm or refute this assertion using TC-RFWM.

Fluorescence quenching. We plan substantial effort to develop accurate predictive models for the quenching of fluorescence from CO $B^1\Sigma^+(v=0)$ and NO $A^2\Sigma^+(v=0)$. This research builds on our previous success using time-resolved ps-LIF to measure temperature- and species-dependent cross sections for these species. We will also develop quenching models for O ($3p^3P$) and H ($n=3$) in support of our work on two-photon ps-LIF detection of these species. We propose to extend our measurements to temperatures approaching 2000 K using premixed, low-pressure flames. Using our time-resolved ps-LIF apparatus, we can very accurately measure fluorescence lifetimes, which will be on the order of 2 ns or longer under low-pressure flame conditions. We will infer quenching cross sections from the measured lifetimes in a series of engineered flames using the computed species concentrations and measured temperature in each flame. The higher-temperature data will enable the development and validation of comprehensive quenching models. Initial work will focus on the design, construction, and characterization of a low-pressure flame facility. A variety of premixed

low-pressure flames, using various fuels, oxidizers, diluents, and flow rates will be utilized to achieve the desired conditions.

Quench-free imaging via prompt ps-LIF. We propose to investigate fluorescence lifetime imaging and the feasibility of prompt ps-LIF imaging for quantitative concentration measurements of NO. These experiments will use a gated (<100 ps FWHM) intensified camera to detect the LIF signal generated by 50-ps excitation of NO in flames. By scanning the gate with respect to the laser pulse, a two-dimensional image of the time-resolved fluorescence can be obtained in steady or periodically forced flames. Measured lifetimes will be compared to those predicted by quenching model that we are developing. Furthermore, it should be possible to obtain single-shot quench-free images by gating the detection to overlap with the laser pulse. We propose to evaluate critically the feasibility of this application.

References

- [1] X. Chen, B. D. Patterson, T. B. Settersten, *Chem. Phys. Lett.* **388**, 358 (2004).
- [2] J. W. Daily, W. G. Bessler, C. Schulz, V. Sick, T. B. Settersten, *AIAA J.* **43**, 458.
- [3] T. B. Settersten, R. L. Farrow, J. A. Gray, *Chem. Phys. Lett.* **370**, 204 (2003).
- [4] C. Morter, C. Domingo, S. Farhat, E. Cartwright, G. Glass, R. Curl, *Chem. Phys. Lett.* **195**, 316 (1992).
- [5] D. A. Ramsay, P. Thistlethwaite, *Can. J. Phys.* **44**, 1381 (1966).
- [6] A. Fahr, P. Hassanzadeh, B. Laszlo, R. E. Huie, *Chem. Phys.* **215**, 59 (1997).
- [7] D. B. Atkinson, J. W. Hudgens, *J. Phys. Chem. A* **103**, 4242 (1999).

BES-Supported Publications (2003-present)

- T. B. Settersten, R. L. Farrow, J. A. Gray, "IR-UV double-resonance spectroscopy of OH in a flame," *Chem. Phys. Lett.* **369**, 584 (2003).
- T. B. Settersten, R. L. Farrow, J. A. Gray, "IR-UV double-resonance spectroscopy of CH₃ in a flame," *Chem. Phys. Lett.* **370**, 204 (2003).
- T. B. Settersten, A. Dreizler, B. D. Patterson, P. E. Schrader, R. L. Farrow, "Photolytic interference affecting two-photon laser-induced fluorescence detection of atomic oxygen in hydrocarbon flames," *Appl. Phys. B* **76**, 479 (2003).
- A. N. Karpets, T. B. Settersten, R. W. Schefer, and R. S. Barlow, "Laser imaging system for determination of three-dimensional scalar gradients in turbulent flames," *Opt. Lett.* **29**, 355 (2004).
- X. Chen, B. D. Patterson, T. B. Settersten, "Time-domain investigation of OH ground-state energy transfer using picosecond two-color polarization spectroscopy," *Chem. Phys. Lett.* **388**, 358 (2004).
- J. H. Frank, B. D. Patterson, X. Chen, T. B. Settersten, "Comparison of nanosecond and picosecond excitation for two-photon LIF imaging of atomic oxygen in flames," *Appl. Opt.*, **43**, 2588 (2004).
- J. H. Frank, T. B. Settersten, "Two-photon LIF imaging of atomic oxygen in flames with picosecond excitation," *Proc. Combust. Instit.*, in press (2004).
- J. W. Daily, W. G. Bessler, C. Schulz, V. Sick, T. B. Settersten, "Role of non-stationary collisional dynamics in determining nitric oxide LIF spectra," *AIAA J.*, **43**, 458 (2005).

Theoretical Studies of Potential Energy Surfaces and Computational Methods

Ron Shepard
Chemistry Division
Argonne National Laboratory
Argonne, IL 60439
[email: shepard@tcg.anl.gov]

Program Scope: This project involves the development, implementation, and application of theoretical methods for the calculation and characterization of potential energy surfaces (PES) involving molecular species that occur in hydrocarbon combustion. These potential energy surfaces require an accurate and balanced treatment of reactants, intermediates, and products. This difficult challenge is met with general multiconfiguration self-consistent-field (MCSCF) and multireference single- and double-excitation configuration interaction (MR-SDCI) methods. In contrast to the more common single-reference electronic structure methods, this approach is capable of describing accurately molecular systems that are highly distorted away from their equilibrium geometries, including reactant, fragment, and transition-state geometries, and of describing regions of the potential surface that are associated with electronic wave functions of widely varying nature. The MCSCF reference wave functions are designed to be sufficiently flexible to describe qualitatively the changes in the electronic structure over the broad range of molecular geometries of interest. The necessary mixing of ionic, covalent, and Rydberg contributions, along with the appropriate treatment of the different electron-spin components (e.g. closed shell, high-spin open-shell, low-spin open shell, radical, diradical, etc.) of the wave functions are treated correctly at this level. Further treatment of electron correlation effects is included using large scale multireference CI wave functions, particularly including the single and double excitations relative to the MCSCF reference space. This leads to the most flexible and accurate large-scale MR-SDCI wave functions that have been used to date in global PES studies.

Electronic Structure Code Maintenance, Development, and Applications: A major component of this project is the development and maintenance of the COLUMBUS Program System. The COLUMBUS Program System computes MCSCF and MRSDCI wave functions, MR-ACPF (averaged coupled-pair functional) energies, MR-AQCC (averaged quadratic coupled cluster) energies, spin-orbit CI energies, and analytic energy gradients. Geometry optimizations to equilibrium and saddle-point structures can be done automatically for both ground and excited electronic states. The COLUMBUS Program System is maintained and developed collaboratively with several researchers including Isaiah Shavitt (University of Illinois), Russell M. Pitzer (Ohio State University), Thomas Mueller (Central Institute for Applied Mathematics, Juelich, Germany), and Hans Lischka (University of Vienna, Austria). The COLUMBUS Program System of electronic structure codes is maintained on the various machines used for production calculations by the Argonne Theoretical Chemistry Group, including Macintosh personal computers, IBM RS6000 workstations, DEC/COMPAC ALPHA workstations, the parallel IBM SP at NERSC, and the Group's 64-CPU Linux cluster. Most recently, the codes have been ported to the 512-CPU Linux cluster, Chiba City, and

to the 320-CPU JAZZ Teraflop facility at Argonne. Ports to the Cray X1 and to the IBM Blue Gene machines are in progress. The parallel sections of the code are based on the single-program multiple-data (SPMD) programming model with explicit message passing using the portable MPI library, and the portable Global Array Library is used for data distribution. These computer codes are used in the production-level molecular applications by members and visitors of the Argonne Theoretical Chemistry Group. The next major release of the COLUMBUS codes will begin to incorporate the newer language features of F90/F95. This will facilitate future development and maintenance effort.

Nonadiabatic Coupling: In collaboration with David Yarkony (Johns Hopkins University) and Hans Lischka (University of Vienna), the ability to compute nonadiabatic coupling between different electronic states of molecules has been incorporated into the COLUMBUS Program System. This results in the ability to compute branching ratios of chemical reactions that involve PES cusps and crossings. It will also allow for the automatic location of cusp and crossing conformations and of the noncrossing conformations of the PES that maximize the nonadiabatic coupling. Table I shows the timings for a single iteration of the geometry optimization step to locate the minimum-energy conformation of the crossing seam for two excited states of the formaldehyde molecule. Note in particular that the computational effort required for the analytic energy gradients for the individual states and for the nonadiabatic coupling between the states is a small fraction of the effort required for the energy and wave function optimization. This important feature is due to the ability to exploit the Hellmann-Feynman theorem for the variational MR-SDCI and MR-AQCC wave functions within COLUMBUS.

Table I. Gradient and Nonadiabatic Coupling

Computational Step	Time ^a	
AO Integrals (DALTON)	9	
MCSCF	17	
MR-SDCI (42 iterations, 3 states)	5567	
Gradient State 1		
CIDEN	191	
CIGRD	23	
TRAN	10	
AO Gradient Integrals (DALTON)	26	
Gradient State 1 Total	250	
Gradient State 2 Total	246	
Nonadiabatic Coupling State1-2	249	
Energy Total	5593	88%
Gradient+Coupling Total	745	12%
Grand Total	6338	

a) Timings in seconds for one geometry iteration cycle for the determination of the minimum-energy conformation of the crossing seam of the 1^1B_1 and 2^1A_1 states of H_2CO with a MR-SDCI wave function using a cc-pVTZ orbital basis.

Computation of Eigenvalue Bounds: During the development of the Subspace Projected Approximate Matrix (SPAM) diagonalization method (described last year), it was necessary to compute bounds of approximate eigenvalues and eigenvectors. This work resulted in the development of a general computational procedure to compute rigorous eigenvalue bounds for general subspace eigenvalue methods. This method consists of the recursive application of a combination of the Ritz Bound, the Residual Norm Bound, the Gap Bound, and the Spread Bound. In addition to application within the SPAM method, this method may also be applied to the Davidson method as used in CI calculations and to the Lanczos method as used in the computation of vibrational eigenvalues. This software will be distributed using anonymous ftp and through the *Computer Physics Communications* program library.

Linear Combination of Product Wavefunctions: A practical limitation of standard MCSCF wave function optimization is the extension to active orbital spaces beyond the 12 to 14 orbital range. This range is sufficient for small molecules and for particular molecular reactions of larger molecules for which the orbitals involved in the reaction are localized and with relative unchanging nature. However, when the nature of the active orbitals changes significantly (e.g. strong valence-Rydberg mixing, or strong charge redistribution), then larger active orbital spaces are necessary. In order to allow larger active orbital spaces, we are investigating the use of a nonlinear wave function form. The important feature of this wave function form is that very long linear wave function expansions, \mathbf{v} , are parameterized in terms of a much smaller number of optimization parameters $\{\Phi\}$. Wave functions of this general form include the perfect-pairing GVB wave functions and the geminal product wave functions.

Our method is more flexible than these previous wave function forms for three reasons. First, open-shell functions are included in our expansions, which are formulated directly in terms of spin-eigenfunctions. This will allow our new method to be used for the reactions that are important to combustion chemistry (i.e. involving radicals and other open-shell electronic states) without introducing spin contamination. Second, we place no restrictions on the orbital occupations, so our products are not restricted to only geminals or to other molecular fragments. Third, we use linear combinations of product wave functions (LCPW) rather than a single expansion term. This allows our method to be used for both ground and excited electronic states, the increased wave function flexibility will lead to more accurate wave functions, and it will allow the computation of transition moments, nonadiabatic coupling, and other properties that at present can only be computed reliably with MCSCF and MR-SDCI approaches.

For our formulation $\text{Dim}(\Phi) \ll \text{Log}(\text{Dim}(\mathbf{v}))$. The critical new feature of our proposed method is that scalar products $\langle ab \rangle$ between two wave function expansion terms can be computed with an effort that is proportional to the dimension of Φ rather than the much larger dimension of \mathbf{v} . We also take advantage of this scalar product relationship to reduce the effort required in the computation of hamiltonian matrix elements $\langle aH|b \rangle$ and in the computation of reduced one- and two-particle transition density matrices, $\langle a|E_{pq}|b \rangle$ and $\langle a|e_{pqrs}|b \rangle$ which will allow the computation of molecular properties such as expectation values, response properties, and analytic energy gradients. We plan to apply this new method to MCSCF, Full-CI, and MR-SDCI wave function

optimizations. At the present time, we can optimize the nonlinear parameters $\{\Phi\}$ and the expansion coefficients c_M in order to minimize the least-squares error in the quantity $\sigma^2 = |\mathbf{v} - \mathbf{v}^{ref}|^2$ with $\mathbf{v} = \sum_{M=1}^{N_\alpha} c_M |L(\Phi^M)\rangle$ where $L(\Phi^M)$ is the representation within the underlying linear wave function expansion space of the of the M -th expansion term.

Public Distribution of Software: The COLUMBUS Program System is available using the *anonymous ftp* facility of the internet. The codes and online documentation are available from the web address <http://www.itc.univie.ac.at/~hans/Columbus/columbus.html>. In addition to the source code, the complete online documentation, installation scripts, sample calculations, and numerous other utilities are included in the distribution. A partial implementation of an IEEE POSIX 1009.3 library has been developed and is available from <ftp://ftp.tcg.anl.gov/pub/libpxf>. This library simplifies the porting effort required for the COLUMBUS codes, and also may be used independently for other Fortran programming applications. The SPAM code described above is available from <ftp://ftp.tcg.anl.gov/pub/spam>.

This work was supported by the U.S. Department of Energy, Office of Basic Energy Sciences, Division of Chemical Sciences, under Contract No. W-31-109-ENG-38.

Publications:

- “Analytic Evaluation of Nonadiabatic Coupling Terms at the MR-CI Level. I: Formalism,” H. Lischka, M. Dallos, P. G. Szalay, D. R. Yarkony, and R. Shepard, *J. Chem. Phys.* **120**, 7322-7329 (2004).
- “Analytic Evaluation of Nonadiabatic Coupling Terms at the MR-CI Level. II. Minima on the Crossing Seam: Formaldehyde and the Photodimerization of Ethylene,” M. Dallos, H. Lischka, R. Shepard, D. R. Yarkony, and P. G. Szalay, *J. Chem. Phys.* **120**, 7330-7339 (2004).
- “An Ab Initio Study of AmCl⁺: f-f Spectroscopy and Chemical Binding,” Jeffrey L. Tilson, Conrad Naleway, Michael Seth, Ron Shepard, Albert F. Wagner, and Walter C. Ermler, *J. Chem. Phys.* **121**, 5661-5675 (2004).
- “Computing Eigenvalue Bounds for Iterative Subspace Methods,” Y. Zhou. R. Shepard, M. Minkoff, *Computer Physics Comm.* **167**, 90-102 (2005).
- “Software for Computing Eigenvalue Bounds for Iterative Subspace Methods,” R. Shepard, M. Minkoff, Y. Zhou. *Computer Physics Comm.* (in press).

COMPUTATIONAL AND EXPERIMENTAL STUDY OF LAMINAR FLAMES

M. D. Smooke and M. B. Long
Department of Mechanical Engineering
Yale University
New Haven, CT 06520
mitchell.smooke@yale.edu

Program Scope

Our research has centered on an investigation of the effects of complex chemistry and detailed transport on the structure and extinction of hydrocarbon flames in coflowing axisymmetric configurations. We have pursued both computational and experimental aspects of the research in parallel. The computational work has focused on the application of accurate and efficient numerical methods for the solution of the boundary value problems describing the various reacting systems. Detailed experimental measurements were performed on axisymmetric coflow flames using two-dimensional imaging techniques. Spontaneous Raman scattering and laser-induced fluorescence were used to measure the temperature, major and minor species profiles. Laser-induced incandescence has been used to measure soot volume fractions. Our goal has been to obtain a more fundamental understanding of the important fluid dynamic and chemical interactions in these flames so that this information can be used effectively in combustion modeling.

Recent Progress

The major portion of our work during the past year has focused on a combined computational and experimental study of time varying, axisymmetric, laminar unconfined methane-air diffusion flames and on a combined computational and experimental study of the formation of soot in axisymmetric, laminar ethylene-air diffusion flames. The time varying systems can bridge the gap between laminar and fully turbulent systems. In addition, time varying flames offer a much wider range of interactions between chemistry and fluid dynamics than do steady-state configurations. The sooting flames can enable the investigator to understand the detailed inception, oxidation and surface growth processes by which soot is formed in hydrocarbon flames.

Soot Modeling: Soot kinetics are modeled as coalescing, solid carbon spheroids undergoing surface growth in the free molecule limit. The particle mass range of interest is divided into sections and an equation is written for each section including coalescence, surface growth, and oxidation. For the smallest section, an inception source term is included. The transport conservation equation for each section includes thermophoresis, an effective bin diffusion rate, and source terms for gas-phase scrubbing. The gas and soot equations are additionally coupled through non-adiabatic radiative loss in the optically-thin approximation. The inception model employed here is based on an estimate of the formation rate of two- and three-ringed aromatic species (naphthalene and phenanthrene), and is a function of local acetylene, benzene, phenyl and molecular hydrogen concentrations. Oxidation of soot is by O_2 and OH . The surface growth rate is based upon that of Harris and Weiner [1] with an activation energy as suggested by Hura and Glassman [2]. Using planar laser imaging, we obtain two-dimensional fields of temperature, fuel concentration, and soot volume fraction in the C_2H_4/N_2 flames. The temperature field is determined using the two scalar approach of Stårner *et al.* [3]. The soot volume fraction field is determined by laser-induced incandescence (LII). In our initial work, probe measurements of the soot volume fraction were used for calibration. More recently, absorption measurements are being coupled with the LII measurements both as a check for the calibration and as an independent

measurement of the soot volume fraction profile. The use of multiple measurement techniques should improve our overall confidence in the results as well as provide better estimates of the accuracy of the measured results.

The chemical kinetic mechanism utilized in the modeling work was a 65 species mechanism based upon the work of Sun *et al.* [4]. Fuel and nitrogen are introduced through the center tube (4 mm id) and air through the outer coflow with plug flow velocity profiles. Both velocity profiles were those employed in the experiments. Flames containing 32% (68%), 40% (60%), 60% (40%) and 80% (20%) mole fractions of ethylene (nitrogen) with a bulk-averaged velocity of 35 cm/sec were studied. The coflow air velocity was 35 cm/sec. Reactant temperatures were assumed to be 298 K. Calculations were performed on an AMD Dual Opteron 240 system.

In our recent studies [5,6], we investigated the changing soot field as the dilution fuel fraction in the central tube changed. We were able to predict soot volume fractions along the wings of the flame in good agreement with experimental measurements; but we underpredicted soot volume fractions along the centerline. This deficiency was particularly true for the flames with higher fuel mole fractions. The transition from peak soot along the centerline to peak soot volume fractions along the wings (observed both in our experiments and our modeling) is qualitatively consistent with the early work of Santoro and coworkers [e.g., 7,8], although in the prior work, the fuel jet was undiluted and the transition in the soot field was observed by increasing the fuel jet velocity.

To help understand the reasons for the disagreement between the model and the experiments, we identified two principal deficiencies of the soot model. Our model allowed particles to grow by coalescence and surface growth without any size limit contrary to experimental data, which show the maximum primary particle size to be 20-30 nm. In addition, large diameter soot particles slowed the oxidation process and were the direct cause of the extended wings. In effect, the model did not treat primary particle aggregation (and hence underestimated surface area for larger volume fractions) and ageing. In an attempt to remedy these deficiencies, we turned off coalescence and surface growth at a pre-selected particle size of 25 nm. These modifications made a significant improvement in the computed soot volume fraction distributions. Second, the model implemented an optically thin radiation model. In principle, some re-absorption of thermal emissions can occur. This optical thickness effect reduces the net rate of thermal radiation energy loss. Utilizing the discrete transfer method of Lockwood and Shah [9], we directed a number of rays from the boundaries through the body of the flame. We then determined path-integrated radiative fluxes along rays using the program RADCAL [10]. This energy source rate was then employed as a fixed correction term in the energy equation and the process iterated. The small changes to the temperature profiles modified the ratio of the peak soot along the centerline to the peak overall soot so that the values were more in line with the experiments.

While these modifications help improve the comparison between the model and the experiment, they do not explain the reason for the transition. To this end, we began an investigation of the relative rates of inception, surface growth, and oxidation, along with a particle residence time analysis as a function of fuel fraction. The results help to explain the shift of soot away from the centerline as the fuel fraction increases. While inception tends to peak on the centerline, the maximum in surface growth migrates from the centerline to the wings of the flame as the fuel fraction increases. Concurrently, the relative importance of surface growth and inception reverses. This change in the relative importance of these two subprocesses is due to the significant increase in residence time available for soot growth in the flame wings. Moreover, even with a significant increase in residence time along the centerline (and the local increase in fuel fraction) associated with the less diluted flames, the ageing of the soot particles and the lower temperatures inhibit the enhanced soot inception and growth along the centerline.

Time-Varying Flames: Atmospheric pressure, overventilated, axisymmetric, coflowing, nonpremixed laminar flames were generated with a burner in which the fuel flows from an uncooled 4.0 mm inner diameter vertical brass tube (wall thickness 0.038 mm) and the oxidizer flows from the annular region between this tube and a 50 mm diameter concentric tube. The oxidizer is air while the fuel is a mixture containing methane (nitrogen) 65% (35%) by volume, to eliminate soot. The burner includes a small loudspeaker in the plenum of the fuel jet, which allows a periodic perturbation to be imposed on the exit parabolic velocity profile. Perturbations of 30% and 50% of the average velocity have been investigated. Because the flame is slightly lifted, there is no appreciable heat loss to the burner. Two-dimensional profiles of temperature, mixture fraction, and mole fractions of N_2 , CO_2 , CH_4 , H_2 , CO , and H_2O as well as CH^* emission have been measured in the time-varying flame.

As we move toward the investigation of soot formation in these time-varying flames, we will need to adopt different diagnostics in sooty regions of the flame, since the presence of soot will interfere with the Raman- and Rayleigh-based diagnostics that we have used thus far. We have investigated the potential application of a relatively low-cost, color digital camera, for use as a three-color optical pyrometer for measuring soot temperatures within the flame. The use of the built-in color filter array (CFA) of the digital camera allows for two-dimensional imaging of flame emission at the wavelengths of the color filters. The image data provide pixel-by-pixel spectral and spatial information, which are then used to calculate the two-dimensional flame temperatures. The filter profiles of the CFA were characterized to provide a calibration for the two-color method used to calculate the temperatures. Images were taken of sooting, axisymmetric laminar ethylene flames, and the two-dimensional temperature field was calculated. Comparisons were made to temperature and soot distributions provided by our calculations.

Future Plans

During the next year we hope to expand our research in several areas. We will continue our study of sooting hydrocarbon flames with the goal of understanding the differences in soot distribution between the computational and experimental results. A significant portion of the modeling work will address soot aggregation and ageing. The goal will be to include a detailed soot model into the gas phase system so as to predict soot volume fractions as a function of time. Experimentally we will continue our work on improving the accuracy of our soot volume fraction measurements, as well as applying other diagnostic techniques that can provide information on the soot such as primary particle size and aggregation. We will continue to develop the soot pyrometry by improving the characterization of the camera's color filter array. Finally, in the time-varying flames, we will perform phase-averaged particle image velocimetry to allow a comparison of measured and computed velocity fields

References

1. Harris, S.J., and Weiner, A.M., *Combust. Sci. Tech.*, **31**, p. 155, (1983).
2. Hura, H.S. and Glassman, I., *Proceedings of the Combustion Institute*, **22**, p. 371, (1988).
3. Starner, S., Bilger, R. W., Dibble, R. W., Barlow, R. S., *Combust. Sci. Tech.*, **86**, p. 223, (1992).
4. Sun, C. J., Sung, C. J., Wang, H., and Law, C. K., *Comb and Flame*, **107**, p. 321, (1996).
5. Smooke, M. D., McEnally, C. S., Pfefferle, L. D., Hall, R. J., and Colket, M. B., *Comb. Flame*, **117**, p. 117, (1999).
6. Smooke, M. D., Hall, R. J., Colket, M. B., Fielding, J., Long, M. B., McEnally, C. S., and Pfefferle, L. D., *Comb. Theory and Modelling*, **8**, p. 593, (2004).
7. Santoro, R. J., Semerjian, H. G., and Dobbins, R. A., *Comb. Flame*, **51**, p. 203, (1983).
8. Santoro, R. J. and Semerjian, H. G., *Proceedings of the Combustion Institute*, **20**, p. 997, (1984).
9. F.C. Lockwood and N.G. Shah, *Proceedings of the Combustion Institute*, **18**, p. 1405, (1981).
10. Grosshandler, W.L., *RADCAL: A Narrow-Band Model for Radiation Calculations in a Combustion Environment*, NIST Technical Note 1402 (1993).

DOE Sponsored Publications since 2003

1. S. V. Naik, N. M. Laurendeau, J. A. Cooke and M. D. Smooke, "A Soot Map for Methane-Oxygen Counterflow Diffusion Flames," *Combust. Sci. and Tech.*, **175**, (2003).
2. S. V. Naik, N. M. Laurendeau, J. A. Cooke, and M. D. Smooke, "Effect of Radiation on Nitric Oxide Concentrations Under Sooting Oxy-Fuel Conditions," *Comb. and Flame*, **134**, (2003).
3. J. A. Cooke, M. D. Smooke, M. Bellucci, A. Gomez, A. Violi, T. Faravelli and E. Ranzi, "Computational and Experimental Study of a JP-8 Counterflow Diffusion Flame," *Proceedings of the Combustion Institute*, **30**, (2004).
4. V. V. Toro, A. V. Mokhov, H. B. Levinsky and M. D. Smooke, "Combined Experimental and Computational Study of Laminar, Axisymmetric Hydrogen-Air Diffusion Flames," *Proceedings of the Combustion Institute*, **30**, (2004).
5. K.T. Walsh, J. Fielding, M.D. Smooke, A. Linan and M.B. Long, "A Comparison of Computational and Experimental Lift-Off Heights of Coflow Laminar Diffusion Flames," *Proceedings of the Combustion Institute*, **30**, (2004).
6. F. Laurent, V. Santoro, M. Noskov, M. D. Smooke, A. Gomez and M. Massot, "Accurate Treatment of Size Distribution Effects in Polydisperse Spray Diffusion Flames: Multi-Fluid Modelling, Computations and Experiments," *Comb. Theory and Modelling*, **8**, (2004).
7. M. Noskov and M. D. Smooke, "An Implicit Compact Scheme Solver with Application to Chemically Reacting Flows," *J. Comp. Physics*, **203**, (2004).
8. M.D. Smooke, R.J. Hall, M.B. Colket, J. Fielding, M.B. Long, C.S. McEnally, and L.D. Pfefferle, "Investigation of the Transition from Lightly Sooting towards Heavily Sooting Coflow Ethylene Diffusion Flames," *Comb. Theory and Modelling*, **8**, (2004).
9. M. J. H. Anthonissen, B. A. V. Bennett and M. D. Smooke, "An Adaptive Multilevel Local Defect Correction Technique with Application to Combustion," to be published *Comb. Theory and Modelling*, (2005).
10. S. A. Kaiser, J. H. Frank, and M. B. Long, "Use of Rayleigh Imaging and Ray Tracing to Correct for Beam-Steering Effects in Turbulent Flames," to be published *Appl. Opt.* (2005).
11. J. H. Frank, S. A. Kaiser, and M. B. Long, "Multiscalar Imaging in Partially Premixed Jet Flames with Argon Dilution," submitted to *Combust. Flame* (2005).
12. M. D. Smooke, M. B. Long, M. B. Colket and R. J. Hall, "Soot Formation in Laminar Diffusion Flames," submitted to *Combust. Flame* (2005).

Universal and State-Resolved Imaging Studies of Chemical Dynamics

Arthur G. Suits
Department of Chemistry
Wayne State University
5101 Cass Ave
Detroit, MI 48202
asuits@chem.wayne.edu

Program Scope

The focus of this program is on combining universal ion imaging probes providing global insight, with high-resolution state-resolved probes providing quantum mechanical detail, to develop a molecular-level understanding of chemical phenomena. Particular emphasis is placed upon elementary reactions important in understanding and predicting combustion chemistry. This research is conducted using state-of-the-art molecular beam machines, photodissociation, reactive scattering, and vacuum ultraviolet lasers in conjunction with ion imaging techniques. An ongoing parallel effort is made to develop new tools and experimental methods with which to achieve these goals.

Recent Progress

Roaming atoms. We performed a high-resolution slice imaging study of the dissociation of formaldehyde in the vicinity of the threshold for H atom loss (the “radical channel”). Photolysis of formaldehyde was carried on the 2^14^1 and 2^14^3 bands (S_0 - S_1). The CO fragments were ionized using (2+1) REMPI on various rotational states of CO ($v=0$, $j_{CO}=10$ -40) and were imaged using DC slice imaging. The correlated H_2 rovibrational levels were resolved in the images and the corresponding translational energy distributions. Dissociation on the 2^14^1 band, below the radical threshold, showed the formation of H_2 in vibrational levels 0-4, consistent with previous studies and implying dissociation to molecular products via the well-known distorted transition state. Photolysis on the 2^14^3 band just above the radical threshold, followed by imaging on $j_{CO} = 15$, however, showed formation of highly excited H_2 , ($v=5$ -8, $j_{H_2} = 7$ -15), almost to its dissociation limit. Results obtained for intermediate rotational levels show both contributions (Fig. 1). The results provide strong evidence in support of a conjecture by van Zee et al. that there exists a second molecular channel in formaldehyde dissociation that is related to the radical H elimination channel¹, i.e., an intramolecular H abstraction mechanism. These results have been interpreted with the aid of theoretical calculations from the Bowman group at Emory, revealing the process involves near loss of the H atom, which then roams in the vicinity of the HCO fragment until it abstracts the remaining H atom.

Current efforts are directed to measurements of the energy dependence of this “roaming atom” mechanism in formaldehyde. Results have been obtained for numerous additional excitation energies, both below and above the radical threshold. In addition, photofragment excitation scans have been performed for several rotational levels of CO to obtain detailed wavelength dependence for the roaming atom channel.

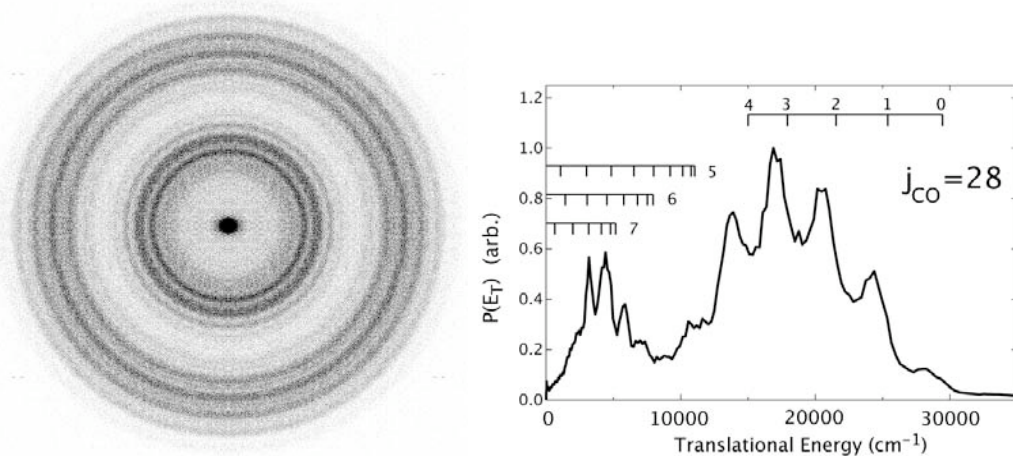


Figure 1. DC sliced image of CO ($v=0, j=28$) from H_2CO photodissociation on the $2^1_4^3$ transition at 31340 cm^{-1} (left); translational energy distribution obtained from image shown with combs indicating H_2 cofragment vibrational ($v=0-4$) or rovibrational level ($v=5-7$) (right).

Application of DC slice imaging to orbital polarization measurements. We have recently adapted the DC slice imaging approach to obtain the absolute speed-dependent angular momentum polarization anisotropy parameters as well as the alignment-free angular and translational energy distributions in photodissociation experiments. Results for ozone photodissociation show that the $\text{O}(^1\text{D})$ produced in ozone photodissociation at 266nm is strongly aligned, with the angular momentum vector preferentially perpendicular to the recoil direction. This is consistent with earlier results from the Houston group: this alignment is largely incoherent in origin, and likely results from diabatic dissociation on the initially excited “B” surface.² We have also measured the orientation of the $\text{O}(^1\text{D})$ atom at a number of wavelengths throughout the Hartley band, and we see a strong coupling of this orientation with the recoil speed of the atom, with the coherent parallel/perpendicular term actually changing sign with the vibrational level of the O_2 cofragment. Results compiled at the peak of each vibrational level for all dissociation wavelengths are shown in Fig. 2 as a function of O atom recoil speed. The abrupt change seen for recoil speeds of 1300 m/s and higher suggests a sudden change from adiabatic behavior.

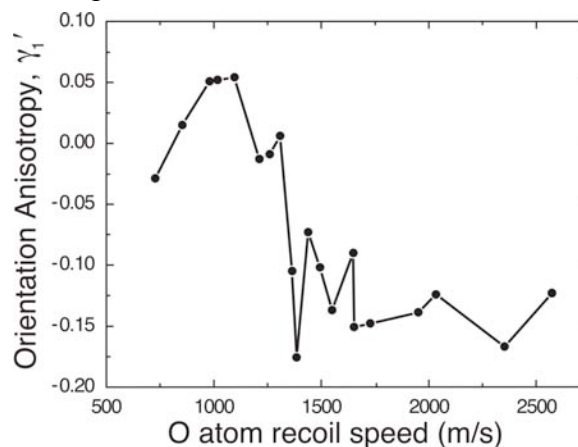


Figure 2. Speed dependence of coherent parallel/perpendicular orientation anisotropy parameter.

Taken together, these results provide evidence of a crossing between the initially prepared “B” surface and the “A” surface. Although the initial

excitation is exclusively to the “B” surface, because this excitation contains both parallel and perpendicular components of the transition moment, a coherence is created that can then be used to trace the subsequent evolution across the two surfaces even though both yield the same asymptotic state of the O atom.

Selected Future Plans

Roaming atom reaction dynamics. We will perform DC slice imaging of CN+O₂ reaction dynamics in crossed beams. The reaction of O₂ with CN represents a prototypical radical-radical reaction with two major product channels: barrierless O atom abstraction to give radical products NCO + O, and formation of CO + NO, a strongly exothermic process yielding closed-shell products with a room temperature branching fraction of 0.22 reported.³ The observation of the latter channel is significant in that a large barrier has been reported (and is expected) for the four-center transition state, and a “dynamical” mechanism⁴, analogous to the roaming atom pathway we have seen in H₂CO dissociation, has been adduced to account for this. We will focus on the molecular channel, and we can measure both state-resolved CO and NO with slice imaging. The correlated internal state distribution in these products can then be used to characterize the reaction mechanism by comparison to theoretical dynamics studies.

State-correlated photochemistry of HCCO. A new system of interest for our high-resolution photochemistry studies, building upon our previous success with ketene itself, is the ketylenyl radical, HCCO. There is a marvelous body of work on the spectroscopy and dynamics of this system. However, the dynamics measurements were obtained at fairly low translational energy resolution. Nevertheless, they provide a roadmap for rich correlated state imaging measurements of the CO. This radical system has the great advantage that metastable levels of the state may be excited state-specifically, so that even employing a photolytic radical source we need not worry about contamination by dissociation of excited radicals. Small changes in photolysis energy are seen to change the branching between dissociation on the doublet and quartet surfaces quite dramatically. Again, quantum state specific probing of the CO product will provide correlated internal state information on the rovibrational levels of both ground state (X²Π) and electronically excited (a⁴Σ⁺) CH product, allowing detailed investigation of ground state dissociation and intersystem crossing dynamics in this system.

References

1. R. D. van Zee, M. F. Foltz and C. B. Moore, *J. Chem Phys.*, **99** 1664 (1993).
2. S. M. Dylewski, J. D. Geiser and P. L. Houston, *J. Chem. Phys.*, **115** 7460 (2001).
3. K. T. Rim and J. F. Hershberger, *J. Phys. Chem. A*, **103** 3721 (1999).
4. F. Mohammad, V. R. Morris, W. H. Fink and W. M. Jackson, *J. Phys. Chem.*, **97** 11590 (1993).

DOE Publications 2003-present

W. Li, L. Poisson, D. S. Peterka, M. Ahmed, R. Lucchese and A. G. Suits, "Dissociative photoionization dynamics in ethane studied by velocity map imaging," *Chem. Phys. Lett.* **374**, 334 (2003).

R. L. Gross, X. Liu and A. G. Suits, " $O(^3P)$ versus $O(^1D)$ Reaction Dynamics with n-Pentane: A Crossed-Beam Imaging Study," *Chem. Phys. Lett.* **376**, 710 (2003).

W. Li, R. Lucchese, A. Doyuran, Z. Wu, H. Loos, G. E. Hall and A. G. Suits, "Superexcited state dynamics probed with an extreme ultraviolet free electron laser," *Phys. Rev. Lett.*, **92** 083002 (2004).

X. Liu and A. G. Suits, "The dynamics of hydrogen abstraction in polyatomic molecules," in **Modern Trends in Chemical Reaction Dynamics**, X. M. Yang and K. Liu, eds. (World Scientific, Singapore: 2004)

D. Townsend, S. A. Lahankar, S. K. Lee, S. D. Chambreau, A. G. Suits, X. Zhang, J. Rheinecker, L.B. Harding and J. M. Bowman, "The roaming atom: Straying from the reaction path in formaldehyde decomposition," *Science* **306**, 1158 (2004) (10.1126/science.1104386).

S. K. Lee, D. Townsend, O. S. Vasyutinskii and A. G. Suits, " $O(^1D)$ orbital orientation in the ultraviolet photodissociation of ozone," *Phys. Chem. Chem. Phys.*, **7**, 1650, (2005).

Elementary Reaction Kinetics of Combustion Species

Craig A. Taatjes

Combustion Research Facility, Mail Stop 9055, Sandia National Laboratories,
Livermore, CA 94551-0969

cataatj@sandia.gov www.ca.sandia.gov/CRF/staff/taatjes.html

SCOPE OF THE PROGRAM

This program aims to develop new optical methods for studying chemical kinetics and to apply these methods to the investigation of fundamental chemistry relevant to combustion science. The central goal is to perform accurate measurements of the rates at which important free radicals react with stable molecules. Understanding the reactions in as much detail as possible under accessible experimental conditions increases the confidence with which modelers can treat the inevitable extrapolation to the conditions of real-world devices. Another area of research is the investigation and application of new detection methods for precise and accurate kinetics measurements. Absorption-based techniques are emphasized, since many radicals critical to combustion are not amenable to fluorescence detection.

An important part of our strategy is using experimental data to test and refine detailed calculations (working in close cooperation with Stephen Klippenstein and Jim Miller), drawing on the calculational results to gain insight into the interpretation of our results and to guide experiments that will probe key aspects of potential energy surfaces. This methodology has been applied in our investigations of the reactions of alkyl radicals with O₂, where the combination of rigorous theory and validation by detailed experiments has made great strides toward a general quantitative model for alkyl oxidation. Reactions of unsaturated hydrocarbon radicals that may play a role in soot formation chemistry are also targets of investigation.

PROGRESS REPORT

The current efforts of the laboratory center on developing high-sensitivity absorption-based techniques for kinetics measurements, and on applying these techniques to investigate important combustion reactions. A major focus continues to be the application of cw infrared frequency-modulation (FM) spectroscopy to measurements of product formation in reactions of alkyl radicals with O₂ and the exploitation of visible absorption spectroscopy of the vinyl radical for kinetics measurements. A new multiplexed photoionization mass spectrometric reactor has also been installed at the Advanced Light Source, in collaboration with Stephen Leone and Musa Ahmed at Lawrence Berkeley National Laboratory and David Osborn at Sandia.

Measurements of Product Formation in Alkyl + O₂ Reactions

***i*-propyl and *n*-propyl + O₂** In previous work the reactions of *n*-propyl and *i*-propyl radicals with O₂ were measured by using 266 nm photolysis of 1-propyl and 2-

propyl iodides. The initial alkyl radical density was inferred from a simultaneous measurement of the absorption on the spin-orbit transition of the I atom photolysis co-product. In the past year, quantitative comparisons with master equation models revealed discrepancies in the *i*-propyl oxidation. As in previous investigations, the *ab initio* energies are adjusted to produce agreement with the present experimental data and with available literature studies. The isomer-specificity of the present results allowed refinement of the model for $i\text{-C}_3\text{H}_7 + \text{O}_2$ that resulted in improved agreement with experimental measurements of HO_2 production in C_3H_8 oxidation. However, discrepancies persist between the best models and the experimental measurements for the *i*-propyl + O_2 reaction. Recent measurements of the production of DO_2 in Cl-initiated oxidation of deuterated propane have also displayed systematically larger prompt yields and slightly faster secondary production rates than predicted theoretically.

To further clarify these discrepancies studies of the reactions of perdeuterated *n*-propyl and *i*-propyl radicals with O_2 have been carried out using 266 nm photolysis of 1-iodopropane- d_7 and 2-iodopropane- d_7 . The production of DO_2 in the reaction of $n\text{-C}_3\text{D}_7 + \text{O}_2$ is in excellent agreement with master equation models that employ the same stationary-point energies as the successful $n\text{-C}_3\text{H}_7 + \text{O}_2$ model. However, as in the $i\text{-C}_3\text{H}_7 + \text{O}_2$ reactions, the deuterated *i*-propyl + O_2 reaction shows systematic deviation of the experimental DO_2 production and the predictions of the master equation solution, with the experiment showing higher prompt DO_2 yields and faster secondary DO_2 production. These deviations are reflected in the Cl-initiated propane- d_8 oxidation because the $\text{Cl} + \text{C}_3\text{D}_8$ reaction produces predominantly $i\text{-C}_3\text{D}_7 + \text{HCl}$.

Reconciliation of model with experiment has been obtained in other $\text{R} + \text{O}_2$ reactions by adjustment of the stationary point energies within the uncertainty of the *ab initio* calculations. In the case of *i*-propyl + O_2 , this adjustment is constrained not only by the present data but by literature investigations of the reaction, including the high-temperature rate constant determinations by Gulati and Walker (Gulati, S. K.; Walker, R. W. *J. Chem. Soc. Faraday Trans. 2* **1988**, *84*, 401) and the equilibrium constant measurements of Knyazev and Slagle (Knyazev, V. D.; Slagle, I. R. *J. Phys. Chem. A* **1998**, *102*, 1770). More precise agreement with the present results could be obtained by lowering the transition state to formation of HO_2 from *i*-propylperoxy radical. This agreement comes at the cost of making the calculated rate coefficient for *i*-propyl + O_2 to form propene about a factor of 9 higher than the value derived in the experimental work of Gulati and Walker. The uncertainties in the kinetic modeling of the present experiments are not inconsiderable; however, the HO_2 and DO_2 formation results are consistent, suggesting that a reinvestigation of the high temperature rate constant may be constructive.

$\text{C}_3\text{H}_3 + \text{O}_2$ Investigation of reactions of propargyl radicals using infrared absorption probing is continuing. Efforts have begun to characterize the reaction of propargyl with O_2 , concentrating on measurements of both propargyl removal and product (ketene, HCO) formation over a range of pressure and temperature, for comparison to master equation calculations published by Klippenstein and Miller (Hahn,

D. K.; Klippenstein, S. J.; Miller, J. A., *Faraday Discuss.* **2001**, *119*, 79-100). The falloff of the reaction has been measured for He pressures between 2.5 Torr and 100 Torr between room temperature and transition region near 400 K, where the addition reaction begins to equilibrate. Characterization of product formation and analysis of the equilibration is ongoing.

Laser Photolysis/cwLPA Measurements of C₂H₃ Reactions

Long-path absorption spectroscopy in the (A-X) band of C₂H₃ is being applied to investigations of the C₂H₃ self-reaction. Photolysis of vinyl iodide at 266 nm is used to produce vinyl radicals and I atoms. The I atom is measured by infrared absorption on the spin-orbit transition, and the initial vinyl radical concentration is assumed to be equal to the initial I atom concentration. The self-reaction rate constant has been measured between 298 K and 550 K. Preliminary results show a room temperature rate coefficient of $(6 \pm 2) \times 10^{-11} \text{ cm}^3 \text{ molecule}^{-1} \text{ s}^{-1}$ with a slight negative temperature dependence.

Time-resolved Photoionization Mass Spectrometry Measurements

A new reactor coupled to a novel photoionization mass spectrometer (PIMS) has been successfully tested at the Chemical Dynamics Beamline of the Advanced Light Source (ALS) of LBNL, as detailed in David Osborn's abstract. The first experiments have yielded time and energy-resolved mass spectra of CH₃ and C₂H₅ oxidation systems with good signal-to-noise. Because the photon energy dependence and the kinetic behavior of the signals are simultaneously measured, this apparatus may also prove valuable for determining ion energetics. For example, the photoionization efficiency curve of CH₃O₂ has been measured at low resolution (~ 0.25 eV) in the first experiments with this reactor, using 193 nm photolysis of acetone in the presence of a large excess of O₂. An approximate ionization energy of 10.3 eV can be estimated from these measurements. At higher energy (threshold of ~ 11 eV), CH₃⁺ is formed by dissociative ionization of CH₃O₂; this process can be clearly and unambiguously distinguished from either direct ionization of CH₃ or dissociative ionization of the acetone precursor because of the kinetic signature given by the time profile of the signal.

FUTURE DIRECTIONS

Characterization of R + O₂ reactions will continue, both in the infrared absorption work and in the new PIMS apparatus. The ability to simultaneously probe various reactants and products will play a key role in extending these measurements. One important extension of the deuterated alkane oxidation work will be to probe OD formation. Because the reaction coordinate for the internal isomerization to QOOH (the precursor to OH formation) involves a large degree of H-atom motion, the deuterium kinetic isotope effect may be larger for OH formation than for HO₂ formation. Further in the future, oxidation of selectively deuterated alkanes may make it possible to distinguish among different internal abstraction pathways in R + O₂ reactions. Interpretation of isotopic labeling experiments will require detection of both HO₂ and DO₂ and an understanding of the kinetic isotope effects on the overall reaction. In the long term,

detection of the hydroperoxy radical intermediate in the $R + O_2 \rightarrow RO_2 \rightarrow QOOH \rightarrow QO + OH$ mechanism might be possible in the infrared.

The application of synchrotron photoionization mass spectrometry to chemical kinetics will continue. The ready tunability of the ALS photon energy permits isotopic discrimination similar to that enjoyed in the current ALS flame experiments, and the kinetics measurements will be designed to exploit this capability. Formation of and reactions of ethenol, addition reactions of propargyl radicals with unsaturated hydrocarbons, and oxidation of cycloalkyl radicals are possible targets of kinetic investigations.

Publications acknowledging BES support 2003-present

1. John D. DeSain, Stephen J. Klippenstein, Craig A. Taatjes, Michael D. Hurley, and Timothy J. Wallington, "Product Formation in the Cl-Initiated Oxidation of Cyclopropane" *J. Phys. Chem. A* **107**, 1992-2002 (2003).
2. Michael D. Hurley, William F. Schneider, Timothy J. Wallington, David Mann, John D. DeSain, and Craig A. Taatjes, "Kinetics of Elementary Reactions in the Chain Chlorination of Cyclopropane," *J. Phys. Chem. A* **107**, 2003-2010 (2003).
3. John D. DeSain, Stephen J. Klippenstein, and Craig A. Taatjes, "Time-resolved Measurements of OH and HO₂ Formation in Pulsed-Photolytic Chlorine Atom Initiated Oxidation of Neopentane," *Phys. Chem. Chem. Phys.* **5**, 1584 - 1592 (2003).
4. John D. DeSain, Andrew D. Ho, and Craig A. Taatjes, "High Resolution Diode Laser Absorption Spectroscopy of the O-H stretch overtone band (2,0,0) ← (0,0,0) of the HO₂ Radical," *J. Mol. Spectrosc.* **219**, 163-169 (2003).
5. John D. DeSain, Stephen J. Klippenstein, James A. Miller and Craig A. Taatjes, "Measurement, Theory, and Modeling of OH Formation From the Reactions of Ethyl and Propyl Radicals with O₂," *J. Phys. Chem. A* **107**, 4415-4427 (2003).
6. John D. DeSain and Craig A. Taatjes, "Infrared Laser Absorption Measurements of the Kinetics of Propargyl Radical Self-Reaction and the 193 nm Photolysis of Propyne," *J. Phys. Chem. A* **107**, 4843-4850 (2003).
7. Frank Striebel, Leonard E. Jusinski, Askar Fahr, Joshua B. Halpern, Stephen J. Klippenstein and Craig A. Taatjes, "Kinetics of the Reaction of Vinyl Radicals with NO: Ab Initio Theory, Master Equation Predictions, and Laser Absorption Measurements," *Phys. Chem. Chem. Phys.* **6**, 2216 - 2223 (2004).
8. Terrill A. Cool, Koichi Nakajima, Craig A. Taatjes, Andrew McIlroy, Phillip R. Westmoreland, Matthew E. Law and Aude Morel, "Studies of a Fuel-Rich Propane Flame with Photoionization Mass Spectrometry," *Proc. Combust. Inst.* **30**, 1631-1638 (2004).
9. Craig A. Taatjes, David L. Osborn, Terrill A. Cool, Koichi Nakajima, "Synchrotron Photoionization of Combustion Intermediates: The Photoionization Efficiency of HONO," *Chem. Phys. Lett.* **394**, 19-24 (2004).
10. Marc J. L. de Lange, Steven Stolte, Craig Taatjes, Jacek Kłos, Gerrit C. Groenenboom, and Ad van der Avoird, "Steric Asymmetry and Lambda-Doublet Propensities in Rotationally Inelastic Scattering of NO (²Π_{1/2}) with He," *J. Chem. Phys.*, **121**, 11691-11701 (2004).
11. Craig A. Taatjes, Stephen J. Klippenstein, Nils Hansen, James A. Miller, Terrill A. Cool, Juan Wang, Matthew E. Law, and Phillip R. Westmoreland, "Synchrotron Photoionization Measurements of Combustion Intermediates: Photoionization Efficiency of C₃H₂ Isomers," *Phys. Chem. Chem. Phys.* **7**, 806-813 (2005).
12. Edgar Estupiñán, Stephen J. Klippenstein, and Craig A. Taatjes, Measurements and Modeling of HO₂ Formation in the Reactions of *n*-C₃H₇ and *i*-C₃H₇ Radicals with O₂," *J. Phys. Chem. B*, *in press* (2005).

THE EXTRACTION OF UNDERLYING MOLECULAR VIBRATIONAL DYNAMICS FROM COMPLEX SPECTRAL REGIONS

H.S. Taylor, Principal Investigator
Department of Chemistry, SSC 704
University of Southern California
Los Angeles, CA 90089-0482
E-mail: taylor@usc.edu
Phone: (213) 740-4112; Fax: (213) 740-3972

This project has as its aim the assignment of the good quantum numbers and the extraction of detailed nuclear motions associated with high vibrational states in complex spectra. By complex we mean experimental and/or theoretical spectra that was uninterpretable by all previous methods of analysis due to multiple resonances among the primary modes. Not only do the usual perturbation based analytic methods fail but even wave functions obtained from difficult quantum calculations are often too complex in appearance to even hint at the nature of the dynamics or the quasiconserved quantities.

Our research over the past six years has resulted in a scheme whereby, if given both a Spectroscopic Hamiltonian fitted to reproduce the complex spectra and its simultaneously produced accompanying eigenfunctions in the number representation, we can meet the above stated aims with sometimes no and always little calculations i.e. by analysis.

The systems studied were the bending spectrum of acetylene^{1,2}, DCO³, N₂O⁴, CHBrClF⁵, CDBrClF⁶ and CF₃CHF⁷. We are now studying SCl₂, using a spectroscopic Hamiltonian developed by Sibert⁹ from Gruebele's⁸ measured spectrum and fitted and computed potential. In this system the six normal modes are (1) the CS stretch, (2) the CCl stretch, (3) the CCl₂ scissor, (4) the out of plane bend, (5) the asymmetric stretch and (6) the CCl₂ rock. We work in the 7000 to 9000 cm⁻¹ region where the spectrum is most complex. For the given Hamiltonian Sibert has supplied three constants of the motion, which we rearranged for simplicity as:

$$N_1 = I_1 + I_2 + I_5, N_2 = 2I_1 + I_3 + I_5 + I_6, N_3 = I_4$$

where I_j is the harmonic action and is related to the quantum number n_j in the usual way. Here a polyad of 252 states with $(N_1, N_2, N_3) = (7, 14, 0)$ is studied. Immediately the six dimension problem is reduced to five by realizing that mode 4 is decoupled in all states and can be separated from the remaining dynamics. Using the Heisenberg semi-classical relations relating the quantum creation-destruction operators to the actions and angles then gives an effective classical Hamiltonian in five actions and five angles $(\bar{I}, \bar{\phi})$. Here we choose to use the two remaining constants of the motion, N_1 and N_2 , to carry out a canonical transform that without approximation eliminates modes 5 and 6 in favor of three reduced space actions and angles, $(\bar{J}, \bar{\psi})$. The Hamiltonian is now a function of these latter variables and parametric in N_1 and N_2 . The specific angle transformations are guided by the nature of the resonance terms. In this problem all mode 3 couplings are weak. The two most heavily weighted resonances are mode 2 with modes 5 and 6 and mode 1 with 5 and 6. The fundamental frequencies, and anharmonicities and the resonances suggest mode locks at $\omega_2 = \omega_5 - \omega_6$ and $\omega_5 = \omega_1 - \omega_6$; both being one mode locking to the difference frequency, that is the beat, of the other two. This suggests choosing $\psi_2 = \phi_5 - \phi_6 - \phi_2$, $\psi_1 = \phi_5 + \phi_6 - \phi_1$ and $\psi_3 = \phi_3$. The reasoning is that at the first resonance since $\omega_j = d_t \psi_j$, $d_t \psi_2$ is zero and at the second resonance $d_t \psi_1$ is zero. Any $d_t \psi_j = 0$ means classically no motion in the ψ_j direction and quantum uncertainty indicates that the wave function will, in the ψ_j direction, be an oscillator localized about some constant value of ψ_j .

In the plots of the wave functions for the largest ladder of states that runs from the top to the center of the polyad the wave function in the ψ_3 direction wraps [classically rotates] about the torus and hence mode 3 is free. The wave function is localized about ψ_3 axis at $\psi_1 = \psi_2 = \pi$, as oscillators in ψ_1 and ψ_2 indicating both resonances are active. The wave function would ideally fit into a ring shaped “box” about ψ_3 with a rectangular cross section. The classical motion in reduced space is seen from the free hand sketched lines (or “guiding” or “supporting” or “effective” periodic orbit or central fiber) drawn through the center of the wave function in the delocalized direction. This line taken, as a trajectory, can be transformed back to full dimensional configuration space revealing the VISIBLE nuclear dynamics. Because of the high dimensionality this dynamics is complex and so far defies simple illustration, Happily it is not needed for the most fundamental reduced dynamics and for assignments.

As we move downward in our inspection of the wave functions the nodes in both direction ψ_1 and ψ_2 increase in number and phase advance of ψ_3 increases thereby supplying the quantum numbers. Here mode 2 marches in phase with the relative phase shift between mode 5 and mode 6 and mode 5 is likewise phase locked to the difference of 1 and 6.

A second ladder beginning and dominating the bottom of the polyad has modes 1 and 3 “rotating” independently around the torus indicating modes 1 and 3 are each free. The wave function is localized with nodes characteristic of an oscillator about a fixed value of $\psi_2 = 0$ indicating that again mode 2 is locked to the phase difference (beat) of modes 5 and 6 albeit with a different relative phase from the top ladder which it overlaps and intersperses and eventually mixes with before ending about one third up the polyad. All these effects cause spectral complexity.

In this way even though the important couplings can be seen in the Hamiltonian, states associated with them can be sorted only in reduced space into two ladders with specific dynamics. Quantum numbers can be assigned. All is done by inspection and analysis without calculation.

REFERENCE

1. M.P. Jacobson, C. Jung and R.W. Field, J. Chem. Phys., 111, 600-618 (1999).
2. C. Jung, M.P. Jacobson and H.S. Taylor, J. Phys. Chem. A, 105, 681-693 (2001).
3. C. Jung, H.S. Taylor and E. Atilgan, J. Phys. Chem. A, 106, 3092-3101 (2002).
4. H. Walkens, C. Jung and H.S. Taylor, J. Phys. Chem., 106, 911-924 (2002).
5. C. Jung, E. Ziemniak and H.S. Taylor, J. Chem. Phys., 115, 2449-2455 (2001).
6. C. Jung, C. Mejia-Monasterio and H.S. Taylor, J. Chem. Phys., 120, 4194-4206 (2004)
7. C. Jung, C. Mejia-Monasterio and H.S. Taylor, PCCP, 6, 3069-3076 (2004).
8. R. Bigwood, B. Milam and M. Gruebele, Chem. Phys. Lett., 287, 333-341 (1998).
9. E.L. Sibert III, J. Chem. Phys., 88, 4378-4390 (1988).

Reference 1-7 was done with DOE support.

Theoretical Chemical Dynamics Studies of Elementary Combustion Reactions

Donald L. Thompson

Department of Chemistry, University of Missouri, Columbia, MO 65211

thompsondon@missouri.edu

Program Scope

There are two major objectives of this theoretical research program: (1) develop practical, facile methods for performing rate calculations by using *ab initio* potential-energy surfaces (PESs) and (2) improve molecular dynamics (MD) methods for treating the full dimensionalities of many-atom systems. The first of these is the core of the project. Our goal is to develop an automatic PES generation algorithm that takes advantage of high-performance computing environments. The initial goal to develop efficient methods for generating global PESs, but the long-term goal is develop methods in which software for rate calculations direct quantum chemistry codes to produce *ab initio* predictions of reaction rates and related dynamics quantities.

Recent Progress

The speed with which quantum chemistry calculations can now be done makes the direct use of *ab initio* forces in MD simulations feasible. However, high-level quantum calculations are often too costly in computer time for practical applications and the levels of theory that must be used are often inadequate for reactions. Thus, among the immediate pressing problems are the efficiency in using expensive high-level quantum chemistry methods (which often do not provide the necessary gradients directly) and ways to correct the errors in *ab initio* energies when necessary. A critical part of the solution is better methods for fitting global potential energy surfaces (PESs) and techniques for making direct dynamics more efficient (e.g., reducing the number of points that must be computed). Within the context of modern quantum chemistry capabilities it is sensible to focus on local fitting schemes.

In the 1970's we proposed a scheme based on local fitting with cubic splines,¹ which provide a flexible and numerically efficient method for fitting a PES with smooth first and continuous second derivatives; however, they require a fairly high density of points for a good fit. A more useful approach is the interpolating moving least squares (IMLS) introduced by Ischtwan and Collins.² It is based on a modified Shepard interpolation, the simplest case of IMLS. The Shepard method is a zero-degree IMLS method. It has a serious problem because the derivative of the interpolant is zero at every data point; however, this problem can be remedied by using Taylor expansions instead of just data points; and the method has been widely applied. Nevertheless, there is a need to explore more efficient and accurate interpolation schemes. We are exploring higher-order IMLS solutions to this problem in collaboration with Drs. Al Wagner and Michael Minkoff at Argonne National Laboratory.

In our initial study,³ we developed the basic IMLS method for efficient and accurate local fitting of discrete energy values to provide global representations of potential energy surfaces (PESs) for many-atom systems. We demonstrated the method with 1-, 2-, 3-D fits of the $\text{HN}_2 \rightarrow \text{N}_2 + \text{H}$ PES. To allow for extensive fitting and testing,

the analytical PES developed by Koizumi *et al.*⁴ was used to generate energy values. Unlike the modified Shepard method this approach does not require derivatives, thus it can be used to fit energies computed using highest-level quantum chemistry methods for which forces are not directly obtainable. Our results showed that this fitting scheme accurately describes the PES, is not computationally time-consuming, can be improved using higher degrees and larger numbers of basis functions, and is straightforward to apply.

We have developed a method in which a zeroth-order PES V_0 is used as a reference surface and IMLS is used to fit the difference $V-V_0$ in it and the *ab initio* PES V .⁵ This allows for the fitting of a much smoother topology than that of the real PES. It is relatively easy to formulate an approximate analytical PES to serve as V_0 , since the main consideration is that it accurately fit the critical points (which can be determined by high-level quantum chemistry calculations). We demonstrated it by using the analytical PES developed by Kuhn *et al.*⁶ for HOOH. The root-mean-square error in the fitting of the 6-D PES is reduced by ~50% for a given number of *ab initio* points by using the reference PES. This approach has great potential for use in an automatic procedure for constructing accurate PES based on *ab initio* results.

Recent Progress

We applied IMLS fitting in classical trajectory simulations to compute rate constants for the O-O bond fission in HOOH.⁷ We find that using a proper coordinate system can be important to accurately describe intramolecular couplings, which affect the reaction rate. For HOOH valence internal coordinates are better than interatomic distances. The efficiency of IMLS can be improved by using a cut-off radius with various selections of the data points and basis elements. Our results indicate that preliminary random samplings of IMLS evaluations with large basis sets can be monitored for basis function coefficient size, and those with small coefficients can be neglected. We found that using a simple fixed cut-off radius encompassing on average a few hundred *ab initio* points leads to good accuracy.⁷ The efficiency and accuracy can be significantly improved by using an adaptive cut-off based on density of points. We have performed extensive testing of strategies for selecting the points to be used in a given fit; this work is being prepared for publication.⁸

In another study⁹ we explored the effects of different degrees and mixed-degree polynomials in the IMLS and of *ab initio* point selection by automatic PES generation schemes for the 6-D PES of the HOOH dissociation reaction. We find that the rms fitting error converges with the number of *ab initio* points in an inverse power law fashion with powers that increase with the IMLS degree. Higher-degree IMLS fits are dominated by cross terms that contribute in only a minor way to the quality of the fit; e.g., using third-degree IMLS with elimination of second-order cross terms along with all cross terms that do not include the reaction coordinate and bond angles gives a fit as good as the full third-degree IMLS. Automatic point selection that optimally picks *ab initio* points to improve a fit approximately halves the root-mean-square error relative to “blindly” selecting points by changing grid increments or by random sampling; e.g., for a 100 kcal/mol range the rms error of 1 kcal/mol can be reached for the full 6-D HOOH PES with a third-degree IMLS fit of ~1350 automatically selected *ab initio* points. Reliable termination procedures of automatic point selection allow pre-selected fit accuracy.

Future Work

The main objective of our research is the development of practical, facile methods for performing rate calculations for many-atom systems by using *ab initio* potential-energy surfaces (PESs). The long-term goal is to develop an automatic PES generation algorithm that takes advantage of high-performance computing environments. We are developing methods in which software for rate calculations will direct quantum chemistry codes to produce *ab initio* predictions of reaction rates and related dynamics quantities. There will be two major aspects of our future work: We will continue the formal and numerical refinements of the methods and we will make practical applications of the methods to reactions important in combustion chemistry. More specifically, we will perform studies of (a) the basic formal and numerical aspects of IMLS methods; (b) practical methods using IMLS for simulating reactions in many-atom systems, with an emphasis on hydrocarbon radical reactions; and (c) explore a method in which IMLS fitting of *ab initio* points of transition state regions is used to join existing analytical PESs of "component" systems to build a PES for a larger reacting system; e.g., the allene/propyne system. All of this work will be done in collaboration with Drs. A. Wagner and M. Minkoff at ANL.

Publications

- Yin Guo and Donald L. Thompson, "Semiclassical Calculations of Tunneling Splitting in Hydrogen Peroxide and its Deuterated Isotopomers," J. Phys. Chem. A **106**, 8374-8377 (2002). (Part of Don Setser Festschrift)
- Yin Guo and Donald L. Thompson, "A Theoretical Study of Cis-Trans Isomerization in HONO Using an Empirical Valence Bond Potential," J. Chem. Phys. **118**, 1673-1678 (2003).
- Gia G. Maisuradze and Donald L. Thompson, "Interpolating Moving Least-Squares Method for Fitting Potential Energy Surfaces: Illustrative Approaches and Applications," J. Phys. Chem. A **107**, 7118-7124 (2003). (Part of Donald J. Kouri Festschrift)
- Yin Guo and Donald L. Thompson, "A Classical Trajectory Study of Bond Dissociation in HONO and HOOH," Chem. Phys. Letters **382**, 654-660 (2003).
- Yin Guo, Akio Kawano, Donald L. Thompson, Albert F. Wagner, and Michael Minkoff, "Interpolating Moving Least-Squares Methods for Fitting Potential Energy Surfaces: Applications to Classical Dynamics Calculations," J. Chem. Phys. **121**, 5091-5097 (2004).
- Gia G. Maisuradze, Akio Kawano, Donald L. Thompson, Albert F. Wagner, and Michael Minkoff, "Interpolating Moving Least-Squares Methods for Fitting Potential Energy Surfaces: Analysis of an Application to a Six-Dimensional System," J. Chem. Phys. **121**, 10329-10338 (2004).
- Akio Kawano, Igor Tokmakov, Donald L. Thompson, Albert F. Wagner, and Michael Minkoff, "Interpolating Moving Least-Squares Methods for Fitting Potential Energy Surfaces: Further Improvement of Efficiency via Cutoff Strategies," J. Chem. Phys., to be submitted.

References

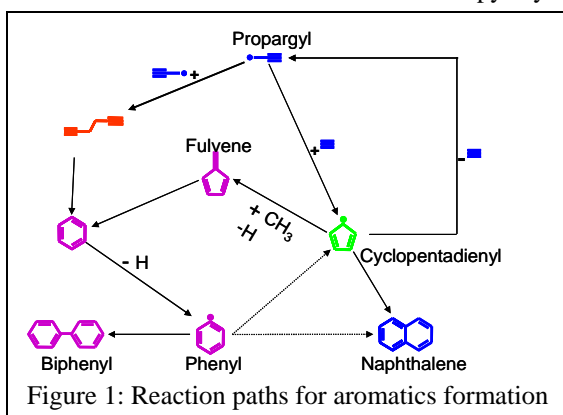
1. D. R. McLaughlin and D. L. Thompson, *J. Chem. Phys.* **59**, 4393 (1973).
2. J. Ischtwan and M. A. Collins, *J. Chem. Phys.* **100**, 8080 (1994).
3. G. G. Maisuradze and D. L. Thompson, *J. Phys. Chem. A* **107**, 7118 (2003).
4. H. Koizumi, G. C. Schatz, and S. P. Walch, *J. Chem. Phys.* **95**, 4130 (2003).
5. A. Kawano, Y. Guo, D. L. Thompson, A. F. Wagner, and M. Minkoff, *J. Chem. Phys.* **120**, 6414 (2004).
6. B. Kuhn, T. R. Rizzo, D. Luckhaus, M. Quack, and M. A. Suhm, *J. Chem. Phys.* **111**, 2565 (1999).
7. Y. Guo, A. Kawano, D. L. Thompson, A. F. Wagner, and M. Minkoff, *J. Chem. Phys.* **121**, 5091 (2004).
8. A. Kawano, I. Tokmakov, D. L. Thompson, A. F. Wagner, and M. Minkoff, "Interpolating Moving Least-Squares Methods for Fitting Potential Energy Surfaces: Further Improvement of Efficiency via Cutoff Strategies," *J. Chem. Phys.*, to be submitted.
9. G. G. Maisuradze, A. Kawano, D. L. Thompson, A. F. Wagner, and M. Minkoff, *J. Chem. Phys.* **121**, 10329 (2004).

Elementary Reactions of PAH Formation

Robert S. Tranter
Chemistry Division
Argonne National Laboratory
Argonne, IL-60439
tranter@anl.gov

Program scope

This program is aimed at elucidating kinetic and mechanistic information over a broad range of temperature and pressure for elementary reactions that are important in combustions systems. In particular the initial research is focused on the web of pyrolytic and oxidative reactions involved in the formation and destruction of small aromatic species in flames such as those illustrated in figure 1.



The approach utilizes two experimental apparatuses whose combined strengths can be exploited to study reactions from near room temperature to flame temperatures at pressures from approximately 1 torr to 500 torr. One apparatus is a low pressure fast flow reactor (LPFFR) and the other a diaphragmless shock tube (DLST). The LPFFR is coupled via a nozzle/skimmer interface to a quadrupole mass spectrometer and the DLST has been designed for coupling to a time-of-flight mass spectrometer (TOF-MS) and for Laser Schlieren (LS).

Recent Progress

DLST/TOF-MS

A new diaphragmless shock tube apparatus ($P_5 < 500$ torr, $T_5 > 900$ K) has been developed for coupling to a TOF-MS to permit species concentrations to be monitored behind reflected shock waves using a 'universal detector'. The principle difference between the DLST and a conventional shock tube is that in the DLST the driven section is separated from the driver section by a plate that covers the end of the driven section instead of a diaphragm being placed between the two sections. The DLST is then fired by quickly moving the plate out of the way. For a shock tube that is coupled to a TOF-MS the DLST design has several advantages. The primary benefits are that it is no longer necessary to expose the tube to air to replace the diaphragm, there are no diaphragm fragments to accumulate inside the shock tube as happens in tubes where the diaphragms are burst spontaneously and more reproducible shocks can be generated than is possible using spontaneously burst diaphragms due to the ability to accurately set the initial conditions in the DLST. For the new DLST, a novel design that is different to that of Matsui et al¹ has been developed using an air driven piston to move the sealing plate from the end of the driven section. This allows the force used to fire the shock tube to be set independently of the driver gas pressure allowing for better control of the piston. A schematic of the DLST/TOFMS is shown in figure 2.

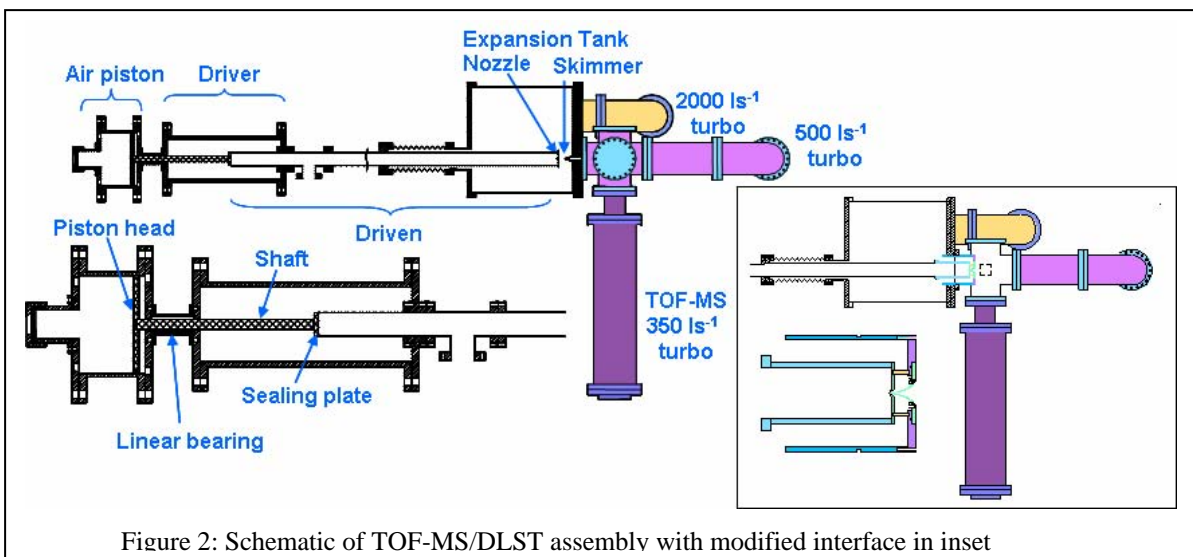


Figure 2: Schematic of TOF-MS/DLST assembly with modified interface in inset

In addition to the TOF-MS the DLST has been equipped with optical ports for laser schlieren studies or possibly other optical diagnostics. The DLST has been constructed and the initial tests will measure, via shock velocity measurements, the ability to create reproducible post shock conditions for given initial conditions and the LS setup will be tested by measuring rate coefficients of a couple of well defined reactions.

The TOF-MS with electron impact ionization and interface to the shock tube has been recently

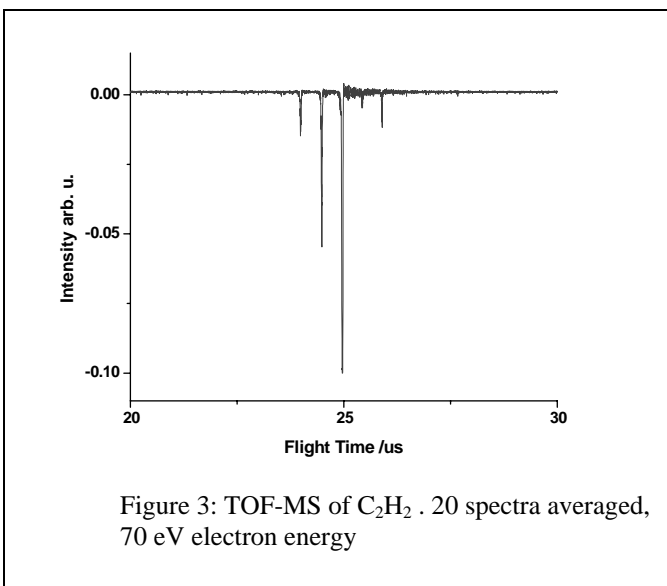


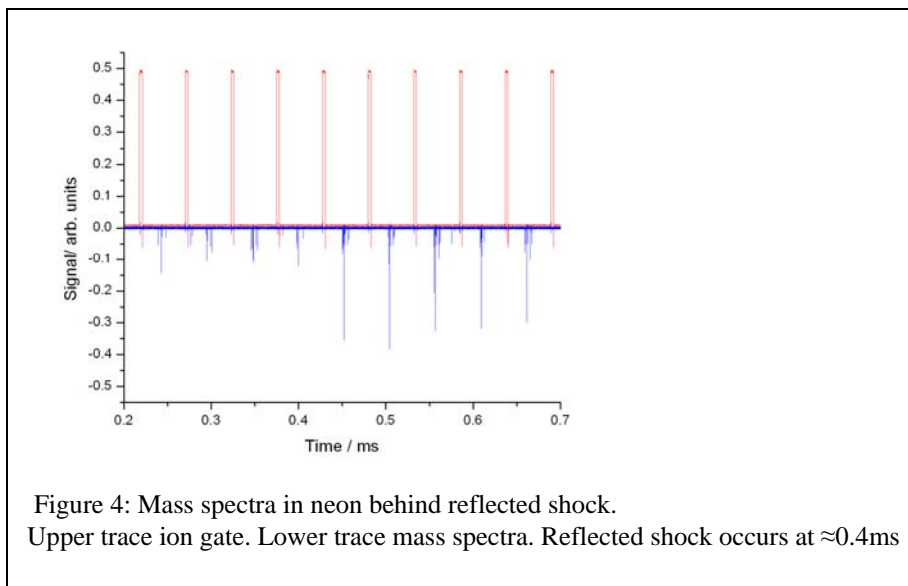
Figure 3: TOF-MS of C_2H_2 . 20 spectra averaged, 70 eV electron energy

constructed in Kiefer's lab at UIC and initial developments were presented in previous progress reports. The apparatus is conceptually similar to Kern's now decommissioned TOF/shocktube system but incorporates many improvements including superior data acquisition that provides better resolution, a differentially pumped nozzle/skimmer interface that permits larger sampling orifices to be used thereby improving sensitivity and minimizing sampling effects due to wall collisions and larger pumps that can handle the increased gas flow from the DLST into the TOF-MS. Electron impact is a reasonable ionization scheme for this apparatus due to the high rep rate that the beam can be pulsed at which permits multiple data points to be acquired in the early stages of reaction as well as the

broad applicability of the technique. However photoionization may yield isomer specific information and the application to shock tube/TOF-MS studies will be explored particularly if very reproducible shocks can be attained with the DLST.

Early tests of the TOF-MS assembly used Kiefer's shock tube as a gas reservoir to supply a constant stream of stable species into the TOF-MS ionization zone. A sample of the measured spectra are shown in fig 3 for C_2H_2 . The spectrum shows well defined, narrow peaks that are well resolved however a couple of points need to be noted. First the spectrum is an average of 20 spectra and in shock tube/TOF-MS experiments only single shot spectra are available due to the rapidly changing gas composition behind the shock waves. Secondly the flight time of the $C_2H_2^+$ ions is around 25 us which is too long if several spectra are to be captured in the first 100 us of reaction. With the initial configuration of the TOF-MS interface

single shot spectra were quite noisy and exhibited low sensitivity even for pressures up to 1×10^{-5} torr in the ion source, obtained with large gas flows from the shock tube.



The poor sensitivity was almost certainly due to the large separation ($\approx 5''$) between the skimmer and the ionization zone of the mass spectrometer. The interface was modified as shown in fig. 2 inset to allow the skimmer to be placed within a few millimeters of the TOF-MS ionization zone.

A large amount of background noise was traced to several faulty insulators in the E-Gun and ion optics. Replacement of these insulators greatly reduced spurious signals and background noise.

With the above modifications the signal shown in figure 4 was recently obtained which shows a series of spectra taken prior to an incident shock wave in neon arriving at the end wall of the shock tube and behind the reflected shock wave ($P_5=280$ torr, $T_5=1380$ K); note the large increase in signal as the reflected shock is generated. The ion gating pulse which introduces ions into the TOF-MS occurred every 50 μ s. The flight time for neon is about 24 μ s (TOF voltages are a little different to the C_2H_2 experiments). While this result is very encouraging and indicates that the apparatus is ready to use for kinetic experiments it can currently only be applied to relatively slow reactions due to the long flight times. To study fast reactions the flight time needs to be shortened which is being addressed with a shortened flight tube and higher accelerating voltages.

The ultimate goal with the DLST/TOF-MS experiment is to perform simultaneous TOF-MS and LS experiments behind incident shock waves so that species data and initial rates of reaction can be obtained in the same experiment. This is not a trivial problem as the sampling time available for the MS part of the experiment will be on the order of a few tens of microseconds.

Low pressure fast flow reactor

The new LPFFR is being developed primarily to study radical molecule reactions under pseudo first order conditions and at temperatures from 300 K to ~ 1200 K and at pressures from <1 torr to ~ 100 torr. The temperature, pressure and residence times in the reactor thereby extend the range of conditions that can be applied to a particular reaction by combining DLST and LPFFR experiments. The detection method (MS) is very suitable for analyzing the mixtures of heavy species that will elute from the reactor under conditions where IR or UV absorption studies would be difficult. The primary detector is a quadrupole mass spectrometer coupled to the reactor via a centerline sampling nozzle/skimmer arrangement that minimizes sampling problems, associated with different flow regimes at different pressures in the reactor². Initially electron impact ionization which is broadly applicable to all molecules and radicals in addition to being simple and inexpensive will be used. However to minimize fragmentation and improve detection of parent ions and discrimination of isomers alternative ionization schemes will be required particularly as the work moves towards larger aromatic species.

The LPFFR is particularly well suited to pseudo first order studies of radical molecule reactions and the use of novel double injectors gives access to a wide variety of radical species via titration reactions

such as stripping of halides with Na atoms at the highest temperatures attainable in the reactor. Currently the LPFFR is being constructed and shortly testing will begin

Future Plans

The TOF-MS, DLST and LPFFR will be tested by using appropriate reactions with well established rate coefficients and following successful tests the TOF-MS will be moved to ANL and coupled to the DLST. One of the first true studies made with the two experiments will be the oxidation and recombination of phenyl radicals that form a key part of PAH production. The oxidation reaction exhibits a shift in mechanism from stabilization of the peroxy adduct to decomposition into phenoxy and p-benzoquinone at around 900 K. So far the shift has not been experimentally observed although previous flow tube experiments at up to 850K indicated the beginnings of a change in mechanism. Additionally the only two shock tube studies of this reaction resulted in rate coefficients that are in broad agreement but differ in activation energy^{3,4}. The formation of biphenyl from phenyl radical combination is an obvious competitor to the oxidation path. Recent theoretical calculations by Harding and Klippenstein⁵ have shown large discrepancies to some of the existing experimental data for this reaction and detailed experimental studies from 300-1200K are needed to augment the existing data set for reliable comparison between theory and experiment. This range is accessible using the combined capabilities of the DLST/TOF-MS and LPFFR. These reactions form the first part of an extensive investigation of the reaction network in fig. 1.

References

1. M. Yamauchi, H. Matsui, M. Koshi, K. Tanaka, S. Tamaki and H. Tanaka, *Bunko Kenkyu* **36**, 388(1987).
2. J.V. Seeley, J.T. Jayne and M.J. Molina, *Int. J. Chem. Kinet.*, **25**,571(1993).
3. S. S. Kumaran and J. V. Michael, *Proceedings of the 21st International Symposium on Shock Waves* A. F. P. Houwing, Ed., Panther Publishing, Fyshwick, Australia, pp. 241-244
4. P. Frank, J. Herzler, Th. Just, and C. Wahl, *Proc. Combust. Inst.* **25**, 833 (1994)
5. L.B. Harding and S. J. Klippenstein, unpublished .

Publications

1. "Dissociation, Relaxation and Incubation in the Pyrolysis of Neopentane: Heat of Formation of the tert-butyl Radical", N. K Srinivasan, J.H. Kiefer and R.S. Tranter, *J.Phys. Chem A* **107**, 1532(2003)
2. "A Shock-Tube, Laser-Schlieren Study of the Pyrolysis of Isobutene: Relaxation, Incubation and Dissociation Rates", S. Santhanam, J.H. Kiefer, R.S. Tranter and N.K. Srinivasan, *Int. J. Chem. Kinet.*, **35**, 381 (2003)
3. "Vibrational Relaxation in Methyl Hydrocarbons at High temperatures: Propane, Isobutene, Isobutane, Neopentane and Toluene" J.H. Kiefer, G.C. Sahukar, S. Santhanam, N. K. Srinivasan and R.S. Tranter, *J. Chem. Phys.* **120**, 918 (2004)
4. "A Shock-Tube, Laser-Schlieren Study of the Dissociation of 1,1,1-trifluoroethane: An Intrinsic non-RRKM Process" J. H. Kiefer, C. Katapodis, S. Santhanam, N. K. Srinivasan and R. S. Tranter, *J. Phys. Chem. A* **108**, 2443 (2004)
5. "Dissociation, Relaxation, and Incubation in the High-Temperature Pyrolysis of Ethane, and a Successful RRKM Modeling", J. H. Kiefer, S. Santhanam, N. K. Srinivasan, and R.S. Tranter, S. J. Klippenstein, and M. A. Oehlschlaeger. *Proc. 30th Int. Symp. Combust.*, 2005
6. "A Shock Tube Study of the High Pressure Thermal Decomposition of Benzene", R. R. Sivaramakrishnan, H. Vasudevan, R.S. Tranter, K. Brezinsky, *In Press, Combustion Science and Technology*, 2005

VARIATIONAL TRANSITION STATE THEORY

Principal investigator, mailing address, and electronic mail

Donald G. Truhlar
Department of Chemistry, University of Minnesota, 207 Pleasant Street SE,
Minneapolis, Minnesota 55455
truhlar@umn.edu

Program scope

This project involves the development of variational transition state theory (VTST) with multidimensional tunneling (MT) contributions and its application to gas-phase reactions. The further development of VTST as a useful tool for combustion kinetics also involves multidimensional tunneling calculations for the transmission coefficient, electronic structure calculations for the input potential energy surfaces, and methods to interface the electronic structure calculations to the dynamics calculations. Our current work has a special emphasis on developing and applying new methods of electronic structure theory and interfacing reaction-path and reaction-swath dynamics calculations with electronic structure theory. The project involves the development of new theory, the development and implementation of practical techniques for applying the theory to various classes of reactions and transition states, and applications to specific reactions, with special emphasis on combustion reactions and reactions that provide good test cases for methods needed to study combustion reactions. A theme that runs through our current work is the development of consistently and generally defined electronic structure methods with empirical elements, including molecular mechanics, density functionals, and scaled-electron-correlation components and the use of these methods in direct or semidirect dynamics calculations of chemical reaction rates.

Recent progress

In order to generate reactive potential energy surfaces with minimal computational effort, we have introduced an algorithm called multiconfiguration molecular mechanics (MCMM). MCMM describes polyatomic potential energy surfaces by several interacting MM configurations (each of which is the analog of a valence bond configuration) and can thus be viewed as an extension of standard MM to chemical reactions. From another point of view, MCMM provides a semiautomatic fitting scheme for electronic structure data and may therefore be considered a form of semidirect dynamics. MCMM fitting is accomplished by combining molecular mechanics potentials for the reactant and product wells with electronic structure data (energy, gradient, and Hessian) at the saddle point and a small number of non-stationary points. We developed a general strategy for placement of the non-stationary points for fitting potential energy surfaces in the kinetically important regions and for calculating rate constants for atom transfer reactions by variational transition state theory with multidimensional tunneling. Then we improved the efficiency of the MCMM method by using electronic structure calculations only for certain critical elements of the Hessians at the non-stationary points and by using interpolation for the other elements at the non-stationary points. We tested this new MCMM strategy for a diverse test suite of reactions involving hydrogen-atom transfer. The new method yields quite accurate rate constants as compared with the standard MCMM strategy employing full electronic structure Hessians and also as compared with straight (uninterpolated) direct dynamics calculations at the same electronic structure level.

Development of exchange and correlation functionals for density functional theory (DFT) is an active research area in theoretical chemistry and physics, but most of this research has neglected the important issue of barrier height prediction. We have embarked on a systematic set of calculations designed to improve the performance of DFT for barrier heights and other thermochemical quantities (such as heats of formation) of interest to combustion modeling. Our current set of databases includes the MGAE109/3 atomization energy database, the IP13/3 ionization potential database, the EA13/3 electron affinity database, the HB6/04 hydrogen

bonding database, the CT7/04 charge transfer database, the DI6/04 dipole interaction database, the WI9/04 weak interaction database, a pi-pi interaction database, and the HTBH38/4 and NHTBH38/04 databases for barrier heights of the following classes of reaction: hydrogen transfer reactions, heavy-atom transfer reactions, nucleophilic substitution reactions, and unimolecular and association reactions. Some DFT methods such as B3LYP, B1B95, and B97-2 are successful for thermochemistry but unsatisfactory for kinetics, whereas our earlier density functionals developed for kinetics (MPW1K and BB1K), although quite accurate for barrier heights, are not as accurate as one would like for the whole set of data. However, we were able to develop some more broadly applicable density functionals. In particular, our new PW6B95 and PWB6K density functionals now appear to be the most broadly accurate density functionals available for combustion chemistry, and they represent a considerable improvement over the most popular functionals in current use.

Software distribution

We have developed several software packages for applying variational transition state theory with optimized multidimensional tunneling coefficients to chemical reactions and for carrying out MCCM calculations, hybrid Hartree-Fock density functional theory calculations, direct dynamics, and MCMM applications. The URL of our software distribution site is comp.chem.umn.edu/Truhlar. The license requests that we fulfilled during the period Jan. 1, 2003–Mar. 31, 2005 for software packages developed wholly or partially under DOE support is as follows:

	<i>Total</i>	<i>academic</i>	<i>government/DoD</i>	<i>industry</i>
GAMESSPLUS	79	71	3	5
GAUSSRATE	81	78	2	1
HONDOPLUS	40	33	5	2
MOPAC-mn	94	78	8	8
MULTILEVEL	20	19	1	0
POLYRATE	178	169	17	2
7 OTHERS	31	28	1	2

Future plans

We have several specific objectives for the next few years. (1) It will be useful, especially for the treatment of small-barrier association reactions, to create a hybrid theory incorporating quantization and multidimensional tunneling into the multifaceted-dividing-surface generalization of the variable reaction coordinate approach to VTST, and research aimed at this objective will be initiated. (2) Projects will be undertaken to develop further improved density functional methods and further improved multi-coefficient correlation methods for using electronic structure theory to calculate potential energy surfaces. (3) We will further develop the multi-configuration molecular mechanics approach as an efficient tool for the semiautomatic fitting of potential energy surfaces for large systems. (4) We will attempt to develop more reliable methods for including anharmonicity at variational transition states, especially for torsions. (5) We will develop new methods for the calculation of substituent effects. Reactions to be considered as test cases include: reactions of hydrogen atoms with hydrogen peroxide, ethanol, acetaldehyde, acetone, 2-butanone, acetylene, methylformate, fluoromethyl formate, and polycyclic aromatic hydrocarbon anions; reactions of C(³P) with allene; hydrogen atom abstraction from fluoroformaldehyde by NO₃; reaction of hydroxyl radical with hydrogen sulfide, dimethyl sulfide, ethylene, benzene, and toluene; reactions of CF₃ with various hydrocarbons; and rearrangement of unsymmetrically substituted *o*-tolylcarbenes. We will also carry out further studies of the reaction of H with methanol. (6) In addition to developing the methods, we are putting them into user-friendly packages that will allow more researchers to carry out calculations conveniently by the new methods.

Publications, 2003-present

Journal articles

1. "Reduced Mass in the One-Dimensional Treatment of Tunneling," D. G. Truhlar and B. C. Garrett, *Journal of Physical Chemistry A* **107**, 4006-4007 (2003).
2. "The Effectiveness of Diffuse Basis Functions for Calculating Relative Energies by Density Functional Theory," B. J. Lynch, Y. Zhao, and D. G. Truhlar, *Journal of Physical Chemistry A* **107**, 1384-1388 (2003).
3. "Robust and Affordable Multi-Coefficient Methods for Thermochemistry and Thermochemical Kinetics: The MCCM/3 Suite and SAC/3," B. J. Lynch and D. G. Truhlar, *Journal of Physical Chemistry A* **107**, 3898-3906 (2003).
4. "Generalized Transition State Theory in Terms of the Potential of Mean Force," G. K. Schenter, B. C. Garrett, and D. G. Truhlar, *Journal of Chemical Physics* **119**, 5828-5833 (2003).
5. "Force Field Variations along the Torsional Coordinates of CH₃OH and CH₃CHO," T. V. Albu and D. G. Truhlar, *Journal of Molecular Spectroscopy* **219**, 129-131 (2003).
6. "H + H₂ Thermal Reaction: Another Solved Problem of Quantum Mechanics," S. L. Mielke, K. A. Peterson, D. W. Schwenke, B. C. Garrett, D. G. Truhlar, J. V. Michael, M.-C. Su, and J. W. Sutherland, *Physical Review Letters* **91**, 063201/1-4 (2003).
7. "Small Representative Benchmarks for Thermochemical Calculations," B. J. Lynch and D. G. Truhlar, *Journal of Physical Chemistry* **107**, 8996-8999 (2003).
8. "Small Basis Sets for Calculations of Barrier Heights, Energies of Reaction, Electron Affinities, Geometries, and Dipole Moments," B. J. Lynch and D. G. Truhlar, *Theoretical Chemistry Accounts* **111**, 335-344 (2004).
9. "Small Representative Benchmarks for Thermochemical Calculations," B. J. Lynch and D. G. Truhlar, *Journal of Physical Chemistry A* **107**, 8996-8999 (2003); erratum: **108**, 1460 (2003).
10. "Benchmark Results for Hydrogen Atom Transfer Between Carbon Centers and Validation of Electronic Structure Methods for Bond Energies and Barrier Heights," A. Dybala-Defratyka, P. Paneth, J. Pu, and D. G. Truhlar, *Journal of Physical Chemistry A* **108**, 2475-2486 (2004).
11. "Tests of Second-Generation and Third-Generation Density Functionals for Thermochemical Kinetics," Y. Zhao, J. Pu, B. J. Lynch and D. G. Truhlar, *Phys. Chem. Chem. Phys.* **6**, 673-676 (2004).
12. "Development and Assessment of a New Hybrid Density Functional Method for Thermochemical Kinetics," Y. Zhao, B. J. Lynch, and D. G. Truhlar, *J. Phys. Chem. A* **108**, 2715-2719 (2004).
13. "Efficient Molecular Mechanics for Chemical Reactions: Multiconfiguration Molecular Mechanics using Partial Electronic Structure Hessians," H. Lin, J. Pu, T. V. Albu, and D. G. Truhlar, *Journal of Physical Chemistry A* **108**, 4112-4124 (2004).
14. "Doubly Hybrid DFT: New Multi-Coefficient Correlation and Density Functional Methods for Thermochemistry and Thermochemical Kinetics," Y. Zhao, B. J. Lynch, and D. G. Truhlar. *Journal of Physical Chemistry A* **108**, 4786-4791 (2004).
15. "Hybrid Meta Density Functional Theory Methods for Thermochemistry, Thermochemical Kinetics, and Noncovalent Interactions: The MPW1B95 and MPWB1K Models and Comparative Assessments for Hydrogen Bonding and van der Waals Interactions," Y. Zhao and D. G. Truhlar, *Journal of Physical Chemistry A* **108**, 6908-6918 (2004).
16. "Use of Block Hessians for the Optimization of Molecular Geometries," *Journal of Computational and Theoretical Chemistry* **1**, 54-60 (2005).
17. "Variational Transition State Theory," B. C. Garrett and D. G. Truhlar, *Journal of Molecular Structure THEOCHEM*, in press.

18. "The 6-31B(d) Basis Set and the BMC-QCISD and BMC-CCSD Multi-Coefficient Correlation Methods," B. J. Lynch, Y. Zhao, and D. G. Truhlar, *Journal of Physical Chemistry A* **109**, 1643-1649 (2005).
19. "Multi-Coefficient Extrapolated Density Functional Theory for Thermochemistry and Thermochemical Kinetics," Y. Zhao, B. J. Lynch, and D. G. Truhlar, *Physical Chemistry Chemical Physics* **7**, 43-52 (2005).
20. "Benchmark Calculations of Reaction Energies, Barrier Heights, and Transition State Geometries for Hydrogen Abstraction from Methanol by a Hydrogen Atom," and D. G. Truhlar, *Journal of Physical Chemistry A* **109**, 773-778 (2005).
21. "Benchmark Database of Barrier Heights for Heavy Atom Transfer, Nucleophilic Substitution, Association, and Unimolecular Reactions and Its Use to Test Theoretical Methods," Y. Zhao, N. González-García, and D. G. Truhlar, *Journal of Physical Chemistry A* **109**, 2012-2018 (2005).
22. "Temperature Dependence of Carbon-13 Kinetic Isotope Effects of Importance to Global Climate Change," H. Lin, Y. Zhao, B. A. Ellingson, J. Pu, and D. G. Truhlar, *Journal of the American Chemical Society*, in press.
23. "Redistributed Charge and Dipole Schemes for Combined Quantum Mechanical and Molecular Mechanical Calculations," H. Lin and D. G. Truhlar, *Journal of Physical Chemistry B*, in press.
24. "Generalized Hybrid Orbital Method for Combined Quantum Mechanical and Molecular Mechanical Calculations Based on Density Functional Theory and Hybrid Density Functional Theory," J. Pu, J. Gao, and D. G. Truhlar, *ChemPhysChem*, in press.
25. "Benchmark Databases for Nonbonded Interactions and Their Use to Test Density Functional Theory," Y. Zhao and D. G. Truhlar, *Journal of Chemical Theory and Computation*, in press.
26. "Dependence of Transition State Structure on Substrate: The Intrinsic C-13 Kinetic Isotope Effect is Different for Physiological and Slow Substrate of the Ornithine Decarboxylase Reaction Because of Different Hydrogen Bonding Structures," D. Sicinska, D. G. Truhlar, and P. Paneth, *Journal of the American Chemical Society*, in press.
27. "Databases for Transition Element Bonding: Metal–Metal Bond Energies and Bond Lengths and Their Use to Test Hybrid, Hybrid Meta, and Meta Density Functionals and Generalized Gradient Approximations," N. E. Schultz, Y. Zhao, and D. G. Truhlar, *Journal of Physical Chemistry*, in press.
28. "The Design of Density Functionals that are Broadly Accurate for Thermochemistry, Thermochemical Kinetics, and Nonbonded Interactions," Y. Zhao and D. G. Truhlar, *Journal of Physical Chemistry A*, received by JPC on Jan. 31, 2005.

Book chapters

1. "Multilevel Methods for Thermochemistry and Thermochemical Kinetics," B. J. Lynch and D. G. Truhlar, *American Chemical Society Symposium Series*, edited by A. K. Wilson, American Chemical Society, Washington, in press.
2. "Variational Transition State Theory and Multidimensional Tunneling for Simple and Complex Reactions in the Gas Phase, Solids, Liquids, and Enzymes," D. G. Truhlar, in *Isotope Effects in Chemistry and Biology*, edited by H. Limbach and A. Kohen (Marcel Dekker, Inc., New York, 2004), to be published.
3. "Bimolecular Reactions," A. Fernández-Ramos, J. A. Miller, S. J. Klippenstein, and D. G. Truhlar, in *Comprehensive Chemical Kinetics*, edited by R. W. Carr and M. R. Zachariah (Elsevier, Amsterdam, 2004), to be published.

KINETIC DATABASE FOR COMBUSTION MODELING

Wing Tsang
National Institute of Standards and Technology
Gaithersburg, MD 20899
wing.tsang@nist.gov

Program Scope or Definition: The fundamentals of combustion are based on fluid dynamics and chemical kinetics. Progress in the treatment of reactive flows have led to the capability of newer computational fluid dynamics programs being able to handle increasing amounts of chemistry. There is the prospect that realistic systems can be simulated and hence the development of powerful design tools that will increasingly take the place of empirical physical testing. The aim of this project is to help develop the chemical kinetic databases for ultimate use in such reactive flow programs. The elements in this work are the rate expressions for the chemical reactions that convert reactants into products through a variety of reaction intermediates and the thermodynamic properties of the molecular entities. The information in the databases represents transferable elements that can be used in a large variety of scenarios. For kinetics, they begin with the thermal rate constants for unimolecular and bimolecular processes. Our work has largely concentrated on the former. We have been particularly concerned with the pyrolytic decompositions that form the smaller unsaturated compounds that are the precursors to soot. Insufficient attention has been paid to these reactions in existing databases since they have been concerned with the initial stages of combustion. It has become particularly important in recent years due to the interest in particle formation from combustion with particular fuels.

Recent Progress: Earlier work has focussed on the decomposition of the aliphatic radicals that are formed from the abstraction of hydrogens from the fuel molecules or the 1-olefins formed from their decomposition. The 1-olefinyl radicals can now decompose to form the dienes that are important precursors of PAH/Soot. Problems involved in assigning rate constants for these processes have been discussed in previous reports. They involve the multichannel nature of the decomposition, the possibility of isomerization and the low reaction thresholds. These create problems for the treatment of the contribution of energy transfer processes during unimolecular decomposition, since such situations are not treated in standard formalisms and neglected in current combustion kinetics databases. Generalization of the standard procedures has been developed and applied to these systems (1). Work during the past year have been concerned with the chemically activated decomposition of the aliphatic radicals formed as a result of the addition of hydrogen atoms to the 1-olefins formed from alkyl radical decomposition, tunneling effects during alkyl radical isomerization and preliminary work on the oxidation of heptane.

(a) Chemically activated radical decomposition: The necessity of considering such processes can be seen in Figure 1. Rate constants of addition reactions are not overtaken by abstraction processes until temperatures in the 700-1000 K range(2). These addition reactions lead to chemically activated molecules with rate constants that are dependent on the rate of relaxation to thermal distributions. This sequence of processes have been neglected in combustion kinetics databases. The high temperatures generate many radicals that can react with unsaturates or other radicals to form hot molecules. Therefore the phenomenon is quite general. Figure 2 summarizes

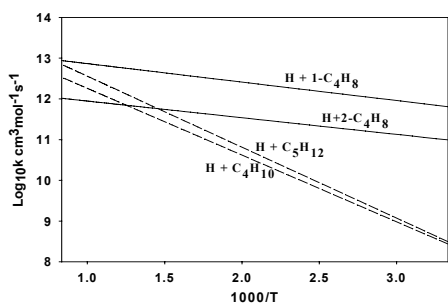


Figure 1: Hydrogen atom additions (solid line) and abstraction rate constants

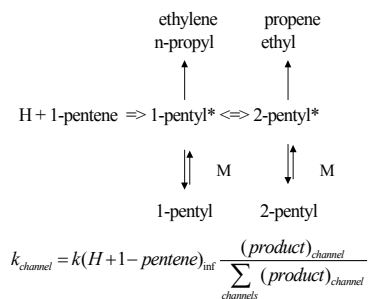


Figure 2: Mechanism for the chemically activated decomposition of 1-pentyl radical and rate constants for individual channels

the reactions of importance as a result of the chemically activated formation of 1-pentyl radicals from the nonterminal addition of H-atom to 1-pentene. The overall effect is to reduce the production of the products from olefinyl radical decomposition into the dienes and increase the small olefin yields. Practically all the past work on chemically activated decompositions has dealt with studies near room temperature (3). The consequence is that there are no contributions from the thermal decomposition of the stabilized molecule. The aim of the present work is to arrive at a general picture of the case where the chemical activation reaction is occurring under combustion temperatures. Figure 3 gives a picture of the physical situation. At the lowest temperatures, subsequent to an initial induction period and before the attainment of a final steady state distribution one obtains the chemically activated decomposition. However at really long time there are indications that yields are beginning to increase again. The physical picture consists of a certain amount of product being decomposed via chemical activation. However much of the activated molecule is being stabilized. As the concentration of stabilized molecule increases some of the stabilized molecules will cross the reaction threshold and decomposition will now occur thermally. There are some indications of this at the lowest temperatures. It becomes more clear at the intermediate temperatures and at the highest temperatures the chemical activation and thermal reactions run into each other. A troublesome problem is the existence of two rate constants as a function of time. We have found that it is possible to divide them into a chemically activated and a thermal rate (in the fall-off region). This is illustrated in Figure 4. Our analysis of the situation shows that even at the highest temperatures the chemical activation component is the dominant one. The distribution of products from the ethylene and propene decomposition channels are relatively invariant whether they are formed from thermally or chemically activated molecules. These results can serve as a guide for subsequent work. They will be particularly important in PAH formation and the initial steps in oxidation mechanisms. Figure 4 contains an Arrhenius plot of the three chemically activated decomposition reactions at 1 bar pressure. These reactions are pressure dependent. The rate constants are much larger than that if purely high pressure rate constants are used.

(b) Contribution of tunneling to radical isomerization: Radical isomerization processes are an important component of the decomposition of larger aliphatic decomposition. There has long been problems in fitting low and high temperature results(4-6). We have found that this is most likely due to neglect of tunneling effects. This will be illustrated for the isomerization reaction 1-hexyl \rightleftharpoons 2-hexyl. These reactions have large rate constants. They are most conveniently studied near room temperature. The measured A-factors are extremely small and it is difficult to construct a reasonable transition state to accommodate such values. Recent higher temperature measurements from this series of studies lead to drastically larger A-factors. The drastic change

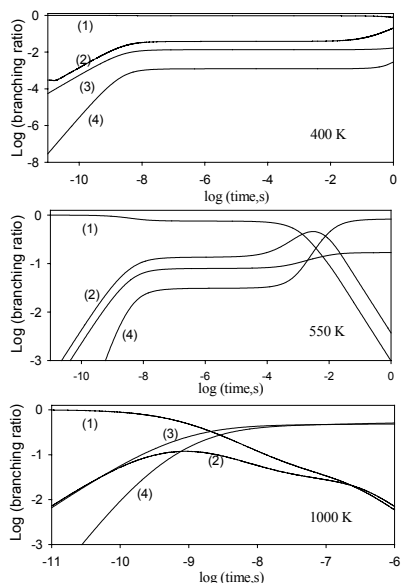


Figure 3: Branching ratios for the four reaction channels during the chemically activated decomposition of 1-pentylradicals: (1) 1-pentyl; (2) 2-pentyl (3)1-pentyl=ethylene + 1-propyl (4)2-pentyl =propene + ethyl

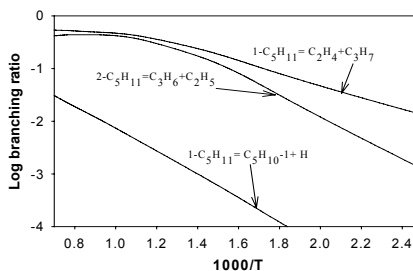


Figure 4: Branching ratio for 1-pentyl radical decomposition as a function of temperature at 1 bar

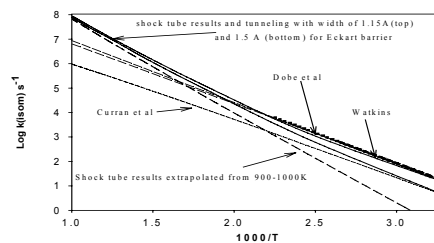


Figure 5: Rate constants for 1-5 hydrogen shift during 1-hexyl radical isomerization. Dobe, Watkins and shock tube studies are experimental results. Curran et al is the recommendation for heptane oxidation

in slope is suggestive of tunneling. Specifically, the measurements at low temperature are almost entirely due to tunneling effects. At 1000 K the tunneling effects represent only 20 % of the rate constant. The situation is summarized in Figure 5. It can be seen that straightforward linear extrapolation from either the high or low temperature results leads to gross errors. Also included are recommendations of Curran et al (7). They lead to drastic errors at high temperatures.

The data can be accommodated with an Eckart potential with a barrier width of 1.15 Angstroms. This leads to a non-Arrhenius T^6 value. In the case of H + methane the non-Arrhenius fact is of the order of T^4 . We can rationalize this in terms of the high reaction barrier and the constraints imposed by the cyclic transition state. This work also illustrates the problems involved in extrapolating data over extended temperature range. Fortunately, these tunneling effects are probably most important for hydrogen transfer reactions. An immediate application that comes to mind is the sequence of oxidation reaction $R^* + O_2 = RO_2 = *QO_2H$, in exact analogy to the alkyl radical isomerization case. We also note that this sequence of reactions involves chemical activation processes. Here again existing combustion databases have not taken this into account.

(c) Heptane Oxidation: We had originally planned to devote much of the current year's effort on the initial steps in heptane oxidation. However in the course of completing work on the pyrolytic module, the issues discussed earlier became evident. Note that the processes treated here are precisely those of concern in the initial oxidation processes. Considerable amount of preliminary work have been carried out. There is much less experimental data to serve as a basis for predictions. However the rate constant for initial processes involving oxygen and small hydrocarbon radicals are beginning to appear (8). The recent theoretical work of Green and coworkers (9) have laid a basis regarding the thermochemistry and some of the chemical kinetics. Existing experimental work on product distribution from oxidation experiments during heptane oxidation(10) should be very useful. Clearly any database must be able to reproduce such observations. It should be possible to extract relative rate constants. Since some of the

products clearly involve beta bond scission and are well understood, it should be possible to use this as a basis to determine absolute rate constants. We are therefore combining our energy transfer calculations with CHEMKIN modeling.

Future Plans: We will continue work on the oxidation of heptane. As noted earlier the initial addition of oxygen and the subsequent isomerization and beta bond scission reactions are all chemical activation processes and has never been treated in this fashion. The isomerization processes involving internal hydrogen abstraction by oxygen is the exact analog of the situation described above for alkyl radical isomerization. An important issue will be the proper treatment of tunneling in the cases where oxygen is substituted for carbon.

Publications: 2003-2005

Roy, K. Awan, I. A., Manion, J. A., "Thermal Decomposition of 2-chloropropene and 2-bromopropene", *Phys. Chem., Chem. Phys.*, 2003, 5, 1806-1810

Tsang, W., "Energy Transfer Effects During Multichannel Decomposition of Ethanol", *Int. J. Chem. Kin.*, 36, 2004 456-465

Babushok, V. and Tsang, W., "Gas Phase Mechanism for Dioxin Formation", *Chemosphere* 2003, 51, 1023-1029

Babushok, V., Tsang, W., McNesby K. L., "Additive Influence on Polycyclic Aromatic Hydrocarbon Formation", *P. Combust. Inst.*, 2003, 29, 2315,-2323

Babushok V. Tsang, W., Kinetic Modeling of Heptane Combustion and PAH Formation, *J. Prop. and Power*", 2004, 20, 403-412

Tsang, W., "Progress in the Development of Combustion Kinetic Databases for Liquid Fuels" *Data Science Journal*, 3, 2004, 1-9

References:

1. Tsang, W., "A Pre-processor for the Generation of Chemical Kinetics Data for Simulations" AAIA-2001-0359, 39th AIAA Aerospace Sciences Meeting and Exhibit, January 8-11, 2001 Reno. NV

2. Kerr, J. A. and Parsonage M. J., "Evaluated Kinetic Data on Gas Phase Addition Reactions. Reactions of Atoms and Radicals with Alkenes, Alkynes and Aromatic Compounds" Butterworths, London, 1972. "Evaluated Kinetic Data on Gas Phase Hydrogen Transfer Reactions of Methyl Radicals Butterworths, London, 1976

3. Robinson, P. J. Holbrook, K. A., "Unimolecular Reactions", Wiley, New York, 1972

4. Dobe, S., Berces T. Reti, F. and Marta, P. *Int. J. Chem. Kin.*, 1987, 19, 895-921

5. Watkins, K. W., *J. Phys. Chem.*, 1973, 77, 2938-2942

6. Tsang, W., "Pathways for the Decomposition of 1-Hexyl Radicals"; *Chemical and Physical Processes in Combustion*, 1996 Fall Technical Meeting, Eastern States Section of the Combustion Institute, Hilton Head, SC., pg 515

7. Curran, H. J., Gaffuri, P., Pitz, W. J., Westbrook, C. K., *Comb. and Flame*, 1998, 114, 149,

8. DeSain, J. D., Klippenstein S. J. Miller, J. A., Taatjes, C. A., *J. Phys Chem., A*, 2003, 107, 4415-4427

9. Griffiths J. F. and Mohamed, C. "Experimental and Numerical Studies of Oxidation Chemistry and Spontaneous Ignition Phenomena", in *Comprehensive Chemical Kinetics, Low Temperature Combustion and Autoignition* (M. J. Pilling, ed) 1997, 545-660

10. Wijaya C.D., Sumathi R, Green W.H., *J. Phys. Chem. A*, 2003, 107, 4908-4920

SINGLE-COLLISION STUDIES OF ENERGY TRANSFER AND CHEMICAL REACTION

James J. Valentini
Department of Chemistry
Columbia University
3000 Broadway, MC 3120
New York, NY 10027
jjv1@columbia.edu

PROGRAM SCOPE

This research program aims to develop an understanding of the dynamics of bimolecular reactions. We are interested in many reactions—ones that are actually important in combustion, those that are prototypes of such reactions, and those that illustrate fundamental dynamical principles that govern combustion reactions. The principal question that we pose in our current work is how "many body" effects influence bimolecular reactions. By many-body effects we mean anything that results from having a reaction with a potential energy surface of more than three mathematical dimensions. For the reactions that we study now there are actually many more than three dimensions, at least 12 and usually many more, and part of our effort is to determine how many of them actually participate in the important dynamics of the reactions. These are polyatomic reactions, that is, reactions in which one or both of the reactants and one or both of the products are molecules with from 4 to 20 atoms. Our major current interest is in reactions for which the reactants offer multiple, identical reaction sites. Though sometimes we are interested in the details particular to one specific reaction, our approach is more commonly to study an entire class of reactions to develop a general understanding of how the factors of energetics, kinematics, and reactant/product structure control the dynamics in a series of analogous systems. As part of developing that understanding we devise and test models that explicate the interplay of these different influences.

Our effort is primarily experimental, but supplemented by computational simulations that help reveal details not accessible to experiments. Our experiments are measurements of quantum-state-resolved partial cross sections under single-collision conditions. We use pulsed uv lasers to produce reactive radical species and thereby initiate chemical reactions. The reaction products are detected and characterized by resonant multi-photon ionization (REMPI) and time-of-flight mass spectroscopy. We have a new capability with an ion imaging detector that allows measurement of partial cross sections resolved by scattering angle and velocity, and provides determination of the correlation of the quantum state of one product with the quantum state of the other.

In a collaborative effort with David Chandler we are studying ways to produce molecules at ultra-low temperatures, and study collisions at the low energies associated with these temperatures.

RECENT PROGRESS

Most of our laboratory effort this year has been in the construction of an ion imaging apparatus for our bimolecular studies. This is designed to allow measurement of quantum-state-resolved differential cross sections for the reactions $\text{H} + \text{RH} \rightarrow \text{H}_2 + \text{R}$, where RH is an alkane. The resolution of the apparatus should allow us to make measurements of correlations of the quantum states of the two reaction products, or, when the density of states is too great, the correlation of the internal energy of the radical product with the quantum state of the H_2 product.

The apparatus is designed for ion "slicing" of the H_2 reaction product. This represents a stringent design criterion on the instrument. We have met that using a large microchannel plate detector—120 mm diameter—with a large-aperture, long-axial-length einzel lens. This allows us to slice the velocity distribution of the high-velocity H_2 product quite effectively. We just got this detection system working and have observed H_2 product from $\text{H} + \text{HBr}$ as a test case of a system for which the product velocity and angular distributions are known. We are now looking at H_2 product from $\text{H} + \text{C}_3\text{H}_6$ for which we think the velocity and angular distributions will be particularly interesting.

While building up this apparatus this year we have carried out an extensive series of quasiclassical trajectory calculations aimed at testing a kinematic model of suprathreshold collision energy abstraction reactions. We developed that model a few years ago as a way of explaining a particularly interesting feature of the energy disposal in such reactions, namely the observation that only a fraction, sometimes a very small fraction, of the energetically-allowed product quantum states are actually populated even when the collision energy is far above the reaction barrier height. We were able to show that a simple kinematic constraint could explain the bounding of the product rovibrational energy. We were able to quantitatively predict the highest energy populated quantum state in all reactions for which state-to-state dynamics measurements had been made. Our QCT results show that some aspects of the model are correct, but key elements of it are contradicted by the trajectory results. This leaves us searching for another dynamical source for the kinematic correlations that are remarkable in their ability to predict product energy disposal.

We have continued the collaboration with David Chandler to produce ultracold molecules by velocity cancellation in molecular collisions. The experiment takes advantage of the fact that in some molecular collisions the velocity vector of a scattered product in the center-of-mass frame is exactly the negative of the velocity vector of the center-of-mass, yielding a lab-frame product velocity that is identically zero. We have succeeded in making NO in selected rotational states with a velocity spread that represents a temperature of less than 1K, in collisions of NO with Ar, and reduction in that temperature seems readily achievable.

FUTURE PLANS

We will begin to use the new ion imaging capability to try to obtain state-to-state differential cross sections, starting with $\text{H} + \text{C}_3\text{H}_6 \rightarrow \text{H}_2 + \text{C}_3\text{H}_5$ that gave such interesting scalar state-to-state results—evidence that the allyl radical is an

important product and that the energy released by allyl formation can find its way to the H₂ product. Our intermediate-term goal is the H + CH₄ → H₂ + CH₃ reaction. We believe that we will have enough velocity resolution to observe the population of individual vibrational states of the CH₃ product in the translational energy distribution of the H₂(v',j'). Lacking that, we should be able to determine the rotational and vibrational states of the H₂ product that are formed paired with particular quantum states of the CH₃ product if we do REMPI on the CH₃. Measurements on H₂ from the H + HBr reaction test case are encouraging in this regard.

We will continue our cold molecule studies with David Chandler on two fronts: exploring different collisional systems and attempting to trap the cold molecules that we have already produced. Simple analysis of the kinematics and energetics of the scattering in a crossed beam arrangement indicates that there are particular combinations of scattering partners and collision energies that are very favorable for production of zero-lab-velocity products.

PUBLICATIONS

1. N. S. Shuman, A. Srivastava, C.A. Picconatto, D.S. Danese, P.C. Ray, and J.J. Valentini, "Evidence of a Surprising Channeling of Ring-Opening Energy to the H₂ Product in the H + c-C₃H₆ → H₂ + C₃H₅ Abstraction Reaction," J. Phys. Chem. 107, 8380-8382 (2003).
2. M.S. Elioﬀ, J.J. Valentini, and D.W. Chandler, "Subkelvin Cooling NO Molecules via "Billiard-Like" Collisions with Argon," Science 302, 1940-1943 (2003).
3. M.S. Elioﬀ, J.J. Valentini, and D.W. Chandler, "Formation of NO(j'=7.5) Molecules with Sub-Kelvin Translational Energy via Molecular Beam Collisions with Argon using the Technique of Molecular Cooling by Inelastic Collisional Energy-Transfer," European Physical Journal D: Atomic, Molecular and Optical Physics 31, 385-393 (2004).

Molecular Dynamics as seen through Rydberg States

Peter M. Weber
Department of Chemistry
Brown University, Providence, Rhode Island 02912
Peter_Weber@brown.edu

1. Program Scope

In our research, we explore new ways to characterize the structure of molecules, with special emphasis on the development of new time resolved techniques. At the present time, two interesting techniques are at the forefront of our research: time-resolved electron diffraction and time-resolved spectroscopy.

The electron diffraction technique uses ultrashort pulsed electrons to probe the molecular structure at specific points in time. A laser pulse initiates a structural rearrangement, either by exciting the molecule to an excited state with a different geometry, or by inducing a chemical reaction. In the context of this experiment, we are now exploring the applicability of the technique to nanoscale objects by pairing the time resolution with spatial resolution. In addition, we are investigating the use of very high energy (megaelectron volt) electrons for the purpose of time-resolved diffraction.

In the second technique, we are using pump-probe multi-photon ionization/photoelectron spectroscopy to map out the energy level structure of Rydberg levels. We discovered that in addition to a direct excitation, we can access Rydberg states via a two- or three-photon process involving superexcited states. In addition, we found that the energy level structure of the Rydberg states provide a unique glimpse of the molecular structure, as seen through the eye of the Rydberg electrons. This Rydberg fingerprint spectroscopy, as we call it, therefore has a place next to other spectroscopic techniques that primarily measure energy levels, but can be interpreted in a structural sense, namely NMR and IR spectroscopy. It turns out, however, that the Rydberg electrons are uniquely sensitive to particular aspects of molecular structure. Some of these unique aspects are briefly described in this account.

2. Recent Progress

Rydberg fingerprint spectroscopy as a structural tool

The Rydberg fingerprint spectroscopy rests on the idea that while electrons in Rydberg states spend much of their time far away from the charge center, occasionally they do pass the ion core. This passage is associated with a scattering event, which induces a phase shift in the electron's wave function. Over the course of a round trip, the electron wave function has to constructively interfere with itself, which implies that the energy of the orbit is sensitive to the phase shift. Since the latter depends on the spatial arrangement of atoms and functional groups within the molecule, the energy of a Rydberg level must depend on the geometrical structure of the molecular ion core. While in electron diffraction an unbound electron is scattered, the energies of Rydberg levels

relate to the scattering of a bound electron. The energies of Rydberg states are conveniently described by the quantum defect formula,

$$E_B = \frac{Ry}{(n - \delta)^2},$$

where Ry is the Rydberg constant, n is the principal quantum number, and δ is the quantum defect. The following sections briefly describe the peculiar ways in which Rydberg electrons spy on the molecular structure.

A. Location of the charge center

The Rydberg states are sensitive toward the molecular structure, i.e. the positions of atoms with respect to the center of charge in a molecule. It stands to reason that, if a molecule with a specific structure has two possible charge sites, then the Rydberg spectrum observed with each of those sites should be distinct. We tested this hypothesis on the example of 2-phenyl ethyl-N,N-dimethylamine (PENNA). PENNA can have its charge center either at the amine site, or at the aromatic ring. Figure 1 shows the comparison of the Rydberg spectrum of the PENNA molecule, with two molecules that simulate one or the other charge site. Clearly, the PENNA spectrum very much resembles that of the amine, and is not at all like that of the aromatic ring. We conclude that ionization of PENNA, using the 400 nm pulses chosen for figure 1, is characterized by ionization at the amine site.

Interestingly, when we ionize PENNA using 266 nm pulses, we find a Rydberg fingerprint resembling the one of toluene: apparently, that wavelength ionizes via the aromatic ring. In addition, the lines are broadened, presumably on account of a very fast charge transfer process. Details are described in reference 2.

The experiments on PENNA show that the Rydberg fingerprints are sensitive probes of the charge site, and able to reveal ultrafast charge transfer reactions. Additionally, we found a method to control the ionization center in a bifunctional molecule by tuning the laser wavelength.

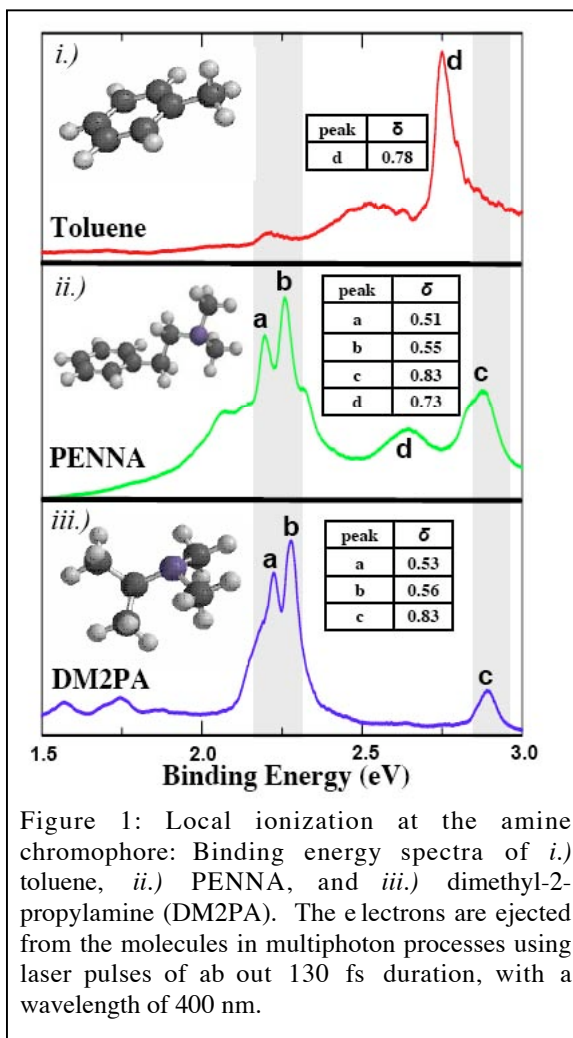


Figure 1: Local ionization at the amine chromophore: Binding energy spectra of *i.*) toluene, *ii.*) PENNA, and *iii.*) dimethyl-2-propylamine (DM2PA). The electrons are ejected from the molecules in multiphoton processes using laser pulses of about 130 fs duration, with a wavelength of 400 nm.

B. Global Structure Sensitivity

Rydberg orbitals can have a large diameter. Therefore, even atoms and functional groups that are far removed from the charge center can contribute phase shifts, and therefore affect the quantum defects. Thus we surmise that the Rydberg fingerprints ought to be sensitive to the global molecular structure.

To test his hypothesis, we measured the Rydberg fingerprint spectra of a series of diamines. The ionization is localized on one of the amine sites of the symmetric molecules. Figure 2 shows that the Rydberg fingerprint spectra of the diamines are distinct. Since the only differences of molecules relate to the changing molecular composition at parts of the molecule far removed from the charge center, the spectra clearly support the notion of global structure sensitivity.

C. Intramolecular Charge Distributions

The electron in a Rydberg orbital revolves around the center of the charge, with perturbations in the potential stemming from the charge distributions as given by the positions of the atoms. Thus, the spectra ought to be sensitive toward the exact distribution of charges within the molecule.

We measured the Rydberg fingerprint spectra of 2-, 3-, and 4- fluorophenol using 400 nm laser pulses. The spectra of 2- and 4- fluorophenol are well resolved (figure 3, top and bottom). The Rydberg fingerprints are distinct, reflecting the expected sensitivity toward the positioning of the atoms in the molecule.

Surprisingly, the spectrum of 3-fluorophenol was congested to the extent that our femtosecond lasers could not resolve the spectrum (figure 3, middle). We now understand the congestion as resulting from two isomeric forms of 3-fluorophenol, with the hydroxyl hydrogen atom being either syn or anti with respect to the fluorine atom. To understand why the Rydberg fingerprints of those molecules could be so distinct, we calculated the positions of the charge centers. It turns out that since the hydroxy hydrogen atom has a large fractional positive charge, the placement of this atom on one or the other side of the oxygen atom dramatically changes the center of the charge with respect to the aromatic ring. Since the Rydberg electron experiences the Coulomb field arising from that charge, the syn and anti forms of 3-fluorophenol appear to be very different molecules as seen from the perspective of the Rydberg electron!

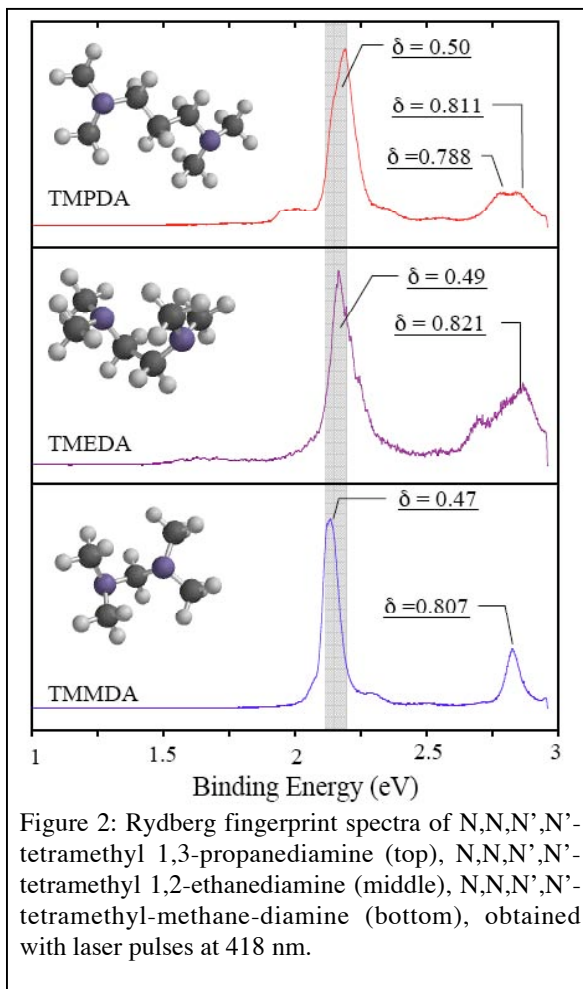


Figure 2: Rydberg fingerprint spectra of N,N,N',N'-tetramethyl 1,3-propanediamine (top), N,N,N',N'-tetramethyl 1,2-ethanediamine (middle), N,N,N',N'-tetramethyl-methane-diamine (bottom), obtained with laser pulses at 418 nm.

3. Future Plans

Both the Rydberg fingerprint spectroscopy and the pump-probe electron diffraction provide views of molecular structure from unique vantage points. We continue to explore these unique aspects with both techniques. Current experiments investigate the dissociation dynamics of amines on Rydberg surfaces. Separately, we explore the applicability of Rydberg fingerprint spectroscopy to observe the folding dynamics of floppy molecules.

4. Publications resulting from DOE sponsored research (2004 & 2005)

1. "Rydberg Fingerprint Spectroscopy: A New Spectroscopic Tool With Local And Global Structural Sensitivity," J. L. Gosselin and Peter M. Weber, in print, *J. Phys. Chem.*
2. "Control of local ionization and charge transfer in the bifunctional molecule 2-phenylethyl-N,N-dimethylamine using Rydberg fingerprint spectroscopy," W. Cheng, N. Kuthirummal, J. Gosselin, T. I. Sølling, R. Weinkauff, and P. M. Weber, *Journal of Physical Chemistry*, *109*, pp 1920 – 1925 (2005).
3. "Experimental and theoretical studies of pump-probe electron diffraction: time-dependent and state-specific signatures in small cyclic molecules," Peter M. Weber, Ray C. Dudek, Seol Ryu, and Richard M. Stratt, in *Femtochemistry and Femtobiology: Ultrafast Events in Molecular Science*, Eds. M. Martin and J. T. Hynes, Elsevier, p. 19, (2004).
4. "Probing reaction dynamics with Rydberg states: The ring opening reaction of 1, 3-cyclohexadiene," N. Kuthirummal and P. M. Weber, in *Femtochemistry and Femtobiology: Ultrafast Events in Molecular Science*, Eds. M. Martin and J. T. Hynes, Elsevier, p. 37 (2004).
5. "Centering of ultrafast time-resolved pump-probe electron diffraction patterns" J. D. Cardoza, R. C. Dudek, R. J. Mawhorter, and P. M. Weber. *Chemical Physics*, *299*, 307 – 312 (2004).
6. "Electron diffraction of molecules in specific quantum states: a theoretical study of vibronically excited s-tetrazine" S. Ryu, R. M. Stratt, K. K. Baeck and P. M. Weber, *Journal of Physical Chemistry A*, *108*, 1189 – 1199 (2004).

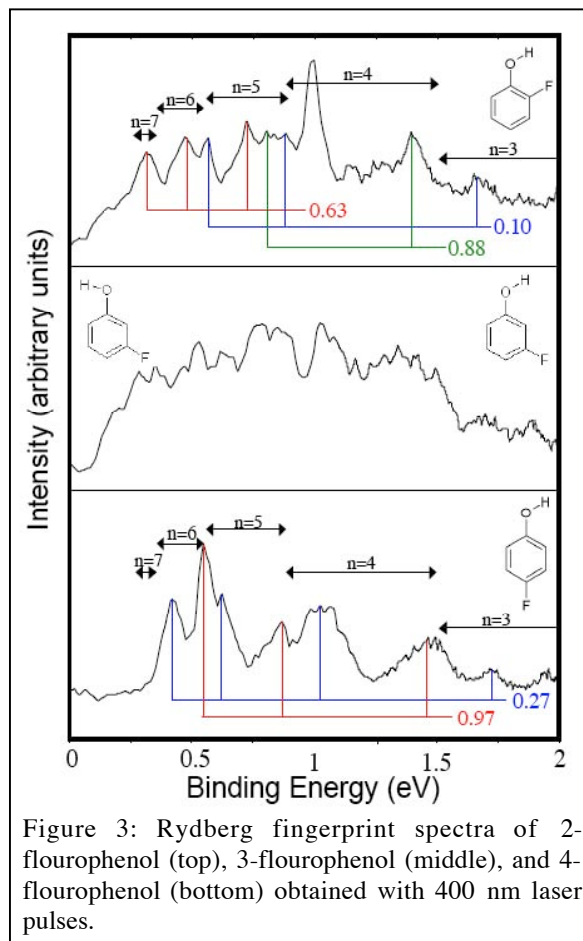


Figure 3: Rydberg fingerprint spectra of 2-fluorophenol (top), 3-fluorophenol (middle), and 4-fluorophenol (bottom) obtained with 400 nm laser pulses.

Chemical Kinetic Modeling of Combustion Chemistry

Charles K. Westbrook and William J. Pitz
Lawrence Livermore National Laboratory

Program Scope

Our research project focuses on developing detailed chemical kinetic reaction mechanisms for the combustion of a wide variety of fuels and other chemical species. These reaction mechanisms are intended to be applicable over extended ranges of operating conditions, including temperature, pressure, and fuel/oxidizer ratio, making them so-called “comprehensive” reaction mechanisms. They can then be systematically reduced in size and complexity as needed for specific types of modeling applications. We also use these detailed kinetic mechanisms to carry out modeling studies of practical combustion systems, and we also contribute basic chemical information on thermochemical and kinetic data.

Recent Progress

During the past year, we have developed detailed kinetic mechanisms and carried out kinetic modeling studies in several interconnected areas, including kinetics of oxygenated hydrocarbons and their importance in diesel soot production, kinetic flame inhibitors, and kinetics of high explosives.

A major combustion problem associated with diesel engine combustion is the production and emission of soot. We have carried out kinetic modeling studies [1] that have shown that soot is a product of very rich hydrocarbon ignition, and others have identified the kinetic reaction species and pathways that produce soot under fuel-rich conditions. Recent experimental engine studies with a variety of diesel fuel additives have shown that addition of many oxygenated hydrocarbon species such as ethanol, ethers and others can reduce the soot emissions from those engines. We have developed detailed kinetic models for oxygenated hydrocarbons including methanol, ethanol, dimethyl ether, dimethoxy methane, and more complex oxygenated species including dibutyl maleate (DBM), tripropylene glycol monomethyl ether (TPGME), dimethyl carbonate, and a surrogate biodiesel fuel methyl butanoate, using standard rate and thermochemical parameter estimation tools, and we have used these kinetic models to study the details of soot production and its variations as oxygenated species are included in the diesel fuel. We used n-heptane as the surrogate for diesel fuel, and our kinetic models reproduced the reduction in soot production as the oxygenated additive concentration in the fuel is increased. Our kinetic models reproduced all of the experimental results, and we were also able to show how different additives were not equally effective in reducing soot formation. We were also able to show how these additives kinetically reduced soot production by reducing the fraction of carbon atoms that were available to participate in soot formation reactions. We also used accelerator mass spectrometry [2] to extend our understanding of the kinetic details of oxidation

of DBM. We placed C14 at different locations within the DBM molecules used as additives for diesel combustion and then monitored the C14 fate in soot and in This work permitted us to refine the branching ratios between competitive reaction pathways in the DBM reaction mechanism.

Interestingly, soot production is also a problem for the military who must dispose of unwanted explosive materials. Common past practice has been to blow up old munitions in remote areas, but it has been found that this practice produces large amounts of soot that then drift downwind and create pollution problems. We have addressed this problem with kinetic modeling, but it has required us to develop kinetic reaction mechanisms for the explosives being destroyed. We have developed a kinetic reaction mechanism for the oxidation of tri-nitro toluene (TNT), a very commonly used explosive in itself and a component in many other important explosives. This required an extensive amount of thermochemical and kinetic rate parameter development, and a considerable amount of work was based on analogies with similar molecules for which kinetic research had been done in the past. We compared the soot production from TNT with that from other explosives, including RDX, HMX, TATB and CompB, and our kinetic models were able to distinguish between the sooting tendencies of each energetic material. We were able to show that the procedure used by the military of burying munitions to reduce soot production is not likely to result in reduced emissions, and we have developed a method to predict sooting tendencies of important mixtures of explosive molecules. Perhaps even more important, we have shown that the kinetics of soot production in explosive material combustion is essentially identical with soot production in diesel engines and in rich premixed and diffusion flames.

Following a long history of kinetic modeling of flame inhibition with additives such as halogens HBr, HCl, HI, CH₃Br, and CF₃Br, we have built an inhibition mechanism for organophosphorous compounds. We modeled [3,4] methane and propane laminar flames with different amounts of trimethyl phosphate (TMP) and di-methyl methyl phosphonate (DMMP), to go along with previous studies of di-isopropyl methyl phosphonate (DIMP). Although there are many ways to introduce phosphorous atoms into a flame, we showed that all of them are essentially the same in their interactions with hydrocarbon kinetics. The effect of phosphorous atoms is to introduce an atom with multiple oxidation states which accordingly has multiple reaction pathways to produce radical recombination for radicals such as H, OH and O and reduce the overall rate of combustion. In addition to explaining the inhibition due to phosphorous, this kinetic modeling work offers the possibility of explaining why such species as iron pentacarbonyl are so effective in reducing combustion rates, by having multiple oxidation states and multiple reaction pathways that also promote radical recombination. All of these organophosphate inhibitors are closely related to the fluorinated organophosphate compounds that are noted as toxic chemical warfare agents, for which we have previously developed the only kinetic reaction mechanisms in the past.

We continued our studies of the soot reduction properties of oxygenated hydrocarbons in diesel engine combustion. The most recent oxygenated fuel for which we developed a detailed chemical kinetic reaction mechanism in the past year has been dimethyl carbonate [5], which we predict to be somewhat less effective per oxygen atom than many other oxygenates at reducing sooting in diesel combustion. When we first started this project several years ago, it was commonly believed that all oxygenates reduced sooting at virtually the same rate, when measured on the basis of how many oxygen atoms are introduced into the diesel combustion. However, we have gradually found that this effect is more complex, and that some oxygen atoms are less effective than others, depending on the details of the molecular structure of the oxygenated additive. We have been able to identify those types of bonding structures that are more and less effective ways to include oxygen in additive fuels, so that it is possible to evaluate soot reduction potential of oxygenated species simply by visual inspection of the structure of the additive molecule.

We have continued to refine our basic kinetic submodels that form the core of our large molecule mechanisms. We refined and updated the most basic submodel, the H_2/O_2 submodel [6] by including recent research on thermochemistry, particularly heats of formation of small radicals including OH. We also provided kinetic modeling support for a recent experimental study of dimethyl ether (DME) combustion in opposed flow diffusion flames [7]. Finally, we helped celebrate the 50th anniversary of the Combustion Institute by being asked to deliver one of the five special anniversary plenary lectures at the International Symposium on Combustion in Chicago, with the subject being Computational Combustion [8]. Together with experimental collaborators at Sandia National Laboratories in Livermore, we also received the Arch Colwell Award of Merit from the Society of Automotive Engineers for a paper on oxygenates on reducing diesel soot production [9], identifying this paper as one of the best 4 -6 papers in 2003 out of more than 4000 SAE papers in 2003.

Future Plans

We will continue to carry out chemical kinetic modeling studies of a wide variety of combustion problems, developing new kinetic reaction mechanisms when they do not already exist. We have found a powerful connection between soot production kinetics in diesel engines and in explosives incineration, a unifying principle that provides important and fundamental information. We will continue to pursue similar unifying chemical kinetic principles.

Charles K. Westbrook
LLNL, L-090
P. O. Box 808
Livermore, CA 94550

westbrook1@llnl.gov
925-422-4108

William J. Pitz
LLNL, L-091
P. O. Box 808
Livermore, CA 94550

pitz1@llnl.gov
925-422-7730

References to publications of DOE sponsored research in 2003-2005

1. Flynn, P.F., Durrett, R.P., Hunter, G.L., zur Loye, A.O., Akinyemi, O.C., Dec, J.E., and Westbrook, C.K., "Diesel Combustion: An Integrated View Combining Laser Diagnostics, Chemical Kinetics, and Empirical Validation", Society of Automotive Engineers Transactions, Section 3, Volume 108, pp. 587-600 (1999).
2. Buchholz, B.A., Mueller, C.J., Upatnieks, A., Martin, G.C., Pitz, W.J., and Westbrook, C.K., "Using Carbon-14 Isotope Tracing to Investigate Molecular Structure Effects of the Oxygenate Dibutyl Maleate on Soot Emissions from a DI Diesel Engine", **Soc. Auto. Eng.** 2004-01-1849 (2004).
3. Jayaweera, T.M., Melius, C.F., Pitz, W.J., Westbrook, C.K., Korobeinichev, O.P., Shvartsberg, V.M., Shmakov, A.G., Rybitskaya, I.V., and Curran, H.J., "Flame inhibition by phosphorus-containing compounds over a range of equivalence ratios", **Combust. Flame** 140, 103-115 (2005).
4. Korobeinichev, O.P., Shvartsberg, V.M., Shmakov, A.G., Bolshova, T.A., Jayaweera, T.M., Melius, C.F., Pitz, W.J., and Westbrook, C.K., "Flame Inhibition by Phosphorus-Containing Compounds in Lean and Rich Propane Flames", **Proc. Combust. Inst.** 30, 2350-2357 (2004).
5. Glaude, P.-A., Pitz, W.J., and Thomson, M.J., "Chemical Kinetic Modeling of Dimethyl Carbonate in an Opposed-Flow Diffusion Flame", **Proc. Combust. Inst.** 30, 1111-1118 (2004).
6. O'Conaire, M., Curran, H.J., Simmie, J.M., Pitz, W.J., and Westbrook, C.K., "A Comprehensive Modeling Study of Hydrogen Oxidation", **Int. J. Chem. Kinet.** 36, 603-622 (2004).
7. Zheng, X.L., Lu, T.F., Law, C.K., Westbrook, C.K., and Curran, H.J., "Experimental and computational study of nonpremixed ignition of dimethyl ether in counterflow", **Proc. Combust. Inst.** 30, 1101-1109 (2004).
8. Westbrook, C.K., Mizobuchi, Y., Poinso, T., Smith, P.A., and Warnatz, J., "Computational Combustion", **Proc. Combust. Inst.** 30, 125-157 (2004).
9. Mueller, C., Pickett, L., Pitz, W.J., and Westbrook, C.K., "Effects of Oxygenates on Soot Processes in DI Diesel Engines: Experiments and Numerical Simulations", Society of Automotive Engineers SAE-2003-0193 (2003).
10. Kubota, A., Harris, L., Mundy, C.J., Pitz, W.J., Melius, C., Westbrook, C.K., and Caturla, M.-J., "Combined Monte Carlo and Molecular Dynamics Methods to Study the Long-Time-Scale Evolution of Particulate Matter and Molecular Structures under Reactive Flow Conditions: Hydrocarbon Soot Nanoparticulate Matter Inception, Growth and Aging", Nineteenth International Colloquium on the Dynamics of Explosions and Reactive Systems, Hakone, Japan, July 2003.

PROBING FLAME CHEMISTRY WITH MBMS, THEORY, AND MODELING

Phillip R. Westmoreland

Department of Chemical Engineering
University of Massachusetts Amherst
159 Goessmann Laboratory, 686 N. Pleasant
Amherst, MA 01003-9303

Phone 413-545-1750
FAX 413-545-1647
westm@ecs.umass.edu
<http://www.ecs.umass.edu/che/westmoreland.html>

Program Scope

Our objective is obtaining kinetics of hydrocarbon combustion and molecular-weight growth in flames. Our approach combines molecular-beam mass spectrometry (MBMS) experiments on low-pressure flat flames; *ab initio* thermochemistry and transition-state structures; rate constants predicted by transition-state and chemical activation theories; and whole-flame modeling using mechanisms of elementary reactions. The MBMS technique is powerful because it can be used to measure a wide range of species quantitatively, including radicals. Our electron-impact-ionization quadrupole MS at UMass provides species profiles with high signal sensitivity and mass resolution, and we are obtaining extraordinarily specific isomer identifications and their profiles using a time-of-flight MS with VUV photoionization that we co-developed at the Advanced Light Source (ALS) at LBNL.

Flame chemistry for stoichiometric cyclohexane combustion

Cyclohexane is a significant fuel component whose combustion and pollutant-forming chemistry is important. For example, it makes up 8.6% of the European Unleaded Certified gasoline. Chemically, it is interesting for being cyclic and also for being an alkane that has only secondary hydrogens. At low temperatures, it has distinct boat and chair configurations, but at flame conditions, inversion of these forms is sufficiently fast to make cyclohexane dynamically flat and symmetrical; thus, all of its hydrogens are equivalently accessible for abstraction.

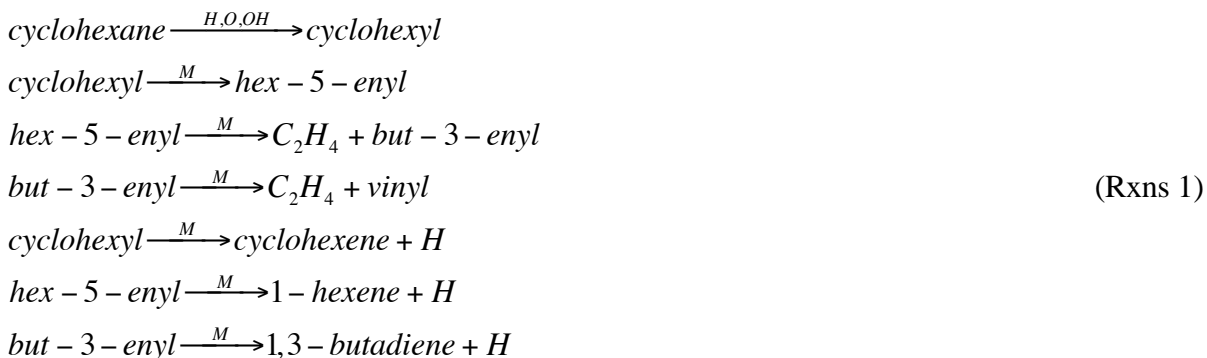
We mapped a stoichiometric cyclohexane flame with 32.5% argon at 30.00 torr and 35.0 cm/s feed gas velocity (at 300 K). The intent was to test and obtain kinetics for abstraction and radical decomposition at conditions where O and OH were the dominant radicals and where molecular-weight growth was not interfering.

The first set of data was with the UMass apparatus, where mass resolution, signal sensitivity, and detectability of certain radicals is better. Our quadrupole mass spectrometer (Extrel) can resolve masses in three different ranges: $m/z = 1-50$ daltons (ultra-high resolution of $m/\Delta m=1000$), 1-500, and 4-2000. Positive and negative ions can be measured from radicals and molecules using either analog (continuous) or pulse-counting detection. The latter method allows the high sensitivity of single-ion detection from the beam. We can also measure H, O, and OH, which has not yet been possible in the ALS apparatus (a present limitation that we expect to resolve). Also, temperature measurements are better performed in the UMass apparatus.

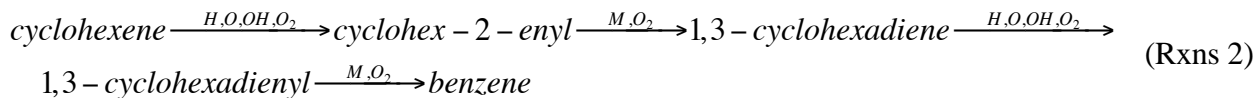
With the ALS apparatus, isomer analyses and profiles were mapped for the same flame. This apparatus has been built in collaboration with Terry Cool of Cornell, Andy McIlroy of Sandia, and the staff of the Chemical Dynamics Beamline at Lawrence Berkeley National Laboratory (<http://www.chemicaldynamics.lbl.gov/es3/flamediagnostics.htm>); a larger group of users is now involved (see refs. 2 and 10). That system's remarkable capability is its specificity of ionization threshold detection. That is made possible by spectroscopic energy resolution of the high flux of tunable vacuum-ultraviolet photons at 7 to 16.5 eV. They are resolved to energies as precise as

± 0.013 eV. Many isomers have close ionization energies (ionization potentials). Although electron-impact ionization can identify ionization energies of single species to ± 0.2 eV, resolution of isomers requires at least 2 eV difference in ionization energies because of the thermal distribution of electron energies. Tunable VUV photons from lasers can offer the same energy resolution, but the range and flux of photons is much higher from the ALS.

Seventy species were detected and mapped (Table 1). Species identifications pointed to reaction paths that are occurring. Cyclohexane is only consumed by abstraction. Beta scissions to C_2 species may then occur, along with channels forming alkenes+H:



This general picture is sufficiently supported by modeling such that we will be able to determine improved kinetics for the steps. At the same time, the presence of cyclic C_6H_6 to C_6H_{10} species indicates dehydrogenation steps leading to benzene even at this stoichiometric condition:



Fulvene is also detected, implying some C_3H_3 combination. We find further evidence of pathways from the presence and profiles of other species in Table 1.

Our modeling supports these hypotheses. We have built a reaction set based substantially on Carrière et al. [ref. 1] with cyclohexane and related reactions added, including those reactions above. We are using this set to test and extract improved kinetics. Many predictions are in good agreement with the data, but the initially predicted H, O, and OH profiles did not show the radical overshoot (superequilibrium behavior) and post-flame decay that are present in these and most flame data. For H_2 , C_2H_4 , and other fuels, such misprediction is also seen near stoichiometric conditions, which are technologically very important compositions. We are examining homogeneously catalyzed radical combinations as the most likely reason.

Usually, aromatics formation is not significant at stoichiometric conditions, but benzene reaches a mole fraction of $5E-4$ here. Quantitative analyses of the benzene data and modeling shows that the cyclo- C_6 dehydrogenation sequence (2) predicts benzene within a factor of three. C_3H_3 combination was tested using the modeled and experimental C_3H_3 mole fractions. It proved to be a small contributor, comparable to the slightly smaller, later $C_4H_3 + C_2H_2$ route.

The detailed species analysis and modeling are making this flame very useful for developing and improving reaction kinetics. Several oxygenates are also of interest, newly identified by the increased mass resolution at UMass or increased ionization resolution at the ALS (e.g., the widely occurring but previously unmodeled enols [ref. 9]).

Table 1. Species measured for stoichiometric cyclohexane/oxygen/32.5% argon flame in UMass EI/MBMS system and ALS PI/MBMS system.

Mass	Species	UMass	ALS	Mass	Species	UMass	ALS
1	H	Profile	-	52	C ₄ H ₄	Profile	Profile
2	H ₂	Profile	Profile	53	C ₄ H ₅	Profile	Profile
13	CH	Profile	-	54	C ₄ H ₆	Profile	Profile
14	CH ₂	Profile	-	55	C ₄ H ₇	Profile	Profile
15	CH ₃	Profile	-	56	C ₄ H ₈	Profile	Profile
16	CH ₄	Profile	-	58	vinylmethyl ether	-	Profile
16	O	Profile	-	58	acetone	-	Profile
17	OH	Profile	-	65	C ₅ H ₅	Profile	Profile
18	H ₂ O	Profile	Profile	66	C ₅ H ₆	Profile	Profile
26	C ₂ H ₂	Profile	Profile	67	C ₅ H ₇	Profile	Profile
27	C ₂ H ₃	Profile	Profile	68	C ₅ H ₈	Profile	Profile
28	C ₂ H ₄	Profile	Profile	69	C ₅ H ₉	Profile	Profile
28	CO	Profile	Profile	70	C ₅ H ₁₀	-	Profile
29	HCO	Profile	Profile	70	C ₄ H ₆ O	-	Profile
30	C ₂ H ₆	Profile	Profile	71	C ₄ H ₇ O	-	Profile
30	H ₂ CO	Profile	Profile	72	C ₄ H ₈ O	-	Profile
32	CH ₃ OH	Profile	Profile	76	C ₆ H ₄	Profile	-
32	O ₂	Profile	Profile	77	C ₆ H ₅	Profile	-
33	HO ₂	Profile	-	78	fulvene	-	Profile
34	H ₂ O ₂	Profile	-	78	benzene	-	Profile
39	propargyl (C ₃ H ₃)	Profile	Profile	79	C ₆ H ₇	-	Profile
40	Ar	Profile	Profile	80	1,3-cyclohexadiene*	-	Profile
40	allene (1,2-propadiene)	-	Profile	80	C ₅ H ₄ O	-	Profile
40	propyne	-	Profile	81	C ₆ H ₉	-	Profile
41	C ₃ H ₅	Profile	Profile	82	cyclohexene	-	Profile
41	HCCO	Profile	Profile	82	C ₆ H ₁₀	-	Profile
42	C ₃ H ₆	Profile	-	83	cyclohexyl	-	Profile
42	CH ₂ CO	Profile	-	83	C ₆ H ₁₁	-	Profile
43	CH ₃ CO	-	Profile	84	cyclohexane	Profile	Profile
43	CH ₂ CHO	-	Profile	92	toluene	-	Profile
44	CH ₂ CHOH	-	Profile	94	phenol	-	Profile
44	CH ₃ CHO	Profile	Profile	94	C ₇ H ₁₀	-	Profile
44	CO ₂	Profile	Profile	96	C ₆ H ₈ O	-	Profile
50	C ₄ H ₂	Profile	Profile	96	C ₇ H ₁₂	-	Profile
51	C ₄ H ₃	Profile	Profile	98	C ₆ H ₁₀ O	-	Profile

*No 1,4-cyclohexadiene threshold was detected (8.82 eV from literature).

Other work of interest

Other flame measurements. With our collaborators at the ALS in our July and January beam cycles, we have also probed fuel-rich and fuel-lean flames of several fuels. We have made detailed maps of stoichiometric and fuel-rich flames of allene, of propyne, and of cyclopentene. Our initial measurements for fuel-rich cyclohexane show a large number of detectable species extending up to the three-ring polycyclics acenaphthylene and fluorene.

Identification of C₃H₂ species. Our group has long been intrigued that C₃H₂ is often of the same magnitude as the important radical C₃H₃ and that it could have some quite analogous

molecular-weight-growth chemistry. However, it has a number of isomers, and C_3H_2 ionization energies measured in different flames have implied that unidentified different isomers might dominant.

In Ref. 7, we now have identified the dominant C_3H_2 isomers using recent data from the ALS apparatus, our past measurements at MIT and UMass, and quantum-chemistry calculations by our Sandia colleagues and us. The lowest-energy isomer, triplet propargylene (HCCCH, prop-2-ynylidene), was shown to be dominant in our previous fuel-rich C_2H_2 measurements, while our previous fuel-rich C_2H_4 , C_3H_6 , and C_6H_6 flames were shown to be a mixture of isomers. When a small amount of allene was added to a rich ethene flame, C_3H_2 appeared to be dominated by singlet propadienylidene (H_2CCC), suggesting formation by 1,1- H_2 elimination from the allene.

Future work

While we analyze and model the data from the two MBMS systems, we are also measuring temperatures, area-expansion ratios, and mole fraction profiles for the fuel-rich cyclohexane flame in the UMass MBMS system. This summer, we plan to resolve isomers within that flame at the ALS and to begin measurements on toluene. Model development is focused on adding these chemistries to the existing set, modeling other of the ALS flames, and resolving the radical predictions in stoichiometric flames.

Publications of DOE-sponsored Research, 2002-2005

1. T. Carrière, P.R. Westmoreland, A. Kazakov, Y.S. Stein, and F.L. Dryer, "Modeling Ethylene Combustion from Low to High Pressure," *Proc. Combust. Inst.*, **29**, 1257-1266 (2002).
2. A. Morel, M. E. Law, P. R. Westmoreland, T. A. Cool, K. Nakajima, T. A. Mostefaoui, F. Qi, A. McIlroy, L. Poisson, D. S. Peterka, M. Ahmed. "Selective detection of isomers using a new photoionization MBMS apparatus," *Chem. Phys. Proc. Comb.*, 281-284 (2003).
3. M. E. Law, A. Morel, P. R. Westmoreland, T. A. Cool, C. Taatjes. "Selective Detection of C_3H_4 and C_6H_6 Isomers in Flames," *Chem. Phys. Proc. Comb.*, 285-288 (2003).
4. T. A. Cool, K. Nakajima, T. A. Mostefaoui, F. Qi, A. McIlroy, P. R. Westmoreland, M. E. Law, L. Poisson, D. S. Peterka, and M. Ahmed, "Selective Detection of Isomers with Photoionization Mass Spectrometry for Studies of Hydrocarbon Flame Chemistry," *J. Chem. Phys.* **119**:16, 8356-8365 (2003).
5. T.A. Cool, K. Nakajima, C.A. Taatjes, A. McIlroy, P.R. Westmoreland, M.E. Law, A. Morel, "Studies of a Fuel-Rich Propane Flame with Photoionization Mass Spectrometry," *Proc. Comb. Inst.* **30**(1), 1681-1688 (2004).
6. M.E. Law, T. Carrière, P.R. Westmoreland, "Allene Addition to a Fuel-Lean Ethylene Flat Flame," *Proc. Comb. Inst.* **30**(1), 1353-1361 (2004).
7. C.A. Taatjes, S.J. Klippenstein, N. Hansen, J.A. Miller, T.A. Cool, J. Wang, M.E. Law, P.R. Westmoreland, "Synchrotron Photoionization Measurements of Combustion Intermediates: Photoionization Efficiency of C_3H_2 Isomers," *Phys. Chem. Chem. Phys.* **7**, 806-813 (2005).
8. B. Ruscic, J. E. Boggs, A. Burcat, A. G. Czàszàr, Jean Demaison, R. Janoschek, J. M. L. Martin, M. L. Morton, M. J. Rossi, J. F. Stanton, P. G. Szalay, P. R. Westmoreland, F. Zabel, T. Bérces, "IUPAC critical evaluation of thermochemical properties of selected radicals - Part I," *J. Phys. Chem. Ref. Data* (in press).
9. C.A. Taatjes, N. Hansen, A. McIlroy, J.A. Miller, J.P. Senosiain, S.J. Klippenstein, F. Qi, L. Sheng, Y. Zhang, T.A. Cool, J. Wang, P.R. Westmoreland, M.E. Law, T. Kasper, K. Kohse-Höinghaus, "Enols Are Common Intermediates in Hydrocarbon Oxidation" (submitted).

Photoinitiated Processes in Small Hydrides

Curt Wittig
Department of Chemistry
University of Southern California
Los Angeles, CA 90089
U. S. A.
wittig@usc.edu

During the past year we have continued to study the role of curve crossings in the photochemistry of small hydride systems. Most of our work this year has concentrated on the role of relativistic effects in hydrides that contain heavy atoms. Molecules with heavy atoms can have qualitatively different potential energy surfaces than their lighter counterparts, for example, due to strong spin-orbit coupling. To this end, we have continued our study of the H₂Te system, aided by recent high-level theoretical calculations,¹ and we have started experiments on SbH₃. Continuing our study of the H₂O \tilde{X}/\tilde{B} conical intersection, we have begun to integrate a four-wave mixing scheme for the generation of tunable VUV light.

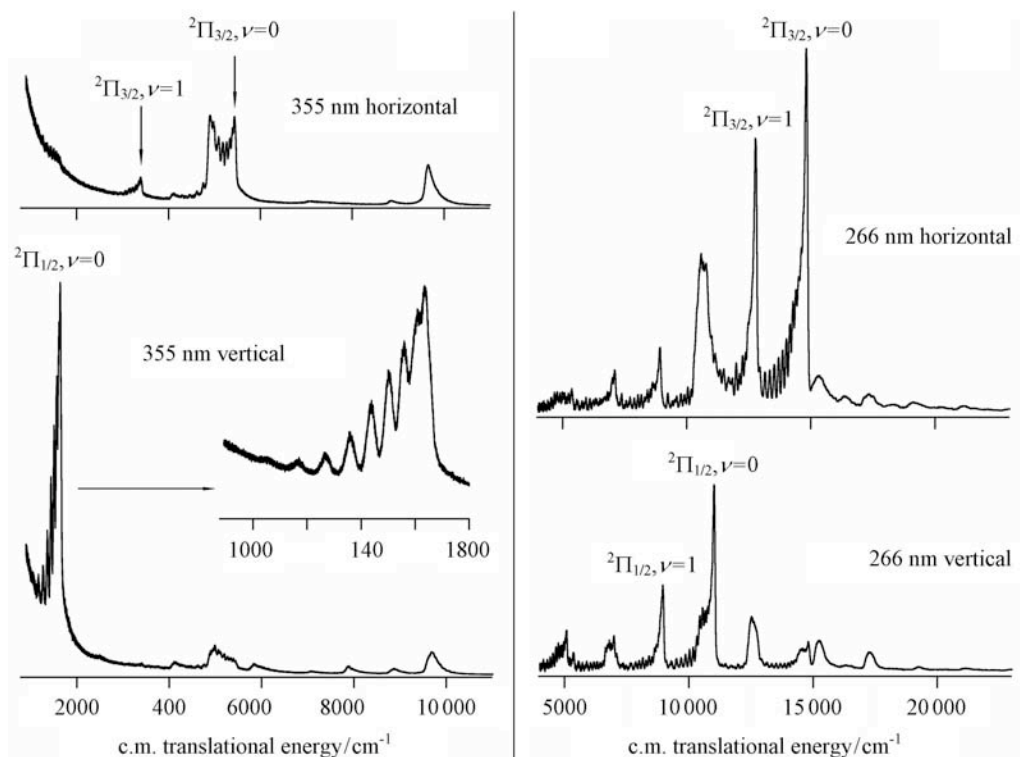
I. H₂Te absorption spectrum and photodissociation dynamics

A detailed analysis of the absorption spectrum and photodissociation experiments (both primary and secondary processes) has been carried out,² and the most important results are summarized here. H₂Te is a model system for studying relativistic effects. It is isoelectronic with HI, and the lighter isovalent dihydrides in the group, H₂O, H₂S, and H₂Se, have been studied in varying degrees of detail. Three product channels are energetically accessible in the first absorption band of H₂Te: (i) H₂ + Te; (ii) H + TeH(²Π_{3/2}, *v*, *N*); (iii) H + TeH(²Π_{1/2}, *v*, *N*). Spin-orbit excited TeH(²Π_{1/2}) lies 3815 cm⁻¹ above the TeH ground state. Our photodissociation experiments are sensitive only to channels (ii) and (iii). Center-of-mass translational energy distributions for photolysis at 266 and 355 nm obtained with high-*n* Rydberg time-of-flight (HRTOF) spectroscopy are shown below.

These experiments are also sensitive to secondary photolysis of the TeH products that are formed via the primary photolysis channels (ii) and (iii) described above. Following H₂Te photolysis, the nascent TeH diatoms can absorb a second photon and dissociate yielding H + Te(³P_{2,1,0}) and/or H + Te(¹D₂). Analyses of the secondary photolysis products in this study determine that $D_0 = 64.8 \pm 0.4$ kcal/mole (22,300 cm⁻¹ ± 150 cm⁻¹), in good agreement with theoretical predictions.³

Alekseyev et al. have recently calculated the low-lying potential energy surfaces and transition dipole moments in the H–TeH coordinate.¹ One of the most striking features is the weakly bound $3A'$ surface. Its large- r shape is remarkably similar to that of the $^3\Pi_{0+}$ curve in the isoelectronic HI system.⁴

We previously proposed that there should exist a state that is similar to the HI($^3\Pi_{0+}$) curve in the H–TeH coordinate.⁵ Because the $\Omega = 1/2$ state has a larger degree of spherical symmetry than the $\Omega = 3/2$ state, TeH($^2\Pi_{1/2}$) is not inclined to form either strongly bonding or anti-bonding orbitals with a H-atom. This results in a shallow van der Waals-like well on the $3A'$ surface at large r that leads to spin-orbit excited products. Calculations in the H–TeH coordinate predict that the $3A'$ surface is bound by ~ 1600 cm^{-1} . We attribute the long-wavelength structure observed in the absorption spectrum taken in our labs to vibrations of H_2Te on the $3A'$ surface.



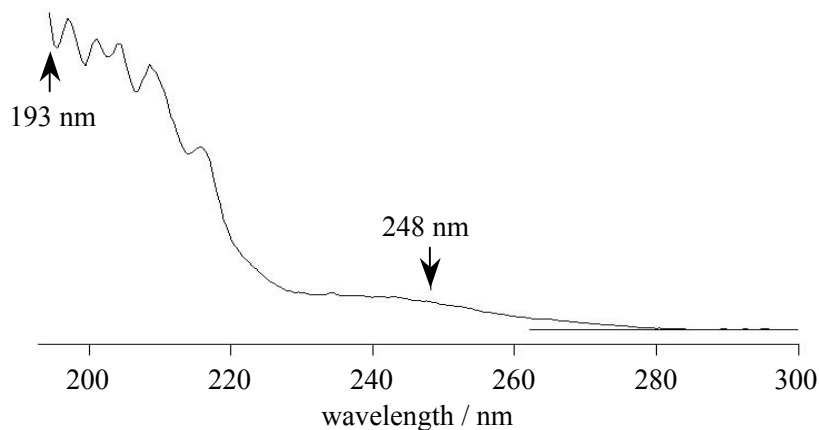
Photodissociation with horizontally polarized 266 nm radiation yields primarily TeH($^2\Pi_{3/2}$). This transition is due to a transition dipole moment out of the plane of the molecule, and this is assigned to the $4A'' \leftarrow \tilde{X}A'$ transition. The large anisotropy indicates that the TeH($^2\Pi_{1/2}$) channel results from a transition to a distinct electronic state, rather than from coupling of $4A''$ to another state in the exit channel that leads to the spin-orbit excited products. The $3A'$, $4A'$, and $3A''$ states correlate with the spin-

orbit excited channel, but the $3A' \leftarrow \tilde{X}A'$ transition moment is in the plane of the molecule, so $3A'$ is unlikely to be involved. Near the Franck-Condon region, the $4A''$ state has a larger transition dipole moment, but absorption to $3A'$ is also possible.

At 355 nm, $\sim 65\%$ of the photoproducts dissociate to yield the spin-orbit excited channel. This is due to the role of the $3A'$ state. In the Franck-Condon region, the $3A' \leftarrow \tilde{X}A'$ and $2A' \leftarrow \tilde{X}A'$ transition dipole moments are weak, as both transitions are of primarily singlet to triplet character.¹ The preference for long-wavelength photodissociation via the spin-orbit excited channel is due to the behavior of the transition dipole moment outside the Franck-Condon region. The $3A' \leftarrow \tilde{X}A'$ transition moment increases quickly with H–TeH distance, due primarily to increasing singlet character at large r of the $3A'$ state.¹

II. Another heavy hydride: SbH_3

One of the challenges to working with systems containing heavy atoms is that they can be quite unstable. SbH_3 is no exception.⁶ We have succeeded in synthesizing it and are currently carrying out HRTOF experiments with 193 nm photolysis radiation. A room temperature absorption spectrum taken in our labs is shown below. Note that as in H_2Te , a long wavelength tail is observed.



Experiments are underway to photolyze SbH_3 with 193 nm radiation and probe the H atom products using the HRTOF method. This energy is sufficient to break two of the Sb–H bonds. Though none of the bond energies have been measured, theoretical calculations predict D_e values of 63.3, 55.8, and 53.9 kcal/mole for each of the successive Sb–H bonds.⁷ The HRTOF results will provide information about the dissociation dynamics of SbH_3 as well as experimentally determine D_0 for two of the Sb–H bonds. Photolysis at 248 nm should prove to be interesting as well. At this

wavelength not only will the long wavelength tail of the absorption spectrum be accessed, but the energy in the system will be near the region where only one of the Sb–H bonds can be broken. Photodissociation dynamics in this region may be quite different than those observed at higher energies.

III. Probing the \tilde{X}/\tilde{B} conical intersection in H₂O

Tunable VUV is desirable to probe the \tilde{X}/\tilde{B} conical intersection in H₂O at energies lower than those studied to date.⁸ We are integrating a four-wave mixing scheme to generate radiation from ~ 140 to 133 nm. An added benefit of such a system is that it can also replace the current method we use for generation of the Lyman- α probe radiation (non-resonant tripling in Kr). The four-wave mixing scheme has significantly higher efficiencies, thereby increasing our sensitivity in the heavy atom studies.

References*

- (1) Alekseyev, A. B.; Liebermann, H.-P.; Wittig, C. *J. Chem. Phys.* **2004**, *121*, 9389.
- (2) Underwood, J.; Chastaing, D.; Lee, S.; Wittig, C. *J. Chem. Phys.* in preparation.
- (3) Setzer, K. D.; Fink, E. H.; Alekseyev, A. B.; Liebermann, H.-P.; Buenker, R. J. *J. Mol. Spectrosc.* **2001**, *206*, 181.
- (4) Alekseyev, A. B.; Liebermann, H.-P.; Kokh, D. B.; Buenker, R. J. *J. Chem. Phys.* **2000**, *113*, 6174.
- (5) Underwood, J.; Chastaing, D.; Lee, S.; Boothe, P.; Flood, T. C.; Wittig, C. *Chem. Phys. Lett.* **2002**, *362*, 483.
- (6) Todd, M. A.; Bandari, G.; Baum, T. H. *Chem. Mater.* **1999**, *11*, 547.
- (7) Dai, D.; Balasubramanian, K., *J. Chem. Phys.* **1990**, *93*, 1837.
- (8) Underwood, J.; Wittig, C. *Chem. Phys. Lett.* **2002**, *386*, 190, and references therein.

* References 1, 2, 5, and 7 were supported by DOE.

Theoretical Studies of the Reactions and Spectroscopy of Radical Species Relevant to Combustion Reactions and Diagnostics

David R. Yarkony

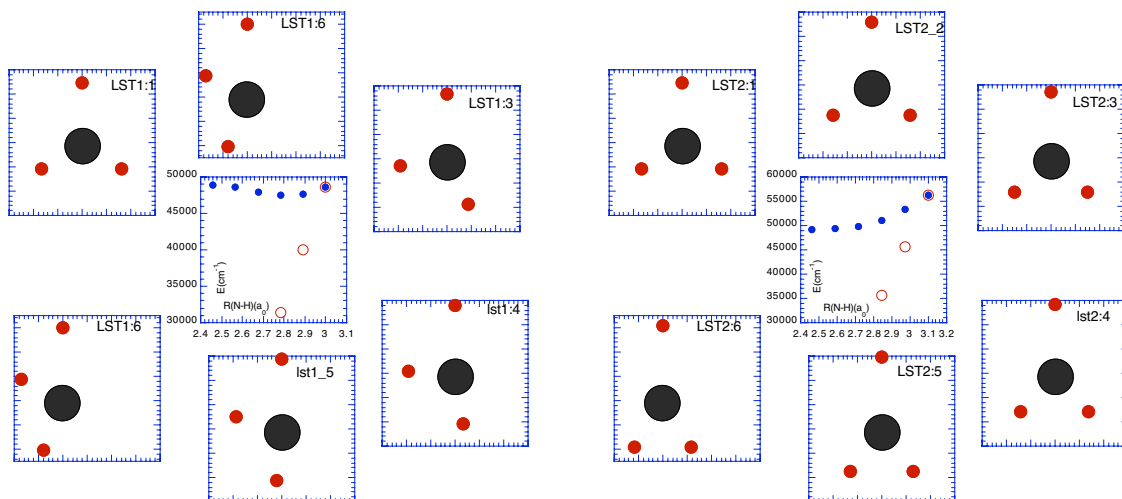
Department of Chemistry, The Johns Hopkins University, Baltimore, MD 21218
yarkony@jhu.edu

Our research employs computational techniques to study electronically nonadiabatic processes involving radical species. relevant to combustion reactions and combustion diagnostics.

Photodissociation of H_2NH

The demonstration by Fleming Crim's group¹ of profound mode specific effects, in the photodissociation of the \bar{A}^1A_2 state of NH_3 led us to initiate a study of this process in which conical intersections play a key role.

The analysis of Crim's and previous experiments is based on a 1987 study² which reported portions of the $1^1A - 2^1A$ seam of conical intersection with C_{2v} symmetry. The figures below, illustrative of the results obtained to date, show additional portions of the seam of conical intersection, portions without C_{2v} symmetry, relevant to Crim's experiments. The structures forming the outer loop represent a linear synchronous transit path from an approximate transition state to a point of conical intersection of the 1^1A-2^1A state. The conical intersection point for the loop on the right, denoted $\mathbf{R}^{x,C_{2v}}$ has C_{2v} symmetry and is typical of the previous *ab initio* results. The conical intersection point on the left denoted \mathbf{R}^{x,C_s} has C_s symmetry and has not been reported previously. Note that $E_2(\mathbf{R}^{x,C_s}) < E_2(\mathbf{R}^{x,C_{2v}})$ when the longest $R(\text{N-H})$ is in the range $[3.0, 3.1] a_0$ and that the lowest energy C_{2v} conical intersections occur for $R(\text{N-H}) \sim 3.7 a_0$. Since for ground state NH_3 $R(\text{N-H}) \sim 2.1 a_0$ these C_s conical intersections which energetically accessible in Crim's experiments, may be sampled before the system has a chance to reach the energetically accessible C_{2v} symmetry intersections!



Linear synchronous transit path from approximate transition state on S_1 to a point of conical intersection. Energies of the 1^1A (2^1A) state open (filled) circles along the path are in the center of the plate. Left hand plate general C_s symmetry conical intersection while for the right hand plate the terminus is a C_{2v} conical intersection.

The present results evince the need for more detailed calculations on this system. We will be particularly interested in factors, pitch, tilt and asymmetry parameters,³ that affect the efficiency of conical intersections in inducing nonadiabatic transitions. These electronic structure calculations

are expected to be only part of the story. We will also consider the role of nuclear dynamics, including the possibility of dynamical bottlenecks or preferred routings, in producing the enormous selectivity observed by Crim. This will be done in collaboration with Michael Collins using his GROW⁴ technology to guide the selection of points on the potential energy surfaces.

Photodissociation of H₂COD

Hanna Reisler's group at the University of Southern California observed that the spectrum of the H₂COD 2²A state, which begins at ~ 3.2 eV, is quite diffuse.⁵ This result was somewhat surprising in view of the fact that in this region the excited state has 3s Rydberg character and the core of 3s Rydberg wave function is the bound cation H₂COH⁺. We showed that Reisler's observations are a consequence of conical intersections of the 2²A and 1²A states.⁶ The relevant region of the 2²A -1²A seam of conical intersections occurs for R(O-D) long and can lead to ground state H₂CO + D.

Of current concern is whether the origin of the diffuse spectrum is an intrinsic property of the 2²A potential energy surface or a consequence of Franck-Condon factor limitations (the O-H bond is significantly stretched at the conical intersection). Further Reisler's group also observed that at higher energies both H and D are produced when H₂COD is photodissociated through the 2²A state. This too appears to be a consequence of 2²A -1²A conical intersections, although in this case R(C-H) is large. To confirm this hypothesis more reliable energetics are required.

Thus we anticipate the 1²A-2²A seam of conical intersections is mechanistically significant in two distinctly different regions of nuclear coordinate space. A quantitative treatment of radiationless decay of the 2²A state requires a more complete and accurate characterization of this seam in the region between these two extremes. Further at the points of conical intersection located to date the electronic states have ²A" and ²A' symmetry. Thus as shown in our DoE funded study of conical intersections in HNCO in these regions intersecting branches of the same seam of conical intersections, confluences, may exist. The existence of confluences which would have important consequences for nuclear dynamics. We are currently investigating whether energetically accessible confluences exist for the H₂COH conical intersection.

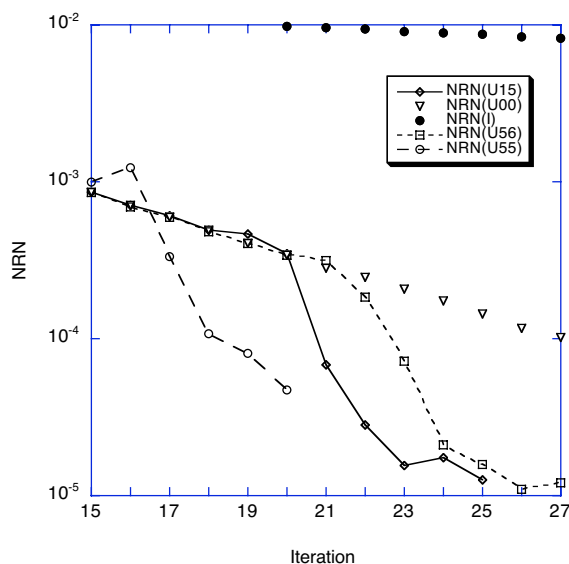
Locating Conical Intersections

Points of conical intersection are not isolated but are continuously connected forming seams. The seams are $N^{int} - 2$ dimensional subspaces in the N^{int} dimensional space of internal nuclear coordinates. For general polyatomic molecules $N^{int} - 2$ is a large number and it is desirable to determine sections of these seams for which the energy has been minimized. While it is relatively straightforward to locate points of conical intersection, energy optimization is more costly to achieve. We attribute this difficulty to the erratic behaviour of the algorithmic parameters along the search path which precludes extrapolation. This erratic behaviour might seem intrinsic to the problem since it is a consequence of the singular character of the conical intersection which is the object of the search. Fortunately this is not the case. We have recently introduced extrapolatable functions, a set of functions that are well-behaved along the search path.⁷ These functions form the basis for a simple, virtually no-additional cost, algorithm that uses hessian updating to significantly improve convergence to an energy minimized point of conical intersection.

The figure below illustrates the improvement measured relative to a unit hessian, denoted $M = I$, of the method $M=Uab$ which updates the entire hessian provided $\Delta E_{ij} < a \cdot 10^{-b}$ and otherwise updates the part corresponding to the average energy. This figure illustrates the importance of at least some approximation to the hessian since the solid circles, which indicate $M=I$, approach their updated counterparts slowly at best. The data for NRM clearly shows how updating the entire hessian - (a,b) \neq (0,0) improves convergence relative to the minimal updating U00.

COLUMBUS

We have continued our collaborative effort⁸ with Ron Shepard (Argonne) and Hans Lischka(Vienna) to incorporate into the COLUMBUS⁹ suite of electronic structure codes our algorithms for locating and analyzing conical intersections. During the captioned performance period we enhanced the capability to locate energy minimized two and three state conical intersection with the introduction of our extrapolatable function techniques described above. During the current performance period we will continue to fine tune these procedures.



Plot of NRN(M) for M = I, Uab, where NRM \rightarrow 0 at convergence.

References

- 1 A. Bach, J. M. Hutchison, R. J. Holiday, and F. F. Crim, J. Chem. Phys. **116**, 4955 (2002); A. Bach, J. M. Hutchison, R. J. Holiday, and F. F. Crim, J. Chem. Phys. **118**, 7144 (2003).
- 2 M. I. McCarthy, P. Rosmus, H.-J. Werner, P. Botschwina, and V. Vaida, J. Chem. Phys. **86**, 6693 (1987).
- 3 D. R. Yarkony, J. Chem. Phys. **114**, 2601 (2001).
- 4 K. C. Thompson, M. J. T. Jordan, and M. A. Collins, J. Chem. Phys. **108**, 8302 (1998).
- 5 L. Feng, X. Huang, and H. Reisler, J. Chem. Phys. **117**, 4820 (2002); L. Feng, A. V. Demyanenko, and H. Reisler, J. Chem. Phys. **118**, 9623 (2003).
- 6 B. C. Hoffman and D. R. Yarkony, J. Chem. Phys. **116**, 8300 (2002).
- 7 D. R. Yarkony, Faraday Discussions 127 (2004).
- 8 H. Lischka, M. Dallos, P. Szalay, D. R. Yarkony, and R. Shepard, J. Chem. Phys. (2004); M. Dallos, H. Lischka, P. Szalay, R. Shepard, and D. R. Yarkony, J. Chem. Phys. (2004).
- 9 H. Lischka, R. Shepard, I. Shavitt, R. Pitzer, M. Dallos, T. Müller, P.G.Szalay, F. B. Brown, R. Alhrichs, H. J. Böhm, A. Chang, D. C. Comeau, R. Gdanitz, H. Dachsel, C. ERhard, M. Ernzerhof, P. Höchtel, S. Irle, G. Kedziora, T. Kovar, V. Parasuk, M. Pepper, P. Scharf, H. Schiffer, M. Schindler, M. Schüller, and J.-G. Zhao, COLUMBUS, An ab initio Electronic Structure Program (2003).

PUBLICATIONS SUPPORTED BY DE-FG02-91ER14189: 2002 - present

- 1 *Conical Intersections and the Spin-Orbit Interaction*, Spiridoula Matsika and David R. Yarkony, in **The Role of Degenerate States in Chemistry**, Advances in Chemical Physics, Michael Baer and Gert. D. Billing, eds, J. Wiley, New York, 2002, pp. 557-583
- 2 *Conical Intersections: Their description and consequences*, David. R. Yarkony, in **Conical Intersections: Electronic Structure, Dynamics and Spectroscopy**, Wolfgang Domcke, David R. Yarkony and Horst Köppel, eds. World Scientific Publishing, Singapore, (2004).

- 3 *Determination of potential energy surface intersections and derivative couplings in the adiabatic representation* David. R. Yarkony, in **Conical Intersections: Electronic Structure, Dynamics and Spectroscopy**, Wolfgang Domcke, David R. Yarkony and Horst Köppel, eds. World Scientific Publishing, Singapore, (2004)
- 4 *Photodissociation of the Hydroxymethyl Radical I. The Role of Conical Intersections in Line Broadening and Decomposition Pathways*
Brian C. Hoffman and David R. Yarkony, *J. Chem. Phys.* **116** 8300-8306, (2002).
- 5 *Spin-orbit Coupling and Conical Intersections. IV: A perturbative determination of the electronic energies, derivative couplings and a rigorous diabatic representation near a conical intersection. The general case*
S. Matsika and D. R. Yarkony, *J. Phys. Chem B.* **106** 8108-8116 (2002)
- 6 *Photodissociation of the vinyloxy radical through conical and avoided intersections*
S. Matsika and D. R. Yarkony, *J. Chem. Phys.* **117**, 7198 (2002)
- 7* *Accidental Conical Intersections of three states of the same symmetry: Location and Relevance*
S. Matsika and D. R. Yarkony, *J. Chem. Phys.* **117**, 6907-6910 (2002)
- 8 *Beyond two-state conical intersections. Three-state conical intersections in low symmetry molecules: The allyl radical*
S. Matsika and D. R. Yarkony, *J. Amer. Chem. Soc.* **125**, 10672-10676 (2003)
- 9 *The analytic evaluation of nonadiabatic coupling terms at the MR-CI level I; Determination of minima on the crossing seam*
Dallos, M.; Lischka, H.; Szalay, P.; Shepard, R.; Yarkony, D. R. *J. Chem. Phys.* (2004).
- 10 *Marching along ridges. Efficient location of energy minimized conical intersections of two states using extrapolatable functions*
D. R. Yarkony, *J. Phys. Chem. A* (2004).

GAS-PHASE MOLECULAR DYNAMICS: QUANTUM MOLECULAR DYNAMICS OF COMBUSTION REACTIONS AND MOLECULAR SPECTROSCOPY CALCULATIONS

Hua-Gen Yu

Chemistry Department, Brookhaven National Laboratory

Upton, NY 11973-5000

hgy@bnl.gov

Program Scope

The goal of this program is the development of computational methods for studying chemical reaction dynamics and molecular spectroscopy in the gas phase. We are interested in developing rigorous quantum dynamics algorithms for small polyatomic systems and in implementing approximate approaches for complex ones. Particular focuses are on the dynamics and kinetics of chemical reactions and on the rovibrational spectra of species involved in combustion processes. This research also explores the potential energy surfaces of these systems of interest using state-of-the-art quantum chemistry methods.

Recent Progress

Quantum molecular dynamics of bimolecular reactions in the gas phase

Recently, we have developed an efficient and accurate quantum molecular dynamics (QMD) program for studying the dynamics of complex reactions. The QMD method treats the electronic structures of systems quantum mechanically while the sluggish nuclei are described using a classical molecular dynamics method. Our QMD program has implemented four major techniques: the predictor-corrector symplectic reversible integrator of Martyne and Tuckerman [Martyne & Tuckerman, *J. Chem. Phys.* **102** (1995) 8071] for solving Hamilton's equations of nuclear motion, the CASSCF method (if necessary) for obtaining correct initial electronic wave functions of each trajectory propagation at beginning, an accurate dual-level *ab initio* method for electronic structure calculations, and graph theory for analyzing and characterizing molecular structure and fragments of the system "on the fly" as a function of time. The symplectic integrator calls forces only once in every time propagation step, and allows a large time step without significantly sacrificing accuracy. Therefore, the algorithm is very efficient because thousands of time steps are usually required in dynamical simulations. In addition, we also programmed an option for the CASSCF method to produce the initial wave functions in electronic structure calculations. This option is very useful especially for open shell radical-radical reactions, such as the OH + HOCO reaction, that are common in combustion environments. This circumvents the deficiency of both HF SCF and single determinant-based post-SCF methods at a large separation of two open-shell species in bimolecular reactions.

The forces used in the QMD studies are calculated using a general dual-level *ab initio* method,

$$E_{DL} = f_1 E_1 + f_2 E_2,$$

where f_i are two constant parameters. Here E_i are the potential energies of the collision system calculated with two quantum chemistry methods or basis sets. If the same basis set is employed, this dual-level approach becomes a variant of Truhlar et al.'s "scaling all correlation" (SAC) method [Gordon & Truhlar, *J. Am. Chem. Soc.* **108** (1986) 5412]. The common implementation of the SAC/MP2 (or SAC/CCD) method has employed HF and MP2 (or CCD) calculations as the two *ab initio* levels of theory. On the other hand, if the same *ab initio* theory is employed

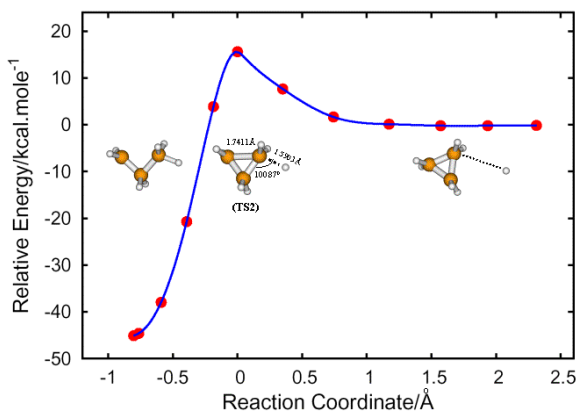
together with two different basis sets, such a dual-level approach can be considered as a basis set extrapolation or interpolation scheme. One example is the MP2/complete basis set method based on the MP2/cc-pVDZ and MP2/cc-pVTZ calculations. In particular, both dual-level approaches are affordable in practice, and provide accurate potential energy surfaces.

The program has successfully been applied to the study of the $O(^1D) + CH_4$ reaction at a collision energy of 6.8 kcal/mol using the SAC/CCD method with a D95(d,p) basis. The dynamical results reveal two reaction mechanisms, direct and long-lived ones, for the $O(^1D) + CH_4 \rightarrow OH + CH_3$ reaction. Combined with the RRKM calculations, the results show that the products are dominated by the OH and H channels.

Additionally, a quantum molecular dynamics study was also carried out for the $^1CH_2 + C_2H_2$ reaction using a SAC/CCSD method. This reaction is an important combustion reaction that yields the product propargyl radical (C_3H_3). The propargyl radicals are believed to be the precursor of soot in hydrocarbon combustion. The results show that the thermal rate constants are predicted to exhibit a negative temperature dependence, which is in excellent agreement with the previous results. However, the temperature dependence is consistent with the earlier RRKM results but weaker than the experimental observations at high temperatures. The reaction occurs via long-lived intermediates, and the lifetime of the cyclopropene intermediate is predicted to be 3.2 ± 0.4 ps.

Searching for the reaction pathway to the fast H_2 in the $H + cyc-C_3H_6$ reaction

The molecular beam experiment of Valentini and co-workers [J. Phys. Chem. A **107**, 8380 (2003)] shows that the reaction of a hydrogen atom with cyclopropane ($cyc-C_3H_6$) can produce a significant fraction (about 15%) of extremely hot H_2 except for normal H_2 products. The translational energy of these hot hydrogen molecules exceeds the total released energy if the reaction occurs via a normal direct H-abstraction mechanism in which the coproduct is the cyclopropyl radical. To understand this unusual behavior, we have performed a high level *ab initio* calculation with the CCSD(T)/CBS method. Besides the direct hydrogen-abstraction, a hydrogen addition/ring-opening reaction pathway (shown in the figure) was found. This pathway will lead to an $n-C_3H_7$ radical, which can result in a variety of products such as $CH_3 + C_2H_4$, $H + CH_3CHCH_2$ and $H_2 + C_3H_5$, etc. Its VAG barrier height was obtained as 16.49 kcal/mol, which is only 3.46 kcal/mol higher than that of the direct H-abstraction reaction. In particular, since the H_2 product is formed after the ring opening of cyclopropane, the hydrogen molecule can pick up some ring-opening energy during the reaction. As a result, the H_2 molecule has more translational energy than usually expected.



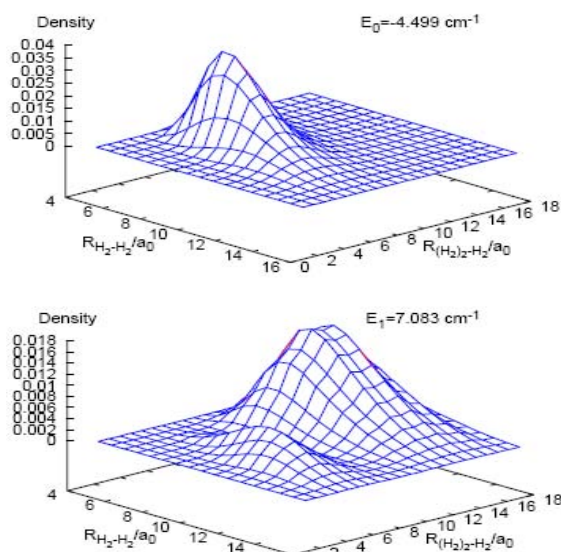
The CCSD(T)/CBS minimum energy path for the $H + cyc-C_3H_6$ reaction. The geometries of the transition state (TS2) and two points near either reactants or products are inserted.

Converged quantum dynamics calculations of vibrational energies of CH₄ and CH₃D

We have performed exact variational calculations of vibrational energies of CH₄ and CH₃D using a two-layer Lanczos algorithm based on the *ab initio* potential energy surface of D. W. Schwenke and H. Partridge, *Spectrochim. Acta, Part A* **57**, 887 (2001). Well converged vibrational energy levels are reported for CH₄ up to 6600 cm⁻¹, and for CH₃D up to 5000 cm⁻¹ from the ground state, respectively, together a comparison with experimental results and/or previous theoretical calculations. Our results show that the best previous theoretical calculations have errors as large as 7.5 cm⁻¹ for CH₄.

Full-dimensional quantum calculations of the vibrational spectra of six-atom molecules

Two quantum mechanical Hamiltonians have been derived in polyspherical coordinates for the study of the vibrational energies of six-atom molecules. They are expressed in an explicit Hermitian form in the spatial representation. Since one employs a set of orthogonal coordinates, which can be formed by Jacobi and/or Radau vectors, *etc.*, the Hamiltonians are very compact. In particular, the large amplitude motions of a molecule are naturally described. The matrix representation of the Hamiltonians is described in both mixed grid/basis and full-grid representations. Using the two-layer Lanczos iteration algorithm, we have in our initial application of this approach determined the vibrational energy levels of the hydrogen trimer (H₂)₃. Results show that a rigid-H₂ approximation can underestimate the binding energy of the trimer by 27%. This research has also extended the two-layer Lanczos algorithm to be capable of computing the eigenvectors of the system with minor efforts.



Two-dimensional wave functions of the vibrational ground (upper panel) and first excited (lower panel) states of (*p*-H₂)₃. The first excited state is not stable w.r.t. the dissociation limit.

The first excited state is not stable w.r.t. the dissociation limit.

Future Plans

Quantum molecular dynamics study of radical-radical reactions

We will still develop the quantum molecular dynamics program, and apply it to some important combustion reactions. Particular interests are the dynamics and kinetics of radical-radical reactions. One application for the OH + HOCO reaction, in collaboration with J. Francisco (Purdue Univ.), is in progress. This research mainly addresses the temperature dependence of the thermal rate constant and the reaction mechanism.

A coherent discrete variable representation method

During the past two decades, the discrete variable representation (DVR) technique has been widely used in quantum dynamics studies in chemical physics. In particular, the potential-optimized DVR (PODVR) of Echave and Clary has proved to be one of most efficient methods for a single degree of freedom representation because the PODVR points are well adapted to the potential energy surface. The high efficiency of the PODVR method has spurred us to search for

multidimensional PODVR basis functions. Only a little progress has previously been made. There is no exact multidimensional PODVR available.

We are currently exploring a coherent discrete variable representation (ZDVR) method for constructing a multidimensional PODVR basis. In this approach, inspired by a coherent-state formalism in momentum and conjugate coordinates, the multidimensional quadrature pivots are obtained by diagonalizing a complex coordinate operator matrix in a finite basis set, which is spanned by the lowest eigenstates of a two-dimensional reference Hamiltonian. Here a *c-norm* condition is used in the diagonalization procedure. The orthonormal eigenvectors define a collocation matrix connecting the localized ZDVR basis functions and the finite basis set. The convergence and properties of the ZDVRs are being explored. In addition, a zeroth order approximation method has been derived and will be tested.

Acknowledgment

This work was performed at Brookhaven National Laboratory under Contract DE-AC02-98CH10886 with the U.S. Department of Energy and supported by its Division of Chemical Sciences, Office of Basic Energy Sciences.

Publications since 2004

- H.-G. Yu and J.T. Muckerman, *MRCI calculations of the lowest potential energy surface for CH₃OH and direct ab initio dynamics calculations of the O(¹D) + CH₄ and OH + CH₃ reactions*, J. Phys. Chem. A **108**, 8615 (2004).
- H.-G. Yu and J.T. Muckerman, *Exploring the multiple reaction pathways for the H + cyc-C₃H₆ reaction*, J. Phys. Chem. A **108**, 10844 (2004).
- H.-G. Yu and J.T. Muckerman, *Ab initio and direct dynamics studies of the reaction of singlet methylene with acetylene, and the lifetime of the cyclopropene complex*, J. Phys. Chem. A **109**, 1890 (2005).
- H.-G. Yu, J.T. Muckerman and J.S. Francisco, *Direct ab initio dynamics study of the OH + HOCO reaction*, J. Phys. Chem. A (submitted, 2005).
- H.-G. Yu, *Full-dimensional quantum calculations of vibrational spectra of six-atom molecules. I. Theory and numerical results*, J. Chem. Phys. **120**, 2270 (2004).
- H.-G. Yu, *Converged quantum dynamics calculations of vibrational energies of CH₄ and CH₃D using an ab initio potential*, J. Chem. Phys. **121**, 6334 (2004).
- H.-G. Yu, *A coherent discrete variable representation method for multidimensional systems in physics*, J. Chem. Phys. (in press, 2005).

Experimental Characterization of the Potential Energy Surfaces for Conformational Isomerization in Aromatic Fuels

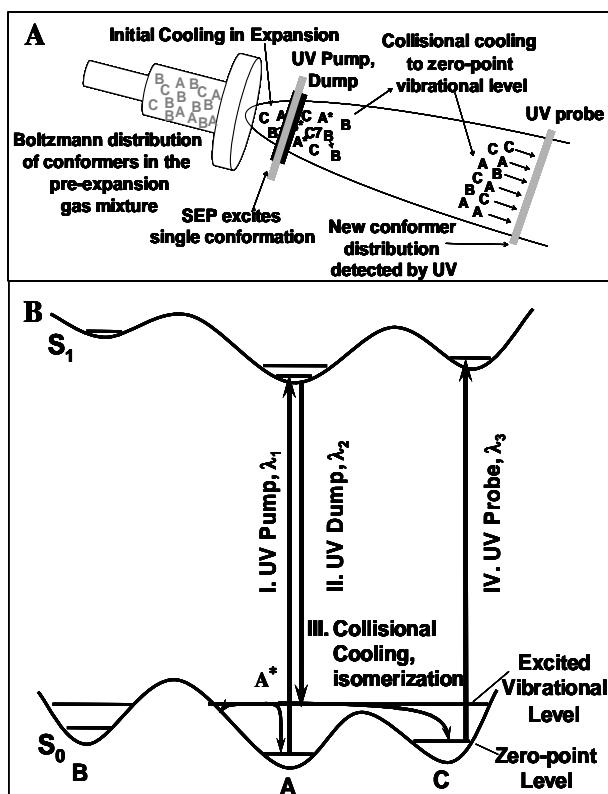
Timothy S. Zwier

Department of Chemistry, Purdue University, West Lafayette, IN 47907-2084
zwier@purdue.edu

Program Definition and Scope

Gasoline and diesel fuels are complicated mixtures containing about 30% aromatics, including alkylbenzene, alkenylbenzene, and alkynylbenzenes of various chain lengths. The combustion of these molecules is influenced by their structural and conformational make-up, and by the rates of isomerization between them. The objective of this research program is to develop and utilize laser-based methods to characterize the spectroscopy and isomerization dynamics of conformational isomers of aromatic derivatives that play a role in soot formation. We have recently demonstrated a new experimental method that will enable us to study the isomerization dynamics in new ways. Stimulated emission pumping (SEP) is being used to selectively excite a single conformation of the molecule of interest to a well-defined vibrational energy early in the supersonic expansion. The excited molecules are re-cooled in the expansion before isomer-specific detection in LIF or R2PI. By tuning the SEP dump laser in a 20-10-20 Hz laser configuration, it is possible to directly measure the magnitude of the population transfer between individual A→B reactant-product isomer pairs as a function of internal energy in the reactant.

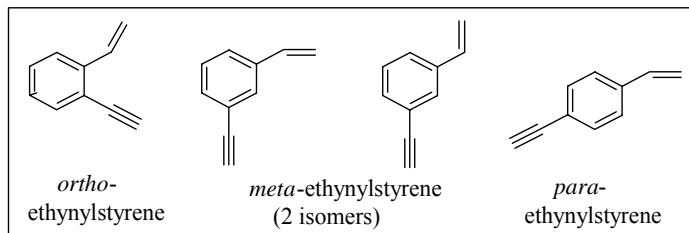
In this project, these methods are being employed to study conformational isomerization in substituted benzenes spanning a range of types and degrees of conformational flexibility. As a first step in all these studies, UV-UV hole-burning and resonant ion-dip infrared (RIDIR) spectroscopy is being used to determine the number and identity of the conformations present, based on their ultraviolet and infrared spectral signatures. These structural studies then serve as a foundation for studies of the dynamics of conformational isomerization using SEP population transfer spectroscopy (SEP-PTS). From such studies, we seek to determine the energy thresholds for isomerization in specific X→Y reactant-product isomer pairs, the relative energies of the minima, and, in cases where there are several flexible sites, the efficient isomerization pathways on the multidimensional surface. From near-threshold intensity measurements we hope to explore the rate of isomerization relative to collisional cooling as a function of energy above threshold. These results can provide new tests of RRKM descriptions of isomerization in large molecules.



Recent Progress

A. Spectroscopy and isomerization of *ortho*-, *meta*-, and *para*-ethynylstyrene

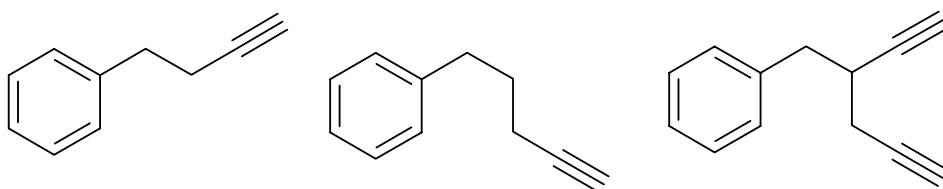
The infrared and ultraviolet spectroscopy of *ortho*-, *meta*-, and *para*-ethynylstyrene (*o*ES, *m*ES, and *p*ES) have been studied by a combination of methods, including resonant two photon ionization (R2PI), UV-UV hole-burning spectroscopy (UVHB), resonant ion-dip



infrared spectroscopy (RIDIRS), and rotationally resolved fluorescence excitation spectroscopy. In addition, the newly-developed method of stimulated emission pumping-population transfer spectroscopy (SEP-PTS) was used to place direct experimental bounds on the barrier to conformational isomerization in *meta*-ethynylstyrene. The $S_1 \leftarrow S_0$ origin transitions of *o*ES and *p*ES occur at 32369 cm^{-1} and 33407 cm^{-1} , respectively. In the R2PI spectrum of *m*ES, the two most prominent peaks (32672 cm^{-1} and 32926 cm^{-1}) were confirmed by UVHB spectroscopy to be $S_1 \leftarrow S_0$ origins of these two conformers. The red-shifted conformer was identified as the *cis* structure by least squares fitting of the rotationally resolved fluorescence excitation spectrum of the origin band, recorded in collaboration with Pratt and co-workers. There are also two possible conformations of *o*ES, but transitions due to only one were observed experimentally, as confirmed by hole-burning spectroscopy. Ground state infrared spectra in the C-H stretch region ($3000\text{--}3300\text{ cm}^{-1}$) of each isomer were obtained using resonant ion-dip infrared spectroscopy (RIDIRS). In all three structural isomers, the acetylenic C-H stretch fundamental was split by Fermi resonance. Infrared spectra were also recorded in the excited electronic state using a UV-IR-UV version of RIDIR spectroscopy. In all three isomers the acetylenic C-H stretch fundamental was unshifted from the ground state, but no Fermi resonance was seen. The barrier to *cis* \rightarrow *trans* isomerization in *meta*-ethynylstyrene was determined to be in the range $990\text{--}1070\text{ cm}^{-1}$ using SEP-PT spectroscopy. The analogous *trans* \rightarrow *cis* barrier was in the same range ($989\text{--}1065\text{ cm}^{-1}$), indicating that the relative energies of the zero-point levels of the two isomers are $(E_{\text{ZPL}}(\textit{cis}) - E_{\text{ZPL}}(\textit{trans})) = -75 - +81\text{ cm}^{-1}$. Both the barrier heights and relative energies of the minima are close to those determined by DFT Becke3LYP/6-31+G* calculations.

B. The single-conformation spectroscopy of a series of alkynylbenzenes

We are also nearing completion of a study of the single-conformation spectroscopy of 4-phenyl-1-butyne, 5-phenyl-1-pentyne, and 3-benzyl-1,5-hexadiyne, whose structures are shown below.



4-phenyl-1-butyne (4PB) 5-phenyl-1-pentyne (5PP) 3-benzyl-1,5-hexadiyne (BHD)

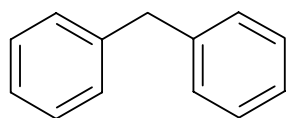
This series of molecules spans an interesting range of size and conformational complexity. A combination of vibronic level R2PI spectroscopy, rotational band contour analysis, UV-UV hole-burning, and RIDIR spectroscopy have been employed to obtain firm conformational assignments. There are two conformations of 4PB, in which the acetylenic group is anti or gauche with respect to the ring. Three conformations of 5PP are observed, while five conformations are present in BHD. In all cases, the $S_1 \leftarrow S_0$ origin transitions of the conformers

are spread over about 150 cm^{-1} . The magnitude and direction of the electronic frequency shift reflect the types of interactions of the side chains with the phenyl ring. CIS calculations correctly predict the direction of the transition moment in these alkylbenzenes, aiding in the rotational band contour fitting of the observed bands. In BHD, the two acetylenic groups produce acetylenic CH stretch fundamentals that reflect the relative orientation of these groups in the hexadiyne side chain. Single vibronic level dispersed fluorescence spectra, SEP spectra, and SEP-PT spectroscopy will be carried out on this triad of molecules using the new fluorescence-based chamber (Sec. D).

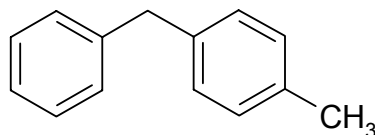
C. 5-phenyl-1-pentene and diphenylmethane

5-phenyl-1-pentene is a close analog of 5-phenyl-1-pentyne, substituting a vinyl group for the acetylenic group at the end of the 5-carbon chain. Previous photochemical studies have identified unusual photochemistry associated with addition of the vinyl group across the phenyl ring to form bicyclic products (C.D.D. Ho and H. Morrison, *J. Am. Chem. Soc.* **127**, 2114 (2005)). We have subjected 5-phenyl-1-pentene to our methods in order to determine the conformations present and to search for conformation-specific behavior in the excited state lifetimes or isomerization dynamics. We have completed our spectroscopic studies, identifying five conformational isomers in the R2PI spectrum, and assigning the observed transitions to specific conformers based on rotational band contour analysis of the $S_1 \leftarrow S_0$ origin transitions and a comparison with 5-phenyl-1-pentyne.

Finally, we are presently completing our analysis of the ultraviolet spectroscopy of diphenylmethane and 4-methyldiphenylmethane, shown below.



Diphenylmethane (DPM)



4-methyl-diphenylmethane (4-mDPM)

These molecules have fascinating and complicated electronic spectroscopy because the two aromatic chromophores are insulated by the CH_2 group that connects them, yet close enough to interact with one another significantly. The calculated barrier to internal rotation of the phenyl rings is only about 150 cm^{-1} . In DPM, the S_0 - S_1 and S_0 - S_2 origins are split by 123 cm^{-1} . Despite this small splitting, there is clear evidence in the dispersed fluorescence spectrum for electronic energy transfer between S_2 and S_1 even at the S_2 origin. In collaboration with D. Plusquellic at NIST, we have recorded the high resolution electronic spectrum of the $S_1 \leftarrow S_0$ origin transition. The rotational constants are consistent with a C_2 geometry for DPM with a 60° angle between the two phenyl rings. The direction of the transition moment is different than in toluene (70:30 a:c hybrid band), indicating that the coupling across the methylene group is sufficient to rotate the transition moment from the direction anticipated based on toluene. In 4-mDPM, the electronic excitation is localized on either of the two rings, with a splitting between S_1 and S_2 states of 662 cm^{-1} . At the S_2 origin of 4-mDPM, electronic energy transfer to S_1 is complete on the timescale of the fluorescence.

D. Construction of a new fluorescence-based chamber for hole-filling experiments

We are nearing completion of the construction of a new fluorescence-based chamber that will be used to carry out population transfer spectroscopy experiments. The chamber is outfitted with fluorescence collection optics that will collect 30% of the fluorescence, and image it in one direction onto a fluorescence excitation PMT and in the opposite direction onto the entrance slit of a $\frac{3}{4}$ -meter monochromator equipped with a CCD detector. This chamber will be coupled into our roots blower pumping line in order to facilitate population transfer studies that require the high throughput of the roots blower.

Publications acknowledging DOE support, 2002-present

Christopher Ramos, Paul R. Winter, Timothy S. Zwier, and Stephen T. Pratt, "Photoelectron Spectroscopy via the $1^1\Delta_u$ state of Diacetylene", *J. Chem. Phys.* **116**, 4011 (2002).

Allison G. Robinson, Paul R. Winter, and Timothy S. Zwier, "The singlet-triplet spectroscopy of 1,3-butadiene using cavity ring-down spectroscopy", *J Chem. Phys.* **116** (18): 7918-7925 (2002).

Allison G. Robinson, Paul R. Winter, and Timothy S. Zwier, "The Ultraviolet Photochemistry of Diacetylene with Styrene", *J. Phys. Chem. A* **106** (24): 4789-4796 (2002).

Jaime A. Stearns and Timothy S. Zwier, "The infrared and ultraviolet spectroscopy of jet-cooled *ortho*-, *meta*-, and *para*-diethynylbenzene", *J. Phys. Chem. A* **107**, 10717-10724 (2003).

Bruce C. Garrett, et al., "The Role of Water on Electron-Initiated Processes and Radical Chemistry: Issues and Scientific Advances", *Chemical Reviews* **105**, 355-389 (2005).

Talitha M. Selby, Jasper R. Clarkson, Diane Mitchell, James A.J. Fitzpatrick. H. Daniel Lee, David W. Pratt, and Timothy S. Zwier, "Conformation-specific Spectroscopy and Conformational Isomerization Energetics of *ortho*-, *meta*-, and *para*-Ethynylstyrenes", (submitted).

Talitha M. Selby, Alope Das, and Timothy S. Zwier, "Conformation-specific spectroscopy of 3-benzyl-1,5-hexadiyne", (submitted).

Talitha M. Selby, Nathan R. Pillsbury, and Timothy S. Zwier, "Conformation-specific spectroscopy of 4-phenyl-1-butyne and 5-phenyl-1-pentyne", (submitted).

Participants

Dr. Wesley Allen
Center for Computational Chemistry
University of Georgia
Athens, GA 30602
wdallen@ccqc.uga.edu (706)542-7729

Dr. Linda Blevins
Combustion and Plasma Systems Program
National Science Foundation
4201 Wilson Blvd.
Arlingtn, VA 22230
lblevins@nsf.gov 703-292-8371

Dr. Nancy Brown
Environmental Technologies Division
Advanced Energy Technology
Lawrence Berkeley Laboratory MS 70-108B
One Cyclotron Road
Berkeley, California 94720
njbrown@lbl.gov (510)486-4241

Dr. Robert Carling
Combustion Research Facility
Sandia National Laboratories
Livermore, California 94551-0969
rwcarli@sandia.gov 925.294.2206

Dr. Jacqueline H. Chen
Combustion Research Facility
MS9051
Sandia National Laboratories
Livermore, California 94551-0969
jhchen@sandia.gov 925.294.2586

Professor Terrill A. Cool
College of Engineering
School of Applied & Engineering Physics
Cornell University
Ithaca, New York 14853-1301
tac13@cornell.edu 607/255-4191

Dr. Michael Davis
Chemistry Division
Argonne National Laboratory
9700 South Cass Avenue
Argonne, Illinois 60439
davis@tcg.anl.gov 630.252.4802

Professor G. Barney Ellison
Department of Chemistry
University of Colorado
Boulder, Colorado 80309-0215
barney@jila.Colorado.EDU 303.492.8603

Professor Robert W. Field
Department of Chemistry
Room 6-219
Massachusetts Institute of Technology
77 Massachusetts Ave.
Cambridge, Massachusetts 02139
rwfield@mit.edu 617.253.1489

Professor Michael Frenklach
Department of Mechanical Engineering
Lawrence Berkeley Laboratory
University of California at Berkeley
Berkeley, California 94720-1740
myf@me.berkeley.edu (510)643-1676

Professor Tomas Baer
Department of Chemistry
University of North Carolina
Chapel Hill, North Carolina 27599-3290
baer@unc.edu (919)962-1580

Professor Joel M. Bowman
Department of Chemistry
Emory University
1515 Pierce Drive
Atlanta, Georgia 30322
jmbowma@emory.edu (404)727-6590

Professor Alexander Burcat
Faculty of Aeospace Engineering
Technion - Israel Inst of Technology
Haifa 32000 Israel
aer0201@technix.technion.ac.il (630) 252-7666

Professor Barry K. Carpenter
Department of Chemistry
Cornell University
Ithaca, NY 14853-1301
bkc1@cornell.edu (607)255-3826

Dr. Robert K. Cheng
Energy and Environment Division
University of California
Lawrence Berkeley Laboratory
One Cyclotron Road
Berkeley, California 94720
rkcheng@lbl.gov 510.486.5438

Professor F. Fleming Crim
Department of Chemistry
University of Wisconsin
1101 University Avenue
Madison, Wisconsin 53706
fcrim@chem.wisc.edu (608)263-7364

Professor H. Floyd Davis
Department of Chemistry
Baker Laboratory
Cornell University
Ithaca, New York 14853-1301
hfd1@cornell.edu 607-255-0014

Professor Kent M. Ervin
Department of Chemistry/216
1664 N. Virginia St.
University of Nevada, Reno
Reno, Nevada 89557-0020
ervin@chem.unr.edu 775.784.6676

Professor George Flynn
Department of Chemistry
Mail Stop 3109
Columbia University
3000 Broadway
New York, New York 10027
flynn@chem.columbia.edu (212)854-4162

Dr. David Golden
Department of Mechanical Engineering
Bldg. 920
Stanford University
Stanford, CA 94305-3030
david.golden@stanford.edu 650-723-5009

Dr. Robert S. Barlow
Combustion Research Facility
MS9051
Sandia National Laboratories
Livermore, California 94551-0969
barlow@ca.sandia.gov 925.294.2688

Professor Kenneth Brezinsky
Chemical Engineering Dept.
810 S. Clinton
The University of Illinois at Chicago
Chicago, Illinois 60607-7022
kenbrez@uic.edu (312)996-9430

Professor Laurie J. Butler
The James Franck Institute
The University of Chicago
5640 S. Ellis Avenue
Chicago, Illinois 60637
L-Butler@uchicago.edu 773.702.7206

Dr. David W. Chandler
Combustion Research Facility
MS 9055
Sandia National Laboratories
Livermore, California 94551-0969
chand@sandia.gov 925.294.2091

Professor Robert E. Continetti
Department of Chemistry, 0340
University of California, San Diego
9500 Gilman Drive
La Jolla, CA 92093-0340
rcontinetti@ucsd.edu 858.534.5559

Professor Hai-Lung Dai
Department of Chemistry
University of Pennsylvania
Philadelphia, Pennsylvania 19104-6323
dai@sas.upenn.edu 215.898.5077

Professor Frederick L. Dryer
Department of Mechanical & Aerospace Engineering
Princeton University
Princeton, New Jersey 08544
fldryer@princeton.edu (609)258-5206

Dr. Askar Fahr
Chemical Sciences and Technology Lab
Natl. Inst. of Standards and Technology
Gaithersburg, MD 20899
askarfahr@hotmail.com (301)975-2511

Dr. Jonathan H. Frank
Combustion Research Facility
MS 9051
Sandia National Laboratories
Livermore, California 94551
jhfrank@ca.sandia.gov 925.294.4645

Dr. Stephen K. Gray
Chemistry Division
Argonne National Laboratory
9700 South Cass Ave.
Argonne, Illinois 60439
gray@tcg.anl.gov 630.252.3594

Participants

Dr. Gregory E. Hall
Chemistry Department
Brookhaven National Laboratory
Upton, New York 11973
gehall@bnl.gov 631.344.4376

Dr. Alex Harris
Chemistry Department
Building 555
Brookhaven National Laboratory
P.O. Box 5000
Upton, NY 11973-5000
alexh@bnl.gov 631-344-4301

Dr. Jan P. Hessler
Chemistry Division
Bldg. 200, Room R119
Argonne National Laboratory
9700 South Cass Avenue
Argonne, Illinois 60439
hessler@anl.gov 630-252-3717

Professor Philip M. Johnson
Department of Chemistry
State University of New York at Stony Brook
Stony Brook, New York 11794
Philip.Johnson@sunysb.edu (631)632-7912

Professor Michael E. Kellman
Department of Chemistry
University of Oregon
Eugene, Oregon 97403
kellman@oregon.uoregon.edu 541.346.4196

Dr. Stephen J. Klippenstein
Combustion Research Facility
MS 9055
Sandia National Laboratories
Livermore, California 94551-0969
SJKLIIPP@sandia.gov (925)294-2289

Professor Marsha I. Lester
Department of Chemistry
University of Pennsylvania
231 South 34th Street
Philadelphia, Pennsylvania 19104-6323
milester@sas.upenn.edu (215)898-4640

Professor Ming-Chang Lin
Department of Chemistry
Emory University
1515 Pierce Drive
Atlanta, Georgia 30322
chemmcl@emory.edu (404)727-2825

Dr. R. Glen Macdonald
Chemistry Division
Argonne National Laboratory
9700 South Cass Avenue
Argonne, Illinois 60439
RGMacDonald@anl.gov (630)252-7742

Dr. Joe V. Michael
Chemistry Division
Argonne National Laboratory
9700 South Cass Avenue
Argonne, Illinois 60439
jmichael@anl.gov (630)252-3171

Dr. Nils Hansen
Combustion Research Facility
Sandia National Laboratories
Livermore, California 94551-0969
nhansen@sandia.gov 925.294.6272

Professor Martin Head-Gordon
Department of Chemistry
University of California at Berkeley
Berkeley, California 94720
mhg@cchem.berkeley.edu 510.642.5957

Dr. Richard L. Hilderbrandt
SC-14 Germantown Building
U. S. Department of Energy
1000 Independence Ave. SW
Washington, DC 20585-1290
richard.hilderbrandt@science.doe.gov 301-903-0035

Professor Ralf I. Kaiser
Department of Chemistry
The University of Hawaii at Manoa
2445 The Mall
Honolulu, HI 96822
kaiser@gold.chem.hawaii.edu (808)956-5731

Dr. Alan R. Kerstein
Combustion Research Facility
MS9051
Sandia National Laboratories
Livermore, California 94551-0969
arkerst@sandia.gov 925.294.2390

Dr. Allan Laufer
Retired - Guest Worker at NIST
allan.laufer@nist.gov 301.975.2062

Professor William A. Lester, Jr.
Department of Chemistry
University of California at Berkeley
Berkeley, California 94720-1460
walester@lbl.gov 510.643.9590

Professor Marshall B. Long
Department of Mechanical Engineering
Yale University
P.O. Box 208284
New Haven, Connecticut 06520-8284
long-marshall@yale.edu 203.432.4229

Dr. Andrew
Combustion Research Facility
Sandia National Laboratories
Livermore, California 94551-0969
amcrlr@sandia.gov 925 294-3054

Dr. Terry Michalske
Combustion Research Facility
Sandia National Laboratories
Livermore, California 94551-0969
tamicha@sandia.gov 925.294.2122

Dr. Lawrence Harding
Chemistry Division
Argonne National Laboratory
9700 South Cass Avenue
Argonne, Illinois 60439
harding@anl.gov (630)252-3591

Professor John Hershberger
Department of Chemistry
North Dakota State University
Fargo, ND 58105-5516
john.hershberger@ndsu.nodak.edu (701)231-8225

Professor Paul L. Houston
Department of Chemistry
122 Baker Laboratory
Cornell University
Ithaca, New York 14853-1301
plh2@cornell.edu 607.255.4303

Dr. Andrei Kazakov
Department of Mechanical & Aerospace Engineering
Princeton University
Princeton, New Jersey 08544
andrei@princeton.edu 609-258-5280

Professor John Kiefer
Department of Chemical Engineering
University of Illinois at Chicago
Chicago, Illinois 60607
kiefer@uic.edu (312)996-5711

Professor Stephen R. Leone
Department of Chemistry
209 Gilman Hall
University of California at Berkeley
Berkeley, California 94720-1460
srl@cchem.berkeley.edu 510.643.5467

Professor John C. Light
The James Franck Institute
The University of Chicago
5640 S. Ellis Avenue
Chicago, Illinois 60637
j-light@uchicago.edu 773.702.7197

Professor Robert P. Lucht
Department of Mechanical Engineering
Purdue University
Lafayette, Indiana
lucht@purdue.edu 765-494-5623

Professor Alexander Mebel
Department of Chemistry and Biochemistry
Florida International University
11200 8th Street
Miami, FL 33199
mebela@fiu.edu (305)348-1945

Dr. Hope Michelsen
Combustion Research Facility
M/S 9055
Sandia National Laboratories
Combustion Research Facility
Livermore, CA 94551
hamiche@ca.sandia.gov 925.294.2335

Participants

Professor Terry A. Miller
Department of Chemistry
Ohio State University
140 West 18th Avenue
Columbus, Ohio 43210
tamiller+@osu.edu 614.292.2569

Dr. John Miller
SC-14 Germantown Building
U. S. Department of Energy
1000 Independence Ave. SW
Washington, DC 20585-1290
John.Miller@science.doe.gov 301-903-5806

Dr. Habib N. Najm
Combustion Research Facility
MS9051
Sandia National Laboratories
Livermore, California 94551-0969
hnnajm@sandia.gov 925.294.2054

Dr. Joseph Oefelein
Combustion Research Facility
Sandia National Laboratories
Livermore, CA 94551
oefelei@sandia.gov

Professor Stephen B. Pope
Mechanical and Aerospace Engineering
Cornell University
106 Upson Hall
Ithaca, New York 14853
pope@mae.cornell.edu (607)255-4314

Dr. Larry Rahn
Combustion Research Facility
Sandia National Laboratories
Livermore, California 94551-0969
rahn@sandia.gov 925 294 2091

Dr. Gregory Rosasco
Physical and Chemical Properties Division
NIST, 838.00
1000 Bureau Drive 8380
Gaithersburg, MD 20899-8380
gregory.rosasco@nist.gov 301-975-2483

Professor Henry Frederick Schaefer III
Department of Chemistry
University of Georgia
Athens, Georgia 30602
hfs@uga.edu (706)542-2067

Dr. Ron Shepard
Chemistry Division
Argonne National Laboratory
9700 South Cass Avenue
Argonne, Illinois 60439
shepard@tcg.anl.gov 708.252.3584

Dr. Craig Taatjes
Combustion Research Facility
MS 9055
Sandia National Laboratories
Livermore, California 94551-0969
cataatj@sandia.gov 925.294.2764

Professor William H. Miller
Department of Chemistry
213 Gilman Hall
University of California at Berkeley
Berkeley, California 94720
millerwh@berkeley.edu (510)642-0653

Dr. James Muckerman
Chemistry Department
Brookhaven National Laboratory
Upton, NY 11973
muckerma@bnl.gov 631.344.4368

Professor Daniel M. Neumark
Department of Chemistry
University of California at Berkeley
Berkeley, California 94720
dan@radon.cchem.berkeley.edu 510.642.3502

Dr. David L. Osborn
Combustion Research Facility
MS 9055
Sandia National Laboratories
Livermore, California 94551-0969
dlosbor@sandia.gov 925-294-4622

Dr. Stephen Pratt
Chemistry Division
Argonne National Laboratory
9700 South Cass Avenue
Argonne, Illinois 60439
spratt@anl.gov 630.252.4199

Professor Hanna Reisler
Department of Chemistry
University of Southern California
Los Angeles, California 90089-0482
reisler@usc.edu (213)740-7071

Professor Klaus Ruedenberg
Department of Chemistry
Iowa State University of Science and Technology
Ames, Iowa 50011
ruedenberg@iastate.edu (515)294-5253

Dr. Trevor Sears
Chemistry Department
Brookhaven National Laboratory
Upton, New York 11973
sears@bnl.gov 631.344.4374

Professor Mitchell Smooke
Department of Mechanical Engineering
Yale University
P.O. Box 208284
New Haven, Connecticut 06520-8284
mitchell.smooke@yale.edu (203)432-4344

Professor Donald L. Thompson
Department of Chemistry
125 Chemistry Building
University of Missouri-Columbia
Columbia, Missouri 65211
thompsondon@missouri.edu 573.882.8374

Dr. James A. Miller
Combustion Research Facility
MS-9055
Sandia National Laboratories
Livermore, California 94551-0969
jamille@sandia.gov 925.294.2759

Professor Amy S. Mullin
Department of Chemistry
Boston University
590 Commonwealth Avenue
Boston, Massachusetts 02215-2507
mullin@chem.bu.edu 617.353.8477

Professor Cheuk-Yiu Ng
Department of Chemistry
One Shields Avenue
University of California at Davis
Davis, CA 95616
cyng@chem.ucdavis.edu (530)754-9645

Professor David S. Perry
Department of Chemistry
University of Akron
Akron, Ohio 44325
dperry@uakron.edu 330.972.6825

Dr. Martin Quack
Laboratory for Physical Chemistry
ETH Hönggerberg HCI E 235
Wolfgang-Pauli-Str. 10
CH-8093 Zürich, Switzerland
quack@phys.chem.ethz.ch +41 1 632-4421

Dr. Eric Rohlfing
SC-14 Germantown Building
U. S. Department of Energy
1000 Independence Ave. SW
Washington, DC 20585-1290
eric.rohlfing@science.doe.gov 301-903-8165

Dr. Branko Ruscic
Chemistry Division
Argonne National Laboratory
9700 South Cass Avenue
Argonne, Illinois 60439
ruscic@anl.gov 630.252.4079

Dr. Thomas B. Settersten
Combustion Research Facility
MS 9056
Sandia National Laboratories
Livermore, California 94551-0969
tbsette@sandia.gov 925.294.4701

Professor Arthur G. Suits
Department of Chemistry
5101 Cass Avenue
Wayne State University
Detroit, MI 48202
asuits@chem.wayne.edu (313)577-9008

Dr. Robert Tranter
Chemistry Department
Argonne National Laboratory
9700 S. Cass Avenue
Argonne, IL 60439
tranter@anl.gov (630)252-6505

Participants

Professor Donald G. Truhlar
Department of Chemistry
139 Smith Hall
University of Minnesota
207 Pleasant St. SE
Minneapolis, Minnesota 55455
truhlar@umn.edu (612)624-7555

Professor James J. Valentini
Department of Chemistry
Columbia University
3000 Broadway, MC 3120
New York, New York 10027
jjv1@columbia.edu (212)854-7590

Dr. Charles K. Westbrook
Chemistry and Materials Science
Lawrence Livermore National Laboratory
P. O. Box 808, L-090
Livermore, California 94550
westbrook1@llnl.gov 925.422.4108

Professor Curt Wittig
Department of Chemistry
University of Southern California
Los Angeles, California 90089-0484
wittig@usc.edu (213)740-7368

Professor Timothy S. Zwier
Department of Chemistry
Purdue University
West Lafayette, Indiana 47907
zwier@purdue.edu (765)494-5278

Dr. Wing Tsang
Center for Chemical Technology
A147 Chemistry Building
Natl. Inst. of Standards and Technology
Gaithersburg, Maryland 20899
wing.tsang@nist.gov (301)975-2507

Dr. Alber Wagner
Chemistry Division
Bldg. 200, R105
Argonne National Laboratory
9700 S. Cass Avenue
Argonne, IL 60439
wagner@tcg.anl.gov 630-252-3570

Professor Phillip R. Westmoreland
Department of Chemical Engineering
University of Massachusetts
Amherst, Massachusetts 01003
westm@ecs.umass.edu (413)545-1750

Professor David R. Yarkony
Department of Chemistry
Johns Hopkins University
Charles and 34th Streets
Baltimore, Maryland 21218
yarkony@jhu.edu 410.516.4663

Dr. Frank Tully
SC-14 Germantown Building
U. S. Department of Energy
1000 Independence Ave. SW
Washington, DC 20585-1290
frank.tully@science.doe.gov (301)903-5998

Professor Peter M. Weber
Department of Chemistry
Brown University
Box H
Providence, Rhode Island 02912
Peter_Weber@brown.edu (401)863-3767

Dr. Kevin Wilson
Advanced Light Source Division
Lawrence Berkeley National Labs
One Cyclotron Road, MS 6R2100
Berkeley CA, 94720-8226
krwilson@lbl.gov 510-495-2474

Dr. Hua-Gen Yu
Chemistry Department
Brookhaven National Laboratory
Upton, NY 11973
hgy@bnl.gov (631)344-4367

Author Index

Baer, T.....1	Leone, S.R.....160	Valentini, J.J.....307
Barlow, R.S.5	Lester, M.I.....164	Weber, P.M.310
Bowman, C. T.....112	Lester, Jr., W.A.168	Westbrook, C.K.314
Bowman, J. M.9	Light, J.C.....171	Westmoreland, P.R.318
Brezinsky, K.13	Lin, M.C.....175	Wittig, C.....322
Brown, N.J.17	Long, M.B.277	Yarkony, D.R.326
Butler, L. J.....21	Lucht, R.P.179	Yu, H.G.....330
Carpenter, B.K.25	Macdonald, R.G.183	Zwier, T.S.334
Chandler, D.W.29	Mebel, A.187	
Chen, J.H.....33,133	Michael, J.V.191	
Cheng, R.K.....37	Michelsen, H.A.195	
Continetti, R.E.41	Miller, J.A.199	
Cool, T.A.45	Miller, T.A.202	
Crim, F.F.....49	Miller, W.H.....206	
Dai, H.L.52	Muckerman, J.T.210	
Davis, H.F.56	Mullin, A.S.....214	
Davis, M.J.59	Najm, H.N.....218	
Dryer, F.L.....63	Neumark, D.M.222	
Ellison, G.B.....67	Ng, C.Y.225	
Ervin, K.M.73	Oefelein, J.229	
Fahr, A.77	Osborn, D.L.233	
Field, R.W.80	Perry, D.S.....237	
Flynn, G.84	Pitz, W.J.314	
Frank, J.H.....88	Pope, S.B.....241	
Frenklach, M.92	Pratt, S.T.245	
Gordon, M.S.....253	Reisler, H.249	
Gray, S.K.96	Ruedenberg, K.253	
Green, Jr., W.H.100	Ruscic, B.257	
Hall, G.E.104	Rutland, C.J.....133	
Hansen, N.....108	Sankaran, R.33	
Hanson, R.K.....112	Schaefer III, H.F.261	
Harding, L.B.116	Sears, T.J.....265	
Hawkes, E.R.....33	Settersten, T.A.269	
Head-Gordon, M.120	Shepard, R.....273	
Hershberger, J.F.124	Smooke, M.D.277	
Houston, P.L.129	Suits, A.G.....281	
Im, H.G.133	Taatjes, C.A.285	
Johnson, P.M.....137	Taylor, H.S.....289	
Kaiser, R.I.140	Thompson, D.L.291	
Kellman, M.E.....144	Tranter, R.S.....295	
Kerstein, A.R.148	Trouve, A.133	
Kiefer, J.H.152	Truhlar, D.G.....299	
Klippenstein, S.J.156	Tsang, W.303	